Late-Stage C−H Activation of Spiropiperidines *via* Evolved $P450_{BM3}$ Mutants and its Application to Fragment-Based Drug Discovery

A thesis submitted to the

Board of the Faculty of the Mathematical, Physical and Life Sciences

in partial fulfilment of the requirements for the degree of

Doctor of Philosophy of the University of Oxford

Ka Wing Alethea Lee

St. Peter's College

Hilary Term 2023

Abstract

Late-Stage C−H Activation of Spiropiperidines *via* Evolved $P450_{BM3}$ Mutants and its Application to Fragment-Based Drug Discovery

Ka Wing Alethea Lee — D.Phil.
St. Peter's College — Hilary Term 2023

This thesis describes the synthesis of spirocyclic piperidines, specifically 6-azaspiro[4.5]decane and 7-azaspiro[4.5]decane, and the late-stage functionalisation of the synthesised piperidines *via* $P450_{BM3}$ mutants. Utilisation of the newly-installed hydroxyl group as a synthetic handle was also explored, with the aim of demonstrating the potential of $P450_{BM3}$ catalysis to Fragment-Based Drug Discovery.

Chapter 1 provides an introduction to Fragment-Based Drug Discovery and a review of the major synthetic studies towards spirocyclic piperidines. Subsequently, the significance of C−H functionalisation and the various aspects of $P450_{BM3}$ applications are discussed.

Chapter 2 describes the synthesis of 6-azaspiro[4.5]decane and its substrate engineering to access hydroxylated products at various unactivated positions. Molecular Dynamics simulations and molecular docking were employed to investigate the underlying ligand-protein interactions.

Chapter 3 describes the synthesis of 7-azaspiro[4.5]decane and its substrate engineering to access hydroxylated products. Analogous to Chapter 2, computational methods were also employed to study ligand-protein interactions.

Chapter 4 explores the utilisation of the hydroxyl group introduced by $P450_{BM3}$ mutants as a synthetic handle for functional group diversification. Numerous synthetic reactions were performed and the results are discussed.

Finally, Chapter 5 details the protein engineering of $P450_{BM3}$ mutants to optimise the conversion and selectivity of a selected metabolite *via* docking-guided mutagenesis. Computational and experimental results were compared by considering different factors in the docking algorithms.

Table of Contents

Acknowledgment ..... **i**

Abbreviations ..... **iii**

Amino Acid Codes ..... **viii**

Chapter 1: Introduction **1**

1.1 The Evolution of Drug Discovery 1

1.1.2 Fragment-Based Drug Discovery 3

1.1.3 Spiropiperidines 14

1.3 C(sp^3)-H Activation 21

1.3.1 Significance of C(sp^3)−H Activation 21

1.3.2 Hydrogen Atom Transfer 22

1.3.3 Metal-Catalysed Carbene and Nitrene Transfer 22

1.3.4 Directed Transition-Metal-Catalysed C−H Activation 24

1.3.5 Biocatalysis in C(sp^3)-H Activation 26

1.4 Cytochrome P450 and $P450_{BM3}$ 28

1.4.1 Background and Significance 28

1.4.2 The Catalytic Cycle of P450s 30

1.4.3 $P450_{BM3}$ (CYP102A1) 32

1.4.4 $P450_{BM3}$ in Synthesis 34

1.5 Aims and Proposed Work 46

Chapter 2: *N*-Protected 6-azaspiro[4.5]decane (2-spiro) analogue **48**

2.1 Overview 48

2.2 First Generation Route *via* Curtius Rearrangement 48

2.3 Second Generation Route *via* Beckmann Rearrangement 50

2.4 Third Generation Route *via* Reductive Amination 52

2.5 Fourth Generation Route *via* Reductive Bis-alkylation 53

2.6 Screening of *N*-protected 6-azaspiro[4.5]decane with $P450_{BM3}$ 58

2.6.1 Screening of *N*-Ms-protected Spiroamine 2.37 59

2.6.2 Screening of *N*-Bn-protected Spiroamine 2.45 61

2.6.3 Screening of *N*-Boc-protected Spiroamine 2.24 62

2.6.4 Screening of *N*-Tfa-protected Spiroamine 2.55 66

2.7 Computational Docking Studies on Substrates 2.24 and 2.55 71

2.8 Conclusion and Future Work on the 2-Spiroamine Series 80

Chapter 3: *N*-protected 7-azaspiro[4.5]decane (3-spiro) analogue **84**

3.1 Overview 84

3.2 Retrosynthesis 84
3.4 Screening of *N*-protected 7-azaspiro[4.5]decane with $P450_{BM3}$ 90
3.4.1 Screening of *N*-Boc-protected Spiroamine 3.10 92
3.4.2 Screening of *N*-Ips-protected Spiroamine 3.11 96
3.4.3 Screening of *N*-Ms-protected Spiroamine 3.5 99
3.4.4 Screening of *N*-DEP Protected Spiroamine 3.12 101
3.4.5 Computational Studies on 3.10 and 3.11 103
3.4.6 Screening of Unprotected Spirocyclic Lactam 3.6 110
3.4.7 Screening of *N*-Bn-protected Spirocyclic Lactam 3.13 111
3.4.8 Computational Studies on 3.13 115
3.5 Conclusions and Future Work on the 3-Spiroamine and 3-Spirolactam Series 118
Chapter 4: Diversification of a $P450_{BM3}$ Metabolite 122
4.1 Overview 122
4.2 Fragment Diversification 122
4.2.1 Titre Screen of Substrate 122
4.2.2 Diversification from Alcohol 3.13a 123
4.2.3 Diversification from Ketone 4.57 138
4.2.4 Conclusion and Future Work on Fragment Diversification 145
4.3 Screening of *N*-protected 4-azaspiro[2.5]octane with $P450_{BM3}$ 148
4.3.1 *N*-Bn-protected 4-azaspiro[2.5]octane (*N*-Bn [6.3]spirocycle, 4.56) 148
4.3.2 *N*-Boc-protected 4-azaspiro[2.5]octane (*N*-Boc [6.3]-spirocycle, 4.58) 150
4.3.3 Computational studies on *N*-Bn and *N*-Boc [6.3]-spirocycle 4.56 and 4.58 152
4.3.4 Conclusion and Future Work on the [6.3]-Spirocycle Series 155
Chapter 5: Docking-guided Mutagenesis 157
5.1 Overview 157
5.2 Initial Docking Study for *N*-Boc 3-spiroamine 157
5.2.1 First Generation Mutagenesis (R19/A184I/A328L) 157
5.2.2 Second Generation Mutagenesis (R19/A184I/A328L/T268S) 161
5.2.4 Fourth Generation Mutagenesis (R19/A184I/A328L/T268S/L437F) 167
5.3 Weighted Docking Selectivity 168
5.3.1 Cluster population 169
5.3.2 The Affinity Energy (AE) of Binding Poses 173
5.4 Conclusion and Future Work on Docking-guided Mutagenesis 177
5.4.1 Conclusion 177
5.4.2 Implications and Future Work 178
Chapter 6: Summary and Future Work 180

Chapter 7: Experimental.....182
7.1 General Experimental 182
7.1.1 General Experimental for Chemical Syntheses..... 182
7.1.2 General Experimental for Enzymatic Reactions and Molecular Biology 183
7.2 Enzymatic Hydroxylation Procedures 184
7.2.1 Enzymatic Screening 184
7.2.2 General Procedure-1 (GP-1) for Preparative Scale Reactions 185
7.2.3 Enzyme Expression and Quantification..... 186
7.2.4 Mutagenesis and DNA Preparation..... 187
7.2.4 MD Simulations and Molecular Docking 189
7.3 Compounds from Chapter 2..... 192
7.4 Compounds from Chapter 3..... 217
7.5 Compounds from Chapter 4..... 236
7.6 Single Crystal X-Ray Data..... 262
7.6.1 Crystal Data for Compound 3.10a 262
7.6.2 Cystal Data for Compound 4.57 263
7.7 Mosher Ester NMR Analysis..... 264
7.7.1 Metabolite 3.10a from Mutant RT2 264
7.7.2 Metabolite 3.11a from Mutant R19/F87I..... 265
7.7.3 Metabolite 3.11b from Mutant GV/L188Q..... 266
7.7.4 Metabolite 3.11c from Mutant R19/F87I..... 267
7.7.5 Metabolite 3.13a from Mutant R19/F87I..... 268
7.7.7 Metabolite 3.13b from Mutant R19/F87A/A184I..... 269
7.8 Chiral GC Data 270
7.8.1 Chiral GC Trace of 3.10a from Mutant R19/F87I 270
7.8.2 Chiral GC Trace of 3.10b..... 270
7.8.3 Chiral GC Trace of 3.10c..... 270
7.9 NOESY Spectra 271
7.9.1 Metabolite 2.24a from Mutant KT2/L188G/I263G 271
7.9.2 Metabolite 2.24b from Mutant GL/L188Q/I263G/A264G 271
7.9.3 Metabolite 2.55a from Mutant A330P 272
7.9.4 Metabolite 3.10a from Mutant R19/F87I..... 272
7.9.5 Metabolite 3.10c from Mutant RT2 273
7.9.6 Metabolite 3.11a from Mutant R19/F87I..... 273
7.9.7 Metabolite 3.11b from Mutant R19/F87I..... 274
7.9.8 Metabolite 3.13a from Mutant R19/F87I..... 274

7.9.9 Compound 4.5 275
7.9.10 Compound 4.9 275
Chapter 8: Appendices 276
8.1 Screening Data 276
8.1.2 *N*-Ms Protected Spiroamine 2.37 276
8.1.3 *N*-Boc Protected Spiroamine 2.24 277
8.1.4 *N*-Tfa Protected Spiroamine 2.55 280
8.1.5 *N*-Boc-protected Spiroamine 3.10 282
8.1.6 *N*-Ips-protected Spiroamine 3.11 284
8.1.7 *N*-Ms-protected Spiroamine 3.5 286
8.1.8 *N*-DEP Protected Spiroamine 3.12 287
8.1.9 Unprotected Spirocyclic Lactam 3.6 289
8.1.10 *N*-Bn-protected Spirocyclic Lactam 3.13 291
8.2 Selectivity of α′-OH from Mutagenesis 292
8.2.1 First Generation Mutagenesis 292
8.2.2. Second Generation Mutagenesis 293
8.2.3 Third Generation Mutagenesis 293
8.2.4 Fourth Generation Mutagenesis 294
8.3 Flexible Residues in ADFR Docking Studies 295
8.3.1 *N*-Bn [6.3]-spirocycle 4.56 295
8.3.2 Flexible Residues for Docking-Guided Mutagenesis Studies 295
References 306

Acknowledgment

Firstly, my biggest thanks go to Professor Jeremy Robertson. Thank you for all your patience and continuous guidance throughout these four years. Your immense chemistry knowledge never fails to amaze me and I truly respect and admire you from the bottom of my heart. Being part of your group certainly made my DPhil journey a lot more enjoyable and tolerable. I am eternally grateful to receive your mentorship and my future success would not have made possible without the foundation that you have helped me laid.

Secondly, I would like to thank Professor Luet Wong, for making this project a successful collaboration. Thank you for your guidance on all the enzymatic work, especially when I first began my DPhil and had no clue about P450 catalysis. Thank you for proofreading my thesis in such a busy time, particularly in providing some very valuable insights on molecular docking. This thesis has certainly become a better one with your input.

I would also like to thank everyone in the Robertson and Wong groups, both present and past members, for bringing laughter and lightness, and fostering such a relaxed and friendly environment which certainly brightened up my bad days. To Xinxin, for being effortlessly humorous and a good friend both inside and outside of the lab. To Alice, for all the encouragement throughout my DPhil and I hope we don't have to work on weekends and late-nights ever again. To Melody, for your angelic voice that brings livelihood to the lab, don't ever stop singing! To Wenyu and Yuan, for all the support with my enzyme work and being such good mentors. To Mary, for all your patience with my chemistry problems and your amazing baking. To Vicky, for sharing your passion in spirolactams and I hope

you overcome your obstacles in your fragment diversification. To Yini, for all the fun conversation and life lessons.

Thirdly, I would like to thank Celeste Hung. I am so glad that we met and thankful for how far we have come. Thank you for all your continuous support and putting up with my late-night complaints. Thank you for being so creatively entertaining, which brought me a lot of laughter and joy. Most importantly, thank you for being by my side and all of this would not have been possible without your presence.

Lastly, I would like to thank my parents, for your unconditional love and support that they have been for me. There are not enough words to express how grateful I am for everything you have done for me. Everything I have and everything I am, I owe it all to you.

Abbreviations

°C	Degree Celsius
δ	NMR chemical shift
ν_{max}	Infrared absorption maximum
µM	Micromolar
µL	Microlitre
Å	Angstrom
Ac	Acetyl
ACN	Acetonitrile
A.D.	Anno Domini
aq.	Aqueous
B.C.	Before Christ
Bn	Benzyl
Boc	*tert*-Butoxycarbonyl
Br	Broad
Bu	Butyl
cal	Calories
CAN	Ceric ammonium nitrate
cat.	Catalyst
CDI	Carbonyldiimidazole
COSY	Homonuclear correlation spectroscopy
Conc.	Concentrated
cm^{-1}	Wavenumbers
Conv.	Conversion
Cp	Cyclopentadienyl
Cy	Cyclohexyl
CYP	Cytochromes P450
d	Doublet
d	Days
Da	Dalton
DAST	Diethylaminosulfur trifluoride
DCE	Dichloroethane

DCM	Dichloromethane
d.e.	Diastereomeric excess
DEP	Diethyl phosphonate ester
DIBAL-H	Diisobutyl aluminium hydride
DIPEA	*N*,*N*-Diisopropylethylamine
DMA	*N*,*N*-Dimethylacetamide
DME	Dimethoxyethane
DMF	Dimethyl formamide
DMP	Dess–Martin periodinane
DNA	Deoxyribonucleic acid
dNTP	Deoxyribonucleotide triphosphate
DPPA	Diphenylphosphoryl azide
d.r.	Diastereomeric ratio
DTBP	Di-*tert*-butyl peroxide
DMSO	Dimethyl sulfoxide
EC_{50}	Half maximal effective concentration
e.e.	Enantiomeric excess
Equiv.	Equivalents
ESI	Electrospray ionisation
Et	Ethyl
et al.	And others
Et_3N	Triethylamine
EtOAc	Ethyl acetate
FAD	Flavin adenine nucleotide
FB	Flavobacterium
FID	Flame ionisation detector
FMN	Flavin mononucleotide
g	Gram
GC	Gas chromatography
GDH	Glucose dehydrogenase
h	Hour
HFIP	Hexafluoroisopropanol
HIV	Human immunodeficiency virus

HRMS	High resolution mass spectrometry
HSQC	Heteronuclear Single Quantum Coherence
Hz	Hertz
IC_{50}	Half maximal inhibitory concentration
i	Iso
Ips	Isopropyl sulfonyl
IPTG	Isopropylthio-β-galactoside
IR	Infrared
J	Coupling constant
J	Joules
k	Kilo
K_D	Dissociation constant
K	Equilibrium constant
kan	Kanamycin
L	Litre
LB	Lysogeny broth
LOGSY	Ligand Observed via Gradient Spectroscopy
m	Multiplet
M	Molar
m-CPBA	*meta*-chloroperoxybenzoic acid
Me	Methyl
mg	Milligram
MHz	Megahertz
min	Minutes
mmol	Millimolar
MOM	Methoxymethyl
MOMTPPC	(Methoxymethyl)triphenylphosphonium chloride
m.p.	Melting point
Ms	Methanesulfonyl
MSA	Methanesulfonic acid
MS	Molecular sieves
MS	Mass spectrometry
m/*z*	Mass/charge ratio

n-	Normal
NADH	Nicotinamide adenine dinucleotide
NADPH	Nicotinamide adenine dinucleotide phosphate
NIS	*N*-Iodosuccinimide
NMR	Nuclear magnetic resonance spectroscopy
NOE	Nuclear Overhauser Effect
NOESY	Nuclear Overhauser Effect Spectroscopy
p	Para
PCR	Polymerase chain reaction
Ph	Phenyl
Piv	Pivaloyl
Press.	Pressure
ppm	Parts per million
Pr	Propyl
PTTL	*N*-phthaloyl-*tert*-leucinate
Pyr	Pyridine
q	Quartet
quant.	Quantitative
R	Generic group
R_f	Retention factor
Rpm	Revolution per minute
RT	Room temperature
s	Singlet
S	Spin state
Sat.	Saturated
Select.	Selectivity
SOC	Super optimal broth with catabolite repression
S_N2	Substitution nucleophilic bimolecular
STD	Saturation-transfer difference
t	Triplet
t	Tertiary
TBAB	Tetrabutylammonium bromide
TBAF	Tetrabutylammonium fluoride

TBTU	*N*,*N*,*N*′,*N*′-Tetramethyl-O-(benzotriazol-1-yl)uronium tetrafluoroborate,
TCE	Tetrachloroethane
Temp.	Temperature
TES	Triethylsilyl
THF	Tetrahydrofuran
Tf	Trifluoromethanesulfonyl
Tfa	Trifluoroacetyl
TFA	Trifluoroacetic acid
TFAA	Trifluoroacetic anhydride
TLC	Thin layer chromatography
TMS	Trimethylsilyl
TON	Turnover number
TPPC	Triphenylphosphonium chloride
Ts	4-Toluenesulfonyl
UDP	Uridine diphosphate
vs.	Versus
WT	Wild type

Amino Acid Codes

Amino Acid	Three Letter Code	One Letter Code
Alanine	Ala	A
Arginine	Arg	R
Asparagine	Asn	N
Aspartic Acid	Asp	D
Cysteine	Cys	C
Glutamic acid	Glu	E
Glycine	Gly	G
Histidine	His	H
Isoleucine	Ile	I
Leucine	Leu	L
Lysine	Lys	K
Methionine	Met	M
Phenylalanine	Phe	F
Proline	Pro	P
Serine	Ser	S
Threonine	Thr	T
Tryptophan	Trp	W
Tyrosine	Tyr	Y
Valine	Val	V

Chapter 1: Introduction

1.1 The Evolution of Drug Discovery

For thousands of years, humans have depended on nature to fulfil their fundamental needs, including the production of food, clothing and shelter. Plants have played a significant role in sophisticated traditional medicine systems that have existed throughout the ages. The first record, dated from about 2600 B.C., were oils of *Cedrus* species (Cedar) and *Cupressus sempevirens* (cypress), all of which are still used today as treatment ranging from coughs and colds to parasitic infections.[1] Later in 130 – 200 A.D., Galen authored over 30 books on the use of medicinal herbs and related topics. He became well-known for his intricate prescriptions and formulas used in drug compounding, which were based on the Hippocratic theory, stating that all illness were based on an imbalance of four primary "humours".[1]

The formal codification of these work, among others, can be traced back to the publication of the *London Pharmacopoeia* in 1618.[2] The concept of using "pure" compounds as drugs can be attributed to the isolation of active components from commonly used plants and herbs, such as morphine, atropine, strychnine, and colchicine, during the early 1800s. These isolations paved the way for the production of the first commercial natural product in its pure form, morphine, by Emanuel Merck in 1826.[1]

Some of the most crucial foundations in chemical theory were established by 1870.[3] These included the birth of the periodic table framework, created by Mendeleev, and the pioneering theory of chemical structure, particularly benzene, developed by Kekulé.[4,5] These remarkable discoveries propelled the maturity of chemistry and provided the opportunity to allow its application to expand beyond chemistry itself, which also marked the beginning of drug discovery.

Later in 1905, J. N. Langley formulated the theory of drug receptors, which can be traced back to the original idea proposed by Ehrlich in the period of 1872−1874.[6,7] Langley concluded that receptors bound by drugs or transmitter substances can accept signals and generate responses that result in pharmacological effects.[6,7] Until this day, the basis of this theory continues to lie at the very heart of pharmacology. In that pre-NMR and pre-computational chemistry era, however, medicinal chemistry tools were somewhat limited and one can argue that chance was the basis for drug discovery. A notable example was the discovery of penicillin in 1928 by Fleming[8] which stimulated the development of antibiotics research.

From the late 1980s onwards, advances in synthetic, analytical, and purification technology,[9,10] along with the advent of combinatorial chemistry and automated high-throughput screening,[11] hugely benefited the process of "lead discovery" to "lead optimisation". In 2003, the completion of the human genome project[12,13] and a rapid growth in molecular biology revolutionised the pharmaceutical industry. We now have a better understanding of molecular pathways and the way is paved for drug discovery to be increasingly successful.

Overall, with the process of drug discovery having previously operated from a relatively small knowledge base and being dependent on serendipity, drugs were mainly derived from natural products without prior knowledge of their toxicity. Today, with alliances spanning various disciplines, drug discovery is more streamlined, often incorporating large compound libraries and high-throughput screening to greatly improve the success rate in finding useful therapeutics.

1.1.2 Fragment-Based Drug Discovery

1.1.2.1 Fragment-Based Drug Discovery vs. High-Throughput Screening

High-throughput screening (HTS) serves as a useful tool in present day drug discovery, coming into play at the stages of "hit identification" and "hit to lead" development (Figure 1.1). This process enables a large number of biological modulators and effectors to be screened and assayed against selected and specific targets in a short period of time.[14] By the early 2000s, HTS led to many drugs leads, especially against established classes of targets; however, when encountering newer or more difficult targets, HTS yielded fewer hits and even false positives.[15,16]

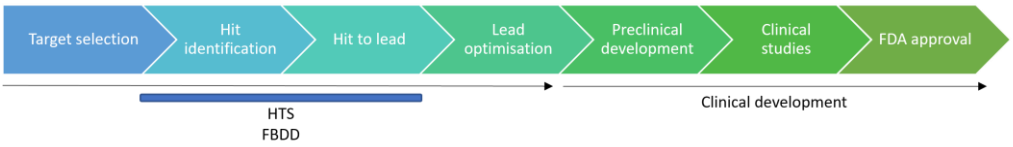

Figure 1.1 Flow chart of modern drug discovery and the significance of HTS and FBDD.

The success rates of identifying hits from HTS are generally agreed to be around 50%,[17,18] with the lack of success in HTS being attributed in part to the dominance of sp^2-rich, flat compounds present in compound libraries.[19,20] With recent advancements in structural biology, fragment-based drug discovery (FBDD) has become increasingly popular in target-based drug discovery (Figure 1.1)[21,22] because it is more efficient at sampling chemical space by limiting the size and physiochemical properties of potential candidates.[23,24] Unlike HTS, which screens millions of compounds to find a drug-sized starting point, FBDD begins with a chemical fragment and a much smaller library,[25,26] generally containing only a few thousand molecules.[16] Fragment-sized molecules are compounds with low molecular weight (<300 Da) and complexity, and have fewer than 20 heavy atoms.[27] The initial fragment hits generally have a low affinity towards the therapeutic target, usually in a μM−mM range.[18] Once an initial fragment binding event

is identified, it can be either elaborated or combined with other fragments to generate a hit (Figure 1.2).

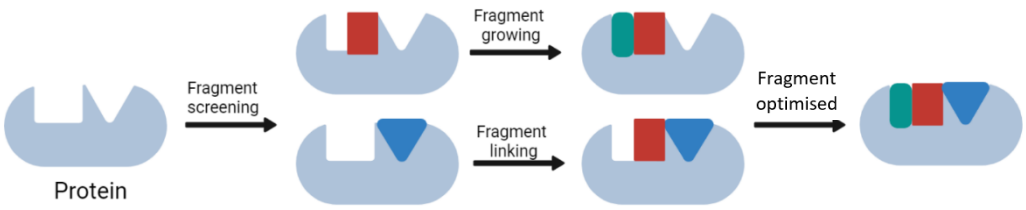

Figure 1.2 Illustration of the concept of FBDD.

An early estimate suggested that there are approximately 10^{63} drug-like molecules with up to 30 heavy atoms,[28] as opposed to about 10^{6} fragments with less than or equal to 160 Da.[29] In other words, given the vast number of compounds that can theoretically be made, and the limited structures that can be available for screening (*ca.* 10^{8} structures),[30] the screening of fragments would be more efficient than small molecules (Figure 1.3).

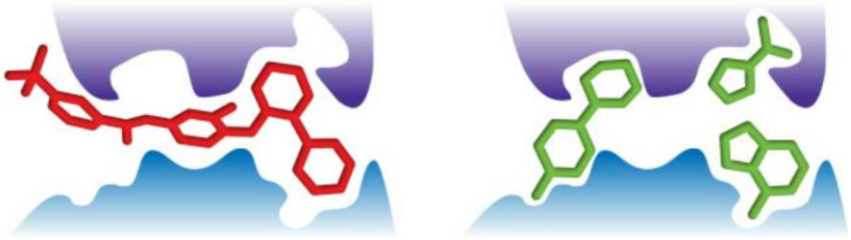

Figure 1.3 Comparison of HTS (red) and FBDD (green).

The second advantage of FBDD is that the resulting lead provides a higher ligand efficiency (LE) than leads discovered through HTS. LE is defined as "the binding energy per non-hydrogen atom of a ligand to its binding partner",[31] the concept being inspired by a study conducted by Kuntz *et al*. which revealed that the free energy of binding ($\Delta\Delta G$) increased linearly with increasing ligand size up to about 15 non-hydrogen atoms; beyond this, the increments were minimal. To depict this trend more clearly, Reynolds *et al.* extracted affinity data from the BindingDB database developed at the University of Maryland Biotechnology Institute.[32] By focusing on only the most potent ligands at each

size, it became apparent that LE dropped dramatically as size increased beyond a certain threshold (Figure 1.4). Furthermore, Reynolds reported a positive correlation between LE and compounds assembled from fragments.[33] This physical phenomenon can be explained by the greater accessible surface area per atom of a ligand with fragment-sized molecules, as well as fewer constraints presented in the ligand binding sites.

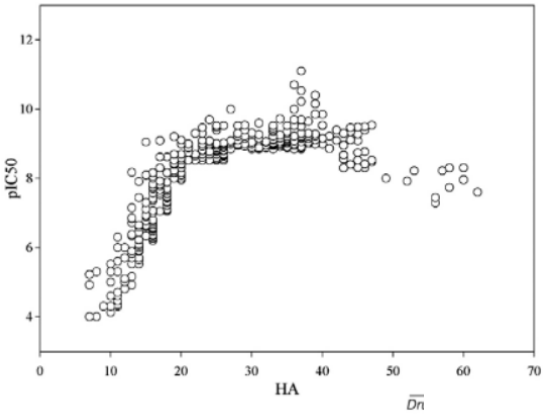

Figure 1.4 Plot of the most potent ligands of various sizes as extracted from Binding DB. The pIC_{50} reflects the "maximal affinity" of the ligands and increases rapidly up to 20 heavy atoms (HA), but plateaus beyond 25.[32]

1.1.2.2 Examples of FBDD

At present, there are four FDA-approved drugs known to have been developed by FBDD (Scheme 1.4A): Vemurafenib **1.24**[34] – treatment for late-stage melanoma; Pexidartnib **1.25**[35] – treatment for adults with symptomatic tenosynovial giant cell tumour (TGCT); Venetoclax **1.26**[36] – treatment for adults with chronic lymphocytic leukemia; and Erdafitinib **1.27**[37] – treatment for adults with urothelial cancer. Although most fragment libraries are diverse, work is still dedicated towards the development of libraries that are less "flat".[38] In 2013, several UK non-profit drug discovery groups, have collaborated to form the 3D Fragment Consortium,[38] with the goal of incorporating the element of three-dimensionality into existing fragment libraries. Commercial databases were combined to give 13.4 million compounds where, after numerous rounds of selection based on the guideline criteria set by the consortium on the features of 3D fragments, a final collection

of 200 compounds was delivered. The process of selection suffered from attrition at various stages, which involved the removal of ≥90% of commercial samples due to their failure to meet the criteria, and fragments with increased three-dimensionality occurred at a much lower frequency. Efforts are still ongoing on synthesising more 3D drug-like fragments. Furthermore, the effect of more "shaped" fragments was reflected from work reported by Jorgensen and co-workers,[39] where propitious conformational changes were induced by the addition of a methyl group to various lead compounds (Scheme 1.4B), leading to significantly improved potencies and LEs.

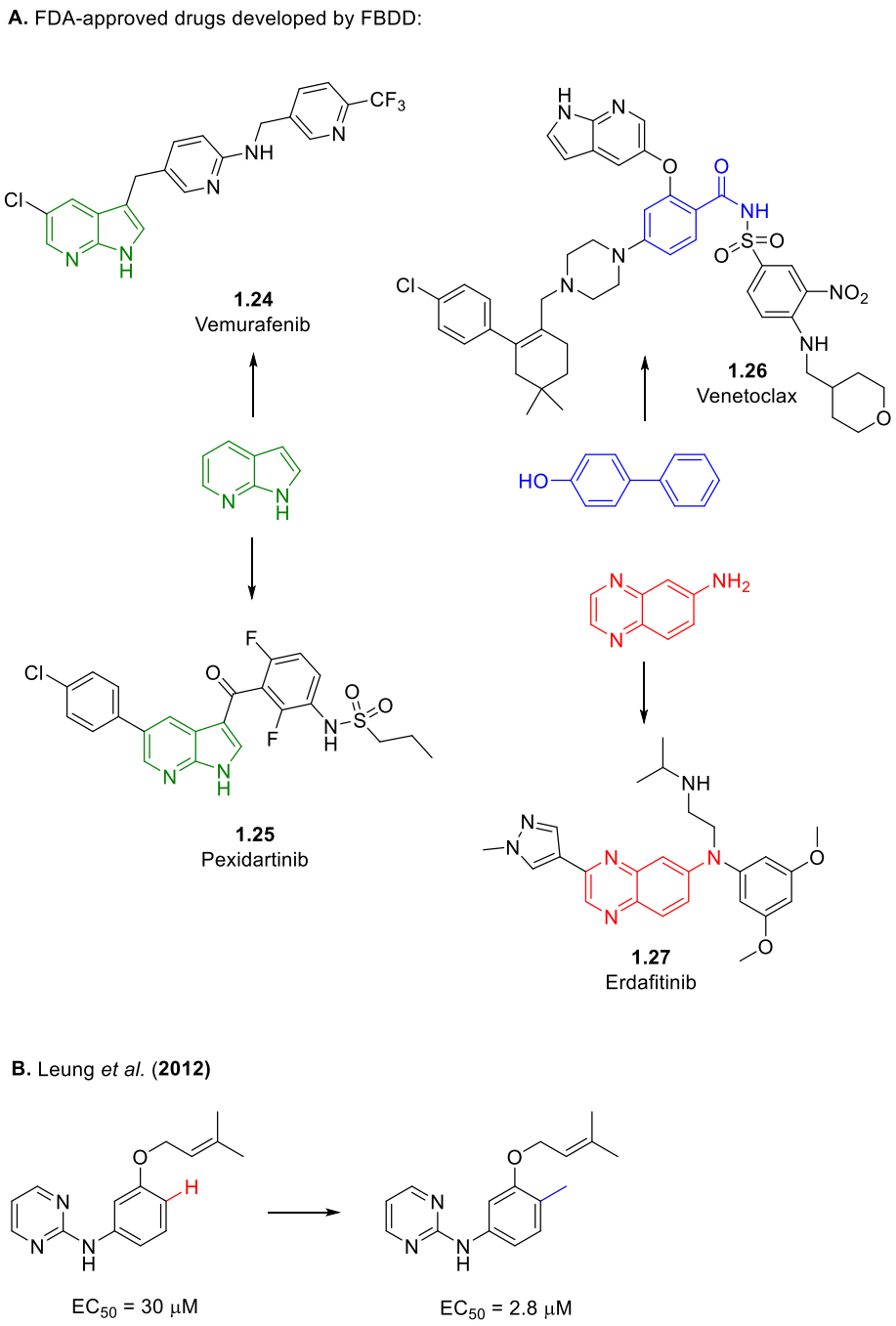

Scheme 1.1 (a) Four FDA-approved drugs derived from FBDD and their corresponding fragments; (b) An example of the effect of the addition of a methyl substituent to a lead compound on EC_{50}*.[39]

* EC_{50} is a measure of the concentration of a drug effective in producing 50% of the maximal response.

1.1.2.3 Fragment Optimisation

Fragment hits usually bind weakly to targets and exhibit minimal inhibitory effects. Further modifications are required for hits to be developed into strongly-binding leads that exhibit high potency. The three most frequently utilised strategies for fragment optimisation are fragment growing, fragment linking and fragment merging or scaffold hopping.

Fragment growing, by adding various functional groups, is the most commonly employed method to generate high molecular weight lead compounds with high potencies. As an example, Zhao *et al.* reported the discovery of potent and highly selective c-Jun NH_2 terminal kinase (JNK) inhibitors,[40] initiating with an HTS hit, acylaminopyridine derivative **1.1** (IC_{50}* = 0.84 μM), that qualified as a fragment (Scheme 1.1). Further chemical elaboration found phenylacetylamide **1.2** to be an improvement, with an IC_{50} of 45 nM; however, this compound (**1.2**) suffered from poor metabolic stability and oral bioavailability. Then, after a series of fragment optimisations through chemical modifications based on previous results, Zhao discovered that 2-pyridinecarboxamide analogues (**1.6**−**1.9**) displayed improved cellular activity compared to analogue **1.2**, with IC_{50} values ranging from 12 nM−0.27 μM.

* IC_{50} reflects the amount of drug needed to inhibit a given biological process by 50%

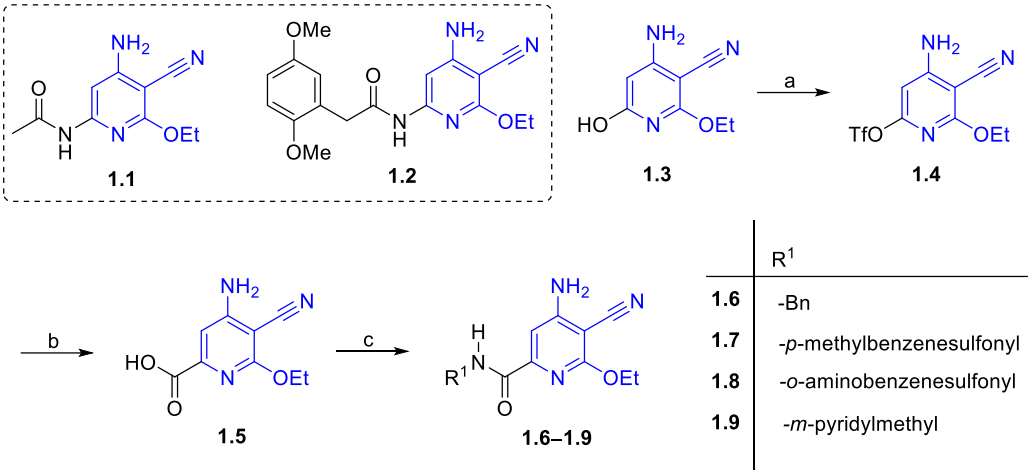

Scheme 1.2 Synthesis of analogues **1.6−1.9**. (a) $PhNTf_2$, Et_3N, RT, 60%; (b) (1) CO, $PdCl_2(dppf)$-CH_2Cl_2, MeOH, 50 °C, 50%; (2) LiOH, MeOH-H_2O, RT, 76%; (c) For **1.6−1.9**, R^1NH_2, TBTU, Et_3N, DMF, RT.[40]

On the other hand, Ellman *et al.* described a new fragment-based method, Substrate Activity Screening (SAS),[41] in identifying protease inhibitors. A library of *N*-acyl aminocoumarins with low molecular weight *N*-acyl fragments was screened to identify protease substrates (Scheme 1.2) then the activities of the weak protease substrates were optimised through rapid analogue synthesis and evaluation. Finally, the optimised substrates were converted into inhibitors by the addition of protease active-site traps. Application of this method led to the discovery of two distinct classes of novel, nonpeptidic inhibitors that exhibited >8000-fold improvements in cleavage efficiency of protease cathepsin S, which is involved in antigen presentation and immune response.[42]

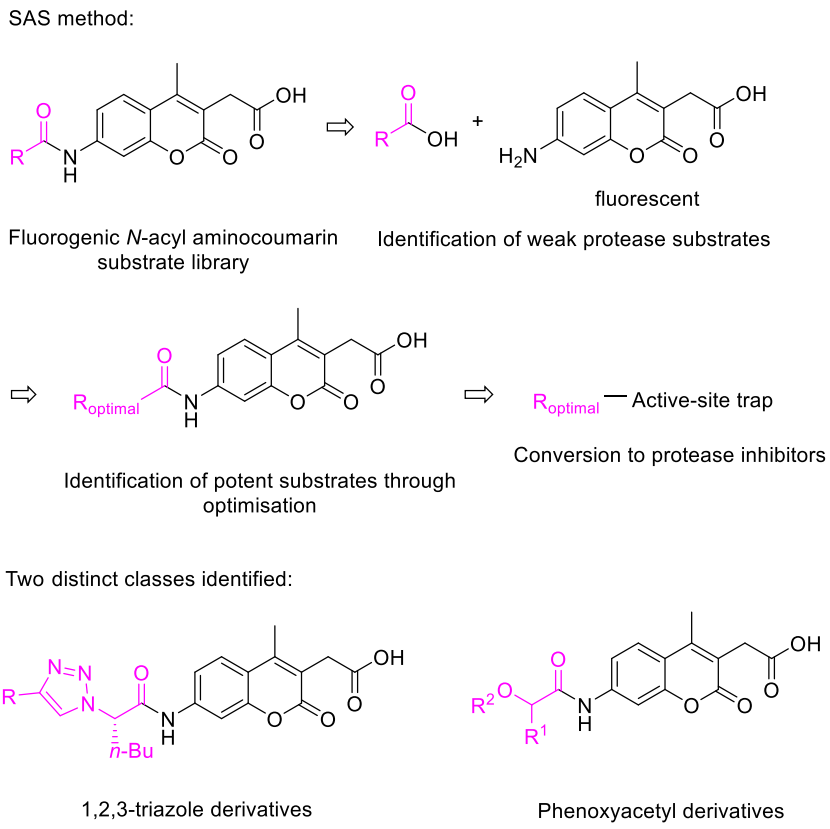

Scheme 1.3 Steps involved in SAS which led to the identification of two distinct classes of potent inhibitors of cathepsin S.[41]

NMR spectroscopy also acts as a useful tool in guiding and providing information on fragment optimisation. A major strength of NMR-based screening methods lies in its ability to use changes in one or more of several different NMR parameters to detect associations,[43] including chemical shifts (e.g. ^{1}H, ^{15}N), cross-relaxation between fragments and protein-bound water molecules (e.g. water-LOGSY), and in the protein-fragment complex (e.g. STD-NMR). Forino *et al.* have taken advantage of highly sensitive heteronuclear NMR techniques (^{19}F-1D NMR) to detect the inhibition of *Bacillus anthracis* lethal factor (LF) metalloproteinase,[44] an integral component in the causation of inhalation anthrax, a deadly disease that has no effective treatment. By using fluorinated peptide as an enzymatic substrate, ^{19}F NMR spectroscopy was employed to monitor cleavage events and LF kinetics. Starting from a library of only around 300 fragments, application of this strategy led to the identification of inhibitor **1.10** (Scheme

1.3) which, through further chemical elaboration, gave rise to three extremely potent inhibitors, **1.11**−**1.13**.

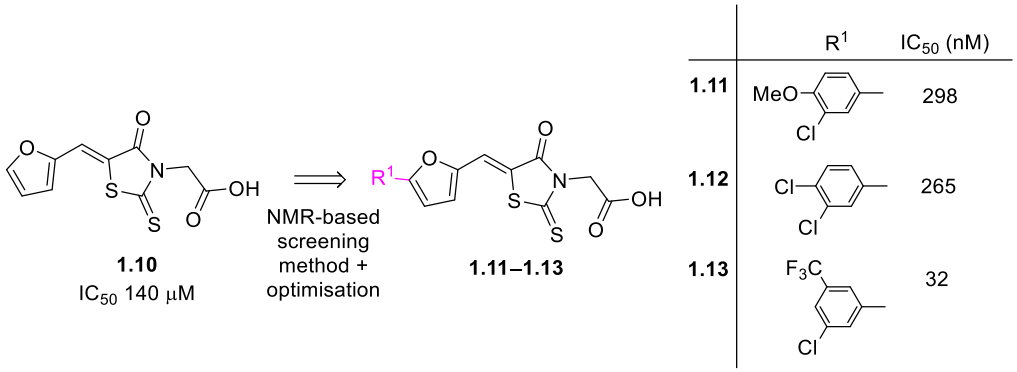

Scheme 1.4 Discovery of highly potent LF inhibitors **1.11**−**1.13** through NMR-based screening methods, as reported by Forino *et al.*[44]

Aside from fragment growing, there have also been considerable advances in fragment merging and linking. McCoy and co-workers reported the use of structure-based NMR spectroscopic screening approaches (SbN) in identifying drug-like fragment hits from customised libraries.[45] In search of inhibitors of the single-chain hepatitis C virus NS3 protease/NS4A cofactor complex (ns4a-ns3p), 3639 compounds were screened against uniformly ^{15}N-labelled ns4a-ns3p. Sixteen fragment hits were found and two were linked together to produce a highly potent inhibitor.

Sunesis Pharmaceuticals Inc. developed a combinatorial technology, "extended tethering", as a platform for drug discovery.[46] The first step of this strategy involves the covalent modification of a cysteine residue in or near the active site of the targeted protein with an "extender", a small molecule that possesses an inherent affinity to the Cys residue and that also contains a protected thiol group (Figure 1.5). Next, the thiol group is deprotected, and the protein-extender complex is screened against a library of disulfide-containing small molecules. Fragment hits showing affinity towards the regions of the protein near the extender form stable disulfide bonds, and such complexes can be identified by mass spectrometry. The selected fragments could then be combined with

binding elements from the extender to test for inhibition of the targeted protein. Tethering identified two novel fragments, **1.14** and **1.15**, to generate a unique inhibitor of caspase-1,[47] which plays a central role in cell immunity. The direct linking of each fragment significantly reduced the secretion of interleukin 1β (IL-1β), whose increase in production leads to a number of autoinflammatory syndromes.[48]

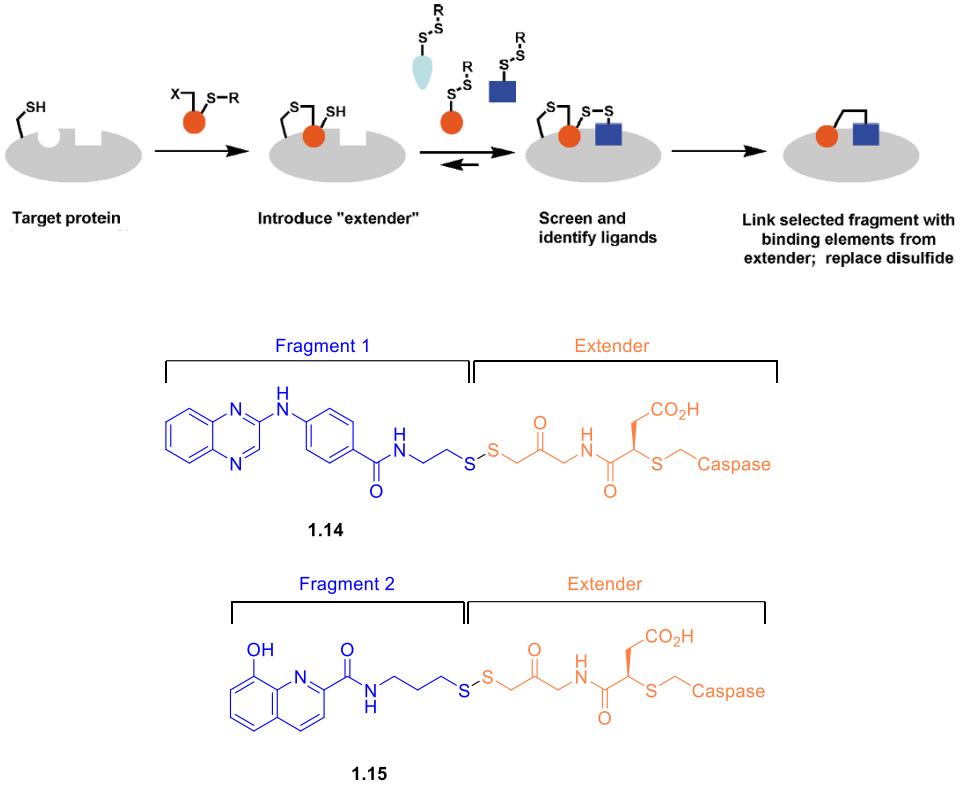

Figure 1.5 Schematic illustration of the process of "extended tethering" and the two novel fragments identified by Sunesis Pharmaceuticals Inc. utilising this strategy.[47]

Last but not least, the fragment merging or scaffold hopping strategy identifies fragment hits that have overlapping binding sites;[49] consequently, the chemical features of the hits can be combined or merged. To determine the binding modes of the identified hits, NMR spectroscopy, X-ray crystallography, or docking methods should be employed. Hudson *et al*. designed a novel type of aminoquinoline inhibitor against a cytochrome P450 enzyme from *Myobacterium tuberculosis* (CYP121).[50] This inhibitor showed high LE and fourfold greater affinity than the natural substrate of CYP121, cYY. Initial screening led to four fragment hits, **1.16**−**1.18** (Figure 1.6a), in which the merging of **1.16** and **1.17**

produced the lead compound 1,2,4-triazolyquinoline **1.20** (Figure 1.6b). The merging of the other fragments, however, did not generate improved results.

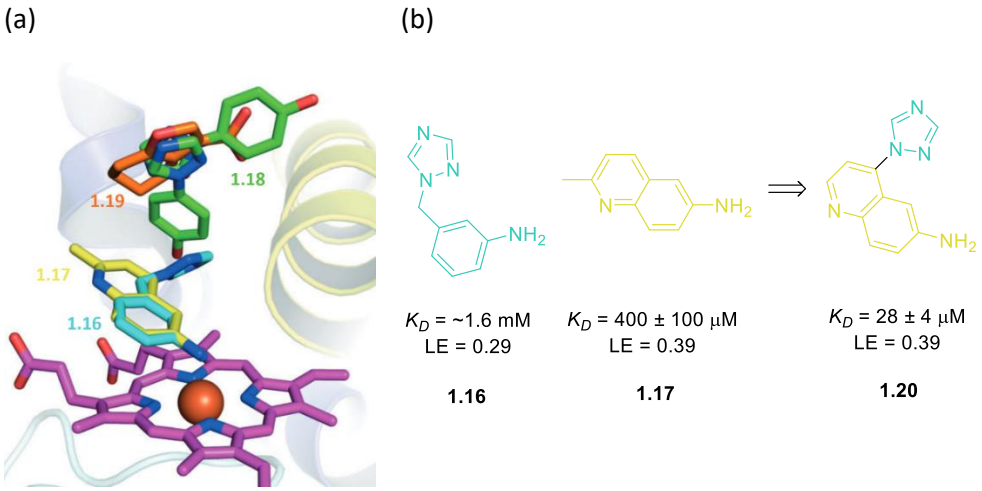

Figure 1.6 (a) Overlay of **1.16**–**1.19** within the active site of the crystal structure of CYP121; (b) Structures of **1.16**, **1.17**, and the combined lead compound **1.20**. K_D represents the dissociation constant and is used to describe drug/receptor interactions. A low K_D value indicates that the drug has a high affinity for the receptor and fewer molecules of the drug are required to occupy 50% of the receptor. LE is expressed in the unit of kcal/mol per non-hydrogen atom.[50]

Suzuki and co-workers also reported a fragment-based merging strategy in the discovery of highly potent and cell-active histone lysine demethylases (KDMs) inhibitors.[51] Modifications in KDMs are associated with epigenetic gene expression and are involved in biological events such as oncogenesis.[52] Compound **1.21** was a previously identified KDM inhibitor, with moderate KDM5 selectivity and IC_{50} value (Figure 1.7).[53] With α-ketoglutarate being the natural substrate for KDM5, various α-ketoglutarate mimic scaffolds were then synthesised and screened. Based on an analysis of the superimposed crystal structures of inhibitor **1.21** and a series of α-ketoglutarate mimic scaffolds, as well as molecular docking experiments, structures **1.21** and **1.22** were merged. The resulting product **1.23** exhibited strong competitive inhibitory activity with α-ketoglutarate and KDM5 selectivity.

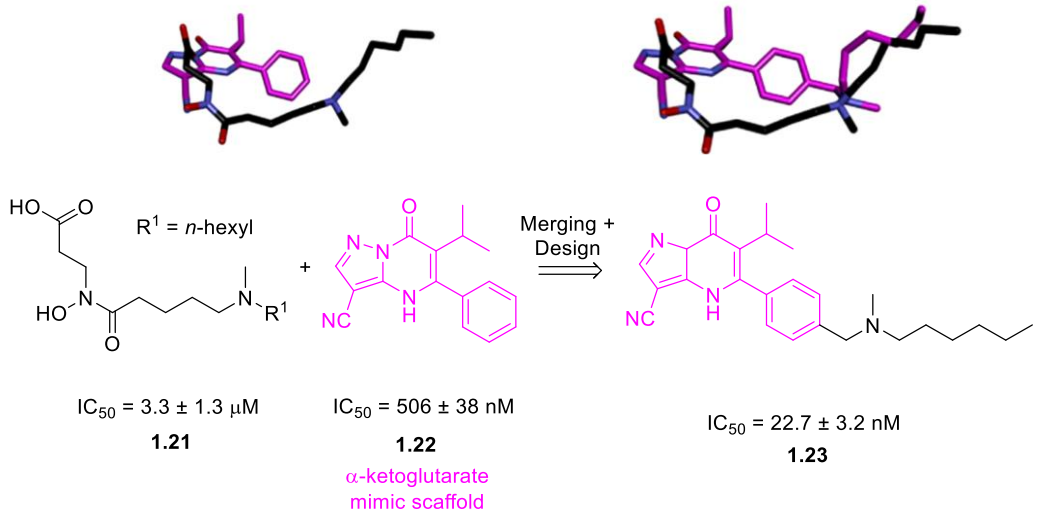

Figure 1.7 Fragment merging of inhibitor **1.21** and α-ketoglutarate mimic scaffold **1.22**, and the corresponding superimposed crystal structures.[51,53]

In summary, different hit identification methods have their strengths and weaknesses, and only by judicious integration of these approaches can the chance of successful lead development be maximised. Nevertheless, the versatility of FBDD permits its application in assessing the druggability of diverse targets and carries immense potential for the future of drug discovery.

1.1.3 Spiropiperidines

1.1.3.1 Significance of Spiropiperidines (Spiroamines)

The over-representation of sp^2-rich, flat aromatic scaffolds in HTS has led to the increasingly wide application of FBDD. Although to date, FBDD has not generated any 3D FDA-approved drugs, the exploration and exploitation of chemical space in FBDD continues, with an emphasis on three-dimensionality. Spirocycles represent an important class of non-aromatic ring systems, and an avenue to "escape from the flatland".[54] As a consequence of the two orthogonal planes and multiple exit vectors possible, which give rise to their inherent three-dimensionality and rigidity, spirocycles are frequently present within pharmacophores in drug discovery.[55,56]

More than 85% of all biologically-active chemical entities contain heterocycles;[57] in particular, nitrogen-based heterocycles occupy an exclusive position as a valuable source of therapeutic agents. Vitaku *et al.* compiled a database of all FDA-approved pharmaceuticals and showed that nearly 75% contained an *N*-heterocycle (Scheme 1.5),[58] presumably because of the relative ease of synthesis and the ability of the nitrogen atom to form hydrogen bonds with biological targets.[59] In Vitaku's analysis, piperidine was the most prevalent nitrogen ring system, followed by pyridine and piperazine.[58] Accordingly, combining the unique 3D-features of spirocycles with the biological activity of piperidines, harnessing the potential of spiropiperidines could greatly broaden the scope of drug development and deliver useful candidates for FBDD.

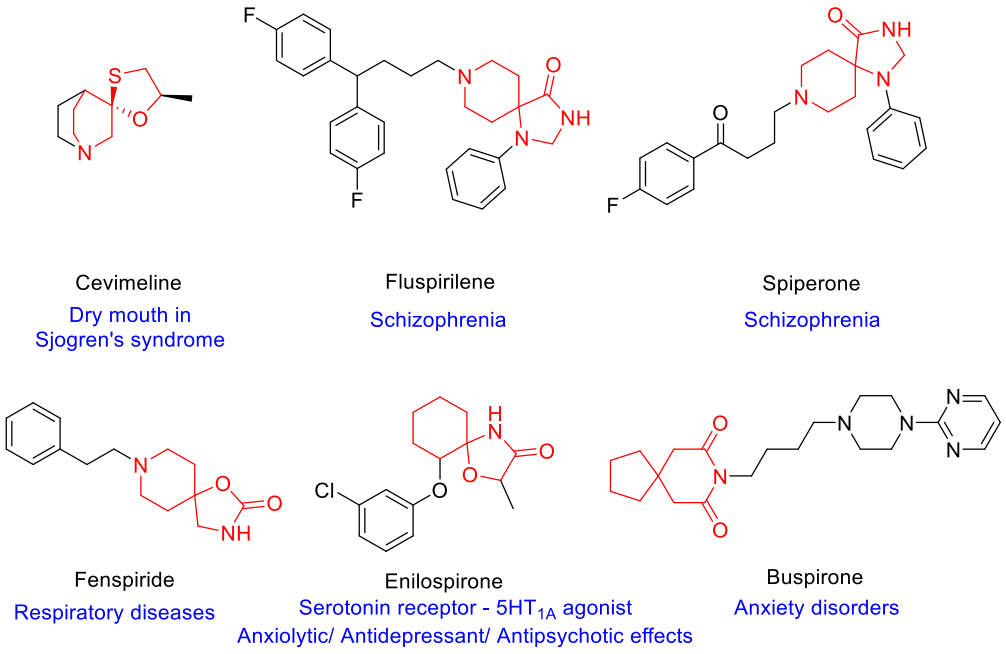

Scheme 1.5 Examples of marketed drugs containing spirocyclic scaffolds.[60,61,62]

1.1.3.2 Synthesis of Spiropiperidines

Recognition of the biological potential of azaspirocycles has resulted in their increasing incorporation into fragment-screening libraries and has sparked a recent surge of interest in the synthesis of spiropiperidines for drug discovery purposes.[63,64]

There are, however, synthetic challenges associated with spirocyclic scaffolds, which are likely due to the generation of the quaternary carbon centre with control of regio- and stereoselectivity; synthetic routes are generally linear and long. Consequently, a lack of effective synthetic strategies has hampered the implementation of spirocyclic moieties in drug development.[65]

The synthesis of spiroamines is typically achieved by amide formation or other classical C–N bond-forming reactions. For instance, building blocks containing the nitro-group are commonly employed because of their ability to form new C–C bonds by α-alkylation then new C–N bonds after reduction. The first preparation of *N*-Boc-4-nitropiperidinone **1.30** was reported by Mullen *et al*. in 2010 (Scheme 1.6)[66,67] by oxidation of its precursor oxime. Michael addition to methyl (meth)acrylate afforded nitroester **1.31** (R = H or Me), and subsequent catalytic reduction with Raney-Ni as catalyst generated spirolactams **1.34** and **1.35**. Mullen demonstrated the synthetic utility of the product by preparing an analogue (**1.36**) of the triazolyl aza[3.2.1]bicyclic component of maraviroc, an antiretroviral medication for treating HIV infection.

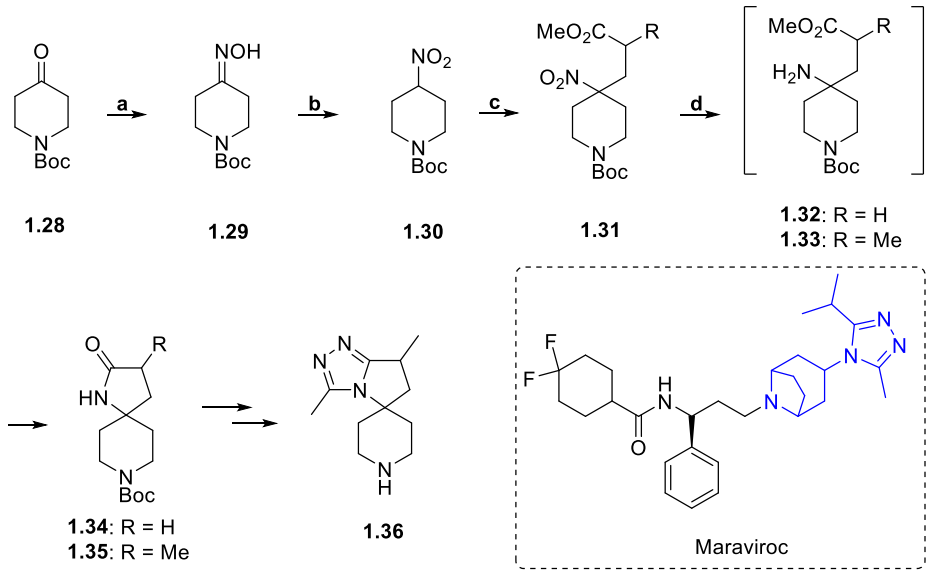

Scheme 1.6 Synthesis of *N*-Boc spirolactam **1.34** and its relevance to the antiviral medication maraviroc. (a) $NH_2OH{\cdot}HCl$, EtOH, reflux, 1.5 h, quant.; (b) TFAA, H_2O_2, urea, acetonitrile, reflux, 2 h, 55%; (c) $CH_2{=}CRCO_2Et$, K_2CO_3, EtOH, RT, 6 h (R = H) or TBAF, THF, reflux, 15 h (R = Me); (d) Raney-Ni, H_2, 50 °C, 12 h, **1.34**: 82%; **1.35**:

85%.[66]

A similar approach was described by De Clercq and co-workers in the synthesis of various aminoadamantane derivates (Scheme 1.7),[68] some of which have proven to be active against the influenza A H2N2, H3N2, and H1N1 strains. The synthetic route began with commercially available 2-nitroadamantane **1.37**, followed by Michael condensation with acrylic ethyl ester, purification by saponification, and esterification of the intermediate carboxylic acid to afford methyl ester **1.38**. A four step sequence was used to homologate this ester to key intermediate **1.42**, which was reduced with Raney-Ni catalyst and $LiAlH_4$, respectively, to give rise to spirocycle **1.43** and then derivatives **1.44** and **1.45**.

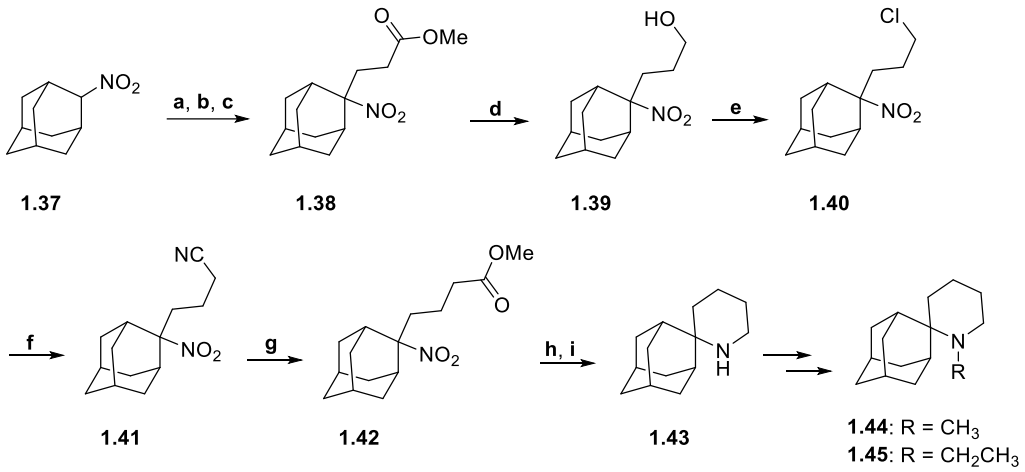

Scheme 1.7 Synthesis of aminoadamantane derivatives **1.44** and **1.45**. (a) CH_2=$CHCO_2Et$, Triton B, *t*-BuOH, 55 °C; (b) NaOH, EtOH-H_2O, reflux; (c) HCl gas, MeOH, RT, 97% in 3 steps; (d) $NaBH_4$, dioxane-H_2O (1:1), 87%; (e) $SOCl_2$, toluene, 90 °C, 96%; (f) KCN, 18-crown-6, acetonitrile, reflux, 99%; (g) HCl gas, MeOH, reflux, then H_2O, reflux, 92%; (h) (1) Raney-Ni, H_2, EtOH, 50 °C, (2) EtOH, reflux; (i) $LiAlH_4$, DME, reflux, 85% in 2 steps.[68]

Ring-closing metathesis (RCM) is widely employed in spiroamine synthesis. For example, Lesma *et al.* reported the synthesis of an unprecedented chiral spiropiperidine oxindole system (Scheme 1.8)[69] with RCM as a key step. *N*-Acetylation and *N*-allylation of oxindole derivative **1.46**[69] led to the formation of the RCM precursor **1.48** from which Grubbs II-catalysed RCM afforded 2-spiropiperidine **1.49**. Such spiropiperidine-3,3′-

oxindole scaffolds have found application as type-II β-turn peptide isosteres including, for example, compound **1.50**.

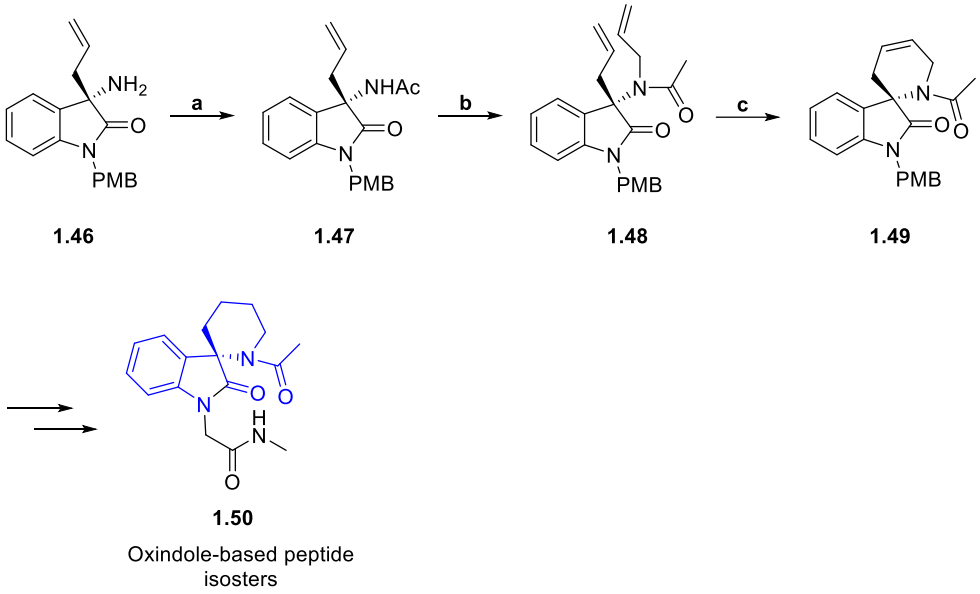

Scheme 1.8 Synthesis of spiropiperidine oxindole **1.49** and its relevance to peptidomimetics. (a) Ac_2O, DIPEA, DCM, RT, 85%; (b) allyl bromide, NaH, TBAB, DMF, 0 °C, 70%; Grubbs II cat., toluene, reflux, 79%.[69]

Martinez-Alsina *et al.* described an application of a diastereoselective Overman rearrangement to form the spirocyclic centre, followed by RCM (Scheme 1.9A).[70] The resulting 4-spiropiperidine intermediate **1.54** was used in studies of the structure-activity relationship (SAR) of β-secretase (BACE) inhibitors. Sveiczer *et al.* also developed an RCM-based method for the formation of novel spirocyclic scaffolds comprising pharmacophore heterocycles and carbocycles (Scheme 1.9B).[63] Using this strategy, Sveiczer constructed a library of 28 spirocyclic fragments and compared it to the commercially available Maybridge core fragment library with principal moments of inertia analyses.[71,72] The results revealed that the synthesised fragments demonstrated high levels of rigidity, three-dimensionality, and stereochemical diversity.

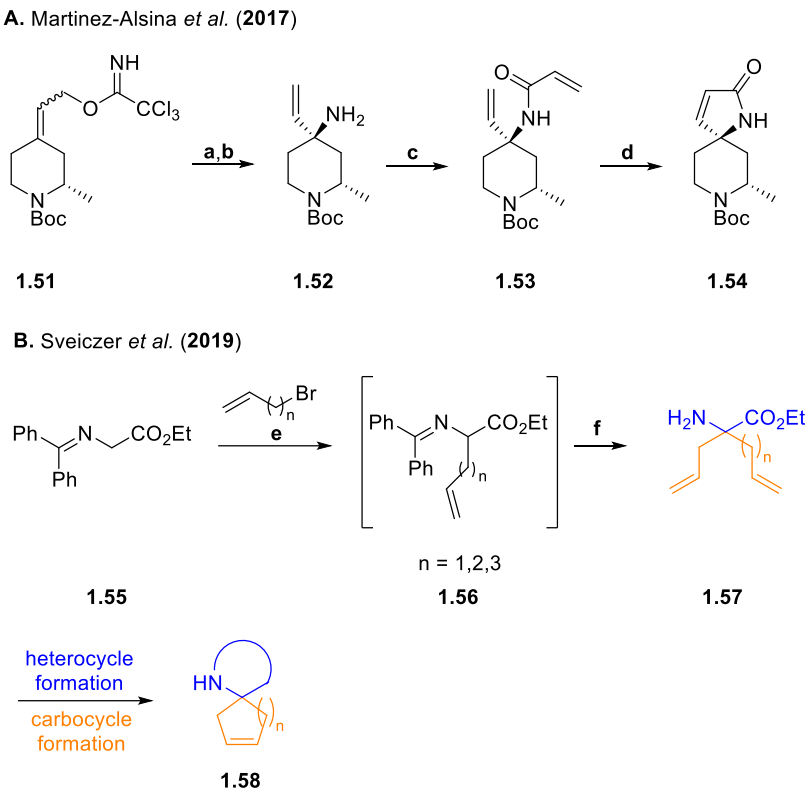

Scheme 1.9 RCM-based synthesis of spirocyclic scaffolds **1.54** and **1.58**. (a) K_2CO_3, xylenes, 140 °C, 63%; (b) DIBAL-H, −78 °C, 88%; (c) acryloyl chloride, Cs_2CO_3, THF, 0 °C, 99%; (d) Grubbs II cat., toluene, 80 °C, 81%; (e) *t*-BuOK, THF; (f) (1) *t*-BuOK, THF, (2) HCl, THF/H_2O, then Na_2CO_3, 31%−67%.[70,63]

Aiming to develop synthetic methods for lead library generation in drug discovery, Jenkins *et al.* reported a novel bromine-mediated cyclisation in the synthesis of *N*-Boc protected 4-spiropiperidine scaffolds (Scheme 1.10).[73] Following allyl Grignard addition to imine **1.59**, and formation of the HBr salt **1.61**, bromination furnished spiro[4.5]bicyclic product **1.62**. A one-pot deprotection-protection and reduction of the 2°-bromide led to spirocyclic diamine **1.63**. Jenkins proposed that the cyclisation reaction proceeded *via* bromine addition to the olefin then 5-*exo*-*tet* cyclisation (via **1.64**) to form intermediate **1.62**. The authors described the transformation as unprecedented and it was later employed by Melnykov *et al.* in the multigram-scale preparation of spirocyclic pyrrolidines.[65]

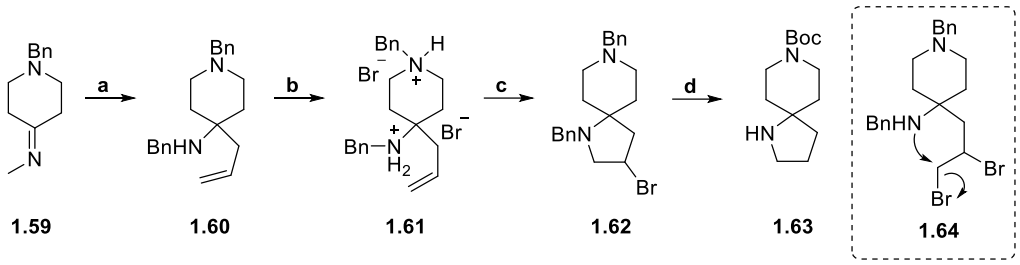

Scheme 1.10 Bromine-mediated cyclisation. (a) Allyl magnesium bromide, toluene, 0 °C, 92%; (b) HBr; (c) (1) Br_2, (2) aq. K_2CO_3, 90%; (d) H_2, Pd, Boc_2O, *i*-PrOH, 75 °C, 38%.[73]

Metal-mediated and -catalysed cyclisations are also commonly employed. For instance, Pfefferkorn *et al.* described the synthesis of 3-spiropiperidines – for use as a scaffold in drug discovery – via Pd-catalysed intramolecular α-arylation[74] (Scheme 1.11A). Separately, Guazzelli developed a Sm(II)-mediated conjugate reduction-aldol cyclisation in the stereoselective synthesis of spirocyclic keto-lactams (Scheme 1.11B).[75]

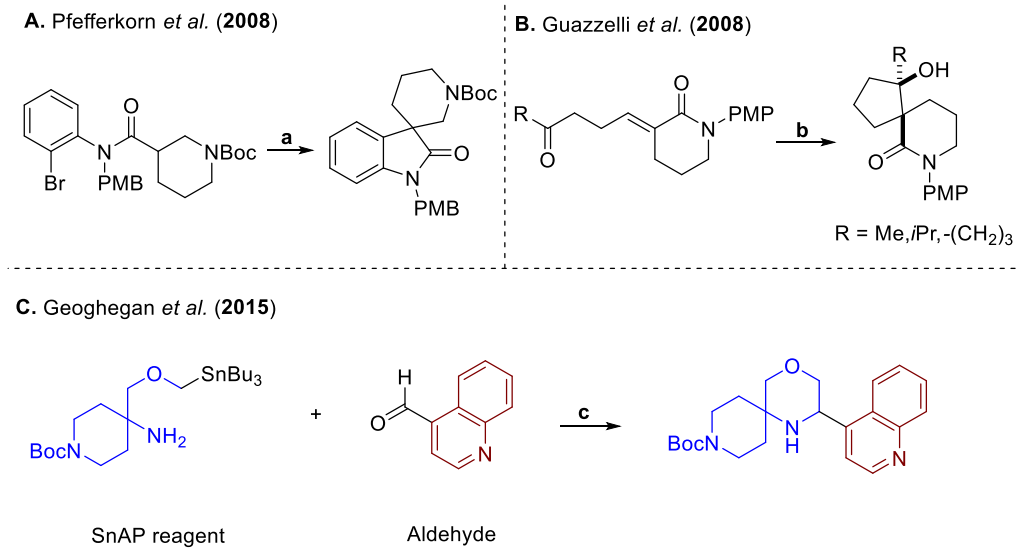

Scheme 1.11 Metal-mediated and -catalysed spirocyclisation reactions. (a) $Pd(OAc)_2$ cat., PCy_3, KO*t*-Bu, dioxane/THF (10:1), 85 °C, 16 h, 54%; (b) SmI_2, THF, MeOH, 0 °C to RT, 18 h, Me: 79%, *i*Pr: 64%, -$(CH_2)_3$: 82%; (c) (1) 3 Å MS, DCM, 15 h, RT, (2) $Cu(OTf)_2$, 2,6-lutidine, DCM/HFIP (4:1), 15 h, RT, 87%.[74,75,64]

In summary, there are many conceivable approaches regarding the synthesis of 2-, 3-, and 4-spiropiperidines. Other strategies include: radical cyclisation using commercially-available saturated *N*-heterocyclic (SnAP) reagents [Sn (tin) Amine Protocol] (Scheme 1.11C);[76,77] metal catalyst-free conditions;[78] and rearrangements.[79] Numerous excellent

reviews provide a comprehensive overview of various synthetic approaches to spirocyclic scaffolds.[80,81,60]

1.3 C(sp^3)-H Activation

1.3.1 Significance of C(sp^3)−H Activation

The field of organic synthesis provides a logical framework for the generation of a vast number of compounds and chemists have a clear understanding of how to design new routes based on, primarily, the manipulation of functional groups. Within this context, the beginning of the twenty-first century has witnessed a truly revolutionary trend in organic chemistry: the activation and functionalisation of C−H bonds (Figure 1.8).[82,83] Undoubtedly, strategic use of reactions that achieve the direct transformation of C−H bonds, particularly C(sp^3)−H bonds, can render synthetic routes more efficient and atom-economical. This approach has the potential to be applied in many areas of chemistry including the late-stage diversification of various scaffolds, ranging from small molecules to organic polymers.

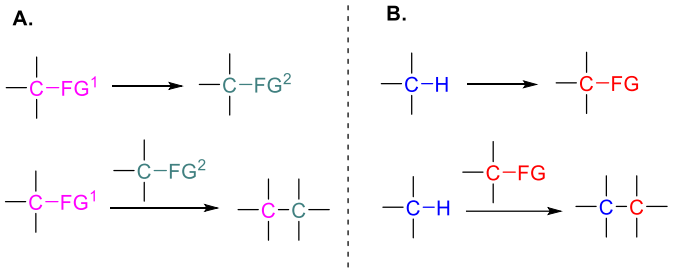

Figure 1.8 (A) Traditional approaches to organic synthesis centre on manipulating functional groups (FG); (B) modern organic synthesis by (catalytic) C−H bond functionalisation.

The ubiquity of aliphatic C(sp^3)−H bonds imposes selectivity issues; however, countless publications have documented successful efficient C(sp^3)−H functionalisation based on three main strategies as outlined below.

1.3.2 Hydrogen Atom Transfer

The use of free radical reactivity to achieve C(sp^3)-H activation is long-known and continues to be investigated extensively. Here, an H-atom is transferred from a C−H bond to a highly reactive radical species usually one centred on oxygen, nitrogen, or an sp^2-carbon (vinyl, aryl). The thermodynamic driving force in this process is the formation of a stronger X−H bond than the C−H bond broken.[84] Kinetically, intramolecular events are often favoured over analogous intermolecular reactions due to their lower entropic cost. In most cases, 1,5-hydrogen atom transfer (1,5-HAT) is the predominant pathway for such an event since a preferred near-linear arrangement of [C···H···X]$^{\bullet}$ is just attainable within the six-membered cyclic transition state and entropic losses are lower than for more remote 1,n-abstractions.[84] In fact, early approaches to the functionalisation of unactivated C(sp^3)-H bonds involve 1,5-HAT steps; for example, the Hofmann–Löffler–Freytag and Barton reactions form saturated *N*-heterocycles and δ-nitroso alcohols, respectively (Scheme 1.12).[85]

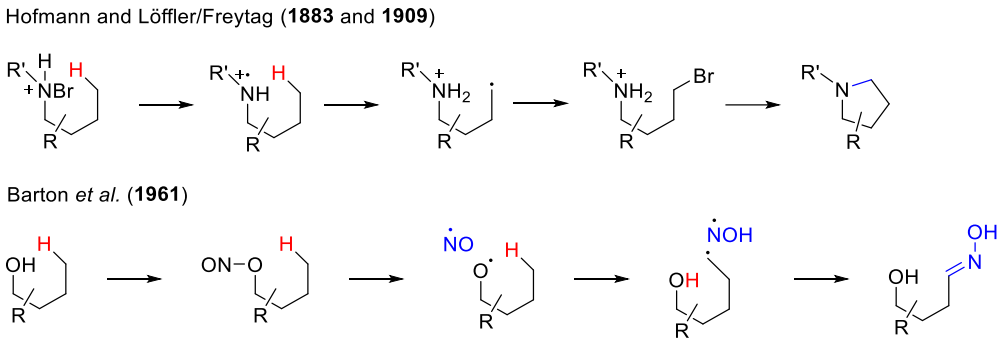

Scheme 1.12 Early C−H activating reactions *via* radical processes.

1.3.3 Metal-Catalysed Carbene and Nitrene Transfer

Apart from radicals, carbenes and nitrenes can act as reactive intermediates for the activation of C(sp^3) −H bonds by C−H insertion. The lack of an octet configuration renders them highly electrophilic and sufficiently energetic to break unactivated C−H bonds.[84] Transition metal carbenoids (and nitrenoids) constitute relatively stabilised

versions of the free reactive intermediates leading to more controlled reactions. For example, the combination of a diazo precursor and Rh(II) catalysis is reliable for accomplishing intramolecular insertions.[82] Hong's synthesis of the natural product (–)-incarviatone A **1.67** (Scheme 1.13)[86] made use of a highly diastereoselective Rh-catalysed intramolecular C−H insertion as an early key step to yield the indane core **1.66**.

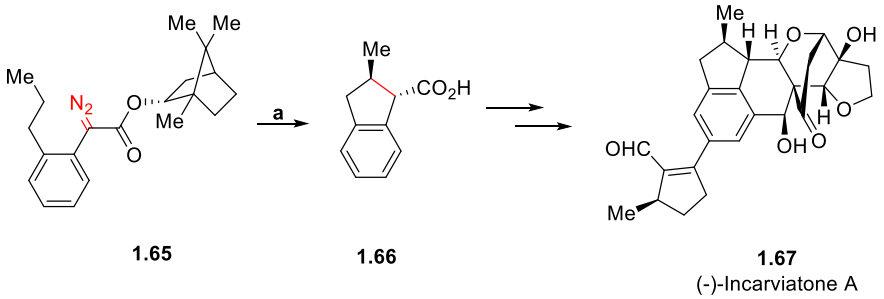

Scheme 1.13 Synthesis of (–)-incarviatone A. (a) Rh_2(*R*-PTTL)$_4$, toluene, then LiOH, MeOH, 70%.[86]

Pioneered by Breslow in 1983[87] and subsequently developed by Du Bois and co-workers,[88,89] transition-metal-catalysed nitrenoid C(sp^3)−H insertions have also been extensively studied from sulfonamide and carbamate precursors. Du Bois and co-workers showed that intramolecular C−N bond formation from such substrates could be achieved reliably using $Rh_2(OAc)_4$ as catalyst in the presence of $PhI(OAc)_2$ as stoichiometric oxidant and MgO as a combined base and drying agent.[88,89] Two different substrate classes were explored, namely sulfonamides and carbamates, which were used interchangeable depending on the starting alcohol and subsequent transformations followed (Scheme 1.14A).[90] The approach was applied to the synthesis of vildagliptin analogue **1.70** as reported by Hrdina *et al.* (Scheme 1.14B) [91]

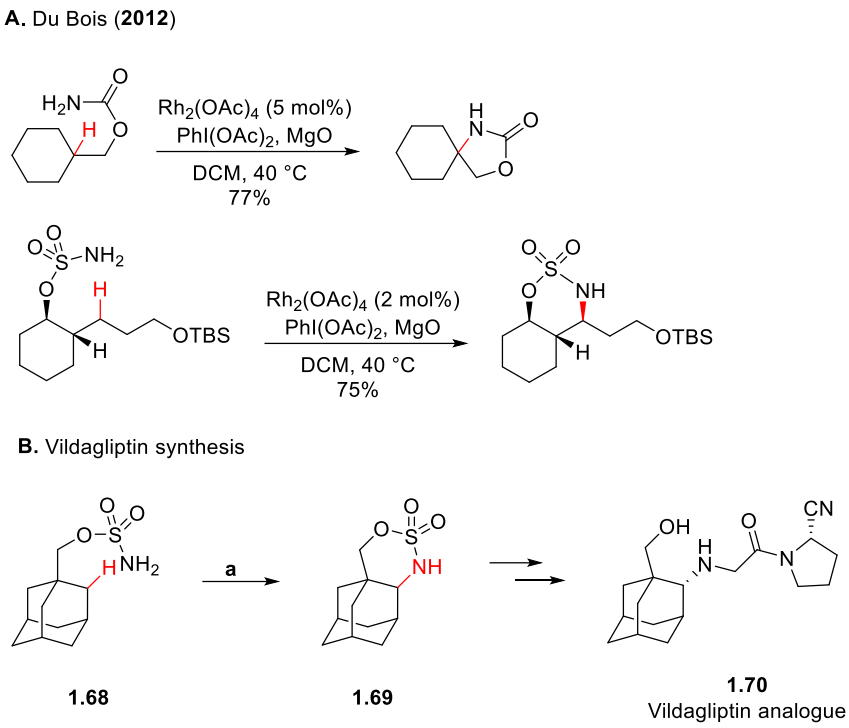

Scheme 1.14 (A) Du Bois's protocol for Rh(II)-catalysed intramolecular C−H amination with carbamates and sulfamates; (B) Application of a Du Bois C−H amination in the synthesis of vildagliptin analogue **1.70**. (a) $Rh_2(OAc)_4$ (1 mol%), $PhI(OAc)_2$, MgO/DCM, 95%.[90, 91]

1.3.4 Directed Transition-Metal-Catalysed C−H Activation

Transition-metal catalysis is one of the predominant approaches to C(sp^3)−H activation. Coordination between a transition-metal and a Lewis-basic directing group brings the catalyst into close proximity to the C−H bond to be activated; this agostic interaction thus lowers the energy barrier for the bond cleavage to take place.[84] Aryl halides and triflates are often used as traceless directing groups. Kreutzer *et al.* have demonstrated the use of vinyl halides as traceless directing groups in the formation of bicyclic pyrrolidone **1.72** through a Pd(0)-catalysed intramolecular cyclisation of vinyl bromide **1.71** (Scheme 1.15A).[92] Pd catalysts are also employed in amines functionalisation, where an electron-withdrawing group is installed on the *N*-atom to generate a directing group. Topczewski *et al.* exploited Pd-catalysed transannular C−H activation for the derivatisation of medicinally-relevant heterocyclic amine **1.75** (Scheme 1.15B).[93] The perfluorinated amide component within piperidine **1.73** acts as the directing group for arylation with 4-

iodoanisole (**1.74**, Scheme 1.15C); [94] subsequent removal of the directing group can be achieved by reductive cleavage with SmI_2. Alongside C−C and C−N bond formations, metal-catalysed C−O bond formations were also reported. For example, in the synthesis of paspaline **1.78** the local desymmetrisation of the *gem*-dimethyl unit in precursor **1.76** was attributed to the proximity of the oxime directing group to the equatorial methyl group (Scheme 1.15).

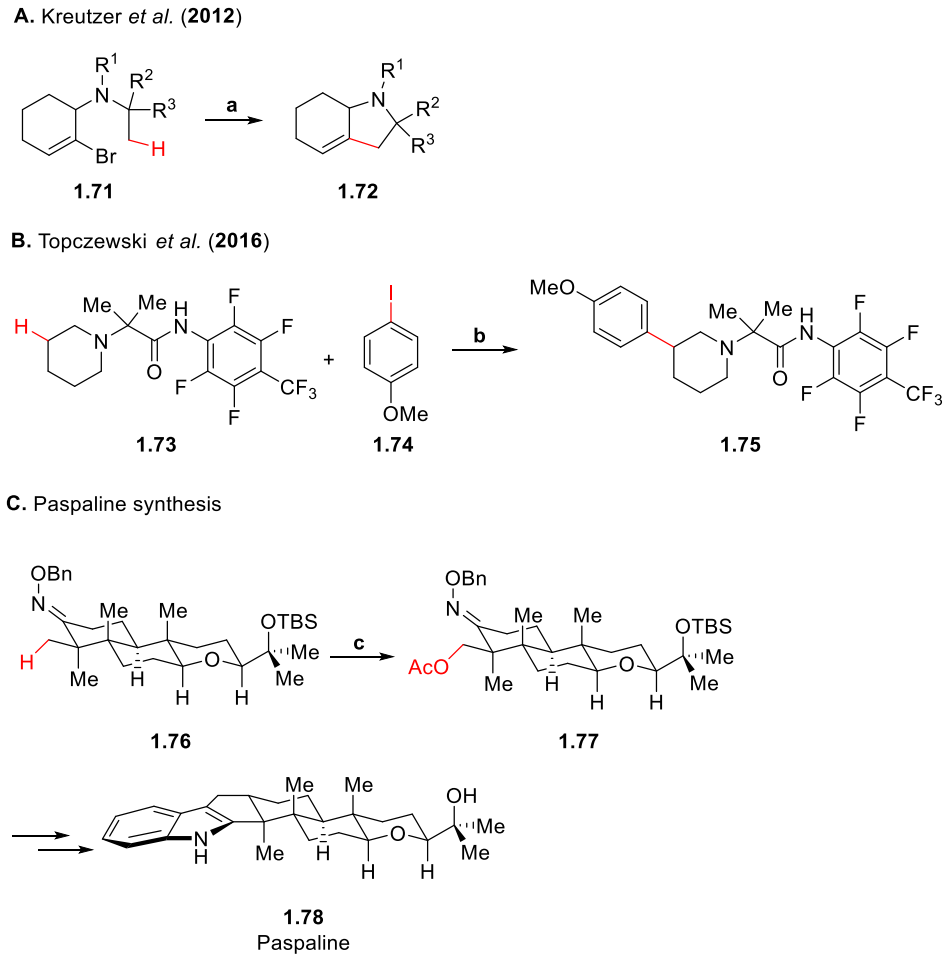

Scheme 1.15 (A) Synthesis of hexahydroindoles from alkenyl bromides, (a) $Pd(OAc)_2$ (10 mol%), $PCy_3{\cdot}HBF_4$ (20 mol%), Rb_2CO_3, PivOH (30 mol%), toluene, 120 °C, 75%; (B) Transannular C−H activation of alicyclic amines, (b) $Pd(OAc)_2$ (10 mol%), CsOPiv, neat, 150 °C, 55%; (C) Synthesis of paspaline utilising an oxime directing group for C−O bond formation, (c) $Pd(OAc)_2$ (15 mol%), $PhI(OAc)_2$, AcOH/Ac_2O (1:1), 100 °C, 79%, *d.r.* > 20:1.[95,93,94]

Other transition-metal catalysts based on Iridium(I),[96] Rhodium(III),[97] and Nickel(II)[98] have also been reported for C−H activation reactions. Chu *et al.*[84] and Chatani *et al.*[99]

published comprehensive reviews on various directed transition-metal catalysed C−H activation methodologies.

1.3.5 Biocatalysis in C(sp^3)-H Activation

The field of biocatalysis makes use of Nature's catalytic repertoire to facilitate chemical transformations and is constantly being explored. Terms such as "environmentally benign" are frequently claimed in biocatalysis publications[100] because enzyme-mediated reactions are usually carried out under mild, aqueous conditions. Enzymes can be engineered to achieve desired selective conversions in diverse non-natural substrates which has led to their application in building block synthesis and mid- and late-stage functionalisation (LSF).

Enzymatic catalysis of C−O bond formation has proven to be successfully employed in target molecule synthesis.[101,102] For example, in 2018, Zwick *et al.* highlighted the potential of a leucine 5-hydroxylase (GriE) in the synthesis of a rare alkaloid, manzacidin C **1.81**.[103] In this synthesis, azide **1.79** was hydroxylated at one of the diastereotopic methyl groups to yield **1.81** with >95% conversion and >99% *d.e* (Scheme 1.16A). An example of biocatalysis in late-stage functionalisation is found in the first enantioselective total synthesis of nigelladine A **1.83** via engineered cytochrome P450-catalysed allylic C−H oxidation of imine **1.82** (Scheme 1.16B).[104] This biocatalytic selective late-stage oxidation circumvented the need for extensive generational screening and reaction optimisation through numerous rounds of protein engineering and mutagenesis.

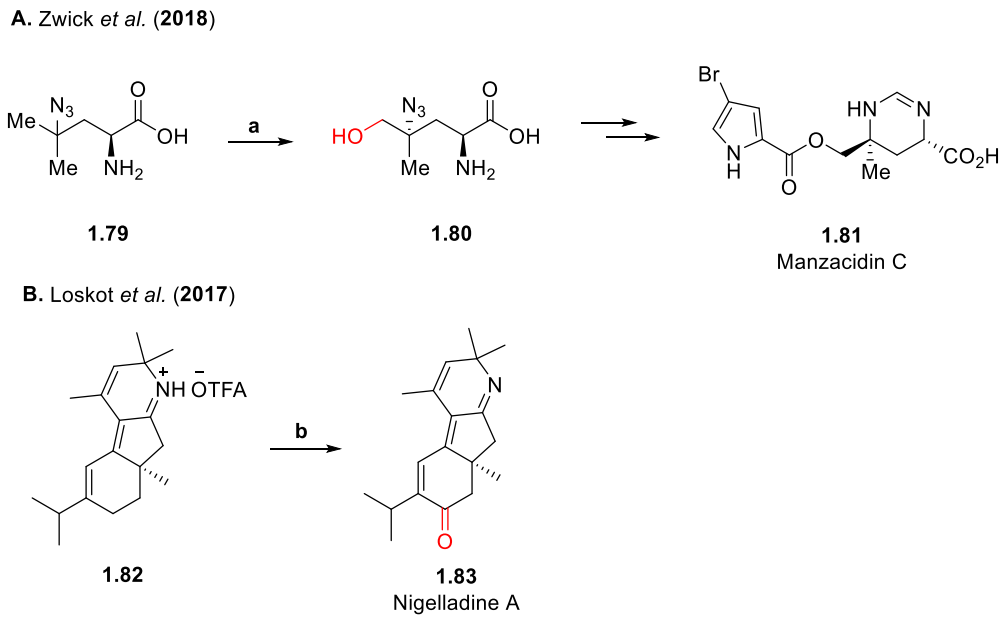

Scheme 1.16 (A) Chemoenzymatic synthesis of manzacidin C including δ-hydroxylation, (a) GriE (0.15 mol%), α-ketoglutarate, Fe^{2+}, >95% conversion; (B) First enantioselective synthesis of nigelladine A through a late-stage allylic oxidation by a cytochrome P450, (b) (1) P450 8C7 (0.02−0.04 mol%), NADP (10 mol%), *i*PrOH, alcohol dehydrogenase, 2.5% DMSO in potassium phosphate buffer (pH 8), 23 °C, 12 h, (2) DMP, DCM, 0 °C, 4 h, 21% over two steps.[103,104]

Apart from C−O bond-forming processes, biocatalytic C(sp^3)-H aminations are also documented. Singh *et al.* reported the use of engineered cytochrome P450 enzymes to effect an intramolecular C−H amination reaction (Scheme 1.17A),[105] resulting in oxazolidinones from the cyclisation of carbonazidates with mutant P450 FL#62. Singh's work provided early insights into the mechanism of P450-mediated C−H aminations. Furthermore, the direct primary amination of benzylic and allylic C(sp^3)-H bonds was developed by Jia *et al.*,[106] using P411 enzymes, where the Cys axial ligand in P450 was replaced by a Ser (Scheme 1.17B). The Cys → Ser substitution increases the reduction potential of the haem iron, enabling the amination to occur under physiological conditions without additional reductants.[106] This process was demonstrated to be efficient and selective, with TON up to 3930 and a 96% *e.e.*

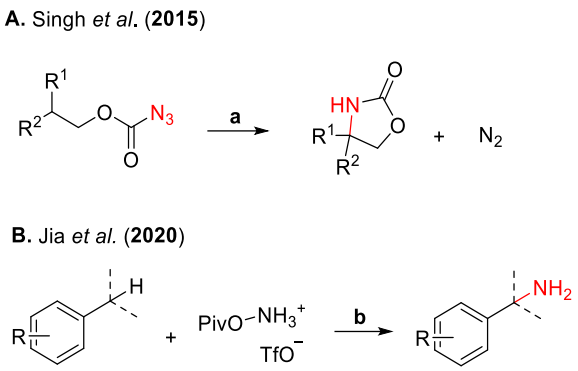

Scheme 1.17 (A) Biocatalytic formation of oxazolidinones by C−H amination, (a) P450 FL#62 (0.05 mol%), potassium phosphate buffer (pH 8.0), 25 °C, 16 h; (B) Enzyme-mediated amination of C(sp^3)-H, (b) P411 variant, M9-N medium (pH 7.4), 10 °C, 12 h.[105,106]

Enzymatic C−H functionalisation has also been applied to achieve halogenations,[107,108] alkylations,[109] and desaturation,[110] with unique reactivity profiles that are often unmatched by conventional chemcal catalysts.

1.4 Cytochrome P450 and $P450_{BM3}$

1.4.1 Background and Significance

The cytochrome P450 enzymes (CYPs) are a superfamily of haem *b*-dependent monooxygenases.[111] They were first discovered by Klingenberg in 1945[112] and their abilities to carry out hydroxylation reactions was confirmed by Cooper and co-workers in 1965.[113] Cooper also revealed the absorption maximum of CYPs at a reduced state while in complex with CO to be at 450 nm, hence the term "CYP450s".[113]

CYPs are identified in most biological species from all five kingdoms (monera, protoctista, fungi, plantae and animalia).[114] They are classified by their gene sequences: a family number (e.g. CYP1), a subfamily letter (e.g. CYP1A), and a number for the individual enzyme (e.g. CYP1A1).[115] CYPs share a highly conserved tertiary structure and common topology (Figure 1.9a).[116] The conserved structural core comprises three parallel helices, namely D, L, and I, and one anti-parallel helix E.[116] Despite the similarities, only one

amino acid residue is invariant – the cysteine residue axially ligated to the haem group (Figure 1.9b).[117]

(a) (b)

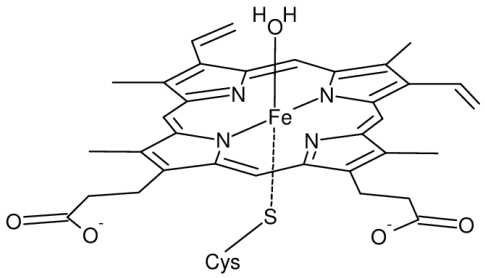

Figure 1.9 (a) The tertiary structure of CYPs is highly conserved. The substrate-recognition site (SRS) is shown in black, the helices mentioned are labelled; (b) The haem iron is axially ligated with a conserved cysteine residue and water, and equatorially ligated to four nitrogen ligands from the porphyrin ring.[114,115]

The majority of reactions catalysed by CYPs are oxidations, in particular hydrocarbon hydroxylation, the most characteristic oxidation of CYPs.[118] In this process, one of the oxygen atoms from molecular oxygen is inserted into a C−H bond of the substrate and the other oxygen is inserted (formally) into H_2.[118] In humans, CYPs are found at the highest concentration in the liver[119] and are, in general, responsible for the biotransformation of endogenous compounds, pharmaceutical agents, and environmental xenobiotics.[120] There are several ways that drugs can be metabolised by CYPs; they may be activated or deactivated, and metabolised by one or multiple CYPs, examples being shown in Scheme 1.18A. Metoprolol **1.65**, a medication for angina and hypertension, is α-hydroxylated exclusively by CYP2D6 to its active form **1.66**.[121] On the other hand, phenytoin **1.67**, an anti-seizure medication, is primarily metabolised to its inactive form 5-(4′-hydroxyphenyl)-5-phenylhydantoin (*p*-HPPH) **1.68** by CYP2C9 and CYP2C19, which is then glucuronidated by UDP-glucuronosyltransferase (UGT) to **1.69** for excretion into the urine (Scheme 1.18B).[122] Apart from hydroxylations, CYPs are also capable of catalysing less generally discussed reactions such as reduction, desaturation,

rearrangements, and coupling reactions.[123] Furthermore, they are crucial in the biosynthesis of a multitude of natural products as exemplified by the steroid hormones derived from successive oxidations of chloesterol (Scheme 1.18C).[124]

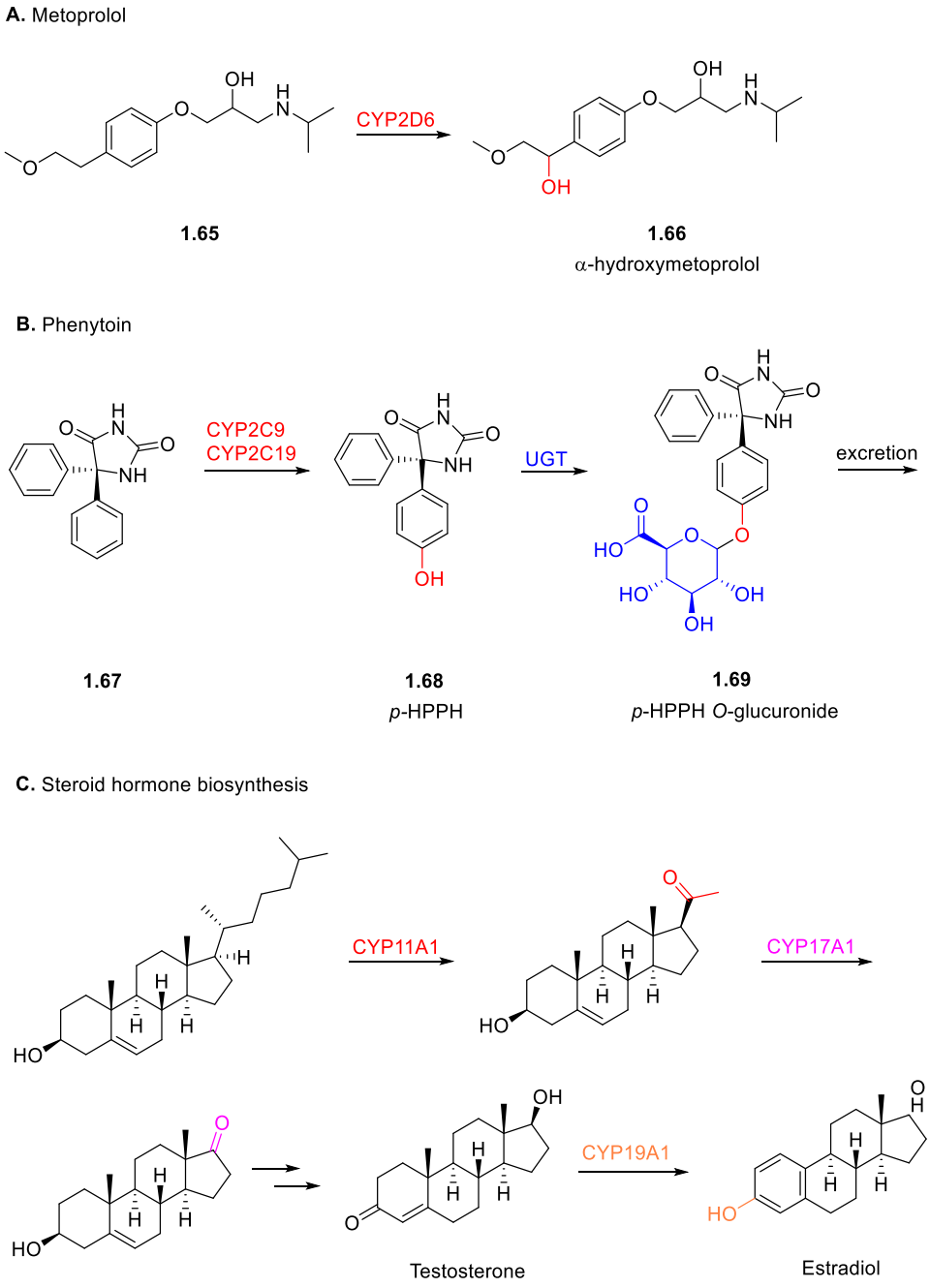

Scheme 1.18 Metabolism of (A) metoprolol and (B) phenytoin by CYPs in humans; (C) Biosynthesis of testosterone and estradiol from cholesterol by CYPs.[121,122,124]

1.4.2 The Catalytic Cycle of P450s

The catalytic cycle of the CYPs has been extensively studied and the generally accepted form is shown in Scheme 1.19.[125] The cycle begins when the substrate enters the active

site and interacts with the resting state, complex **I**, where the low-spin (S = 1/2) ferric iron coordinates to a water molecule at the axial position, along with four equatorial nitrogen ligands from the porphyrin ring. Once the substrate begins to interact with the active site, the water molecule from the axial position is displaced; whether this displacement occurs through induced conformational changes or direct displacement originating from the bulkiness of the substrate remains unclear. This displacement causes the ferric spin state to increase from low-spin to high-spin (S = 5/2) due to the change from a six-coordinated iron to five-coordinated, forming complex **II** and lowering the reduction potential of the haem to make it more oxidising. Complex **II** accepts an electron, often from NADH or NADPH, which converts it to the ferrous state complex **III**. Dioxygen rapidly binds and yields the oxyferrous-complex **IV**, followed by another one-electron reduction, creating ferric peroxy complex **V**. At this point, the terminal oxygen atom of complex **V** is protonated to give the hydroperoxy adduct **VI**, also known as "compound 0". An additional proton is accepted which triggers the loss of a water molecule *via* the heterolytic cleavage of the O−O bond, generating complex **VII**, also known as "compound I". The active species in P450-catalysed oxidations. Compound I is capable of abstracting hydrogen atoms from R−H, forming a substrate radical R' and the iron(IV)-hydroxo-species **VIII** ("compound II"), after which R˙ rebound generates the alcohol R−OH and a ferric heme. The hydroxylated product is then replaced in the active site by a water molecule, thus restoring the enzyme to its resting state complex **I**.

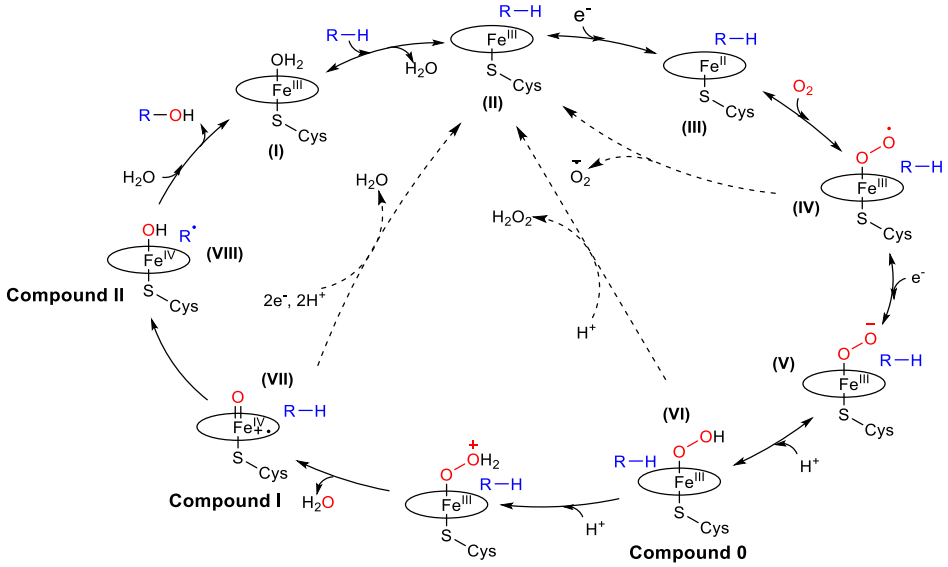

Scheme 1.19 Generally accepted catalytic cycle of CYPs.[125]

1.4.3 P450$_{BM3}$ (CYP102A1)

P450$_{BM3}$ was first discovered by Fulco and co-workers in the 1970s as the third P450 to be isolated from the gram-positive bacterium, *Bacillus megaterium*.[126,127,128] Characterisation of the full-length 120 kDa enzyme revealed that the 55 kDa haem domain (BMP) of P450$_{BM3}$ is fused to a 65 kDa reductase domain (BMR) containing two prosthetic flavin groups, FAD and FMN, in a 1:1 molecular ratio (Figure 1.10a).[129,130,131] As illustrated in Scheme 1.19, two electrons are required as part of the catalytic cycle. The FAD group of the reductase domain of P450$_{BM3}$ accepts a hydride from NADPH and transfers two electrons sequentially to FMN which in turn transfers the electrons to the haem in the two separate reduction steps of the catalytic cycle. This is a stochiometric requirement; P450-catalysed oxidations *in vitro* for product characterisation are carried out in the presence of a cofactor recycling system to regenerate NADPH and NADP$^+$, the most commonly used system is glucose with glucose dehydrogenase (Figure 1.10b). While many other CYPs (e.g. human CYPs) contain a redox partner as a separate protein,[132] the naturally fused nature of P450$_{BM3}$ gives rise to its unique characteristic of being "self-sufficient". As a result, P450$_{BM3}$ is regarded as the benchmark CYP with the

combination of high catalytic rates and self-sufficiency making it an ideal candidate for academic research.

(a) (b)

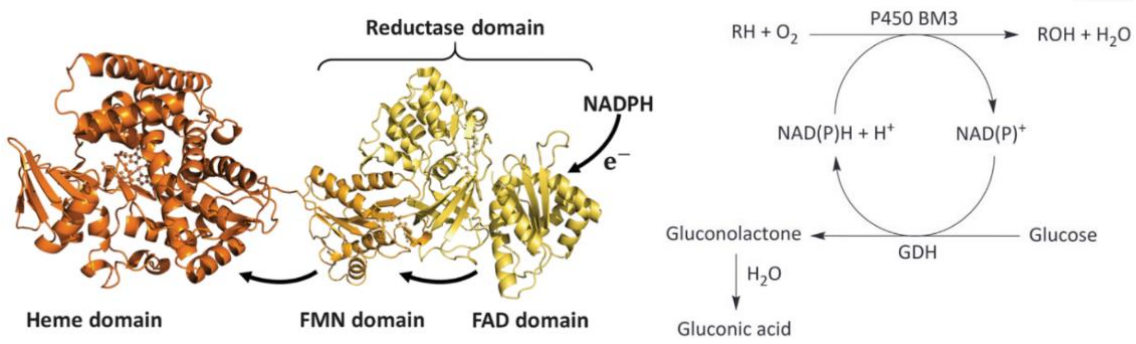

Figure 1.10 (a) Cartoon of the "self-sufficient" system of $P450_{BM3}$; (b) Turnover of the reductase domain with glucose as the stochiometric reductant catalysed by GDH.[131,133]

1.4.3.1 Key Residues

When Fulco first reported $P450_{BM3}$ he postulated the presence of a hydrophilic binding region in order to tether the carboxylate group of its native long-chain fatty acid substrates.[128] This hypothesis was later proven to be correct, with Arg47 and Tyr51 being found to be responsible for the interaction (Figure 1.11).[134] These residues are situated at the mouth of the substrate access channel, and are proposed to be the gatekeepers to the active site.[135,136] Double substitution of these residues (R47A/Y51F) led to a two-thirds decrease in catalytic efficiency;[137] such double mutations of R47 and Y51 have also been found to decrease substrate specificity.[138]

Phe87 was also found to be a key residue in $P450_{BM3}$ catalysis. The benzyl group in F87 extends into the lumen of the substrate access channel and is in close proximity to the haem iron.[125] The residue undergoes a 90° rotation upon substrate binding and this motion is speculated to be responsible for the displacement of the axial water ligand from the coordination site during the catalytic cycle.[139] Stemming from the bulky and non-polar nature of Phe, F87 helps to maintain a hydrophobic environment within the active site by

discouraging water molecules or other polar solvents from entering.[140] Mutations in F87 have been shown to reduce substrate specificity,[135] hence substitutions at this position (F87V and F87A) are commonly present in $P450_{BM3}$ variants to aid the oxidation of unnatural and hydrophilic substrates.

Located as part of the I-helix, the carbonyl oxygen of Ala264 is hydrogen-bonded to the water molecule in the closest proximity to the haem-iron,[125] regardless of whether the active site has substrate bound or not. This suggests its pivotal role in conformational changes upon substrate binding.

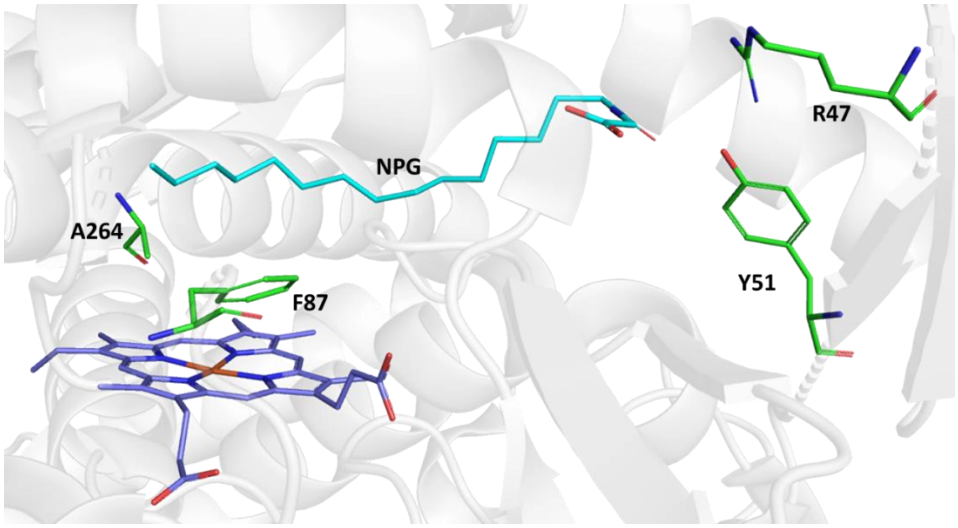

Figure 1.11 *N*-Palmitoylglycine- (NPG-) bound $P450_{BM3}$ crystal structure (PDB ID: 1JPZ), with the key residues discussed highlighted in green.[139]

1.4.4 $P450_{BM3}$ in Synthesis

$P450_{BM3}$ possesses a number of unique features that shape it into a competent candidate for the synthesis of fine chemicals and various metabolites. First, as mentioned above, $P450_{BM3}$ is one of the few known CYPs to have a fused haem and reductase domain.[131,141] Additionally, as a microbial CYP, $P450_{BM3}$ is stable, soluble and readily expressed.[142] The substrates of wild-type $P450_{BM3}$ are largely limited to the native long chain fatty acid substrates, but numerous mutagenesis efforts have been dedicated towards engineering $P450_{BM3}$, with the aim of expanding the substrate scope.

1.4.4.1 Substrate Engineering

Directing Group and Chemical Auxiliaries

Typical substrate engineering involves linking a non-native substrate to a directing or anchoring group that allows the productive binding of the engineered substrate. Pioneering work on substrate engineering to improve conversion in CYPs focused on PikC (CYP107L1), from the bacterium *Streptomyces venezuelae*. Structural studies revealed that the ionic interactions and hydrogen bonding network between the desoamine moiety in PikC's native substrates and certain residues in the BC loop and FG helices of the enzyme play a crucial role in substrate recognition (Figure 1.12).[143,144]

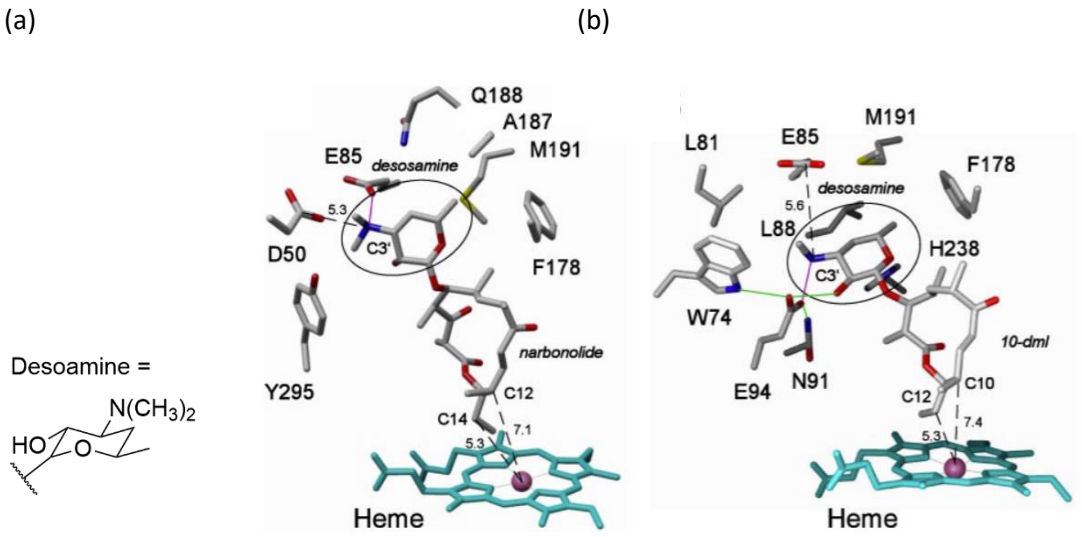

Figure 1.12 Interactions between PikC active site residues and the desosamine moiety of its native substrates (a) narbomycin and (b) YC-17. Hydrogen bonds are shown as light green lines, salt bridges are shown as magenta lines, distances are given in Å.[143,144]

Li *et al.* later harnessed this desoamine anchoring and constructed a series of carbocyclic rings linked to desoamine glycosides (known as "carbolides") (Scheme 1.20A).[145] The results fully demonstrated the potential of substrate engineering, in which hydroxylations took place in a regioselective manner. Meanwhile, substrate engineering was also applied to the optimisation of the regioselectivity of substrate oxidation. Thus, Ménard *et al.* explored the use of nicotinate esters on various hydrocarbon substrates as chemical

auxiliaries to control the hydroxylation regioselectivity achieved by CYP2E1 (Scheme 1.20B).[146]

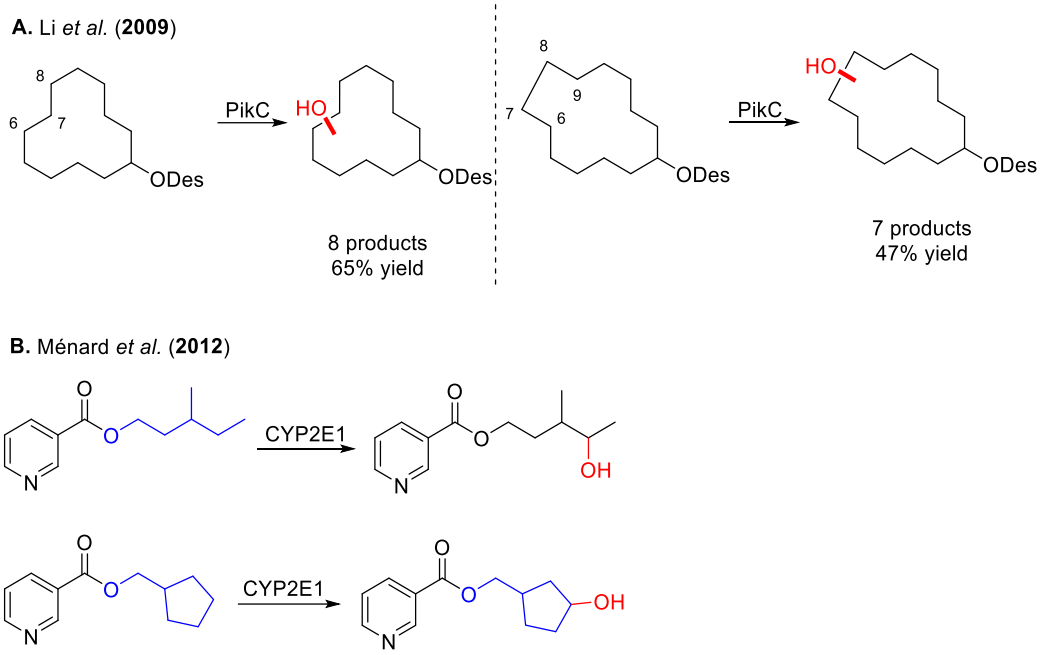

Scheme 1.20 (A) Application of desoamine anchoring in carbocyclic rings for hydroxylations at the C6−C9 positions. Yields are for the combined products and were calculated following LC-MS analysis; (B) Nicotinate esters as chemical auxiliaries in controlling the regioselectivity of CYP2E1-mediated hydroxylations. Des = desoamine.[145,146]

Docking and Protecting Groups

The use of protecting groups is also widely applied in substrate engineering for effective biohydroxylation reactions. In fact, the concept of substrate engineering was first derived from the docking and protecting (d/p) groups introduced by Grengl and co-workers.[147,148] The purpose of these d/p groups was to achieve better substrate recognition by providing a docking site and to minimise undesired side reactions[147] as illustrated in Scheme 1.21. In these examples, the biotransformations were carried out on otherwise unreactive substrates after the installation of different d/p groups which were subsequently removed.

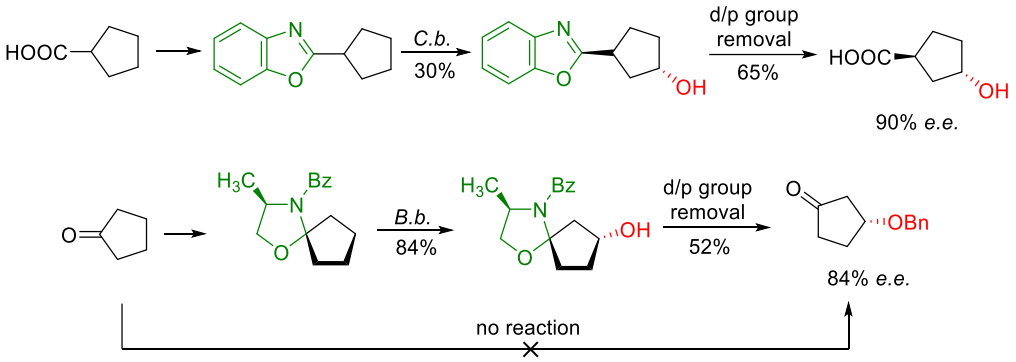

Scheme 1.21 The use of d/p groups (green) as introduced by Grengl *et al. C.b.* and *B.b.* are the fungal species *Cunnighamella blakesleeana* and *Beauveria bassiana*, respectively.[147,148]

In combination with protein engineering, Arnold's group applied this approach to the efficient and selective biohydroxylation of achiral carboxylic acid derivatives with $P450_{BM3}$ variants[149,150] from which derivatives **1.86** and **1.87** served as intermediates in the synthesis of (–)-carbovir **1.88**.

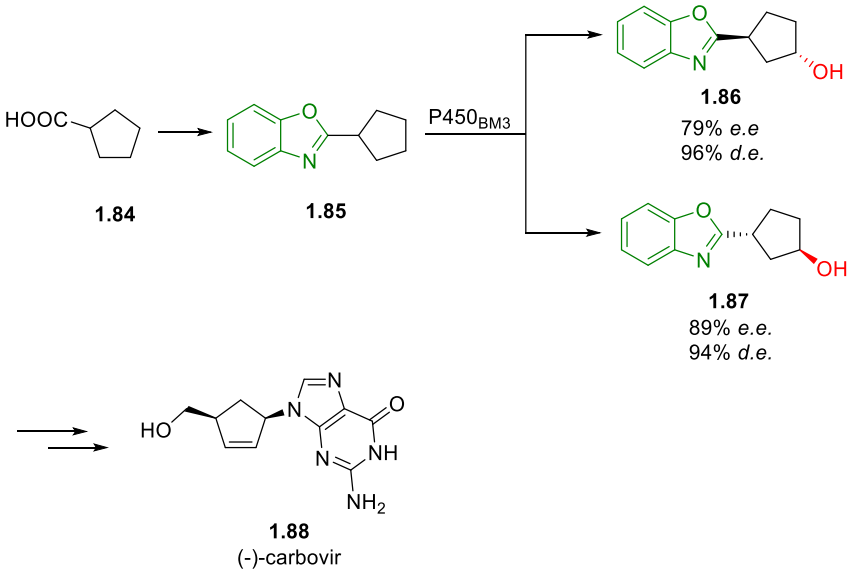

Scheme 1.22 Synthesis of (–)-carbovir **1.88** via derivatives **1.86** and **1.87** formed using the d/p group approach.[150]

1.4.4.2 Protein Engineering

Directed Evolution

Protein engineering entails introducing modifications of the residues based on the folding principles of proteins, with the goal of improving properties such as selectivity, catalytic rates, and substrate tolerance.[151] Pioneered by Stemmer and Arnold in the mid to late 1990s, an approach that involves modifying biocatalysis through an *in vitro* version of Darwinian evolution was introduced,[152] which is now known as "directed evolution".

This approach was applied to esterases by Arnold and co-workers.[153] Previous studies showed that the high catalytic activity of the esterase, *p*-nitrobenzyl esterase, is incompatible with its stability at high temperatures. To probe the relationship between stability and activity of this esterase, six generations of random mutagenesis were carried out, where thermostabilising mutations were identified throughout each generation and incorporated into the enzymes. The cumulative influence of each small contribution from amino acid substitutions led to a >14 °C increase in melting temperature (T_m) of the esterase. This strategy mimics natural evolution while circumventing the need for detailed structural and mechanistic information.

In combination with error-prone PCR and DNA shuffling, directed evolution was used to engineer $P450_{BM3}$ for activity in alkane oxidation.[154,155,156] Five generations of mutagenesis and screening were performed, leading ultimately to $P450_{BM3}$ mutant 139-3,[155] which exhibited significantly higher TON than the WT (Figure 1.13a) as well as superior catalytic activity compared to known, naturally occurring alkane monooxygenases on their most preferred substrates (Figure 1.13b). Building on the 139-3 mutant with more rounds of random and site-saturation mutagenesis, mutant 35E11 was identified, which enhanced propane oxidation activity even further to a TON of approximately 6,000.[156]

(a) (b)

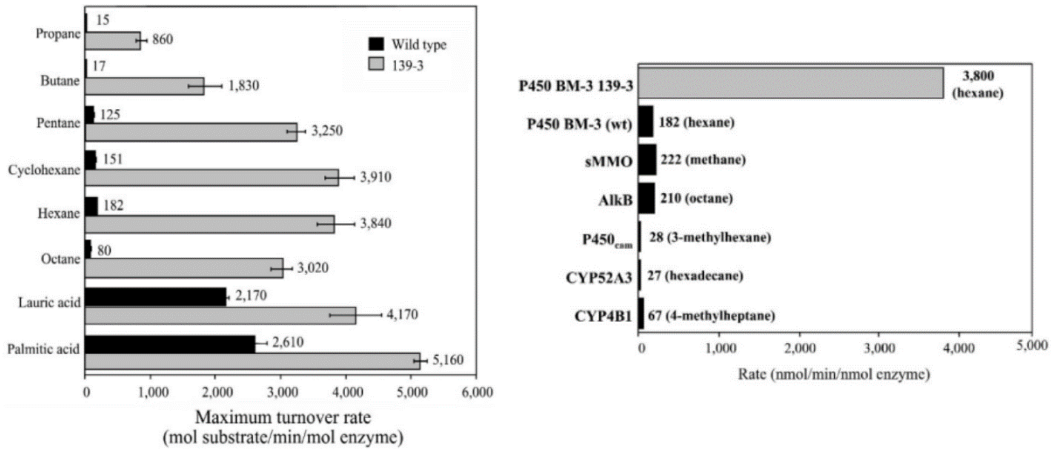

Figure 1.13 (a) Maximum TON for WT $P450_{BM3}$ and $P450_{BM3}$ mutant 139-3 for oxidations of various alkanes; (b) Maximum rates for alkane hydroxylation for different alkane monooxygenases and $P450_{BM3}$ 139-3.[155]

Fasan's group deployed an alternative strategy,[157] domain-based directed evolution, in developing a highly efficient engineered $P450_{BM3}$ for propane oxidation ($P450_{PMO}$). $P450_{PMO}$ was built from mutant 35E11 mentioned previously in which the haem, FMN and FAD reductase domains were evolved separately by different methods of mutagenesis, and beneficial mutations were combined in a final step. The success of this approach was demonstrated by the production of $P450_{PMO}$ which achieved an impressive catalytic efficiency (TON ~45,000). Wang *et al.* further applied this strategy and resulted in the discovery of mutant BM3-Hstar, [158] an engineered $P450_{BM3}$ variant with a histidine residue in place of cysteine at position 400. BM3-Hstar was shown to be an efficient and enantioselective cyclopropanation catalyst, then used in the synthesis of the cyclopropyl core structure in approved drug levomilnacipran (Scheme 1.23A). A change from histidine to serine (C400S) led to variant $P411_{BM3}$[159,160,161] in which the reduction potential of the ferric to ferrous state is raised, abolishing its native monooxygenase activity and enabling non-natural carbene and nitrene insertions (Scheme 1.17). The P411 mutant is capable of carrying out reactions such as highly efficient styrene cyclopropanation with $P411_{BM3}$-CIS[161] (Scheme 1.23B) and indole alkylation with $P411_{BM3}$-HF (Scheme 1.23C).[162]

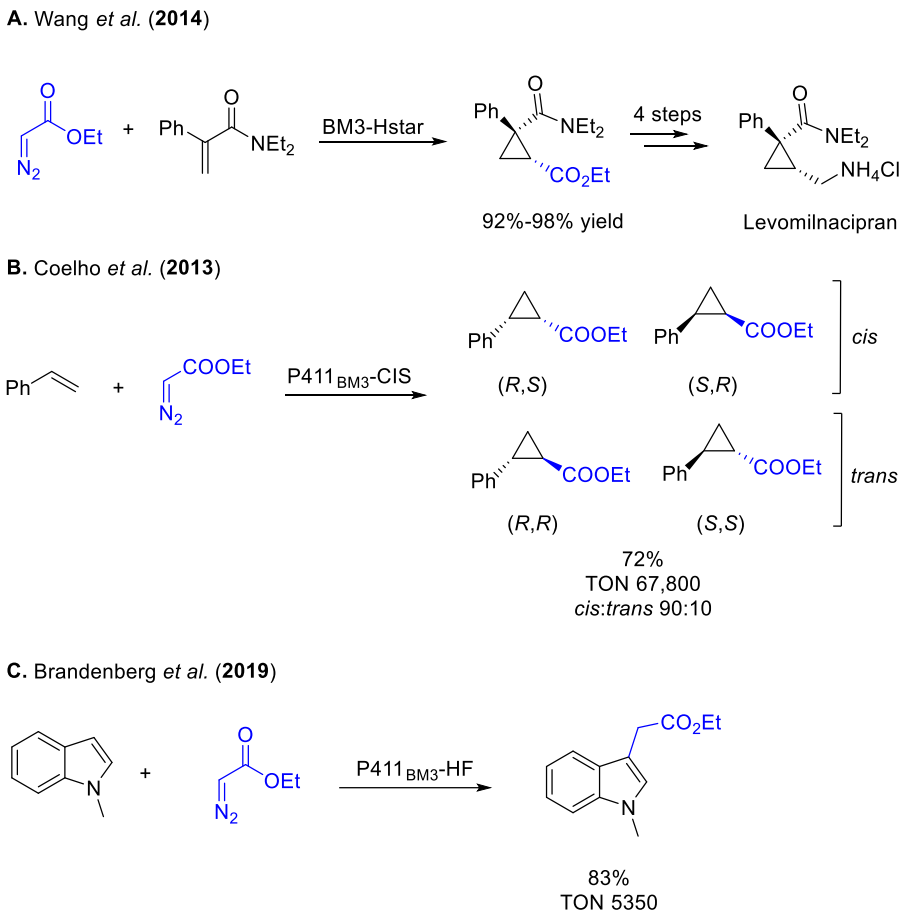

Scheme 1.23 (A) Synthesis of levomilnacipran via the metabolite of BM3-Hstar; (B) Cyclopropanation with P411$_{BM3}$-CIS; (C) Indole alkylation with P411$_{BM3}$-HF.[158, 161,162]

Rational Protein Design

While directed evolution requires no prior knowledge of the structural information of the protein, the alternative strategy of rational protein design does. This approach requires detailed knowledge of the structure and function of the protein in order to allow target selections for mutagenesis. One of the first rational design approaches, reported by Hecht *et al.* in 1990,[163] used qualitative analysis, such as designing sequences that are native-like in pattern and composition, and incorporating natural structural motifs. Hecht successfully designed the *de novo* protein Felix, which was "native-like" in terms of its protein sequence and closely resembled the designed three-dimensional structure. Bryson *et al.* described this type of approach as a "hierarchal" design,[164] in which a progressing level of complexity is introduced iteratively, based on new insights gathered on the fundamental structure and function of the protein from previous rounds of mutagenesis.

In 2009, Pleiss and co-workers constructed a small library comprising just 24 $P450_{BM3}$ variants by combining five hydrophobic residues (Ala, Val, Phe, Leu, Ile) at two positions.[165] These residues are located in the vicinity of positions 87 and 328, both of which were identified by the analysis of crystal structures and sequences, as well as molecular dynamics simulations. Variants from this library showed enhanced activity towards four terpene substrates: geranylacetone, neryl acetate, (4*R*)-limonene and (+)-valencene.

Wong and co-workers developed a library of approximately 100 $P450_{BM3}$ mutants,[166,167] derived from five base mutants:

A330P,
K19 H171L/Q307H/N319Y,
RP R47L/Y51F/I410P,
RT2 R47L/Y51F/A191T/N239H/I259V/A276T/L353I, and
GVQ A74G/F87V/L188Q,

with additional mutations at between two and four active site residues in order to engineer various shapes and sizes of the substrate pocket giving rise to improved binding with unnatural substrates.[168,169,170,171] Screening with this library showed high selectivity and catalytic activity against drug molecules (diclofenac **1.89** and naproxen **1.92**),[168] drug core motifs (substituted tetrahydroquinolines **1.95** and quinolines **1.97**),[171] and diterpenes (eleuthoside precursor **1.99**) (Scheme 1.24).[170]

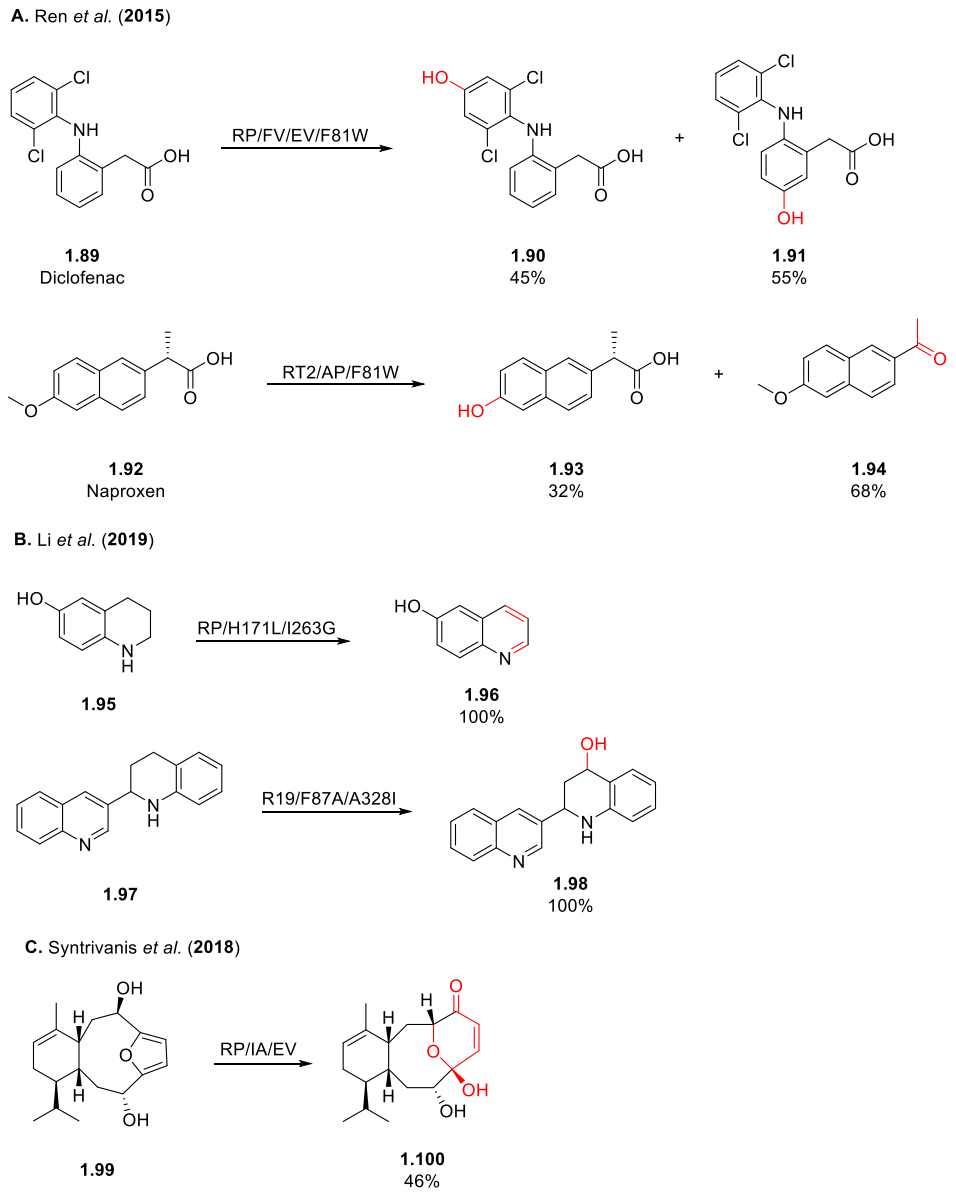

Scheme 1.24 Examples of metabolites from a selection of substrate types with the corresponding $P450_{BM3}$ variant shown for each transformation. The selectivity for each metabolite is shown as a percentage.[168,171,170]

Molecular Dynamics Simulations and Substrate Docking

The strategies in protein engineering discussed so far involve continuous rounds of mutagenesis and large screening efforts; prior knowledge of protein structure and residue functions are required to a certain extent. Although crystal structures provide unparalleled information on stable enzyme-substrate binding modes and have had significant impacts on protein design, enzymatic functions are often influenced by the dynamics between the residues and substrates, which crystal structures are unable to capture.

Molecular dynamics (MD) simulations and computational substrate docking have emerged as powerful tools in understanding and predicting ligand-protein interactions. Based on a classical mechanics treatment of interatomic interactions,[172,173,174] MD simulations predict how each atom in a molecular system will move over time. Such simulations are capable of capturing a wide range of important biomolecular processes, with examples including protein folding and conformational changes. MD simulations calculate the forces exerted on each atom by all other atoms in a biomolecular system such as a protein solvated by water molecules.[174] The first MD simulation of a protein dates back to 1977 by McCammon *et al.* on a bovine pancreatic trypsin inhibitor.[175] Since then, this approach has been applied to modelling many complex biological systems.[176]

Molecular docking is used to model interactions between small molecules and proteins, e.g. drugs and target enzymes, and between proteins.[177] Small molecule docking into proteins, involves two steps: (1) prediction of the conformations, orientations and position of the ligands within the active site (commonly referred to as "poses"); and (2) assessment of the binding affinities of each pose to generate a ranking.[178] These two steps use sampling algorithms and scoring schemes, respectively.[178] Most of the earlier docking approaches treated both ligand and receptor as rigid bodies, following Fischer's lock-and-key mode;[179] however, molecular systems are more suited to Koshland's induced-fit model (Figure 1.14), wherein the receptor optimises the binding interface through physical interactions to form the final complex.[180] Most modern docking methodologies adopt this latter model, in which the flexibilities of both ligand and receptor components are considered. In this project, docking programmes Autodock Vina and Autodock Flexible Receptors (ADFR) were employed, as discussed in detail later in the thesis (§2.8, 4.3.3). The D.Phil. thesis of Zhang[174] and a review published by Cui *et al.*[178] together provide a comprehensive summary of the mechanism and algorithms behind MD simulations and molecular docking.

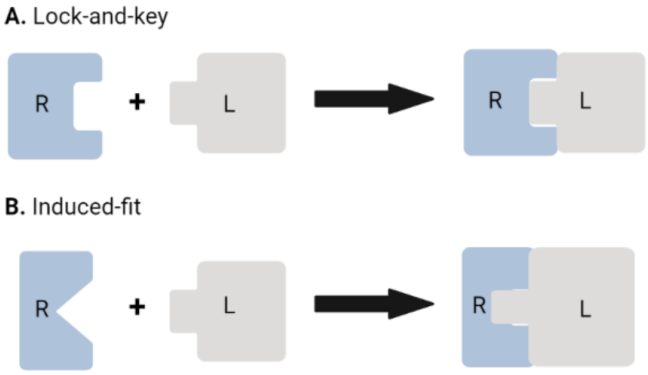

Figure 1.14 Illustration of the lock-and-key and induced-fit models.

Early applications of MD simulations and docking approaches focused mainly on investigating ligand binding orientations. For example, Kille *et al.* performed MD simulations and docking experiments to rationalise the origin of regio- and stereoselectivity of the $P450_{BM3}$ hydroxylation of testosterone (TST).[181] Two variants, KSK-2 and KSK-14, were selective against for the production of 2β-(OH) (94% selectivity) and 15β-(OH) TST (96% selectivity), respectively. Computational analysis revealed that only a single active positional orientation of the substrate was observed in each case, leading to the aforementioned isolated products (Figure 1.15).

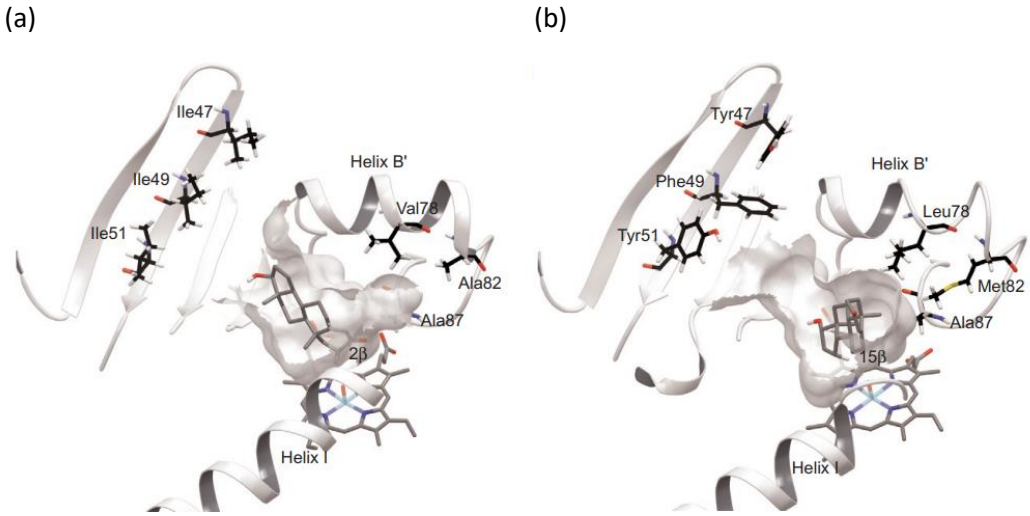

Figure 1.15 Computational results of MD simulations and dockings, showing (a) 2β-(OH) TST-selective mutant KSK-2, and (b) 15β-(OH) TST-selective mutant KSK-14, in which the hydroxylated carbons in each pose were in the ideal proximity to the haem-iron.[181]

Chen *et al.* employed docking strategies to understand the influence of glycine mutations on the hydroxylation of androstenedione (AD) in $P450_{BM3}$ variants.[182] MD simulations and molecular docking were performed on a $P450_{BM3}$ variant, K19/F87A/A82M/I263G/A264G, which was one of the most selective mutants for the production of 2β-(OH) AD (59%). The results revealed that the binding poses consistent with oxidation at the 2β- position were indeed the most populated for this variant, according with experimental data.

Recently, Li *et al.* engineered $P450_{BM3}$ variants *in silico*, with MD simulation and docking as a guide (Scheme 1.25).[183] Variant LG-23 (R47W/S72W/F77Y/V78L/F81I/A82L/F87G/T88S/M177T/M185Q/L188Q/I209T/A328G/A330W) achieved an increase in selectivity towards 11α-(OH) 9-dehydronandrolone **1.102** was from 78% to 92%. This metabolite acted is an intermediate in the synthesis of trenbolone **1.103**, a versatile anabolic-androgenic steroid.

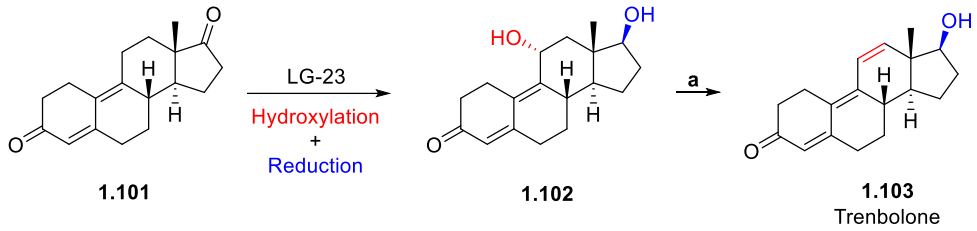

Scheme 1.25 Chemoenzymatic synthesis of trenbolone. (a) *p*-TsOH, $CHCl_3$, RT, 90%.[183]

To summarise, the combination of MD simulations and molecular docking provides insights into substrate-ligand interactions, helping to guide the rational design of variants by P450 engineering. Application to protein design remains greatly under-explored but, compared with traditional methods such as random mutagenesis or rationally designed libraries, MD simulations and docking significantly reduce the resource needed for extensive screening efforts. Most of these approaches are substrate-specific and further research is needed to develop a more general and applicable strategy for *in silico* design.

1.5 Aims and Proposed Work

This work builds on research previously undertaken within the Robertson and Wong groups[174] in which it was discovered that the position of hydroxylation of spirocyclic and bridged bicyclic amines varies depending on the protecting groups (PG) installed on the *N*-atom. In order to establish a complete profile for the *N*-protected azaspiro-series, this project aimed to explore the functionalisation of *N*-protected 2- and 3-spiroamine analogues *via* $P450_{BM3}$-mediated hydroxylation (Scheme 1.26A). Following the synthesis of both spirocycles, enzymatic screening with panels of $P450_{BM3}$ variants was proposed to be conducted with substrates bearing four representative PGs: Boc, Ms, Ips and DEP. The screening results would allow the identification of mutants deemed worthy of further study based on high conversion and/or high selectivity. Preparative-scale oxidations with these mutants would then provide sufficient quantities of the products for complete characterisation. In the achiral system of both spiroamines, the introduction of a hydroxyl group confers chirality and serves as a synthetic "handle". The chemical properties of the "handle" would then be exploited to construct a set of diversified fragment compounds. In addition, MD simulations and molecular docking were proposed to be performed on selected variants for protein engineering.

As discussed earlier, in §1.1.3, piperidines are "privileged" structural units in pharmaceutical compounds and spirocycles are gaining increasing importance in the drug discovery industry. Combining the unique characteristics of spiropiperidines and biocatalysis, the ultimate goal of this project is to elucidate the potential of utilising $P450_{BM3}$ as a tool for constructing fragment-sized libraries by performing chemical transformations that are difficult or unachievable in conventional synthetic chemistry, thus showcasing its potential application within FBDD (Scheme 1.26B).

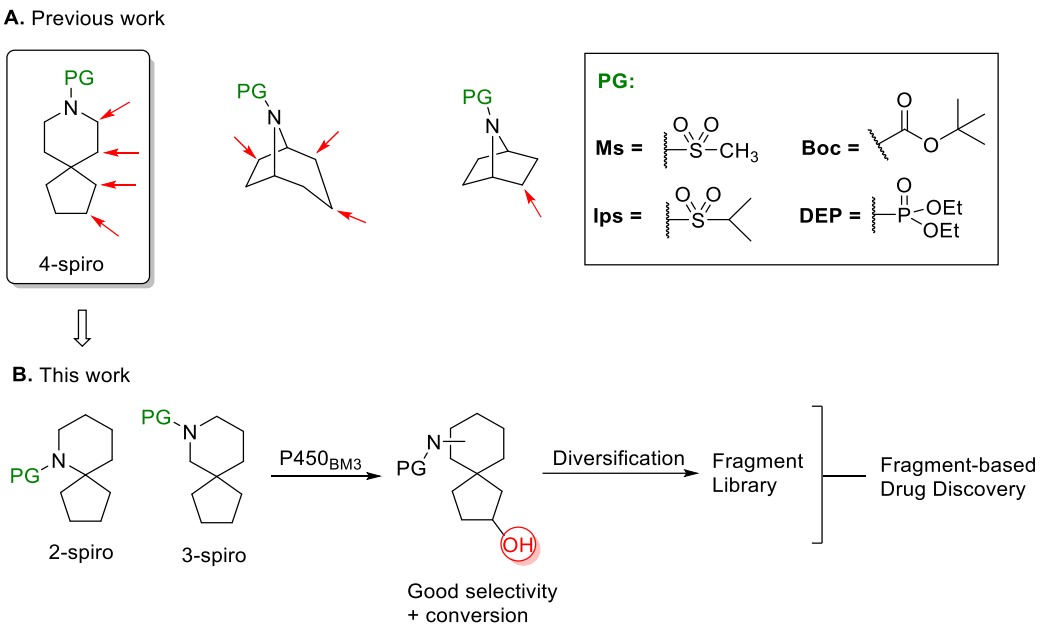

Scheme 1.26 (A) Previous work; oxidation sites are indicated by red arrows; (B) Overall aims of this work.

Chapter 2: *N*-Protected 6-azaspiro[4.5]decane (2-spiro) analogue

2.1 Overview

This chapter discusses various synthetic routes towards the 2-spiro system, enzymatic reactivity, and the metabolites identified from the substrates bearing different protecting groups. Results from MD simulations and molecular docking are also discussed.

2.2 First Generation Route *via* Curtius Rearrangement

An initial route to spirocycle **2.1** was envisaged to begin with alkylation of methyl cyclopentanecarboxylate **2.4**, followed by Curtius rearrangement of derived acid azide **2.2** then cyclisation (Scheme 2.1).

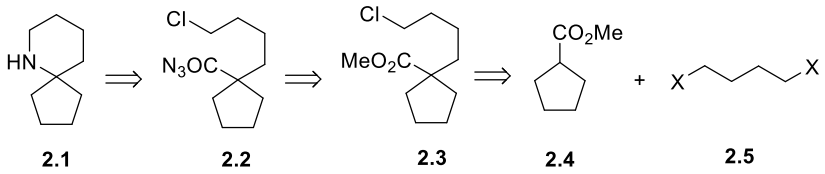

Scheme 2.1 First generation retrosynthetic route of spirocycle **2.1**.

Ester **2.4** was synthesised from carboxylic acid **2.6** *via* Fischer esterification (Scheme 2.2),[184, 185] then enolate alkylation with 1-chloro-4-iodopropane furnished ester **2.3** efficiently. Before continuing with the next step, the ester to amine conversion *via* Curtis rearrangement was tested with model substrate **2.9** which afforded carbamate **2.12** without complication.[186]

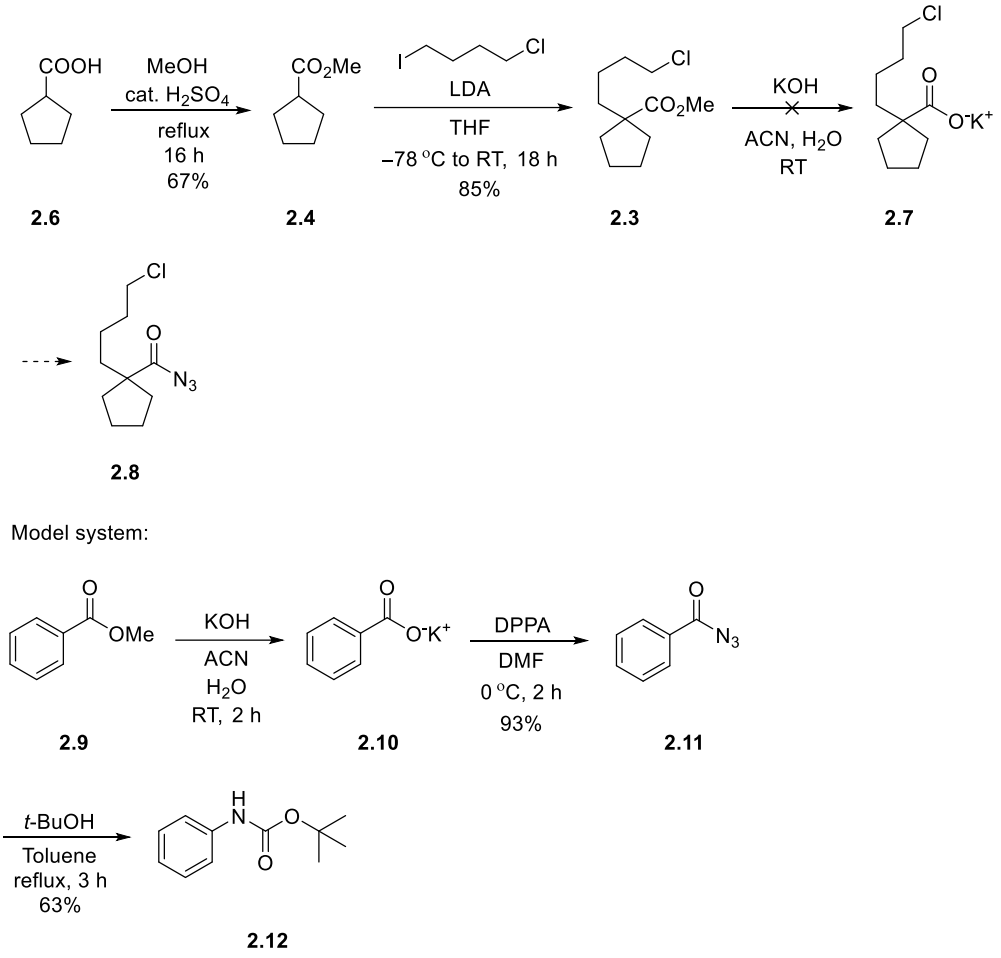

Scheme 2.2 Progress towards spirocycle **1** and a model for the Curtius rearrangement.

Although the reaction was successful for the model compound, negligible conversion was achieved, despite various modifications, when attempting to convert ester **2.3** into carboxylate salt **2.7**, (Table 2.1). It was speculated that the quaternary carbon centre and the bulky alkyl chain impeded the addition of hydroxide ion, even under forcing conditions.

Entry	Temperature (˚C)	KOH (equiv.)	Time	Conversion (%)
1	RT	1.1	5 h	0
2	RT	2.2	24 h	0
3	30	2.2	3 days	0
4	50	2.2	5 days	Trace
5	Reflux	2.2	7 days	Decomposed

Table 2.1 Reaction conditions screened for hydrolysis of ester **2.3**.

2.3 Second Generation Route *via* Beckmann Rearrangement

The second generation route (Scheme 2.3) is based on steps optimised within the group by previous D.Phil. student, Cook.[187] In the forward sense, alkylated cyclopentanone **2.15** would be synthesised from an alkylation/decarboxylation sequence from β-ketoester **2.16**. The cyclisation of **2.15**, followed by a condensation reaction with hydroxylamine would give spiro-oxime **2.14**, from which Beckmann rearrangement would give lactam **2.13** and then spirocycle **2.1** after reduction.

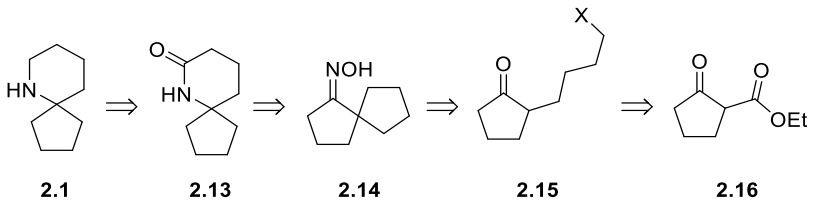

Scheme 2.3 Second generation route to spirocycle **2.1**.

Commercially available ketoester **2.16** was alkylated with 1,4-dibromobutane (→ **2.17**, Scheme 2.4)[4] then decarboxylation and a base-mediated cyclisation produced spirocycle **2.19** via bromoketone **2.18**. This ketone was conveniently transformed into oxime **2.14** which, under standard conditions with $SOCl_2$, formed the abnormal Beckmann products **2.22** and **2.23** in a 20:1 ratio, respectively. The formation of these products likely arises because the stability of the carbocation (**2.21**) derived from chlorosulfite ester **2.20** makes the E1 pathway favourable.[188]

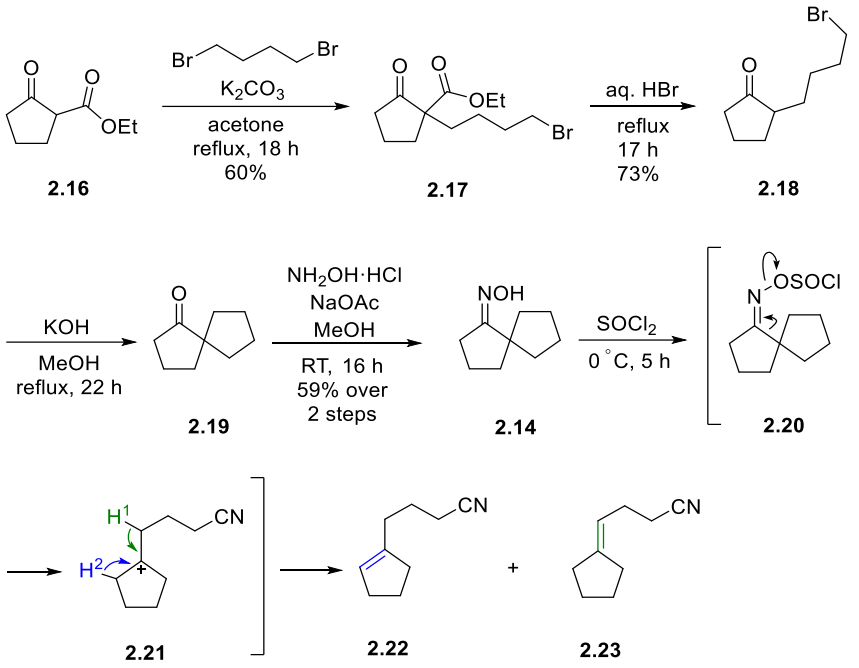

Scheme 2.4 Progress towards spirocycle **2.1** based on Beckmann rearrangement.

It has been reported that the partially-characterised ethyl ester of polyphosphoric acid, so-called polyphosphate ester (PPE), is an effective dehydrating reagent and mediator of the Beckmann rearrangement of ketoximes.[189,190,191,192] PPE was prepared from P_2O_5 and diethyl ether according to the reported procedure[193] and combined with oxime **2.14** (Scheme 2.5); lactam **2.13** was successfully synthesised and isolated with a 34% yield, along with nitriles **2.22** and **2.23**, which comprised about 30% of the total isolated mass. Despite the unsatisfactory yield, the synthetic route was maintained to synthesise *N*-Boc protected **2.24** through $LiAlH_4$-mediated reduction of **2.13** in poor yield.[187] Overall, however, this route was deemed impractical because: (i) the product from each step required purification; (ii) the volatility of ketone **2.19** and the loss of product from purification in previous steps significantly lowered the yield of oxime **2.14**; and (iii) preparation of PPE was time-consuming and a large excess of it was required.

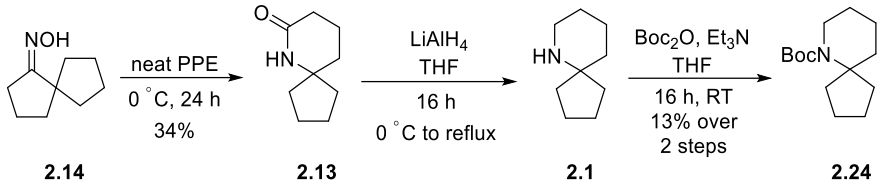

Scheme 2.27 Synthesis of Boc-protected **2.24** through PPE-mediated Beckmann rearrangement of **2.14**.

2.4 Third Generation Route *via* Reductive Amination

A different approach was then explored (Scheme 2.6), in which the spirocycle would be installed by reductive amination of nitro-aldehyde **2.25**, which could, in principle, derive from the hydrolysis of enol ether **2.26**, the product of an alkylation/Wittig homologation sequence from nitrocyclopentane **2.27**.

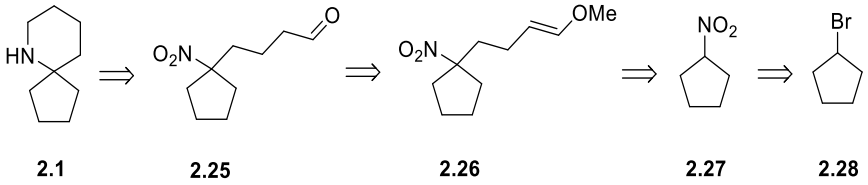

Scheme 2.6 Third generation route to spirocycle **2.1**.

Nitrocyclopentane **2.27** was prepared from the commercially available bromide **2.28** (Scheme 2.7).[194] Alkylation with acrolein then furnished aldehyde **2.29**[195] which was homologated *via* Wittig reaction and hydrolysis to give the aldehyde **2.25**.[196] The next step required the sequential reduction of the nitro group and the aldehyde moiety after cyclic imine formation. Literature procedures of this type of process are scarce and not, in any case, directly applicable to this substrate.[197,198] Nonetheless, reduction was still attempted with Raney nickel which, by analysis of the ^{1}H NMR spectrum of crude product, afforded a complex crude mixture containing a trace of the reduced aminoalcohol.

This route was also deemed impractical due to the long reaction time required for the alkylation step to compound **2.29**, as well as its inefficiency that, in part, arose from polymerised acrolein that complicated product purification.

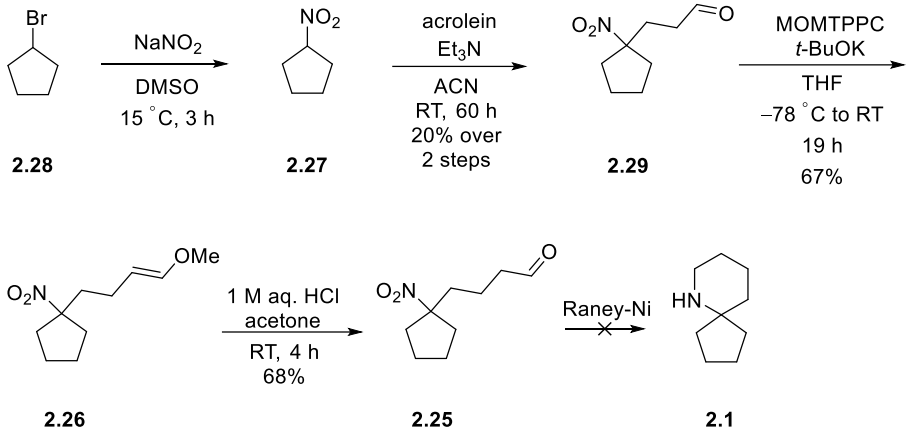

Scheme 2.7 Progress towards spirocycle **2.1** based on reductive amination.

2.5 Fourth Generation Route *via* Reductive Bis-alkylation

The fourth generation synthetic route commenced from commercially available δ-valerolactam **2.33** (Scheme 2.8). In this route, the free lactam would be protected and subjected to a reductive bis-alkylation to form diallylated product **2.31** from which a tandem RCM/transfer hydrogenation sequence was expected to furnish protected spirocyclic amine **2.30**. Depending on the PG chosen, the corresponding deprotection procedure can be performed in order to install a different PG.

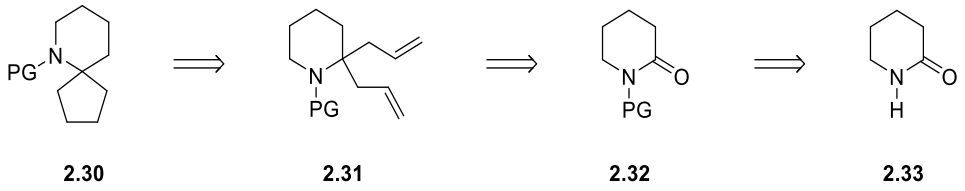

Scheme 2.8 Fourth generation route to *N*-protected spirocyclic amine **2.30**.

δ-Valerolactam **2.33** was converted into imidoyl chloride **2.34** using PCl_5 (Scheme 2.9),[199] then Grignard reaction with allyl magnesium chloride, and mesylation generated diallylated amine **2.36**.[200,187] The *N*-mesylated spirocyclic amine **2.37** was finally achieved by the proposed tandem RCM/transfer hydrogenation reaction.[201]

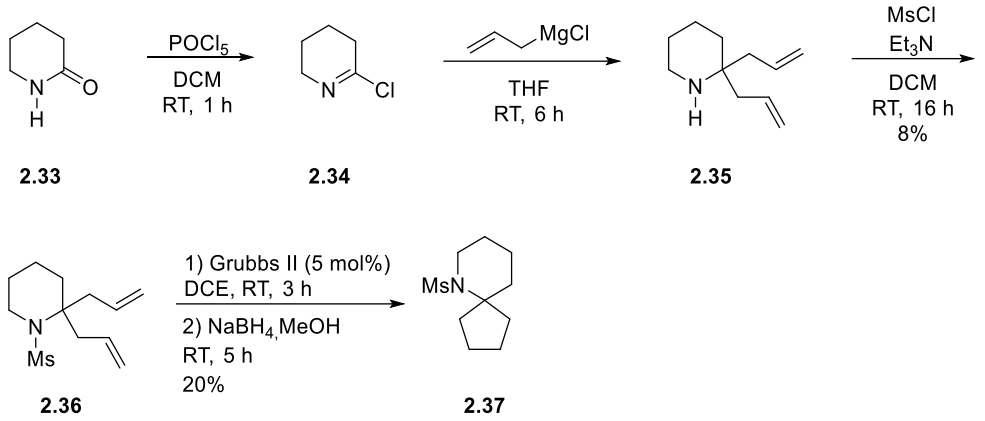

Scheme 2.9 An optimized route to spirocyclic amine **2.37**.

The overall yield of spirocycle **2.37** was disappointing but attempts to improve individual steps were not successful. During this process, an impurity was observed that carried through the route, complicating purification; this was later identified as mesylated dodecyl **2.42**, resulting from the ring-opening of the solvent THF (Scheme 2.10). It was postulated that the Schlenk equilibrium between allylmagnesium chloride and diallymagnesium **2.38** would provide Lewis acidic $MgCl_2$ to promote the ring-opening of THF, ultimately leading to alcohol **2.40** which was then mesylated to intermediate **2.41**. dodecyl mesylate **2.42** would then be produced during the RCM/hydrogenation step;[201] its presence was supported by ^{1}H NMR analysis (δ 3.00, s; 4.25, t, J = 6.5 Hz) that indicated the methyl moiety on the Ms- group and a -CH_2OX substructure, respectively. MS data were also consistent (m/z = 359.5).

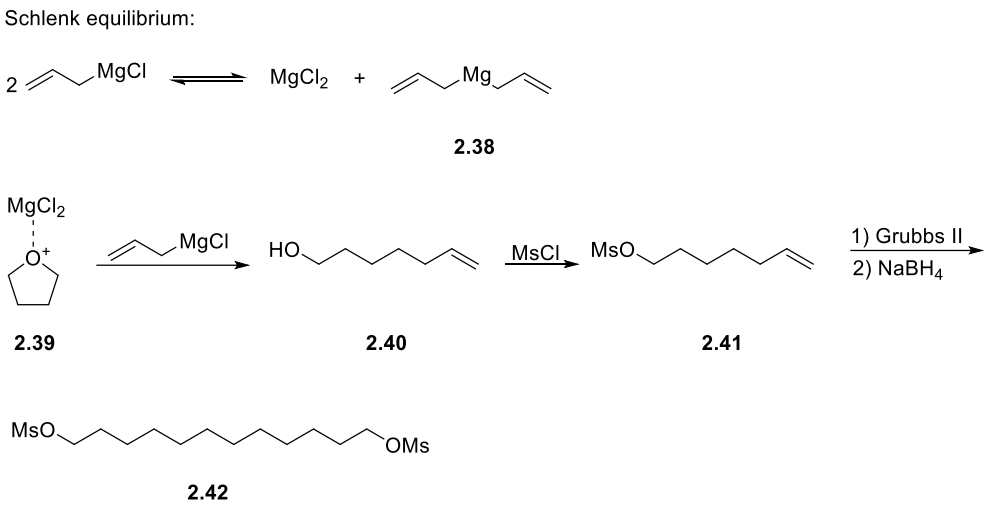

Scheme 2.10 THF ring-opening and alkylation with allylmagnesium chloride.

To circumvent this problem, the route was slightly amended (Scheme 2.11). *N*-Benzyl lactam **2.43**[202] was subjected to TFAA-mediated reductive bis-alkylation,[203] via the electrophilic iminium intermediate **2.47**. Sequential addition of one allyl group, ionisation, and addition of a second allyl group formed piperidine derivative **2.44** which underwent the RCM/hydrogenation sequence to give spirocycle **2.45**.[201] One-pot deprotection/protection then afforded the *N*-Boc protected 2-spiro analogue **2.24**.[204]

Although some yields remained stubbornly moderate, the route was applicable to gram-scale and sufficient *N*-Boc protected 2-spiroamine **2.24** was prepared to study the enzymatic hydroxylation.

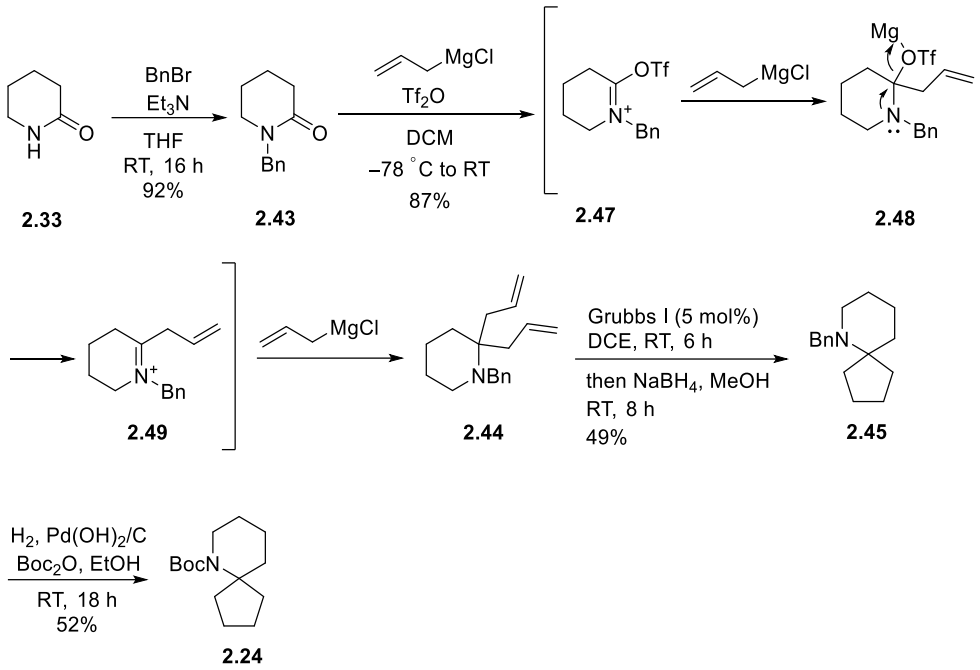

Scheme 2.11 Modified fourth generation route via reductive bis-alkylation.[20]

With the *N*-Ms **2.37** and *N*-Boc **2.24** 2-spiroamines in hand, attention turned to installing the Ips and DEP PGs. Three different approaches were undertaken but all failed (Scheme 2.12): (i) deprotection of the Bn group[205] and reprotection of amine **2.1** with Ips;[206] (ii) deprotection of Boc to obtain TFA salt **2.54**,[207] and reprotection with Ips or DEP;[206] and (iii) debenzylation with *N*-dealkylating agent ethyl chloroformate[206] ready for reprotection. In the latter case, NMR spectroscopic analysis of the crude product revealed that the benzyl group remained intact but the chloroacyl group appeared to have been cleaved to an unknown moiety. It was apparent that *N*-activation led to the formation of carbocation **2.52** leading to olefinic structures **2.53** in a 2:1 *endo*:*exo* ratio. The reasons behind the unsuccessful Ips and DEP protections are not understood but it was speculated that the spirocyclic centre presented steric hindrance; however, the same issue was not observed with the *N*-Boc amine **2.24** and further investigations are necessary to pinpoint the problems.

During the attempts to synthesise protected 2-spiroamine **2.30** (PG = DEP), trifluoroacetyl amine **2.55** was obtained in 57% yield.

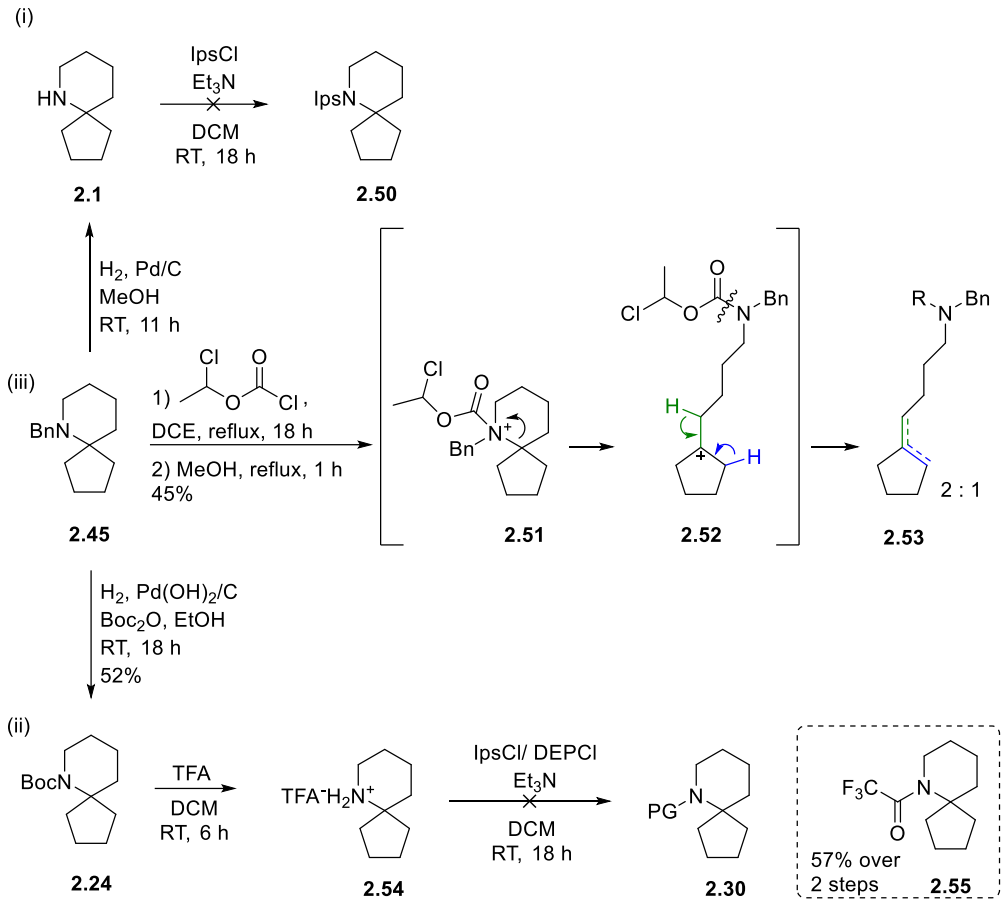

Scheme 2.12 Failed attempts to achieve Ips and DEP protection.

After the unexpected formation of trifluoroacetyl derivative **2.55**, it was decided to employ this product as a hydroxylation substrate for which it was deliberately synthesised from the trifluoroacetate salt **2.54** (Scheme 2.13).

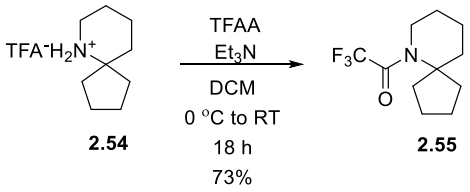

Scheme 2.13 Synthesis of *N*-trifluoroacetyl protected 2-spiroamine **2.55**.

2.6 Screening of *N*-protected 6-azaspiro[4.5]decane with $P450_{BM3}$

Prior to the isolation of major metabolites, screening was carried out for each substrate. The underlying idea in this method is to identify variants that show high conversion and selectivity, which are then selected for preparative-scale reactions for metabolite identification (see Experimental for details). Screening was conducted in 24-well plates, with varying substrate/enzyme ratio and on a timescale of 5−24 h. Four different substrates, namely **2.37** (Ms), **2.45** (Bn), **2.24** (Boc), and **2.55** (Tfa), were screened against libraries of either 24 or 48 $P450_{BM3}$ mutants (full screening data in Chapter 8: Appendix). These libraries consisted of variants that have exhibited diverse metabolite formation from a variety of substrate types.[208,171] At the outset, it was intended that screening rounds resulting in low conversion rates or non-selective reactions would be followed by further screening with more specialised enzyme variants. All the major metabolites isolated from each substrate are listed in Table 2.2, along with the corresponding conversion, selectivity, yield, and enantioselectivity if applicable. The basis for assigning 'major' metabolites was moderate conversion (≥50%) and selectivity (≥50%), since poor conversion and selectivity present difficulties in isolating the metabolite. Unless otherwise stated, all metabolites were isolated as a single diastereomer.

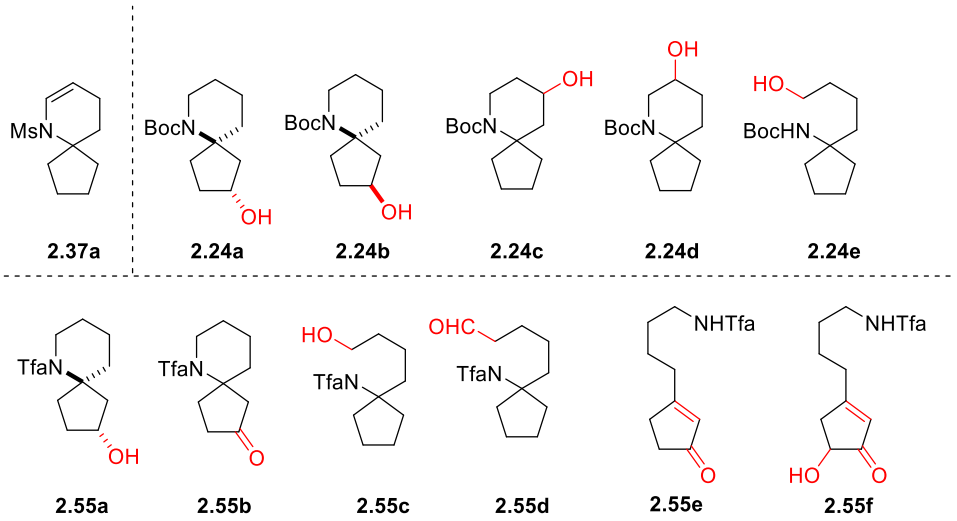

PG	Variant	Conv. (%)	Prod.	Select. (%)	e.e. (%)	Substrate : Enzyme Ratio	Yield[b] (%)
Ms- (2.37)	R19/F87A/A184I/ A264G	98	**2.37a**	43	-	1000:1	38
Boc- (2.24)	KT2/L188G/ I263G	91	**2.24a**[a]	66	-		11
	GL/L188Q/ I263G/A328G	93	**2.24b**[a]	14	-		3
	R19/F87I/ L437LV	95	**2.24c**	56	-		7
	R19/F87I/E267F	100	**2.24d**	32	-		4
	R19/A330W	93	**2.24e**	36	-		11
Tfa- (2.55)	A330P	100	**2.55a**	97[c]	1		52
	R19/F87A/T260G	99		46[c]	8		29
	GV/L188Q/ A264G	100		30[c]	18		31
	VQ/S72G/A330W	99	**2.55b**	61	-		13
	RP/A82M/I263A	99	**2.55c**	48	-		11
		80	**2.55d**	30	-	5000:1	11
	R19/F87I	100	**2.55e**	28	-	1000:1	7
	VQ/S72G/A330W	100	**2.55f**	18	-		7

Table 2.2 Summary of all metabolites identified from preparative-scale reactions for substrates **2.37**, **2.45**, **2.24**, and **2.55**; [a] The stereochemical configurations for metabolites **2.24a** and **2.24b** are relative and refer only to products from the mutants listed; [b] Isolated yields; [c] Selectivity shown incorporates the derived secondary products, i.e. **2.55b**, **2.55e**, and **2.55f**.

2.6.1 Screening of *N*-Ms-protected Spiroamine 2.37

The *N*-Ms protected 2-spiro analogue **2.37** was screened against 46 variants at the substrate/enzyme ratio 1000:1. Preparative-scale reactions were then carried out with 0.1

mmol substrate. In the event, only one significant metabolite was identified, enamine **2.37a** (Figure 2.1) produced by α-hydroxylation and elimination.

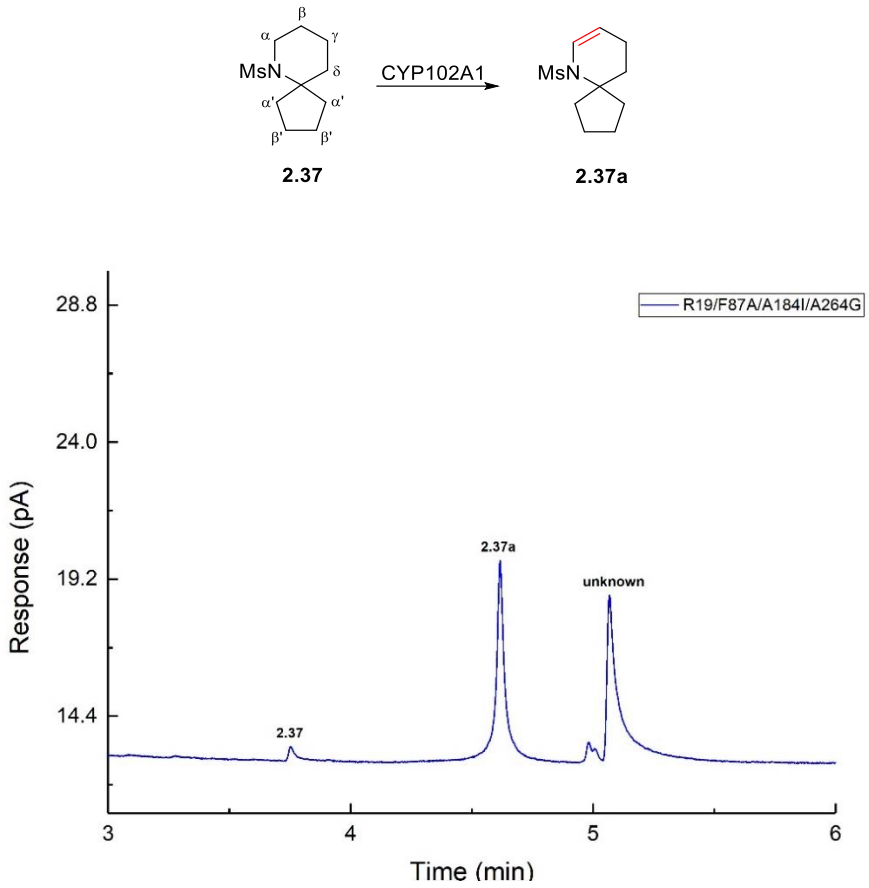

Figure 2.1 GC analysis of the product mixture from substrate **2.37** with the selected variant shown, giving oxidation product **2.37a**.

During screening, 25 out of 46 variants gave >50% conversion of substrate **2.37** based on GC integration. The substrate was initially screened against 24 variants that were from the "common" library, which were known to show conversion to diverse substrate profiles; however, since only two major products were observed (GC, Figure 2.1), 23 further variants were screened that were chosen for their increased activity, for example towards steroids. Even so, the major metabolites remained the same two observed previously. The peak at around 5 min was present in the enzymatic screen but absent from the preparative-scale reaction and it was suggested that this peak corresponded to the α-

hydroxylated metabolite which spontaneously dehydrates during product isolation to form the enamine **2.37a**.

Mutation A82M/A328G encouraged the elimination of the precursor α-OH to **2.37a** with a selectivity of 91% in variant K19/F87A/A82M/I263G/A328G (Table 2.3, Entry 2). Mutation A264G enhanced the selectivity by a further 6% on template K19/F87A/A82M/A264G/A328G (Entry 3). The substitution of an Ala residue with Val also appeared to promote enamine formation (Entry 5). On base mutant R19, the F87A mutation promoted the production of enamine **2.37a**, whereas F87I discouraged it (Entries 7 and 8).

Entry	Mutant	Conv. (%)	2.37a (%)	Others (%)
1	K19/F87A/I263G	100	0	100
2	K19/F87A/A82M/I263G/A328G	100	91	9
3	K19/F87A/A82M/A264G/A328G	100	97	3
4	K19/F87V	72	28	72
5	K19/F87V/A328V	35	64	36
6	R19	4	0	100
7	R19/F87A	100	59	41
8	R19/F87I	36	0	100

Table 2.3 Selected screening data for substrate **2.37**. Full data in Chapter 7.

2.6.2 Screening of *N*-Bn-protected Spiroamine 2.45

The *N*-Bn protected 2-spiro analogue **2.45** was screened against 47 variants at a substrate/enzyme ratio of 1000:1; however, there was no conversion observed in the majority of variants (Figure 2.2). One variant, R19/F87I, showed minimal conversion (in blue). Preparative-scale reactions with this mutant using a longer reaction time (48 h) and an increased enzyme/substrate ratio did not produce sufficient metabolite to be characterised.

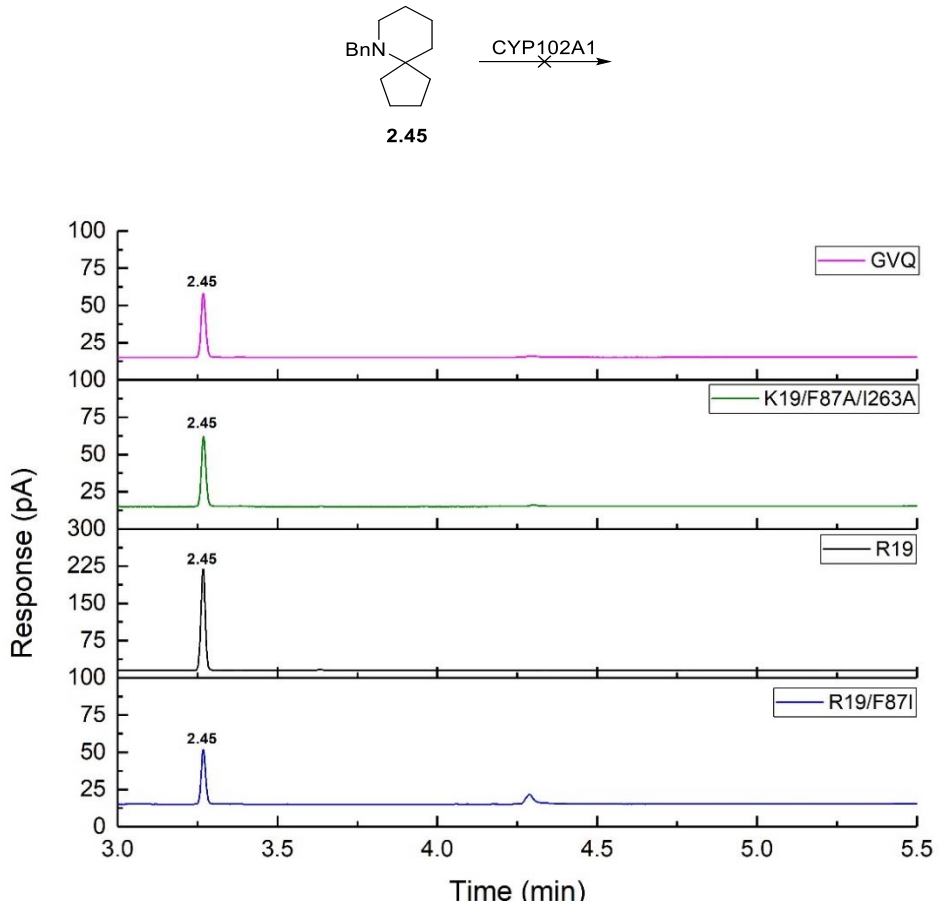

Figure 2.2 GC reaction profile for selected variants that showed some conversion of substrate **2.45** to at least one new product.

The low reactivity of substrate **2.45** is likely attributable to interaction of the nitrogen lone electron pair with the iron centre at the P450 active site, which would cause the substrate to be trapped in the binding pocket thus hampering enzyme activity. A similar issue was not observed with the *N*-Bn protected lactams (§3.4.7) in which the nitrogen lone pair is delocalised into a carbonyl group.

2.6.3 Screening of *N*-Boc-protected Spiroamine 2.24

The *N*-Boc protected 2-spiro analogue **2.24** was initially screened against 47 variants at a substrate/enzyme ratio of 1000:1, and five major products were identified (Figure 2.3). One metabolite, alcohol **2.24c**, was produced with the lowest selectivity across all 47 variants, so further screening was conducted with 23 more variants based on the R19/F87I

mutations. The five metabolites were characterised as β′-OH **2.24a**, its diastereomer **2.24b**, γ-OH **2.24c**, β-OH **2.24d**, and α-OH (then reduction) **2.24e**.

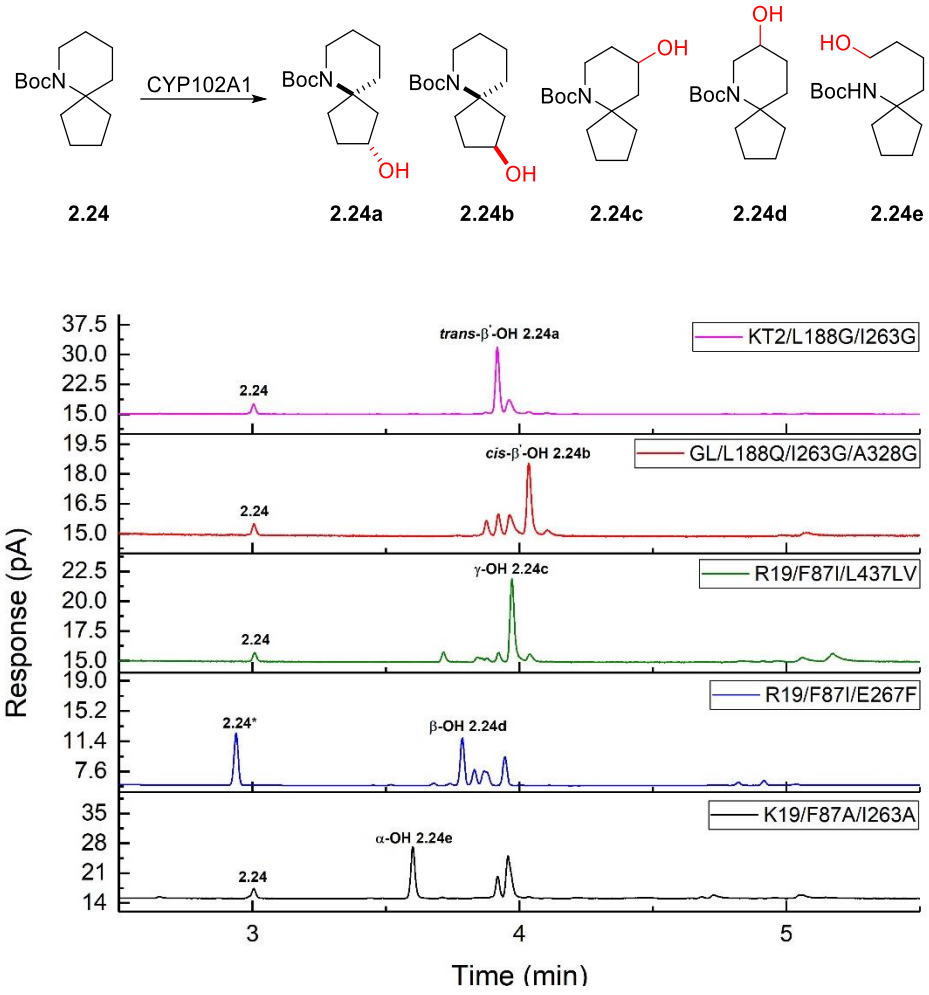

Figure 2.3 GC analysis of the product mixture from the reactions of selected variants with substrate **2.24**; the GC trace for R19/F87I/E267F is shifted due to a change of GC column.

The relative stereochemical configurations were assigned through NOE analysis. The observed NOEs showed the proximity of the *CH*OH in **2.24a** and the more shifted H-1, which correlated to the axial H-9, consistent with the *trans*-diastereomer of the β′-OH (Scheme 2.14a). In contrast, *cis*-diastereomer **2.24b** exhibited proximity of the *CH*OH and the less shifted H-1, which in turn correlated to the H-7. Ambiguity in the NMR data regarding regiochemistry, particularly in the case of γ-OH **2.24c**, DMP-mediated oxidation was carried out in order to eliminate complications from diastereotopic proton resonances (Scheme 2.14b). A prominent singlet at 2.56 ppm was seen in the ^{1}H NMR

spectrum, corresponding to H-6 in ketone **2.24c1** and supporting the hydroxylated site to be at the γ-position.

a)

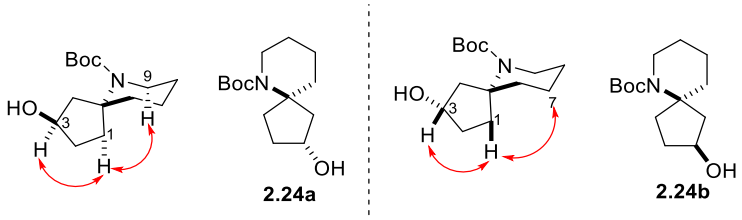

b)

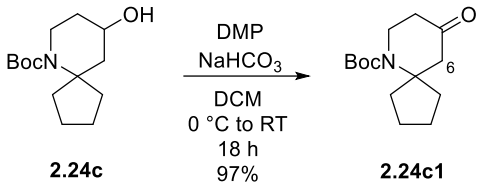

Scheme 2.14 a) Characteristic NOE correlations in **2.24a** and **2.24b**; c) DMP oxidation of **2.24c** to **2.24c1**.

Substrate **2.24** showed the highest reactivity against the enzyme libraries and 48 out of 66 variants gave >50% selectivity. Compared with the cases of substrates **2.37** and **2.45**, the metabolite profile was also more diverse, achieving hydroxylations at several chemically unactivated positions around both rings.

The combinations of A184I/A328L and I263A/A328L raised selectivity towards *trans*-β′-OH diastereomer **2.24a**when introduced on base mutant R19 (Table 2.4, Entries 5 & 6), suggesting that L328 could be a key residue in influencing the formation of this metabolite. On the other hand, mutation E267V on template K19/F87V discouraged β′-oxidation (Entry 17); however, with the addition of V78I, β′-oxidation was favoured (Entry 18).

The *cis*-β′OH diastereomer **2.24b** was formed with lower selectivity than the *trans*-diastereomer. Computational analysis later revealed that in the pro-*cis*-binding

configuration, the angles between the hydrogen in the C**H** bond of the β′-carbon and the ferryl oxygen are relatively strained with respect to criteria (2) and (3) as stated in §2.7, thus hampering such a hydroxylation inside the binding pocket of the enzyme. Most mutants that promoted the generation of this isomer (**2.24b**) disfavoured the generation of the *trans*-isomer **2.24a**. For instance, mutations I263G and E267V increased selectivity for isomer **2.24b** but decreased that for isomer **2.24a** (Entries 2 and 17). With the respective addition of A328L and V78I, selectivity in favour of the *cis*-hydroxylation product (**2.24b**) was even higher (Entries 3 and 18).

Mutations that had substitutions with a Gly residue were shown to promote the selectivity for γ-hydroxylation product **2.24c**, particularly for variants R19/F87A/A328G/A264G and R19/F87A/A328G/P329G/A330G (Entries 9 and 10), perhaps by allowing more flexibility of substrate binding within a more open active site. On the other hand, when introduced on mutant K19/F87V/A264G, the A264G mutation did not lead to an increase in selectivity for metabolite **2.24c** (Entry 16). The substitution to a larger residue such as A184I/A328L also did not encourage γ-oxidation (Entry 5).

β-Hydroxylation product **2.24d** was formed with the second lowest selectivity among the five products identified. Extensive screening had to be performed to find mutants with sufficient selectivity to allow isolation of this product. Variants with base mutations R19 promoted β-oxidation; in particular, mutations A330W, F87A/S72W/A328I, and E267F gave higher selectivity towards **2.24d** (Entries 7, 11 and 14). It has been reported that in base mutation R19 (R47L/Y51F/H171L/Q307H/N319Y), R47 and Y51 facilitate the binding of carboxylate-containing substrates in $P450_{BM3}$, possibly due to hydrogen-bonding with the substrate's carboxylate.[209,210] This could provide a plausible explanation of the increase in enzymatic activity for **2.24d** from R19-based mutants, as well as other metabolites such as **2.24c**.

α-Hydroxylation proceeded with the lowest selectively, with the isolated product (**2.24e**) being formed by reduction of the ring-opened aldehyde form; this was not observed in the 3-spiro analogue (§3.4.1). Most variants gave no α-oxidation and, from the data gathered, it can only be determined that mutations A184I/T260G/A328G seem to promote this pathway.

Entry	Mutant	Conv. (%)	2.24					Other (%)
			a (%)	b (%)	c (%)	d (%)	e (%)	
1	GV/L188Q	98	12	3	56	2	0	27
2	GV/L188Q/ I263G	94	10	37	43	3	0	8
3	GV/L188Q/I263G /A328L	96	9	51	30	4	0	6
4	R19	22	26	0	66	7	1	0
5	R19/A184I/A328L	100	86	0	12	0	0	3
6	R19/I263A/A328L	96	78	0	22	0	0	0
7	R19/A330W	100	31	0	54	14	0	0
8	R19/F87A	100	14	0	46	1	0	39
9	R19/F87A/A328G/ A264G	96	5	0	95	0	0	0
10	R19/F87A/A328G/ P329G/A330G	97	8	3	85	0	0	3
11	R19/F87A/S72W/ A328I	95	44	5	34	10	0	8
12	R19/F87A/A184I/T 260G/A328G	95	8	1	67	1	20	3
13	R19/F87I	100	5	9	21	5	5	55
14	R19/F87I/E267F	100	11	0	8	32	1	48
15	K19/F87V	93	20	7	70	4	0	0
16	K19/F87V/A264G	100	12	0	5	4	0	78
17	K19/F87V/E267V	91	8	12	22	4	0	54
18	K19/F87V/V78I/ E267V	73	33	22	35	10	0	0

Table 2.4 Selected screening data for substrate **2.24**. Full data in Chapter 7.

2.6.4 Screening of *N*-Tfa-protected Spiroamine 2.55

The *N*-Tfa 2-spiro substrate **2.55** was initially screened against 48 variants at a substrate/enzyme ratio of 1000:1; however, it was discovered that this substrate was extremely active towards the panel of mutants and many of the primary products were further oxidised. The screening was then repeated with less enzyme (5000:1) and a shorter

reaction time (5 h) and, as expected, the metabolite profile varied depending on the enzyme ratio and the reaction time. Even so, further oxidation products were already present before the substrate reached full conversion and the major products were secondary oxidation products once full substrate conversion had been achieved. A further 23 more specialised variants were screened, based on mutant R19/F87I, since previous screening results showed that R19/F87I-based variants were the most active towards spiroamines, but no new metabolites were discovered. Overall, six major products were characterised: β′-hydroxylation product **2.55a**, the derived β′-ketone **2.55b**, the α-hydroxylation/reduction product **2.55c** arising from aldehyde intermediate **2.55d**, enone **2.55e**, arising from β-elimination in ketone **2.55b**, and its further oxidised derivative **2.55f**.

The conversion rates of **2.55** were extremely high, with 46 out of 48 variants showing >85% conversion over 24 h. Substitutions at I263 and A328 were found to promote β′-oxidation (Table 2.5, Entries 3, 8 and 12), with the A330W mutation favouring selectivity for the alcohol **2.55a** (Entry 9), enhanced by the addition of S72G (Entry 10). NOE analysis revealed coupling between the *CH*OH and H-1 located at 2.18 ppm, which showed proximity to the C-9 protons, suggesting that the hydroxyl group is *trans*- to the -NBoc group. On the other hand, the majority of variants exhibited relatively low selectivity for metabolite **2.55b**, suggesting that not all mutants were able to form further oxidised products within the given reaction time. Among these variants, mutations V78I/E267V, and F87I showed the most rapid oxidation to **2.55b** from **2.55a** (Entries 6 and 16), in which the selectivities of **2.55b** were 38% and 34%, respectively, but 0% for **2.55a**. In particular, the F87I mutation promoted the rapid elimination of **2.55b** to enone **2.55e**, as reflected by a higher proportion of **2.55e** in mutant R19/F87I (Entry 16).

Substitution of A264 to a smaller residue Gly enhanced the reduction by the reductase domain of $P450_{BM3}$ of α-oxidation product aldehyde **2.55d** generating alcohol **2.55c** (Entries 2 and 5).

Apart from mutation F87I, as mentioned earlier, A328I also promoted enone production, as seen with the R19/F87A/S72W/A328I and R19/F87A/V78I/A328I variants (Entries 14 and 15), whereas further oxidation of enone **2.55e** was promoted by mutation A328L (Entry 13). As a general comparison, among all the base mutants, those that contain an F87 substitution such as GV (A74G/F87V) and K19/F87V displayed higher proportions of both enones **2.55e** and **2.55f**, as opposed to R19 (R47L/Y51F/H171L/Q307H/N319Y), which does not contain an F87 mutation.

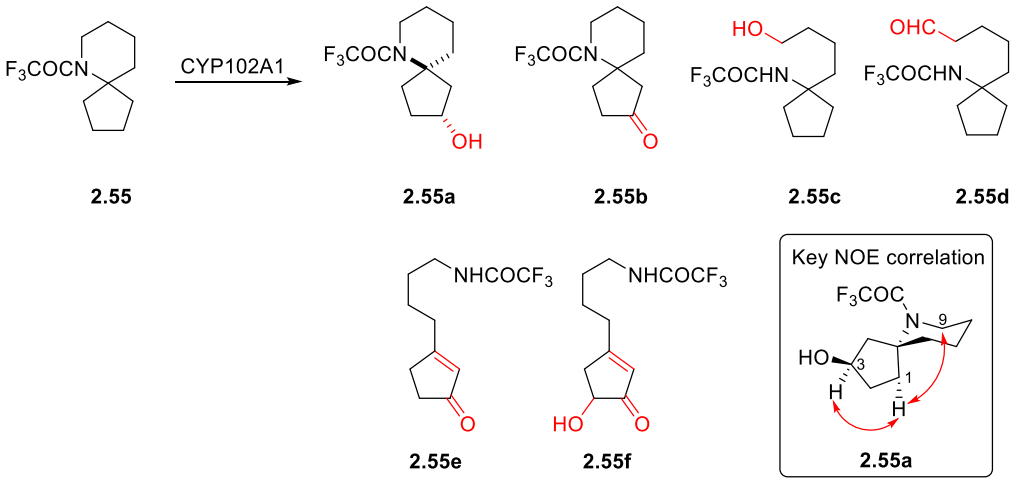

Entry	Mutant	Conv. (%)	2.55 a (%)	b (%)	c (%)	d[a] (%)	e (%)	f (%)	Others (%)
1	GV/L188Q	100	0	5	0	0	10	37	47
2	GV/L188Q/ A264G	100	15	15	13	22	15	1	40
3	GV/L188Q/ I263G/A328L	100	28	26	0	0	13	4	28
4	K19/F87V	100	0	7	0	0	13	47	33
5	K19/F87V/ A264G	100	33	1	10	16	12	1	43
6	K19/F87V/V78I /E267V	100	0	38	0	0	22	10	30
7	R19	61	0	0	0	0	0	0	100
8	R19/I263A/ A328L	100	88	0	0	0	0	0	12
9	R19/A330W	100	72	5	4	6	0	0	19
10	R19/S72G/ A330W	100	81	3	4	5	2	0	10
11	R19/F87A	100	0	0	0	3	4	7	88
12	R19/F87A/ A184I/T260G/ A328G	100	46	13	4	5	13	0	23
13	R19/F87A/ A328L	100	0	8	0	2	22	63	7
14	R19/F87A/ S72W/A328I	100	17	29	6	9	25	4	18
15	R19/F87A/V78I /A328I	100	11	15	3	9	25	11	34
16	R19/F87I	100	0	34	0	0	28	4	35

Table 2.5 Selected screening data for substrate **2.55**; [a] Selectivity for this metabolite was achieved at a substrate/enzyme ratio of 5000:1 and a reaction time of 5 h; Full data in Chapter 7.

To better understand the course of reaction, a time-course experiment was carried out

with mutant VQ/S72G/A330W, as initial screening showed that this mutant produced all the identified metabolites with oxidations at unactivated positions (Figure 2.4).

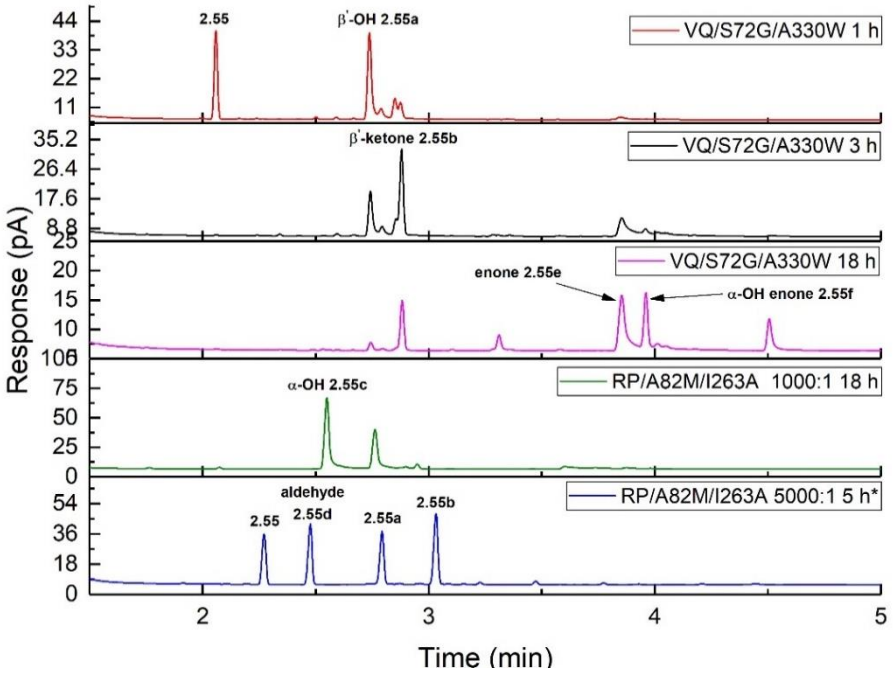

Figure 2.4 GC analysis of the product mixture from the reactions of selected variants with substrate **2.55**; the GC trace for RP/A82M/I263A is shifted due to change of GC column.

It can be seen from Figure 2.4 that at 1 h reaction time (top trace) approximately 50% conversion was already achieved. At 3 h reaction time (second trace), the initially-formed β′-hydroxylation product **2.55a** had become almost fully oxidised to ketone **2.55b**. When the reaction was left for 18 h overall (third trace), this ketone (**2.55b**) underwent elimination to enone **2.55e**, which was then hydroxylated to form **2.55f** as time progressed. With enzyme variant RP/A82M/I263A, at a substrate/enzyme ratio of 1000:1 and the same extended reaction time (fourth trace), the α-hydroxylation/reduction product **2.55c** was isolated; at the higher substrate/enzyme ratio (5000:1, bottom trace) and shorter reaction time (5 h) the intermediate aldehyde **2.55d** persisted in the product profile and the reduced form (**2.55c**) was not produced, suggesting that the primary alcohol arose from the reduction of the aldehyde.

Overall, the majority of oxidation on the *N*-Tfa protected substrate **2.55** took place at the β′- and α-sites. The β′-OH product **2.55a** was prone to oxidation to form ketone **2.55b**, where the strongly electron-withdrawing Tfa group on the *N*-atom further promoted the elimination of **2.55b** to generate enone **2.55e**. Additionally, the Tfa moiety led to instability of the cyclic hemiaminal form of the α-hydroxylated product, hence the ring-opened metabolite **2.55d** was produced. With an increased concentration of enzyme and longer reaction times, the ring-opened aldehyde **2.55d** was reduced to primary alcohol **2.55c** by the reductase domain in $P450_{BM3}$, where this type of chemistry was commonly observed in similar substrates.

2.7 Computational Docking Studies on Substrates 2.24 and 2.55

Using docking methodology developed within the group,[211] MD simulations were performed on the variants that hydroxylated unactivated positions in substrates **2.24** and **2.55**. MD simulations were conducted for three to four replicas for each mutant, after which each replica consisted of 10,000 simulated structures. Each replica was further grouped into three clusters per replica based on similarity of the structures. The docking process employed the rigid docking approach, where the bond angles, bond lengths, and torsion angles at each amino acid residue are not modified at any stage of the docking round, i.e. only one amino acid conformer is present in each cluster. In AutoDock Vina, the substrate was then docked into each cluster, and the nine lowest energy poses were presented. Each pose was analysed and assigned as "productive" or "non-productive". The criteria for designating a productive pose are: (1) the distance between the ferryl oxygen and the closest carbon must be 3.5–4.2 Å; (2) the Fe-O-H angle must be within 95–165°; (3) the (Fe)O-H-C angle must be within 100–180°. The pose was deemed non-productive if it did not satisfy any of the above criteria. Note that the docking process of all substrates and affinity energies of different poses discussed herein only considered the

starting substrate, i.e. further oxidised products were not submitted for docking, hence only mono-hydroxylations were predicted and calculated for affinity energies.

The *trans*-diasteromer **2.24a** of β′-hydroxylation was isolated from mutant KT2/L188G/I263G; therefore, four replicas were generated for this variant, giving rise to 12 clusters and 108 poses. Among the 108 poses, 14 were productive (Figure 2.5). Although the most-populated productive poses represented β′-hydroxylation, the numbers of *cis*- and *trans*- β′- poses were equal so this analysis did not suggest that the major diastereomer would arise from hydroxylation *trans*- to the amine functionality. Moreover, the computational selectivity for **2.24a** was 29%, which was inconsistent with the experimental selectivity of 66% (Table 2.2).

On the other hand, the *cis*-diastereomer **2.24b** arising from β′-hydroxylation was isolated from the reaction with mutant GL/L188Q/I263G/A328G. There were 50 productive poses among the 81 poses generated (3 clusters, 3 replicas/cluster, 9 poses/cluster) (Figure 2.6). Similar to variant KT2/L188G/I263G, the most populated poses again corresponded to β′-hydroxylation, then β-oxidation, although this was not observed experimentally; however, only two poses corresponded to production of the *cis*-diastereomer, as opposed to 23 corresponding to production of the *trans*-diastereomer. Additionally, the computational selectivity for the *cis*-diastereomer **2.24b** (4%) was not consistent with the experimental results (14%) (Table 2.2).

Mutant R19/F87I/L437LV produced the γ-hydroxylation product **2.24c**. Among the 81 poses computed (3 replicas, 3 clusters/replica, 9 poses/replica), only 15 were productive (Figure 2.7) in which four corresponded to γ-oxidation. The majority of poses were non-productive, and the most likely hydroxylation site was predicted to be at β′-, not γ-. The experimental selectivity for compound **2.24c** was 56% (Table 2.2), approximately twice that (27%) calculated by the docking output.

Finally, β-hydroxylation was also observed in the Boc-protected spirocycle, forming metabolite **2.24d** from the reaction with variant R19/F87I/E267F. Computationally, oxidation at all methylene sites around the spirocycle was predicted and 55 productive poses were identified. The most populated poses represented β′-oxidation (20/55) (Figure 2.8), with the second most populated poses (17/55) consistent with β-oxidation. The computational selectivity for metabolite **2.24d**, was comparable to that observed experimentally: 31% and 32%, respectively (Table 2.2).

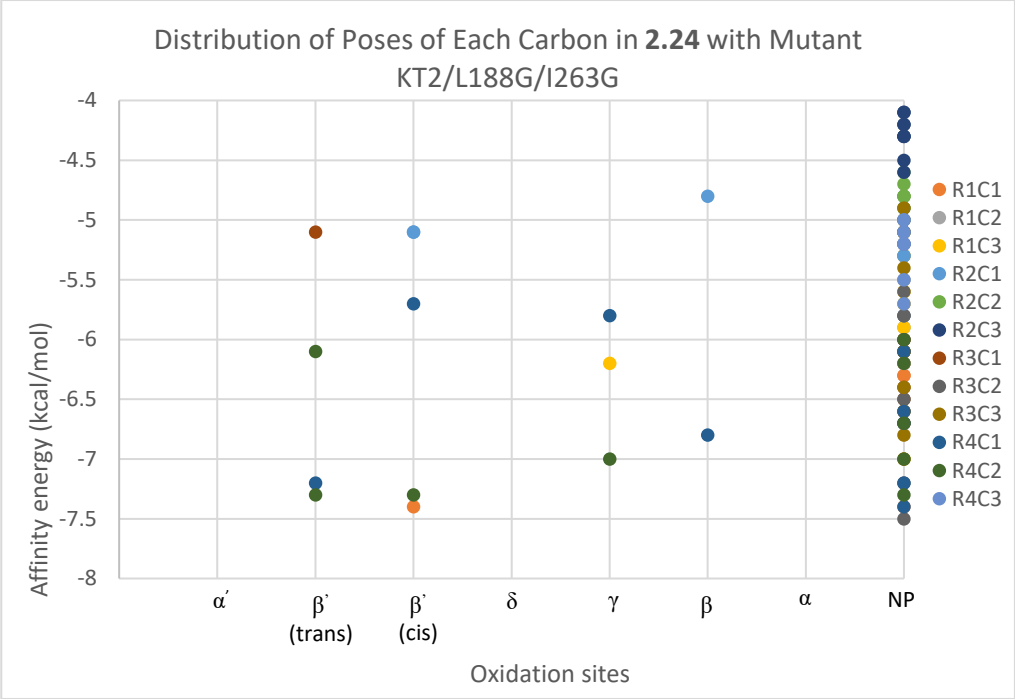

Figure 2.5 Distribution of poses, and calculated affinity energies, for oxidation at each carbon in *N*-Boc substrate **2.24** with mutant KT2/L188G/I263G; (trans) and (cis) refer to the relative disposition of the new hydroxyl group and the C−Nboc bond; NP = non-productive.

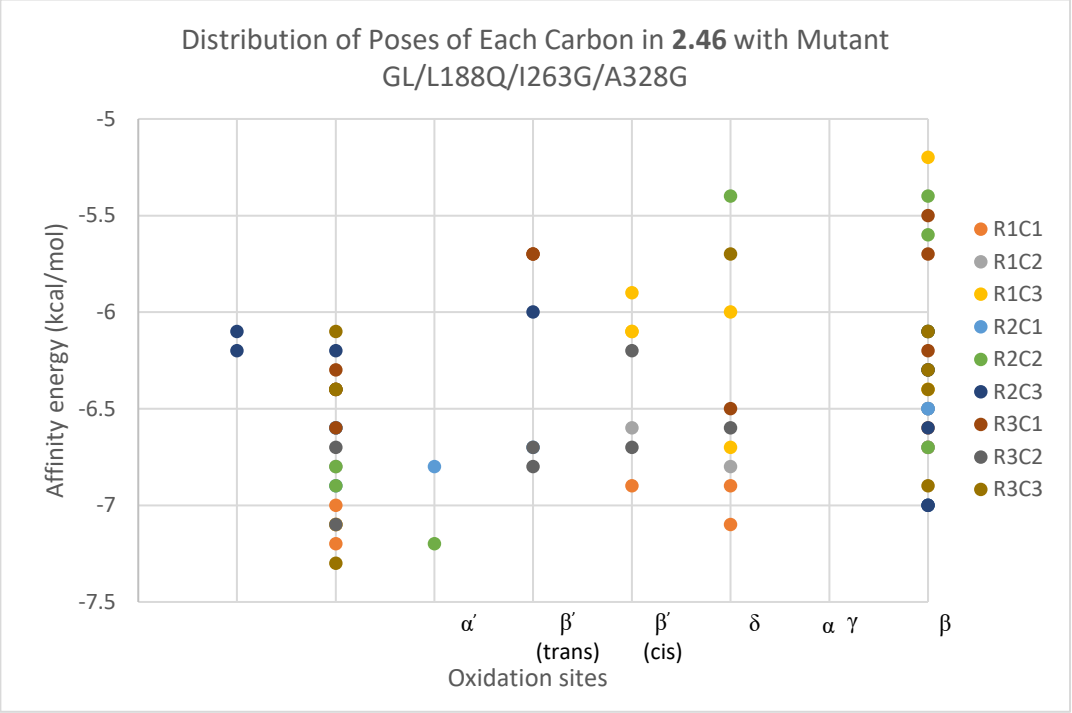

Figure 2.6 Distribution of poses, and calculated affinity energies, for oxidation at each carbon in *N*-Boc substrate **2.24** with mutant GL/L188Q/I263G/A328G.

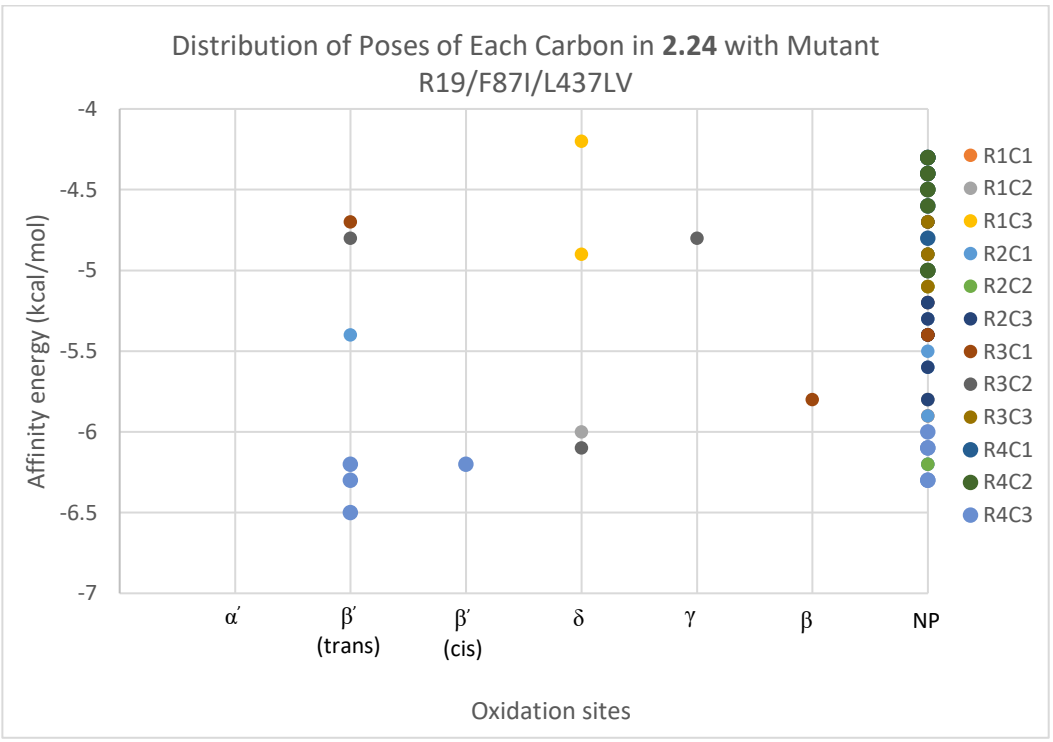

Figure 2.7 Distribution of poses, and calculated affinity energies, for oxidation at each carbon in *N*-Boc substrate **2.24** with mutant R19/F87I/L437LV.

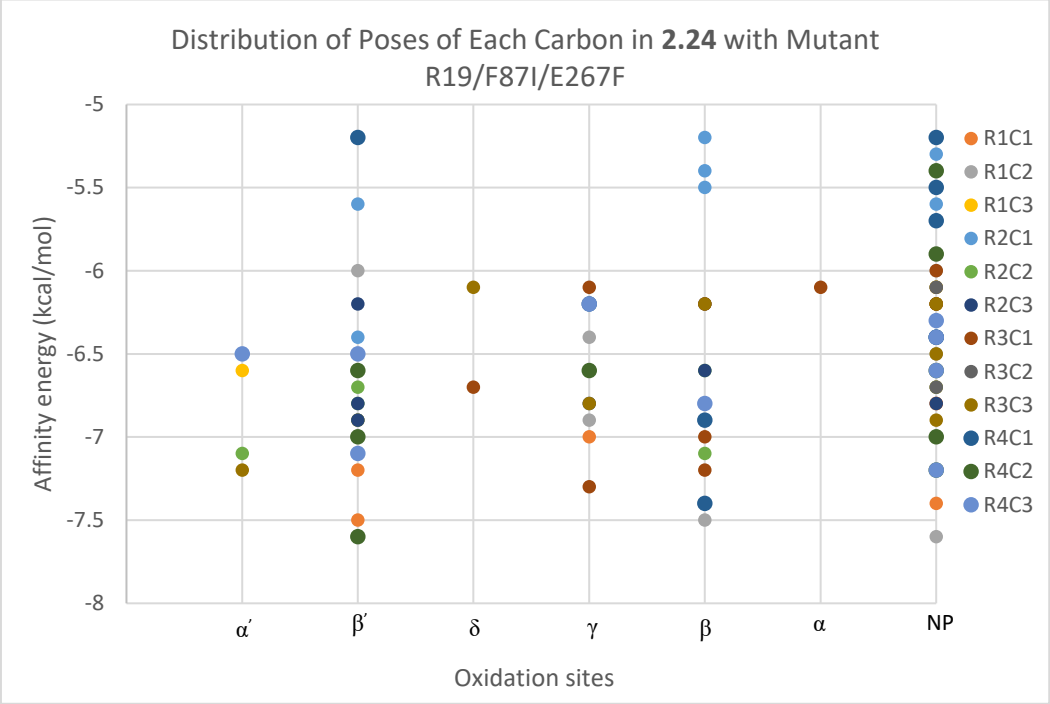

Figure 2.8 Distribution of poses, and calculated affinity energies, for oxidation at each carbon in *N*-Boc substrate **2.24** with mutant R19/F87I/E267F.

Regarding the *N*-Tfa-protected substrate **2.55**, only one metabolite with hydroxylation at an unactivated position was identified, which was β′-alcohol **2.55a**; however, the proportions of further oxidation products **2.55b**, **2.55e**, and **2.55f** should also contribute towards the selectivity of alcohol **2.55a**, since they also arise from the same precursor.

Experimentally, the selectivity for alcohol **2.55a** was the highest in mutant A330P (98%) (Table 2.2). Computationally, there were only eight productive poses among 81 poses generated (Figure 2.9) within which the dominant product was predicted to be β′-hydroxylated, with 63% selectivity, followed by β-hydroxylation.

The least selective variant for alcohol **2.55a** was GV/L188Q/A264G (30%) (Table 2.2); however, the predicted selectivity was computed to be 44%. Nonetheless, there were significantly more productive poses than A330P, with 54 out of 81 poses (Figure 2.10). The most populated poses with this variant also represented β′-oxidation, particularly

trans- to the C−Ntfa group, predicting this to be the major stereoisomer, consistent with experimental results.

Mutant R19/F87A/T260G gave the highest proportion of productive poses, with 72 out of 81 poses (Figure 2.11). The most populated poses corresponded to β-oxidation, comprising 16 poses among all productive poses, but this was not observed experimentally. A similar number (15) of poses corresponded to β′-oxidation, with poses consistent with oxidation *trans*- to the C−Ntfa group dominating once more. There was a significant discrepancy between the computational and experimental selectivity – 21% and 68%, respectively.

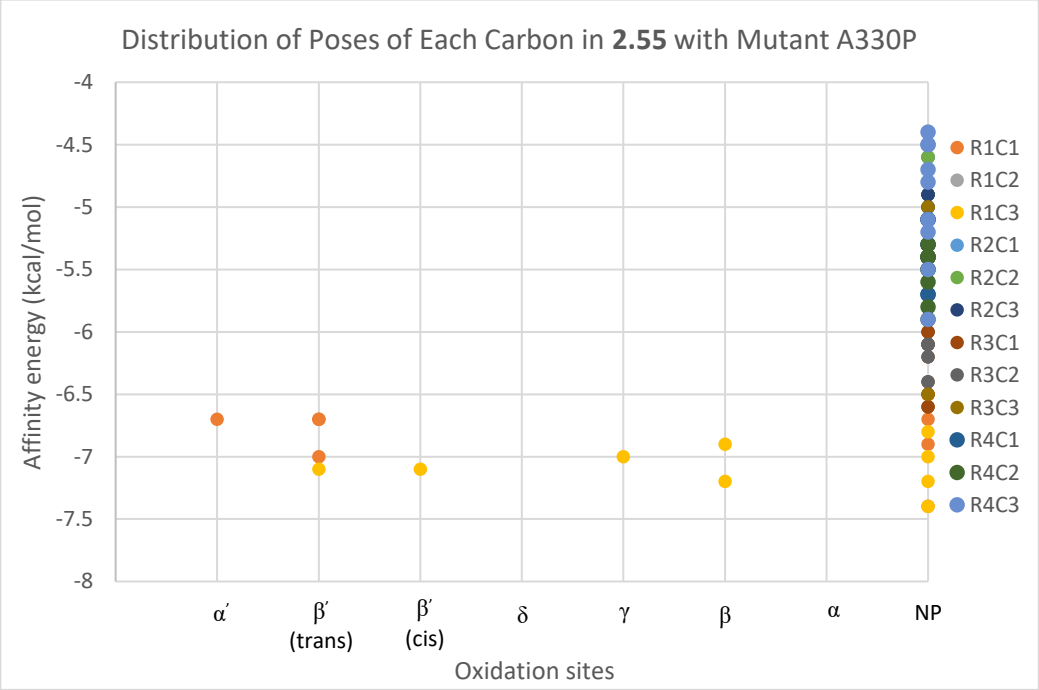

Figure 2.9 Distribution of poses, and calculated affinity energies, for oxidation at each carbon in *N*-Boc substrate **2.55** with mutant A330P.

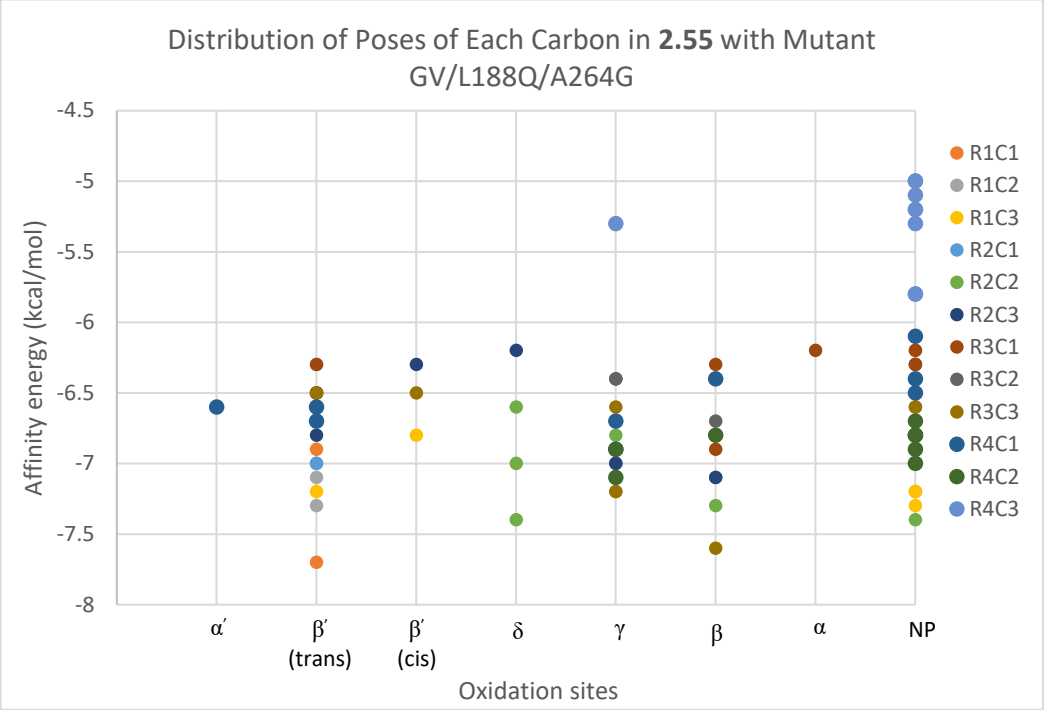

Figure 2.10 Distribution of poses, and calculated affinity energies, for oxidation at each carbon in *N*-Boc substrate **2.55** with mutant GV/L188Q/A264G.

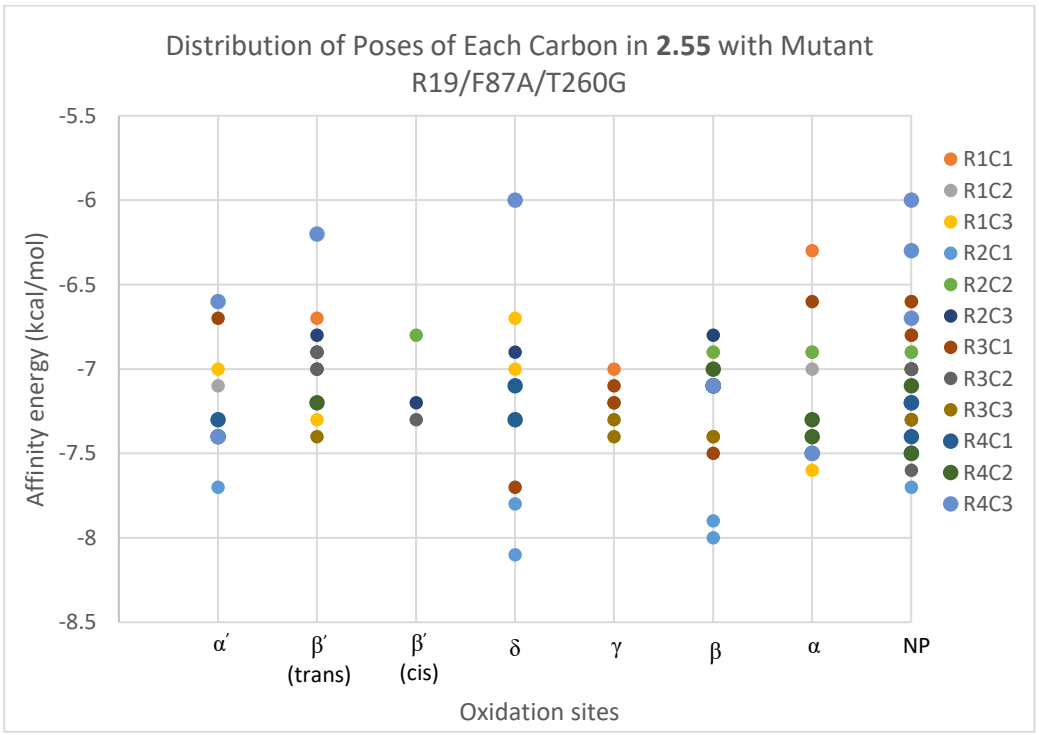

Figure 2.11 Distribution of poses, and calculated affinity energies, for oxidation at each carbon in *N*-Boc substrate **2.55** with mutant R19/F87A/T260G.

As a visual aid, all the productive poses corresponding to metabolites that were hydroxylated at unactivated positions (**2.24a**–**2.24d**, **2.55a** and, by implication, those

deriving from this primary product) were overlaid and are shown in Figures 2.12a–g. It can be seen that both the Boc and Tfa substrates are relatively flexible in the binding pocket, within which their bound orientations varied drastically, particularly in variants KT2/L188G/I263G, R19/F87I/L437LV, and R19/F87A/T260G (Figures 2.12 a, c and g). Stabilisation by hydrogen-bonding (2.0−2.5 Å) was only observed in mutant GL/L188Q/I263G/A328G with the Boc- substrate (black dashed lines, Figure 2.12b), between the Ser72 hydroxyl group and the C=O and C−O components in the Boc- group. Besides H-bonding, the remaining poses were stabilised by van der Waals forces from vicinal residues around the substrate (in yellow). All the key residues identified were similar for both substrates **2.24** and **2.55** despite the different protecting groups. In these models, van der Waals contact mainly originates from hydrophobic residues in the active site, such as F/I/V87, I263, A264, and L437. It should also be noted that the substrate access channel of $P450_{BM3}$ consists largely of hydrophobic residues,[212,213] with only a few residues, such as S72, bearing side chains capable of H-bonding.

In summary, the overlaid poses suggest a large degree of conformational flexibility to be present within the active site. Practically, the observed selectivity would be refined by the presence of active site water molecules, other small molecules such as the substrate, and subtleties in the Fe=O···H−C(substrate) distances and angles leading to variations in reaction rates from different poses, which are not easily reflected at this level of analysis. The bond dissociation energy of the C−H bonds being hydroxylated will also likely have a profound influence on the rate of every hydroxylation process. A deeper understanding of the interactions between poses and the residues within the active site may come from a machine learning approach; however, one must have a clear grasp of the parameters to be considered in order for sensible correlations to be made.

(a)

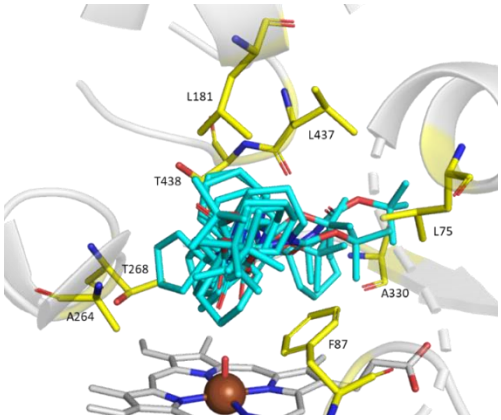
L181
L437
T438
L75
T268
A330
A264
F87

(b)

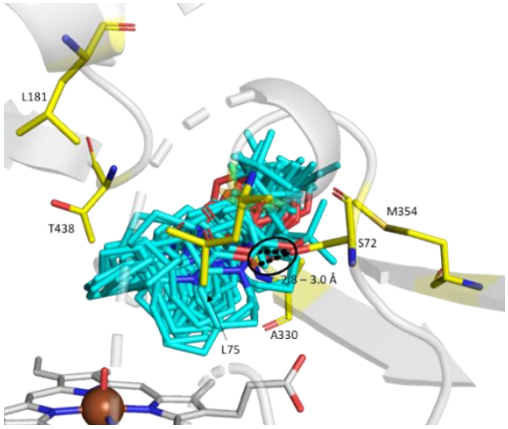
L181
T438
M354
S72
2.8 – 3.0 Å
A330
L75

(c)

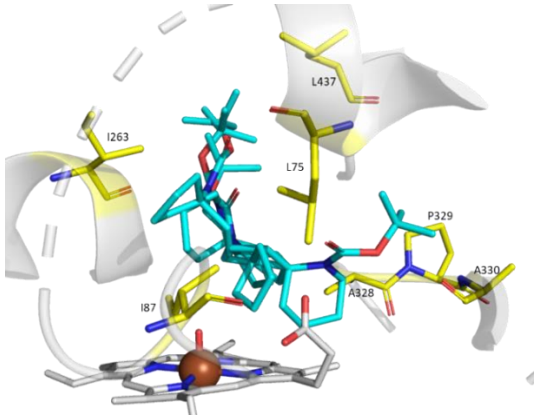
L437
I263
L75
P329
A330
A328
I87

(d)

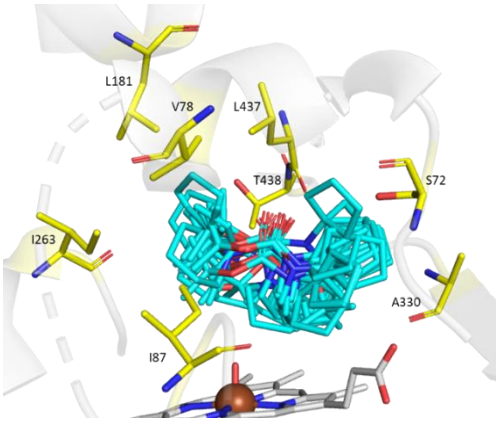
L181
V78
L437
T438
S72
I263
A330
I87

(e)

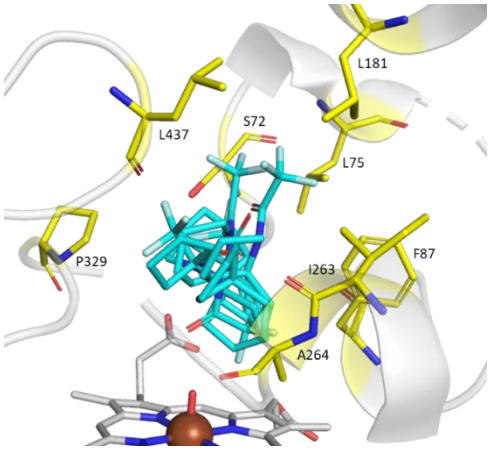
L181
L437
S72
L75
P329
F87
I263
A264

(f)

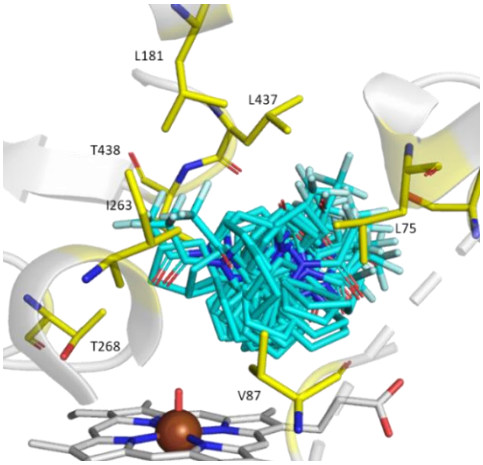
L181
L437
T438
I263
L75
T268
V87

(g)

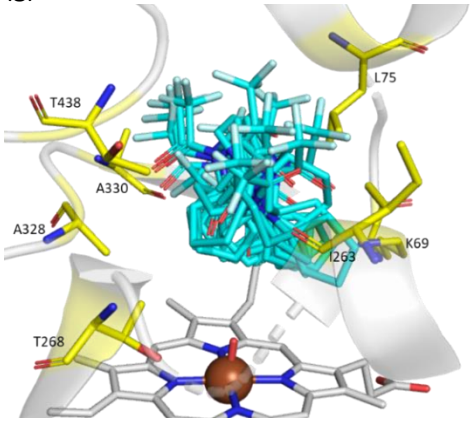
L75
T438
A330
A328
I263
K69
T268

Figure 2.12 (a) Overlay of all 14 β′-oxidation poses from 12 clusters of variant KT2/L188G/I263G with substrate **2.24**; (b) overlay of all 50 β′-oxidation poses from nine clusters of variant GL/L188Q/I263G/A328G with substrate **2.24**; (c) overlay of all 15 γ-oxidation poses from 12 clusters of variant R19/F87I/L437LV with substrate **2.24**; (d) overlay of all 55 β-oxidation poses from 12 clusters of variant R19/F87I/E267F with substrate **2.24** (e) overlay of all 8 β′-oxidation poses from 12 clusters of variant A330P with substrate **2.55**; (f) overlay of all 54 β′-oxidation poses from 12 clusters of variant GV/L188Q/A264G with substrate **2.55**; (g) overlay of all 72 β′-oxidation poses from 12 clusters of variant R19/F87A/T260G with substrate **2.55**. Key contact residues are shown in yellow, hydrogen bonding in (b) is indicated by black dashed lines.

The predicted selectivity for each metabolite was calculated based on this docking process but numerous factors influence the prediction. Overall, the results are primarily useful as a guiding tool and to provide insights into potentially important substrate-enzyme interactions; additionally, these studies advanced our understanding of the differences between the experimental and the computational outcomes so that improved algorithms can be developed. Additional parameters that can be taken into account when interpreting computational results will be further discussed in Chapter 5. It was deemed important that the dominant products predicted by docking were qualitatively comparable to those suggested by the screening data.

2.8 Conclusion and Future Work on the 2-Spiroamine Series

Four 2-spiro substrates **2.24**, **2.37**, **2.45** and **2.55** were screened against 46−71 $P450_{BM3}$ variants. Hydroxylations at the unactivated β-, γ-, β′-, and activated α-positions were observed in the Boc and Tfa derivatives, but oxidations at the δ and α′- positions were not observed in these 2-spiroamines. Further screening with other PGs was considered essential in order to provide access to the aforementioned oxidation positions. Nonetheless, screening results have proven that differently protected substrates can appear as vastly altered molecules to the same panel of enzymes. This suggests that a greater variety of products and selectivity patterns can potentially be attained without the need of a massive screen.

The likelihood of hydroxylation at each methylene position around the *N*-Boc- and *N*-Tfa-protected spirocyclic amines is summarised in Figure 2.13. As the pie charts show, the majority of oxidation sites belong to further oxidation products, in which the 2-Tfa substrate contributed a substantial portion since it led to products of secondary processes that were not seen with other PGs. Next, are the γ- and β′-hydroxylation products. The Boc-protected substrate was the only one from which both β′-OH diastereomers were observed; this feature could be investigated further in order to optimise the diastereoselectivity and enantioselectivity of this metabolite.

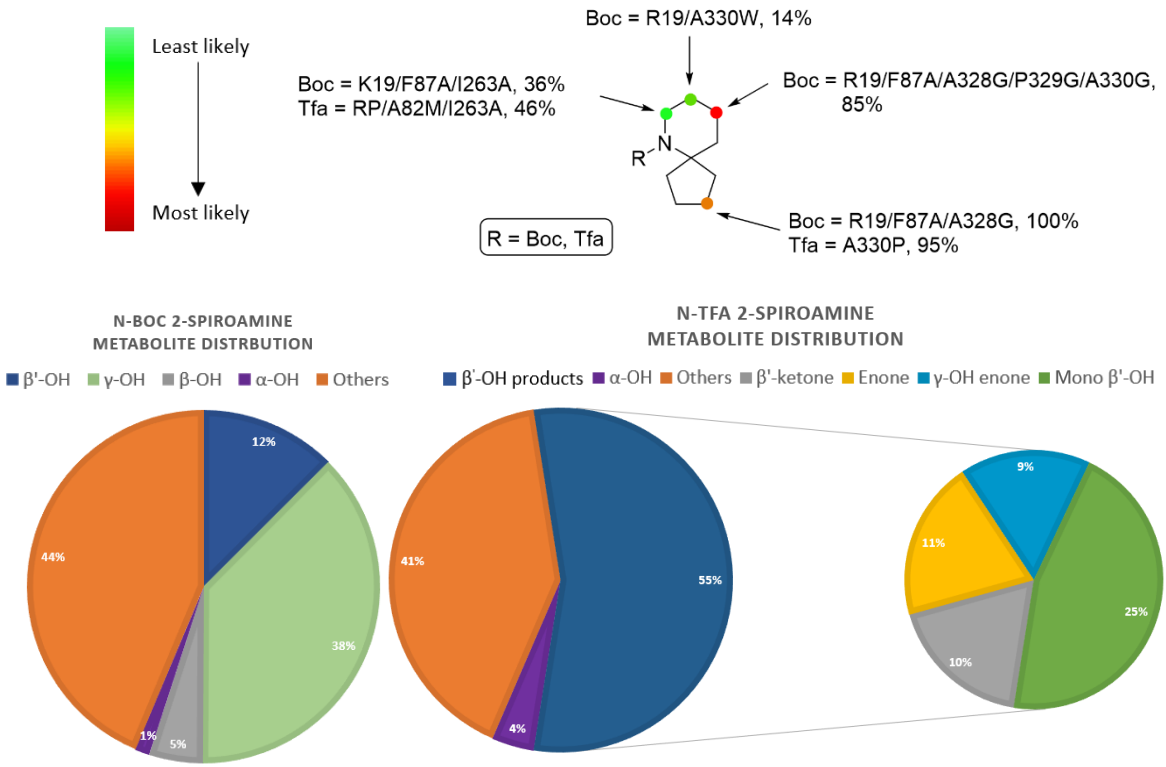

Figure 2.13 Summary of the distribution of hydroxylations at various positions in the 2-spiro series and the respective mutant with the highest selectivity.

The activity of the Tfa-bearing substrate **2.55** suggests that it may have value in large-scale reactions, where relatively shorter reaction times and lower enzyme concentrations are desirable; however, it also suffers from the production of secondary products whose occurrence would have to be controlled by further optimising the reaction conditions. Currently, the Boc- protecting group is considered more useful as it confers a lower

tendency towards further oxidation and elimination, and because it leads to a greater diversity of mono-hydroxylation products.

The docking results are summarised in Table 2.6. The selectivity acquired through experimental and computational means differed significantly for most metabolites in the 2-spiro series; however, as mentioned earlier, there are many factors that were not considered when predicting the selectivity computationally and future work will aim to account for some of these.

Metabolite / mutant	**Experimental select. (%)**	**Docking select. (%)**
2.24a / KT2/L188G/I263G	66	29
2.24b / GL/L188Q/I263G/A328G	15	4
2.24c / R19/F87I/L437LV	56	27
2.24d / R19/F87I/E267F	31	32
2.55a / A330P	98 (3% from **2.55b**)	63
2.55a / R19/F87A/T260G	30 (15% from **2.55b**)	44
2.55a / GV/L188Q/A264G	68 (8% from **2.55b**)	21

Table 2.6 Experimental and docking selectivity for metabolites from the 2-spiro series.

Turning to the major products predicted by docking (Table 2.7), most of the experimental and computational data were in agreement. Other docking methods, such as AutoDock for Flexible Receptors (ADFR), could be employed in order to investigate whether the discrepancy can be narrowed.

PG (substrate)	Mutant	Experimental dominant product	Docking dominant product
Boc (**2.46**)	KT2/L188G/I263G	*trans*- β′-OH	*cis*- and *trans*- β′-OH
	GL/L188Q/I263G/A328G	*cis*-β′-OH	*trans*- β′-OH
	R19/F87I/L437LV	γ-OH	β′-OH
	R19/F87I/E267F	β-OH	β′-OH
Tfa (**2.55**)	A330P	β′-OH	β′-OH
	GV/L188Q/A264G	β′-OH	β′-OH
	R19/F87I/E267F	β′-OH	β′-OH

Table 2.7 Dominant product experimentally and computationally from substrates **2.24** and **2.55**.

As discussed earlier, improvements in the algorithm for the prediction of hydroxylation sites can be developed in order to narrow the gap between experimental and computational results. There are numerous variables that could be considered, such as water molecules surrounding the MD simulated structures; however, these variables cannot be easily computed nor estimated due to the dynamic environment within the enzyme-ligand complex. In conclusion, a balance has to be achieved between the level of accuracy of the results and the practicality of the computational time and resources that are required.

Chapter 3: *N*-protected 7-azaspiro[4.5]decane (3-spiro) analogue

3.1 Overview

This chapter discusses the syntheses of the 3-spiro analogues and their reactivity towards oxidation by the panel of $P450_{BM3}$ variants. MD simulations and docking studies, performed to provide insights on substrate binding, are also discussed.

3.2 Retrosynthesis

An initial route had been explored by a previous rotation student, Cook,[187] in which the spirocyclic centre was to be installed by the alkylation of aldehyde **3.3** with acrylonitrile, itself obtained from a Grignard reaction of **3.4** (Scheme 3.1). Cyclisation would then be achieved by reductive amination of **3.2** to furnish spiroamine **3.1**.

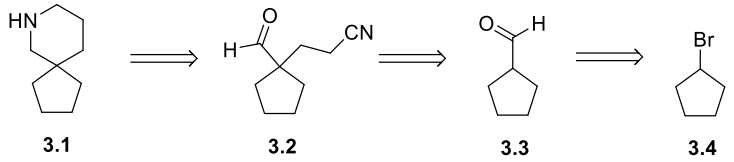

Scheme 3.1 Initially planned route towards 7-azaspiro[4.5]decane **3.1**.

In practice, this route (Scheme 3.2) was found to be extremely inefficient. The volatility of aldehyde **3.3** and the polymerisation of acrylonitrile contributed to the poor yield of cyanoaldehyde **3.2**. The formation *in situ* of a cobalt boride complex during the subsequent reductive amination step led to the trapping by the reagent of a large proportion of the free amine product **3.1**, which ultimately rendered a disappointing overall yield of 0.1% of the *N*-Ms protected amine **3.5**.

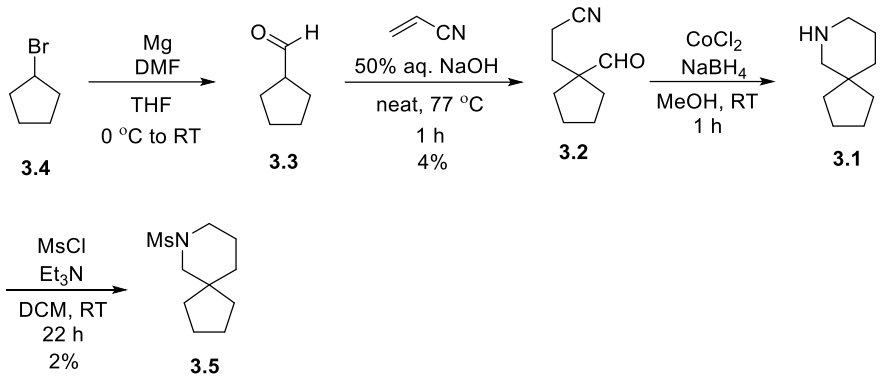

Scheme 3.2 Previous attempt to prepare a 7-azaspiro[4.5]decane substrate.

In this project, a route similar to that used for the 2-spiro analogue was designed (Scheme 3.3) that started with enolate alkylation of methyl ester **2.4** with dihalide **3.0**. The alkylated cyclic ester was then to be converted into amide **3.7** which was envisaged to cyclise to form lactam **3.6** and then amine **3.1**.

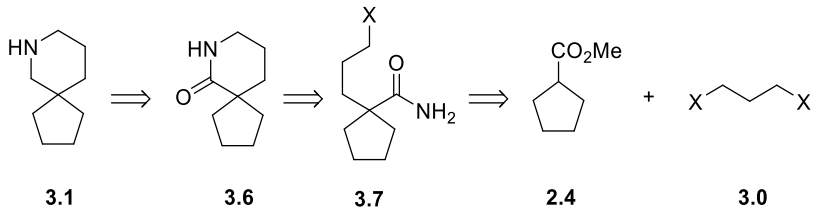

Scheme 3.3 A modified route towards 7-azaspiro[4.5]decane **3.1**.

With **3.1** in hand, various PGs would be installed on the *N*-atom. The aim was, as with the 2-spiro isomer described in the previous chapter, to build a detailed profile of the hydroxylated compounds by varying PGs, and identifying $P450_{BM3}$ mutants facilitating high conversion and selectivity during the enzymatic oxidation of these *N*-protected 3-spiro analogues.

3.3 Synthesis of *N*-protected 7-azaspiro[4.5]decane

The first two steps of the synthesis were identical to those of the 2-spiro analogue, and furnished ester **3.8** efficiently (Scheme 3.4).[184,185] The conversion of the ester moiety to

the corresponding amide, and its subsequent cyclisation to lactam **3.6**, was explored, expecting that the aminolysis could be carried out with aq. NH_3.[214]

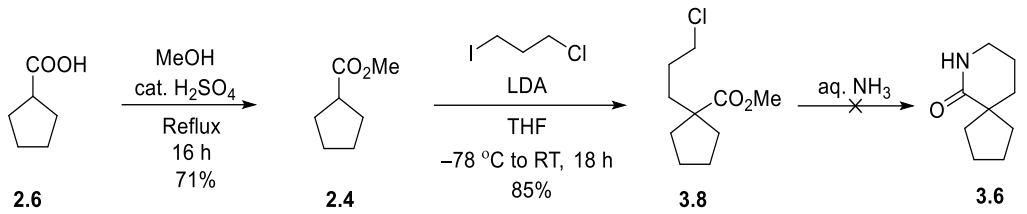

Scheme 3.4 Synthesis of alkylated ester **3.8** and the envisaged conversion to lactam **3.6**.

Various conditions for this reaction were explored based on literature procedures (Table 3.1),[185] and all attempts showed partial or no cyclisation at all. Initially, it was thought that the poor solubility of ester **3.8** in aq. NH_3 limited the reactivity of the substrate; however, more vigorous stirring along with longer reaction times did not improve the percentage conversion to the cyclised product.

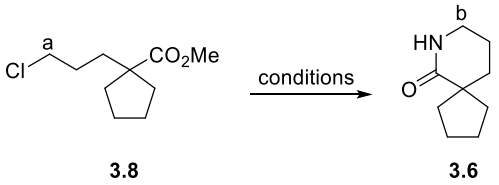

Entry	Conditions	Results (% of cyclisation product **3.6**)
1	2 d, 50 °C, aq. NH_3 (121 equiv.)	55%
2	3 d, 50 °C, aq. NH_3 (121 equiv.)	27%
3	4 d, 50 °C, aq. NH_3 (121 equiv.)	6%
4	6 d, 60 °C, 0.5 M aq. NH_3 in THF (6 equiv.)	None

Table 3.1 Aminolysis reaction to **3.6**.

As depicted in the stacked ^{1}H NMR spectra (Figure 3.1), spirolactam **3.6** can be distinguished by the distinct triplet of doublets (blue box) at 3.31 ppm, representing the CH_2NH on C_b. By comparing the integration of this resonance to that for the CH_2Cl on C_a at approximately 3.5 ppm, the percentage conversion to **3.6** was found to peak and then decrease as the reaction time was extended. In addition, adding THF to aid the

substrate solubility (Table 3.1, Entry 4) failed to promote the nucleophilic addition and no conversion was observed. The unsuccessful attempts of this reaction suggested that the product might be unstable to the reaction conditions, presumably eventually hydrolysing with the extended reaction time and being lost in the work-up procedure. Test reactions with methyl 4-bromobenzoate as a model substrate (see Experimental) proved successful in the amide synthesis with no starting material remaining, further suggesting the instability of **3.6** under the same reaction conditions. Alternative approaches to this reaction could be *via* the acyl chloride form of **3.8**. which is more reactive than its ester,[215,216] or through ester hydrolysis, and a subsequent peptide coupling.[217]

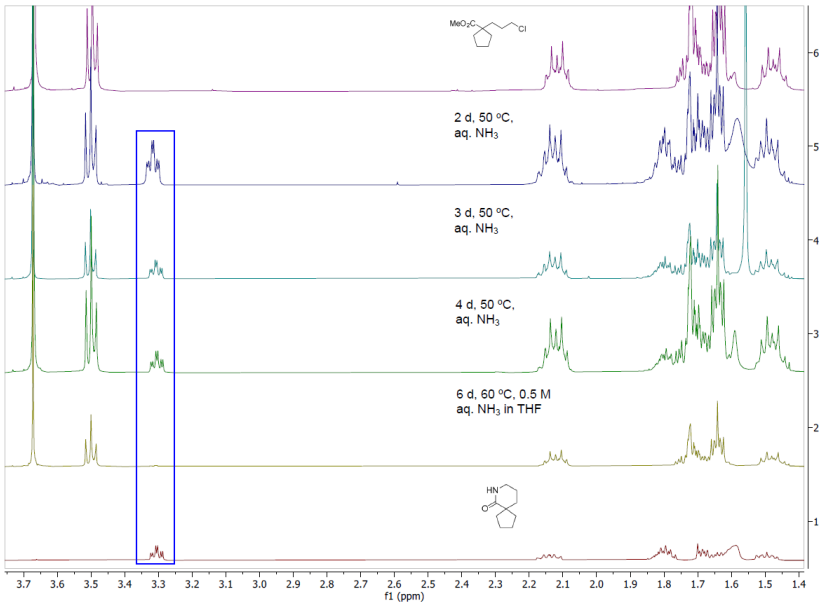

Figure 3.1 Comparison of ^{1}H NMR spectra from various conditions of the conversion of **3.8** to **3.6**.

Instead, the chloroalkyl ester was converted into azide **3.9** (Scheme 3.5)[218] which was reduced and cyclised *in situ* to form lactam **3.6** using the $NaBH_4/CuSO_4$ system reported by Göksu *et al.*[219]

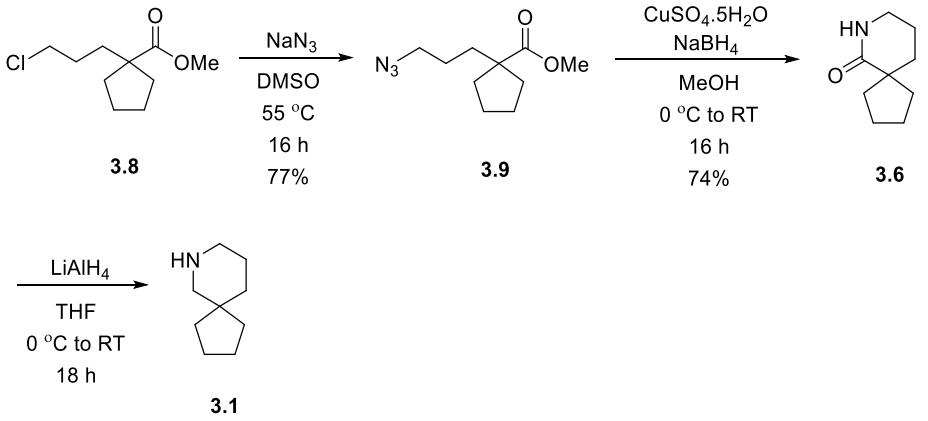

Scheme 3.5 Synthesis of spiroamine **3.1**.

A conventional Staudinger reaction (triphenylphosphine then iminophosphorane hydrolysis)[218,220] was considered for this reduction/cyclisation but the $NaBH_4/CuSO_4$ method has the advantage that no further purification was needed. Using 5 mol% of $CuSO_4$ with a large excess of $NaBH_4$ in methanol as the solvent, the azide reduction was reproducible and efficient. The mechanistic details of this process are not well understood; however, $NaBH_4$ is incapable of reducing azides to amines under normal conditions but its reducing power can be enhanced by added transition metal salts.[221,222] In such reactions, metal borides are proposed as the active reducing agent, mimicking catalytic hydrogenation.[223,224,225] On this basis, a speculated radical-mediated mechanism is proposed (Scheme 3.6).

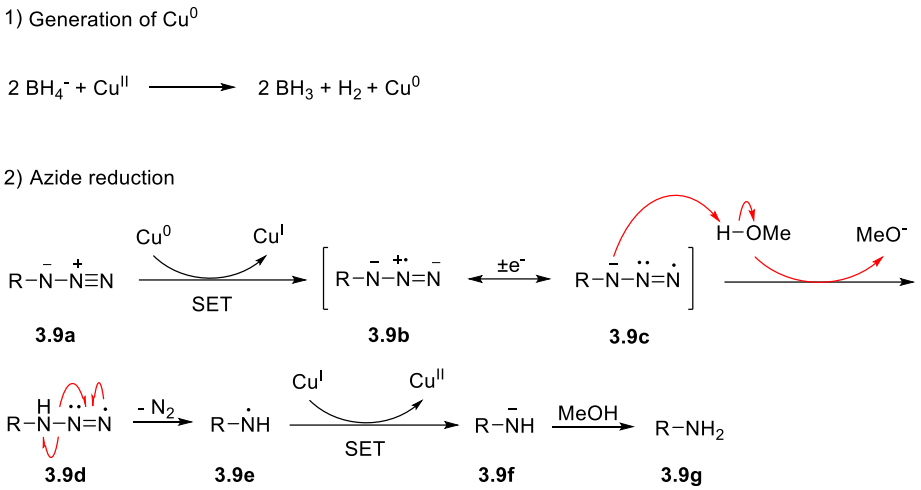

Scheme 3.6 Proposed mechanism of Cu(II)-catalysed azide reduction.

Some support for this mechanism, related to the Sandmeyer reaction,[226] comes from the production of H_2 gas, apparent since vigorous bubbling was observed shortly after the addition of $NaBH_4$ into the $CuSO_4$ solution. Alternatively, the H_2 produced in step 1 may be responsible for the azide reduction.

In practice, this route was relatively efficient since most steps proceeded without purification, and could be performed on gram scale. Lactam **3.6** was therefore synthesised on large-scale, and was reduced to amine **3.1** by $LiAlH_4$ as needed.[187] Due to its volatility, the amine product was immediately protected to furnish derivatives **3.5**, and **3.10**–**3.12** (Scheme 3.7). These four *N*-protected 3-spiro analogues were screened for reactivity against a panel of $P450_{BM3}$ mutants. Since preliminary work in the Wong group at the time showed that lactams can offer complementary reactivity to amines, benzylated lactam **3.13** was also screened with the $P450_{BM3}$ panel.

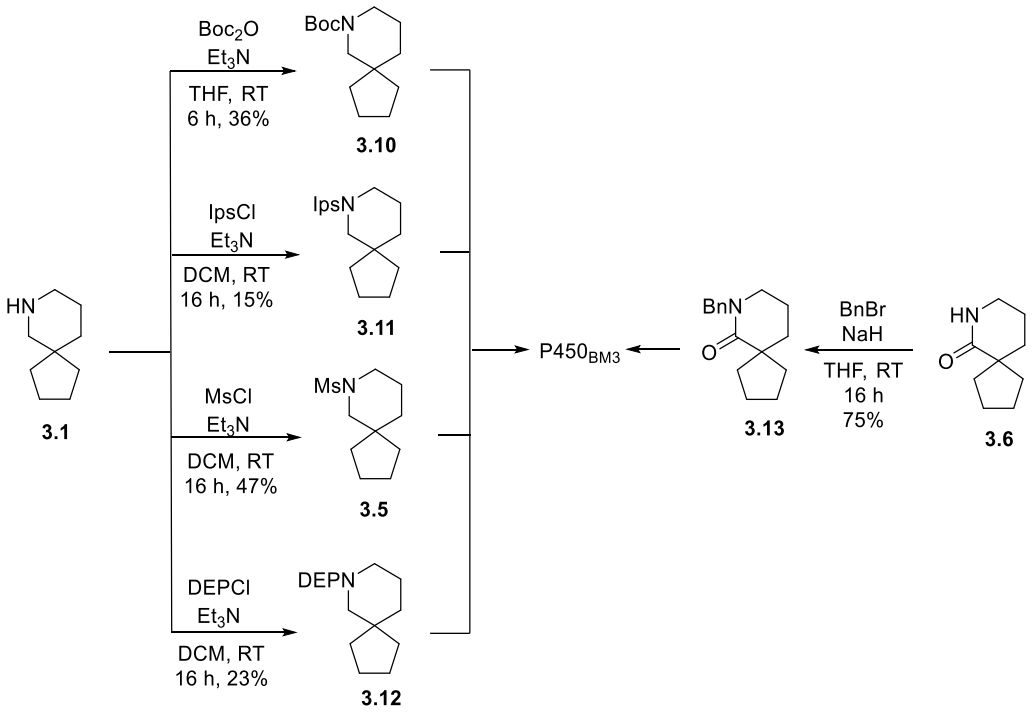

Scheme 3.7 Protection of spiroamine **3.1** and spirolactam **3.6**.

3.4 Screening of *N*-protected 7-azaspiro[4.5]decane with P450$_{BM3}$

The five substrates, namely **3.5**, and **3.10**–**3.13** were screened initially with a panel of 24–48 P450$_{BM3}$ variants that had previously shown varied metabolite profiles, as well as high selectivity towards diverse classes of substrates, including steroids and amines.[208,171] For the 3-spiroamine substrates, screening was conducted at a substrate/enzyme ratio of 2000:1, and on a varying standard timescale which will be discussed for each substrate. At the outset, it was intended that where the conversion and/or selectivity of the metabolites were deemed unsatisfactory, further screening would be carried out with mutants that are more substrate-specific, and mutagenesis studies would follow. A summary of all the major metabolites identified is presented in Table 3.2 and the full screening data can be found in Chapter 6. The basis of metabolite selection for full characterisation was summarised in §2.6. A discussion of the screening of each substrate follows the Table and the full screening data are presented in Chapter 8 (Appendix).

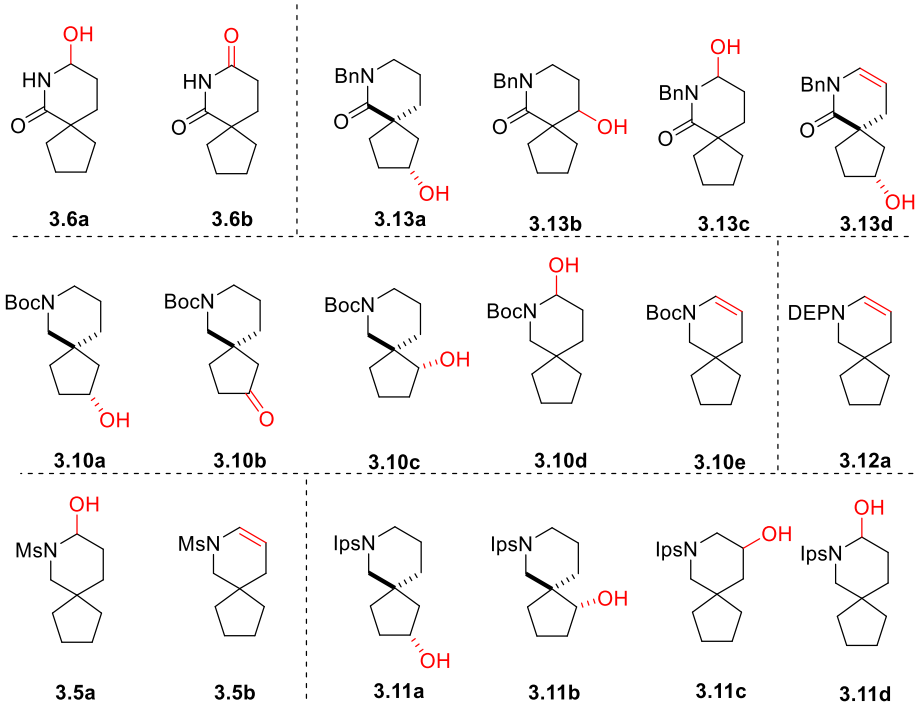

Substrate Type	PG	Mutant	Conv. (%)	Prod.[a]	Select. (%)	e.e. (%)	Yield[g] (%)
Lactam	**None (3.6)**	R19/F87A/ A184I	94	**3.6a**	75	-	47
				3.6b	25	-	10
	Bn- (3.13)	R19/F87I	91	**3.13a**	54	55[b]	31
				3.13d	11	-	6
		R19/F87A/ A184I	100	**3.13b**	1	47[b,f]	0.3
		RT2	70	**3.13c**	59	-	13
Amine	**Boc- (3.10)**	R19/F87I	98	**3.10a**	43	40[c]	11
				3.10b	5	37[c]	3
		RT2	92	**3.10c**	22	11[c]	15
				3.10a	45[e]	28[b]	-
		K19/F87A/ I263A	93	**3.10d**	56	-	23[d]
				3.10e	6	-	
	DEP- (3.12)	R19/F87A/ I263G	94	**3.12a**	31	-	29
	Ms- (3.5)	GV/L188Q	96	**3.5a**	56	-	28[d]
				3.5b	6	-	
	Ips- (3.11)	R19/F87I	86	**3.11a**	58	8[b]	47
				3.11c	13	6[b]	10
		GV/L188Q	61	**3.11b**	5	47[b]	1
				3.11c	3	-	-
				3.11d	61	-	34

Table 3.2 Summary of all metabolites identified from preparative-scale reactions for substrates **3.5**, **3.6**, and **3.10**–**3.13**; All reactions were carried out at a substrate/enzyme ratio of 2000:1. [a] The stereochemical configurations for metabolites **3.10a**, **3.10a**, **3.10c**, **3.11a** and **3.11b** are relative; [b] % e.e. was obtained by Mosher's ester analysis; [c] % e.e. was obtained by chiral GC analysis; [d] **3.5d** and **3.5e** were isolated as a 1:1 equilibrium mixture, the yield being calculated assuming **3.5d** was the only product; [e] Selectivity

shown for **3.10a** incorporates the selectivity of derived oxidation product **3.10b**; [f] Only one Mosher ester was made due to insufficient sample; [g] Isolated yield

3.4.1 Screening of *N*-Boc-protected Spiroamine 3.10

The *N*-Boc-protected 3-spiro analogue **3.10** was first screened against 55 variants at a substrate/enzyme ratio of 2000:1, as previous work in the Wong group showed that this protecting group is well-tolerated across the library of $P450_{BM3}$ mutants. In order to isolate the metabolites from suitable variants, preparative-scale reactions were carried out on a 0.1–0.4 mmol scale, and with a timescale of 7−23 h. Five major products were characterised: β′-OH **3.10a**, β′-ketone **3.10b**, α′-OH **3.10c**, α-OH **3.10d**, and enamine **3.10e** (Figure 3.2). The relative configuration in alcohols **3.10a** and **3.10c** was confirmed *via* the diagnostic NOE correlations to H-9, suggesting the *trans*- conformations for both metabolites.

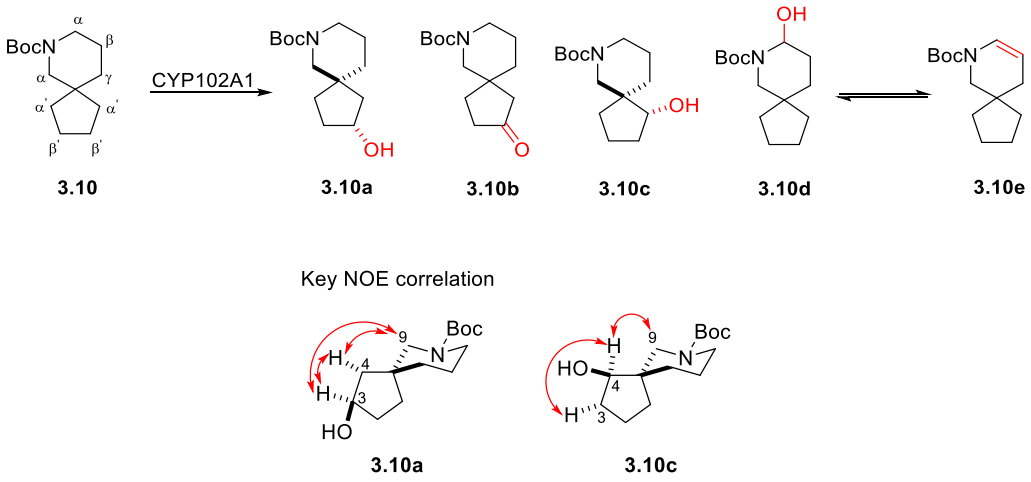

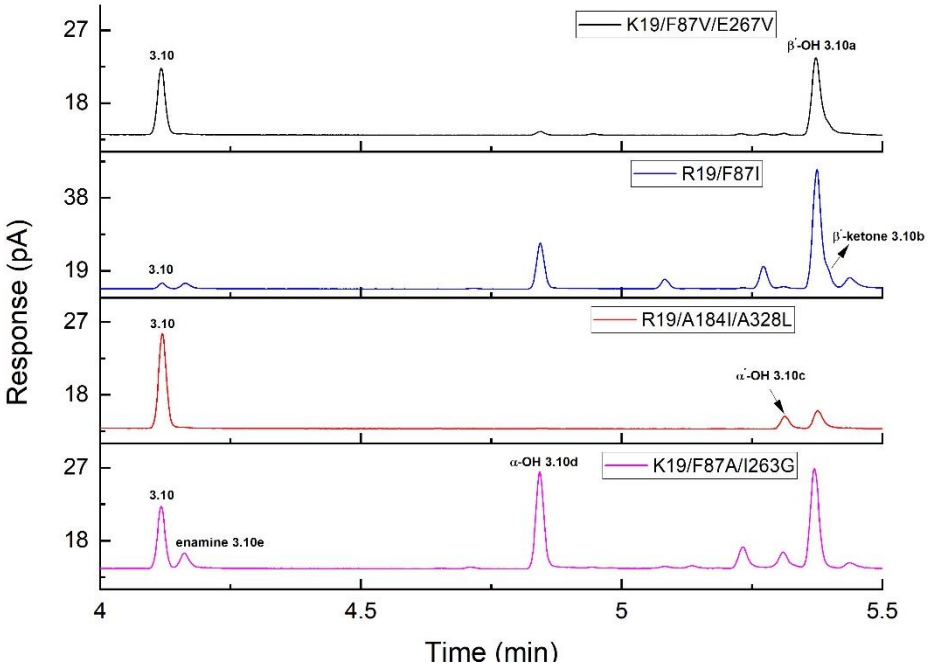

Figure 3.2 GC analysis of the product mixture from the reactions of selected variants with substrate **3.10**.

During screening, 33 out of 55 mutants showed ≥60% conversion of substrate **3.10** based on GC integration. This is consistent with previous results from the Wong group with Boc-protected amine substrates, where generally good (≥60%) conversions were observed, along with a diverse profile of products.

The conversion rates illustrated that mutations of F87 to a smaller residue (I/V/A) were important in promoting the oxidation of **3.10** (Table 3.3, Entries 6, 10, 17, 20 & 23), with the highest being 98% (Entry 10). This was likely due to the removal of steric congestion around the haem group, thus allowing more flexibility for the substrate's orientation in the binding pocket.[227] The most common product across the library was β′-OH **3.10a**. Combinations of mutations of A328 and I263 appear to promote β′-oxidation, as seen with variants R19/A328L/I263A and GV/L188Q/I263G/A328L (Entries 3 & 22). Among the two substitutions, mutation I263G could be the more influential in increasing selectivity for **3.10a**, since the selectivity increased significantly when introduced in mutants K19/F87V/I263G, K19/F87A/A82M/I263G, and GV/L188Q/I263G (Entries 14,

19 & 21). Mutation E267V also dramatically improved selectivity for this metabolite (Entry 12); however, when used in combination with V78I, the selectivity was not enhanced prominently (Entry 13).

Variants containing F87V/I mutations tend to promote further oxidation to form β′-ketone **3.10b**, whereas F87A deterred this further oxidation (Entries 2, 13, 16–19). On the other hand, the F87A mutation favours α-oxidation to form α-OH **3.10d** instead (Entries 16–19).

The combination of A184I/A328L increased the selectivity in favour of α′-OH **3.10c** by 40%, while I263A/A328L did not improve selectivity at all (Entries 3 & 4). Although these observations might suggest the importance of the mutation A184I for α′-hydroxylations, the selectivity decreased to 0% when it was introduced in mutant RP/H171L/A184I/I263G (Entry 25), which implied the importance of the base mutants chosen.

Mutations A328G, A264G, and insertion mutation G265GG enhanced the selectivity for α-OH **3.10d** by approximately 30% (Entries 6 & 7, 15). As mentioned above, none of these mutants showed further oxidation of **3.10a** to form ketone **3.10b**.

Finally, substitution A328V and insertion mutation L437LV facilitated the formation of enamine **3.10e**, where the selectivity doubled and tripled, respectively (Entries 9 & 11). In contrast, mutation I263G disfavoured enamine formation, where the selectivity decreased to 0–5% when present in variants R19/F87A/I263G, K19/F87V/I263G, and GV/L188Q/I263G (Entries 8, 14 & 21).

Entry	Mutant	Conv. (%)	3.10 a (%)	b (%)	c (%)	d (%)	e (%)	Others (%)
1	R19	93	44	0	31	17	2	7
2	R19/F87I	98	43	5	0	16	0	35
3	R19/I263A/ A328L	30	100	0	0	0	0	0
4	R19/A184I/ A328L	28	58	3	40	0	0	0
5	R19/F87A	74	5	0	1	1	8	85
6	R19/F87A/A328G	93	26	0	5	36	8	25
7	R19/F87A/ G265GG	74	45	0	4	37	4	11
8	R19/F87A/I263G	26	25	0	3	25	5	42
9	R19/F87I/ L437LV	67	65	2	7	4	12	10
10	K19/F87V	98	5	0	2	4	3	85
11	K19/F87V/A328V	73	56	0	5	26	9	5
12	K19/F87V/E267V	62	100	0	0	0	0	0
13	K19/F87V/E267/ V78I	77	43	11	0	3	4	39
14	K19/F87V/I263G	72	53	1	2	7	0	36
15	K19/F87V/A264G	57	32	1	4	36	3	23
16	K19/F87A/A82M	82	8	0	3	24	6	59
17	K19/F87A/I263A	93	14	0	0	56	6	24
18	K19/F87A/I263G	85	34	0	5	29	8	24
19	K19/F87A/A82M /I263G	66	53	0	0	36	5	6
20	GV/L188Q	95	34	5	7	27	5	21
21	GV/L188Q/I263G	69	75	0	0	6	0	18
22	GV/L188Q/I263G /A328L	88	86	2	0	2	1	9
23	GV/A184I	94	23	0	0	38	2	36
24	RP/H171L/I263G	34	58	0	18	4	0	20
25	RP/H171L/I263G/ A184I	14	100	0	0	0	0	0

Table 3.3 Selected screening data for substrate **3.10**. Full data in Chapter 7.

Metabolite **3.10a** was successfully crystallised by liquid-liquid diffusion (DCM/heptane) and the structure was determined by single crystal X-ray crystallography, confirming the relative configuration established by NOE experiments. This product was isolated from mutant RT2 with 28% *e.e.* as determined by Mosher ester analysis (Table 3.2, §6.7 for full data) but, as the diagram shows, it crystallised as the racemate (Scheme 3.8).

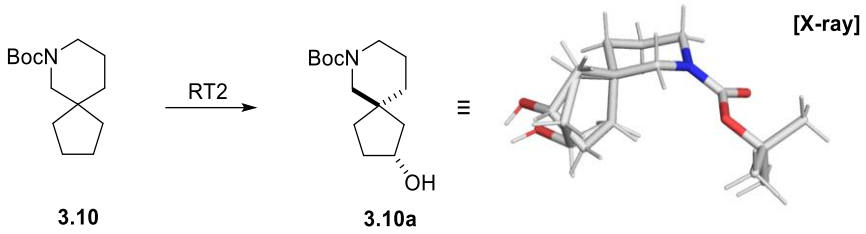

Scheme 3.8 X-ray crystal structure of **3.10a**.

3.4.2 Screening of *N*-Ips-protected Spiroamine 3.11

The *N*-Ips-protected 3-spiro analogue **3.11** was next screened against 54 variants with a substrate/enzyme ratio of 2000:1. A further 21 mutants were screened to optimise the formation of metabolites **3.11b** and **3.11c**. Preparative-scale reactions were carried out on a 0.1–0.4 mmol scale to enable metabolite isolation and characterisation, and on a timescale of 5−16 h. Four metabolites were identified: β′-OH **3.11a**, α′-OH **3.11b**, β-OH **3.11c**, and α-OH **3.11d** (Figure 3.3). The relative configuration in alcohols **3.11a** and **3.11b** was established by identical NOE correlations as observed for **3.11a** and **3.11c**.

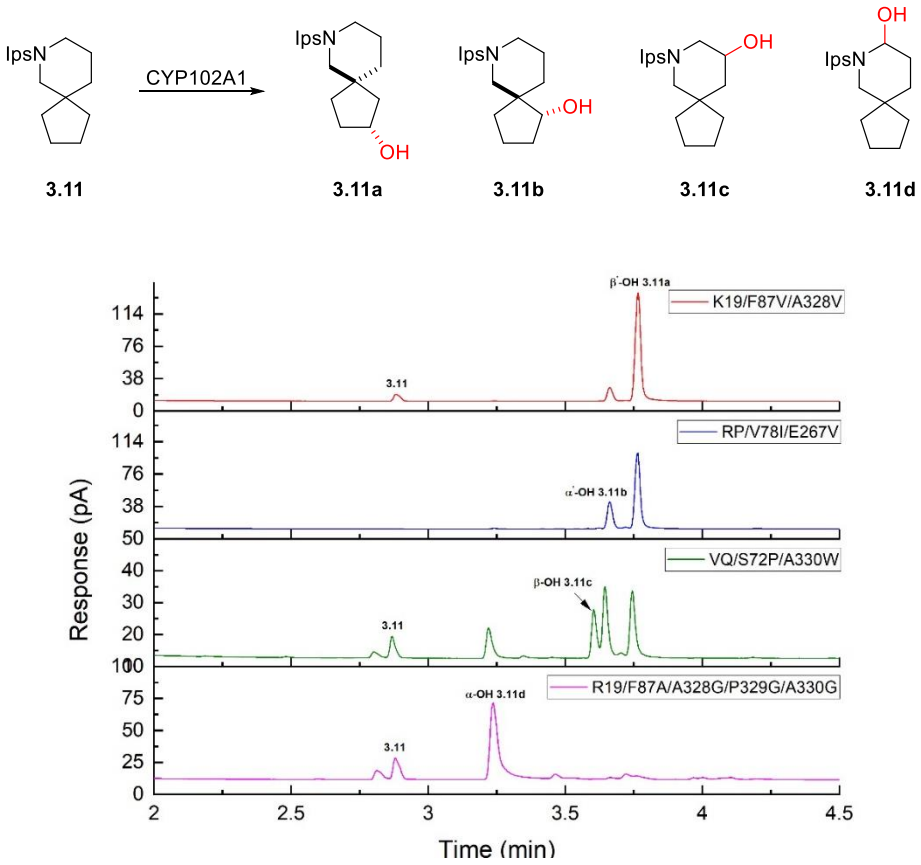

Figure 3.3 GC analysis of the product mixture from the reactions of selected variants with substrate **3.11**.

N-Ips protected amine **3.11** showed lower reactivity during screening than Boc-protected substrate **3.10**, with only 47 out of 75 variants giving >50% conversion; however, hydroxylation at the β-position was achieved (**3.11c**) while this position in the Boc-protected substrate was not accessible to the enzyme library.

From Table 3.4, it can be seen that most of the variants that gave full conversion consisted of F87 mutations (Entries 10, 11, 14, 16 & 18). It has been reported that variants with F87 substitutions have activity-enhancing capacities[228] or improve the development of preparative-scale reactions.[229] Similarly to the *N*-Boc protected spiroamine **3.10**, β′-OH metabolite **3.11a** was one of the major products; however, further oxidation to generate the β′-ketone was not observed.

Base mutant R19 showed no activity at all (Entry 1), but the introduction of an F87I/A mutation led to good conversion. Specifically, F87I and F87I/L437F mutations increased

the selectivity in favour of β′-OH **3.11a** by 69% and 88%, respectively (Entries 2 & 3). The combination of I263A/A328L also dramatically improved **3.11a** selectivity, although with only a 12% conversion (Entry 6). Mutation E267V on base K19 promoted β′-oxidation, while maintaining 100% conversion (Entry 11), yet the addition of a V78I mutation decreased the conversion to 78%, while maintaining the selectivity for **3.11a** (Entry 13). The introduction of mutations I263G/A328L in mutant GV/L188Q/I263G/A328L promoted selectivity for **3.11a** whereas A328G reduced it (Entries 15 & 17).

The selectivity for the production of α′-OH **3.11b** was generally low across the mutant panel. Mutation A330W appeared to raise this selectivity, as indicated when it was introduced in mutants R19/A330W and GV/L188Q/A330W (Entries 4 & 16). Mutation A264G also promoted α′-oxidation, although only to a slight extent (Entry 12).

Selectivity for metabolite β-OH **3.11c** was the lowest among all the products identified, hence it was difficult to establish any trends. Mutation F87I increased **3.11c** selectivity from 0% to 16% when introduced in mutant R19/F87I (Entry 2). Insertion mutation L437LV also promoted β-oxidation (Entry 7). Interestingly, mutants which promoted α-oxidation appeared to disfavour β′-oxidation, possibly due to the substrate orientation of α- and β′-hydroxylations; further investigations including computational studies are required in order to understand the underlying mechanism.

Mutation A330W increased the selectivity for α-OH **3.11d**, as seen in mutant R19/A330W (Entry 4); however, mutant R19/A330S did not give a higher selectivity for **3.11d** (Entry 5). In fact, changing the residue from W to S lowered the mutant's overall reactivity (Entry 5). The combination of mutations A328G/P329G/A330G was found to favour α-oxidation, along with mutations A328G, and I263G/A264G (Entries 9, 15, 19).

Entry	Mutant	Conv. (%)	3.11 a (%)	b (%)	c (%)	d (%)	Others (%)
1	R19	0	0	0	0	0	0
2	R19/F87I	100	69	3	16	2	9
3	R19/F87A	100	12	6	0	1	82
4	R19/A330W	87	7	42	0	34	17
5	R19/A330S	1	0	0	0	11	89
6	R19/I263A/A328L	12	91	0	0	0	9
7	R19/F87I/L437LV	37	72	4	15	3	7
8	R19/F87I/L437F	94	88	2	0	1	9
9	R19/F87A/A328G/ P329G/A330G	56	2	1	0	67	30
10	K19/F87V	100	14	7	0	0	79
11	K19/F87V/E267V	100	55	5	0	0	40
12	K19/F87V/A264G	63	54	11	1	21	13
13	K19/F87V/E267V/V78I	78	52	4	0	2	41
14	GV/L188Q	100	56	8	0	0	36
15	GV/L188Q/A328G	99	5	5	1	33	56
16	GV/L188Q/A330W	100	28	32	2	0	38
17	GV/L188Q/I263G/ A328L	61	80	1	0	0	19
18	GV/A184I	100	35	6	0	0	59
19	GV/A184I/I263G/A264G	67	1	1	5	36	57

Table 3.4 Selected screening data for substrate **3.11**. Full data in Chapter 7.

3.4.3 Screening of *N*-Ms-protected Spiroamine 3.5

The *N*-Ms protected analogue **3.5** was screened against 56 variants at a substrate/enzyme ratio of 2000:1. Preparative-scale reactions were carried out on a 0.1–0.4 mmol scale in order to isolate and identify the metabolites, and on a standard timescale of 23 h. The only two major metabolites identified were α-OH **3.5a** and its enamine form **3.5b** (Figure 3.4). In sharp contrast to the Boc- and Ips- protecting groups, hydroxylations at unactivated positions were not observed.

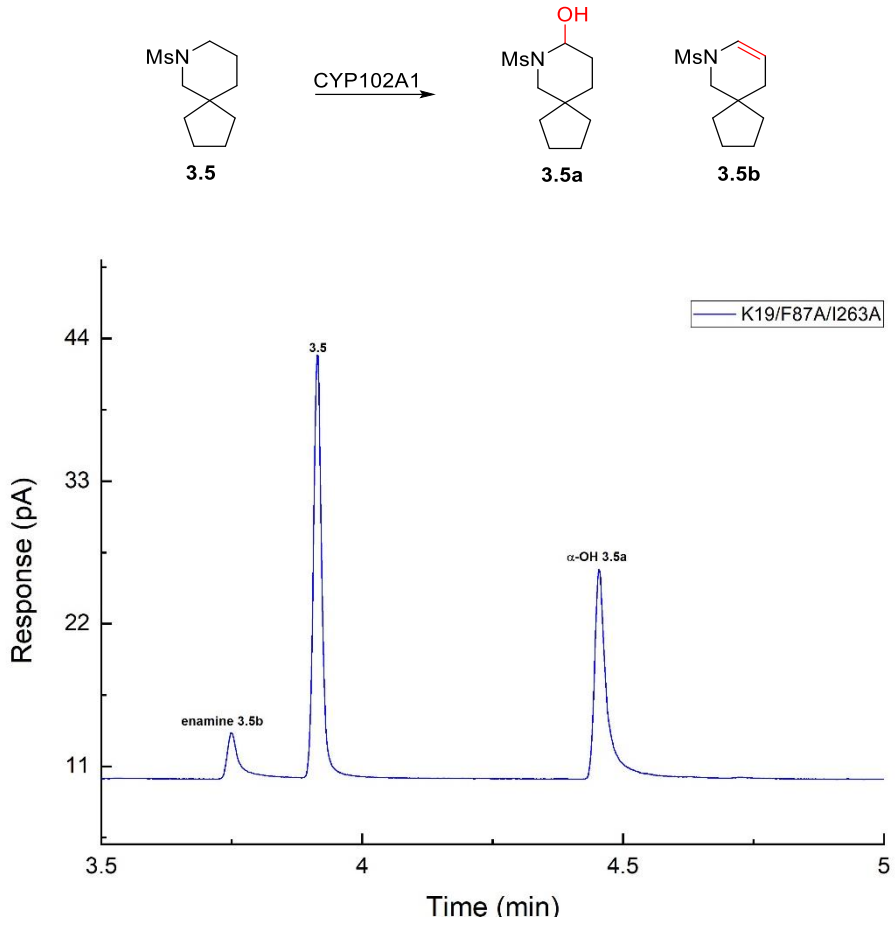

Figure 3.4 GC analysis of the product mixture from the reactions of selected variant with substrate **3.5**.

Ms-protected spiroamine **3.5** showed extremely high oxidation activity, with 34 out of 56 variants giving >90% conversion, and the remaining mutants giving >80%. From Table 3.5, it can be seen that mutation A184I promoted α-oxidation to form **3.5a**, where the selectivity increased by more than 60% (Table 3.5, Entries 3 & 20). In mutant R19/V78I/F87A/A328I, the combination of V78I/A328I further enhanced the selectivity for **3.5a** to 87% (Entry 4); moreover, the substitution of an Ala (A) residue in base mutant R19 was generally better than an Ile (I) residue in promoting α-hydroxylation (Entries 2 & 8). Mutation I263G was also found to increase the selectivity in favour of **3.5a**, as seen with mutants R19/F87A/I263G, K19/F87V/I263G, K19/A82M/F87A/I263G, and GV/L188Q/I263G (Entries 6, 12, 14 & 16). Although I263G was shown to improve the selectivity for **3.5a**, along with mutation A264G, the formation of enamine **3.5b** was

promoted instead (Entry 7). Additionally, mutation at residue A328 appeared to encourage the dehydration of **3.5a** to form enamine **3.5b** (Entries 5 & 18).

Entry	Mutant	Conv. (%)	3.5a (%)	3.5b (%)	Others (%)
1	R19	0	0	0	0
2	R19/F87A	100	54	9	37
3	R19/F87A/A184I	89	77	15	8
4	R19/F87A/V78I/A328I	60	87	13	0
5	R19/F87A/A328L	98	32	40	29
6	R19/F87A/I263G	100	56	10	34
7	R19/F87A/I263G/A264G	100	17	82	1
8	R19/F87I	98	46	13	41
9	K19/F87V	99	50	9	41
10	K19/F87V/E267V	100	0	0	100
11	K19/F87V/E267V/V78I	79	51	6	42
12	K19/F87V/I263G	95	78	11	11
13	K19/F87A/A82M	100	0	0	100
14	K19/F87A/A82M/I263G	100	41	8	51
15	GV/L188Q	96	56	6	38
16	GV/L188Q/I263G	87	77	13	10
17	GV/A184I	100	5	0	95
18	GV/A184I/I263G/A328G	43	72	18	10
19	RP/H171L/I263G	100	18	3	79
20	RP/H171L/I263G/A184I	40	73	11	17

Table 3.5 Selected screening data for substrate **3.5**. Full data in Chapter 7.

3.4.4 Screening of *N*-DEP Protected Spiroamine 3.12

The *N*-DEP protected analogue **3.12** was initially screened against 63 variants at a substrate/enzyme ratio of 2000:1, and with a standard timescale of 5 h. Similar to the *N*-Ms protected substrate **3.5**, the phosphonate ester spiroamine did not give rise to a diverse profile of metabolites. Only one major product was characterised: enamine **3.12a**, and hydroxylations at unactivated positions were not found (Figure 3.5). The DEP-protected amine also produced a number of minor metabolites that were not identified due to their low selectivity and hence difficulty to obtain pure samples.

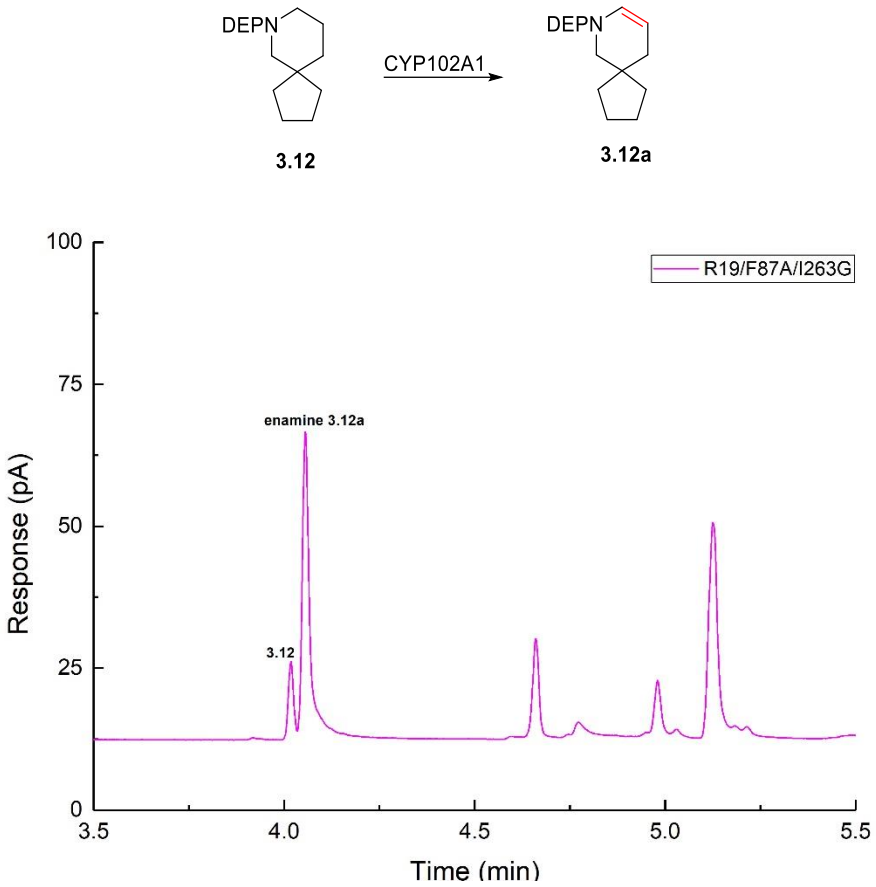

Figure 3.5 GC analysis of the product mixture from substrate **3.12** with the selected variant shown, giving metabolite **3.12a** and unidentified products.

The reactivity towards oxidation of substrate **3.12** was not as high as that for substrate **3.5**, with only 21 out of 63 variants showing >50% conversion. From Table 3.6, it can be seen that F87A and F87I significantly increased conversion rates (Entries 2 & 5). The combination of I263G/A328L increased the selectivity for **3.12a** from 0% to 52% (Entry 14). Mutation I263G on its own did not give the same outcome (Entry 13); however, when present in mutant K19/F87A/A82M/I263G, the selectivity was enhanced, suggesting the effect of base mutants chosen (Entry 11). Mutations E267V and E267V/V78I also improved selectivity for the enamine, as seen from mutant K19/F87V (Entries 8 & 9). The influence of V78I on enamine production can further be seen from base mutant R19/F87A where the combination of V78I/A184I increased the selectivity by 53% (Entry 4). Conversely, A328G decreased selectivity when present in mutant R19/F87A/A328G (Entry 3), whereas L437F increased it (Entry 6).

Entry	Mutant	Conv. (%)	3.12a (%)	Others (%)
1	R19	0	0	0
2	R19/F87A	99	17	83
3	R19/F87A/A328G	100	5	95
4	R19/F87A/V78I/A184I	53	70	30
5	R19/F87I	100	72	29
6	R19/F87I/L437F	99	89	11
7	K19/F87V	100	1	99
8	K19/F87V/E267V	100	68	32
9	K19/F87V/E267V/V78I	95	69	31
10	K19/F87A/A82M	49	37	63
11	K19/F87A/A82M/I263G	50	61	39
12	GV/L188Q	100	12	88
13	GV/L188Q/I263G	0	0	0
14	GV/L188Q/I263G/A328L	14	52	48

Table 3.6 Selected screening data for substrate **3.12**. Full data in Chapter 7.

3.4.5 Computational Studies on 3.10 and 3.11

In a similar manner to the 2-spiro substrates, rigid docking was performed in order to provide insights on substrate-enzyme interactions as well as comparisons between computational and experimental results. Nine clustered structures were generated from the three replicas of each variant. MD simulations were not performed on variants that gave hydroxylated products at the activated *N*-α-position since they are of lesser interest. To summarise, MD simulations were performed on variants generating metabolites *N*-boc β′-OH **3.10a**, and α′-OH **3.10c**, and *N*-Ips β′-OH **3.11a**, α′-OH **3.11b**, and β-OH **3.11c**. A dot plot was generated for each variant, illustrating the carbons that were hydroxylated in each cluster, as predicted by computational algorithms, and their respective affinity energies.

Metabolite β′-OH **3.10a** was produced from mutant R19/F87I; accordingly, *N*-Boc protected 3-spiro analogue **3.10** was docked in the nine clusters of this variant. Out of the 81 poses, 23 were classified as productive poses, in which the criteria for "productive" were identical to those summarised in §2.7. The productive poses indicated α′-, β′-, γ-,

and α-oxidations (Figure 3.6). Within these productive poses, β′-poses were the most populated, which was consistent with experimental results. On the other hand, γ- and α-oxidations were not observed experimentally. The majority of the poses indicated β′-oxidation with *trans*-configuration (the OH group *trans* on the cyclopentane ring to the CH_2N group), which was consistent with the major diastereomer, metabolite **3.10a**. Combining both the *cis*- and *trans*- selective poses for β′-hydroxylation, the selectivity computed from MD simulation was 36%, which was similar to the experimental selectivity of 48% (including the selectivity for **3.10b**) (Table 3.2).

α′-OH **3.10c** was produced from mutant RT2. Among the 81 poses generated, 19 were productive and indicated oxidations at the α′-, β′-, β-, and α- positions (Figure 3.7). The number of poses that corresponded to α′ and β′-hydroxylations were similar, nine and eight, respectively. The majority of α′ poses were consistent with the *trans*-alcohol (as defined above), in agreement with the relative configuration found experimentally for metabolite **3.10c**. The computational selectivity obtained by MD simulation was 35%, comparable to the experimental selectivity of 22% (Table 3.2).

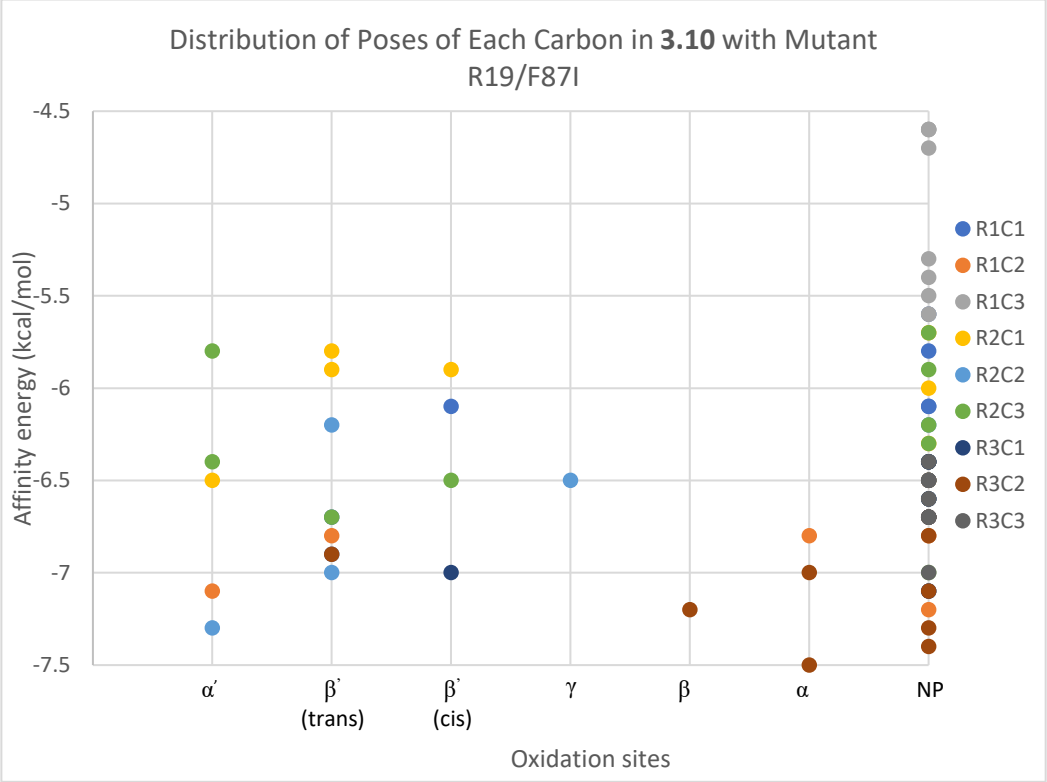

Figure 3.6 Distribution of poses, and calculated affinity energies, for oxidation at each carbon in *N*-Boc substrate **3.10** with mutant R19/F87I; (trans) and (cis) refer to the relative disposition of the new hydroxyl group and the C–CH_2N bond; NP = non-productive poses.

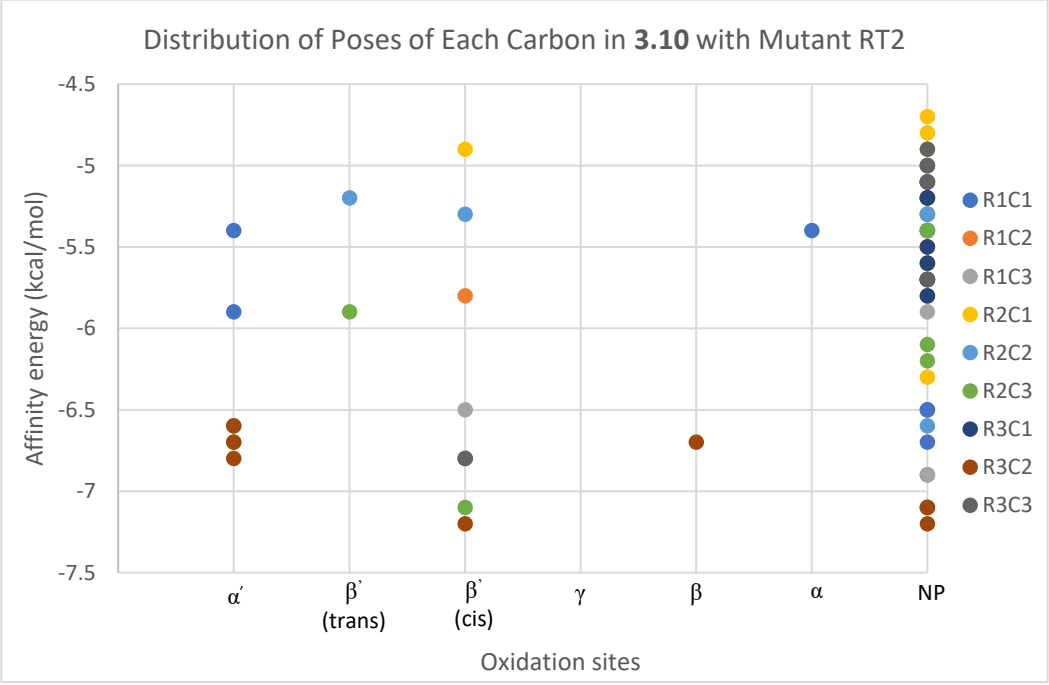

Figure 3.7 Distribution of poses, and calculated affinity energies, for oxidation at each carbon in *N*-Boc substrate **3.10** with mutant RT2.

Metabolite β′-OH **3.11a** was produced from mutant R19/F87I. MD simulations were performed on this mutant and the substrate **3.11** was docked into the nine clusters generated. Of the 81 poses, there were 31 productive poses, indicating oxidations at α′-, β′-, γ-, β-, and α- (Figure 3.8). Poses corresponding to β′-oxidation were the most populated, in which five out of 13 poses gave the *cis*-stereochemistry, and eight out of 13 poses gave the *trans*-stereochemistry, consistent with **3.11a**. Metabolite β-OH **3.11c** was also produced from this variant; however, poses representing β-oxidation were significantly fewer in number than those for β′-, with only six poses. Nonetheless, the β-position still remained the second most likely site to be oxidised based on docking results, followed by oxidations at the α′-, α-, and γ- positions. The computational selectivity for **3.11a** and **3.11c** were 39% and 13%, respectively, similar to the experimental selectivity of 58% and 13% (Table 3.2).

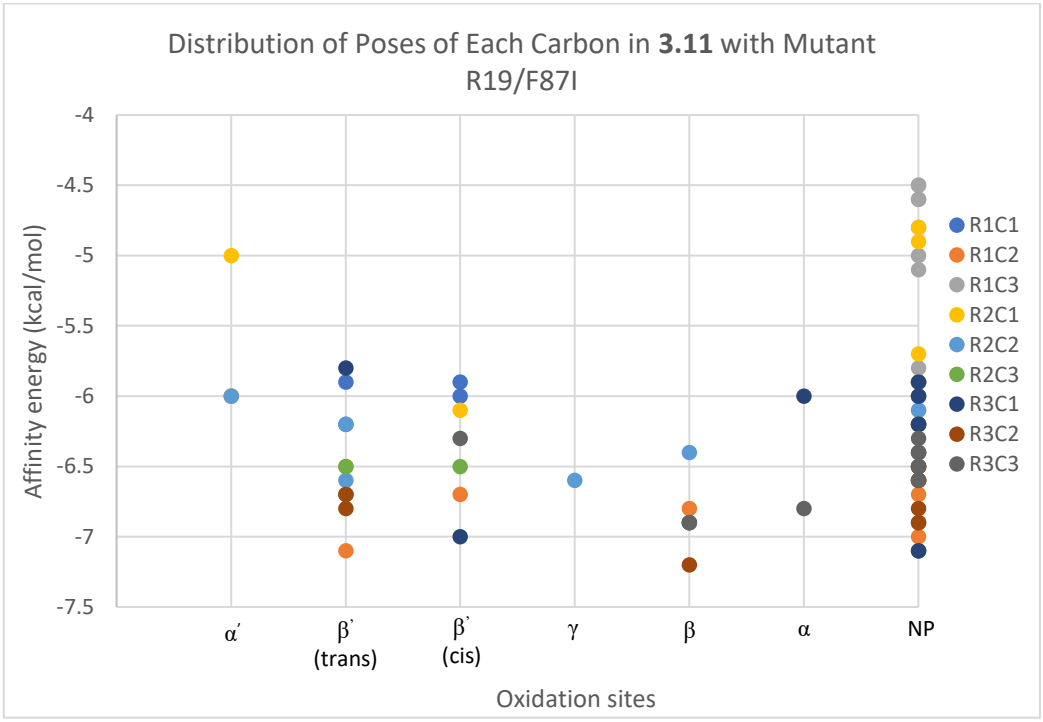

Figure 3.8 Distribution of poses, and calculated affinity energies, for oxidation at each carbon in *N*-Ips substrate **3.11** with mutant R19/F87I.

Metabolite α′-OH **3.11b** was isolated from variant GV/L188Q. Among the 81 poses generated, 41 poses were productive and 18 poses represented α′-oxidation, which was

the most populated oxidation site (Figure 3.9). The *trans*-OH outcome among the α′-poses was favoured from the docking results, since there were 16 such poses, among the 18 α′-oxidation poses. The computational selectivity of α′-oxidation was 37%, with the experimental selectivity being 5% (Table 3.2).

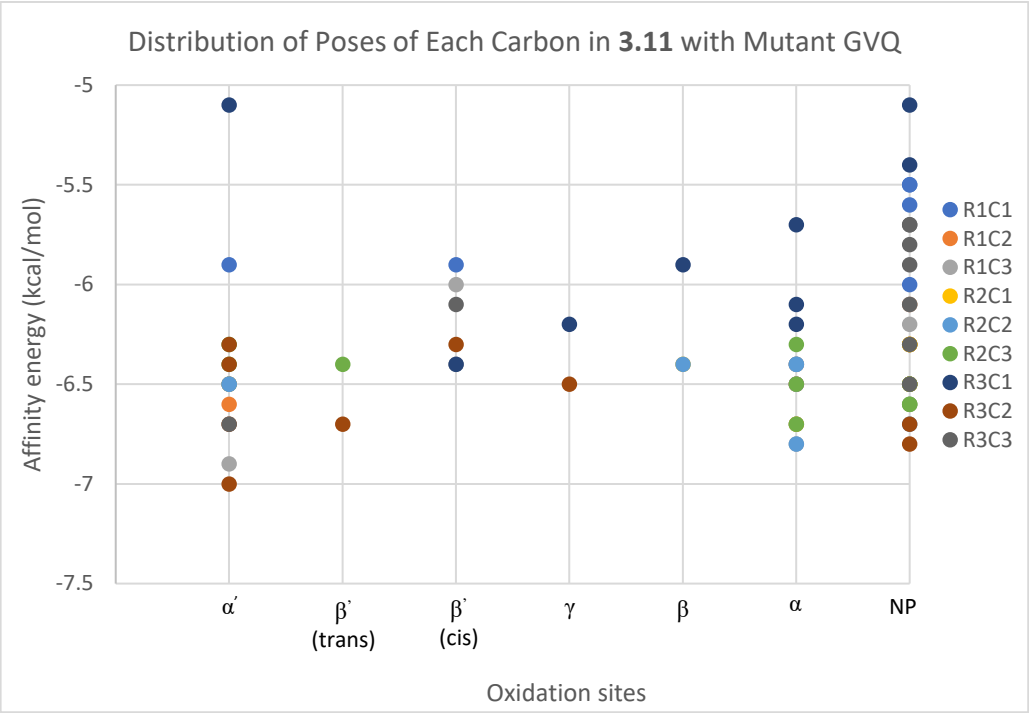

Figure 3.9 Distribution of poses, and calculated affinity energies, for oxidation at each carbon in *N*-Ips substrate **3.11** with mutant GV/L188Q.

In order to gain more information on substrate-enzyme interactions, all the productive poses corresponding to 3-Boc β′-OH **3.10a**, 3-Boc α′-OH **3.10c**, 3-Ips β′-OH **3.11a**, and 3-Ips α′-OH **3.11b** were overlaid (Figures 3.10a–e). Both 3-Boc **3.10** and 3-Ips **3.11** substrates were relatively flexible in the active site, as reflected by their various binding orientations in the binding pocket. Residue Ser72 played an important role in the stabilisation of the binding poses; the side-chain OH of S72 can form hydrogen bonds with the C=O from the Boc-protecting group in **3.10** and the S=O from the Ips-protecting group in **3.11** (Figures 3.10a–c, e), with distances between 2.2–3.1 Å. The residues that were within van der Waals contact were similar between the two substrates, despite their different protecting groups. For instance, Phe87, which is close to the haem centre,

strongly influences specificity and product selectivity;[230,231,232] it is one of the most commonly mutated residues, and the substitution of Phe to a smaller amino acid residue creates space for substrates to approach the haem in the binding pocket.[233,234,235] Other active site residues – such as I263, L437, and A264 – were also within the distance of van der Waals contact with the substrate. An overlay of all the productive poses for 3-Boc β′-OH **3.10a** (in green), 3-Boc α′-OH **3.10c** (in cyan), 3-Ips β′-OH **3.11a** (in blue), 3-Ips β-OH **3.11c** (in magenta) and 3-Ips α′-OH **3.11b** (in purple) is shown in Figure 3.10f, which illustrates the locations of the protecting groups (Boc- group in salmon; Ips- group in orange) in different mutants that gave each product. All of the poses clustered closely, wherein the protecting groups concentrated at the upper left (as presented) of the haem-iron; however, metabolites that were only observed in the 3-Ips substrate **3.11**, namely α′-OH **3.11b** and β-OH **3.11c** (black arrows), occupied the opposite orientation compared to the majority of poses, with the protecting groups found at the upper right (as presented) of the haem-iron. The variation in product orientations suggests that the protecting groups also serve as anchoring groups and indeed directing groups. Residues in the vicinity of selected poses can therefore be identified to alter product selectivity. For instance, mutations at V26, M354 and P329 (Figure 3.10f) could potentially lead to higher selectivity for metabolites **3.11b** and **3.11c**, through the substitution with larger amino acids in order to shift the protecting groups further away from the haem, hence favouring α′-OH and β-OH poses. Future mutagenesis work can follow such a rationale to generate diverse substrate pocket shapes and sizes for accepting unnatural substrates.

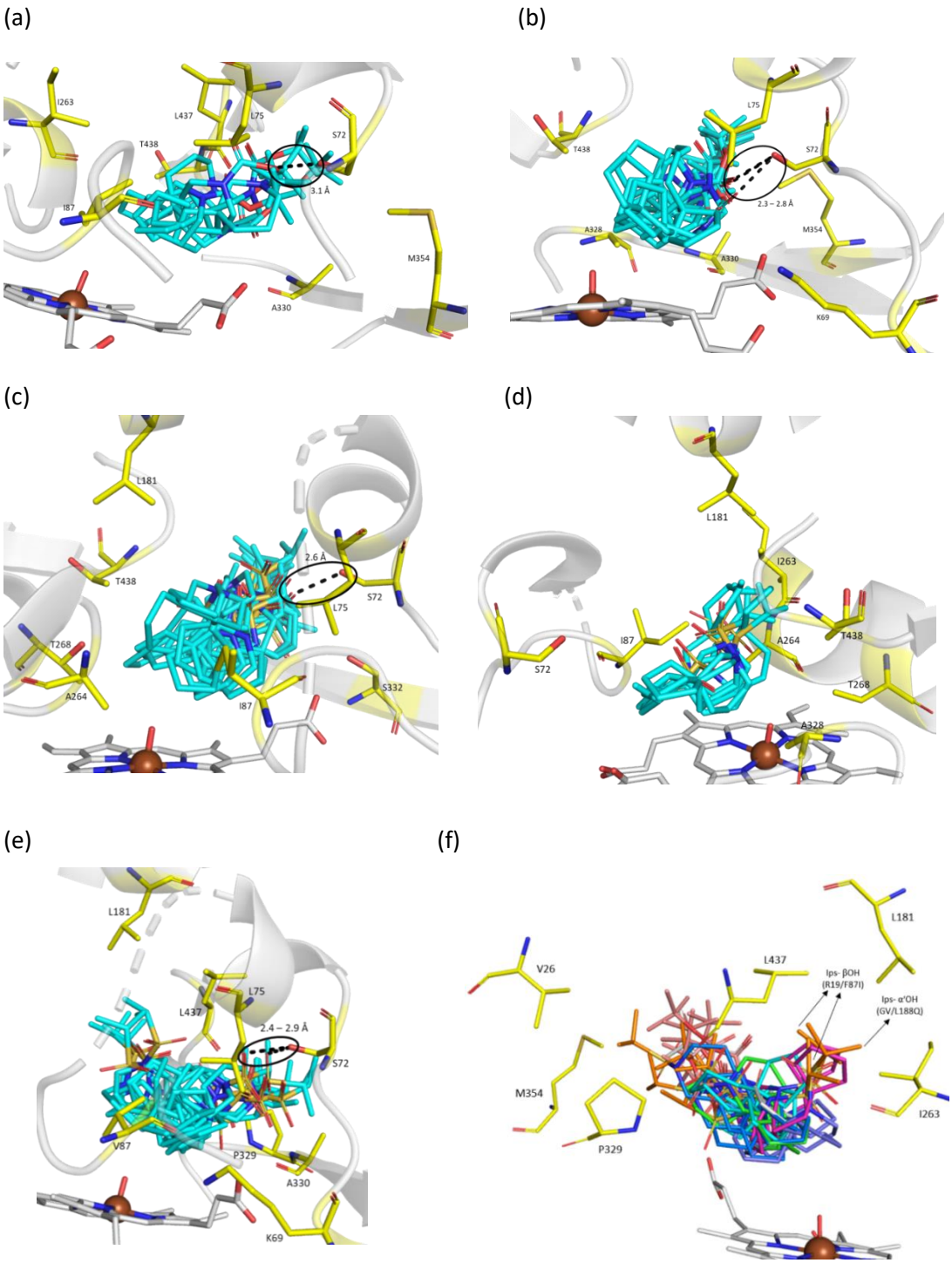

Figure 3.10 (a) Overlaid poses of all 23 β′-oxidation poses from nine clusters of variant R19/F87I with substrate **3.10**; (b) Overlaid poses of all 19 α′-oxidation poses from nine clusters of variant RT2 with substrate **3.10**; (c) Overlaid poses of all 18 β′-oxidation poses from nine clusters of variant R19/F87I with substrate **3.11**; (d) Overlaid poses of all six β-oxidation poses from nine clusters of variant R19/F87I with substrate **3.11** (e) Overlaid poses of all 14 α′-oxidation poses from nine clusters of variant GV/L188Q with substrate **3.11**; (f) Overlay of all productive poses for 3-Boc β′-OH **3.10a** (in green), 3-Boc α′-OH **3.10c** (in cyan), 3-Ips β′-OH **3.11a** (in blue), 3-Ips β-OH **3.11c** (in magenta) and 3-Ips α′-OH **3.11b** (in purple), Boc-protecting groups are shown in salmon, Ips-protecting groups are shown in orange. Key contact residues are shown in yellow; hydrogen bonding in (a), (b), (c), (e) is indicated by black dashed lines.

3.4.6 Screening of Unprotected Spirocyclic Lactam 3.6

As mentioned above, lactam intermediate **3.6** was also of interest since similar oxidation activities were expected compared to the spiroamine substrates. Initially, unprotected lactam **3.6** was therefore screened against 56 variants at a substrate/enzyme ratio of 2000:1, and with a standard timescale of 18 h. Two major metabolites were identified: α-OH **3.6a** and its further oxidised imide **3.6b** (Figure 3.11). Hydroxylations at unactivated positions were not observed.

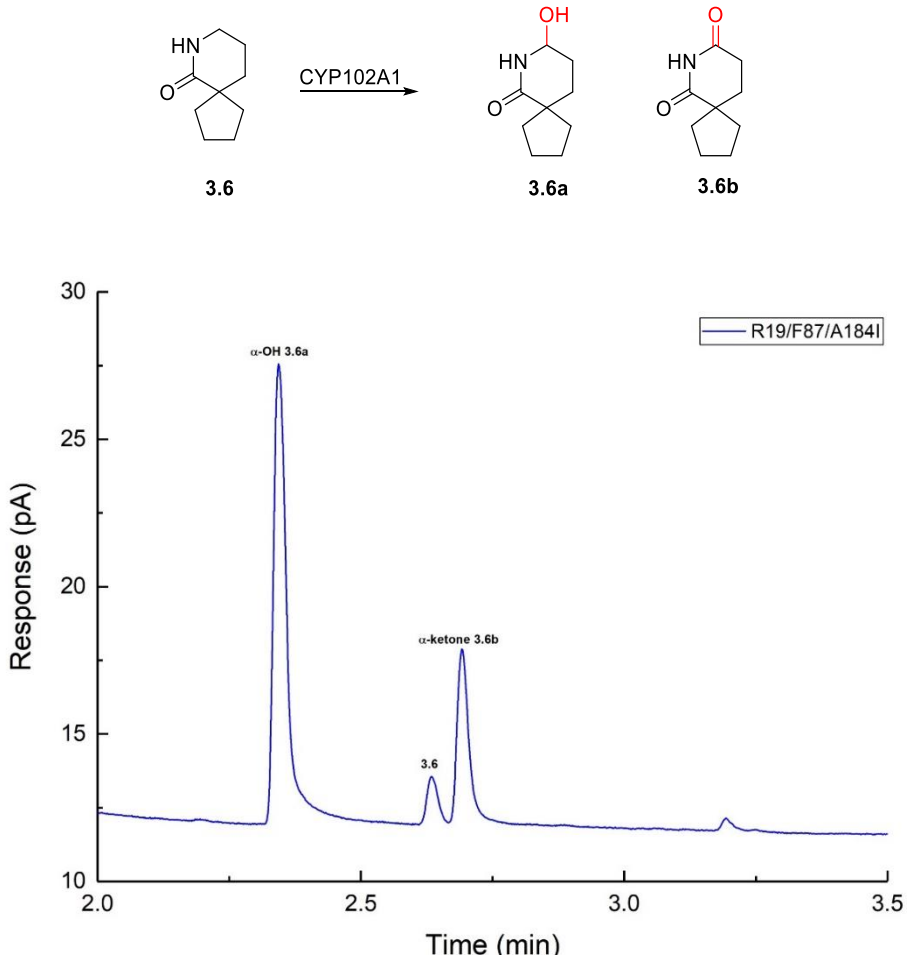

Figure 3.11 GC analysis of the product mixture from the reactions of the selected variant shown with substrate **3.6**.

The distribution of conversion rates for this substrate was relatively even, where 27 mutants gave >50% conversion, and the other 29 gave <50% conversion. Mutations F87I/A significantly improved conversion rates, as well as selectivity for α-OH **3.6a**

(Table 3.7, Entries 2 & 3). When present in mutant K19/F87A/A82M/A330W, mutation A330W greatly increased the selectivity in favour of **3.6a** from 0% to 86% (Entries 8 & 9). Such an increase was also seen with mutant R19/A330W where the selectivity was 57% (Entry 4). When A330W was introduced in mutant GV/L188Q/A330W, α-oxidation was discouraged (Entry 13). In fact, base mutant GV/L188Q gave the highest selectivity for **3.6a** when no other mutations were introduced (Entries 11–13). From the base mutant K19/F87V, additional mutation A328V greatly promoted α-hydroxylation (Entry 7), whereas I263G did not (Entry 10). Mutant GV/L188Q/I263G also exhibited lower selectivity towards **3.6a** compared to GV/L188Q (Entry 12). On the other hand, the selectivity for further oxidised imide **3.6b** was relatively low across the panel of mutants, with the highest being 27%, from mutant R19/F87A/S72W/A328I (Entry 5). This showed that substrate **3.6** was not particularly prone to further oxidation with these variants.

Entry	Mutant	Conv. (%)	3.6a (%)	3.6b (%)	Others (%)
1	R19	11	0	0	100
2	R19/F87A	73	58	20	22
3	R19/F87I	91	70	19	11
4	R19/A330W	11	57	0	43
5	R19/F87A/S72W/A328I	57	69	27	4
6	K19/F87V	88	70	18	12
7	K19/F87V/A328V	36	100	0	0
8	K19/F87A/A82M	100	0	0	100
9	K19/F87A/A82M/A330W	98	86	11	2
10	K19/F87V/I263G	73	51	20	29
11	GV/L188Q	75	80	20	0
12	GV/L188Q/I263G	9	0	0	100
13	GV/L188Q/A330W	85	45	18	37

Table 3.7 Selected screening data for substrate **3.6**. Full data in Chapter 7.

3.4.7 Screening of *N*-Bn-protected Spirocyclic Lactam 3.13

Following the unremarkable screening results with unprotected spirolactam **3.6**, it was decided to derivatise the free lactam to change the nature of the functional group, removing its ability to serve as a hydrogen bond donor. Based on previous and ongoing work in the groups, a benzyl group was installed and the protected lactam substrate **3.13**

was screened against 56 variants at the usual substrate/enzyme ratio of 2000:1, and on a standard timescale of 4−5 h. As Figure 3.12 shows, the benzylated lactam gave a relatively diverse metabolite profile compared to that from free lactam **3.6**. The major products were characterised as β′-OH **3.13a**, γ-OH **3.13b**, α-OH **3.13c**, and enamine **3.13d** (Figure 3.12). The relative configuration was assigned based on NOE correlations, where the CHO*H* on C-3 showed proximity to the proton that is *cis*- to the hydroxyl group on C-4. Additionally, H-4 also showed proximity to the C-6 methylene protons, further supporting the proposed relative configuration.

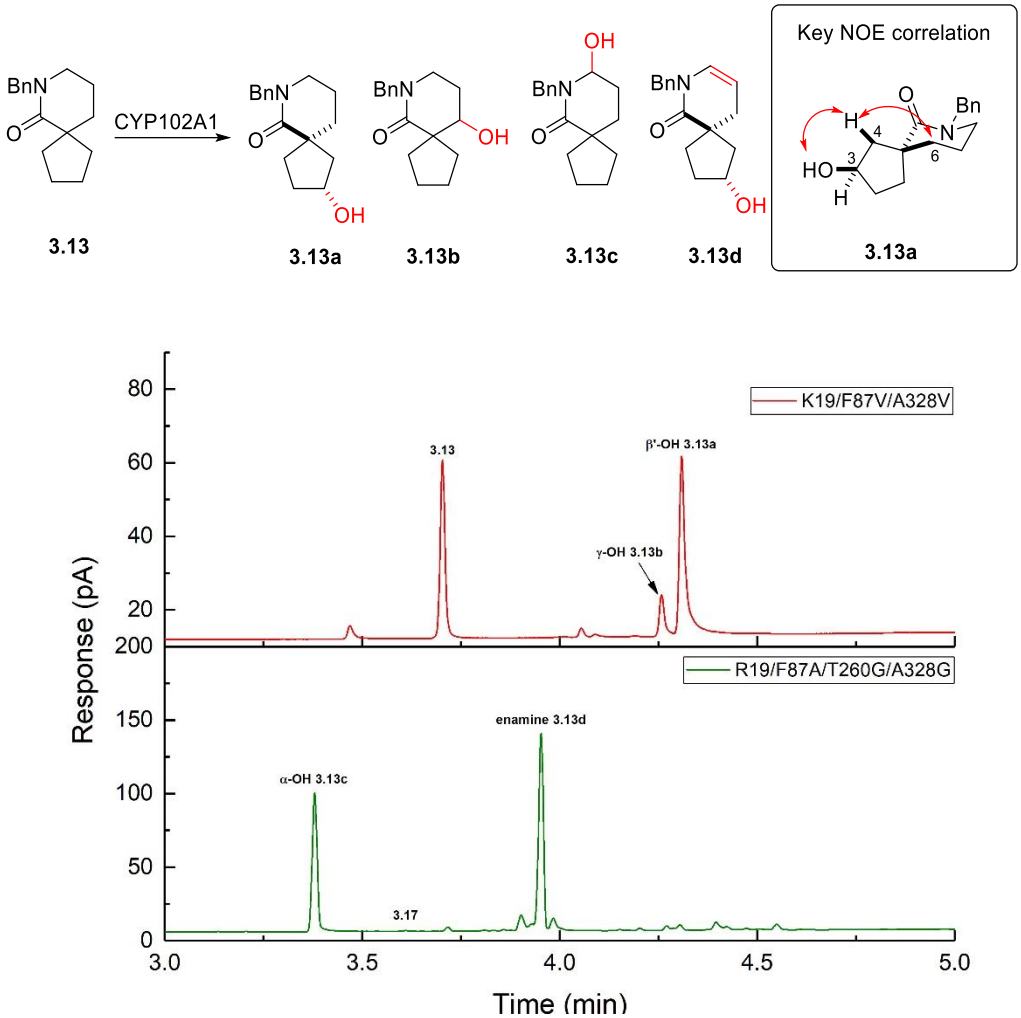

Figure 3.12 GC analysis of the product mixture from the reactions of the selected variants shown with substrate **3.13**.

The conversion rates of Bn-lactam **3.13** were relatively high, with 36 out of 56 variants showing ≥80% conversion. From Table 3.8, it can be seen that mutation A328 promotes

oxidation at the β′-position, generating β′-OH **3.13a**. Variants containing A328 mutations, such as R19/A328L/I263A, K19/F87V/A328V, and GV/L188Q/I263G/A328L, generally had high selectivity for **3.13a** (Entries 2, 13 & 19). Insertion mutation L437LV also increased the selectivity for **3.13a**, without affecting the conversion rate (Entry 11). In contrast, despite mutation S72W improving β′-OH selectivity by 57% (compare Entries 6 and 7), it decreased the conversion by 87% when present in mutant R19/F87A/S72W/A184I (Entry 7).

On the other hand, γ-OH **3.13b** was produced with the lowest selectivity by the panel of mutants screened. Mutation A330W promoted γ-oxidation, as seen with variant K19/F87A/A82M/A330W (Entry 16). Mutation I263G also increased selectivity, along with conversion, when present in mutant R19/F87A/330W, but decreased conversion when incorporated into template K19/F87V (Entries 8 & 14). A similar effect was seen with the combination of S72W/A184I in mutant R19/F87A/S72W/A184I (Entry 7).

Apart from promoting γ-OH selectivity, mutation A330W or a combination of A328G/P329G/A330G enhanced α-OH selectivity as well (Entries 3, 9 & 16); its effect was further enhanced by the addition of S72G (Entry 4).

Substrate **3.13** was the only substrate that gave a hydroxylated enamine as a product. Metabolite **3.13d** could potentially originate from the further oxidation of **3.13a** or **3.13c**. The relative configuration of the metabolite is discussed below. Interestingly, selectivity towards **3.13d** and α-OH **3.13c** appeared to increase proportionally. For instance, mutation A330W promoted the selectivity of the enamine as well (Entry 3 & 4).

Entry	Mutant	Conv. (%)	3.13 a (%)	b (%)	c (%)	d (%)	Others (%)
1	R19	1	0	0	0	0	100
2	R19/A328L/I263A	100	83	0	8	5	4
3	R19/A330W	90	2	4	39	47	9
4	R19/S72G/A330W	83	3	3	46	42	6
5	R19/F87A	100	1	0	17	28	53
6	R19/F87A/A184I	100	4	1	37	22	35
7	R19/F87A/S72W/ A328I	23	61	11	6	6	16
8	R19/F87A/I263G	100	4	11	4	17	64
9	R19/F87A/A328G/ P329G/A330G	1	0	0	50	36	14
10	R19/F87I	91	53	6	14	11	17
11	R19/F87I/L437LV	96	79	2	0	1	18
12	K19/F87V	100	2	1	13	10	73
13	K19/F87V/A328V	66	75	14	5	3	4
14	K19/F87V/I263G	92	36	6	12	12	34
15	K19/F87A/A82M	100	9	0	4	16	71
16	K19/F87A/A82M/ A330W	91	13	10	43	22	12
17	GV/L188Q	100	3	1	8	9	79
18	GV/L188Q/I263G	3	0	0	0	0	100
19	GV/L188Q/I263G/ A328L	100	69	0	0	0	31
20	GV/L188Q/I263G/ V78L	19	4	0	48	12	36

Table 3.8 Selected screening data of substrate **3.13**. Full data in Chapter 6.

To investigate the formation of hydroxy-enamine **3.13d**, a time-course reaction with mutant R19/F87I was performed (Figure 3.13). It was evident that both α- and β′-OH metabolites were formed after 30 min, and full conversion was achieved after 1 h. Based on GC analysis, enamine **3.13d** presumably originated from the further oxidation of β′-OH **3.13a**, since its peak area was inversely proportional to that of **3.13d**, suggesting it being the major contributor to the further oxidised metabolite. In contrast, the peak area of α-OH **3.13c** gradually plateaued as the reaction progressed. It can therefore be concluded that lactam **3.13** was likely first β′-hydroxylated, followed by α-hydroxylation, which was subsequently dehydrated to form enamine **3.13d**. Furthermore, the relative configuration of the metabolite can be confirmed based on the identical GC retention time as **3.13a** as seen from the time-course.

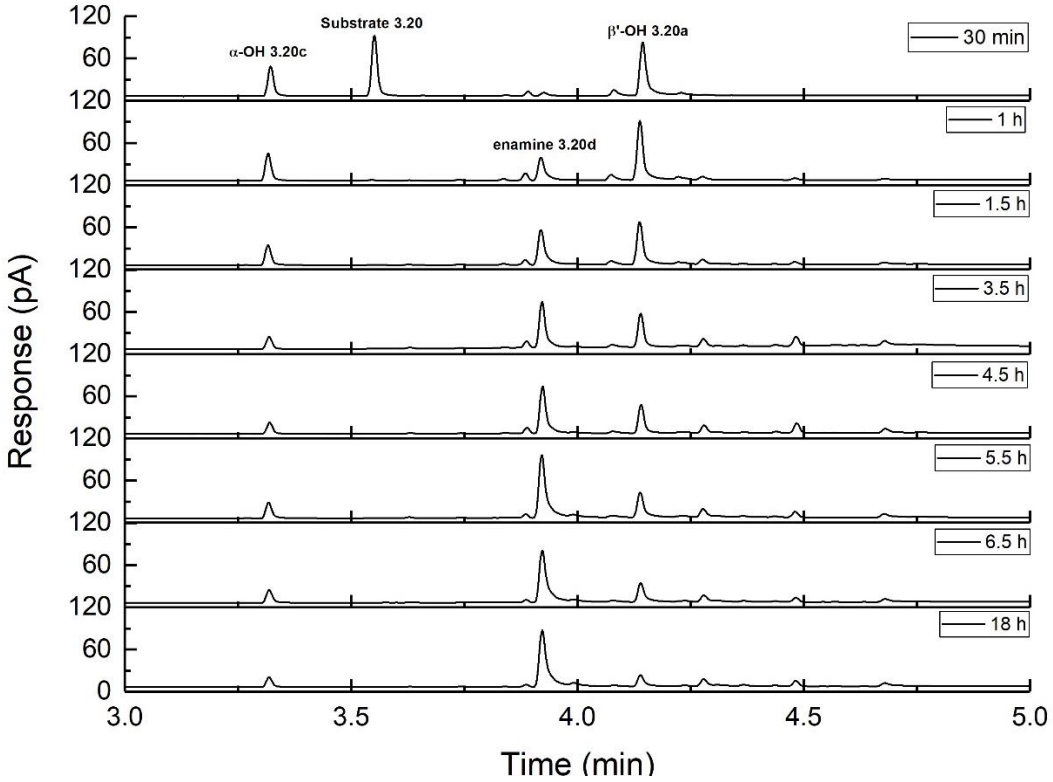

Figure 3.13 Time-course reaction of substrate **3.13** with mutant R19/F87I.

3.4.8 Computational Studies on 3.13

By analogy to the approach discussed in §3.4.5, MD simulations were performed on variants that gave high conversion and selectivity, as well as hydroxylations at unactivated positions; namely, R19/F87I and R19/F87A/A184I, which produced β′-OH **3.13a** and γ-OH **3.13b**, respectively. Nine clusters were generated from the three replicas of each variant.

Among the 81 poses from mutant R19/F87I, 27 productive poses were present that indicated α′-, β′-, and α-oxidation. Poses corresponding to β′-oxidation were the most populated, with 17 poses in total (Figure 3.14). In addition, out of the 17 poses, poses that suggested the *trans*-stereochemical outcome (between the hydroxyl group and the C–CO bond) were dominant, in agreement with the experimental results. The selectivity for β′-OH **3.13a** calculated computationally was 37%, which was not consistent with the

experimental selectivity of 65% (incorporating the selectivity of its further oxidised product, enamine **3.13d**) (Table 3.2).

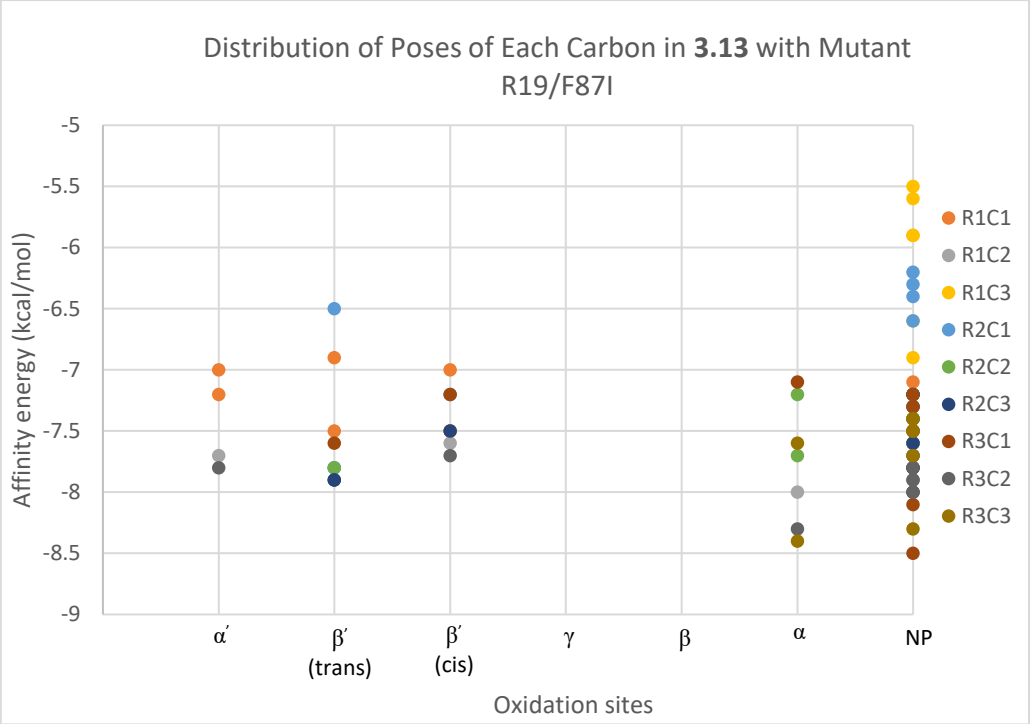

Figure 3.14 Distribution of poses, and calculated affinity energies, for oxidation at each carbon in *N*-Bn substrate **3.13** with mutant R19/F87I.

Metabolite γ-OH **3.13b** was produced from mutant R19/F87A/A184I. Of the 81 poses generated, 33 were productive (Figure 3.15). The most populated pose was γ-oxidation, with 10 out of 33 poses, which was in agreement with the metabolites isolated. The selectivity calculated from docking results for **3.13b** was 30%; compared to the experimental selectivity for this metabolite (0.6%, Table 3.2), the discrepancy is significant.

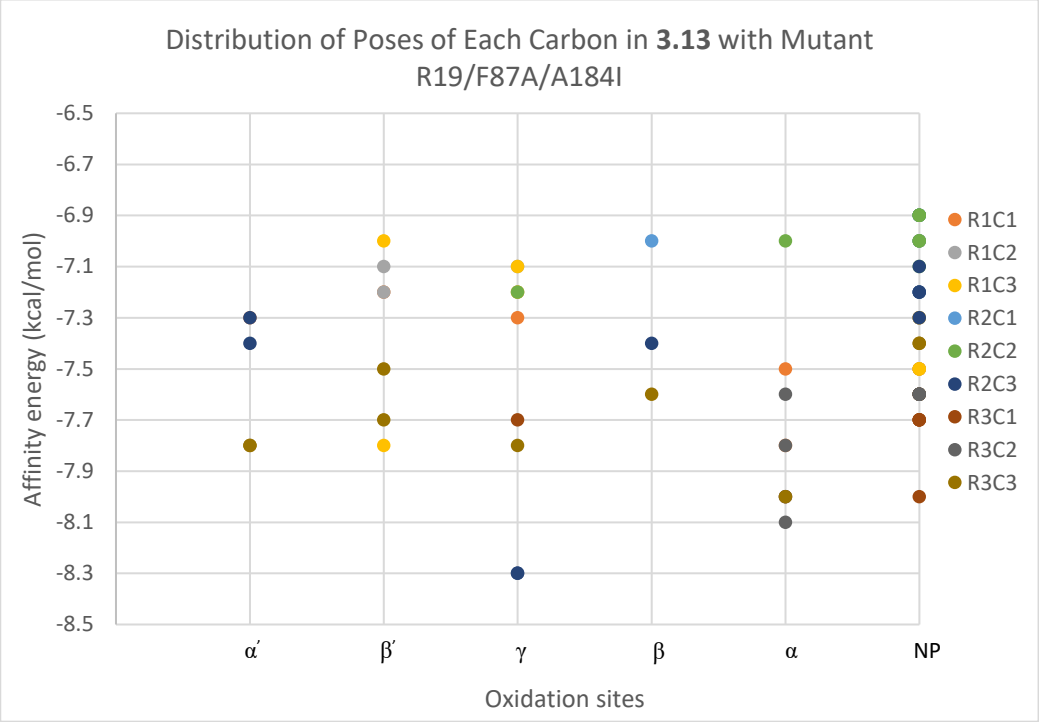

Figure 3.15 Distribution of poses, and calculated affinity energies, for oxidation at each carbon in *N*-Bn substrate **3.13** with mutant R19/F87A/A184I.

All the productive poses corresponding to 3-Bn spirolactam β′-OH **3.13a**, and γ-OH **3.13b** are overlaid in Figures 3.16a & b. The residues that are in van der Waals contact with the substrate are comparable with ones found in the 3-spiroamine substrates, such as L75, I263, and L437. Furthermore, similar to the spiroamines, residue S72 seems to play a crucial role in hydrogen-bonding interactions inside the binding pocket (Figure 3.16a), as reflected in the H-bond present between the -OH group on the amino acid and the lactam carbonyl oxygen. Conversely, H-bonding was absent in mutant R19/F87A/A184I (Figure 3.16b), as the Ser72 residue is too distant (>2.5Å) for such contact to occur. As a result, in these models stabilisation of the substrate is dominated by van der Waals forces. On the other hand, with the benzyl group being the largest protecting group employed thus far, investigations into the influence or potentially advantages of the phenyl group were conducted. The productive poses from substrates 3-Bn spirolactam **3.13** and 3-Boc spiroamine **3.13** were overlaid (Figure 3.16c); however, docking results did not reveal any anchoring aromatic stacking or other extensive van der Waals interactions that were

not observed in the protected spiroamines. Furthermore, the orientations of both protecting groups, Bn (in grey) and Boc (in salmon), and the carbocyclic rings were similar. All of the above implications suggest that no superior interactions were identifed in the benzylated substrates, and further analysis is deemed necessary to guide future mutagenesis work.

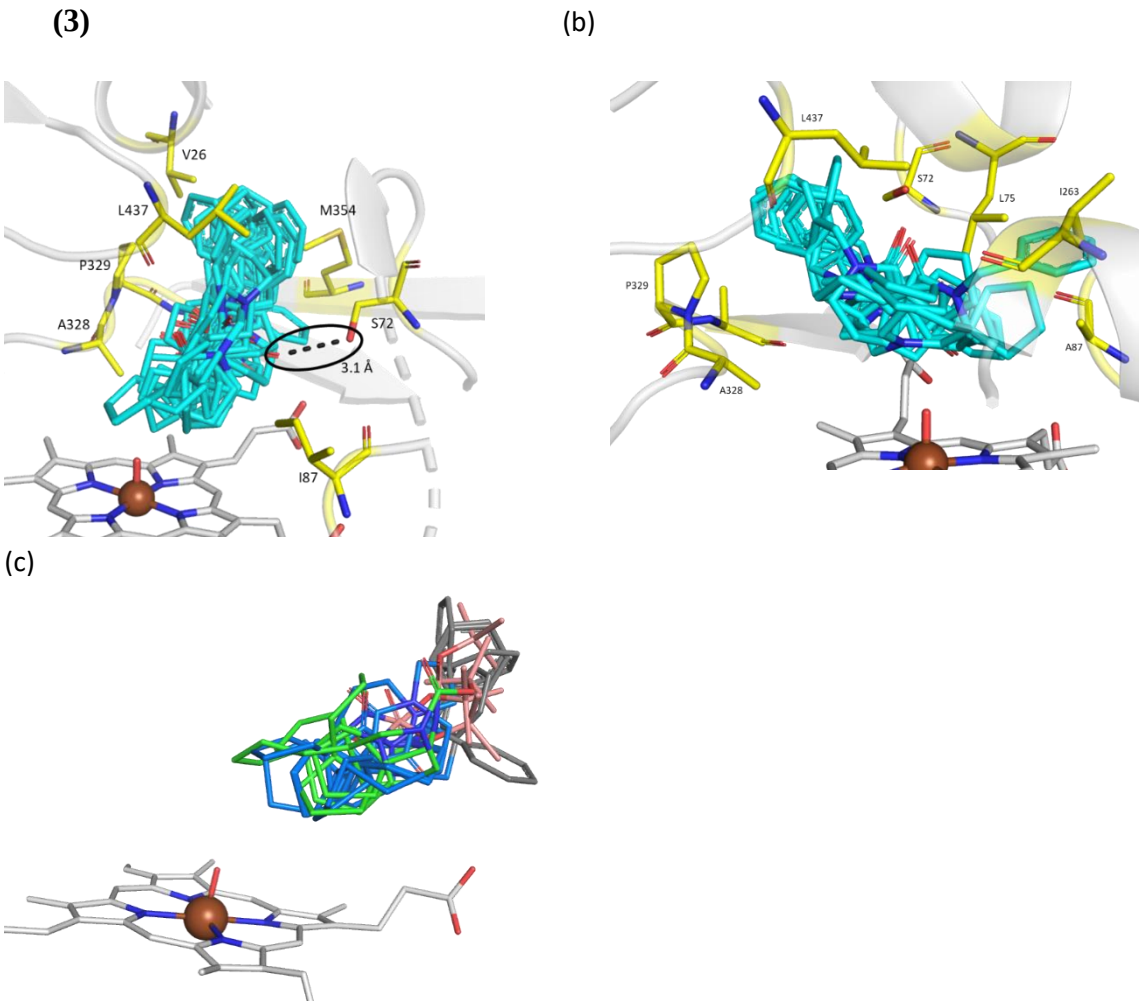

Figure 3.16 (a) Overlaid poses of all 17 β′-oxidation poses from nine clusters of variant R19/F87I with substrate **3.13**; (b) Overlaid poses of all 10 γ-oxidation poses from nine clusters of variant R19/F87A/A184I with substrate **3.13**; (c) Overlaid productive poses from substrates **3.13** (in green) and **3.11** (in blue), Boc- protecting groups are shown in salmon, Bn protecting groups are shown in grey. Key contact residues are shown in yellow; hydrogen bonding in (a) is indicated by a black dashed line.

3.5 Conclusions and Future Work on the 3-Spiroamine and 3-Spirolactam Series

Four 3-spiroamine substrates **3.5**, **3.10**–**3.12** and two 3-spirolactam substrates **3.6** and **3.13** were screened against panels of 55–75 variants to produce a variety of hydroxylated

metabolites. Combining the experimental results across the amine and lactam series, hydroxylations were observed at all unactivated positions for the Boc and Ips analogues (Figure 3.17). The two types of substrates are interchangeable, since cyclic amines can be oxidised to the corresponding lactam with oxidising agents such as $KmnO_4$,[236,237] and lactams can be reduced to the corresponding cyclic amine with, for example, $LiAlH_4$.[238,239]

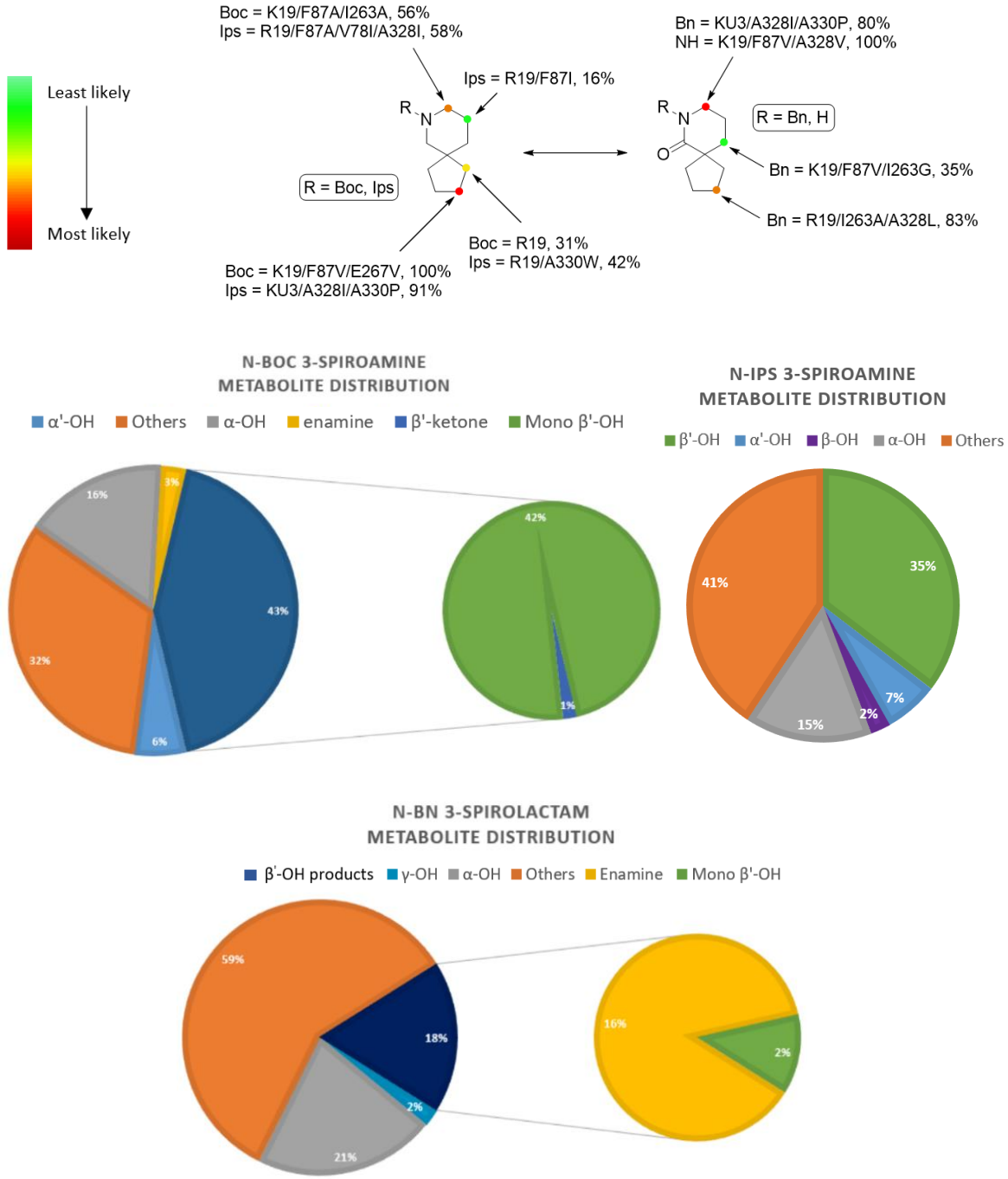

Figure 3.17 Summary of the distribution of hydroxylations at various positions in the 3-spiro series and the respective mutant with the highest selectivity.

According to the pie charts, both *N*-Boc and *N*-Ips amines were most prone to β′-hydroxylation, with the Boc-protected substrate having the minor pathway of further oxidation to the β′-ketone (Figure 3.17). The oxidation profile of the *N*-benzyl lactam, on the other hand, contained 59% of further oxidised products, as well as unidentified minor metabolites; here, the α-position was the most favourably hydroxylated, followed by the β′-position, the product of which was then extremely prone to further conversion into enamine **3.13d** (16%). The least likely sites to be hydroxylated for the *N*-Boc and *N*-Ips amines, and the *N*-benzyl lactam were the α′-, β-, and γ-positions, respectively.

The selectivities computed from docking for most of the metabolites were comparable, at least qualitatively, with the experimental results (Table 3.10). This indicates that docking can be a useful tool for the 3-spiro series, in providing insights in substrate-enzyme interactions, as well as a reference for future mutagenesis in a predictive sense; however, experimental and corresponding computational data with more variants are needed in order to establish the validity and reliability of rigid docking as an effective guide in the 3-spiro series.

Metabolite / mutant	**Experimental select. (%)**	**Docking select. (%)**
3.13a / R19/F87I	65 (11% from **3.13d**)	37
3.13b / R19/F87A/A184I	1	30
3.10a / R19/F87I	48 (5% from **3.10b**)	36
3.10c / RT2	22	35
3.11a / R19/F87I	58	39
3.11b / GV/L188Q	5	37
3.11c / GV/L188Q	13	13

Table 3.10 Experimental and docking selectivity for metabolites from the 3-spiro series.

Additionally, the dominant products as predicted by docking and obtained by screening were partly congruent, with a few outliers (Table 3.11), further supporting the potential

of rigid docking as a guide for mutation design for the selective oxidation of the 3-spiro substrates.

Substrate type	PG (substrate)	Mutant	Experimental dominant product	Docking dominant product
Lactam	Bn- (**3.13**)	R19/F87I	β′-OH	β′-OH
		R19/F87A/A184I	β′-OH	γ-OH
Amine	Boc- (**3.10**)	R19/F87I	β′-OH	β′-OH
		RT2	β′-OH	α′-OH
	Ips- (**3.11**)	R19/F87I	β′-OH	β′-OH
		GV/L188Q	β′-OH	α′-OH
			β′-OH	β′-OH

Table 3.11 Dominant product obtained experimentally and calculated computationally from each 3-spiro substrate.

As discussed in Chapter 2, improved algorithms can be developed for the prediction of hydroxylation sites; moreover, mutagenesis can be conducted in order to improve the selectivity of the least likely hydroxylated sites for each substrate according to the pie charts. Substrate engineering remains an aspect to further explore, which could potentially allow the access of a wider range of products with differently protected substrates. Reaction engineering could also lead to improvements in chemoselectivity control (less or further oxidation), agitation, aeration, concentrations and ratios, and general scaleability.

Chapter 4: Diversification of a $P450_{BM3}$ Metabolite

4.1 Overview

The hydroxyl group introduced by $P450_{BM3}$ mutants can be used as a synthetic "handle" for chemical elaboration and diversification of a core structure. A representative metabolite, the β′-hydroxylated 3-spirolactam **3.13a**, was chosen for a focused diversification programme in which the compound was subjected to widely applicable chemical reactions, allowing the construction of a set of more diverse fragment compounds. Various aspects of the attempted reactions are discussed in this chapter.

4.2 Fragment Diversification

4.2.1 Titre Screen of Substrate

Mutant R19/F87I led to the formation of β′-OH **3.13a** from spirolactam **3.13** (Chapter 3). In order to obtain a sufficient quantity of this metabolite for subsequent diversification, a large-scale enzyme reaction was necessary. To improve the practicality of this step, a titre screen was carried out to identify an optimal substrate concentration and reduce the final reaction volume.

While maintaining an enzyme ratio of 2000:1 and a reaction time of 18 h, substrate concentrations of 2 mM, 4 mM, 8 mM, and 16 mM were screened (Figure 4.1). It was found that the selectivity for metabolite **3.13** increased slightly with substrate concentration, whereas the conversion rate dropped away. The total turnover number peaked at 8 mM (TON = 484). Using this information, a gram-scale reaction with mutant R19/F87I was performed using a 10 mM substrate concentration, and an enzyme ratio of 2000:1 to afford metabolite **3.13a** in 67% yield based on substrate converted and an e.e. of 55%, as established by Mosher's ester analysis (Chapter 3).

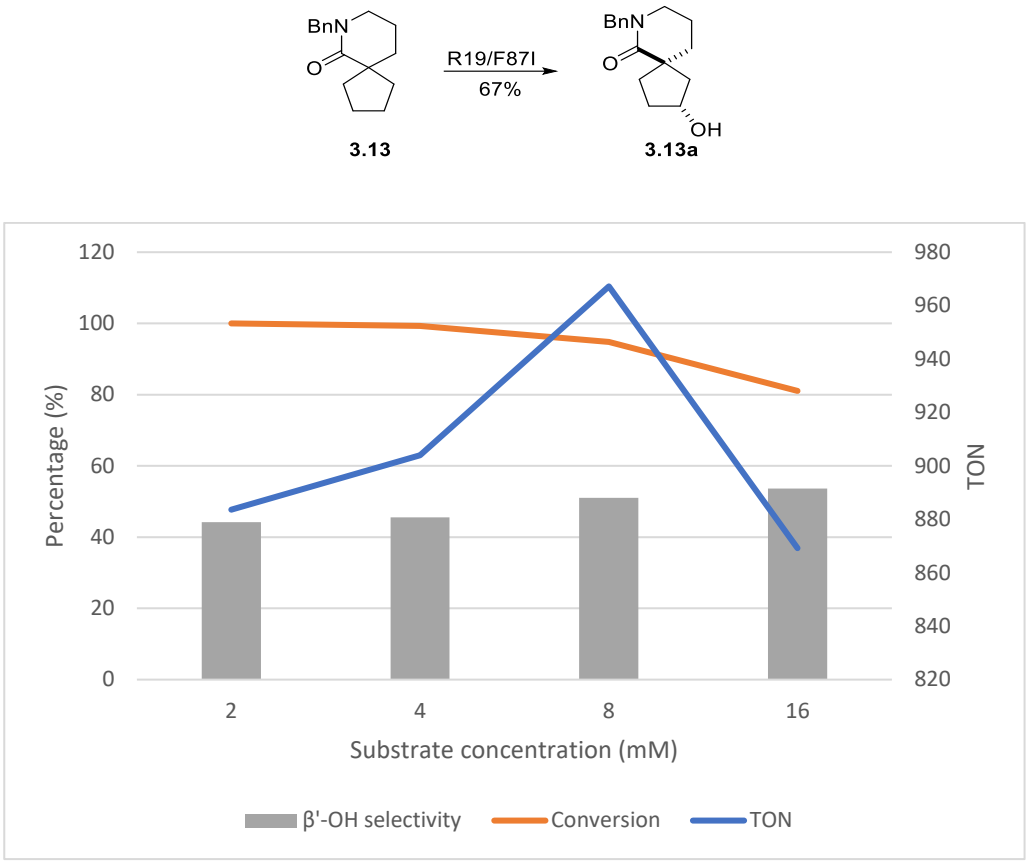

Figure 4.1 Titre screen of substrate **3.13** with mutant R19/F87I, and the respective conversion rate, selectivity, and TON.

4.2.2 Diversification from Alcohol 3.13a

A variety of representative diversification reactions were carried out using alcohol **3.13a** as substrate.

4.2.2.1 Benzyl Deprotection

The removal of the benzyl group provide access to the free spirolactam metabolite. Initially, a formic acid-mediated debenzylation was attempted as reported by Semple *et al.*;[240] however, formate ester **4.1** (Scheme 4.1) was formed instead, and the debenzylation failed to proceed.

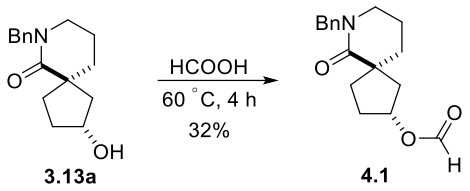

Scheme 4.1 Formation of formate ester **4.1**.

Approaches using catalytic hydrogenolysis with various palladium sources were explored using *N*-benzyl 2-piperidinone **2.43** as a model substrate (Table 4.1) to evaluate different reaction conditions. Palladium catalysts Pd/C, $Pd(OH)_2/C$, and Pd black were used, along with different solvents, H_2 pressure, and reaction times (Table 4.1a, Entries 1–5).[241,242] None of the combinations achieved the desired reaction, and only starting material **2.43** was recovered in each case. Combined Pd-catalyst systems were also trialled (Table 4.1a, Entries 6 and 7)[243] but the results remained disappointing. Finally, hydrogenation with Pt/C as catalyst was performed but the aromatic ring was reduced to generate **4.2** (Table 4.1a, Entry 8).[244] Alternative methods were conducted without success (Table 4.1b, Entries 1–5).[245,246,247,248,249,250] Reductive debenzylation under Birch conditions was attempted (Table 4.1b, Entry 6)[251] but NMR spectroscopic analysis of the crude product indicated only partial reduction of the benzene ring.

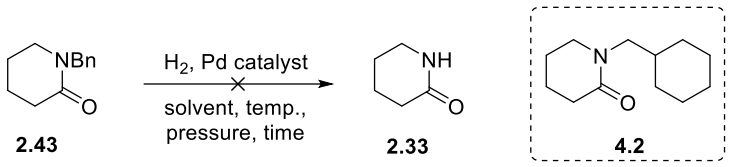

Entry	Pd cat.	Solvent	Temp. (°C)	Press. (bar)	Time (h)	Outcome
1	Pd/C	EtOH	RT	1	16	**2.43**
2			60			
3		MeOH	RT	6	6	
4	$Pd(OH)_2$/C	EtOH	60	1	16	
5	Pd black	EtOH	RT			
6	Pd/C:Pd$(OH)_2$/C 1:1.5	DCM:MeOH:H_2O 1:2:10				
7	Pd/C:Pd$(OH)_2$/C 1:1	THF:*i*PrOH 3:1				
8	Pt/C	MeOH				**4.2**

Table 4.1a Hydrogenolytic debenzylation conditions attempted.

Entry	Conditions	Outcome
1	CAN, ACN-H_2O, 5:1, RT, 5 h	**2.43**
2	Oxone, KBr, $MeNO_2$, 30 °C, 16 h	
3	TfOH, Toluene, 150 °C, 16 h	
4	MSA, 110 °C, 16 h	
5	BCl_3, DCM, −78 °C to RT, 16 h	
6	Na, $NH_{3(l)}$, THF, −78 °C, 4 h	Partial reduction

Table 4.1b Non-hydrogenolytic debenzylation conditions attempted.

With these inexplicable negative results with the model lactam, it was decided that *N*-debenzylation should be conducted after reduction of the lactam carbonyl. This proved successful and aminoalcohol **4.4** was obtained in excellent yield in two steps via the *N*-benzyl piperidine **4.3** (Scheme 4.2).

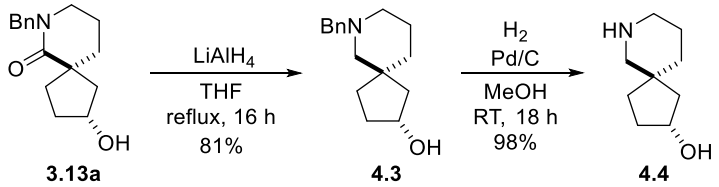

Scheme 4.2 *N*-debenzylation *via* reduced lactam **4.3**.

4.2.2.2 Fluorination

The number of fluorine-containing active pharmaceuticals approved has increased steadily over the last 50 years,[252] and more than 300 are currently registered globally, with the blockbuster statin drug Lipitor[253] being a notable example. In light of the pharmaceutical relevance of fluorine-containing compounds, a fluorination reaction with DAST was carried out on metabolite **3.13a**. The NMR spectroscopic data for the sole product formed in this reaction were incompatible with the expected product, as reflected by a lack of apparent coupling to ^{19}F in both the ^{1}H and ^{13}C NMR spectra. In fact, the spectroscopic and MS data confirmed the production of the corresponding chloride **4.5** (Scheme 4.3). The relative configuration in this compound was shown to be retained from the precursor alcohol as supported by NOE correlation, where proximity between the *CH*Cl and the protons *cis*- to the carbonyl group, i.e. H-2 and H-4, were observed. Moreover, the proton on C-4 that is *trans*- to the carbonyl group in turn correlated with H-6, further suggesting the proposed relative configuration.

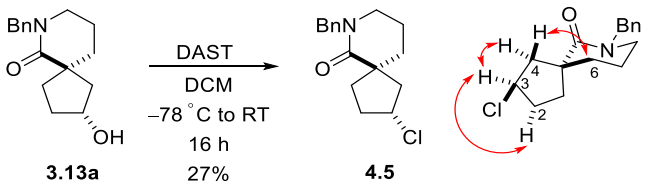

Scheme 4.3 Unexpected formation of chlorinated lactam **4.5**.

The reason for the formation of this product is unclear since DAST is one of the most commonly employed fluorinating reagents and literature precedent for such a chlorination process was not found. Given also the retained configuration, it was reasoned that the outcome results from the particular structural features of the spirolactam in which the lactam carbonyl shields the (C–O)σ* orbital in proposed intermediate **4.7** (Scheme 4.4) preventing displacement by fluoride ion. Instead, the lactam functionality may act as a

neighbouring group to provide a cationic intermediate (**4.8** or an equivalent species) that is sufficiently reactive to sequester chloride from the solvent (DCM), present in excess.

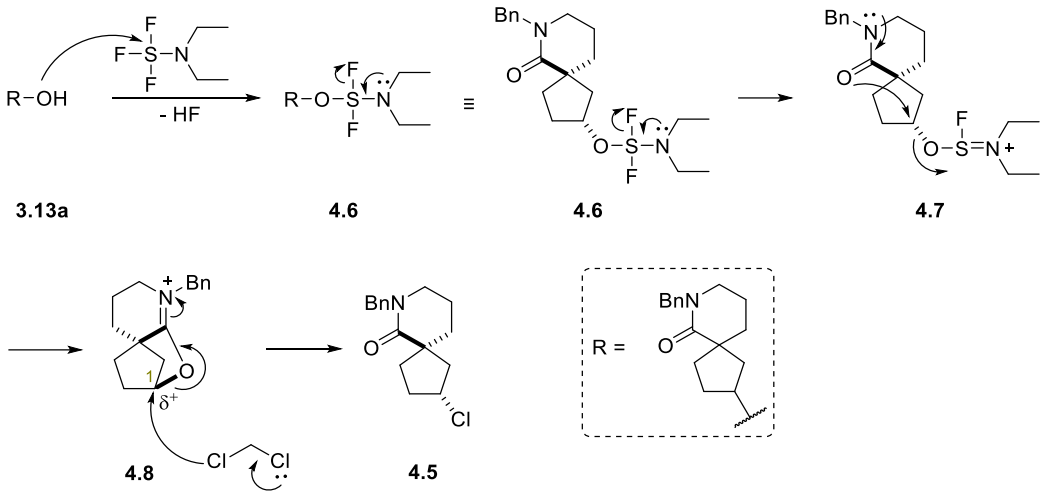

Scheme 4.4 Proposed mechanism for forming chloride **4.5** from alcohol **3.13a** with DAST.

Rodríguez *et al.* have reported the use of dihalomethane solvents as sources of halide ion to intercept cyclohexenyl cation intermediates (Scheme 4.6),[254,255] and the synthesis of Schwartz's reagent,[256] in which Cp_2ZrH_2 is treated with DCM to give Cp_2ZrHCl, is mechanistically related.

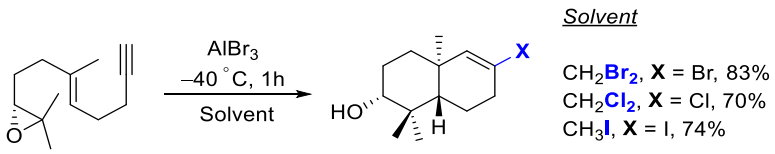

Scheme 4.5 Use of solvents for halide delivery reported by Rodríguez *et al.*

4.2.2.3 Hydrogen-borrowing Transamination

Many commonly employed strategies for overall *N*-alkylation with alcohols require multistep approaches in which the hydroxyl moiety is either activated as a leaving group for subsequent substitution, or is oxidised for reductive amination. In contrast, the hydrogen-borrowing catalysis approach enables efficient, one-step, functionalisation of alcohols in a variety of C−C and C−N bond-formation reactions.[257] Iridium-catalysed

hydrogen-borrowing transamination with aniline was performed to afford amine **4.9** in a moderate yield (Scheme 4.7).[258] With a catalyst loading of 2.5 mol%, the reaction was relatively clean and gave no other significant side products. The assigned relative configuration was based on NOE correlations, where the proton on C-4 that is *trans*- to the carbonyl group coupled to H-6, and H-3 coupled to the more shifted protons on C-4, i.e. protons that are *cis*- to the carbonyl group.

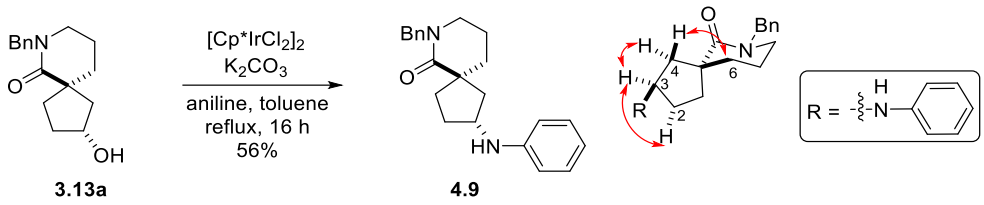

Scheme 4.6 Iridium-catalysed hydrogen borrowing amination.

4.2.2.4 Reductive Bis-alkylation

By analogy with the synthesis of 2-spiro substrate **2.44**, reductive bis-alkylation was attempted with lactam **3.13a** to afford α,α-dialkyl derivatives.[259] The hydroxyl group present was expected to interfere with the added Grignard reagent, ethylmagnesium bromide; therefore, it was protected as its TES derivative **4.10**.[260] In the event, the bis-alkylation conditions led to ethoxy lactam **4.11** with a 21% yield (Scheme 4.8); although its origin is unclear, it seems reasonable given the low yield to propose that ethyl triflate **4.12** formed from EtOMgBr potentially present in the Grignard reagent could alkylate the TES ether cleavage product **4.14**.

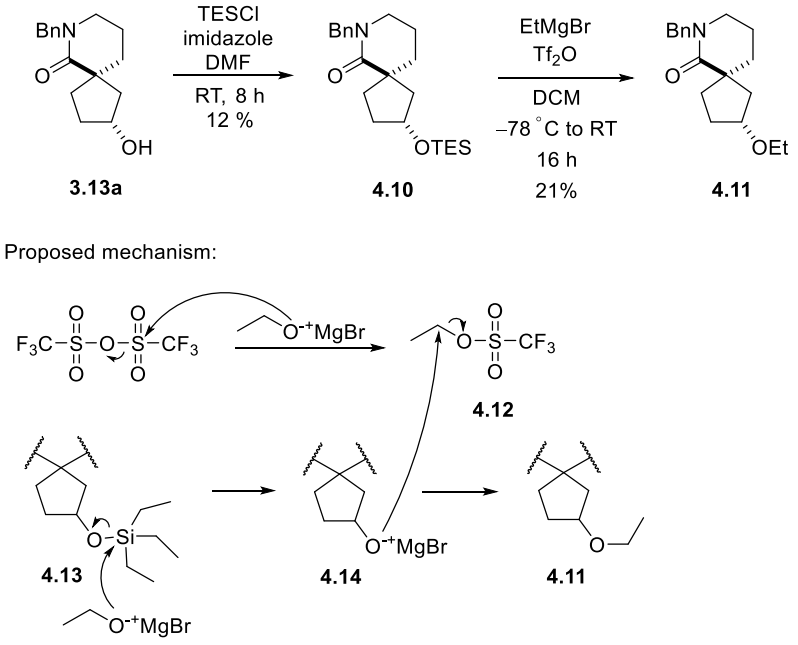

Scheme 4.7 Proposed mechanism for the formation of ethyl ether **4.11**.

4.2.2.5 Intramolecular C−H Amination

The ability of P450s to oxidise unreactive C−H bonds provides tremendous potential for this system to be harnessed in synthetic strategies based on C−H functionalisation. Turner *et al.* reported a one-pot, three-enzyme, biocatalytic cascade for the amination of unfunctionalised cycloalkanes through hydroxylated P450 metabolites.[261] $P450_{BM3}$ is employed for the first oxidation step, then an alcohol dehydrogenase (ADH) in combination with a reductive aminase (RedAm) is used to achieve the subsequent amination step (Scheme 4.9).

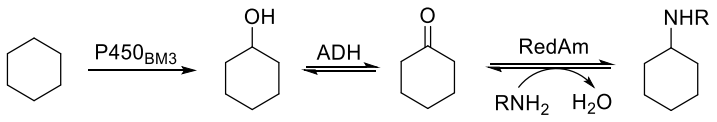

Scheme 4.8 One-pot, three-enzyme, biocatalytic amination reported by Turner *et al.*[261]

The introduction of amine moieties into pharmacophores improves their biological activities,[262] and C−N bond-forming reactions, particularly at inert C−H bonds, have been

heavily studied and continuously evolved throughout the past decades.[263] In this project, we studied the usage of the newly formed hydroxyl group as a tether for secondary C−H insertion processes, resulting in the double functionalisation of a bare -CH_2CH_2- linkage.

Rh(II)-catalysed aminations at unactivated C−H bonds, *via* oxidative cyclisation of sulfamates utilising Du Bois's chemistry, were found to be unsuccessful in unbiased substrates and only starting material was recovered (Scheme 4.10).[264] An extensive substrate and Rh(II)-catalyst scope was conducted by a previous D.Phil. student in the group, Zhang;[260] in this, results were disappointing.

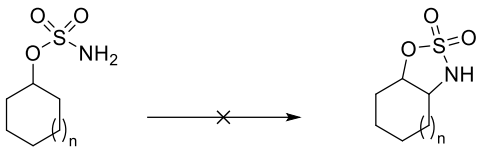

4.15 (*n*=1)
4.16 (*n*=2)

4.17 (*n*=1)
4.18 (*n*=2)

Scheme 4.9 Failed Rh(II)-catalysed C−H insertion of sulfamates in unbiased substrates.

In this project, the alternative approach reported by Schomaker *et al.* was explored, which involves intramolecular C−H amidation of β- or γ-C−H bonds through a ligand-controlled Ag catalyst system.[265,266,267] Model substrate pentyl carbamate **4.20**, derived from pentanol **4.19**, was tested (Table 4.2) since this was a direct homologue of one of the substrates reported in Schomaker's work. Using $AgClO_4$ as the pre-catalyst, and iodosobenzene as stoichiometric oxidant, different ratios of β- and γ-C−H inserted cyclic carbamates **4.21** and **4.22**, respectively, were observed as the ligand (**4.23**–**4.26**) was varied. According to Schomaker, the best γ-:β- selectivities were observed with ligands **4.23** and **4.24**, showcasing excellent tunability in activating C−H bonds. In our hands, the reactions proceeded with poor conversion; however, it was evident that pyridine-based ligand **4.23** did, indeed, favour β-C−H insertion but oxazoline-based ligand **4.24** did not promote γ-C−H insertion as reported (Entries 1 & 2). In addition, reactions with ligands **4.25** and **4.26**[266] were attempted (Entries 3 & 4) but these led to either no conversion or

low selectivity; Schomaker did not apply these two ligands on aliphatic systems and the reasons for their poor activity towards alkyl chains is not well elucidated.

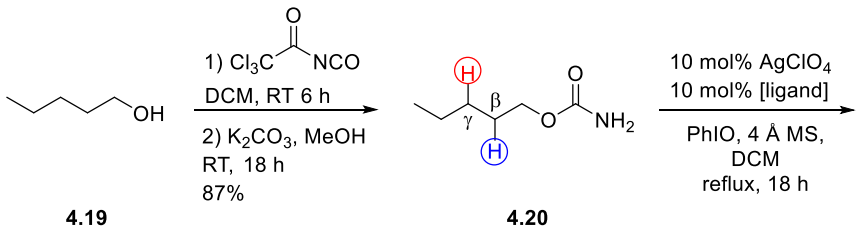

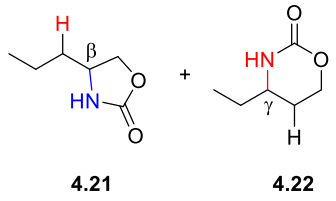

Ligand:

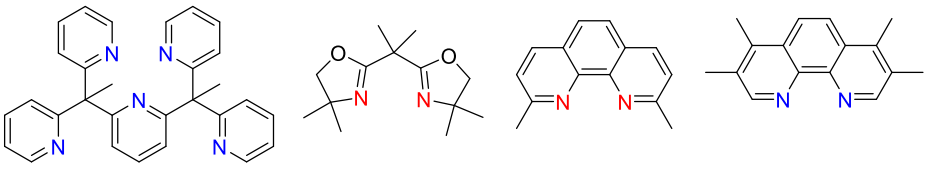

Entry	Ligand	4.20 : 4.21 : 4.22*
1	**4.23**	61 : 39 : 0
2	**4.24**	27 : 57 : 22
3	**4.25**	100 : 0 : 0
4	**4.26**	81 : 5 : 14

Table 4.26 Evaluation in model substrate **4.20** of Schomaker's Ag catalyst system for intramolecular C–H amidation; *Ratios are calculated from relative integrations of key resonances in the ^{1}H NMR spectra of crude products.

Schomaker's system was then tested with ligands Py_5Me_2 **4.23** and dmbox **4.24** on carbamates **4.29** and **4.30** derived from cyclohexanol **4.27** and cycloheptanol **4.28**, respectively (Scheme 4.11); however, the reactions failed to proceed and only starting material was recovered in both cases.

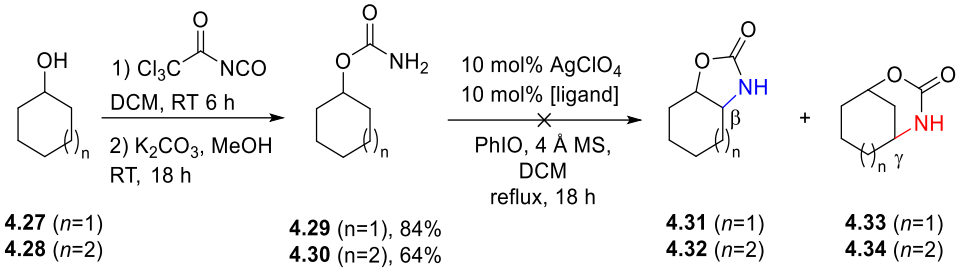

4.27 (*n*=1)
4.28 (*n*=2)

4.29 (n=1), 84%
4.30 (n=2), 64%

4.31 (*n*=1)
4.32 (*n*=2)

4.33 (*n*=1)
4.34 (*n*=2)

Scheme 4.11 Attempted Ag-catalysed C−H insertion reactions from cycloalkyl carbamates.

The same conditions were also tested with carbamate **4.35** (Scheme 4.12) with the same negative results.

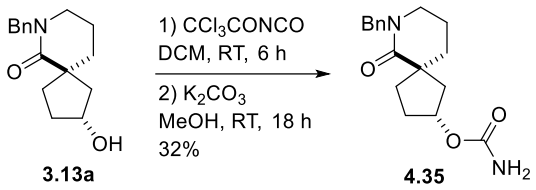

3.13a **4.35**

Scheme 4.12 Synthesis of carbamate **4.35** from lactam **3.13a**.

Alternative methods were then sought to achieve the desired C−H insertion reaction. He *et al.* reported a radical-mediated intramolecular C−H amidation reaction of trichloroacetimidates[268] in a close modification of Nagib's reagent system.[269,270] From Scheme 4.13, He's work followed method (B) and reported a 45% yield of aminoalcohol **4.40**; however, when model substrate **4.37** derived from cyclopentanol **4.36** was subjected to the same conditions, the ^{1}H NMR spectrum of the crude product was complicated and the signature peaks of **4.40** were absent. Subsequent attempts then employed method (A), in which the presumed but unisolated intermediate trichloro-oxazoline **4.38** was hydrolysed with *p*-toluenesulfonic acid as catalyst to furnish acetamide derivative **4.39**,[271] albeit in low overall yield.

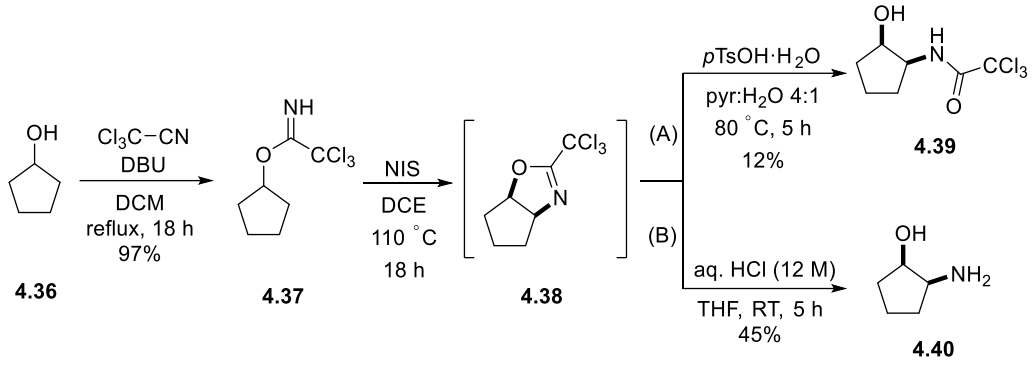

Scheme 4.13 He/Nagib intramolecular C−H amidation.

The mechanism is postulated to proceed by homolytic cleavage of *N*-iodoacetimidate **4.41** to give intermediate imidate radical **4.42** (Scheme 4.14);[268] 1,5-hydrogen atom transfer (HAT) then leads to radical **4.43**, which could then react with NIS or **4.41** to form iodinated **4.44**. Finally, cyclisation of the 1,2-*trans* diastereomer furnishes trichloro-oxazoline **4.38**.

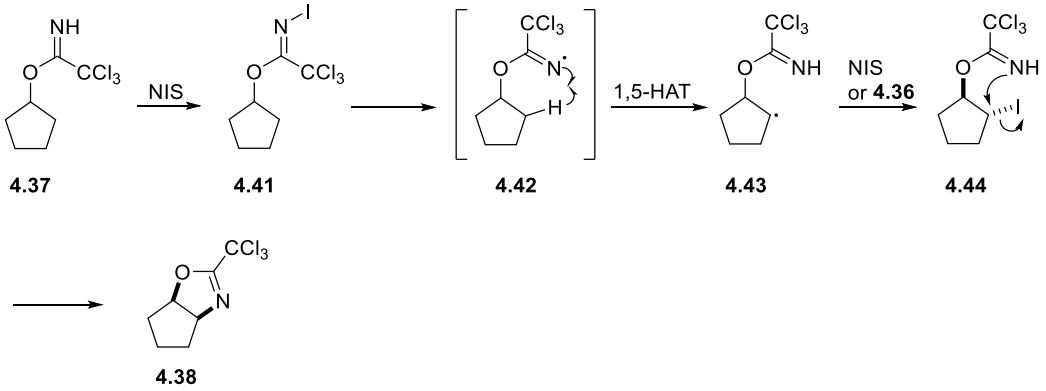

Scheme 4.14 Proposed mechanism of the formation of trichloro-oxazoline **4.38**.[268]

The conversion of metabolite **3.13a** into its imidate derivative **4.45** proceeded in poor yield (Scheme 4.15); however, there was sufficient material to attempt the NIS-mediated C−H insertion with immediate acid-catalysed hydrolysis as before. The ^{1}H NMR spectrum of the crude product showed numerous peaks in the 4.0–5.0 ppm region (Figure 4.2) which indicated the possibility of multiple C−H insertions or a variety of competing reactions. The three-dimensional structure of spirocycle **4.45** could allow insertions into the C−H bonds of the lactam ring, resulting in the formation of bridged-ring systems.

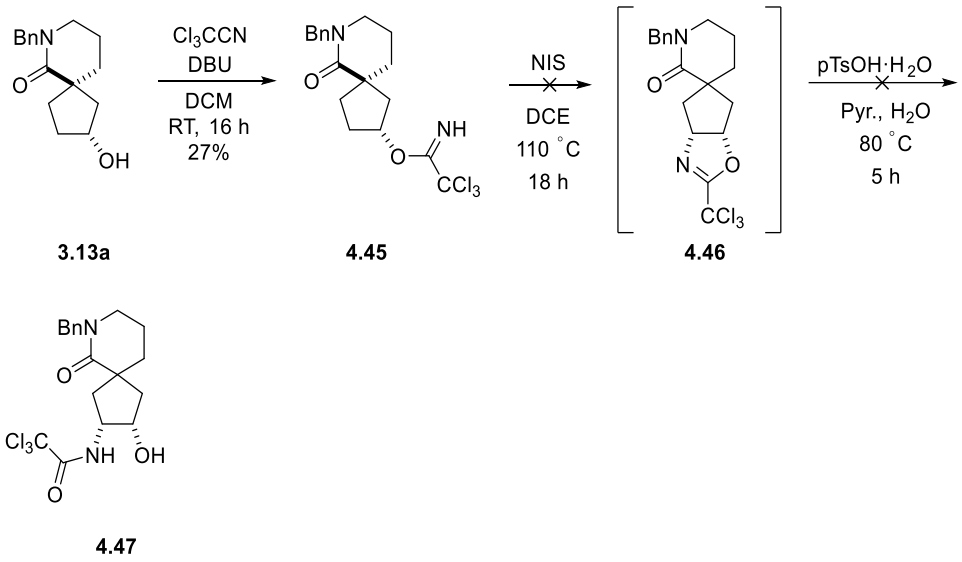

Scheme 4.15 Conversion of **3.13a** into trichloroacetimidate **4.45** and an unsuccessful attempt to achieve C−H amidation.

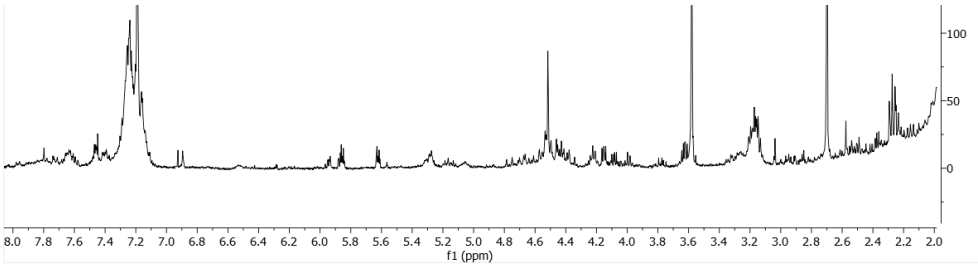

Figure 4.2 ^{1}H NMR spectrum of the crude product from the attempted NIS-mediated C−H insertion and hydrolysis of imidate **4.45**.

It was considered that the substrate might be thermally unstable; therefore, an NMR experiment was performed in which imidate **4.45** was heated with NIS in CD_2Cl_2 at 110 °C and the reaction progress was monitored hourly, looking for evidence of oxazoline intermediate **4.46**. It was evident that the substrate was mostly destroyed within an hour; no starting material was present and the ^{1}H NMR spectrum was already complex (Figure 4.3). The reaction conditions were therefore deemed too harsh and an alternative route was explored.

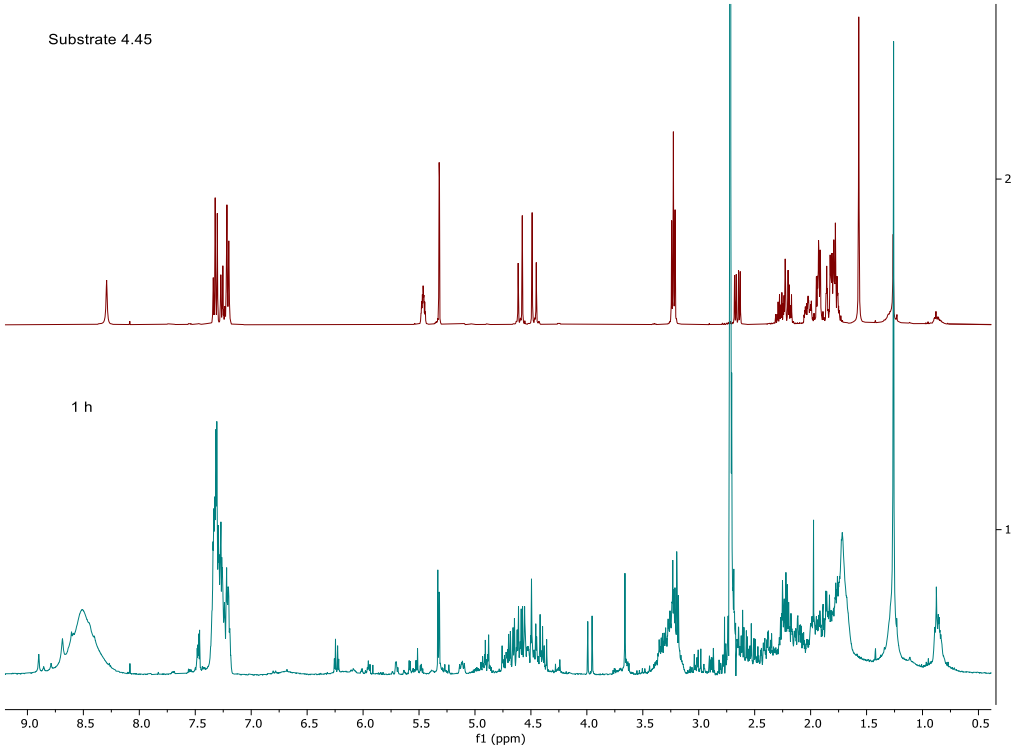

Figure 4.3 ^{1}H NMR spectrum of an attempted C−H insertion of **4.45** after one hour.

The previous D.Phil. student in the group to work on related transformations, Zhang, reported successful but non-selective intramolecular C−H insertions from azidoformates.[260] Azidoformates decompose thermally to eliminate molecular nitrogen, forming electron-deficient acylnitrenes[272] that can insert into proximal C−H bonds to create oxazolidinone derivatives.

Azidoformate derivative **4.48** (Scheme 4.16) was heated at reflux in TCE for 4 h to afford regioisomers **4.49** and **4.50** in a 2:1 ratio but within a complex product mixture. The formation of both products was confirmed by NMR analysis. Protons H-2 from both stereoisomers **4.49** and **4.50** overlapped at 5.27 ppm, which showed ^{1}H-^{1}H COSY coupling to protons H-3 (4.47 ppm) and H-1 (4.36 ppm) from **4.49** and **4.50**, respectively. Furthermore, both H-2 and H-3 from **4.49** coupled to H-1 and H-4 at 1.77 ppm and 2.63 ppm, respectively. On the contrary, H-2 in **4.50** only showed coupling to H-3 at 2.36 ppm. This marked the first successful C−N bond formation originating from a C−H insertion

product, underlining the potential of such an approach for the generation of structurally diverse scaffolds.

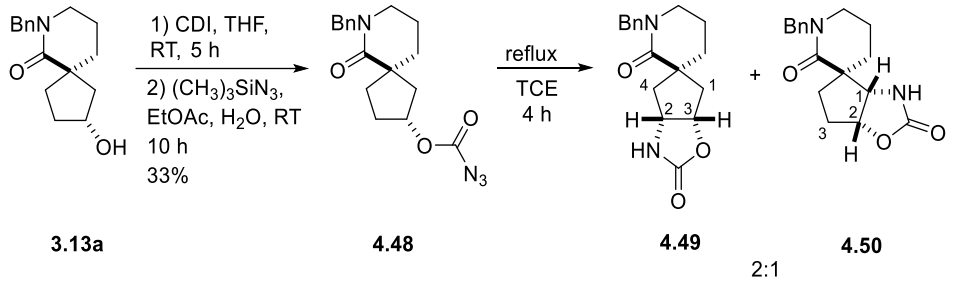

Scheme 4.16 Intramolecular C−H insertion *via* azidoformate **4.48**.

4.2.2.6 Kulinkovich–de Meijere Cyclopropanation

There has been a recurring appearance of cyclopropyl scaffolds in pharmaceutical compounds[273] and this is the 10th most frequent ring system incorporated in small molecule drugs.[273,274] The C−H bonds in cyclopropane are stronger (106 kcal/mol) compared to those in ethane (101 kcal/mol),[275] which implies that increased metabolic stability is achievable through cyclopropyl derivatives, since hydrogen atom abstraction by P450s would be more difficult.[273] Cyclopropane scaffolds can be found within drugs such as tasimelteon, a treatment for non-24 h sleep-wake disorder, and the anti-HIV drug nevirapine (Scheme 4.17).

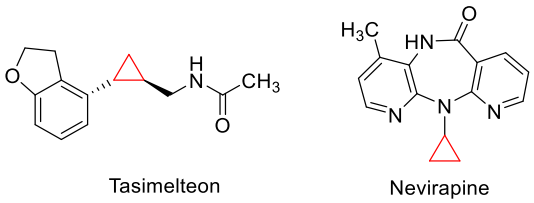

Scheme 4.17 Drugs containing cyclopropane scaffolds.

Prior to applying the reaction conditions on lactam **3.13a**, a test reaction was performed on *N*-benzyl δ-valerolactam **2.43** to give the expected cylopropanation product **4.52** efficiently (Scheme 4.18).[276] The product identity was supported by mutually coupling ^{1}H NMR resonances at 0.36 and 0.61 ppm consistent with the cyclopropane methylenes

in product **4.52**. It was considered that this product would be an interesting substrate for enzymatic screening (see §4.3) since it presents an opportunity to test the hydroxylation on a substrate containing a scaffold of pharmacological interest. To generate a more diverse substrate library, the *N*-Boc protected cyclopropane **4.53** was also sought; however, the Kulinkovich–de Meijere conditions applied to **4.51** led to ring-opened product **4.54**. It appears that isopropoxide ion liberated from the Ti(IV) reagent reacted with the more electrophilic carbonyl group in this substrate. The desired *N*-Boc spirocyclopropane **4.53** was prepared instead from **4.52** by a deprotection/protection sequence by analogy to that discussed in Chapter 2.

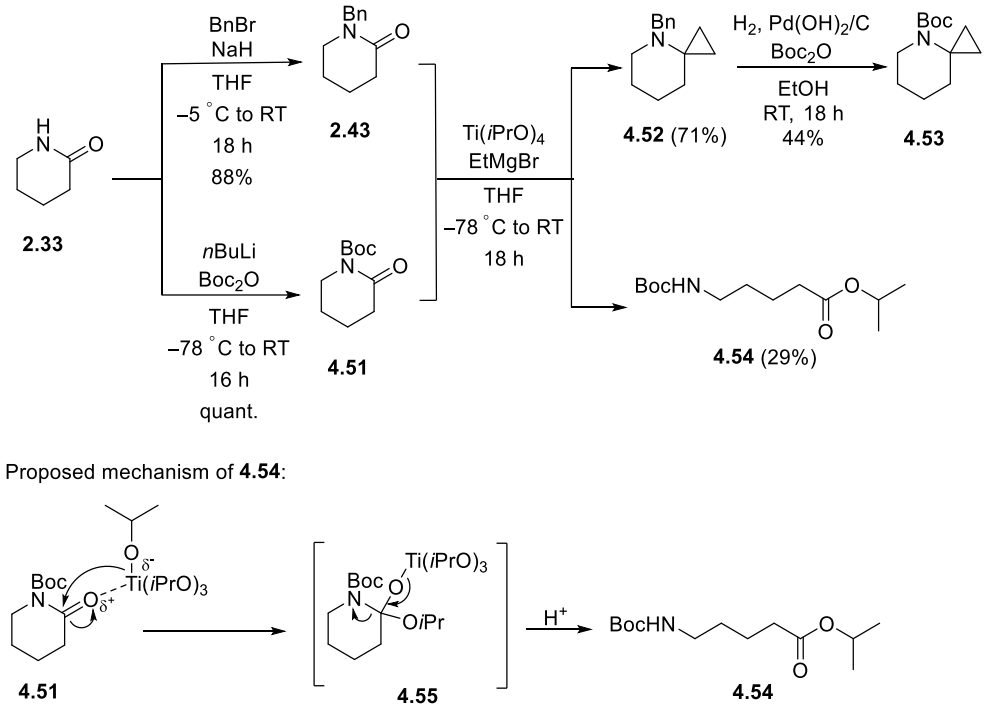

Scheme 4.18 Synthesis of simple substrates for Kulinkovich–de Meijere cyclopropanation and their reactions.

With this background, the Kulinkovich–de Meijere reaction conditions with titanium isopropoxide and ethylmagnesium bromide were applied to metabolite **3.13a** in an attempt to form cyclopropyl a mine derivative **4.56** (Scheme 4.19).[276] In practice, a complex mixture of products was obtained according to ^{1}H NMR spectroscopic analysis, which suggested the possible generation of unidentified diastereomeric side-products.

This crude mixture was treated with DMP in order to eliminate the stereogenic centre at the hydroxyl group and ease product characterisation but the ^{1}H NMR spectrum remained complex and no firm conclusion could be reached on the success or otherwise of the reaction.

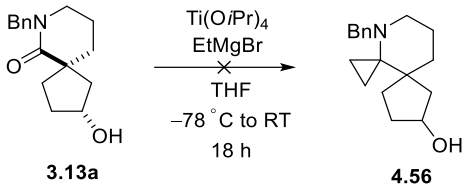

3.13a **4.56**

Scheme 4.19 Unsuccessful attempt of the Kulinkovich–de Meijere cyclopropanation on **3.13a**.

4.2.3 Diversification from Ketone 4.57

The ketone derived from the hydroxylated metabolite **3.13a** was also considered to have significant potential for diversification. To begin, metabolite **3.13a** was oxidised to ketone **4.57** with DMP (Scheme 4.20).[260] The ^{1}H NMR spectrum showed the crude product to be relatively pure apart from the by-product mono-acetoxy iodinane [δ_H = 7.72 (1H, td, *J* = 7.5, 1.0 Hz), 7.90 – 7.95 (1H, m), 8.00 – 8.03 (1H, m), 8.27 (1H, dd, *J* = 7.5, 1.5 Hz)], and no side products derived from the starting lactam were visible. The merely moderate isolated yield (48%) was explained by losses during purification, particularly from the need of multiple washes of the crude product in order to remove the iodinane by-product.

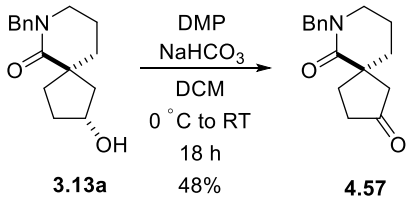

3.13a **4.57**

Scheme 4.20 DMP-mediated oxidation of **3.13a** to ketone **4.57**.

4.2.3.1 Baeyer–Villiger Oxidation

The Baeyer–Villiger (BV) oxidation achieves the conversion of ketones into esters and cyclic ketones into lactones,[277] providing general access to δ- and ε- lactones from cyclopentanones and cyclohexanones, respectively. Lactones **4.58** and **4.59** were successfully prepared from ketone **4.57** using mCPBA as oxidant and TFA as acid catalyst (Scheme 4.21).[278] As expected, there was little selectivity in this process, and the regioisomers were isolated as a 40:60 mixture. Assignment of each regioisomer was based on ^{1}H NMR spectroscopic analysis. The more shifted a-CH_2 resonances in lactone **4.58** were seen at 4.18 (d, J = 11.5 Hz) and 4.67−4.70 (d, J = 11.8 Hz) ppm, and showed no coupling to other protons. On the other hand, the a-CH_2 resonances in lactone **4.59** were seen at 4.36 (dt, J = 11.5, 5.0 Hz) and 4.51−4.58 (m) ppm, and exhibited clear coupling to the b-CH_2 multiplets at 1.71−1.80 and 2.35−2.40 ppm.

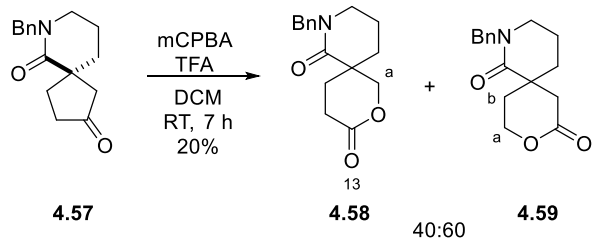

Scheme 4.21 Baeyer−Villiger oxidation of ketone **4.57**, forming lactones **4.58** and **4.59**.

4.2.3.2 Beckmann-type Rearrangement

The Beckmann rearrangement is a ubiquitous method for efficient conversion of acyclic ketooximes into amides and cyclic ketoximes into lactams and has gained prominence in the synthesis of pharmaceutical compounds and natural products.[279] One of its most important applications is in the synthesis of ε-caprolactam, the raw material in the production of Nylon-6.[279]

Beckmann rearrangement was attempted from ketone **4.57** using hydroxylamine-*O*-sulfamic acid (HOSA),[280] in which the activated amino group acts as a nucleophile,

leading to the formation of the corresponding oxime-*O*-sulfonic acid, from which subsequent Beckmann rearrangement would be catalysed by acetic acid as solvent to form the desired ring-expanded lactam(s). Unexpectedly, α,β-unsaturated ketone **4.60** was formed instead (Scheme 4.22), as reflected from the distinct doublets at 6.26 (J = 5.5 Hz) and 7.57 (J = 5.5 Hz) ppm corresponding to the alkene protons; such reactivity with this reagent does not appear to be documented in the literature. Again, it is proposed that this unusual outcome originates in the particular structural features of the substrate; here, it is proposed that the initial oxime-*O*-sulfonic acid **4.61** is in tautomeric equilibrium with enamine form **4.62** then 1,4-elimination of H_2SO_4, possibly facilitated in some way by the lactam functionality (see below), would lead to enone **4.60** via easily-hydrolysed imine **4.63**.

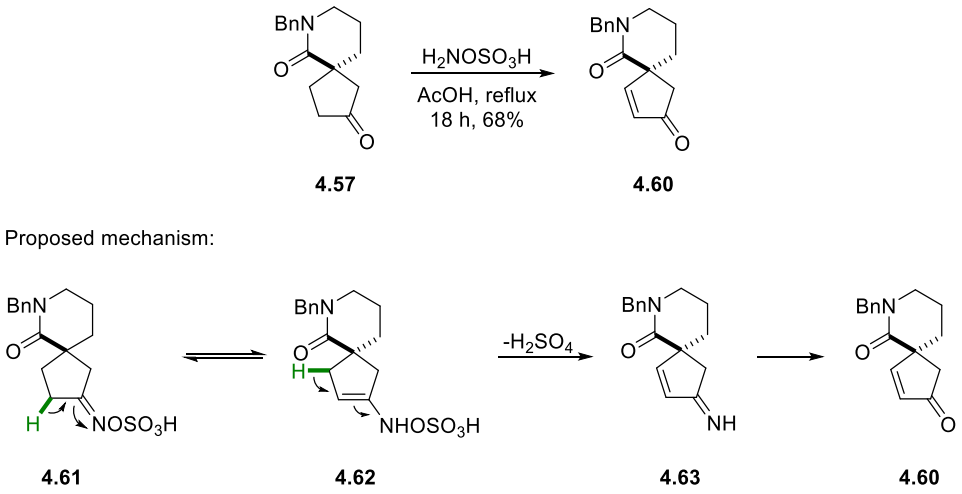

Scheme 4.22 Proposed mechanism for the formation of enone **4.60**.

Applying the same conditions to substrates **4.64** and **4.65**, however, successfully furnished Beckmann products **2.33**, **4.66**, and **4.67** (Scheme 4.23),[280,281] supporting the idea that the spirocyclic ketolactam **4.57** possesses special reactivity as a consequence of its structure.

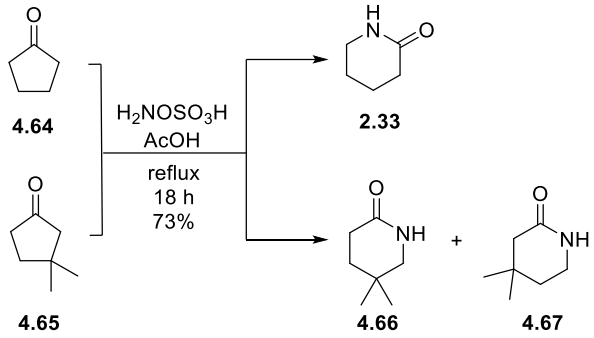

Scheme 4.23 Beckmann rearrangement test reactions.

During this study ketone **4.57** was able to be crystallised as a single diastereomer by solvent diffusion (DCM/heptane) and the structure was confirmed by single crystal X-ray crystallography (Figure 4.4). The structure reveals the proximity of the lactam carbonyl to *cis*-disposed protons on the cyclopentanone ring. A computer model of an enamine corresponding to intermediate **4.62** was constructed, with N-OH present instead of N-OSO_3H. A conformational search[*] was performed and the lowest energy conformations revealed the proximity of the C=O group to H_a on the beta C−H bond; therefore, in principle it can act as a general base catalyst for the conversion of intermediate **4.62** into **4.63** and and hence product **4.60**. This provides an explanation for the analogous reactions of non-spirocyclic substrates **4.64** and **4.65** that did not generate α,β-unsaturated ketones.

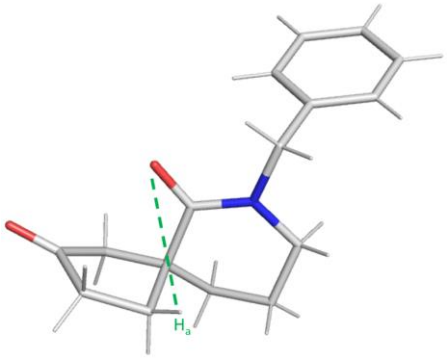

Figure 4.4 X-ray crystal structure of ketone **4.57** showing the proximity of the lactam oxygen with *cis*-disposed protons in the cyclopentanone ring.

[*] Calculations performed by J. Robertson using *Spartan'20*. A Monte Carlo conformation search was performed using the MMFF forcefield; the lowest 10 conformations were individually energy minimised using DFT (B3LYP/6-31G*). The lowest energy conformations showed the C=O bond to be close to the β C−H bonds, indicating the possibility of the carbonyl group to act as a general base for the 1,4-elimination.

4.2.3.3 Beckmann Rearrangement

After the unsuccessful attempt to effect the Beckmann rearrangement as a one-step process with HOSA, the reaction was conducted in two steps via oxime **4.68** (Scheme 4.24) [282] to afford lactam regioisomers **4.69** and **4.70** in a 1:1 ratio.[283]

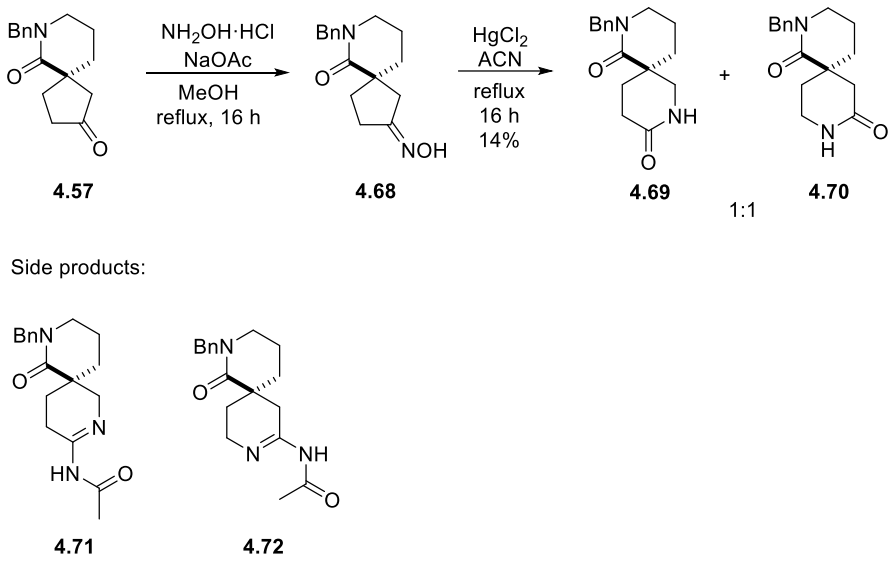

Scheme 4.24 Beckmann rearrangement *via* oxime **4.68**.

Acetamides **4.71** and **4.72** were identified as side-products of the reaction. The proposed mechanism for their formation, mediated by solvated[284] Hg(II) ion, is outlined in Scheme 4.25. Rearranged cations equivalent to **4.74** and **4.76** cannot be well stabilised by the adjacent nitrogen because the so-formed nitrilium ions would be too strained; consequently, their high reactivity leads to rapid trapping by CAN to generate the much more stable linear nitrilium ions **4.75** and **4.77** that are sufficiently long-lived to be trapped by water liberated in the first step of the process.

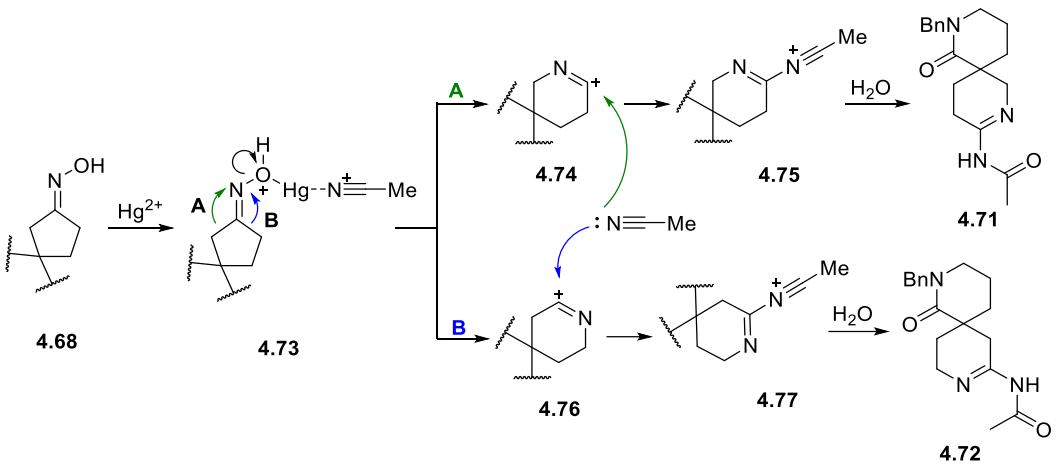

Scheme 4.25 Proposed mechanism for the formation of side-products **4.71** and **4.72**.[283]

4.2.3.4 Grignard Reaction

The Grignard reaction is one of the most widely employed processes for C−C bond formation[285] and Grignard reagents are central for organic synthesis in academia and in industry.[284] A representative example of such a reaction was conducted with ethynylmagnesium bromide in order to provide a functionalised carbon substituent from which many further transformations could be envisaged (deprotonation/alkylation, Sonogashira cross-coupling, hydrolysis, hydroboration and oxidation, reduction and cross metathesis, etc). The product, alkyne **4.78** was successfully prepared as a mixture of unassigned diastereomers in a ratio of 2:1 (Scheme 4.26).[286] This was confirmed by the ^{1}H NMR resonance of the alkynyl proton, which appeared as singlets at 2.43 and 2.51 ppm for the minor and major diastereomer, respectively.

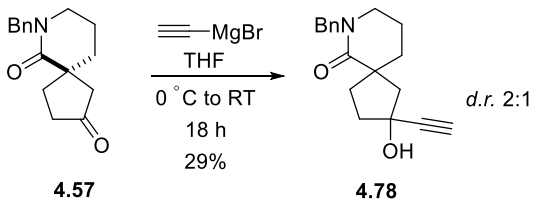

Scheme 4.26 Grignard reaction of **4.57** with ethynylmagnesium bromide for the formation of terminal alkyne **4.78**.

4.2.3.5 Carbonyl Olefination

The regiospecific synthesis of olefins from carbonyl derivatives is another essential transformation in organic synthesis[287] for which the Wittig reaction is one of the most popular options. When applied to a model substrate (**4.79**),[288] Wittig product **4.80** was achieved and isolated in moderate yield (Scheme 4.27); however, application of the same conditions to ketone **4.57** led only to the recovery of starting material. Horner–Wadsworth–Emmons (HWE) and Peterson olefinations, with phosphonate salts and α-silyl carboanions,[289,286] respectively, similarly gave no desired products and only ketone **4.57** was recovered.

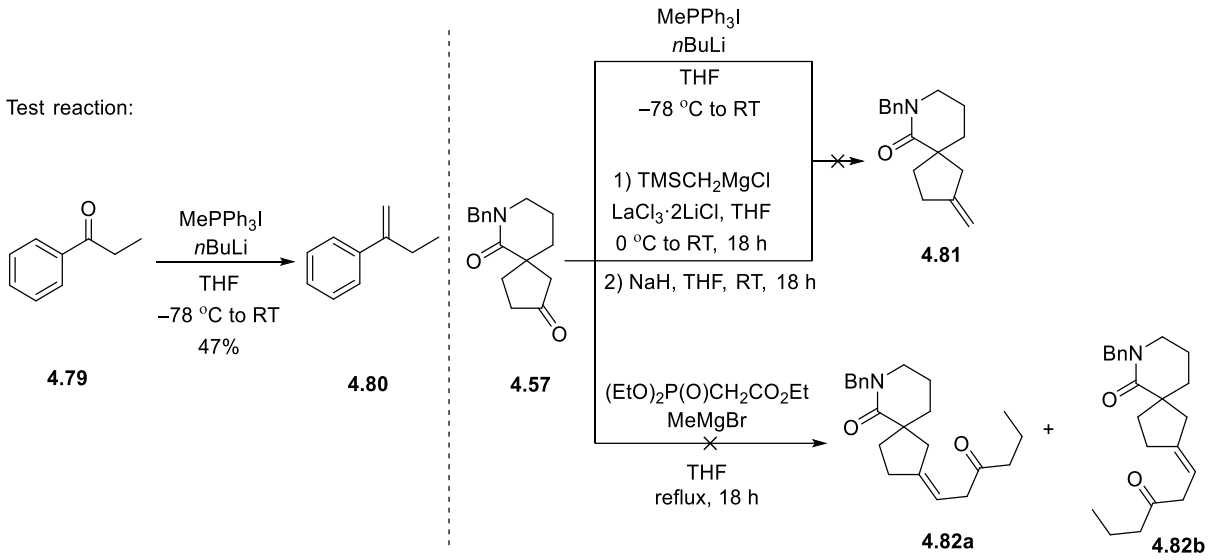

Scheme 4.27 Attempted Wittig, Peterson, and HWE reactions.

Finally, the Petasis olefination with dimethyltitanocene was tested successfully to afford *exo*-olefin **4.83** in 54% yield, as supported by the olefinic resonances at 4.90 ppm (m) in the ^{1}H NMR spectrum (Scheme 4.28).[290]

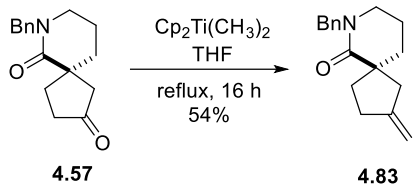

Scheme 4.28 Petasis olefination of **4.57**.

The reason for the failed olefinations using methods with relatively basic carbon nucleophiles (phosphorus ylid, phosphonate salt, α-silyl carbanion) is most likely due to the steric hindrance imparted by the lactam carbonyl (*cf.* Figure 4.4); this both impedes access to the carbonyl carbon and destabilises the transition state leading to the primary (tetrahedral) adduct. Because carbonyl addition is slowed, basic reagents probably deprotonate α-ketonic hydrogens, leading to epimerisation if the site is a chiral centre, and either return of starting ketone upon work-up or secondary reactions. The Petasis reagent has the unique advantage of being relatively non-basic, hence does not risk epimerising α-keto stereogenic centres, and effectively smaller which renders it more capable of reacting with sterically hindered carbonyl groups.[291]

4.2.4 Conclusion and Future Work on Fragment Diversification

From metabolite **3.13a**, the use of the hydroxyl group as a synthetic handle to carry out further diversifications has been exemplified by a series of non-trivial transformations, as summarised in Schemes 4.29 and 4.30.

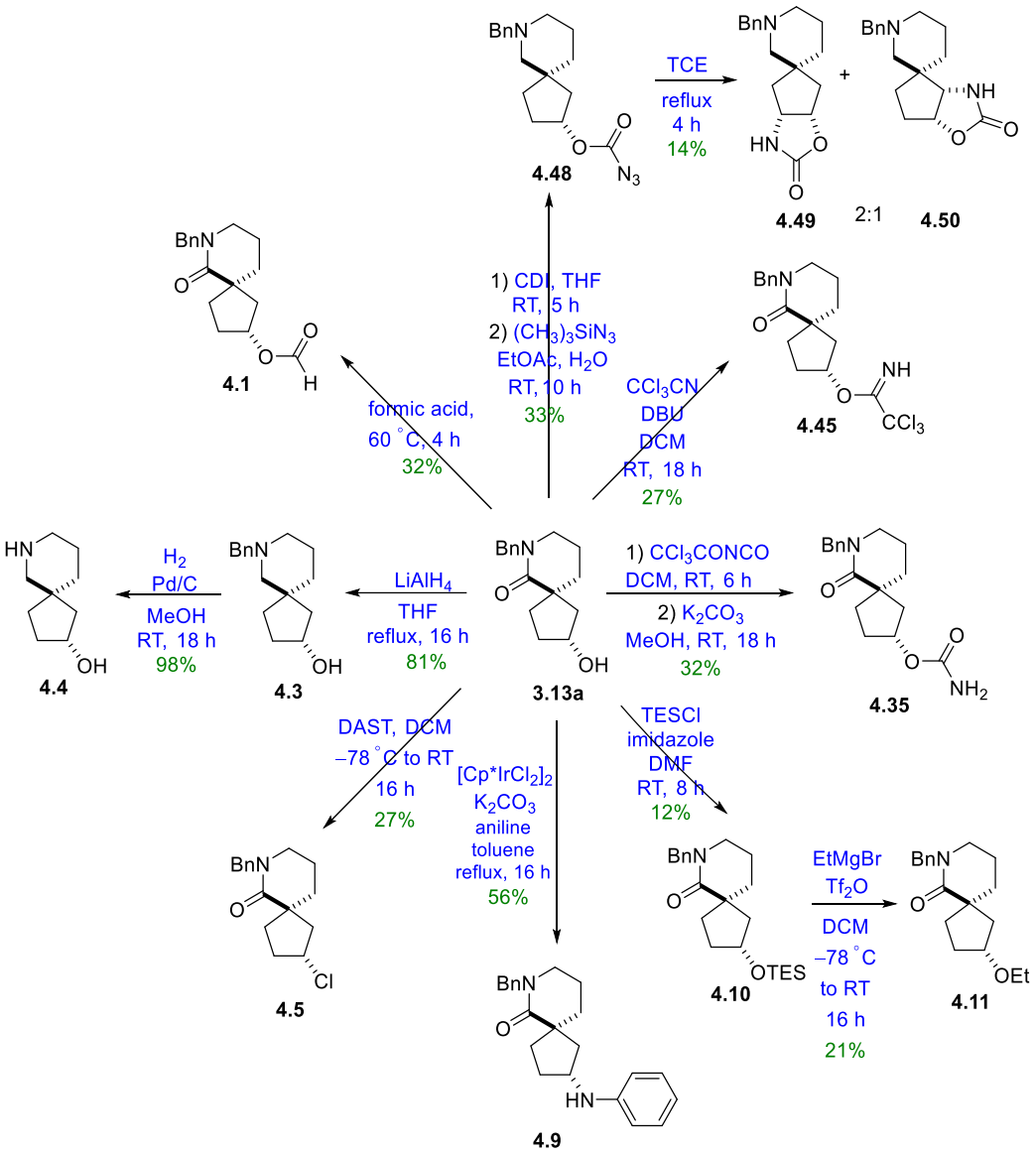

Scheme 4.29 Summary of successful diversification reactions with alcohol **3.13a** as substrate.

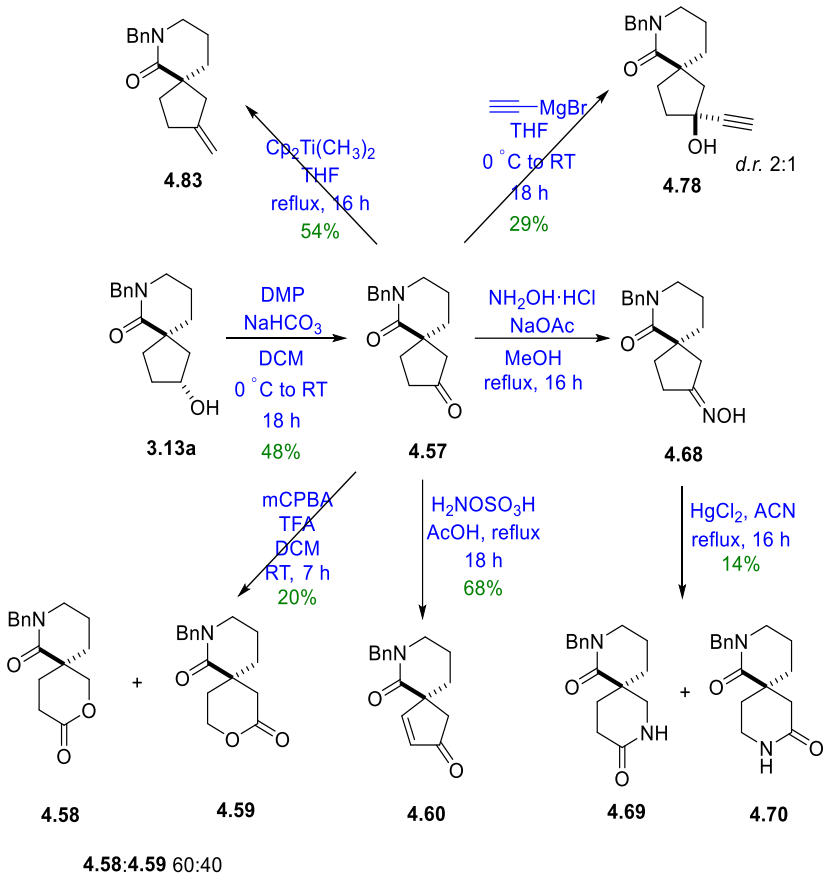

Scheme 4.30 Successful diversification reactions with ketone **4.57** as substrate.

A variety of reactions were conducted – from the widely-employed Grignard reaction to more complex transformations such as C−H insertions and hydrogen-borrowing aminations – that, collectively, illustrate the possibility of creating a focused fragment-molecule library *via* hydroxylated metabolites from $P450_{BM3}$ catalysis. Future investigations could focus on expanding such a library by exploring more sophisticated transformations including further biocatalytic reactions or oxidative functionalisation of the C(OH)-H bond by radical addition (Scheme 4.31).[292]

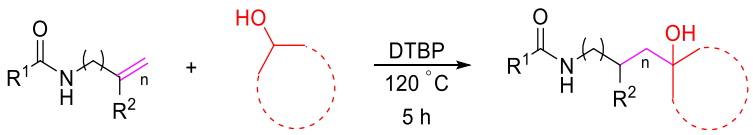

Scheme 4.31 DTBP-promoted oxidative functionalisation of C(OH)-H bonds.

4.3 Screening of *N*-protected 4-azaspiro[2.5]octane with P450$_{BM3}$

The *N*-Bn and *N*-Boc protected [6.3]-spirocycles **4.56** and **4.58**, respectively, were screened against 48 variants from the "common" plates at an enzyme ratio of 1000:1. The main objective was to investigate the possibility of cyclopropane hydroxylations, since cyclopropane motifs are highly significant in drug discovery and biologically active natural products.[293] In the event, none of the major metabolites indicated hydroxylations on the cyclopropane ring (Table 4.3), probably as a consequence of the inaccessibly high C−H bond strength (106 kcal/mol).[275]

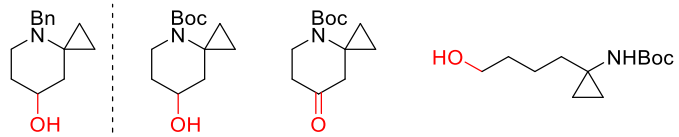

4.56a **4.58a** **4.58b** **4.58c**

PG	Mutant	Conv. (%)	Product	Select. (%)	e.e. (%)	Yield (%)
Bn-	R19/I263A/A328L	34	**4.56a**	92	33	11
Boc-	GV/A184I	100	**4.58a**	20	-	14
	K19/F87A/I263G	100	**4.58b**	19	-	8
	R19/S72G/A330W	97	**4.58c**	63	-	10

Table 4.3 Summary of all metabolites identified from substrates **4.56** and **4.58**.

4.3.1 *N*-Bn-protected 4-azaspiro[2.5]octane (*N*-Bn [6.3]spirocycle, 4.56)

In order to isolate the major metabolites from substrate **4.56**, preparative scale reactions were carried out on a 0.2 mmol scale. Similar to the *N*-Bn 2-spiro analogue **2.45** discussed in Chapter 2, spirocycle **4.56** also did not exhibit a diverse metabolite profile. The only major metabolite was characterised as γ-OH **4.56a** (Figure 4.5). Despite the low conversion, as depicted by the GC trace (in blue), mutant R19/A184I/A328L gave the highest selectivity for the product (92%). The preparative-scale reaction was, therefore, compromised by the need for a longer reaction time to allow greater substrate conversion.

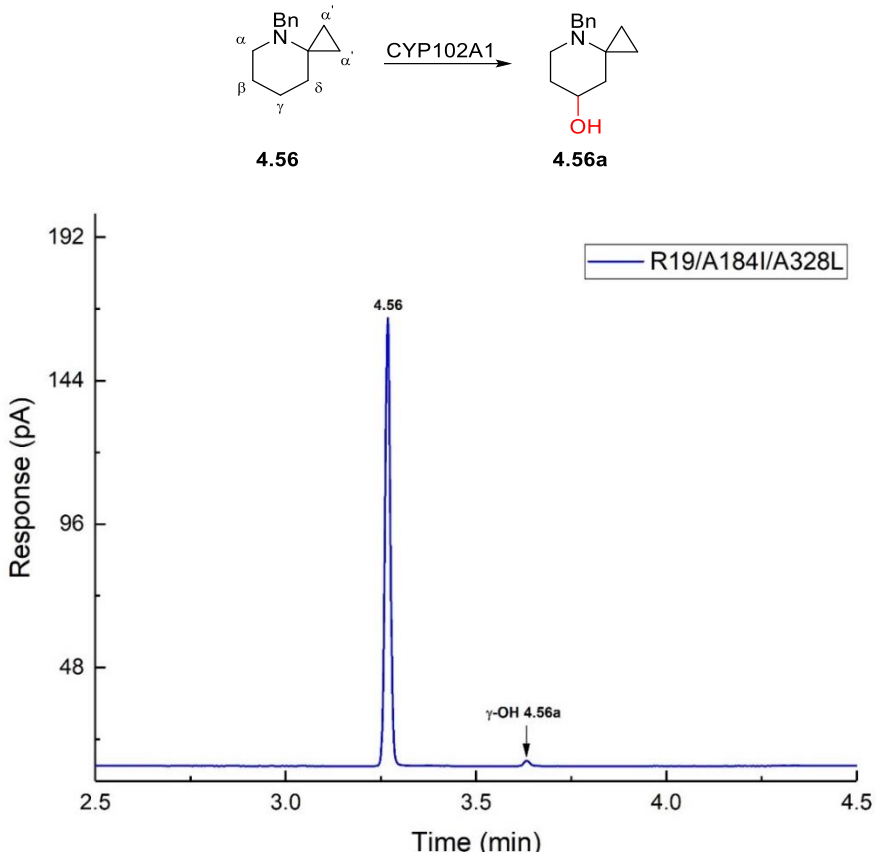

Figure 4.5 GC analysis of the product mixture from substrate **4.56** with the selected variant shown, giving oxidation product **4.56a**.

The conversion rates for substrate **4.56** were all low, with only two out of 48 mutants showing ≥50% conversion. As mentioned in Chapter 2, the low activity could be due to the basicity of the *N*-atom, which interacts with the haem system, causing the enzyme-substrate complex to be rendered inactive. Similar results reporting the low reactivity of *N*-benzyl-protected amines were found previously in the Wong group. There were no obvious trends on mutations that promoted higher conversion.

From Table 4.4, it is evident that the combination of mutations on residues I263 and A328 enhanced γ-oxidation (Entries 2, 5 & 8). Specifically, the change of residue I263 to a smaller residue, i.e. Gly and Ala, promoted the effect. Each individual mutation, i.e. I263 and A328, in mutants GV/L188Q/I263G and R19/F87A/A328L, however, did not demonstrate effects as pronounced as when combined together (Entries 4 & 10). In some cases, the selectivity for **4.56a** even decreased (Entries 4 & 12). This suggests that the combination of I263 and A328 might exhibit certain synergistic effects.

Entry	Mutant	Conv. (%)	4.56a (%)	Others (%)
1	GV/A184I	34	0	100
2	GV/A184I/I263G/A328G	3	20	80
3	GV/L188Q	6	14	86
4	GV/L188Q/I263G	14	0	100
5	GV/L188Q/I263G/A328L	26	54	46
6	GV/L188Q/A328G	6	7	93
7	R19	13	11	89
8	R19/I263A/A328L	34	92	8
9	R19/F87A	25	5	95
10	R19/F87A/A328L	2	38	62
11	K19/F87V	5	13	87
12	K19/F87V/I263G	19	0	100

Table 4.4 Selected screening data for substrate **4.56**. Full screening data in Chapter 7.

4.3.2 *N*-Boc-protected 4-azaspiro[2.5]octane (*N*-Boc [6.3]-spirocycle, 4.58)

The *N*-Boc [6.3]-spirocycle **4.58** gave a more diverse metabolite profile in comparison with the *N*-Bn substrate **4.56**. The enzymatic activity towards **4.58** was also significantly higher, with 43 out of 48 variants showing >90% conversion. Preparative-scale reactions were carried out on a 0.2 mmol scale and the major metabolites were identified as γ-OH **4.58a**, γ-ketone **4.58b**, and α-OH-derived **4.58c**. (Figure 4.6).

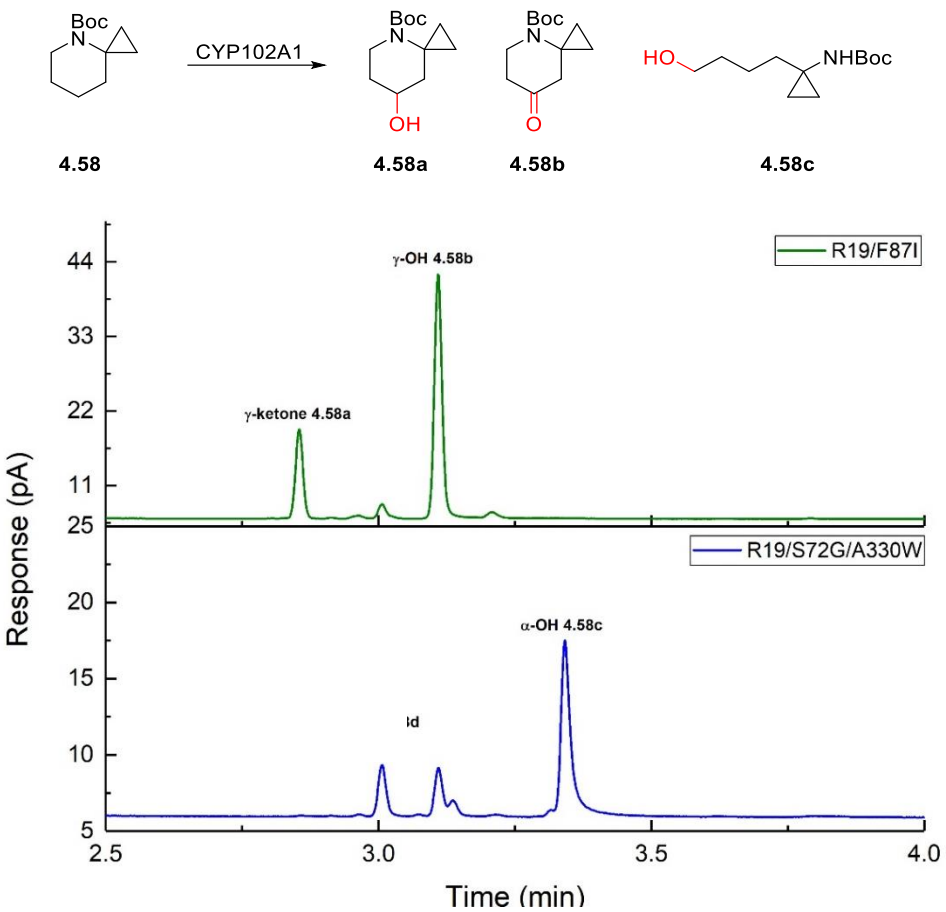

Figure 4.6 GC analysis of the product mixture from the reactions of selected variants with substrate **4.58**.

Akin to Bn-protected spiroamine **4.56**, the change of I263 to a smaller residue and substitution on A328 promoted γ-oxidation to form alcohol **4.58a** (Table 4.5, Entries 2, 4 & 10). The combination of V78I/A328I within mutant R19/V78I/F87A/A328I also increased selectivity for **4.58a** (Entry 14). In these combinations, further oxidation of the product to generate γ-ketone **4.58b** is disfavoured (Entries 2, 4, 10 & 14). On the other hand, mutations E267V and Q403P within mutant K19/F87V/E267V/Q403P encouraged further oxidation of the γ-OH product (Entry 7 & 8). Mutation A330W appeared to promote selectivity for α-OH-derived **4.58c** (Entry 11); the addition of S72G further enhanced the effect, increasing the selectivity to 63% (Entry 12).

Entry	Mutant	Conv. (%)	4.58 a (%)	4.58 b (%)	4.58 c (%)	Others (%)
1	GV/A184I	100	20	26	2	52
2	GV/A184I/I263G/A328G	100	45	8	20	11
3	GV/L188Q	99	72	13	0	9
4	GV/L188Q/I263G/A328L	94	64	1	10	22
5	GV/L188Q/I263G	97	54	5	8	13
6	K19/F87V	99	73	12	0	9
7	K19/F87V/E267V	100	37	27	0	34
8	K19/F87V/Q403P	100	41	29	1	29
9	R19	99	67	3	15	6
10	R19/I263A/A328L	95	95	0	0	3
11	R19/A330W	99	15	0	50	8
12	R19/S72G/A330W	97	13	0	63	9
13	R19/F87A	98	15	15	1	66
14	R19/F87A/V78I/A328I	98	80	6	4	8

Table 4.5 Selected screening data for substrate **4.58**. Full screening data in Chapter 7.

4.3.3 Computational studies on *N*-Bn and *N*-Boc [6.3]-spirocycle 4.56 and 4.58

By analogy to the previous spirocyclic analogues screened, docking was performed to provide some insight into substrate-enzyme interactions and comparisons between computational and experimental results.

As mentioned in previous chapters, all the substrates discussed thus far had employed the rigid docking approach; however, when the rigid docking method was employed with mutant R19/I263A/A328L with spirocycle **4.56** as ligand, no productive proses were generated. In rigid docking, ligand flexibility is modelled whereas receptor flexibility is not; i.e., conformational changes at receptor side-chains are not accommodated. This disadvantage of rigid docking becomes more prominent when there are bulky residues present in the active site within the substrate recognition region. In mutant R19/I263A/A328L, no substitutions are made at Phe87, which is found in the lumen of the substrate access channel in $P450_{BM3}$ and in proximity to the haem iron.[125] It is speculated that the large size of the phenyl ring could impose a significant effect on substrate binding, depending on its orientation and the existing amino acid conformer. If the conformation of F87, as computed from MD simulation, is not favoured, a minimal

number of productive poses will be generated when the rigid docking method is applied, since receptor flexibilities are absent. As such, an alternative docking method – AutoDock for Flexible Receptors (ADFR) – was performed. The ADFR programme permits receptor flexibility by allowing explicit specification of a set of receptor side-chains *a priori*. It has been shown that a higher docking success rate can be achieved with ADFR,[294] most likely due to the inclusion of receptor flexibility, which provides an opportunity for specified residues to explore their conformational spaces, while searching for energetically favourable poses for a given ligand.

As Figure 4.7 shows, the differences between the F87 residues from ADFR (orange) and rigid docking (light orange) were not substantial, yet the rigid docking method generated a non-productive pose (blue), while ADFR gave two productive poses (light blue). This further supported the expectation that the orientations of bulky residues present within the active site would exert dramatic effects in ligand binding.

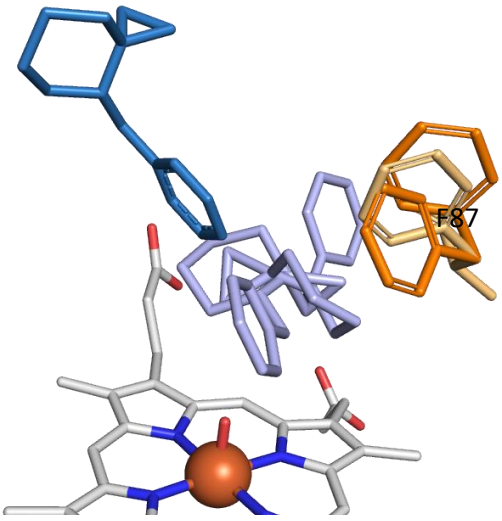

Figure 4.7 Overlaying poses from ADFR (light blue) and rigid docking (blue) of substrate **4.56** on mutant R19/I263A/A328L, along with the difference between the F87 residue from ADFR (orange) and rigid docking (light orange).

Analogous to the work described in previous chapters, a dot plot was generated for substrate **4.56** and mutant R19/I263A/A328L (Figure 4.8) from which it is apparent that the large majority of poses are non-productive and only three poses are productive, of

which two poses are compatible with α′-hydroxylation (that is, of the cyclopropyl group). None of the poses are compatible with γ-hydroxylation, which was the major metabolite produced experimentally.

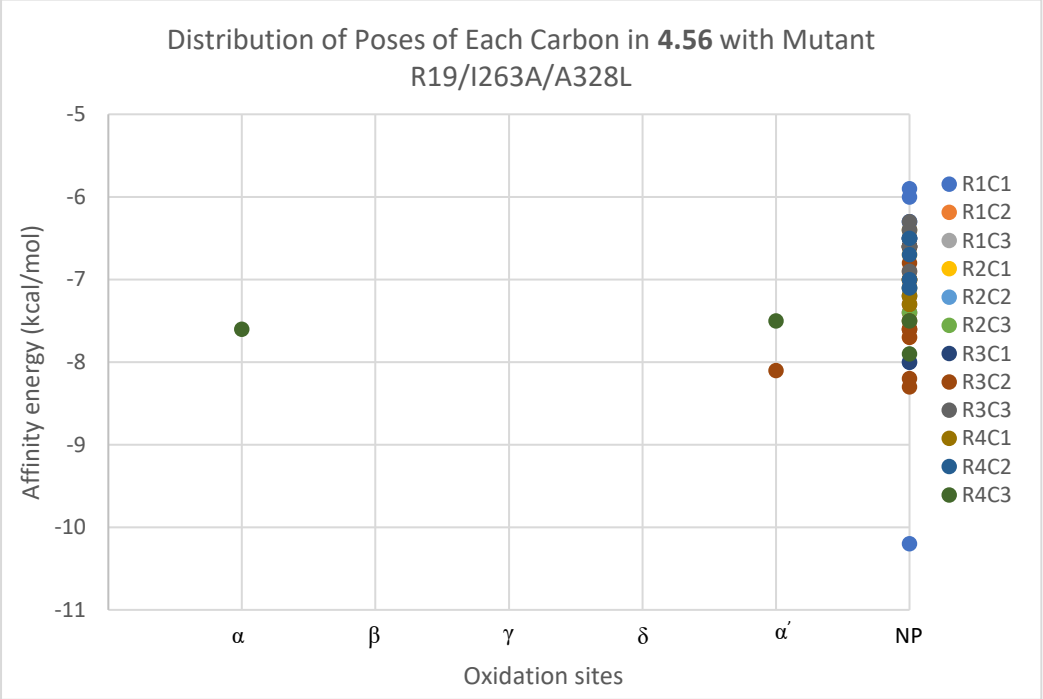

Figure 4.8 Distribution of poses, and calculated affinity energies, for oxidation at each carbon in *N*-Bn substrate **4.56** with mutant R19/I263A/A328L.

For *N*-Boc protected substrate **4.58**, the rigid docking approach was applied, since a substitution was present at F87 (F87V). As Figure 4.9 illustrates, just over half the poses were classified as non-productive (61/108), while the remaining 47 productive. The most likely carbons to be hydroxylated as predicted from docking are the β- and γ-carbons as they shared an equal number of poses (12/47 each). This is broadly consistent with the experimental results, since the γ-alcohol **4.58a** was the major metabolite isolated (Figure 4.4). On the other hand, this docking predicted hydroxylation to be possible on the cyclopropyl ring (the α′-site); however, this was not observed experimentally because of the high cyclopropyl C−H bond strength as mentioned above.

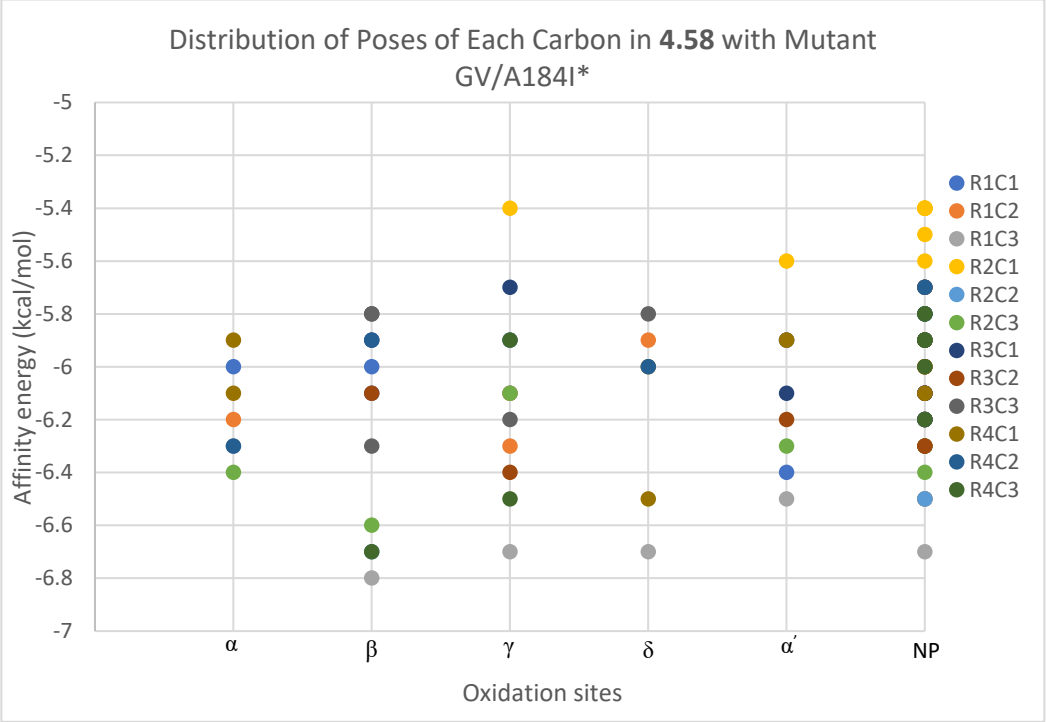

Figure 4.9 Distribution of poses, and calculated affinity energies, for oxidation at each carbon in *N*-Boc substrate **4.58** with mutant GV/A184I. *Numerous poses had identical affinity energies and they are presented under one spot.

4.3.4 Conclusion and Future Work on the [6.3]-Spirocycle Series

Two *N*-protected [6.3]-spirocycles were synthesised and screened against a panel of 48 $P450_{BM3}$ mutants and one (Bn) and four (Boc) metabolites were identified, respectively. The main interest in studying the enzymatic activities of this spiro-series was to explore the potential of achieving hydroxylations on the cyclopropyl ring but none of the major metabolites identified showed such hydroxylation products. As mentioned already, this is almost certainly due to the strong C−H bond dissociation energy (BDE) in cyclopropanes which is the highest (106 kcal/mol) among simple carbocycles such as cyclopentane (~95 kcal/mol) and cyclohexane (~97 kcal/mol).[295,296] In fact, no literature precedent has been found for $P450_{BM3}$-mediated hydroxylations of cyclopropyl rings, further supporting the difficulty of enzymatic oxidation at these positions.

Future research could consider evaluating other enzymes, such as methane monooxygenase, which has been reported to achieve cyclopropane and small-ring

oxidations.[297,298] Substrate engineering can also be explored in order to achieve desired oxidations and product variations.

Chapter 5: Docking-guided Mutagenesis

5.1 Overview

As discussed in Chapter 3, the selectivity in favour of particular metabolites can be optimised by protein engineering, specifically through modifications of the enzymes' amino acid sequences. Molecular docking approaches can be used to model the interactions between the ligand and its binding receptor. This elucidates the structural characteristics of the ligand-receptor complex, which can be used as a guide to the amino acid residues that potentially influence substrate binding. This chapter discusses the results of implementing docking-guided mutagenesis in an attempt to improve the selectivity of one of the metabolites; namely, α′-hydroxylated *N*-Boc 3-spiroamine **3.13c**. In addition, the exploration of different methods of docking and their comparisons with experimental data are discussed.

5.2 Initial Docking Study for *N*-Boc 3-spiroamine

5.2.1 First Generation Mutagenesis (R19/A184I/A328L)

Boc-protected 3-spiroamine **3.13** was chosen due to its diverse profile of metabolites and relatively high reactivity towards the enzyme panel. As noted in Figure 5.1, mutant K19/F87V/E267V gave 100% selectivity for the production of β′-OH **3.13a**, whereas the highest selectivity for metabolite **3.13c** was only 40%, with mutant R19/A184I/A328L. This latter mutant was therefore selected as the starting point from which to perform docking studies.

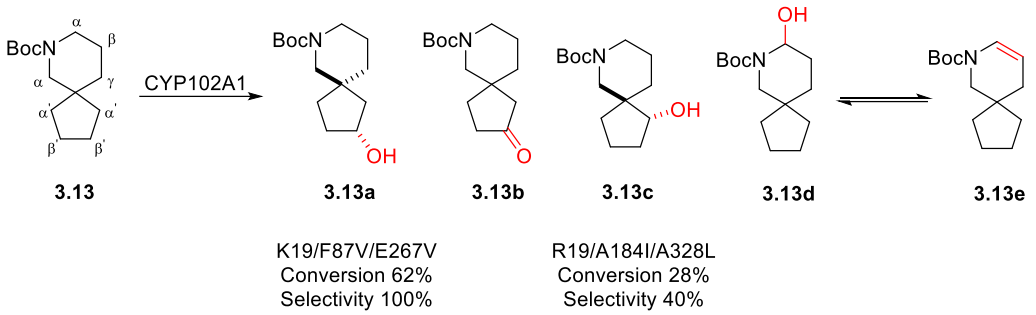

Top five mutants ranked by their selectivity for metabolite **3.13c**:

Entry	Mutant	3.13c Select. (%)	Conv. (%)
1	R19/A184I/A328L	40	28
2	R19	31	93
3	RT2	22	92
4	RP/H171L/I263G	16	68
5	K19/F81W/F87A	11	94

Figure 5.1 The major metabolites isolated from the oxidation of *N*-Boc protected 3-spiroamine **3.13** and the most selective mutants for metabolite **3.13c**.

As discussed in Chapter 3, rigid docking approaches are not ideal when bulky residues are present in the active site of the protein. In R19-based (R47/Y51F/H171L/Q307H/N319Y) variants, Phe87 is present and, as expected, rigid docking did not generate any productive poses; therefore, the ADFR method was implemented and the flexible residues incorporated are listed in §8.3 (Appendix).

Using the method described in previous chapters, MD simulated structures of variant R19/A184I/A328L were generated in four replicas, and further grouped into three clusters per replica. Applying the criteria mentioned in Chapter 2, productive and non-productive (NP) poses were identified and categorised based on the carbon predicted to be hydroxylated.

Mutations were designed based on overlaying non-productive and productive poses corresponding to α′-hydroxylation. Neighbouring residues were then analysed in order to select candidates that would potentially disfavour the undesired poses. Productive poses from this mutant were consistent with α′-, β′-, α-, β-, and γ-hydroxylations. As Figure 5.2a–d shows, the α′-producing poses were found to overlap with poses giving β′-, α-, β-,

and γ-oxidations; hence, it was difficult to identify distinct residues that might disfavour the unwanted poses due to the similar space occupied by the different poses.

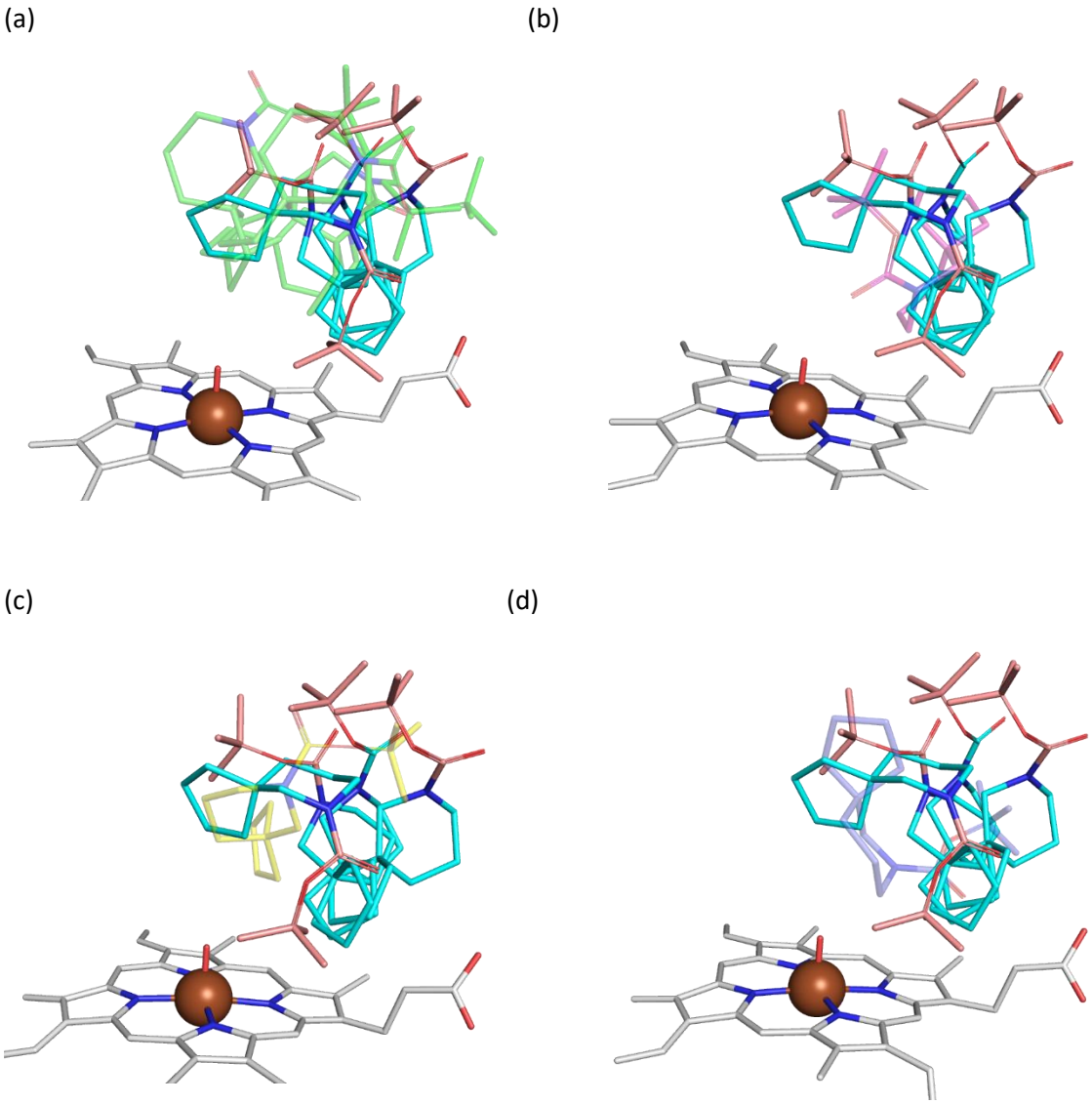

Figure 5.2 Overlap of α′-poses (cyan) and (a) β′- (green); (b) β- (magenta); (c) γ- (yellow); (d) α- (purple) poses. Boc-groups are shown in salmon in α′-poses.

Consequently, as shown in Figure 5.3, the NP (magenta) and productive (cyan) poses were overlaid, and this revealed a more distinct difference. Residues (V26, V178, L181, I263, A264, T268, S332, T436, and T438) in the vicinity of the NP poses were identified as more significant than others, so mutations at these sites were expected to have more influence on selectivity and conversion. It was speculated that altering these residues could potentially disfavour the NP poses. Substitutions with amino acids with bulkier side

chains were explored, since they exert greater steric effects on the spatial orientation of poses.

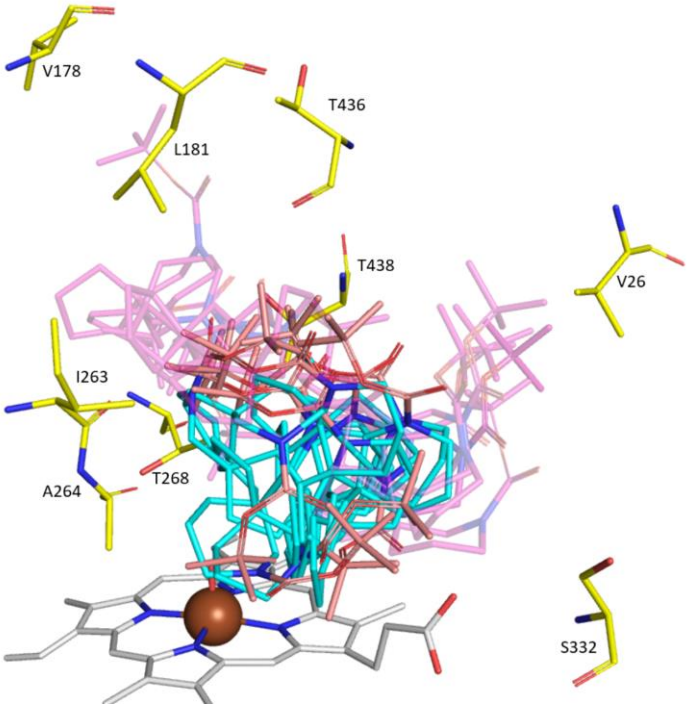

Figure 5.3 Overlay of NP poses (magenta) and poses corresponding to α′-hydroxylation (cyan) from mutant R19/A184I/A328L with neighbouring key residues highlighted (yellow). Boc-protecting groups in α′-poses are shown in salmon.

A panel of 16 mutants was designed, containing mutations at V26, V178, L181, I263, A264, T268, S332, T436 and T438, and the top five mutants ranked by their selectivity for metabolite **3.13c** are listed in Table 5.1. It was found that the substitution T268S increased the selectivity from 40% to 56% (Entry 2) but the conversion was lowered from 28% to 15% (Entry 1).

Entry	Mutant	3.13c Select. (%)	Conv. (%)
1	R19/A184I/A328L	40	28
2	R19/A184I/A328L/T268S	56	15
3	R19/A184I/A328L/V26L	28	30
4	R19/A184I/A328L/T438L	19	20
5	R19/A184I/A328L/T436F	14	29
6	R19/A184I/A328L/I263F	12	4

Table 5.1 Top five R19/A184I/A328L-based mutants ranked by their selectivity for **3.13c**.

Interestingly, previous screening results from the Wong group showed that the Thr268 residue is among those not often targeted for mutagenesis. This residue is one of the few polar residues in the active site and has been implicated in various roles including proton delivery, dioxygen activation, and the stabilisation of intermediates present in the $P450_{BM3}$ catalytic cycle.[299,300, 301] A comparison between Thr and Ser revealed that the methyl group of Thr268 could impose an unfavourable steric clash, due to its close proximity (1.8–1.9 Å) to the α′-productive poses (Figure 5.4). In contrast, substitution to a Ser residue created space which allowed these poses indicating hydroxylation at the desired site, and potentially increasing selectivity.

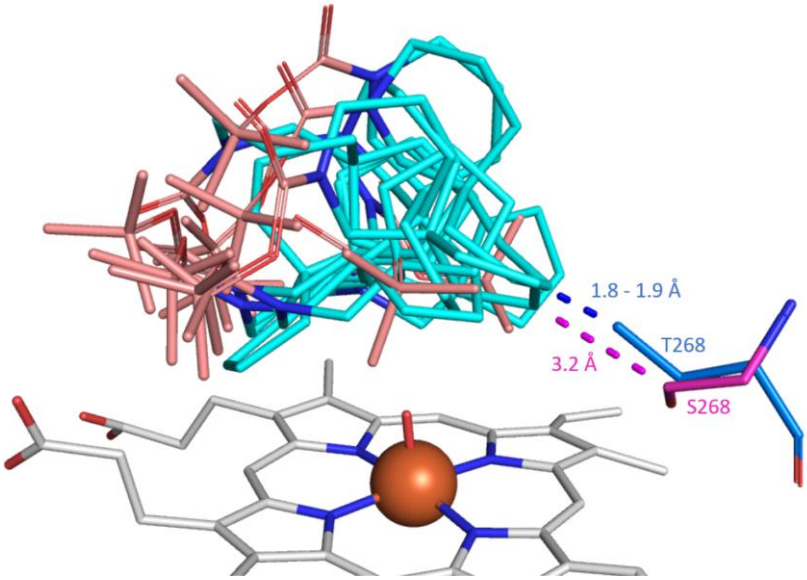

Figure 5.4 Overlay of α′-productive poses in mutant R19/A184I/A328L/T268S (cyan) and a comparison of the shortest distances between the productive pose and residues T268 (blue) in mutant R19/A184I/A328L/T268S and S268 (magenta) in mutant R19/A184I/A328L, showing the potential of a steric clash in the presence of T268 (1.8−1.9 Å). Boc-protecting groups are shown in salmon.

5.2.2 Second Generation Mutagenesis (R19/A184I/A328L/T268S)

The newly-designed mutant with the highest selectivity for **3.13c** (R19/A184I/A328L/T268S, 56%) was then used as the base mutant for second generation mutagenesis. Applying the approach described in §5.2.1, docking results predicted hydroxylation at all methylene carbons. Similar to first generation mutagenesis, poses

other than NP poses overlapped significantly with the desired α′-poses. As a result, only NP poses can be used for the design of new mutants and it was evident that they were somewhat clustered towards the left, as viewed in Figure 5.5, of the α′-productive poses. Based on this trend, key residues (V26, S72, P329, S332, M354, L437) in the vicinity of the NP poses were targeted for mutagenesis with the aim of improving the conversion of **3.13** to products.

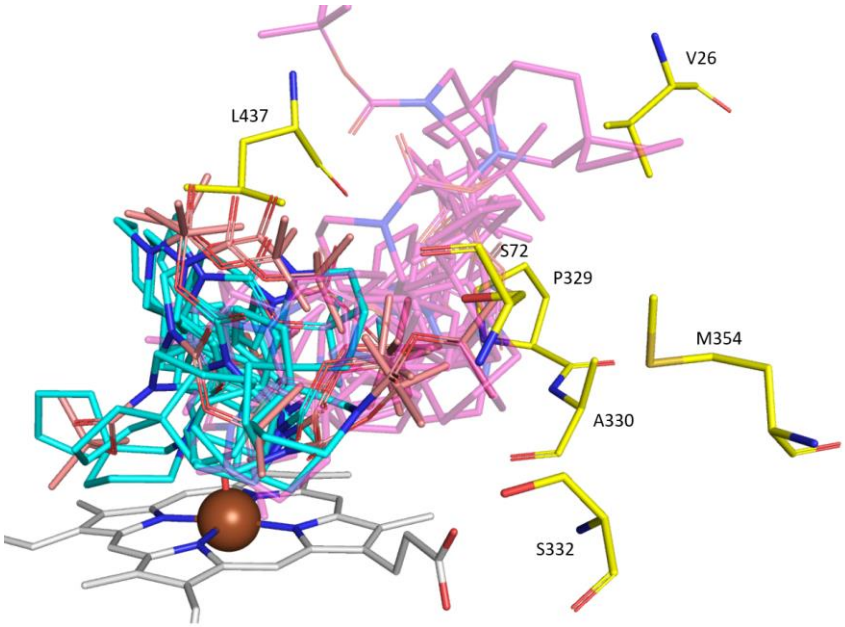

Figure 5.5 Overlay of NP poses (magenta) and poses corresponding to α′-hydroxylation (cyan) from mutant R19/A184I/A328L/T268S and neighbouring key residues (yellow).

A panel of 21 mutants was designed and screened with substrate **3.13**; the five mutants with the highest selectivity for **3.13c** are listed in Table 5.2. The substitution of Val26 to Met or Leu improved the selectivity from 56% to 74% or 68%, respectively (Entries 1 and 2).

Entry	Mutant	3.13c Select. (%)	Conv. (%)
1	R19/A184I/A328L/T268S/V26M	74	15
2	R19/A184I/A328L/T268S/V26L	68	18
3	R19/A184I/A328L/T268S/L437F	67	25
4	R19/A184I/A328L/T268S/L437M	65	33
5	R19/A184I/A328L/T268S/S72W	65	34

Table 5.2 Top five R19/A184I/A328L/T268S-based mutants ranked by their selectivity for **3.13c**.

The NP poses from mutant R19/A184I/A328L/T268S (cyan) were then overlaid with the productive poses for α′-hydroxylation from mutant R19/A184I/A328L/T268S/V26M (magenta) (Figure 5.6a). It was evident that the proximity of Met26 (2.6 Å) could destabilise the NP poses, whereas the distance to Val26 (3.8 Å) could stabilise the poses through van der Waals interactions. Further comparison between the NP poses of both mutants revealed that they were more packed and shifted towards the top left (as viewed) of the ferryl-oxygen as opposed to the mutant with Val26 (Figure 5.6b,c), possibly implicating the underlying effect of the substitution with a bulkier residue.

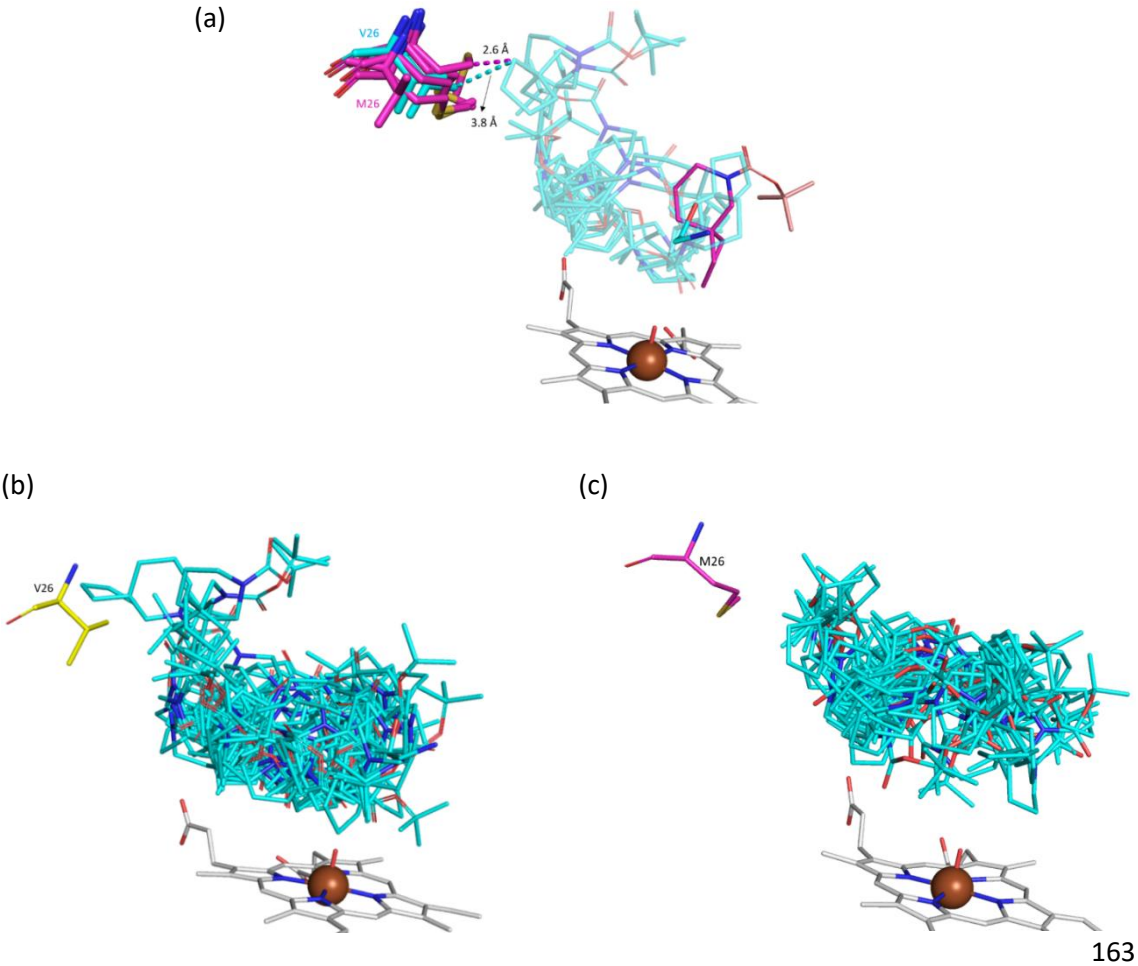

Figure 5.6 (a) Overlay of NP poses from mutant R19/A184I/A328L/T268S (cyan) and α′-productive poses from mutant R19/A184I/A328L/T268S/V26M (magenta), Boc-protecting groups are shown in salmon; (b) Overlay of NP poses from mutant R19/A184I/A328L/T268S (cyan); (c) Overlay of NP poses from mutant R19/A184I/A328L/T268S/V26M (cyan). Magenta dashes with black label denote the distance between M26 and NP poses. Blue dashes with black label denote the distance between V26 and NP poses.

5.2.3 Third Generation Mutagenesis (R19/A184I/A328L/T268S/V26M)

Using R19/A184I/A328L/T268S/V26M as the base mutant, the approach described in the previous two sections was repeated. Docking results predicted hydroxylation at all methylene carbons apart from the β-position. Unlike the first- and second-generation mutagenesis, poses corresponding to other carbons showed less significant overlap with the α′-poses (Figure 5.7a). Two poses in particular (red arrows) , corresponding to β′- and α-hydroxylation, were distinct from the cluster of other productive poses and could be targeted for mutagenesis. Further analysis with the NP poses depicted that they surrounded all of the productive poses to a certain extent (Figure 5.7b). With this information in hand, various residues (violet: V26, S72, L75, V78, L188, P329, A330, S332, M354, L437) were selected as potential candidates to improve selectivity for metabolite **3.13c**.

(a) (b)

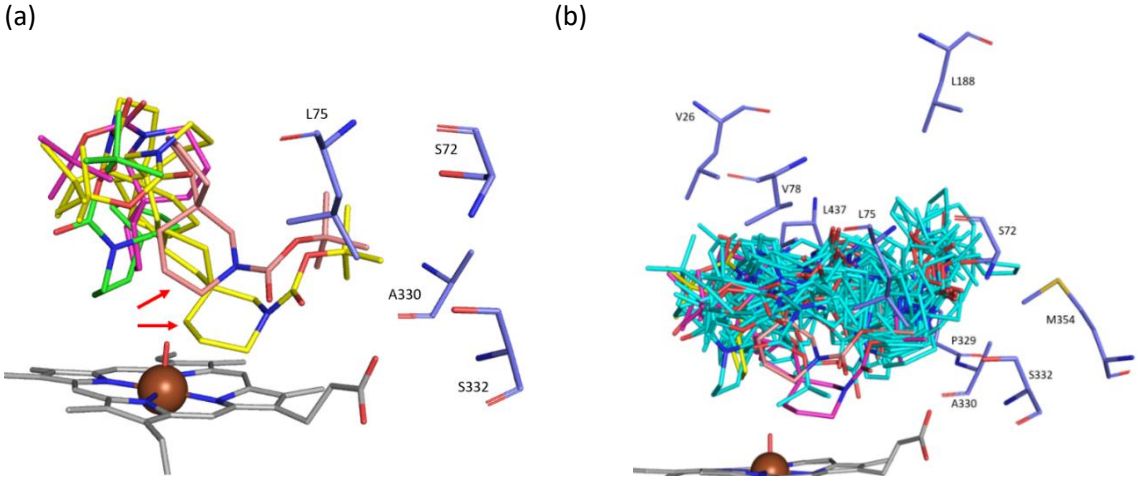

Figure 5.7 (a) Less significant overlap of α′- (magenta) poses and other productive poses: β′- (yellow), α- (salmon), γ- (green). Red arrows indicate the more distinct productive poses from others; (b) Overlay of NP (cyan) and productive poses from mutant R19/A184I/A328L/T268S/V26M. Key residues identified for mutagenesis are shown in

violet.

A panel of 26 mutants was designed with mutations at residues S72, L75, V78, L181, L188, P329, A330, S332, M354, L437, T438, and the five mutants with the highest selectivity for metabolite **3.13c** are shown in Table 5.3. None of the mutants exhibited higher selectivity than the base mutant (74%) but the conversion improved overall, with the highest being 83% from mutant R19/A184I/T268S/A328L/V26M/L75F (§8.2.3: Appendix); the selectivity for this mutant, however, was only 24%. The next step was to combat the decreased conversion from this generation of mutagenesis. The highest-converting of the most selective mutants, R19/A184I/A328L/T268S/V26M/L437F, was therefore chosen as the template for the next generation of mutagenesis (Table 5.3, Entry 1). Despite its lower selectivity compared to the base mutant selected previously (67% vs. 74%), it had a conversion of 57%, which was approximately a four-fold improvement (57% vs. 15%).

Entry	Mutant	3.13c Select. (%)	Conv. (%)
1	R19/A184I/A328L/T268S/V26M/L437F	67	57
2	R19/A184I/A328L/T268S/V26M/L75M	65	48
3	R19/A184I/A328L/T268S/V26M/S72W	64	32
4	R19/A184I/A328L/T268S/V26M/L188F	61	27
5	R19/A184I/A328L/T268S/V26M/M354W	60	12

Table 5.3 Top five R19/A184I/T268S/A328L/V26M-based mutants ranked by their selectivity for metabolite **3.13c**.

To investigate the increase in conversion after the substitution of Leu with Phe at residue 437, NP poses in the R19/A184I/A328L/T268S/V26M variant (cyan) were overlaid with the structure of the R19/A184I/A328L/T268S/V26M/L437F variant (Figure 5.8a), from which it became clear that the Phe437 side chain (magenta) steric clashes with the NP poses in the precursor variant. This could provide a potential explanation for the shifting of NP poses (yellow) within mutant R19/A184I/A328L/T268S/V26M/L437F away from F437, improving the conversion from 15% to 57% (Figure 5.8b).

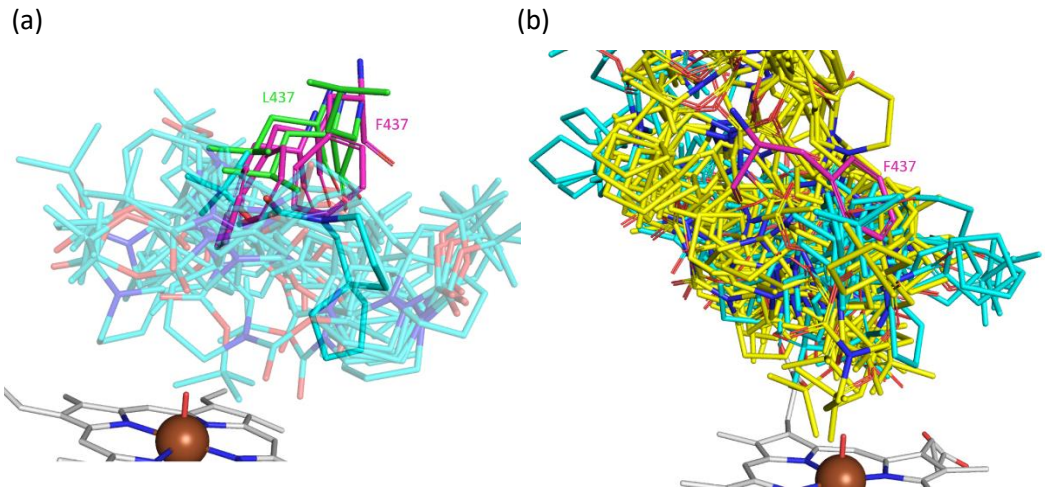

Figure 5.8 (a) NP poses (cyan) from R19/A184I/A328L/T268S/V26M overlaid with the structure of R19/A184I/A328L/T268S/V26M/L437F, illustrating the locations of L437 (green) and F437 (magenta). Only replica 1 for each receptor is shown; (b) Overlay of NP poses from R19/A184I/A328L/T268S/V26M (cyan) and R19/A184I/A328L/T268S/V26M/L437F (yellow), showing exclusion of this upper region of the substrate pocket from binding of substrate **3.13**.

In a further effort to optimise conversion, key residues to mutate (yellow, Figure 5.9) were selected on the basis of disfavouring NP poses that were distinctly distant from the haem-iron.

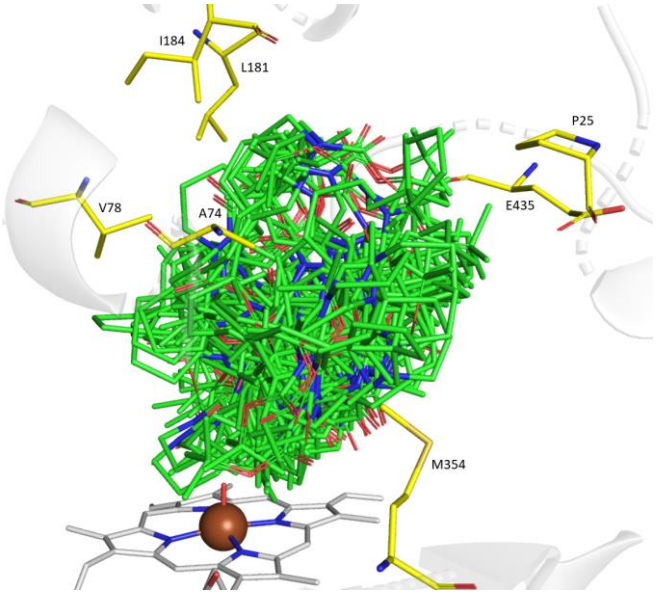

Figure 5.9 Overlay of NP poses (green) from mutant R19/A184I/A328L/T268S/ V26M/L437F and neighbouring key residues (yellow).

5.2.4 Fourth Generation Mutagenesis (R19/A184I/A328L/T268S/L437F)

A panel of 21 mutants was designed using R19/A184I/A328L/T268S/V26M/L437F as the base mutant, with the aim of further enhancing conversion. The five mutants with the highest conversion and selectivity for **3.13c** are shown in Tables 5.4 and 5.5, respectively.

Entry	Mutant	3.13c Select. (%)	Conv. (%)
1	R19/A184I/A328L/T268S/V26M/E435H	17	71
2	R19/A184I/A328L/T268S/V26M/E435Q	17	71
3	R19/A184I/A328L/T268S/V26M/L437F/M354W	17	71
4	R19/A184I/A328L/T268S/V26M/E435M	0	65
5	R19/A184I/A328L/T268S/V26M/L437F/I184M	18	65

Table 5.4 Top five R19/A184I/T268S/A328L/V26M/L437F-based mutants ranked by substrate conversion.

Entry	Mutant	3.13c Select. (%)	Conv. (%)
1	R19/A184I/A328L/T268S/V26M/E435F	73	3
2	R19/A184I/A328L/T268S/V26M/L437F/M354F	65	38
3	R19/A184I/A328L/T268S/V26M/L437F/A74V	64	28
4	R19/A184I/A328L/T268S/V26M/L437F/P25G	62	29
5	R19/A184I/A328L/T268S/V26M/L437F/A74G/V78W	62	0.3

Table 5.5 Top five R19/A184I/T268S/A328L/V26M/L437F-based mutants ranked by their selectivity for metabolite **3.13c**.

These screening results show that the newly-designed mutants gave a higher conversion overall, with 33% of mutants showing >50% conversion, in contrast to 15% from the previous batch (§7.2.3). The highest conversion achieved thus far, 71% from mutant R19/A184I/A328L/T268S/V26M/E435H (Table 5.4, Entry 1), was offset by a corresponding decrease in the selectivity for metabolite **3.13c** to 17%. Similarly, mutant R19/A184I/A328L/T268S/V26M/E435F gave a selectivity of 73% (Table 5.5, Entry 1), but the conversion was extremely poor.

Despite the increase in overall conversion, the selectivity for metabolite **3.13c** did not improve relative to the results from previous rounds of mutagenesis. From a synthetic chemistry perspective, the yield from a reaction is often the target of interest. From a biotcatalysis perspective, therefore, the best outcome (i.e. highest yield) from a mutant can be interpreted as the one with the highest conversion multiplied by the selectivity. Taking this into consideration, the best mutant was R19/A184I/A328L/T268S/V26M/L437F from the third generation of mutagenesis (Table 5.6). This mutant exhibited the greatest balance between conversion and selectivity, implicating that in preparative-scale reactions, the purification of metabolite **3.13c** might be readily achieved with a moderate amount. Future work on further enhancing the selectivity for metabolite **3.13c** and conversion could continue to employ this mutant as the template for mutagenesis.

Entry	Mutant	3.13c Select. (%)	Conv. (%)	Yield (%)
1	R19/A184I/A328L/T268S/V26M/L437F	67	57	38
2	R19/A184I/A328L/T268S/V26M/L75M	67	48	32
3	R19/A184I/A328L/T268S/V26M/L437F/ M354F	65	38	25
4	R19/A184I/A328L/T268S/L437F/P25G	63	29	18.3
5	R19/A184I/A328L/T268S/V26M/L437F/ A74V	64	28	17.9

Table 5.6 Top five mutants ranked by effective yield (**3.13c** selectivity × conversion), expressed as a percentage.

5.3 Weighted Docking Selectivity

Docking studies were carried out on the spiroamine substrates which produced metabolites hydroxylated at unactivated positions as discussed in Chapters 2–4. The docking selectivity for each metabolite was also calculated based on Equation 5.1, where X represents the desired carbon to be hydroxylated:

$$Docking\ selectivity\ for\ a\ metabolite\ from\ mutant\ Y$$

$$= \frac{\sum productive\ poses\ for\ position\ X}{\sum productive\ poses\ across\ all\ replicas} \times 100\%$$

Equation 5.1 Calculation of selectivity based on number of poses.

From the docking selectivities computed thus far, it was apparent that the discrepancy compared with the experimental selectivity fluctuated, and not all substrates reflected agreement with experimental results.

Methods to improve the accuracy of selectivity from docking were therefore explored. In Chapter 2 it was suggested that factors such as the presence of water molecules in the active site and C−H bond dissociation energies would have pronounced effects on both reaction rates and substrate orientation in the active site; however, these aspects cannot be easily considered computationally due to the complexity of the calculations and the limited power of the docking approach implemented herein. Nevertheless, efforts were made to obtain more meaningful calculations of the selectivity for specified metabolites, as detailed below. With this refined method of calculation, the selectivities for the mutants were re-computed and compared with experimental results.

5.3.1 Cluster population

A 100-ns MD simulation was performed for three or four replicas for each mutant, from which 10,000 structures snapshots (taken every 10 ps) were generated per replica. Clustering algorithms have been widely used as a means to reduce such ensembles of MD structures to a manageable size. The clustering method employed herein is known as the Root-Mean-Square Deviation (RMSD)-based clustering, where the RMSD of the C-α atoms of the amino acid residues for each replica was computed. An example from variant R19/A184I/A328L/T268S is depicted in Figure 5.10, which shows that the RMSDs of all simulated structures for the four replicas were approximately in the range 1–2 Å, implying that the deviations between the structures were minimal.

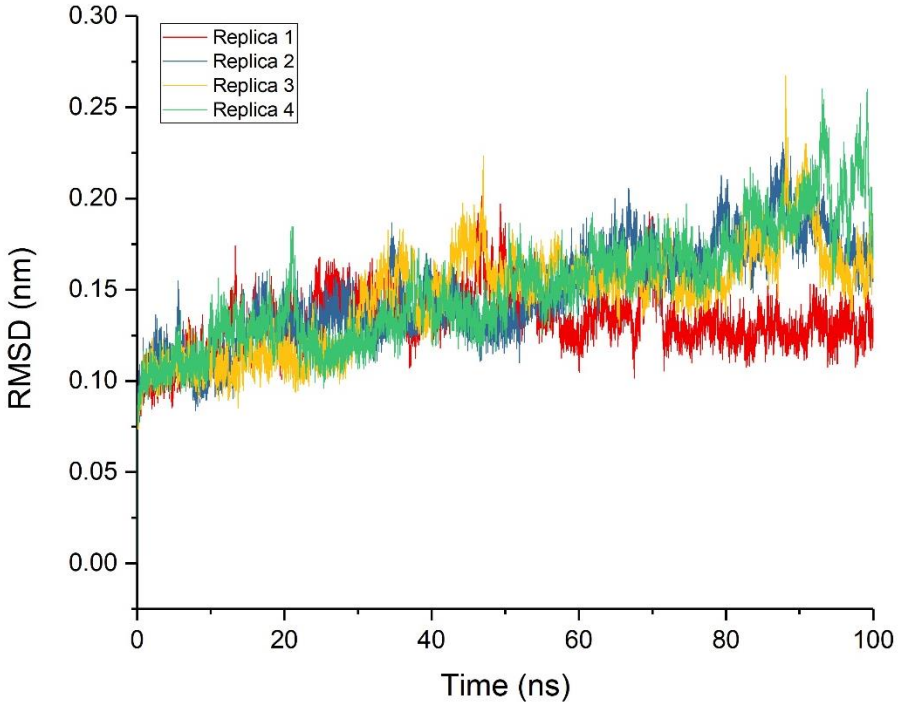

Figure 5.10 RMSD values of the C-α atoms for all recorded structures during four replicas of 100-ns MD simulation for mutant R19/A184I/A328L/T268S.

These structures were then clustered based on the RMSD of the C-α atoms (§7.2.4: Experimental). The number of clusters thus generated varies between replicas, since each cluster consists of a different number of structure snapshots. Only the top three clusters, as ranked by decreasing cluster population, were analysed for each replica, which represented >90% of the total population for each replica of simulation (Table 5.7).

Replica	Cluster (Cluster population)
1	1 (7197)
	2 (1566)
	3 (553)
2	1 (4010)
	2 (2195)
	3 (1769)
3	1 (4334)
	2 (3392)
	3 (771)
4	1 (4550)
	2 (2916)
	3 (780)

Table 5.7 Cluster population for each replica of MD simulated structures for mutant R19/A184I/A328L/T268S.

The substrate was subsequently docked into each cluster, from which the lowest energy nine poses constituted the output. From the perspective of the docking step, only one MD simulated structure was used from each cluster, representing an average of the clusters of several hundreds to thousands of MD structures. In order to take into account the cluster population with respect to each productive pose, the relative likelihood of the corresponding cluster was calculated. This was done by calculating the percentage population of each cluster within each replica (Equation 5.2).

$$Cluster\ population\ weight\ from\ Replica\ \boldsymbol{y}\ Cluster\ \boldsymbol{z} = \frac{cluster\ population\ of\ cluster\ \boldsymbol{z}}{\sum cluster\ population\ of\ replica\ \boldsymbol{y}}$$

Equation 5.2 Calculation of cluster population weight.

As a sample calculation, replica 1 of mutant R19/A184I/A328L/T268S was chosen. Referring to Table 5.7, the cluster population weights of a productive pose from replica 1 clusters 1 and 2 can be calculated as follow (Equation 5.3), where 1 represents the non-weighted productive pose:

Cluster population-weighted productive pose from:

$$R1C1 = 1 \times \frac{7197}{7197 + 1566 + 553} = 0.773$$

$$R1C2 = 1 \times \frac{1566}{7197 + 1566 + 553} = 0.168$$

Equation 5.3 Sample calculations of cluster population-weighted productive poses from R1C1 and R1C2 of mutant R19/A184I/A328L/T268S.

Hence, a productive pose from replica 1 clusters 1 and 2 in mutant R19/A184I/A328L/T268S carries a population weight of 0.773 and 0.168, respectively.

Results from mutants with the lowest and highest experimental selectivity for metabolite **3.13c** from each generation of mutagenesis were compared with the cluster population-weighted selectivities as described above (Figure 5.11). In four cases (bar charts 1, 4, 6

and 8), the computed non-weighted and population-weighted selectivities were higher than obtained experimentally, but in R19/A184I/A328L/T268S/V26M and R19/A184I/A328L/T268S/V26M /L437F/M354F (bar charts 3 and 7), lower. In mutants R19/A184I/A328L/T268S and R19/A184I/A328L/T268S/V26M/L437F (bar charts 2 and 5), however, the computed selectivities resemble the experimental results reasonably well after taking the cluster population into consideration.

Overall, the effect of the population weighting appeared relatively random, where the predicted selectivities were reduced or enhanced in some cases without apparent patterns. Conceptually, however, the cluster population should be included in selectivity predictions because a binding pose indicating a product might come from a clustered structure with a low population and its effect would be over-estimated, and *vice versa*. Moreover, the use of clustered structures, which are generated by averaging thousands of snapshot structures, does not take into account the stability of the structure. Although the cluster population could be considered as an indication of the relative stability of the structure, the evolution of the structure during MD simulation depends on the starting parameters; that is, the clustered structure with a high population could be a local minimum. This possibility of simulations being "trapped" in local minima is partly alleviated by conducting 3−4 replica simulations; more simulations would further reduce the risk of incorrect structures being obtained but at the expense of computational resources. Little could be done to take this into account without data on the relative energies of the clusters from different simulations. Attention, therefore, turned to the potential role of affinity energies of the poses.

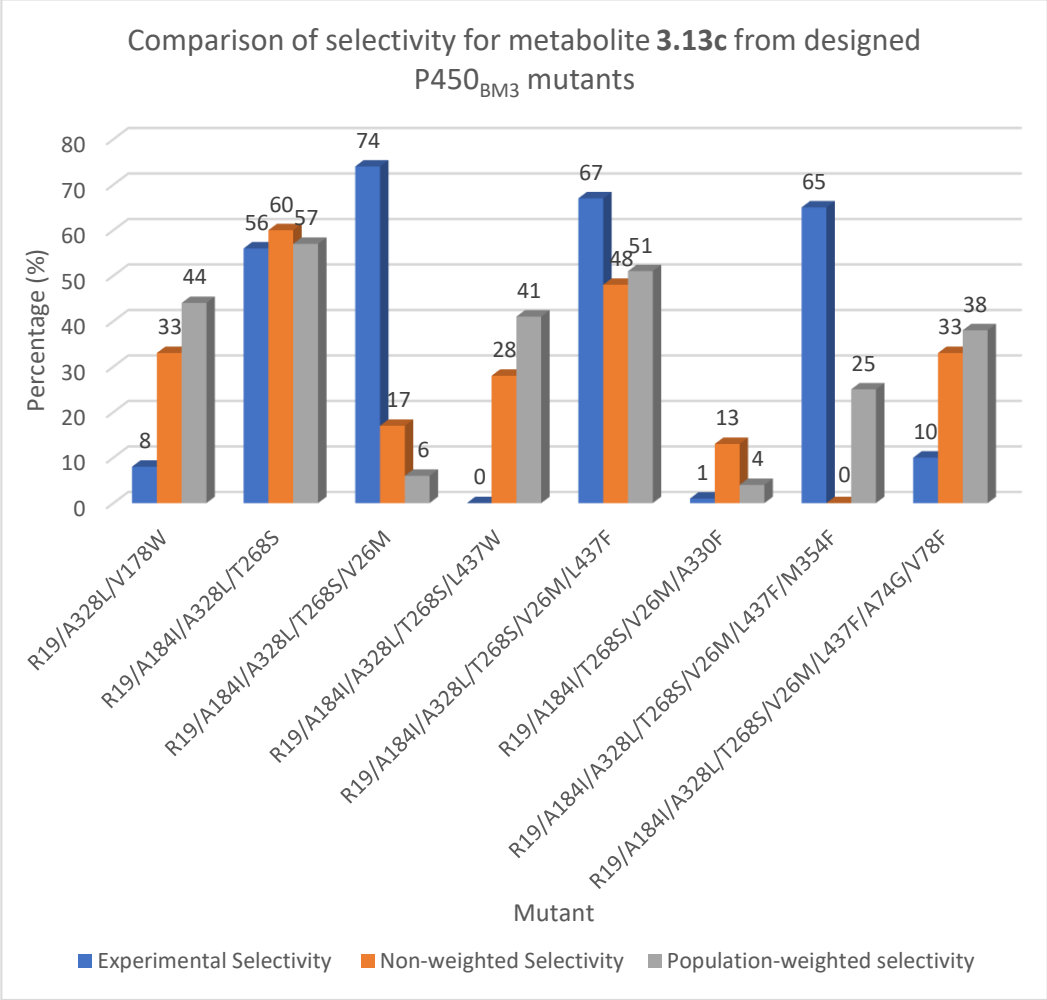

Figure 5.11 Comparison of experimental selectivities with the non-weighted and population-weighted computed selectivities (left → right: bar chart 1 → 8).

5.3.2 The Affinity Energy (AE) of Binding Poses

As mentioned in §1.4.4.2, MD simulated structures are generated with the solvation of water molecules. The process of molecular docking, however, is performed in vacuum, and involves (1) generation of poses based on prediction of factors such as conformations, and (2) assessment and ranking of binding affinities of the poses by scoring functions. These scoring functions are calculations that typically involve estimations to reduce computational time and adopt different assumptions and simplifications. In ADFR, the affinity energy output is a weighted sum of van der Waals, hydrogen bond, electrostatic, and desolvation contributions, which are calculated between pairs of atoms.[294] Figure 5.12 illustrates the computational AE calculated for each pose from substrate **3.13** binding

in mutant R19/A184I/A328L/T268S/V26M/L437F/A74G/V78F. The second lowest energy productive pose was found to correspond to α′-hydroxylation (−34 kJ/mol) and all remaining α′-poses had calculated AEs below −28 kJ/mol.

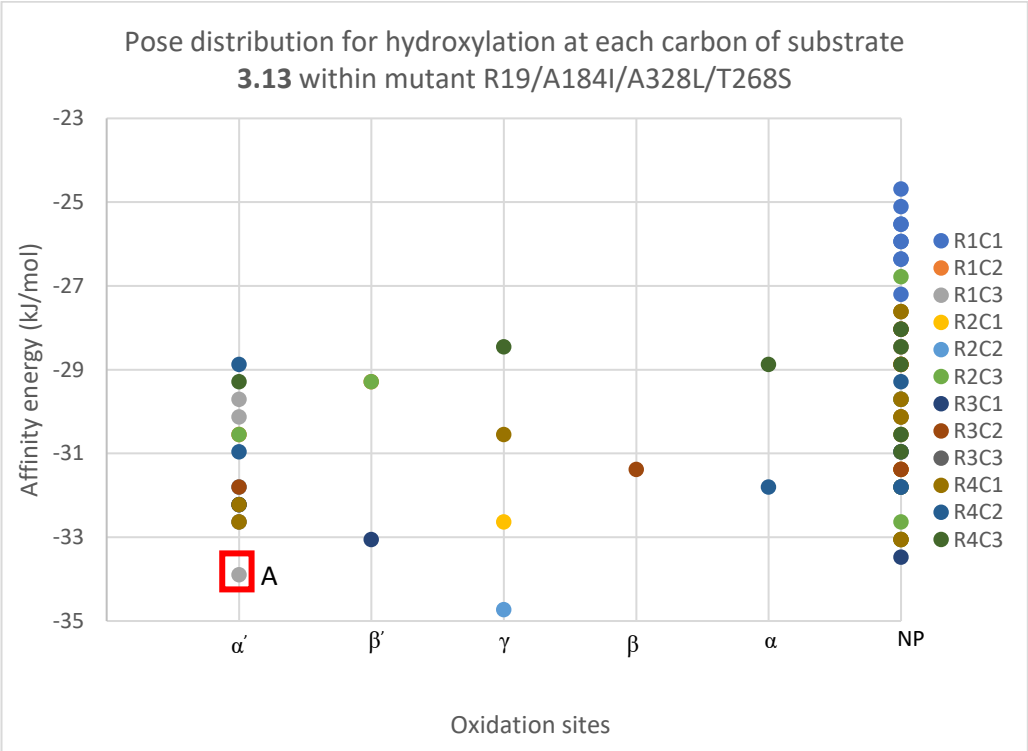

Figure 5.12 Distribution and calculated AEs for poses of substrate **3.13** classified by the predicted oxidation site within mutant R19/A184I/A328L/T268S.

Since the AE of poses differed by up to ~7 kJ/mol, all productive poses were weighted by the AE. The energies are indicative of the change in Gibbs free energy by assuming similar entropy changes for the same enzyme variant, i.e. the effect of ΔS is negligible. Based on $\Delta G^o = -RTlnK$, a value of $\frac{1}{K}$ for each pose was calculated, for ease of comparison, which represents the AE weighting. Assuming the weighting of the most negative energy pose is 1 (Table 5.8, Entry 1), then pose A (highlighted in Figure 5.12), for example, is assigned an AE weight of 0.26 (Entry 2), *etc* (Entries 3−8).

Entry	AE of pose (kJ/mol)	Lowest affinity energy pose among all replicas (kJ/mol)	ΔΔG (kJ/mol)	K	1/K (i.e. AE weight)
1	−33.9	−34.7	0.8	1.40	0.71
2	−31.8		2.9	3.26	0.31
3	−31.0		3.8	4.57	0.22
4	−31.0		3.8	4.57	0.22
5	−30.1		4.6	6.41	0.16
6	−30.1		4.6	6.41	0.16
7	−29.7		5.0	7.59	0.13
8	−29.7		5.0	7.59	0.13
9	−29.7		5.0	7.59	0.13
10	−29.7		5.0	7.59	0.13
11	−28.5		6.3	12.59	0.08

Table 5.8 Sample calculation of AE weight; The lowest-energy pose (AE = −34.7 kJ/mol) was assigned a weighting of 1; R = 8.3144598 J/mol/K, T = 298K, unit conversions applied.

In a further attempt to improve the accuracy of computed selectivity, both population and AE weight were taken into account to calculate a final AE-weighted selectivity (Equation 5.5).

$$Weighted\ selectivity = 1 \times population\ weight \times AE\ weight$$

Equation 5.4 Calculation of AE-weighted selectivity, taking into consideration both the population weight and AE.

The computed selectivities for the mutants listed in Figure 5.11 were re-evaluated with Equation 5.5; the results are presented in Figure 5.13. Compared with the population-weighted selectivity, the AE weighted-selectivity did not appear to show any improvement in correlation with the experimental results. In summary, focusing on only the experimental and AE-weighted selectivity, charts 1, 4 and 8 over-predicted selectivity, whereas charts 3, 5 and 7 under-predicted. On the other hand, charts 2 and 6 were comparable to experimental selectivities, although the effect of AE reduced and increased, respectively. Most of the weighted-selectivities were over-estimated, and there did not seem to be an obvious explanation for the differences between the population-weighted and AE-weighted selectivity. This was not surprising since the docking poses were not

relaxed and energy-minimised by MD simulations in water, and the force field used for affinity energy calculations for such *in vacuo* docking might be too simplistic.

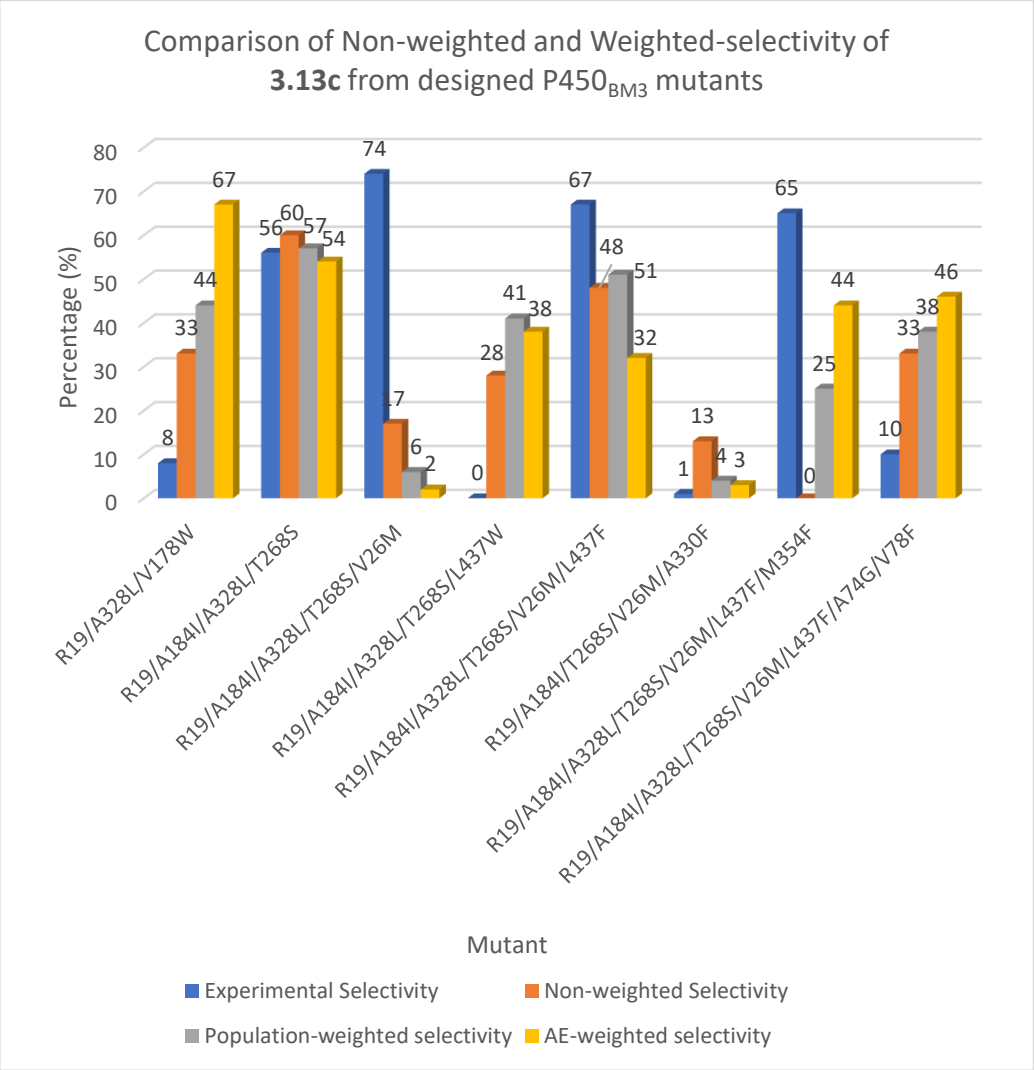

Figure 5.13 Comparison of experimental selectivities with the non-weighted, population-weighted, and AE-weighted computed selectivities (left → right: bar chart 1 → 8).

Finally, a more qualitative comparison of experimental and computationally-predicted selectivities still gives poor alignment between the results (Table 5.9).

Mutant	Experimental major product	Docking major product
R19/A328L/V178W	β′-OH	α′-OH
R19/A184I/A328L/T268S	α′-OH	α′-OH
R19/A184I/A328L/T268S/V26M	α′-OH	γ-OH
R19/A184I/A328L/T268S/L437W	β′-OH	α′-OH
R19/A184I/A328L/T268S/V26M/L437F	α′-OH	α′-OH
R19/A184I/T268S/V26M/A330F	β′-OH	γ-OH
R19/A184I/A328L/T268S/V26M/L437F/M354F	α′-OH	α′-OH
R19/A184I/A328L/T268S/V26M/L437F/A74G/V78F	β′-OH	α′-OH

Table 5.9 Comparison of experimental and docking major products from designed $P450_{BM3}$ mutants.

5.4 Conclusion and Future Work on Docking-guided Mutagenesis

5.4.1 Conclusion

To sum up, the ADFR approach was employed in order to optimise the selectivity for metabolite **3.13c** with the result that the selectivity was improved from 40% (R19/A184I/A328L) to 74% (R19/A184I/A328L/T268S/V26M), although this came at the expense of conversion, which dropped from 28% to 15% with the same two mutants. With designed mutants that gave moderate conversion, the selectivity remained low to minimal; however, it was considered that with selective enzymes, improving the conversion would be relatively straightforward since it can, for example, be achieved by altering reaction conditions. For instance, one can modify the substrate to enzyme ratio or, as found by previous D.Phil. student Harwood,[302] bubbling oxygen through the reaction mixture results in significant, sometimes dramatic, increases in conversion rates.

Correlations between experimental and computed selectivities revealed that non-weighted docking selectivities did not resemble the experimental data at all. The further measures taken – allowing for cluster population and affinity energy – did not improve the accuracy of the resulting docking selectivities which generally were overestimates compared with experiment. The results of simply comparing the major products obtained

experimentally (in screening reactions) with the computed predictions were mostly incongruent.

5.4.2 Implications and Future Work

From the data collected, it can be concluded that docking serves a useful guide for protein engineering, particularly in identifying vicinal residues around the binding site; however, in this work, docking did not demonstrate a close quantitative or even qualitative correlation to the experimental results, likely as a result of the factors mentioned in Chapters 2 and 3. A complete consideration of the dynamic environment of the protein-ligand complex along with the numerous varying parameters that could influence the binding, and the rate of the hydroxylation step, was deemed impractical. For instance, the computational power required to carry out MD simulations in water for all productive docking poses would be extremely large. On the other hand, despite the ADFR approach showing significant improvements over rigid-docking[294] – likely due to accommodating conformational changes in specified side-chain residues – there remains a limit on the number of flexible residues since it directly affects the practicality of such an approach. Previous D.Phil. student Zhang found that the docking run time increases linearly as the number of flexible residues increases;[174] consequently, although increasing the number of flexible residues might lead to a more reliable prediction, a balance must be established between docking run time and a meaningful output. Nevertheless, substrate docking provided information on residues that contacted or were too far away from the substrate, enabling mutations to be designed to attempt to manipulate substrate binding by blocking regions of the substrate pocket that accommodated unwanted binding poses. There were meaningful gains in selectivity and activity. One major advantage of using docking for mutations design is the mutation of residues that would not have been identified as potentially having significant effects because these were not in the screening library of variants. Apart from computational perspectives, factors from the experimental

perspective could also influence *in silico* results, including: the inherent variability in the experimental outcomes, both within screening repeats and comparing screening and scale-ups, change of oxidation profile with experimental parameters (e.g. reaction concentration, presence of organic co-solvents and additives), the different behaviours of racemic and single-enantiomer substrates – which suggest self-association within the active site to a certain extent, the bond dissociation energies of the various C−H bonds being hydroxylated, product inhibition, and further kinetic resolution processes arising by oxidation of the first-formed metabolites.

Future work could explore automating the analysis of the output from docking calculations, such as sorting productive and non-productive poses, or the measurement of distances and angles. This would significantly reduce the time required for mutant design and data analysis, and, in turn, could allow more effort to be invested in longer docking run times by incorporating more flexible residues. Additionally, more refined adjustments of the current parameters can be investigated; for instance, the number of water molecules and force field measurements associated with the protein. Such refinements would perhaps provide more insightful outcomes that would facilitate the identification of usefully-accurate *in silico* predictions. Screening and preparative-scale reactions should also be performed in replicates to minimise the influences from the differences in reaction conditions (e.g. temperature). Moreover, the stereochemistry and enantioselectivity of the substrate should be established wherever possible and practical.

Chapter 6: Summary and Future Work

The main goal of this research was to achieve late-stage C-H activation of the 2- and 3-spiropiamine series by engineered variants of $P450_{BM3}$. The combined strategy of variant screening and substrate engineering were deployed, which led to the generation of a range of metabolites with decent conversion and selectivity (Chapter 2 & 3), along with the identification of hydroxylation hot spots as shown in figure 6.1.

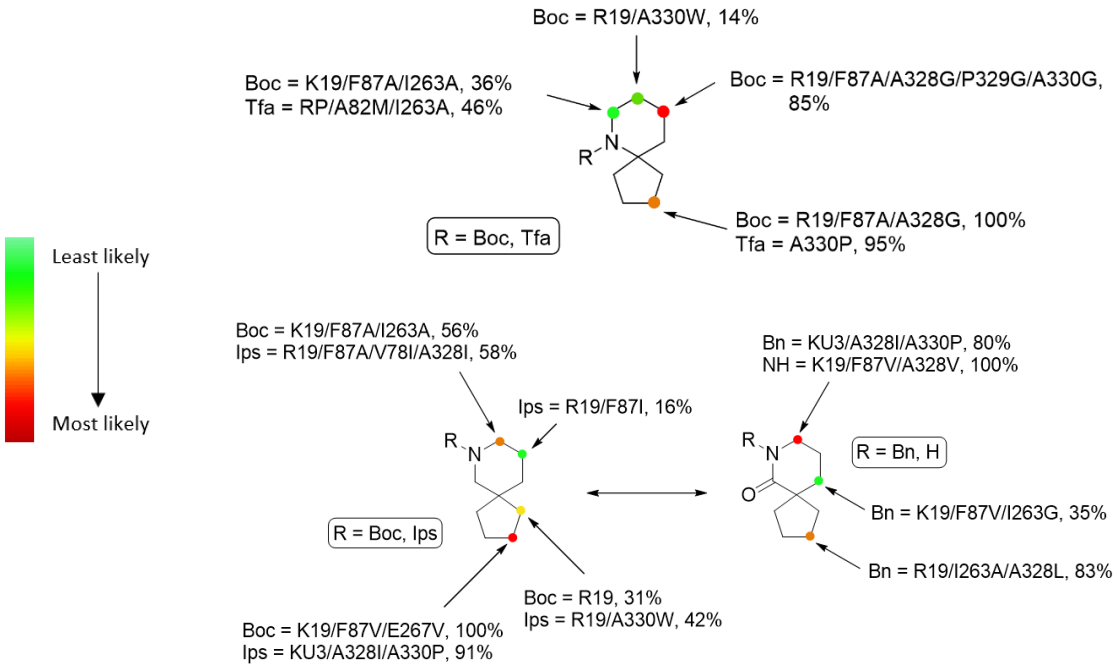

Figure 6.1 Hydroxylation hot spots for the 2- and 3-spiroamine series as reflected by results from variants screening.

In order to shed light on further information regarding ligand-protein interactions, docking studies were also performed on substrates that gave rise to metabolites with hydroxylations at unactivated positions. Combined with results from screening, several key variant residues were identified (Figure 6.2), where the majority are active site residues that reside in the vicinity of the haem iron. These residues could be targeted for future mutagenesis work in order to improve selectivity and/or conversion, in which the effects exerted could potentially be more influential than others.

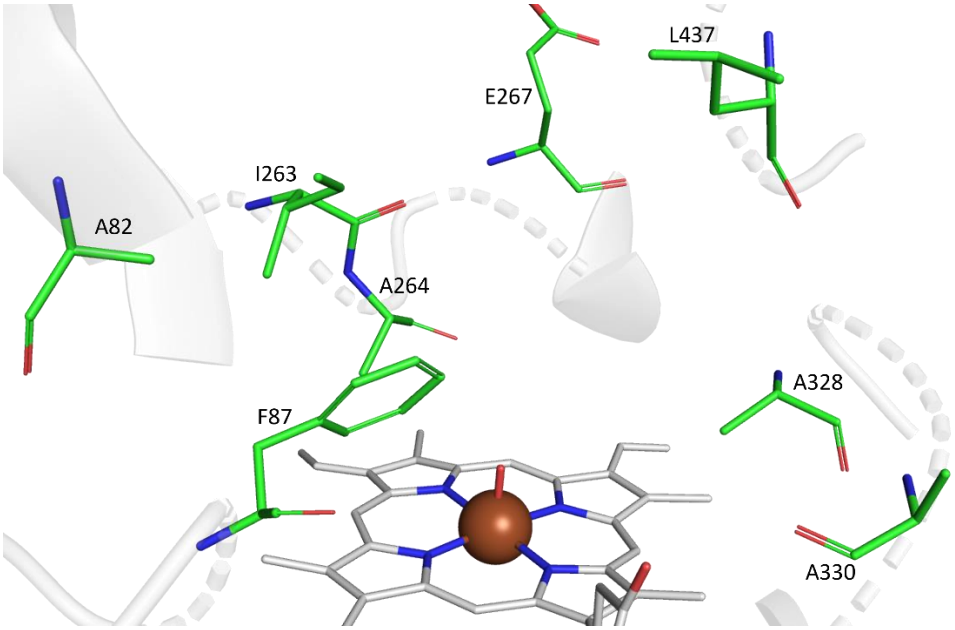

Figure 6.16 Key variant residues identified from docking studies and screening results, where most residues reside in the vicinity of the haem iron.

To demonstrate the synthetic utility of the hydroxylated metabolites, lactam **3.13a** was selected to perform a series of diversification reactions to create a fragment library (Chapter 4, schemes 4.29 & 4.30). The reactions ranged from relatively straightforward Grignard reactions to more complex intramolecular C-H aminations, showcasing the potential of utilising $P450_{BM3}$ in constructing fragment libraries.

Last but not least, docking-guided mutagenesis was employed to optimise the selectivity of metabolite **3.13c** (Chapter 5), where the selectivity and conversion were improved from 40% and 28% (R19/A184I/A328L) to 67% and 57% (R19/A184I/A328L/T268S/V26M/L437F), respectively.

In conclusion, the approach of uniting substrate engineering and using docking as a guidance have proven to be a powerful tool on optimising selectivity and conversion of metabolites. In the larger context, this strategy, together with the essential role of $P450_{BM3}$, has the potential to become a valuable asset in fragment-based drug discovery.

Chapter 7: Experimental

7.1 General Experimental

7.1.1 General Experimental for Chemical Syntheses

All reactions were carried out under a nitrogen atmosphere in oven-dried glassware unless otherwise stated. Solvents were either used as commercially supplied or as purified by standard techniques. THF was freshly distilled over Na and benzophenone prior to use. ACN, DCM, diethyl ether, DMF and toluene were obtained from an MBraun 5 solvent purification system. Hünig's base and triethylamine were distilled over KOH and stored under Ar. All other reagents were used as obtained from the supplier unless otherwise stated. Petrol refers to the fraction of light petroleum ether boiling at 30–40 °C. Ether refers to diethyl ether. Brine refers to a saturated aqueous solution of NaCl.

Column chromatography was performed using Merck Geduran Si 60 silica gel as the stationary phase unless otherwise specified. Thin-layer chromatography (TLC) was performed on Merck DC-Alufolien 60 F254 0.2 mm pre-coated plates and visualised with ultraviolet light (λ_{max} = 254 nm), basic $KMnO_4$, vanillin stain, or phosphomolybdic acid stain. Retention factors (R_f) of each product are quoted with the solvent system used for TLC.

Proton (^{1}H), carbon (^{13}C) NMR, and fluorine (^{19}F) spectra were recorded on a Bruker AVIII600 (600/150 MHz), Bruker AVII500 (500/125 MHz), Bruker AVIII400 (400/100 MHz), or Bruker AV400 (400/100 MHz). Proton chemical shifts (δ_H) are quoted in ppm to the nearest 0.01 ppm and carbon chemical shifts (δ_C) are quoted in ppm to the nearest 0.1 ppm relative to tetramethylsilane ($\delta = 0$) and referenced in MestReNova to the solvent residual, with signal splitting recorded as singlet (s), doublet (d), triplet (t), quartet (q), quintet (quin), sextet (sex), septet (sept), multiplet (m) and broad singlet (br s). Coupling constants (*J*) are measured in Hz to the nearest 0.5 Hz. Assignments are recorded as

follows: ppm (number of protons, multiplicity, coupling constants, assignment). COSY, HSQC and NOESY were obtained and used as necessary to aid assignments. For known compounds, ^{1}H and ^{13}C NMR spectroscopic data were found to be in good agreement with literature. Atom numbering reflects NMR peak assignments and does not in general correspond to IUPAC nomenclature. For the ^{13}C NMR spectra of compounds where mixtures of regioisomers or diastereomers were isolated, an asterisk (*) denotes the signal corresponding to the major isomer, where identifiable. The NMR peaks used for integration in all Mosher ester analysis correspond to the *CH*OH peaks in each metabolite.

Infrared spectra were recorded using a Bruker Tensor 27 FT-IR spectrometer. Absorption maxima are reported in wavenumbers/cm^{-1} and described as strong (s), medium (m), weak (w) and broad (br.) relative to the most intense peak. Low resolution mass spectra were recorded using a Micromass LCT Premier spectrometer (ESI±). High resolution mass spectra were obtained for novel compounds on a Bruker Daltronics MicroTOF spectrometer (ESI/FI). Mass to charge ratios (*m/z*) are reported in Daltons and intensities are recorded as a percentage relative to the most intense peak. The injector temperature was 280 °C and the FID was at 250 °C. Melting points are recorded in °C using a Griffin melting point apparatus; where relevant a range may be specified.

Compound names are as generated by ChemBioDraw Ultra 18.2.

7.1.2 General Experimental for Enzymatic Reactions and Molecular Biology

GC analyses were carried out with a ThermoFisher Scientific Trace 1300 instrument equipped with a FID and an AI1310 autosampler using a J&W DB-1MS fused silica column (30 m × 0.25 mm × 0.25 μm, Agilent Technology, UK) with He as carrier gas at a flow rate of 1.5 mL/min. The injector was held at 280 °C and the FID temperature was 250 °C. GC methods were optimised for each substrate/product combination. Chiral-phase analyses were carried out with a Cyclosil-B fused silica column (30 m × 0.25 mm

× 0.25 × μm, Agilent Technology, UK), using He as the carrier gas at a flow rate of 1.5 mL/min. The injector was held at 200 °C and the FID temperature was 250 °C. GC and chiral-GC methods were optimised for each substrate/product combination.

Sonication was carried out using a Misonix 3000 sonicator and Fisher Scientific FB-505 ultrasonic processor. Mutagenesis and PCR reactions were carried out in a Techne thermocycler or a Cetus thermocycler from Perkin-Elmer. UV-vis spectra were acquired on a Varian CARY50 spectrophotometer using 1 cm pathlength quartz cuvettes.

Bacterial culture media components, kanamycin and IPTG were from Melford Laboratories, UK. Hen egg white lysozyme was from Sigma-Aldrich. NADP+ was from Prozomix, UK, and glucose dehydrogenase (GDH) was supplied by Codexis, California. Oligonucleotides for site directed mutagenesis were supplied by Eurofins Genetic Service, UK. Water (ρ ~14 MΩ/cm) used for bacterial growth and buffers was from a Milipore ELIX-5 system. Buffers for molecular biology experiments were prepared using ultrapure water (ρ > 18 MΩ/cm) from a Millipore Milli-Q system. Media were autoclaved at 121 °C for 30 min. Components sensitive to high temperature were first sterilised via a 0.22 μm syringe filter prior to being added to the autoclaved media (cooled to below 40 °C).

7.2 Enzymatic Hydroxylation Procedures

7.2.1 Enzymatic Screening

Substrates were screened with the initial library containing 48 $P450_{BM3}$ variants on a 1 mL scale. These reactions were conducted in two 24-well plates in 200 mM phosphate buffer (pH 8.0), along with 4 μM NADP+, 100 mM glucose, 2 U/mL GDH, 1 mM substrate, and 1 μM enzyme. Screening plates were prepared by aliquoting 100 μL of the 10 μM enzyme solution into each well along with 900 μL of the solution. The following table describes 1 mM substrate : 1 μM enzyme (1000:1); where lower substrate

concentration are used, buffer is adjusted accordingly to keep a final reaction volume at 1 mL.

Reagent	Stock Concentration	Volume added (µL)	Final Concentration
Phosphate buffer	200 mM	775	-
$NADP^+$	4 mM	10	40 µm
GDH	400 U/ mL	10	4 U/ mL
Glucose	1 M	100	10 mM
Substrate	200 mM (in ethanol)	5	1 mM
Enzyme	10 µM	100	1 µM

Table 7.1 Composition of screening mixtures at a 1000:1 substrate:enzyme ratio.

The plates were then transferred to a platform shaker and shaken at 140 rpm and ambient temperature for 16 hours. After this time, 300 µL of each reaction mixture was pipetted into a 1.5 mL microcentrifuge tube along with 300 µL of EtOAc. The mixtures were vortexed and then centrifuged for 2 minutes at 14,300 g to separate the phases. 150 µL of the organic layer was transferred into a 250 µL glass GC insert and GC analyses were performed.

7.2.2 General Procedure-1 (GP-1) for Preparative Scale Reactions

Preparative scale reactions (50– 500 mL) were carried out for 16–24 h in a 200 mL or 1 L beaker with a stirring bar, with the same concentrations as in the initial screening. Progress of the reaction was monitored by GC. After the reaction had proceeded to >90% conversion (GC), the reaction mixture was extracted with EtOAc (3 × 50 mL). The organic extracts were combined and washed with 50 mL sat. aq. $NaHCO_3$ and then 50 mL brine, dried over $MgSO_4$, filtered, and the solvent removed by rotary evaporation. The residue was dissolved in ~5 mL of EtOAc and transferred to a glass vial. The mixture

was then tested with thin-layer chromatography (TLC) to select the solvent or combination of solvents that could be used for purification.

Oxidation products were purified by flash silica gel column chromatography using Geduran Silica 60, 40−63 μm. The fractions were analysed by TLC, stained with a solution of phosphomolybdic acid in ethanol, and by GC. Fractions containing the same compounds were combined, solvents removed by rotary evaporation, and the purified compound characterised by NMR spectroscopy and MS.

7.2.3 Enzyme Expression and Quantification

7.2.3.1 $P450_{BM3}$ Over-Expression

One colony of transformed *E. coli* BL21 (DE3) or acella competent cells from a LB_{KAN} plate was inoculated into 500 mL FB_{gly} media with addition of 1.5 mL of inoculation solution containing 30 mg/L kanamycin in a 2 L flask and shaken at 160 rpm for 24 h at 37 °C. A 5 mL aliquot of the culture was mixed with 5 mL sterile 50% glycerol in a 15-mL centrifuge tube to prepare a cell bank which was then stored as 1 mL aliquots at −80 °C. The incubator temperature for the overnight culture was then lowered to 20 °C and the culture left to shake for 1 h. Protein production was induced by adding 1 mL of induction solution into each 2 L flask. The culture was grown for a further 48−72 h, shaking at 120 rpm, and 20 °C. Cells were harvested by centrifugation at 9000 g, 4 °C for 10 min.

The cell pellet was re-suspended in 30 mL of potassium phosphate buffer per 500 mL culture, transferred to a beaker on ice and the cells were lysed by sonication with a 5-min programme of 15 s pulses and 30 s cooling, at 45% amplitude. The lysate was centrifuged for 15 min at 9,000 g, 4 °C to pellet the cell debris. The P450 enzyme was recovered from the supernatant by ammonium sulfate fractionation. The amount of ammonium sulphate required to take the concentration to 40% saturation was calculated

(http://www.encorbio.com/protocols/AM-SO4.htm) and added as the solid to the solution at 4 °C and the mixture stirred until all the solids had dissolved. The solution was centrifuged at 9,000 g, 4 °C for 20 min. To the retained supernatant was added the amount of ammonium sulfate to take the solution from 40% to 60% saturation to precipitate the P450 enzyme. The pellet was retained after centrifugation at 9,000 g for 30 min at 4 °C and then dissolved in 5 mL of potassium phosphate buffer. The protein was aliquoted into 1.5-mL tubes and stored at −20 °C.

7.2.3.2 Protein Quantification

Before the P450 enzyme was stored at −20 °C, 50 μL of enzyme was added into 950 μL of potassium phosphate buffer and the UV-Vis spectrum (200−500 nm) was recorded. A few crystals of sodium dithionite were added to reduce the protein and the UV-Vis spectrum was recorded of the reduced protein which was then used to obtain the baseline. 10−15 bubbles of CO were gently bubbled through the reduced protein; and the difference spectrum was recorded. More CO was bubbled through the solution and the spectrum recorded until the characteristic 450 nm peak height was maximised. The concentration of the protein was determined from:

$$[\boldsymbol{P450}]\boldsymbol{\mu M} = \frac{\boldsymbol{20(A_{450} - A_{490})}}{\boldsymbol{91000}} \times \boldsymbol{10^6}$$

Where $\varepsilon_{450-490}$ = 91,000 M^{-1} cm^{-1} is the extinction coefficient.[303]

7.2.4 Mutagenesis and DNA Preparation

7.2.4.1 PCR Reactions

Solutions of both the forward and reverse primers, each at 10 μM concentration, were prepared in ultrapure water. To a 200 μL autoclaved PCR microcentrifuge tube the following components were added: 29 μL water, 5 μL dNTP, 5 μL 10× KOD polymerase buffer, 1−2 μL parent DNA, 4 μL MgSO4, 2 μL DMSO, 1.5 μL forward primer, 1.5 μL

reverse primer and 1 μL polymerase to make a total volume of 50 μL. After being gently pipette-mixed and centrifuged for 5 s at 2,900 g, the microcentrifuge tube was placed in the thermocycler and the following temperature program was run: 94 °C for 20 s for strand separation; 55−65 °C for 20 s for annealing; 72 °C for 160 s for extension; cycle repeated 30 times. The temperature was then kept at 72 °C for 10 min before being reduced to and maintained at 4 °C. The PCR reactions were then analysed by agarose gel electrophoresis.

7.2.4.2 Agarose Gel Electrophoresis

A suspension of agarose powder (0.5 g) in 50 mL 1× TAE (Tris-Acetate-EDTA) buffer in a conical flask was heated to form a clear solution in a microwave (2 × 30 seconds). RedSafeTM DNA gel staining (0.5 μL of a 10000× solution) was added into the solution which was poured into the gel tray with a comb to form sample wells and left to set. The gel was then placed in the electrophoresis apparatus and extra 1× TAE buffer was added until the gel was submerged. 2 μL of the loading dye was mixed with 10 μL of the PCR mixture and then carefully pipetted into a well in the gel; 10 μL of a DNA ladder (1 kbp) solution with DNA fragments of certain length was added to an adjacent well in the gel to provide a reference. A voltage difference of 90 V was applied across the gel for 30 minutes. The gel was then irradiated by a UV transilluminator. A strong band with the same mobility as a linearised 8500 bp fragment suggested a successful PCR step. Then, 1 μL of DpnI, a restriction enzyme which digests methylated DNA instead of the new DNA produced *in vitro* by PCR, was added to digest the template DNA for 2 hours at 37 °C.

7.2.4.3 DNA Transformation

E. coli acella competent cells were stored as 120 μL aliquots in microcentrifuge tubes at −80 °C. One aliquot of cells was defrosted on ice, 10 μL of the DpnI−digested PCR mixture was added into 40 μL of competent cells which were incubated for 45 min on ice.

The cells were heat-shocked at 42 °C for 60 s and then placed back on ice for 2 min. 600 μL of filter-sterilised SOC media was added to the mixture which was then incubated for 2 h in a shaker at 180 rpm, 37 °C. The cells were spread onto a LB_{KAN} agar plate and placed in a 37 °C oven to grow overnight.

7.2.4.4 DNA Purification

One single colony was picked from the plate and inoculated into 5 mL LB_{KAN} media in a 15-mL centrifuge tube at 180 rpm, 37 °C for 16 h. The culture was centrifuged at 9,000 g and 4 °C for 10 min. Plasmid DNA was then purified using a GeneJET plasmid miniprep kit from ThermoFisher Scientific. The purified DNA was recovered in 50 μL of deionised water. The DNA concentration (μg/μL) was determined from 5× A_{260} of a 1:100 diluted sample (5 μL solution in 495 μL water) and the purity was assessed by the ratio A_{260}/A_{280}. If the purity ratio was between 1.5 and 1.8 and concentration greater than 0.1 μg μL^{-1}, then 15 μL of the DNA stock was sent for DNA sequencing by Geneservice, UK using two primers, T7F and BM3FP2, to ensure the presence of the desired mutation(s). If the correct sequence was obtained, the plasmid DNA (0.25 μL) was transformed into 40 μL of competent *E. coli* BL21 (DE3) or acella as described in §6.2.3.1.

Primers	Sequence
T7F	TAATACGACTCACTATAGG
BM3FP2	CTGCAGCGAGCAAATCCAGACGAC

Table 7.2 DNA sequences of the T7F and BM3FP2 primers.

7.2.4 MD Simulations and Molecular Docking

7.2.4.1 MD Simulations

MD simulations were performed for the haem domain of wild type $P450_{BM3}$ and variants that showed high selectivity for relevant products. All structures were relaxed via MD simulations performed in GROMACS 2018.6.[304] Mutations were added to the WT $P450_{BM3}$ (PDB code: 1jpz)[139] or the A330P variant (PDB code: 3m4v)[305] crystal structures

via Pymol. The co-crystallised substrate for the WT structure, NPG, was removed prior to adding mutations. The haem moiety was simulated as the ferryl, Compound I species, using parameters from Shahrokh *et al*.[306] The protein was prepared using the Amber 99SB*-ILDN force field[307] with TIP3P water.[308] The protein was placed into the centre of an octahedral box, with a minimum distance of 10 nm to any box edge, and then solvated with *ca*. 17500 water molecules and the net charge neutralised by addition of corresponding Na^+ ions. Steepest descent energy minimisation was performed until the maximum force was <500 kJ mol^{-1} nm^{-2}. Periodic boundary conditions were used to model the system, with electrostatic interactions treated by the particle mesh Ewald method,[309] and bond lengths involving hydrogen atoms constrained with the LINCS algorithm.[310] Short-range non-bonded interactions were calculated with a 1 nm cut-off and a timestep of 2 fs was used. For equilibration steps, all protein backbone Cα atoms were restrained with a positional restraint force constant of 1000 kJ mol^{-1} nm^{-2}. A NVT equilibration step was performed at 298 K for 100 ps, using the modified Berendsen thermostat.[311] This was followed by an NPT equilibration step for 1250 ps utilising the Berendsen barostat with a time constant of 1 ps.[312] All positional restraints were then removed and 100 ns of production MD was performed in triplicate or quadruplicate using the Parrinello–Rahman barostat[313] with a time constant of 5 ps. Structures were recorded every 10 ps. Stability of the simulations was confirmed by monitoring the RMSD of the backbone Cα atoms.

7.2.4.2 Molecular Docking

The individual MD trajectories were clustered using the Daura algorithm[314] with a RMSD cut-off of 1.2 Å, resulting in typically ~15 clusters, each containing different number of similar clusters. The three most populated clusters, with a population cut-off of 5% of all trajectories, were used as receptor structures for docking studies, which were performed in Autodock Vina (for rigid-body docking),[315] or ADFR (for flexible receptor docking).[294]

All water molecules were removed from the structure prior to the docking calculation. Substrate structures were obtained from PubChem and energy-minimisation was performed by Chem3D. The resulting structures were processed by Autodock Tool to generate the PDBQT file for docking runs. In Autodock Vina, the docking site was defined as a 30 × 30 × 30 Å box centred on the ferryl oxygen, and the calculated binding poses were ranked using the Autodock Vina scoring function. In ADFR, the entire active site is accessible and the side chain of residues at positions 75, 78, 87, 260, 263, 328, 330, 437 and 438 were selected to have full flexibility on the basis that these were most likely to contact a bound substrate. Additional flexible residues for each mutant discussed in this thesis are listed in §8.3.

7.3 Compounds from Chapter 2

6-Azaspiro[4.5]decane (2.1)

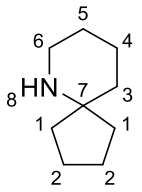

Benzylated amine **2.45** (154 mg, 0.669 mmol) was dissolved in methanol (3.5 mL) and 10% Pd/C (206 mg, 0.194 mmol) was added. The reaction was stirred under hydrogen (balloon) for 18 h at RT. The reaction mixture was filtered through a celite pad and concentrated *in vacuo*. The crude product was used without further purification. **IR** ν_{max} (thin film)/cm^{-1} 3360br, 1591m, 1146m; **^{1}H NMR** δ_H (400 MHz, $CDCl_3$) 1.50 – 1.65 (10H, m, H-1, H-2, H-3, H-4, H-5), 1.65 – 1.76 (4H, m, H-1, H-2), 2.86 (2H, t, J = 5.0 Hz, H-6); **^{13}C NMR** δ_C (100 MHz, $CDCl_3$) 21.9 (C-3), 24.1 (C-2), 25.8 (C-4), 36.7 (C-5), 37.9 (C-1), 42.8 (C-6), 65.9 (C-7); **HRMS (ESI$^+$)** *m/z* $[M+H]^+$ calculated for $C_9H_{18}N$, 140.1434; found, 140.1432.

Methyl 1-(4-chlorobutyl)cyclopentane-1-carboxylate (2.3)[316]

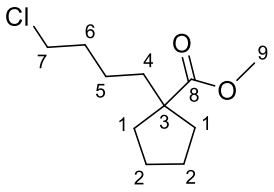

To a stirred solution of DIPEA (1.6 mL, 11.0 mmol) in THF (15 mL) cooled to −78 °C was added *n*BuLi in (6.30 mL, 1.60 M in hexanes, 10.0 mmol) and stirring was continued for 15 min. To this was added ester **2.4** (0.74 mL, 5.0 mmol) at −78 °C. The resulting solution was stirred for 1.5 h then1-chloro-4-iodobutane (1.20 mL, 10.0 mmol) was added and stirring continued for 18 h. The reaction was quenched by the addition of brine (9 mL), and the solution was extracted with ether (3 × 3 mL). The combined organic layers were washed with brine (3 mL) and dried with $MgSO_4$. The solvent was then

removed *in vacuo* to obtain the crude product. Flash chromatography (100% pentane → 30% ether in pentane, with gradient of 10%) afforded the title compound (dark brown oil, 92.4 mg, 85%). **R_f** 0.43 (20% ether in pentane); **IR** ν_{max} (thin film)/cm^{-1} 2950m, 2870w, 1728s, 1453m, 1164s; **^{1}H NMR** δ_H (400 MHz, $CDCl_3$) 1.35 (2H, m, H-5), 1.42 – 1.51 (2H, m, H-1), 1.56 – 1.66 (6H, m, H-2, H-4), 1.69 – 1.78 (2H, m, H-6), 2.06 – 2.15 (2H, m, H-1), 3.51 (2H, t, *J* = 7.0 Hz, H-7), 3.67 (3H, s, H-9); **^{13}C NMR** δ_C (100 MHz, $CDCl_3$) 23.4 (C-5), 25.0 (C-2), 32.3 (C(7)), 36.1 (C-1), 38.4 (C-3), 44.7 (C-7), 51.8 (C-9), 54.0 (C-3), 178.2 (C-8); **HRMS (ESI$^+$)** *m/z* $[M+H]^+$ calculated for $C_{11}H_{20}ClO_2$, 219.1146; found, 219.1147.

Methyl cyclopentanecarboxylate (2.4) [317]

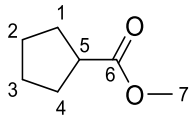

To a stirred solution of cyclopentane carboxylic acid (5.0 g, 44 mmol) in methanol (23 mL) at RT was added conc. sulphuric acid (0.55 mL). The reaction mixture was heated at reflux for 18 h and allowed to cool to RT. The resulting mixture was distilled to remove excess methanol and then diluted with ether (15 mL). The layer was washed with water (20 mL) then sat. aq. $NaHCO_3$ (3 × 20 mL). The combined organic extracts were dried with $MgSO_4$ and evaporated *in vacuo* to afford the desired product (pale yellow oil, 4.0 g, 71%). **R_f** 0.33 (50% ethyl acetate in pentane); **^{1}H NMR** δ_H (400 MHz, $CDCl_3$) 1.50 – 1.93 (8H, m, H-1, H-2), 2.68 – 2.77 (1H, m, H-3), 3.66 (3H, s, H-5); **^{13}C NMR** δ_C (101 MHz, $CDCl_3$) 25.9 (C-2), 30.2 (C-1), 43.9 (C-3), 51.7 (C-5), 177.4 (C-4).

Potassium 4-bromobenzoate (2.10)[318]

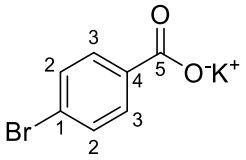

Methyl-4-bromobenzoate (108 mg, 50 mmol) was dissolved in a solution of KOH (30.9 mg, 0.55 mmol) in ACN (3.4 mL) and water (3.4 mL). The reaction mixture was stirred at RT for 2 h then evaporated *in vacuo* to afford the title compound (pale brown solid, 125 mg, quant.). **R**$_f$ 0.59 (50% MeOH in DCM); **mp** >350 ^oC; **^{1}H NMR** δ_H (500 MHz, methanol-d_4) 7.47 – 7.52 (2H, m, H-2), 7.81 – 7.85 (2H, m, H-3); **^{13}C NMR** δ_C (101 MHz, methanol-d_4) 124.2 (C-1), 130.4 (C-2), 130.7 (C-3), 137.0 (C-4), 172.8 (C-5).

4-Bromobenzoyl azide (2.11)[319]

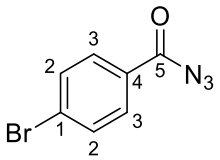

To a stirred solution of carboxylate salt **2.10** (125 mg, 0.500 mmol) in DMF (1.5 mL) at 0 ^oC was added diphenylphosphoryl azide (0.11 mL, 0.50 mmol). The solution was stirred for 2 h at 0 ^oC. Water (11 mL) was added to quench the reaction and diluted with ether (11 mL). The layers were then separated and the aqueous layers were washed with ethyl acetate (3 × 22 mL). The combined organic layers were washed with sat. aq. $NaHCO_3$ (44 mL) followed by brine (44 mL), then dried with $MgSO_4$. The crude product was obtained by evaporation *in vacuo*. Purification by flash chromatography (50% pentane in ethyl acetate) furnished the title compound (yellow oil, 0.105 g, 93%). **R**$_f$ 0.82 (50% ethyl acetate in pentane); **^{1}H NMR** δ_H (400 MHz, $CDCl_3$) 7.58 – 7.63 (2H, m, H-2), 7.86 – 7.91 (2H, m, H-3); **^{13}C NMR** δ_C (101 MHz, $CDCl_3$) 129.6 (C-1), 129.8 (C-3), 130.9 (C-2), 132.1 (C-4), 171.8 (C-5).

tert-Butyl (4-bromophenyl)carbamate (2.12)[320]

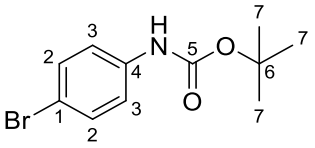

To a stirred solution of acyl azide **2.11** (105 mg, 0.500 mmol) in toluene (1.8 mL) was added *t*-butanol (50 µL, 0.56 mmol). The reaction mixture was heated at reflux for 3 h then cooled to RT. The solvent was evaporated *in vacuo* to obtain the desired product (pale yellow oil, 86.0 mg, 63%). **R_f** 0.80 (20% ethyl acetate in pentane); **^{1}H NMR** δ_H (400 MHz, $CDCl_3$) 1.51 (9H, s, H-7), 6.44 (1H, s, NH), 7.24 (2H, d, *J* = 2.5 Hz, H-2), 7.37 – 7.40 (2H, m, H-3); **^{13}C NMR** δ_C (101 MHz, $CDCl_3$) 27.3 (C-7), 79.9 (C-6), 114.4 (C-1), 119.6 (C-3), 130.9 (C-2), 136.4 (C-4), 151.5 (C-5).

6-Azaspiro[4.5]decan-7-one (2.13)[188]

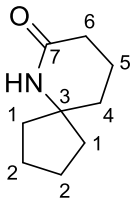

Oxime **2.14** (168 mg, 1.09 mmol) was dissolved in neat PPE (11 mL) and the mixture was stirred for 24 h at 0 ^oC then diluted with cold water (10 mL), and extracted with DCM (3 × 10 mL). The combined organic layers were washed with sat. aq. $NaHCO_3$ (10 mL) then brine (10 mL), and dried with $MgSO_4$. The crude product was concentrated *in vacuo* and purified by flash chromatography (10% ethyl acetate in pentane) to furnish the lactam as a white solid (39.5 mg, 34%). **R_f** 0.23 (10% ethyl acetate in pentane); **IR** ν_{max} (thin film)/cm^{-1} 3286br, 1670m, 1447m; **^{1}H NMR** δ_H (400 MHz, $CDCl_3$) 1.44 – 1.53 (3H, m, H-1, H-2), 1.54 – 1.79 (9H, m, H-1, H-2, H-4, H-5), 2.46 (2H, t, *J* = 8.0 Hz, H-6), 7.54 (1H, s, NH) ; **^{13}C NMR** δ_C (101 MHz, $CDCl_3$) 21.5 (C-5), 25.1 (C-2), 27.0 (C-6), 37.9

(C-1), 39.9 (C-4), 53.1 (C-3), 172.3 (C-7); **HRMS (ESI$^+$)** *m/z* $[M+H]^+$ calculated for $C_9H_{16}NO$, 154.1226; found, 154.1226.

Spiro[4.4]nonan-1-one oxime (2.14) [187]

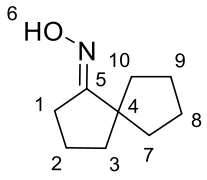

Crude **2.19** (0.119 g, 0.862 mmol) was dissolved in methanol (3.2 mL), followed by the addition of hydroxylamine hydrochloride (0.240 g, 3.45 mmol) and sodium acetate (283 mg, 3.45 mmol). The resultant white suspension was stirred at RT for 16 h, quenched with 0.2 M phosphate buffer pH 7 (4.3 mL), and further stirred for 2 h. The reaction was diluted with DCM and partitioned with water. The aqueous layers were extracted with DCM (4 × 22 mL) and the combined organic layers were washed with brine (22 mL) and dried with $MgSO_4$. The filtrate was concentrated *in vacuo*. Purification by flash chromatography (10% EtOAc in pentane) afforded the oxime as a colourless oil as a single diastereomer (77.9 mg, 59%). **R_f** 0.31 (10% EtOAc in pentane); **^{1}H NMR** δ_H (400 MHz, $CDCl_3$) 1.50 – 1.85 (12H, m, H-2, H-3, H-6, H-7), 2.53 (2H, t, *J* = 7.5 Hz, H-1), 8.35 (1H, br. s, OH); **^{13}C NMR** δ_C (101 MHz, $CDCl_3$) 21.5 (C-2), 25.1 (C-7), 27.1 (C-1), 37.9 (C-6), 40.0 (C-3), 53.1 (C-4), 172.1 (C-5).

Ethyl 1-(4-bromobutyl)-2-oxocyclopentane-1-carboxylate (2.17)

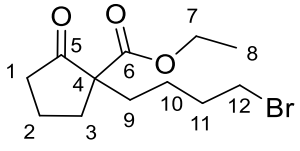

Ethyl 2-oxocyclopentane-1-carboxylate (1.5 g, 10 mmol) was added into a stirring suspension of potassium carbonate (2.76 g, 20.0 mmol) in acetone (20 mL). The mixture was heated at reflux for 18 h and was cooled to RT. Potassium carbonate was filtered and

then washed with EtOAc (*c.a.* 20 mL). The filtrate was concentrated *in vacuo* and purified by flash chromatography (8% → 32% ether in pentane, with a gradient of 5%) to furnish the *title compound* as a colourless oil (1.7 g, 60%). **R_f** 0.76 (20% EtOAc in pentane); **^{1}H NMR** δ_H (400 MHz, $CDCl_3$) 1.25 (3H, t, *J* = 7.0 Hz, H-3), 1.30 – 1.61 (4H, m, H-3, H-9), 1.81 – 2.08 (5H, m, H-2, H-10, H-11), 2.20 – 2.30 (1H, m, H-1), 2.38 – 2.46 (1H, m, H-1), 2.50 – 2.57 (1H, m, H-2), 3.40 (2H, t, *J* = 7.0 Hz, 2H, H-12), 4.16 (2H, qd, *J* = 7.0, 2.0 Hz, H-7); **^{13}C NMR** δ_C (101 MHz, $CDCl_3$) 14.1 (C-8), 19.6 (C-10), 23.4 (C-3), 32.8 (C-2, C-9, C-11), 33.3 (C-12), 37.9 (C-1), 60.3 (C-4), 61.5 (C-7), 170.9 (C-6), 214.8 (C-5); **HRMS (ESI$^+$)** *m/z* $[M+Na]^+$ calculated for $C_{12}H_{19}{}^{79}BrO_3Na$, 313.0410; found, 313.0410.

2-(4-Bromobutyl)cyclopentan-1-one (2.18)[321]

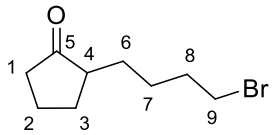

To **2.17** (1.74 g, 5.99 mmol) was added HBr 47–49% (1.0 mL, 9.0 mmol). The resulting solution was then heated at reflux for 17 h. The reaction was cooled to RT and water (35 mL) was added. The mixture was separated with EtOAc (3 × 35 mL) and the combined organic layers were washed with 10% sat. aq. $NaHCO_3$ solution (35 mL), brine (35 mL), dried with $MgSO_4$, and concentrated *in vacuo*. Purification by flash chromatography (10% EtOAc in pentane) afforded the title compound as a yellow oil (0.95 g, 73%). **R_f** 0.61 (10% EtOAc in pentane); **^{1}H NMR** δ_H (400 MHz, $CDCl_3$) 1.23 – 1.33 (1H, m, H-6), 1.45 – 1.56 (3H, m, H-3, H-7), 1.71 – 1.91 (4H, m, H-2, H-6, H-8), 1.97 – 2.16 (3H, m, H-1, H-2), 2.19 – 2.35 (2H, m, H-1, H-3), 3.41 (2H, td, *J* = 7.0 1.0 Hz, H-9); **^{13}C NMR** δ_C (101 MHz, $CDCl_3$) 20.7 (C-2), 26.1 (C-7), 28.8 (C-6), 29.6 (C-3), 32.7 (C-8), 33.6 (C-9), 38.1 (C-1), 49.0 (C-4), 221.1 (C-5).

Spiro[4.4]nonan-1-one (2.19)[322]

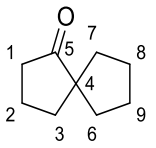

Potassium hydroxide (137 mg, 2.44 mmol) was added to **2.18** (267 mg, 1.22 mmol) in methanol (2.5 mL) whilst stirring. The resultant yellow solution was heated at reflux for 20 h and allowed to cool to RT. The solvent was removed *in vacuo* and the crude mixture was re-dissovled in water (15 mL). The mixture was separated with ether and the aqueous layers were washed with ether (4 × 15 mL). The combined organic layers were washed with brine and dried with $MgSO_4$. The filtrate was concentrated *in vacuo* at 600 mbar at RT to furnish the spiroketone as a yellow oil. Compound was used directly for next step without further purification. **R_f** 0.78 (20% EtOAc in pentane); **^{1}H NMR** δ_H (400 MHz, $CDCl_3$) 1.41 – 1.49 (2H, m, H-6), 1.60 – 1.66 (2H, m, H-7), 1.67 – 1.91 (8H, m, H-2, H-3, H-6, H-7), 2.22 – 2.27 (2H, m, H-1); **^{13}C NMR** δ_C (101 MHz, $CDCl_3$) 19.7 (C-2), 25.9 (C-7), 36.4 (C-6), 37.5 (C-1), 38.2 (C-3), 56.3 (C-4), 224.1 (C-5); **HRMS (ESI$^+$)** *m/z* $[M+H]^+$ calculated for $C_9H_{15}O$, 139.1117; found, 139.1117.

4-(Cyclopent-1-en-1-yl)butanenitrile a (2.22) & 4-Cyclopentylidenebutanenitrile b (2.23)[195,323]

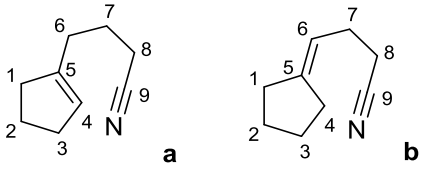

To a solution of oxime **2.14** (77.9 mg, 0.508 mmol) in THF (7.6 mL) was added a solution of thionyl chloride (0.81 mL) in THF (2 mL). The mixture was then stirred at 0 °C for 5 h. Water (3.2 mL) was added and the solution was neutralized with aq. ammonia. The mixture was separated with DCM and the combined extract was washed with water, brine, and dried with $MgSO_4$. The solvent was removed *in vacuo*. Purification by flash

chromatography (10% EtOAc in pentane) afforded the title compound along with the *exo*-isomer as a colourless oil (23.0 mg, 33 %, *endo:exo* 20 : 1, isomer ratio determined by integration of the C(4)H signal in the ^{1}H NMR spectrum). **R_f** 0.5 (10% EtOAc in pentane); **^{1}H NMR** δ_H (400 MHz, $CDCl_3$) 1.73 – 1.57 (2H, m), 1.57 – 1.72 (4H, m), 2.18 – 2.27 (7H, m), 2.27 – 2.37 (5H, m), 5.38 – 5.42 (1H, m, H-4$_A$), 5.22 – 5.28 (1H, m, H-4$_B$); **^{13}C NMR** δ_C (101 MHz, $CDCl_3$) 142.0 (C-5$_A$), 125.4 (C-4$_A$), 115.7 (C-9$_A$), 34.8 (C-1$_A$), 32.4 (C-6$_A$), 30.0 (C-3$_A$), 23.5 (C-2$_A$), 23.4 (C-7$_A$), 14.2 (C-8$_A$).

tert-Butyl 6-azaspiro[4.5]decane-6-carboxylate (2.24)[324]

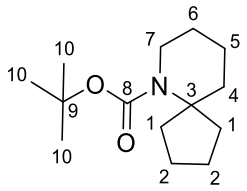

Benzylated-spiroamine **2.45** (656 mg, 2.86 mmol) was dissolved in ethanol (12 mL) and 20% $Pd(OH)_2$/C (86.7 mg) and Boc_2O (936 mg, 4.29 mmol) were added. The mixture was stirred under hydrogen for 18 h at RT. The reaction was then filtered through a celite pad and concentrated *in vacuo*. The filtrate was then dissolved in ethanol (23 mL) and imidazole (195 mg, 2.86 mmol) was added. The mixture was stirred at RT for 1 h and concentrated *in vacuo*. Chloroform (28 mL) was added and the organic layers were washed with 1% HCl aqueous solution cooled to 0 ^{o}C (2 × 10 mL), dried with $MgSO_4$ and concentrated *in vacuo*. Purification by flash chromatography (5% EtOAc in pentane) afforded the title compound as a colourless oil (0.36 g, 52%). **R_f** 0.75 (100% pentane); **^{1}H NMR** δ_H (400 MHz, $CDCl_3$) 1.45 (9H, s, H-10), 1.49 – 1.59 (6H, m, H-2, H-4, H-6), 1.59 – 1.66 (2H, m, H-5), 1.71 – 1.81 (2H, m, H-2), 1.84 – 1.92 (2H, m, H-1), 1.97 – 2.07 (2H, m, H-1), 3.43 – 3.50 (2H, m, H-7); **^{13}C NMR** δ_C (100 MHz, $CDCl_3$) 20.7 (C-5), 23.9 (C-1), 24.7 (C-6), 28.8 (C-10), 34.5 (C-4), 37.5 (C-2), 44.4 (C-7), 66.2 (C-3), 79.3 (C-9), 156.1 (C-8).

***tert*-Butyl (2*R**, 5*R**)-2-hydroxy-6-azaspiro[4.5]decane-6-carboxylate (2.24a)**

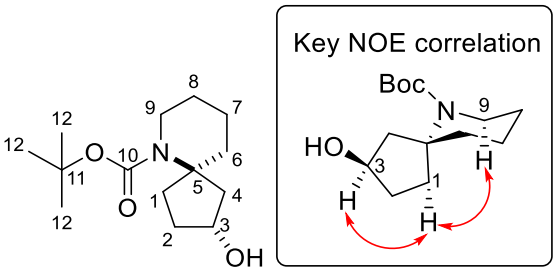

The titled compound was synthesized by following **GP-1** using $P450_{BM3}$ mutant enzyme strain KT2/L188G/I263G on a reaction scale of 50 mL. Reaction was completed after 24 h, as monitored by GC. The crude product was purified by flash chromatography (5% → 25% EtOAc in pentane, with a gradient of 5%) to afford a colourless oil (2.9 mg, 11%). **IR** ν_{max} (thin film)/cm^{-1} 3671br, 1701s, 1365s, 1252m, 1149s; **R_f** 0.48 (70% EtOAc in pentane); **^{1}H NMR** δ_H (500 MHz, $CDCl_3$) 1.45 (9H, s, H-12), 1.52 – 1.54 (2H, m, H-8), 1.55 – 1.56 (1H, m, H-2), 1.60 – 1.67 (2H, m, H-7), 1.73 – 1.79 (3H, m, H-4, H-6), 1.94 – 2.00 (1H, m, H-1), 2.05 – 2.12 (1H, m, H-1), 2.15 – 2.23 (1H, m, H-2), 2.49 (1H, dd, *J* = 14.0, 7.5 Hz, H-4), 3.36 – 3.49 (2H, m, H-9), 4.51 – 4.56 (1H, m, H-3); **^{13}C NMR** δ_C (126 MHz, $CDCl_3$) 19.7 (C-7), 24.2 (C-8), 28.6 (C-12), 34.6 (C-2), 35.7 (C-1), 37.0 (C-6), 43.6 (C-9), 47.3 (C-4), 64.8 (C-5), 73.0 (C-3), 79.3 (C-11), 155.8 (C-10); **HRMS (ESI$^+$)** *m/z* $[M+H]^+$ calculated for $C_{14}H_{26}O_3N$, 256.1907; found, 256.1908.

***tert*-Butyl (2*S**, 5*R**)-2-hydroxy-6-azaspiro[4.5]decane-6-carboxylate (2.24b)**

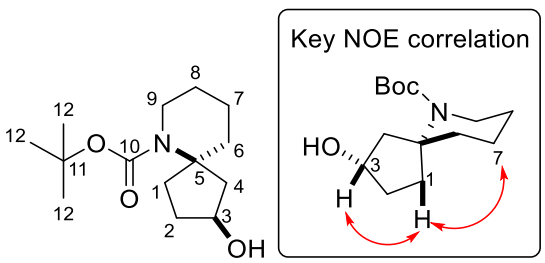

The titled compound was synthesized by following **GP-1** using $P450_{BM3}$ mutant enzyme strain GL/L188Q/I263G/A328G on a reaction scale of 50 mL. Reaction was completed

after 24 h, as monitored by GC. The crude product was purified by flash chromatography (5% → 25% EtOAc in pentane, with a gradient of 5%) to afford a colourless oil (0.8 mg, 3%). **IR** ν_{max} (thin film)/cm^{-1} 3596br, 1702s, 1365m, 1273m, 1150s; **R$_f$** 0.47 (70% EtOAc in pentane); **^{1}H NMR** δ_H (500 MHz, $CDCl_3$) 1.45 (9H, s, H-12), 1.50 – 1.54 (2H, m, H-8), 1.56 – 1.58 (1H, m, H-2), 1.61 – 1.66 (2H, m, H-7), 1.73 – 1.80 (3H, m, H-4, H-6), 1.94 – 2.00 (1H, m, H-1), 2.09 (1H, dt, *J* = 13.0, 8.5 Hz, H-1), 2.15 – 2.22 (1H, m, H-2), 2.49 (1H, dd, *J* = 14.0, 7.5 Hz, H-4), 3.37 – 3.50 (2H, m, H-9), 4.51 – 4.57 (1H, m, H-3); **^{13}C NMR** δ_C (126 MHz, $CDCl_3$) 19.9 (C-7), 24.4 (C-8), 28.7 (C-12), 34.5 (C-1), 35.9 (C-2), 37.2 (C-6), 43.7 (C-9), 47.5 (C-4), 64.5 (C-5), 73.1 (C-5), 79.4 (C-3), 155.9 (C-11); **HRMS (ESI$^+$)** *m/z* $[M+Na]^+$ calculated for $C_{14}H_{25}O_3NNa$, 278.1727; found, 279.0935.

tert-Butyl 1-hydroxy-6-azaspiro[4.5]decane-6-carboxylate (2.24c)

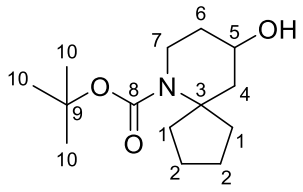

The titled compound was synthesized by following **GP-1** using P450$_{BM3}$ mutant enzyme strain R19/F87I/L437LV on a reaction scale of 50 mL. Reaction was completed after 24 h, as monitored by GC. The crude product was purified by flash chromatography (5% → 25% EtOAc in pentane, with a gradient of 5%) to afford a colourless oil (1.9 mg, 7%). **R$_f$** 0.45 (70% EtOAc in pentane); **^{1}H NMR** δ_H (500 MHz, $CDCl_3$) 1.36 – 1.40 (1H, m, H-6), 1.46 (9H, s, H-10), 1.48 (1H, dd, *J* = 3.0, 1.0 Hz, H-4), 1.51 – 1.52 (1H, m, H-2), 1.58 – 1.62 (1H, m, H-2), 1.68 – 1.73 (2H, m, H-1, H-2), 1.76 – 1.82 (1H, m, H-2), 1.83 – 1.87 (1H, m, H-1), 1.86 – 1.89 (1H, m, H-1), 1.91 – 1.98 (2H, m, H-4, H-6), 2.37 (1H, ddd, *J* = 13.0, 9.0, 8.0 Hz, H-1), 3.03 – 3.10 (1H, m, H-7), 3.92 – 4.02 (2H, m, H-5, H-7); **^{13}C NMR** δ_C (126 MHz, $CDCl_3$) 23.1 (C-2), 28.5 (C-12), 34.7 (C-8), 36.6 (C-1), 42.6 (C-9),

43.6 (C-6), 66.0 (C-5), 66.5 (C-7), 79.6 (C-11), 155.7 (C-10); **HRMS (ESI$^+$)** *m/z* $[M+Na]^+$ calculated for $C_{14}H_{25}O_3NNa$, 278.1727; found *m/z* 278.1728.

tert-Butyl 9-oxo-6-azaspiro[4.5]decane-6-carboxylate (2.24c1)

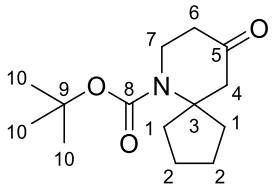

Alcohol **2.24c** (5.1 mg, 0.0200 mmol) was dissolved in DCM (0.5 mL), followed by the addition of $NaHCO_3$ (4.7 mg, 0.0560 mmol). The mixture was cooled to 0 ^oC and DMP (16.9 mg, 0.0399 mmol) was added. The reaction was stirred for 12 h at RT and was washed with 1 M aq. NaOH solution twice. The aqueous layers were washed with DCM (3 × 2 mL) and the combined organic layers were washed with brine (2 mL) and dried with $MgSO_4$. Purification by flash chromatography (40% EtOAc in pentane) afforded the *titled compound* as a pale yellow oil (5.1 mg, 97%); **R$_f$** 0.70 (50% EtOAc in pentane); **IR** ν_{max} (thin film)/cm^{-1} 1727m, 1691s, 1386m, 1227w, 1167m ; **^{1}H NMR** δ_H (400 MHz, $CDCl_3$) 1.49 (9H, s, H-10) 1.57 – 1.65 (4H, m, H-1, H-2), 1.78 – 1.89 (2H, m, H-2), 2.20 – 2.30 (2H, m, H-1), 2.40 (2H, t, *J* = 6.0 Hz, H-6), 2.56 (2H, s, H-4), 3.87 (2H, t, *J* = 6.0 Hz, H-7); **^{13}C NMR** δ_C (125 MHz, $CDCl_3$) 24.3 (C-2), 28.7 (C-10), 38.4 (C-1), 40.4 (C-6), 41.6 (C-7), 51.6 (C-4), 66.0 (C-3), 80.6 (C-9), 155.0 (C-8), 209.2 (C-7); **HRMS (ESI$^+$)** *m/z* $[M+Na]^+$ calculated for $C_{14}H_{23}O_3NNa$, 276.1570; found, 276.1571.

tert-Butyl 8-hydroxy-6-azaspiro[4.5]decane-6-carboxylate (2.24d)

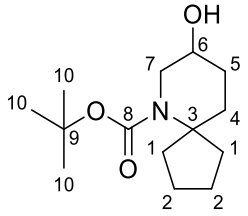

The titled compound was synthesized by following **GP-1** using $P450_{BM3}$ mutant enzyme strain R19/F87I/E267F on a reaction scale of 100 mL. Reaction was completed after 24 h, as monitored by GC. The crude product was purified by flash chromatography (5% → 25% EtOAc in pentane, with a gradient of 5%) to afford a colourless oil (1.8 mg, 4%). **R_f** 0.71 (75% EtOAc in pentane); **IR** ν_{max} (thin film)/cm^{-1} 3439br, 1656m, 1366m, 1250m, 1076w; **^{1}H NMR** δ_H (500 MHz, $CDCl_3$) 1.47 (9H, s, H-10), 1.50 – 1.56 (3H, m, H-2, H-4), 1.60 – 1.67 (1H, m, H-5), 1.73 – 1.79 (3H, m, H-2, H-4), 1.84 – 1.95 (3H, m, H-1, H-5), 1.98 – 2.11 (2H, m, H-1), 3.37 – 3.46 (1H, m, H-7), 3.67 (1H, ddd, *J* = 14.0, 3.5, 1.0 Hz, H-7), 3.79 – 3.84 (1H, m, H-6); **^{13}C NMR** δ_C (126 MHz, $CDCl_3$) 23.7 (C-2), 28.7 (C-10), 29.3 (C-5), 29.9 (C-4), 37.2 (C-1), 47.5 (C-3), 50.2 (C-7), 66.5 (C-6), 79.9 (C-9), 156.(C-8); **HRMS (ESI$^+$)** *m/z* $[M+Na]^+$ calculated for $C_{14}H_{25}O_3NNa$, 278.1727; found, 278.1726.

tert-Butyl (1-(4-hydroxybutyl)cyclopentyl)carbamate (2.24e)

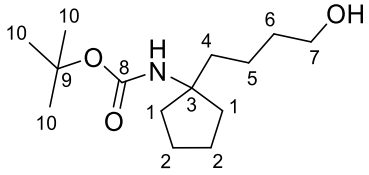

The titled compound was synthesized by following **GP-1** using $P450_{BM3}$ mutant enzyme strain R19/A330W on a reaction scale of 100 mL. Reaction was completed after 24 h, as monitored by GC. The crude product was purified by flash chromatography (5% → 20% EtOAc in pentane, with a gradient of 5%) to afford a yellow oil (5.6 mg, 11%). **R_f** 0.70

(75% EtOAc in pentane); **IR** ν_{max} (thin film)/cm^{-1} 3500br, 3342br, 1689m, 1457w, 1366w, 1250m; **^{1}H NMR** δ_H (400 MHz, $CDCl_3$) 1.32 – 1.40 (2H, m, H-5), 1.43 (9H, s, H-10), 1.50 – 1.60 (4H, m, H-1, H-6), 1.60 – 1.73 (4H, m, H-2), 1.73 – 1.81 (2H, m, H-4), 1.81 – 1.88 (2H, m, H-1), 3.65 (2H, t, *J* = 6.5 Hz, H-7), 4.41 (1H, br s, NH); **^{13}C NMR** δ_C (126 MHz, $CDCl_3$) 21.2 (C-5), 23.8 (C-2), 28.6 (C-10), 33.0 (C-6), 37.5 (C-4), 38.5 (C-1), 62.9 (C-7), 63.9 (C-3), 78.9 (C-9), 154.8 (C-8); **HRMS (ESI$^+$)** *m/z* $[M+Na]^+$ calculated for $C_{14}H_{27}O_3NNa$, 280.1883; found, 280.1883.

4-(1-Nitrocyclopentyl)butanal (2.25)

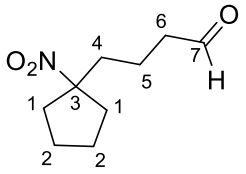

Enol ether **2.26** (47.3 mg, 0.237 mmol) was dissolved in acetone (24 mL) and HCl (0.7 mL, 1.0 M aq. solution 0.71 mmol) was added. The reaction was stirred at RT for 4 h and sat. aq. $NaHCO_3$ solution (15 mL) was added. The mixture was extracted with ether (3 × 20 mL) and the combined organic layers were washed with brine (20 mL). The solvent was removed *in vacuo* to afford the *title compound* as a colourless oil (29.8 mg, 68%). **R$_f$** 0.66 (20% EtOAc in pentane); **IR** ν_{max} (thin film)/cm^{-1} 1723s, 1532s, 1456w, 1356m ; **^{1}H NMR** δ_H (400 MHz, $CDCl_3$) 1.63 – 1.57 (2H, m, H-5), 1.70 – 1.83 (6H, m, H-1, H-2), 1.97 – 2.03 (2H, m, H-4), 2.47 (2H, td, *J* = 7.0, 1.5 Hz, H-6), 2.53 – 2.63 (2H, m, H-1), 9.75 (1H, t, *J* = 1.5 Hz, H-7); **^{13}C NMR** δ_C (101 MHz, $CDCl_3$) 17.4 (C-5), 24.2 (C-2), 37.2 (C-1), 38.8 (C-4), 43.3 (C-6), 99.7 (C-3), 201.2 (C-7); **HRMS (ESI$^+$)** *m/z* $[M+Na]^+$ calculated for $C_9H_{15}O_3NNa$, 208.0944; found, 208.0947.

(E)-1-(4-Methoxybut-3-en-1-yl)-1-nitrocyclopentane (2.26)

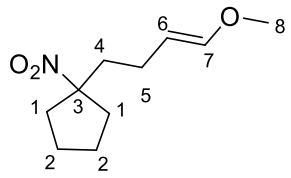

(Methoxymethyl)triphenylphosphonium chloride (1.52 g, 4.43 mmol) was dissolved in THF (17 mL) and *t*-BuOK (4.0 mL, 1.0 M solution in THF, 4.0 mmol) at −78 °C. The mixture was stirred at the same temperature for 30 min. Aldehyde **2.29** (345 mg, 2.01 mmol) in THF (1.7 mL) was then added to the mixture and allowed to warm to RT and stirred for 19 h. Brine (17 mL) was then added and resulting solution was extracted with diethyl ether (3 × 17 mL). The combined organic layers were washed with brine (17 mL) and dried with $MgSO_4$. Solvent was removed *in vacuo* and the crude product was purified by flash chromatography (10% EtOAc in pentane) to furnish a light yellow oil along with the *Z*-isomer (268 mg, 67%, 3:1 *E:Z*, isomer ration determined by integration of the H-5 signal in the ^{1}H NMR spectrum). **R$_f$** 0.58 (20% EtOAc in pentane); **IR** ν_{max} (thin film)/cm^{-1} 1657m, 1534s, 1209m, 1108w, 938m; **^{1}H NMR** δ_H (400 MHz, $CDCl_3$, major isomer) 1.70 – 1.81 (5H, m, H-1, H-2), 1.86 – 1.93 (2H, m, H-5), 2.00 – 2.03 (2H, m, H-4), 2.62 – 2.58 (3H, m, H-1), 3.49 (3H, s, H-8), 4.64 (1H, dt, *J* = 12.5, 7.0 Hz, H-6), 6.28 (1H, dt, *J* = 12.5, 1.0 Hz, H-7); **^{13}C NMR** δ_C (101 MHz, $CDCl_3$) 23.4 (C-5), 24.1 (C-1), 37.2 (C-2), 40.9 (C-4), 56.0 (C-8), 99.8 (C-3), 101.1 (C-6), 147.9 (C-7); **HRMS (ESI$^+$)** *m/z* $[M+Na]^+$ calculated for $C_{10}H_{17}O_3NNa$, 222.1101; found, 222.1102.

Nitrocyclopentane (2.27)[325]

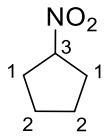

Bromocyclopentane (1.1 mL, 10 mmol) was added to a solution of $NaNO_2$ (1.17 g, 17.0 mmol) in dry DMSO (7 mL). The resulting solution was stirred at 15 °C for 3 h and

quenched with iced water (3 mL). The mixture was separated with petroleum ether (4 × 3 mL) and the organic layers were washed with water (3 mL), brine (3 mL), and dried with $MgSO_4$. The crude product was concentrated *in vacuo* to afford a green oil. Compound was used directly for next step without further purification. **R_f** 0.86 (10% EtOAc in pentane); **^{1}H NMR** δ_H (400 MHz, $CDCl_3$) 1.63 – 1.76 (2H, m, H-1), 1.82 – 1.98 (2H, m, H-1), 2.05 – 2.19 (2H, m, H-2), 2.23 – 2.32 (2H, m, H-2), 4.89 (1H, tt, *J* = 8.0, 4.0 Hz, H-3); **^{13}C NMR** δ_C (101 MHz, $CDCl_3$) 24.7 (C-2), 32.9 (C-1), 86.8 (C-5).

3-(1-Nitrocyclopentyl)propanal (2.29)

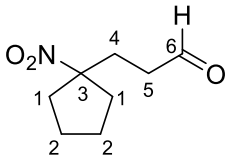

To a solution of **2.27** (930 mg, 8.08 mmol) in ACN (4.1 mL) was added acrolein (0.86 mL, 13 mmol) and triethylamine (0.11 mL, 0.80 mmol). The mixture was stirred at RT for 60 h and quenched with 0.06 M HCl aqueous solution (4 mL). The reaction mixture was extracted with ether (3 × 10 mL) and the combined organic layers were washed with water (10 mL), brine (10 mL) and dried with $MgSO_4$. The crude product was concentrated *in vacuo* and purification with flash chromatography (10% → 20% EtOAc in pentane, with a gradient of 5%) afforded a bright yellow oil (0.349 g, 20% over 2 steps). **R_f** 0.33 (20% EtOAc in pentane); **IR** ν_{max} (thin film)/cm^{-1} 1723m, 1533s 1354w; **^{1}H NMR** δ_H (400 MHz, $CDCl_3$) 1.77 – 1.82 (6H, m, H-1, H-2), 2.28 – 2.35 (2H, m, H-4), 2.48 – 2.54 (2H, m, H-5), 2.54 – 2.60 (2H, m, H-1), 9.77 (1H, t, *J* = 1.0 Hz, H-6); **^{13}C NMR** δ_C (101 MHz, $CDCl_3$) 24.2 (C-2), 31.2 (C-4), 37.3 (C-1), 39.6 (C-5), 98.8 (C-2), 199.8 (C-6); **HRMS (ESI$^+$)** *m/z* $[M+Na]^+$ calculated for $C_8H_{13}O_3NNa$, 194.0788; found, 194.0791.

6-Chloro-2,3,4,5-tetrahydropyridine (2.34)

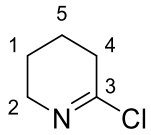

Phosphorus pentachloride (208 mg, 1.00 mmol) was added to a solution of 2-piperidone (90 µL, 1.0 mmol) in DCM (2.1 mL) at RT whilst stirring. After 2 h, the solvent was evaporated *in vacuo* to afford a yellow slurry. Compound was used directly for next step without further purification. **R_f** 0.35 (60% EtOAc in pentane); **IR** ν_{max} (thin film)/cm^{-1} 1640m, 800m; **^{1}H NMR** δ_H (400 MHz, $CDCl_3$) 1.86 - 1.95 (4H, m, H-1, H-5), 2.66 – 2.71 (2H, m, H-4), 3.51 – 3.56 (2H, m, H-2); **^{13}C NMR** δ_C (101 MHz, $CDCl_3$) 18.2 (C-1/C-5), 18.8 (C-1/C-5), 27.4 (C-4), 42.6 (C-2), 177.2 (C-3); **HRMS (ESI)** not found.

2,2-Diallylpiperidine (2.35)[216]

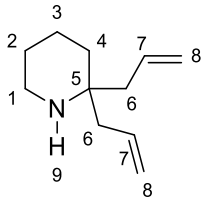

To a solution of imidoyl chloride **2.34** (331 mg, 2.00 mmol) in THF (4.2 mL) was added Allylmagnesium chloride (3.0 mL, 2.0 M solution in THF, 3.0 mmol) at RT. The reaction mixture was stirred for 6 h and quenched with water (31 mL), extracted with ether (3 × 35 mL), and the combined organic layers were washed with water (35 mL) and brine (35 mL). The organic layer was dried with $MgSO_4$ and the solvent was concentrated *in vacuo* to afford a volatile yellow oil. Compound was used directly for next step without further purification. **R_f** 0.6 (20% EtOAc in pentane); **^{1}H NMR** δ_H (400 MHz, $CDCl_3$) 1.35 – 1.44 (2H, m, H-4), 1.44 – 1.50 (2H, m, H-2), 1.53 – 1.60 (2H, m, H-3), 2.11 – 2.44 (4H, m, H-6), 2.77 – 2.84 (2H, m, H-1), 5.08 (4H, ddt, *J* = 8.5, 2.5, 1.0 Hz, H-8), 5.75 – 5.87 (2H, m, H-7); **^{13}C NMR** δ_C (101 MHz, $CDCl_3$) 20.3 (C-3), 26.3 (C-2), 34.2 (C-4), 40.9 (C-1), 41.1 (C-6), 52.9 (C-5), 118.0 (C-8), 134.1 (C-7).

2,2-Diallyl-1-(methylsulfonyl)piperidine (2.36)

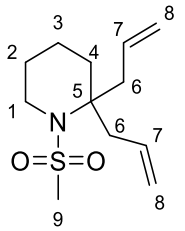

A solution of crude diene **2.35** (331 mg, 2.00 mmol) in DCM (13 mL) was cooled to 0 ^{o}C. Triethylamine (1.4 mL, 10.0 mmol) was added and methanesulfonyl chloride (0.31 mL, 4.0 mmol) was added dropwise. The mixture was warmed to RT and stirred for 5 h. A few drops of sat. aq. $NaHCO_3$ solution was added, followed by water (5 mL). The resulting solution was extracted with DCM and the organic layers were washed with brine and dried with $MgSO_4$. Purification by flash chromatography (10% → 20% EtOAc in pentane , with a gradient of 5%) furnished a yellow oil (38.7 mg, 8%). **R_f** 0.42 (20% EtOAc in pentane); **IR** ν_{max} (thin film)/cm^{-1} 1462m, 1353s, 1252m, 1072m, 827m, 749m; **^{1}H NMR** δ_H (400 MHz, $CDCl_3$) 1.67 – 1.56 (6H, m, H-2, H-3, H-4), 2.45 – 2.52 (2H, m, H-6), 2.86 – 2.91 (2H, m, H-6), 2.92 (3H, s, H-9), 3.30 – 3.35 (2H, m, H-1), 5.10 – 5.12 (2H, m, H-8), 5.12 – 5.17 (2H, m, H-8), 5.80 – 5.92 (2H, m, H-7); **^{13}C NMR** δ_C (101 MHz, $CDCl_3$) 18.7 (C-3), 24.8 (C-2), 32.7 (C-4), 41.4 (C-6), 41.8 (C-9), 44.3 (C-1), 118.6 (C-8), 133.9 (C-7); **HRMS (ESI$^+$)** *m/z* $[M+Na]^+$ calculated for $C_{12}H_{21}O_2NSNa$, 266.1185; found, 266.1187.

6-(Methylsulfonyl)-6-azaspiro[4.5]decane (2.37)

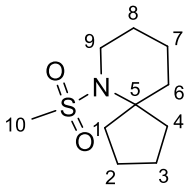

To a solution of diene **2.36** (38.7 mg, 0.159 mmol) in dry and degassed DCE (1.6 mL) was added Hoveyda-Grubbs 2nd generation catalyst (5.0 mg, 0.008 mmol) whilst stirring at RT. After 1 h, an aliquot of the reaction mixture was taken and a NMR spectra was taken to indicate complete conversion to cycloalkene. To the mixture was then added $NaBH_4$ (12.0 mg, 0.318 mmol) and methanol (0.08 mL) and stirred for 4 h. The solvent was concentrated *in vacuo* and purification with flash chromatography (10% → 20% EtOAc in pentane, with a gradient of 10%) afforded the *title compound* as a yellow oil (6.9 mg, 20%). **IR** ν_{max} (thin film)/cm^{-1} 1447m , 1323s, 1058m; **R$_f$** 0.38 (20% EtOAc in pentane); **^{1}H NMR** δ_H (400 MHz, $CDCl_3$) 1.53 – 1.64 (6H, m, H-1, H-4, H-6), 1.64 – 1.72 (2H, m, H-5), 1.73 – 1.83 (2H, m, H-1), 1.90 – 1.97 (2H, m, H-2), 2.06 – 2.16 (2H, m, H-2), 2.95 (3H, s, H-8), 3.47 – 3.50 (2H, m, H-7); **^{13}C NMR** δ_C (101 MHz, $CDCl_3$) 21.1 (C-5), 22.9 (C-1), 25.7 (C(8)), 35.4 (C-2), 44.3 (C-8), 45.9 (C-7), 68.4 (C-3); **HRMS (ESI$^+$)** *m/z* $[M+H]^+$ calculated for $C_{10}H_{20}O_2NS$, 218.1209; found, 218.1212.

6-(Methylsulfonyl)-6-azaspiro[4.5]dec-7-ene (2.37a)

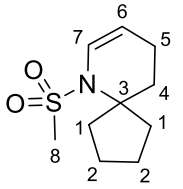

The titled compound was synthesized by following **GP-1** using $P450_{BM3}$ mutant enzyme strain R19/F87A/A184I/A264G on a reaction scale of 50 mL. Reaction was completed after 3 h, as monitored by GC. The crude product was purified by flash chromatography (5% → 15% EtOAc in pentane, with a gradient of 5%) to afford a colourless oil (8.3 mg, 38%). **R$_f$** 0.66 (50% EtAOc in pentane); **IR** ν_{max} (thin film)/cm^{-1} 1655w, 1413m, 1330s, 761m; **^{1}H NMR** δ_H (500 MHz, $CDCl_3$) 1.59 – 1.69 (4H, m, H-1, H-2), 1.72 (2H, t, *J* =

6.5 Hz, H-4), 1.84 – 1.90 (2H, m, H-2), 2.08 (2H, tdd, *J* = 6.5, 3.5, 2.0 Hz, H-5), 2.30 – 2.39 (2H, m, H-1), 2.96 (3H, s, H-8), 4.96 (1H, dt, *J* = 8.0, 3.5 Hz, H-6), 6.61 (1H, dt, *J* = 8.5, 2.0 Hz, H-7); **^{13}C NMR** δ_C (126 MHz, $CDCl_3$) 19.8 (C-5), 23.3 (C-2), 34.2 (C-4), 36.6 (C-1), 42.1 (C-8), 68.1 (C-3), 106.9 (C-6), 126.7 (C-7); **HRMS (ESI$^+$)** *m/z* $[M+Na]^+$ calculated for $C_{10}H_{17}O_2NSNa$, 238.0872; found, 238.0874.

1-Benzylpiperidin-2-one (2.43)[326]

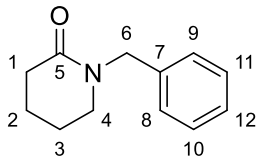

To s solution of piperidin-2-one (920 µL, 10.0 mmol) in THF (23 mL) was added NaH (600 mg, 60% dispersion in mineral oil, 15.0 mmol) at −5 °C. The mixture was stirred for 30 min at 0 °C and BnBr (1.6 mL) was added. The mixture was then warmed to RT and stirred for 16 h. Iced water (8 mL) was added and the solution was extracted with EtOAc (3 × 9 mL). The combined organic layers were washed with brine (9 mL) and dried with $MgSO_4$. The crude product was concentrated *in vacuo* and purification with flash chromatography (1% → 2% methanol in DCM) afforded the title compound as a pale brown oil (1.7 g, 92%). **R_f** 0.39 (4% methanol in DCM); **^{1}H NMR** δ_H (400 MHz, $CDCl_3$) 1.73 – 1.84 (4H, m, H-2, H-3), 2.47 (2H, t, *J* = 6.5 Hz, H-1), 3.16 – 3.23 (2H, m, H-4), 4.60 (2H, s, H-6), 7.23 – 7.34 (5H, m, H-Ar); **^{13}C NMR** δ_C (100 MHz, $CDCl_3$) 21.4 (C-2), 23.1 (C-3), 32.4 (C-1), 47.3 (C-4), 50.1 (C-6), 127.3 (C-Ar), 128.1 (C-Ar), 128.6 (C-Ar), 137.3 (C-7), 169.9 (C-5).

2,2-Diallyl-1-benzylpiperidine (2.44)[203]

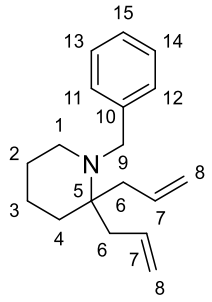

Benzylated-lactam **2.43** (3.0 g, 16 mmol) was dissolved in DCM (159 mL) and cooled to −78 °C. Tf_2O (3.2 mL, 19 mmol) was added dropwise and the solution was stirred at −78 °C for 45 min. Allyl magnesium chloride (24 mL, 2.0 M solution in THF, 48 mmol) was added dropwise and the solution was warmed to RT. The reaction was allowed to stir at RT for 16 h. Sat. aq. NH_4Cl (53 mL) was added and the mixture was extracted with DCM. The combined organic layers were washed with water, brine, and dried with $MgSO_4$. Purification by flash chromatography (25% EtOAc in pentane) afforded the title compound as a pale-yellow oil (3.5 g, 87%). **R_f** 0.56 (10% EtOAc in pentane); **^{1}H NMR** δ_H (400 MHz, $CDCl_3$) 1.41 – 1.58 (6H, m, H-2, H-3, H-4), 2.12 (2H, ddt, *J* = 14.5, 8.0, 1.5 Hz, H-6), 2.38 – 2.47 (2H, m, H-1), 2.62 (2H, ddt, *J* = 14.5, 7.0, 1.5 Hz, H-6), 3.62 (2H, s, H-9), 5.00 – 5.10 (4H, m, H-8), 5.89 – 6.01 (2H, m, H-7), 7.16 – 7.39 (5H, m, H-Ar); **^{13}C NMR** δ_C (100 MHz, $CDCl_3$) 20.6 (C-3), 26.2 (C-2), 32.3 (C-4), 38.0 (C-6), 46.1 (C-1), 52.9 (C-9), 58.2 (C-5), 116.8 (C-8), 126.4 (C-Ar), 128.1 (C-Ar), 128.2 (C-Ar), 135.4 (C-7), 141.0 (C-10).

6-Benzyl-6-azaspiro[4.5]decane (2.45)[216]

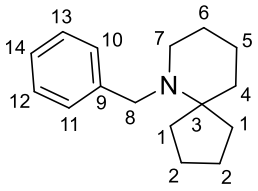

Diallylated lactam **2.44** (1.5 g, 5.9 mmol) was dissolved in dry DCE (59 mL) and Hoveyda-Grubbs first generation catalyst (338 mg, 0.411 mmol) was added. The mixture was stirred at RT for 7 h and $NaBH_4$ (445 mg, 11.8 mmol) and methanol (2.6 mL) was

added. The resulting mixture was stirred at RT for 16 h and diluted with DCM. The combined organic layers were washed with water, brine, and dried with $MgSO_4$. Purification by flash chromatography (20% EtOAc in pentane afforded the title compound as a yellow oil (0.66 g, 49%). **R_f** 0.63 (20% EtOAc in pentane); **^{1}H NMR** δ_H (400 MHz, $CDCl_3$) 1.38 – 1.47 (2H, m, H-6), 1.46 – 1.69 (10H, m, H-1, H-2, H-4, H-5), 1.76 – 1.85 (2H, m, H-2), 2.32 – 2.40 (2H, m, H-7), 3.47 (2H, s, H-8), 7.17 – 7.38 (5H, m, H-Ar); **^{13}C NMR** δ_C (100 MHz, $CDCl_3$) 22.3 (C-5), 25.5 (C-6), 25.9 (C-2), 33.7 (C-1), 39.0 (C-4), 49.0 (C-7), 54.5 (C-8), 66.6 (C-3), 126.4 (C-Ar), 128.1 (C-Ar), 128.4 (C-Ar), 141.6 (C-9).

Trifluoroacetic acid-6-azaspiro[4.5]decane salt (2.54)

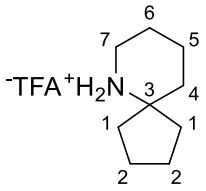

To a stirred mixture of Boc-protected spiroamine **2.24** (0.100 mg, 0.418 mmol) in DCM (2.8 mL) was added trifluroacetic acid (0.14 mL, 1.8 mmol). The resulting solution was stirred for 18 h and concentrated *in vacuo* to afford a yellow oil. Compound was used for the next step without further purification. **^{1}H NMR** δ_H (400 MHz, $CDCl_3$) 1.64 – 1.73 (4H, m, H-2, H-4), 1.75 – 1.86 (8H, m, H-1, H-2, H-5, H-6), 1.90 – 1.96 (2H, m, H-1), 3.10 – 3.17 (2H, m, H-7), 8.21 (1H, br, NH), 9.21 (1H, br, NH); **^{13}C NMR** δ_C (101 MHz, $CDCl_3$) 20.0 (C-4), 22.2 (C-5), 23.9 (C-2), 34.1 (C-6), 36.1 (C-1), 42.1 (C-7), 66.2 (C-3).

2,2,2-Trifluoro-1-(6-azaspiro[4.5]decan-6-yl)ethan-1-one (2.55)

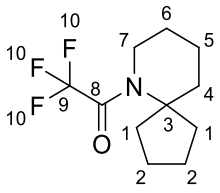

To trifluoroacetate salt **2.54** (818 mg, 3.23 mmol) in DCM (2.6 mL) was added triethylamine (2.3 mL, 16 mmol) dropwise. The mixture was then cooled to 0 °C and TFAA (0.9 mL, 6.5 mmol) was added slowly. The resulting solution was allowed to warm to RT and stirred for 18 h. The organic layers were then washed with 1M HCl, water, and sat. aq. $NaHCO_3$. Purification by flash chromatography (5% EtOAc in pentane) afforded the *title compound* as a yellow oil (0.55 g, 73%). **R_f** 0.64 (5% EtOAc in pentane); **IR** ν_{max} (thin film)/cm^{-1} 2947s, 1691s, 1443m, 1190m, 1135s; **^{1}H NMR** δ_H (500 MHz, $CDCl_3$) 1.52 – 1.61 (2H, m, H-1), 1.65 – 1.72 (6H, m, H-4, H-5, H-6), 1.83 – 1.92 (4H, m, H-1, H-2), 2.08 – 2.19 (2H, m, H-2), 3.52 (2H, t, *J* = 5.5 Hz, H-7); **^{13}C NMR** δ_C (125 MHz, $CDCl_3$) 18.7 (C-5), 24.3 (C-1), 24.7 (C-6), 34.3 (C-4), 36.4 (C-2), 43.5 (q, *J* = 4.0 Hz, C-7), 68.9 (C-3), 116.9 (q, *J* = 290 Hz, C-9), 156.6 (q, *J* = 34.5 Hz, C-8); **^{19}F NMR** δ_F (376 Hz, $CDCl_3$) −69.3 Hz; **HRMS (ESI$^+$)** *m/z* $[M+H]^+$ calculated for $C_{11}H_{17}ONF_3$, 236.1257; found, 236.1257.

2,2,2-trifluoro-1-((2*R,5*R**)-2-hydroxy-6-azaspiro[4.5]decan-6-yl)ethan-1-one (2.55a)**

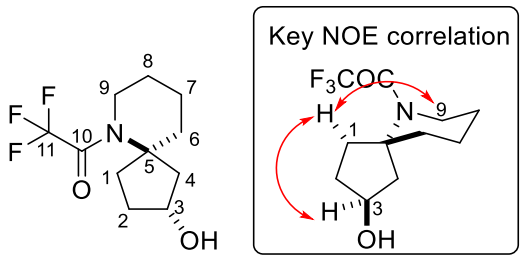

The titled compound was synthesized by following **GP-1** using $P450_{BM3}$ mutant enzyme strain A330P on a reaction scale of 100 mL. Reaction was completed after 24 h, as monitored by GC. The crude product was purified by flash chromatography (5% → 20% EtOAc in pentane, with a gradient of 5%) to afford a colourless oil (26 mg, 52%, *e.e.* 1%). **R_f** 0.60 (50% EtOAc in pentane); **IR** ν_{max} (thin film)/cm^{-1} 3368br, 1685s, 1444m, 1135s, 1047w; **^{1}H NMR** δ_H (400 MHz, $CDCl_3$) 1.59 – 1.67 (1H, m, H-2), 1.69 – 1.74 (4H, m, H-7, H-8), 1.79 (1H, dd, *J* = 14.0, 4.0 Hz, H-4), 1.93 (2H, t, *J* = 6.0 Hz, H-6), 1.96 – 2.00 (1H, m, H-1), 2.18 (1H, dt, *J* = 13.0, 8.0 Hz, H-1), 2.27 – 2.37 (1H, m, H-2), 2.49 (1H,

dd, *J* = 14.0, 7.0 Hz, H-4), 3.46 – 3.54 (2H, m, H-9), 4.60 – 4.66 (1H, m, H-3); **^{13}C NMR** δ_C (126 MHz, $CDCl_3$) 17.9 (C-7), 23.6 (C-8), 35.1 (C-1), 35.2 (C-2), 36.4 (C-6), 42.7 (q, *J* = 4.0 Hz, C-9), 45.9 (C-4), 67.6 (C-5), 73.5 (C-3), 116.7 (q, *J* = 289.5 Hz, C-11), 156.5 (C-10); **^{19}F NMR** δ_F (376 Hz, $CDCl_3$) −69.3 Hz; **HRMS (ESI$^+$)** *m/z* $[M+H]^+$ calculated for $C_{11}H_{17}O_2NF_3$, 252.1206; found, 52.1208. The same metabolite was also isolated from variants GV/L188Q/A264G and R19/F87A/T260G.

6-(2,2,2-Trifluoroacetyl)-6-azaspiro[4.5]decan-2-one (2.55b)

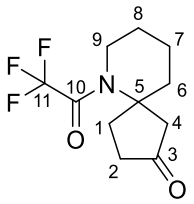

The titled compound was synthesized by following **GP-1** using $P450_{BM3}$ mutant enzyme strain VQ/S72G/A330W on a reaction scale of 50 mL. Reaction was completed after 5 h, as monitored by GC. The crude product was purified by flash chromatography (5% → 20% EtOAc in pentane, with a gradient of 5%) to afford a colourless oil (3.2 mg, 13%) **R_f** 0.53 (50% EtOAc in pentane); **IR** ν_{max} (thin film)/cm^{-1} 1746s, 1683s, 1447m, 1191s, 1133s ; **^{1}H NMR** δ_H (400 MHz, $CDCl_3$) 1.69 – 1.82 (4H, m, H-7, H-8), 1.82 – 1.88 (2H, m, H-6), 2.22 – 2.35 (2H, m, H-1, H-2), 2.41 – 2.50 (2H, m, H-1, H-4), 2.54 – 2.66 (1H, m, H-2), 2.92 – 3.01 (1H, m, H-4), 3.49 – 3.58 (1H, m, H-9), 3.58 – 3.66 (1H, m, H-9); **^{13}C NMR** δ_C (126 MHz, $CDCl_3$) 17.7 (C-7), 23.7 (C-8), 33.0 (C-1), 34.9 (C-6), 37.1 (C-2), 42.5 (q, *J* = 4.0 Hz, C-9), 49.9 (C-4), 64.5 (C-5), 117.5 (q, *J* = 285.5 Hz, C-11), 157.4 (q, *J* = 35.0 Hz, C-10), 214.9 (C-3); **HRMS (ESI$^+$)** *m/z* $[M+H]^+$ calculated for $C_{11}H_{15}O_2NF_3$, 250.1049; found, 250.1050.

2,2,2-Trifluoro-N-(1-(4-hydroxybutyl)cyclopentyl)acetamide (2.55c)

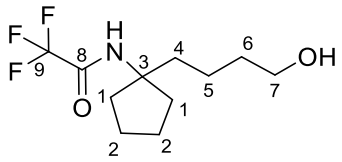

The titled compound was synthesized by following **GP-1** using $P450_{BM3}$ enzyme strain RP/A82M/I263A on a reaction scale of 100 mL. Reaction was completed after 24 h, as monitored by GC. The crude product was purified by flash chromatography (5% → 20% EtOAc in pentane, with a gradient of 5%) to afford a colourless oil (5.6 mg, 11%). **R_f** 0.59 (50% EtOAc in pentane)**; IR** ν_{max} (thin film)/cm^{-1} 3306br, 3079br, 1704s, 1558m, 1459m, 1188s, 1154s; **^{1}H NMR** δ_H (400 MHz, $CDCl_3$) 1.32 – 1.40 (2H, m, H-5), 1.57 (2H, tt, *J* = 8.0, 6.5 Hz, H-6), 1.67 – 1.76 (6H, m, H-1, H-2), 1.84 – 1.91 (2H, m, H-4), 1.94 – 2.03 (2H, m, H-1), 3.65 (2H, t, *J* = 6.5 Hz, H-7), 5.98 (1H, br. s, NH); **^{13}C NMR** δ_C (126 MHz, $CDCl_3$) 21.1 (C-5), 23.7 (C-2), 32.8 (C-6), 36.6 (C-4), 37.8 (C-1), 62.7 (C-7), 66.3 (C-3), 115.8 (q, *J* = 289.5 Hz, C-9), 156.4 (q, *J* = 36.0 Hz, C-8); **^{19}F NMR** δ_F (376 Hz, $CDCl_3$) −76.0 Hz; **HRMS (ESI$^+$)** not found.

2,2,2-Trifluoro-*N*-(1-(4-oxobutyl)cyclopentyl)acetamide (2.55d)

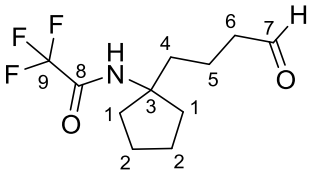

The titled compound was synthesized by following **GP-1** using $P450_{BM3}$ mutant enzyme strain RP/A82M/I263A on a reaction scale of 50 mL at a substrate: enzyme ratio of 5000:1. Reaction was completed after 5 h, as monitored by GC. The crude product was purified by flash chromatography (5% → 20% EtOAc in pentane, with a gradient of 5%) to afford a colourless oil (2.7 mg, 11%). **R_f** 0.49 (50% EtOAc in pentane); **IR** ν_{max} (thin film)/cm^{-1}; **^{1}H NMR** δ_H (600 MHz, $CDCl_3$) 1.57 – 1.62 (2H, m, H-5), 1.68 – 1.75 (6H, m, H-1, H-

2), 1.83 – 1.89 (2H, m, H-4), 1.97 – 2.05 (2H, m, H-1), 2.49 (2H, td, *J* = 7.0, 1.0 Hz, H-6), 6.11 (1H, br. s, NH), 9.78 (1H, t, *J* = 1.0 Hz, H-7); **^{13}C NMR** δ_C (126 MHz, $CDCl_3$) 17.3 (C-5), 23.7 (C-2), 36.4 (C-4), 37.7 (C-1), 43.9 (C-6), 66.1 (C-3), 115.8 (q, *J* = 289.5 Hz, C-9), 156.5 (q, *J* = 36.0 Hz, C-8), 202.1 (C-7); **^{19}F NMR** δ_F (376 Hz, $CDCl_3$) −76.0 Hz; **HRMS (ESI$^+$)** *m/z* $[M+H]^+$ calculated for $C_{11}H_{15}O_2NF_3$, 250.1060; found, 250.1059.

2,2,2-Trifluoro-*N*-(4-(3-oxocyclopent-1-en-1-yl)butyl)acetamide (2.55e)

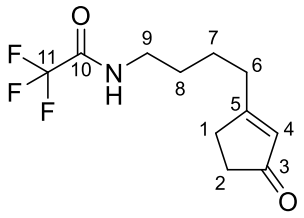

The titled compound was synthesized by following **GP-1** using $P450_{BM3}$ mutant enzyme strain R19/F87I on a reaction scale of 50 mL. Reaction was completed after 24 h, as monitored by GC. The crude product was purified by flash chromatography (5% → 20% EtOAc in pentane, with a gradient of 5%) to afford a colourless oil (1.8 mg, 7%) **R_f** 0.58 (50% EtOAc in pentane); **IR** ν_{max} (thin film)/cm^{-1} 3294br, 1704s, 1676s, 1613m, 1560m, 1440m, 1185m; **^{1}H NMR** δ_H (500 MHz, $CDCl_3$) 1.63 – 1.70 (4H, m, H-7, H-8), 2.39 – 2.43 (2H, m, H-1), 2.45 (2H, t, *J* = 7.0 Hz, H-6), 2.58 (2H, dt, *J* = 7.0, 2.0 Hz, H-2), 3.38 – 3.43 (2H, m, H-9), 5.93 – 5.95 (1H, m, H-4), 6.67 (1H, br. s, NH); **^{13}C NMR** δ_C (126 MHz, $CDCl_3$) 24.2 (C-7), 28.8 (C-8), 31.6 (C-2), 33.0 (C-6), 35.4 (C-1), 39.6 (C-9), 116.0 (q, *J* = 288.0 Hz, C-11), 129.8 (C-4), 157.5 (q, *J* = 37.0 Hz, C-10), 182.1 (C-5), 210.2 (C-3); **^{19}F NMR** δ_F (376 Hz, $CDCl_3$) −75.9 Hz; **HRMS (ESI$^+$)** *m/z* $[M+H]^+$ calculated for $C_{11}H_{15}O_2NF_3$, 250.1049; found, 250.1050.

2,2,2-Trifluoro-*N*-(4-(4-hydroxy-3-oxocyclopent-1-en-1-yl)butyl)acetamide (2.55f)

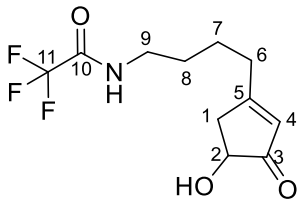

The titled compound was synthesized by following **GP-1** using $P450_{BM3}$ mutant enzyme strain VQ/S72G/A330W on a reaction scale of 100 mL. Reaction was completed after 24 h, as monitored by GC. The crude product was purified by flash chromatography (5% → 20% EtOAc in pentane, with a gradient of 5%) to afford a colourless oil (3.5 mg, 7%). **R_f** 0.42 (50% EtOAc in pentane); **IR** ν_{max} (thin film)/cm^{-1} 3308br, 1704s, 1608m, 1562w, 1443m, 1187m, 1155m; **^{1}H NMR** δ_H (500 MHz, $CDCl_3$) 1.63 – 1.69 (4H, m, H-7, H-8), 2.44 – 2.49 (2H, m, H-6), 2.52 (1H, dt, *J* = 18.0, 2.5 Hz, H-1), 2.93 (1H, dd, *J* = 18.0, 6.5 Hz, H-1), 3.42 (2H, q, *J* = 6.0 Hz, H-9), 4.25 (1H, dd, *J* = 6.5, 3.0 Hz, H-2), 5.97 (1H, t, *J* = 1.5 Hz, H-4), 6.35 (1H, br. s, NH); **^{13}C NMR** δ_C (126 MHz, $CDCl_3$) 23.9 (C-7), 28.9 (C-8), 33.3 (C-6), 39.6 (C-9), 39.8 (C-1), 72.5 (C-2), 115.9 (q, *J* = 288.0 Hz, C-11), 126.6 (C-4), 157.5 (q, *J* = 37.0 Hz, C-10), 179.3 (C-5), 208.8 (C-3); **^{19}F NMR** δ_F (376 Hz, $CDCl_3$) −75.9 Hz **HRMS (ESI$^+$)** *m/z* $[M+Na]^+$ calculated for $C_{11}H_{14}O_3NF_3Na$, 288.0810; found, 288.0819.

7.4 Compounds from Chapter 3

7-Azaspiro[4.5]decane (3.1)

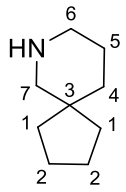

Into round-bottom flask was added lactam **3.6** (253 mg, 1.65 mmol) in THF (8.3 mL) and cooled to 0 °C. To this flask was then added $LiAlH_4$ (313 mg, 8.25 mmol) in THF (17 mL). The reaction mixture was warmed to RT over 30 min whilst stirring and heated to

reflux for 16 h. The reaction was cooled to 0 °C, followed by the addition of water (0.33 mL), 15% NaOH aqueous solution (0.33 mL) and water (0.94 mL). The resultant mixture was diluted with DCM and the organic layers were washed with brine, water, and dried with $MgSO_4$. The filtrate was then concentrated *in vacuo* at 300 mbar at 30 °C to afford the *title compound* as a yellow oil. Compound was used directly for next step without further purification. **R_f** 0.64 (50% EtOAc in pentane); **IR** ν_{max} (thin film)/cm^{-1} 3361m, 2948s, 2862s, 1580m, 1469m, 1019m; **^{1}H NMR** δ_H (500 MHz, $CDCl_3$) 1.32 – 1.39 (2H, m, H-1), 1.42 – 1.61 (10H, m, H-1, H-2, H-4, H-5), 2.24 (1H, br. s, NH), 2.57 (2H, s, H-7), 2.77 (2H, t, *J* = 5.5 Hz, H-6); **^{13}C NMR** δ_C (126 MHz, $CDCl_3$) 24.9 (C-5), 25.8 (C-2, C-4), 37.2 (C-1), 42.2 (C-3), 46.9 (C-6), 57.2 (C-7); **HRMS (ESI$^+$)** *m/z* $[M+H]^+$ calculated for $C_9H_{18}N$, 140.1434; found, 140.1432.

7-(Methylsulfonyl)-7-azaspiro[4.5]decane (3.5)

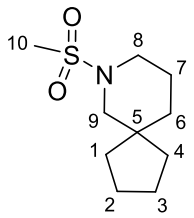

A solution of crude spiroamine **9** in dry DCM (17 mL) was cooled to 0 °C. Triethylamine (1.80 mL, 14.0 mmol) was added and methanesulfonyl chloride (0.390 mL, 5.70 mmol) was added dropwise. The mixture was warmed to RT and stirred for 5 h. A few drops of sat. aq. $NaHCO_3$ solution was added, followed by water (6 mL). The resulting solution was extracted with DCM and the organic layers were washed with brine and dried with $MgSO_4$. The crude product was concentrated *in vacuo* and purification by flash chromatography (25% → 45% ethyl acetate in pentane, with a gradient of 5%) afford the title compound as a white solid (0.160 g, 47% over 2 steps). **R_f** 0.69 (50% ethyl acetate in pentane); **IR** ν_{max} (thin film)/cm^{-1} 1447m, 1328s, 1150s; **mp** 59 °C; **^{1}H NMR** δ_H (400 MHz, $CDCl_3$)1.33 – 1.39 (2H, m, H-1), 1.42 – 1.47 (2H, m, H-4), 1.55 – 1.59 (2H, m, H-

1), 1.59 – 1.66 (4H, m, H-2), 1.66 – 1.72 (2H, m, H-5), 2.74 (3H, s, H-8), 2.88 (2H, s, H-7), 3.13 (3H, t, J = 5.5 Hz, H-6); **^{13}C NMR** δ_C (101 MHz, $CDCl_3$) 23.2 (C-5), 24.8 (C-2), 34.5 (C-8), 36.5 (C-1), 36.6 (C-4), 42.8 (C-3), 46.6 (C-6), 55.7 (C-7); **HRMS (ESI$^+$)** *m/z* $[M+Na]^+$ calculated for $C_{10}H_{19}O_2NNaS$, 240.1029; found, 240.1031.

7-(Methylsulfonyl)-7-azaspiro[4.5]decan-8-ol (3.5a)

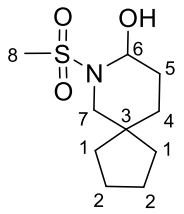

The titled compound was synthesized by following **GP-1** using $P450_{BM3}$ mutant enzyme strain GV/L188Q on a reaction scale of 100 mL. Reaction was completed after 23 h, as monitored by GC. The crude product was purified by flash chromatography (20% → 40% EtOAc in pentane, with a gradient of 5%) to afford a pale yellow oil along with **21b** as a 1:1 mixture (13.0 mg, 28 %). **R_f** 0.74 (50% EtOAc in pentane); **IR** ν_{max} (thin film)/cm^{-1} 3513 br, 1361s, 1214m, 1158s; **^{1}H NMR** δ_H (400 MHz, $CDCl_3$) 1.30 – 1.45 (4H, m, H-1, H-4), 1.59 – 1.69 (4H, m, H-2), 1.71 – 1.88 (4H, m, H-1, H-2, H-5), 2.45 (1H, br. s, OH), 2.91 (3H, s, H-8), 3.01 (1H, dd, J = 11.5, 1.5 Hz, H-7), 3.14 (1H, dd, J = 11.5, 2.0 Hz, H-7), 5.50 – 5.54 (1H, m, H-6); **^{13}C NMR** δ_C (126 MHz, $CDCl_3$) 24.3 (C-2), 30.0 (C-1), 38.6 (C-4), 39.3 (C-8), 42.2 (C-3), 48.9 (C-7), 76.2 (C-6); **HRMS (ESI$^+$)** *m/z* $[M+Na]^+$ calculated for $C_{10}H_{19}O_3NNaS$, 256.0978; found, 256.0979.

7-(Methylsulfonyl)-7-azaspiro[4.5]dec-8-ene (3.5b)

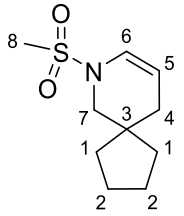

The titled compound was synthesized by following **GP-1** using $P450_{BM3}$ mutant enzyme strain GV/L188Q on a reaction scale of 100 mL. Reaction was completed after 23 h, as

monitored by GC. The crude product was purified by flash chromatography (20% → 40% EtOAc in pentane, with a gradient of 5%) to afford a pale yellow oil along with **3.5a** as a 1:1 mixture (in equilibrium with **3.5a**) **R_f** 0.67 (50% EtOAc in pentane); **IR** ν_{max} (thin film)/cm^{-1} 1651m, 1361s, 716m; **^{1}H NMR** δ_H (500 MHz, $CDCl_3$) 1.29 – 1.37 (4H, m, H-1), 1.48 – 1.56 (4H, H-2), 1.90 – 1.93 (2H, m, H-4), 2.88 (3H, s, H-8), 3.20 (2H, s, H-7), 4.92 (1H, dt, *J* = 8.0, 4.0 Hz, H-5), 6.48 (1H, dt, *J* = 8.0, 2.0 Hz, H-6); **^{13}C NMR** δ_C (126 MHz, $CDCl_3$) 28.3 (C-2), 32.6 (C-1), 33.6 (C-4), 36.8 (C-8), 41.2 (C-3), 51.6 (C-7), 59.4 (C-5), 123.0 (C-6); **HRMS (ESI$^+$)** *m/z* $[M+Na]^+$ calculated for $C_{10}H_{17}O_2NnaS$, 238.0872; found, 238.0872.

7-Azaspiro[4.5]decan-6-one (3.6)[327]

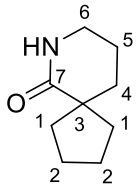

At 0 °C, $NaBH_4$ (0.872 g, 23.1 mmol) was added to a stirred solution of $CuSO_4 \cdot 5H_2O$ (195 mg, 0.781 mmol) in methanol (41 mL). The resulting mixture was allowed to stir for 15 min at 0 °C and a solution of azide **3.9** (3.0 g, 14 mmol) in methanol (34 mL) was added. To this solution was then added more $NaBH_4$ (2.11 g, 55.8 mmol) in four portions and was warmed to RT to stir for 22 h. Methanol was then evaporated *in vacuo* and the mixture was made alkaline with 3 M NaOH aq. solution to pH 12. The organic phase was extracted with EtOAc (3 × 85 mL), washed with brine (85 mL) and dried with $MgSO_4$. Evaporation of solvent gave the desired compound as a white solid (1.52 g, 70 %). **R_f** 0.30 (100% EtOAc); **^{1}H NMR** δ_H (500 MHz, $CDCl_3$) 1.47 – 1.53 (2H, m, H-1), 1.61 – 1.71 (4H, m, H-1, H-2, H-5), 1.77 – 1.83 (4H, m, H-2, H-4), 2.10 – 2.18 (2H, m, H-1), 3.31 (2H, td, *J* = 6.0, 2.5 Hz, H-6), 5.52 (1H, br. s, NH); **^{13}C NMR** δ_C (126 MHz, $CDCl_3$) 20.5 (C-5), 26.0 (C-2), 34.7 (C-4), 38.9 (C-1), 42.9 (C-6), 49.4 (C-3), 179.0 (C-7); **HRMS (ESI$^+$)** *m/z* $[M+Na]^+$ calculated for $C_9H_{16}ON$, 154.1226; found *m/z* 154.1227.

8-Hydroxy-7-azaspiro[4.5]decan-6-one (3.6a)

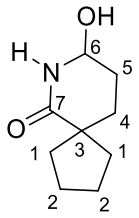

The titled compound was synthesized by following **GP-1** using $P450_{BM3}$ mutant enzyme strain R19/F87A/A184I on a reaction scale of 100 mL. Reaction was completed after 18 h, as monitored by GC. The crude product was purified by flash chromatography (1% → 4% methanol in DCM, with a gradient of 1%) to afford a colourless oil (16 mg, 47%). **R_f** 0.71 (1% methanol in DCM); **IR** ν_{max} (thin film)/cm^{-1} 3300br, 3027br, 1649s, 1344m; **^{1}H NMR** δ_H (500 MHz, $CDCl_3$) 1.45 – 1.62 (3H, m, H-1, H-2, H-4), 1.64 – 1.71 (2H, m, H-1, H-2), 1.72 – 1.87 (3H, m, H-1, H-2, H-5), 1.87 – 1.95 (1H, m, H-4), 1.96 – 2.07 (2H, m, H-2, H-5), 2.14 – 2.28 (1H, m, H-1), 3.00 (1H, br. s, OH), 5.03 (1H, q, J = 4.0 Hz, H-6), 6.28 (1H, s, NH); **^{13}C NMR** δ_C (126 MHz, $CDCl_3$) 25.8 (C-2), 28.4 (C-5), 29.7 (C-4), 38.1 (C-1), 48.5 (C-3), 76.4 (C-6), 179.0 (C-7); **HRMS (ESI$^+$)** *m/z* $[M+H]^+$ calculated for $C_9H_{16}O_2N$, 170.1176; found, 170.1177.

7-Azaspiro[4.5]decane-6,8-dione (3.6b)

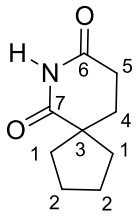

The titled compound was synthesized by following **GP-1** using $P450_{BM3}$ mutant enzyme strain R19/F87A/A184I on a reaction scale of 100 mL. Reaction was completed after 18 h, as monitored by GC. The crude product was purified by flash chromatography (1% → 4% methanol in DCM, with a gradient of 1%) to afford a colourless oil (3.4 mg, 10%). **R_f** 0.68 (1% methanol in DCM); **IR** ν_{max} (thin film)/cm^{-1} 3657br, 1714m, 1690w, 1382m, 1252m; **^{1}H NMR** δ_H (500 MHz, $CDCl_3$) 1.56 – 1.64 (2H, m, H-1), 1.67 – 1.76 (2H, m,

H-2), 1.78 – 1.86 (2H, m, H-2), 1.89 (2H, t, *J* = 6.5 Hz, H-4), 2.13 – 2.21 (2H, m, H-1), 2.63 (2H, t, *J* = 6.5 Hz, H-5), 7.65 (1H, br. s, NH); **^{13}C NMR** δ_C (126 MHz, $CDCl_3$) 25.6 (C-2), 29.8 (C-5), 30.7 (C-4), 36.4 (C-1), 172.4 (C-7), 178.2 (C-6); **HRMS (ESI$^+$)** *m/z* $[M+H]^+$ calculated for $C_9H_{14}O_2N$, 168.1019; found, 168.1020.

Methyl 1-(3-chloropropyl)cyclopentane-1-carboxylate (3.8)

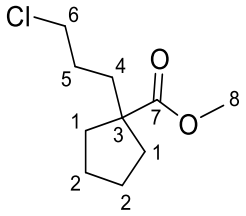

To a stirred solution of DIPEA (11 mL, 77 mmol) in THF (105 mL) cooled to −78 °C was added *n*BuLi in (28 mL, 1.60 M in hexanes, 70 mmol) and stirring was continued for 15 min. To this was added ester **2.4** (5.0 g, 3.5 mmol) at −78 °C. The resulting solution was stirred for 1.5 h then1-chloro-3-iodoproane (7.6 mL, 70 mmol) was added and stirring continued for 18 h. The reaction was quenched by the addition of brine (35 mL), and the solution was extracted with ether (3 × 40 mL). The combined organic layers were washed with brine (40 mL) and dried with $MgSO_4$. The solvent was then removed *in vacuo* to obtain the crude product. Flash chromatography (100% pentane → 30% ether in pentane, with a gradient of 10%) afforded the *title compound* (dark orange oil, 6.12 g, 85%). **R$_f$** 0.47 (20% ether in pentane); **IR** ν_{max} (thin film)/cm^{-1} 2953m, 2872w, 1728s, 1452w, 1166m; **^{1}H NMR** δ_H (400 MHz, $CDCl_3$) 1.43 – 1.52 (2H, m, H-1), 1.60 – 1.77 (8H, m, H-2, H-4, H-5), 2.08 – 2.17 (2H, m, H-1), 3.50 (2H, t, *J* = 6.0 Hz, H-6), 3.67 (3H, s, H-8); **^{13}C NMR** δ_C (101 MHz, $CDCl_3$) 25.0 (C-2), 29.5 (C-5), 36.3 (C-4), 36.5 (C-1), 45.4 (C-6), 52.0 (C-96), 53.7 (C-3), 178.2 (C-7); **HRMS (ESI$^+$)** *m/z* $[M+H]^+$ calculated for $C_{10}H_{18}O_2Cl$, 205.0990; found, 205.0991.

Methyl 1-(3-azidopropyl)cyclopentane-1-carboxylate (3.9)[328]

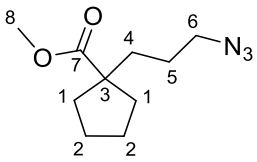

To a stirred solution of ester **3.8** (5.0 g, 25 mmol) in dry DMSO (38 mL) was added NaN_3 (3.03 g, 46.6 mmol). The mixture was then stirred at 50 ^oC for 21 h. The reaction was cooled to RT and was quenched with ice (136 g). The layers were separated and the aqueous layers were extracted with ether (170 mL × 3). The combined organic layers were washed with water (170 mL), brine (170 mL) and dried with $MgSO_4$. The resulting solution was concentrated *in vacuo* to afford a dark yellow oil (3.8 g, 74%). $\mathbf{R_f}$ 0.21 (20% EtOAc in pentane); **^{1}H NMR** δ_H (400 MHz, $CDCl_3$) 1.41 – 1.56 (2H, m, H-1), 1.57 – 1.71 (8H, m, H-2, H-4, H-5), 2.07 – 2.17 (2H, m, H-3), 3.24 (2H, t, J = 7.0 Hz, H-6), 3.67 (3H, s, H-8); **^{13}C NMR** δ_C (101 MHz, $CDCl_3$) 25.1 (C-2), 25.7 (C-5), 36.3 (C-4), 41.2 (C-1), 51.8 (C-6), 52.0 (C-8), 53.8 (C-3), 178.1 (C-7).

***tert*-Butyl 7-azaspiro[4.5]decane-7-carboxylate (3.10)**

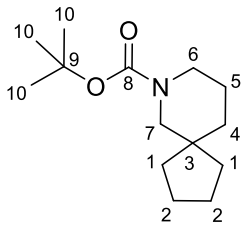

To a solution of crude spiroamine **3.1** in THF (12 mL) was added triethylamine (0.7 mL, 5.0 mmol). The resulting mixture was placed in a cold-water bath and Boc_2O (1.35 g, 6.18 mmol) in THF (12 mL) was added slowly whilst stirring. The reaction was then allowed to warm to RT and stirred for 4 h. THF was removed *in vacuo* and the crude product was re-dissolved in EtOAc. The organic layers were washed with 0.1 M HCl aqueous solution, sat. aq. $NaHCO_3$, brine, and dried with $MgSO_4$. The filtrate was concentrated *in vacuo* and dissolved in ethanol (39 mL). Imidazole (334 mg, 4.90 mmol) was added and the reaction mixture was stirred for 5 min. The solvent was removed *in*

vacuo and chloroform (48 mL) was added. The organic layers were washed with 1% HCl aqueous solution cooled to 0 °C (2 × 15 mL), dried with $MgSO_4$, and concentrated *in vacuo*. Purification by flash chromatography (20% EtOAc in pentane) furnished the Boc-protected spiroamine as a pale yellow oil (50.1 mg, 36% over 2 steps). **R_f** 0.77 (20% EtOAc in pentane); **IR** ν_{max} (thin film)/cm^{-1} 2933m, 2857m, 1692s, 1425s, 1347m, 1153s; **^{1}H NMR** δ_H (400 MHz, $CDCl_3$) 1.20 – 1.29 (4H, m, H-1), 1.45 (9H, s, H-10), 1.46 – 1.54 (4H, m, H-4, H-5), 1.57 – 1.67 (4H, m, H-2), 3.11 (2H, s, H-7), 3.34 (2H, m, H-6); **^{13}C NMR** δ_C (126 MHz, $CDCl_3$) 22.4 (C-5), 23.3 (C-2), 28.5 (C-10), 35.9 (C-4), 37.3 (C-1), 43.3 (C-3), 43.8 (C-6), 53.4 (C-7), 79.0 (C-9), 155.0 (C-8); **HRMS (ESI$^+$)** *m/z* $[M+Na]^+$ calculated for $C_{14}H_{25}O_2NNa$, 262.1778; found, 262.1778.

***tert*-Butyl (2*R**, 5*R**)-2-hydroxy-7-azaspiro[4.5]decane-7-carboxylate (3.10a)**

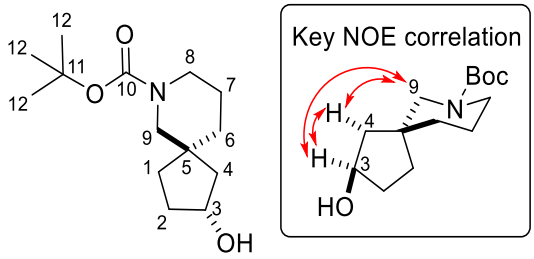

The titled compound was synthesized by following **GP-1** using $P450_{BM3}$ mutant enzyme strain R19/F87I on a reaction scale of 150 mL. Reaction was completed after 23 h, as monitored by GC. The crude product was purified by flash chromatography (20% → 45% EtOAc in pentane, with a gradient of 5%) to afford a pale yellow oil (8.4 mg, 11%, *e.e.* 40%, by chiral GC analysis). **R_f** 0.72 (80% EtOAc in pentane); **IR** ν_{max} (thin film)/cm^{-1} 3451br, 3424br, 1693s, 1478m, 1366m, 1157m; **^{1}H NMR** δ_H (500 MHz, $CDCl_3$) 1.28 – 1.32 (1H, m, H-4), 1.45 (9H, s, H-12), 1.50 – 1.60 (4H, m, H-1, H-7), 1.61 – 1.67 (3H, m, H-2, H-6), 1.80 – 1.87 (1H, m, H-4), 1.87 – 1.95 (1H, m, H-6), 3.10 (2H, s, H-9), 3.24 – 3.44 (2H, m, H-8), 4.32 – 4.43 (1H, m, H-3); **^{13}C NMR** δ_C (126 MHz, $CDCl_3$) 23.1 (C-7), 24.7 (C-2), 28.5 (C-12), 34.5 (C-6), 38.4 (C-1), 44.3 (C-8), 45.7 (C-4), 47.3 (C-5), 53.8 (C-9), 73.4 (C-3), 79.3 (C-11), 110.0 (C-10); **HRMS (ESI$^+$)** *m/z* $[M+Na]^+$ calculated

for $C_{14}H_{25}O_3NNa$, 278.1727; found, 278.1728. The same metabolite was also isolated from mutant RT2 (*e.e.* 28%, by Mosher ester analysis).

tert-Butyl 2-oxo-7-azaspiro[4.5]decane-7-carboxylate (3.10b)

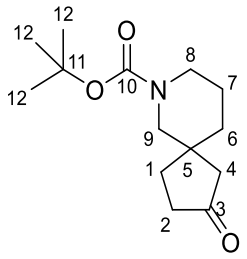

The titled compound was synthesized by following **GP-1** using $P450_{BM3}$ mutant enzyme strain R19/F87I on a reaction scale of 150 mL. Reaction was completed after 23 h, as monitored by GC. The crude product was purified by flash chromatography (20% → 45% EtOAc in pentane, with a gradient of 5%) to afford a pale yellow oil (2.3 mg, 3%, *e.e.* 37%, by chiral GC analysis). **R_f** 0.59 (80% EtOAc in pentane); **IR** ν_{max} (thin film)/cm^{-1} 1743m, 1691s, 1426m, 1037m; **^{1}H NMR** δ_H (500 MHz, $CDCl_3$) 1.44 (9H, s, H-12), 1.53 – 1.55 (1H, m, H-7), 1.59 – 1.63 (3H, m, H-6, H-7), 1.67 – 1.70 (1H, m, H-1), 1.87 – 1.97 (1H, m, H-1), 1.98 – 2.03 (1H, m, H-4), 2.12 – 2.20 (1H, m, H-4), 2.27 – 2.37 (2H, m, H-2), 3.25 (2H, s, H-9), 3.31 – 3.48 (2H, m, H-8); **^{13}C NMR** δ_C (126 MHz, $CDCl_3$) 22.7 (C-7), 28.6 (C-12), 31.6 (C-1), 34.3 (C-6), 36.7 (C-2), 42.4 (C-5), 43.8 (C-8), 48.8 (C-4), 52.3 (C-9), 79.7 (C-11), 122.6 (C-10), 225.8 (C-3); **HRMS (ESI$^+$)** *m/z* $[M+Na]^+$ calculated for $C_{14}H_{23}O_3NNa$, 276.1570; found, 276.1570.

tert-Butyl (1*R**, 5*R**)-1-hydroxy-7-azaspiro[4.5]decane-7-carboxylate (3.10c)

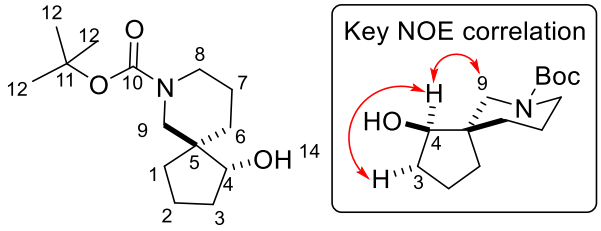

The titled compound was synthesized by following **GP-1** using $P450_{BM3}$ mutant enzyme strain RT2 on a reaction scale of 50 mL. Reaction was completed after 23 h, as monitored by GC. The crude product was purified by flash chromatography (5% → 20% EtOAc in pentane, with a gradient of 5%) to afford a colourless oil (3.8 mg, 15%, *e.e.* 11%, by chiral GC analysis h). **R_f** 0.66 (50% EtOAc in pentane); **IR** ν_{max} (thin film)/cm^{-1} 3442br, 3060br, 1693m, 1365m; **^{1}H NMR** δ_H (500 MHz, $CDCl_3$) 1.45 (9H, s, H-12), 1.47 – 1.54 (5H, m, H-1, H-2, H-6), 1.55 – 1.59 (2H, m, H-7), 1.60 – 1.69 (1H, m, H-3), 1.70 – 1.76 (1H, m, H-2), 1.97 – 2.16 (1H, m, H-3), 3.06 (1H, d, *J* = 13.5 Hz, H-9), 3.14 (1H, d, *J* = 13.5 Hz, H-9), 3.33 – 3.43 (2H, m, H-8), 3.83 – 3.87 (1H, m, H-4); **^{13}C NMR** δ_C (126 MHz, $CDCl_3$) 23.0 (C-7), 28.5 (C-12), 29.7 (C-2), 32.7 (C-6), 33.4 (C-3), 44.1 (C-8), 44.8 (C-5), 51.5 (C-9), 77.0 (C-4), 79.3 (C-11), 154.8 (C-10); **HRMS (ESI$^+$)** *m/z* $[M+Na]^+$ calculated for $C_{14}H_{25}O_3NNa$, 278.1727; found *m/z*, 278.1726.

tert-Butyl 8-hydroxy-7-azaspiro[4.5]decane-7-carboxylate (3.10d)

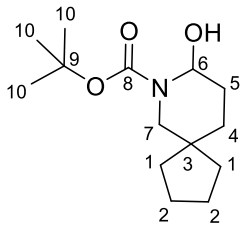

The titled compound was synthesized by following **GP-1** using $P450_{BM3}$ mutant enzyme strain K19/F87A/I263A on a reaction scale of 150 mL. Reaction was completed after 7 h, as monitored by GC. The crude product was purified by flash chromatography (20% → 45% EtOAc in pentane, with a gradient of 5%) to afford a colourless oil along with **19b**

as a 1:1 mixture (17.6 mg, 23%); **R_f** 0.67 (50% EtOAc in pentane); **IR** ν_{max} (thin film)/cm^{-1} 3400br, 1700s, 1418m, 1162m; **^{1}H NMR** δ_H (500 MHz, $CDCl_3$) 1.10 – 1.33 (4H, m, H-1, H-2, H-4), 1.39 (9H, s, H-10), 1.46 – 1.60 (5H, m, H-1, H-2), 1.60 – 1.80 (3H, m, H-4, H-5), 2.85 (1H, d, *J* = 13.0 Hz, H-7), 3.44 (1H, d, *J* = 13.0 Hz, H-7), 5.66 (1H, s, H-6); **^{13}C NMR** δ_C (126 MHz, $CDCl_3$) 24.2 (C-2), 28.4 (C-10), 31.0 (C-4), 33.7 (C-1), 42.1 (C-3), 47.7 (C-7), 74.1 (C-6), 80.0 (C-9); **HRMS (ESI$^+$)** *m/z* $[M+Na]^+$ $C_{14}H_{25}O_3NNa$, 278.1727; found, 278.1728.

tert-Butyl 7-azaspiro[4.5]dec-8-ene-7-carboxylate (3.10e)

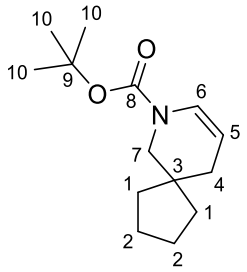

The titled compound was synthesized by following **GP-1** using $P450_{BM3}$ mutant enzyme strain K19/F87A/I263A on a reaction scale of 150 mL. Reaction was completed after 7 h, as monitored by GC. The crude product was purified by flash chromatography (20% → 45% EtOAc in pentane, with a gradient of 5%) to afford a colourless oil along with **3.10d** as a 1:1 mixture (in equilibrium with **3.10d**); **R_f** 0.78 (20% EtOAc in pentane); **IR** ν_{max} (thin film)/cm^{-1} 1700s, 1366m, 1162m; **^{1}H NMR** δ_H (500 MHz, $CDCl_3$) (mixture of 2:1 *N*-Boc rotamers) 1.29 – 1.38 (6H, m, H-1), 1.45 – 1.47 (27H, s, H-10), 1.54 – 1.63 (6H, m, H-1), 1.70 – 1.85 (12H, m, H-2), 1.89 (6H, dd, *J* = 4.0, 2.0 Hz, H-4), 3.23 (2H, s, H-7), 3.27 (4H, s, H-7), 4.75 (2H, dt, *J* = 8.0, 4.0 Hz, H-5), 4.86 (1H, dd, *J* = 8.0, 4.0 Hz, H-5), 6.70 (2H, d, *J* = 8.7 Hz, H-6), 6.83 (1H, d, *J* = 8.5 Hz, H-6); **^{13}C NMR** δ_C (126 MHz, $CDCl_3$) (mixture of 2:1 *N*-Boc rotamers) 23.9 (C-2), 24.18 (C-2), 28.7 (C-10), 29.7 (C-10), 35.9 (C-1), 36.0 (C-1), 34.5 (C-4), 34.2 (C-4), 39.0 (C-3), 39.2 (C-3), 79.3 (C-9),

79.5 (C-9), 103.7 (C-5), 104.4 (C-5), 124.1 (C-6), 124.4 (C-6), 151.9 (C-8), 152.2 (C-8); **HRMS (ESI$^+$)** *m/z* $[M+Na]^+$ calculated for $C_{14}H_{23}O_2NNa$, 260.1621; found, 260.1623.

7-(Isopropylsulfonyl)-7-azaspiro[4.5]decane (3.11)

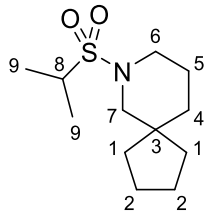

To a solution of crude spiroamine **3.1** (0.166 g, 1.19 mmol) and triethylamine (0.19 mL, 1.34 mmol) in DCM (34 mL) was added 2-Propanesulfonyl chloride (0.15 mL, 1.31 mmol) in DCM (12 mL) at 0 ^oC. The resulting mixture was warmed to RT and stirred for 16 h. The solvent was evaporated *in vacuo* and the resulting semi-solid was re-dissolved in EtOAc (25 mL) and washed with water (25 mL) and brine (25 mL). The combined organic layers were dried with $MgSO_4$ and concentrated *in vacuo*. Purification by flash chromatography (5% → 20% EtOAc in pentane, with a gradient of 5%) afford the title compound as a colourless oil (42.5 mg, 15% over 2 steps). **R_f** 0.60 (20% EtOAc in pentane); **IR** ν_{max} (thin film)/cm^{-1} 1445m, 1269m, 1056m; **^{1}H NMR** δ_H (400 MHz, $CDCl_3$) 1.33 (6H, d, *J* = 7.0 Hz, H-9), 1.54 – 1.66 (10H, m, H-1, H-2, H-5), 3.01 (2H, s, H-7), 3.16 (1H, sept, *J* = 7.0 Hz, H-8), 3.26 (2H, dd, *J* = 6.5, 5.0 Hz, H-6); **^{13}C NMR** δ_C (101 MHz, $CDCl_3$) 16.8 (C-9), 23.7 (C-5), 24.5 (C-1), 36.2 (C-2), 36.6 (C-4), 42.9 (C-3), 47.0 (C-6), 52.9 (C-8), 55.7 (C-7); **HRMS (ESI$^+$)** *m/z* $[M+Na]^+$ calculated for $C_{12}H_{23}NO_2SNa$, 268.1341; found, 268.1342.

(2*R, 5*R**)-7-(Isopropylsulfonyl)-7-azaspiro[4.5]decan-2-ol (3.11a)**

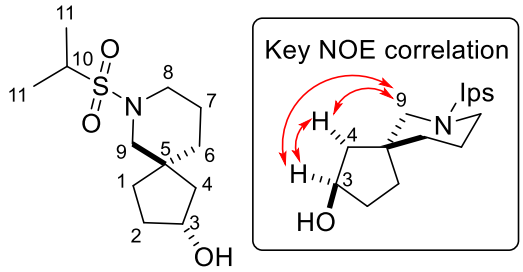

The titled compound was synthesized by following **GP-1** using $P450_{BM3}$ mutant enzyme strain R19/F87I on a reaction scale of 50 mL. Reaction was completed after 16 h, as monitored by GC. The crude product was purified by flash chromatography (10% → 25% EtOAc in pentane, with a gradient of 5%) to afford a colourless oil (12.3 mg, 47%, *e.e.* 8%, by Mosher ester analysis). **R_f** 0.70 (50% EtOAc in pentane); **IR** ν_{max} (thin film)/cm^{-1} 3503br, 1447m, 1320m, 1135m; **^{1}H NMR** δ_H (400 MHz, $CDCl_3$) 1.32 (6H, d, J = 7.0 Hz, H-11), 1.40 (1H, m, H-2), 1.57 – 1.80 (7H, m, H-1, H-4, H-6, H-7), 1.84 – 1.96 (2H, m, H-2, H-4), 2.99 (2H, m, H-9), 3.16 (1H, sept, J = 7.0 Hz, H-10), 3.21 – 3.31 (2H, m, H-8), 4.37 (1H, m, H-3); **^{13}C NMR** δ_C (126 MHz, $CDCl_3$) 16.8 (C-11), 23.6 (C-7), 33.7 (C-1), 34.3 (C-4), 37.8 (C-6), 42.0 (C-5), 45.6 (C-2), 46.9 (C-8), 52.9 (C-10), 56.1 (C-9), 73.3 (C-3); **HRMS (ESI$^+$)** *m/z* $[M+Na]^+$ calculated for $C_{12}H_{23}O_3NSNa$, 284.1291; found *m/z* 284.1290.

(1*R, 5*R**)-7-(Isopropylsulfonyl)-7-azaspiro[4.5]decan-1-ol (3.11b)**

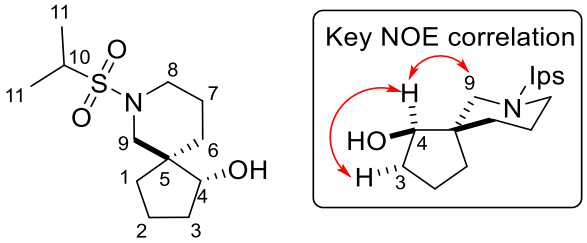

The titled compound was synthesized by following **GP-1** using $P450_{BM3}$ mutant enzyme strain GV/L188Q on a reaction scale of 150 mL. Reaction was completed after 5 h, as monitored by GC. The crude product was purified by flash chromatography (10% → 20% EtOAc in pentane, with a gradient of 5%) to afford a colourless oil (0.80 mg, 1%, *e.e.*

47%, by Mosher ester analysis) . **R_f** 0.64 (50% EtOAc in pentane)**; IR** ν_{max} (thin film)/cm^{-1} 3031br, 1613s, 1451m, 1106m; **^{1}H NMR** δ_H (500 MHz, $CDCl_3$) 1.32 (6H, d, *J* = 7.0 Hz, H-11), 1.41 – 1.47 (1H, m, H-1), 1.54 – 1.56 (1H, m, H-6), 1.60 – 1.67 (4H, m, (H-2, H-3, H-6, H-7), 1.72 – 1.80 (3H, m, H-1, H-2, H-7), 2.04 – 2.12 (1H, m, H-3), 2.95 (1H, d, *J* = 12.5 Hz, H-9), 3.08 (1H, d, *J* = 12.5 Hz, H-9), 3.16 (1H, sept, *J* = 7.0 Hz, H-10), 3.31 (2H, t, *J* = 5.5 Hz, H-8), 3.96 – 4.00 (1H, m, H-4); **^{13}C NMR** δ_C (126 MHz, $CDCl_3$) 17.0 (C-11), 20.2 (C-2), 22.9 (C-7), 29.3 (C-1), 33.2 (C-6), 33.5 (C-3), 46.5 (C-5), 47.1 (C-8), 53.0 (C-10), 54.2 (C-9), 76.9 (C-4); **HRMS (ESI$^+$)** *m/z* $[M+Na]^+$ calculated for $C_{12}H_{23}O_3NSNa$, 284.1291; found, 284.1291.

7-(Isopropylsulfonyl)-7-azaspiro[4.5]decan-9-ol (3.11c)

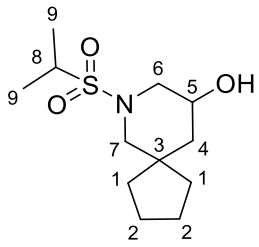

The titled compound was synthesized by following **GP-1** using $P450_{BM3}$ mutant enzyme strain R19/F87I on a reaction scale of 50 mL. Reaction was completed after 16 h, as monitored by GC. The crude product was purified by flash chromatography (10% → 25% EtOAc in pentane, with a gradient of 5%) to afford a colourless oil (2.7 mg, 10%, *e.e.* 6%, by Mosher ester analysis). **R_f** 0.68 (50% EtOAc in pentane); **IR** ν_{max} (thin film)/cm^{-1} 3446br, 1455m, 1322s, 1134m, 1008m; **^{1}H NMR** δ_H (500 MHz, $CDCl_3$) 1.29 – 1.33 (1H, m, H-1), 1.34 (6H, d, *J* = 7.0, H-9), 1.38 – 1.45 (2H, m, H-1, H-2), 1.47 – 1.53 (1H, m, H-2), 1.58 – 1.71 (5H, m, H-1, H-2, H-4), 1.74 – 1.81 (1H, m, H-1), 1.81 – 1.88 (1H, m, H-4), 2.67 – 2.75 (2H, m, H-6, H-7), 3.13 – 3.24 (1H, m, H-7), 3.80 – 3.86 (2H, m, H-5, H-6); **^{13}C NMR** δ_C (126 MHz, $CDCl_3$) 15.8 (C-9), 23.0 (C-2), 34.3 (C-1), 42.5 (C-3), 44.4 (C-4), 51.8 (C-8), 52.3 (C-7), 53.8 (C-6), 64.6 (C-5); **HRMS (ESI$^+$)** *m/z* $[M+H]^+$ calculated for $C_{12}H_{24}O_3NS$, 262.1471; found, 262.1473.

7-(Isopropylsulfonyl)-7-azaspiro[4.5]decan-8-ol (3.11d)

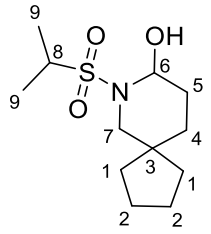

The titled compound was synthesized by **GP-1** using $P450_{BM3}$ mutant enzyme strain GV/L188Q on a reaction scale of 50 mL. Reaction was completed after 16 h, as monitored by GC. The crude product was purified by flash chromatography (10% → 20% EtOAc in pentane, with a gradient of 5%) to afford a colourless oil (8.9 mg, 34%). **R_f** 0.70 (50% EtOAc in pentane)**; IR** ν_{max} (thin film)/cm^{-1} 1449m, 1321s, 1264m; **^{1}H NMR** δ_H (500 MHz, $CDCl_3$) 0.76 – 1.00 (1H, m, H-1), 1.30 – 1.43 (9H, m, H-1, H-4, H-9), 1.60 – 1.72 (6H, m, H-1, H-2), 1.77 – 1.86 (2H, m, H-5), 2.69 (1H, d, *J* = 3.5 Hz, OH), 3.09 (1H, dd, *J* = 12.5, 2.0 Hz, H-7), 3.17 – 3.26 (2H, m, H-7, H-8), 5.33 – 5.39 (1H, m, H-6); **^{13}C NMR** δ_C (126 MHz, $CDCl_3$) 15.6 (C-9), 23.0 (C-2), 27.9 (C-5), 28.7 (C-1), 37.5 (C-4), 48.6 (C-7), 53.2 (C-8), 76.0 (C-6); **HRMS (ESI$^+$)** *m/z* $[M+H]^+$ calculated for $C_{12}H_{24}O_3NS$, 262.1471; found, 262.1803.

Diethyl (7-azaspiro[4.5]decan-7-yl)phosphonate (3.12)

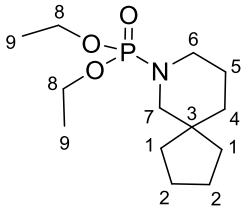

Crude spiroamine **3.1** (266 mg, 1.91 mmol) and triethylamine (0.32 mL, 2.3 mmol) was dissolved in DCM (11 mL) and cooled to 0 °C. Diethylphosphochloridate (0.30 mL, 2.1 mmol) was added dropwise, warmed to RT and stirred for 16 h. A few drops of sat. aq. $NaHCO_3$ was added, followed by water (4 mL). The resulting mixture was extracted with DCM (3 × 6 mL) and the combined organic layers were washed with water, brine, and dried with $MgSO_4$. The solvent was evaporated *in vacuo* and purification by flash

chromatography (20% → 50% EtOAc in pentane, with a gradient of 10%) furnished the product as a yellow oil (113 mg, 23% over 2 steps). **R_f** 0.35 (60% EtOAc in pentane); **IR** ν_{max} (thin film)/cm^{-1} 1255s, 1165m, 1029s; **^{1}H NMR** δ_H (400 MHz, $CDCl_3$) 1.30 (8H, td, *J* = 7.0, 1.0 Hz, H-1, H-9), 1.41 – 1.46 (2H, m, H-4), 1.48 – 1.57 (4H, m, H-1, H-5), 1.57 – 1.63 (4H, m, H-2), 2.81 (2H, d, *J* = 6.0 Hz, H-7), 3.01 (2H, q, *J* = 5.5 Hz, H-6), 3.94 – 4.10 (4H, m, H-8); **^{13}C NMR** δ_C (101 MHz, $CDCl_3$) 16.2 (C-9), 23.6 (C-5), 24.6 (C-2), 36.4 (C-1), 36.9 (C-4), 42.2 (C-3), 45.1 (C-6), 54.5 (C-7), 62.1 (C-8); **HRMS (ESI$^+$)** *m/*z $[M+H]^+$ calculated for $C_{13}H_{27}O_3NP$, 276.1723; found, 276.1722.

Diethyl (7-azaspiro[4.5]dec-8-en-7-yl)phosphonate (3.12a)

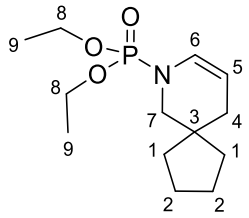

The titled compound was synthesized by following **GP-1** using $P450_{BM3}$ mutant enzyme strain R19/F87A/I263G on a reaction scale of 50 mL. Reaction was completed after 5 h, as monitored by GC. The crude product was purified by flash chromatography (10% → 25% EtOAc in pentane, with a gradient of 5%) to afford a colourless oil (7.8 mg, 29%). **R_f** 0.38 (50% EtOAc in pentane); **^{1}H NMR** δ_H (500 MHz, $CDCl_3$) 1.33 (6H, td, *J* = 7.0, 1.0 Hz, H-9), 1.35 – 1.40 (1H, m, H-2), 1.41 – 1.54 (2H, m, H-2), 1.60 – 1.71 (5H, m, H-1, H-2), 1.86 – 1.90 (2H, m, H-4), 3.04 (2H, d, *J* = 4.5 Hz, H-7), 3.98 – 4.13 (4H, m, H-8), 4.73 (1H, dq, *J* = 8.0, 4.0 Hz, H-5), 6.30 – 6.36 (1H, m, H-6); **^{13}C NMR** δ_C (126 MHz, $CDCl_3$) 16.1 (C-9), 24.8 (C-1), 35.0 (C-4), 37.0 (C-2), 51.7 (C-7), 62.6 (C-8), 103.0 (C-5), 126.5 (C-6); **HRMS (ESI$^+$)** *m/z* $[M+Na]^+$ calculated for $C_{13}H_{24}O_3NPNa$, 296.1386; found, 296.1387.

7-Benzyl-7-azaspiro[4.5]decan-6-one (3.13)

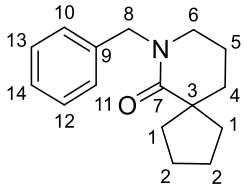

To a solution of **3.6** (1.64 g, 10.7 mmol) in THF (24 mL) was added NaH (642 mg, 60% dispersion in mineral oil, 16.1 mmol) at −5 °C. The mixture was stirred for 30 min at 0 °C and BnBr (1.7 mL) was added. The mixture was then warmed to RT and stirred for 16 h. Iced water (15 mL) was added and the solution was extracted with EtOAc (3 × 20 mL). The combined organic layers were washed with brine (20 mL) and dried with $MgSO_4$. The crude product was concentrated *in vacuo* and purification with flash chromatography (10% EtOAc in pentane) afforded the *title compound* (yellow oil, 1.8 g, 67%); **R_f** 0.73 (50% EtOAc in pentane); **IR** ν_{max} (thin film)/cm^{-1} 1632s, 1280m, 736m; **^{1}H NMR** δ_H (400 MHz, $CDCl_3$) 1.46 – 1.55 (2H, m, H-1), 1.61 – 1.67 (2H, m, H-2), 1.67 – 1.73 (2H, m, H-4), 1.74 – 1.81 (2H, m, H-5), 1.81 – 1.91 (2H, m, H-2), 2.14 – 2.24 (2H, m, H-1), 3.21 (2H, t, *J* = 6.0 Hz, H-6), 4.57 (2H, s, H-8), 7.21 – 7.35 (5H, m, H-Ar); **^{13}C NMR** δ_C (101 MHz, $CDCl_3$) 20.6 (C-5), 26.0 (C-2), 35.0 (C-4), 39.3 (C-1), 47.6 (C-6), 49.1 (C-3), 50.5 (C-8), 127.2 (C-Ar), 127.9 (C-Ar), 128.5 (C-Ar), 137.8 (C-9), 176.7 (C-7); **HRMS (ESI$^+$)** *m/z* $[M+H]^+$ calculated for, 244.1696; found, 244.1697.

(2*R, 5*R**)-7-Benzyl-2-hydroxy-7-azaspiro[4.5]decan-6-one (3.13a)**

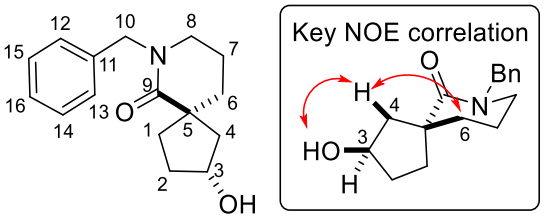

The titled compound was synthesized by following **GP-1** using $P450_{BM3}$ mutant enzyme strain R19/F87I on a reaction scale of 50 mL. Reaction was completed after 4 h, as monitored by GC. The crude product was purified by flash chromatography (1% → 4% methanol in DCM, with a gradient of 1%) to afford a yellow oil (7.9 mg, 31%, *e.e.* 55%,

by Mosher ester analysis). **R_f** 0.66 (1% methanol in DCM)**; IR** ν_{max} (thin film)/cm^{-1} 3031br, 1613s, 1451m, 1106m; **^{1}H NMR** δ_H (500 MHz, acetone-d_6) 1.49 (1H, ddd, *J* = 13.0, 4.0, 1.5 Hz, H-4), 1.63 – 1.74 (2H, m, H-1, H-2), 1.75 – 1.82 (2H, m, H-7), 1.85 – 1.94 (2H, m, H-6), 1.94 – 2.01 (1H, m, H-2), 2.06 – 2.11 (1H, m, H-1), 2.37 (1H, dd, *J* = 13.0, 6.0 Hz, H-4), 3.24 (2H, t, *J* = 6.0 Hz, H-8), 3.58 (1H, dd, *J* = 3.5, 1.0 Hz, OH), 4.40 – 4.45 (1H, m, H-3), 4.50 (1H, d, *J* = 14.5 Hz, H-10), 4.58 (1H, d, *J* = 14.5 Hz, H-10), 7.23 – 7.34 (5H, m, H-Ar); **^{13}C NMR** δ_C (125 MHz, acetone-d_6) 20.4 (C-7), 35.4 (C-2), 36.6 (C-6), 37.0 (C-1), 47.4 (C-4), 47.5 (C-8), 48.2 (C-5), 49.7 (C-10), 73.3 (C-3), 127.6 (C-Ar), 128.4 (C-Ar), 138.5 (C-11), 175.8 (C-9); **HRMS (ESI$^+$)** *m/z* $[M+H]^+$ calculated for $C_{16}H_{22}O_2N$, 260.1645; found, 260.1646; $[\boldsymbol{\alpha}]_{\boldsymbol{D}}^{\mathbf{25}}$ = +3.7 (*c* = 0.0259 g/ mL, DCM).

7-Benzyl-10-hydroxy-7-azaspiro[4.5]decan-6-one (3.13b)

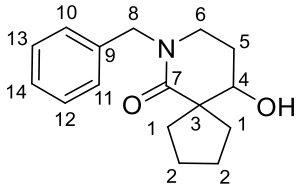

The titled compound was synthesized by following **GP-1** using $P450_{BM3}$ mutant enzyme strain R19/F87A/A184I on a reaction scale of 500 mL. Reaction was completed after 5 h, as monitored by GC. The crude product was purified by flash chromatography (1% → 2% methanol in DCM, with a gradient of 1%) to afford colourless oil (0.84 mg, 0.3%, *e.e.* 78%, by Mosher ester analysis). **R_f** 0.68 (1% methanol in DCM); **IR** ν_{max} (thin film)/cm^{-1} 3398br, 3031s, 1615m, 1495m, 1170w, 732m; **^{1}H NMR** δ_H (400 MHz, $CDCl_3$) 1.55 – 1.80 (5H, m, H-1, H-2), 1.83 – 1.99 (2H, m, H-2, H-5), 1.99 – 2.12 (2H, m, H-1, H-5), 2.17 – 2.26 (1H, m, H-2), 3.09 – 3.18 (1H, m, H-6), 3.43 – 3.52 (1H, m, H-6), 3.81 (1H, dd, *J* = 6.5, 2.5 Hz, H-4), 4.47 (1H, d, *J* = 15.0 Hz, H-8), 4.69 (1H, d, *J* = 15.0 Hz, H-8), 7.26 – 7.33 (5H, m, H-Ar); **^{13}C NMR** δ_C (126 MHz, $CDCl_3$) 26.8 (C-2), 33.3 (C-1), 38.0 (C-5), 42.7 (C-6), 50.3 (C-8), 54.9 (C-3), 70.0 (C-4), 127.2 (C-Ar), 127.8 (C-Ar), 128.6

(C-Ar), 137.6 (C-Ar), 175.7 (C-7); **HRMS (ESI$^+$)** *m/z* $[M+H]^+$ calculated for $C_{16}H_{22}O_2N$, 260.1645; found, 260.1646.

7-Benzyl-8-hydroxy-7-azaspiro[4.5]decan-6-one (3.13c)

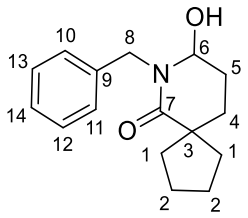

The titled compound was synthesized by following **GP-1** using $P450_{BM3}$ mutant enzyme strain RT2 on a reaction scale of 50 mL. Reaction was completed after 4 h, as monitored by GC. The crude product was purified by flash chromatography (1% → 4% methanol in DCM, with a gradient of 1%) to afford a yellow oil (3.4 mg, 13%). **R_f** 0.70 (1% methanol in DCM); **IR** ν_{max} (thin film)/cm^{-1} 3364br, 1680s, 1355m; **^{1}H NMR** δ_H (500 MHz, $CDCl_3$) 1.43 – 1.54 (3H, m, H-1), 1.60 – 1.73 (4H, m, H-1, H-2, H-4), 1.80 – 1.89 (1H, m, H-2), 1.93 – 2.01 (3H, m, H-2, H-5), 2.18 – 2.21 (1H, m, OH), 2.31 – 2.37 (1H, m, H-2), 4.35 (1H, d, *J* = 15.0 Hz, H-8), 4.90 (1H, dt, *J* = 8.0, 3.5 Hz, H-6), 5.06 (1H, d, *J* = 15.0 Hz, H-8), 7.26 – 7.33 (5H, m, H-Ar); **^{13}C NMR** δ_C (126 MHz, $CDCl_3$) 26.0 (C-2), 28.5 (C-5), 35.0 (C-4), 38.9 (C-1), 47.6 (C-8), 49.2 (C-3), 79.4 (C-6), 127.9 (C-Ar), 128.52 (C-Ar), 128.8 (C-Ar), 137.8 (C-Ar), 177.1 (C-7); **HRMS (ESI$^+$)** *m/z* $[M+H]^+$ calculated for $C_{16}H_{22}O_2N$, 260.1645; found, 260.1647.

7-Benzyl-2-hydroxy-7-azaspiro[4.5]dec-8-en-6-one (3.13d)

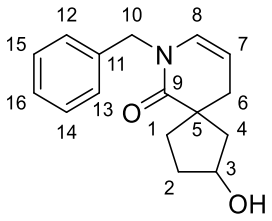

The titled compound was synthesized by following **GP-1** using $P450_{BM3}$ mutant enzyme strain R19/F87I on a reaction scale of 50 mL. Reaction was completed after 4 h, as

monitored by GC. The crude product was purified by flash chromatography (1% → 4% methanol in DCM, with a gradient of 1%) to afford a colourless oil (5.3 mg, 21%). **R_f** 0.42 (1% methanol in DCM); **IR** ν_{max} (thin film)/cm^{-1} 3423br, 1659s, 1231m, 1078w, 700m; **^{1}H NMR** δ_H (600 MHz, $CDCl_3$) 1.54 (1H, ddd, *J* = 14.0, 4.0, 1.5 Hz, H-4), 1.69 – 1.74 (1H, m, H-2), 1.83 (1H, td, *J* = 12.5, 8.0 Hz, H-1), 1.99 – 2.04 (1H, m, H-2), 2.05 – 2.10 (1H, m, H-1), 2.40 (1H, dd, *J* = 4.0, 2.0 Hz, H-6), 2.47 (1H, dd, *J* = 4.0, 2.0 Hz, H-6), 2.48 – 2.52 (1H, m, H-4), 4.49 – 4.53 (1H, m, H-3), 4.67 (2H, q, *J* = 15.0 Hz, H-10), 5.09 – 5.13 (1H, m, H-7), 6.03 (1H, dt, *J* = 7.5, 1.5 Hz, H-8), 7.21 – 7.24 (2H, m, H-Ar), 7.27 – 7.34 (3H, m, H-Ar); **^{13}C NMR** δ_C (151 MHz, $CDCl_3$) 34.4 (C-1), 35.2 (C-6), 35.3 (C-2), 44.9 (C-4), 47.8 (C-5), 49.6 (C-10), 74.3 (C-3), 105.9 (C-7), 127.6 (C-Ar), 127.7 (C-Ar), 128.8 (C-Ar), 129.6 (C-8), 137.7 (C-11), 174.7 (C-9); **HRMS (ESI$^+$)** *m/z* $[M+H]^+$ calculated for $C_{16}H_{20}O_2N$, 258.1489; found, 258.1489.

7.5 Compounds from Chapter 4

(2*R, 5*R**)-7-Benzyl-6-oxo-7-azaspiro[4.5]decan-2-yl formate (4.1)**

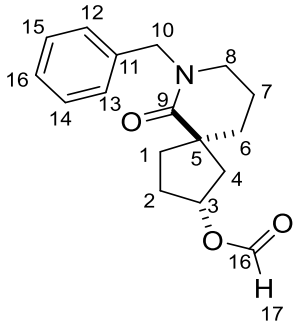

To alcohol **3.13a** (25.9 mg, 0.100 mmol) was added 95% formic acid (1 mL) and was stirred at RT for 2 h. The reaction was then heated to 60 ^{o}C for 4 h and diluted with 10 parts of DCM. The organic layers were washed with water until the washings were neutral (pH 7). The combined organic layers were dried with $MgSO_4$ and concentrated *in vacuo*. Purification with flash chromatography (30% EtOAc in pentane) afforded the *titled compound* as a yellow oil (9.2 mg, 32%). **R_f** 0.89 (30% EtOAc in pentane); **IR** ν_{max} (thin

film)/cm^{-1} 1717s, 1629s, 1355m, 1236m1, 1174s, 733w; **^{1}H NMR** δ_H (400 MHz, $CDCl_3$) 1.63 – 1.69 (1H, m, H-4), 1.70 – 1.83 (3H, m, H-1, H-7), 1.84 – 1.92 (3H, m, H-2, H-6), 2.18 – 2.36 (2H, m, H-1, H-2), 2.68 (1H, dd, *J* = 14.5, 6.5 Hz, H-4), 3.22 (2H, t, *J* = 6.0 Hz, H-8), 4.50 (1H, d, *J* = 14.5 Hz, H-10), 4.61 (1H, d, *J* = 14.5 Hz, H-10), 5.44 – 5.55 (1H, m, H-3), 7.20 – 7.35 (5H, m, H-Ar), 8.02 (1H, s, H-17); **^{13}C NMR** δ_C (101 MHz, $CDCl_3$) 20.5 (C-7), 33.0 (C-2), 35.9 (C-6), 37.6 (C-1), 44.6 (C-4), 47.6 (C-8), 48.6 (C-5), 50.5 (C-10), 77.8 (C-3), 127.3 (C-Ar), 127.9 (C-Ar), 128.6 (C-Ar), 137.5 (C-Ar), 160.7 (C-9), 175.6 (C-16); **HRMS (ESI$^+$)** *m/z* $[M+H]^+$ calculated for $C_{17}H_{22}O_3N$, 288.1593; found, 288.1594.

1-(Cyclohexylmethyl)piperidin-2-one (4.2)

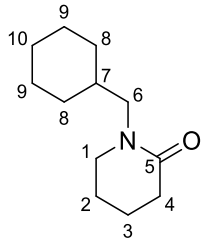

Delta-valerolactam (20.5 mg, 0.100 mmol) was dissolved in methanol (2 mL), and 20 wt. % loading Pt/C (10 mg) was added. The mixture was stirred at a hydrogen atmosphere at RT for 24 h. The mixture was then filtered through a celite pad and concentrated *in vacuo*. Purification by flash chromatography (75% EtOAc in pentane) afforded the *title compound* as a colourless oil (21.8 mg, 85%). **R$_f$** 0.43 (80% EtOAc in pentane); **^{1}H NMR** δ_H (400 MHz, $CDCl_3$) 0.89 – 1.01 (2H, m, H-9), 1.11 – 1.20 (2H, m, H-8), 1.60 – 1.75 (7H, m, H-7, H-8, H-9, H-10), 1.75 – 1.81 (4H, m, H-2, H-3), 2.34 – 2.42 (2H, m, H-4), 3.19 (2H, d, *J* = 7.5 Hz, H-6), 3.23 – 3.27 (2H, m, H-1); **^{13}C NMR** δ_C (101 MHz, $CDCl_3$) 21.4 (C-3), 23.4 (C-2), 25.9 (C-8), 26.5 (C-10), 30.8 (C-9), 32.4 (C-4), 35.8 (C-7), 48.8 (C-1), 53.3 (C-6), 169.9 (C-5); **HRMS (ESI$^+$)** *m/z* $[M+H]^+$ calculated for $C_{12}H_{22}ON$, 196.1696; found, 196.1696.

(2*R, 5*R**)-7-Benzyl-7-azaspiro[4.5]decan-2-ol (4.3)**

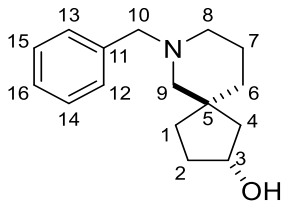

Into round-bottom flask was added lactam **3.13a** (17.7 mg, 0.07 mmol) in THF (0.67 mL) and cooled to 0 °C. To this flask was then added $LiAlH_4$ (12.9 mg, 0.341 mmol) in THF (1.4 mL). The reaction mixture was warmed to RT over 30 min whilst stirring and refluxed for 16 h. The reaction was cooled to 0 °C, followed by the addition of water (10 µL), 15% NaOH aqueous solution (10 µL) and water (30 µL). The resultant mixture was diluted with DCM and the organic layers were washed with brine, water, and dried with $MgSO_4$. The filtrate was then concentrated *in vacuo*. Purification by flash chromatography (25% → 35% EtOAc in pentane, with a 5% gradient) afforded the *title compound* as a yellow oil (13.6 mg, 81%). **R_f** 0.57 (30% EtOAc in pentane); **IR** ν_{max} (thin film)/cm^{-1} 3414br, 2930br, 1453m, 1175s, 740w; **^{1}H NMR** δ_H (500 MHz, $CDCl_3$) 1.32 (1H, dd, *J* = 13.0, 4.5 Hz, H-4), 1.38 – 1.45 (2H, m, H-7), 1.53 – 1.59 (3H, m, H-2, H-6), 1.66 – 1.77 (1H, m, H-6), 1.87 (1H, d, *J* = 13.0 Hz, H-4), 2.24 – 2.38 (2H, m, H-8), 3.39 (2H, s, H-9), 4.14 – 4.20 (1H, m, H-3), 7.15 – 7.28 (5H, m, H-Ar); **^{13}C NMR** δ_C (126 MHz, $CDCl_3$) 23.7 (C-6), 34.6 (C-2), 38.4 (C-7), 42.8 (C-5), 47.1 (C-4), 54.4 (C-8), 63.4 (C-9), 73.8 (C-3), 126.9 (C-Ar), 128.2 (C-Ar), 128.8 (C-Ar), 139.4 (C-11); **HRMS (ESI$^+$)** *m/z* $[M+H]^+$ calculated for $C_{16}H_{24}NO$, 246.1852; found, 246.1853.

(2*R, 5*R**)-7-Azaspiro[4.5]decan-2-ol (4.4)**

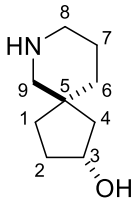

Benzylated amine (14.8 mg, 0.060 mmol) was dissolved in methanol (1 mL) and 10% Pd/C (18.6 mg) was added. The mixture was stirred under hydrogen for 18 h at RT. The reaction was then filtered through a celite pad and concentrated *in vacuo* to afford the *title compound* (9.2 mg, 98%). **IR** ν_{max} (thin film)/cm^{-1} 3289br, 1624w, 1441m, 1192m, 1079m; **^{1}H NMR** δ_H (400 MHz, $CDCl_3$) 1.37 – 1.46 (1H, m, H-4), 1.48 – 1.53 (2H, m, H-7), 1.53 – 1.62 (4H, m, H-1, H-6), 1.61 – 1.68 (1H, m, H-2), 1.77 – 1.90 (2H, m, H-2, H-4), 2.53 (2H, d, *J* = 2.5 Hz, H-9), 2.68 – 2.81 (2H, m, H-8), 4.25 – 4.33 (1H, m, H-3); **^{13}C NMR** δ_C (101 MHz, $CDCl_3$) 24.2 (C-7), 34.5 (C-2), 34.6 (C-1), 38.4 (C-6), 41.4 (C-5), 46.5 (C-8), 46.6 (C-4), 57.2 (C-9), 73.5 (C-3); **HRMS (ESI$^+$)** *m/z* $[M+H]^+$ calculated for $C_9H_{18}ON$, 156.1383; found, 156.1384.

(2*R, 5*R**)-7-Benzyl-2-chloro-7-azaspiro[4.5]decan-6-one (4.5)**

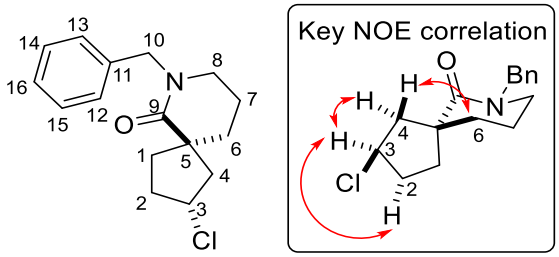

Dissolve alcohol **3.13a** (29.1 mg, 0.100 mmol) in DCM (1.5 mL) and cool the mixture to −78 °C. DAST (16 µL, 0.12 mmol) was added and the resulting solution was stirred at the same temperature for 1.5 h. The solution was then warmed to and stirred for 15 h and diluted with DCM (10 mL). The organic layers were washed with sat. $NaHCO_3$, brine, and dried with $MgSO_4$. The crude product was concentrated *in vacuo*. Purification by flash chromatography (30% EtOAc in pentane) afforded the *titled compound* as a yellow oil (7.5 mg, 27%). **R_f** 0.43 (30% EtOAc in pentane); **IR** ν_{max} (thin film)/cm^{-1} 1632s,

1355m, 1233w, 733m, 700m; **^{1}H NMR** δ_H (400 MHz, $CDCl_3$) 1.74 – 2.07 (7H, m, H-1, H-2, H-4, H-6, H-7), 2.17 – 2.26 (1H, m, H-1), 2.35 – 2.47 (1H, m, H-2), 2.81 (1H, dd, *J* = 14.0, 6.5 Hz, H-4), 3.23 (2H, t, *J* = 6.0 Hz, H-8), 4.49 (1H, d, *J* = 14.5 Hz, H-10), 4.60 (1H, d, *J* = 14.5 Hz, H-10), 4.61 – 4.67 (1H, m, H-3), 7.19 – 7.35 (5H, m, H-Ar); **^{13}C NMR** δ_C (101 MHz, $CDCl_3$) 20.5 (C-7), 36.7 (C-6), 37.5 (C-2), 37.7 (C-1), 47.6 (C-8), 48.7 (C-5), 49.1 (C-4), 50.5 (C-10), 61.6 (C-3), 127.3 (C-Ar), 127.9 (C-Ar), 128.6 (C-Ar), 137.5 (C-11), 175.9 (C-9); **HRMS (ESI$^+$)** *m/z* $[M+H]^+$ calculated for $C_{16}H_{21}ONCl$, 278.1306, 280.1277, 281.1310; found, 278.1305, 280.1276, 281.1310.

(2*R, 5*R**)-7-Benzyl-2-(phenylamino)-7-azaspiro[4.5]decan-6-one (4.9)**

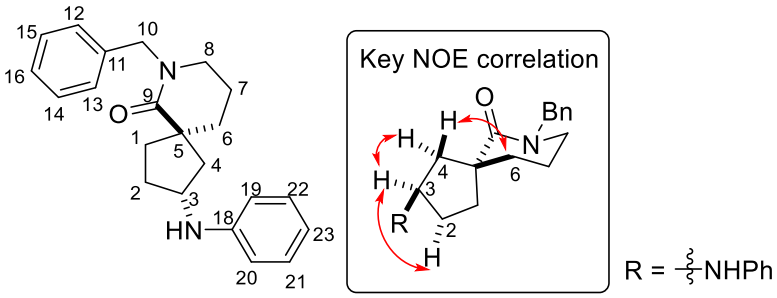

Into a flame-dried vial was added $[Cp^*IrCl_2]_2$ (4.0 mg, 0.005 mmol), and K_2CO_3 (1.4 mg, 0.01 mmol) in toluene (0.1 mL). Alcohol **3.13a** (58.2 mg, 0.20 mmol) and aniline (20 µL, 0.200 mmol) were added and the mixture was refluxed for 12 h. The reaction was extracted with DCM and filtered through a plug of celite. The resulting mixture was concentrated under reduced pressure. Purification by flash chromatography (35% EtOAc in pentane) afforded the *titled compound* as a yellow oil (37 mg, 56%). **R_f** 0.39 (35% EtOAc in pentane); **IR** ν_{max} (thin film)/cm^{-1} 3351br, 1622s, 1602s, 1318m, 749m, 696m; **^{1}H NMR** δ_H (500 MHz, $CDCl_3$) 1.33 (1H, dd, *J* = 13.0, 7.0 Hz, H-4), 1.58 – 1.62 (1H, m, H-2), 1.69 – 1.80 (3H, m, H-1, H-7), 1.81 – 1.87 (2H, m, H-6), 2.23 – 2.30 (1H, m, H-1), 2.32 – 2.39 (1H, m, H-2), 2.73 (1H, dd, *J* = 13.0, 7.0 Hz, H-4), 3.21 (2H, t, *J* = 6.0 Hz, H-8), 3.66 (1H, br. s, NH), 4.17 (1H, quin, *J* = 7.0 Hz, H-3), 4.54 (1H, d, *J* = 14.5 Hz, H-10), 4.62 (1H, d, *J* = 14.5 Hz, H-10), 6.62 – 6.66 (2H, m, H-Ar), 6.66 – 6.70 (1H, m, H-Ar), 7.14 – 7.20 (2H, m, H-Ar), 7.21 – 7.25 (2H, m, H-Ar), 7.27 – 7.30 (1H, m, H-Ar),

7.30 – 7.34 (2H, m, H-Ar); **^{13}C NMR** δ_C (126 MHz, $CDCl_3$) 20.5 (C-7), 33.5 (C-2), 36.4 (C-6), 36.9 (C-1), 46.5 (C-4), 47.6 (C-8), 48.3 (C-5), 50.5 (C-10), 55.2 (C-3), 113.3 (C-Ar), 117.1 (C-Ar), 127.3 (C-Ar), 127.9(C-Ar), 128.6 (C-Ar), 129.3 (C-Ar), 137.6 (C-11), 147.9 (C-Ar), 176.2 (C-9); **HRMS (ESI$^+$)** *m/z* $[M+H]^+$ calculated for $C_{22}H_{27}ON_2$, 335.2118; found, 335.2118.

(2*R, 5*R**)-7-Benzyl-2-((triethylsilyl)oxy)-7-azaspiro[4.5]decan-6-one (4.10)**

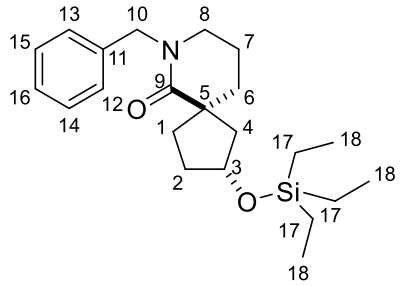

Benzylated alcohol **3.13a** (41.3 mg, 0.159 mmol) was dissolved in DMF (1 mL), followed by the addition of imidazole (65.0 mg, 0.956 mmol) and chlorotriethylsilane (80 µL, 0.48 mmol). The reaction was stirred at RT for 18 h and diluted with 4 parts diethyl ether and washed with water. Purification by flash chromatography (20% EtOAc in pentane) afforded the *title compound* as a yellow oil (7.1 mg, 12%). **R_f** 0.61 (5% EtOAc in pentane); **IR** ν_{max} (thin film)/cm^{-1} 1636s, 1237m, 1197m, 729m; **^{1}H NMR** δ_H (500 MHz, $CDCl_3$) 0.64 – 0.52 (6H, m, H-17), 0.95 (9H, t, *J* = 8.0 Hz, H-18), 1.48 (1H, dd, *J* = 13.0, 5.0 Hz, H-4), 1.63 – 1.69 (1H, m, H-2), 1.69 – 1.71 (1H, m, H-1), 1.73 – 1.81 (2H, m, H-7), 1.84 – 1.92 (2H, m, H-6), 2.00 – 2.07 (1H, m, H-2), 2.08 – 2.17 (1H, m, H-1), 2.38 – 2.47 (1H, m, H-4), 3.20 (2H, t, *J* = 6.0 Hz, H-8), 4.44 – 4.55 (2H, m, H-10, H-3), 4.62 (1H, d, *J* = 14.6 Hz, H-10), 7.19 – 7.34 (5H, m, H-Ar); **^{13}C NMR** δ_C (126 MHz, $CDCl_3$) 4.9 (C-17), 7.0 (C-18), 20.7 (C-7), 36.0 (C-2), 36.6 (C-6), 37.0 (C-1), 37.4 (C-5), 47.8 (C-8), 48.3 (C-4), 50.6 (C-10), 74.6 (C-3), 127.4 (C-Ar), 128.0 (C-Ar), 128.7 (C-Ar), 137.9 (C-Ar), 176.8 (C-9); **HRMS (ESI$^+$)** *m/z* $[M+H]^+$ calculated for $C_{22}H_{36}O_2NSi$, 374.2510; found, 374.2505.

(2*R,5*R**)-7-benzyl-2-ethoxy-7-azaspiro[4.5]decan-6-one (4.11)**

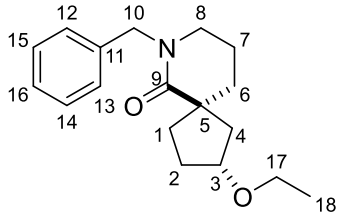

TES-protected lactam **4.10** (22.2 mg, 0.059 mmol) was dissolved in DCM (0.6 mL) and cooled to −78 °C. Tf_2O (10 µL, 0.071 mmol) was added dropwise and the solution was stirred at −78 °C for 45 min. Ethyl magnesium bromide (60 µL, 3.0 M solution in diethyl ether, 0.18 mmol) was added dropwise and the solution was warmed to RT and stirred for 16 h. Sat. aq. NH_4Cl (0.5 mL) was added and the mixture was extracted with DCM. The combined organic layers were washed with water, brine, and dried with $MgSO_4$. Purification by flash chromatography (5% → 30% EtOAc in pentane, with a gradient of 5%) afforded the *title compound* as a pale yellow oil (4.7 mg, 21%). **R_f** 0.58 (30% EtOAc in pentane); **IR** ν_{max} (thin film)/cm^{-1} 1643s, 1492m, 1353m, 1281m, 1197m, 701m; **^{1}H NMR** δ_H (400 MHz, $CDCl_3$) 1.19 (3H, t, *J* = 7.0 Hz, H-18), 1.53 – 1.60 (1H, m, H-4), 1.67 – 1.70 (1H, m, H-1), 1.72 – 1.82 (3H, m, H-2, H-7), 1.83 – 1.90 (2H, m, H-6), 2.04 – 2.18 (2H, m, H-1, H-2), 2.46 (1H, dd, *J* = 13.5, 6.5 Hz, H-4), 3.21 (2H, t, *J* = 6.5 Hz, H-8), 3.46 (2H, qd, *J* = 7.0, 1.5 Hz, H-17), 4.12 – 4.20 (1H, m, H-3), 4.50 (1H, d, *J* = 14.5 Hz, H-10), 4.62 (1H, d, *J* = 14.5 Hz, H-10), 7.20 – 7.30 (5H, m, H-Ar); **^{13}C NMR** δ_C (101 MHz, $CDCl_3$) 15.8 (C-18), 20.6 (C-7), 32.4 (C-2), 36.3 (C-6), 36.9 (C-1), 44.8 (C-4), 47.9 (C-8), 48.3 (C-5), 50.6 (C-10), 64.3 (C-17), 81.5 (C-3), 127.4 (C-Ar), 128.0 (C-Ar), 128.7 (C-Ar), 137.8 (C-Ar), 176.6 (C-9); **HRMS (ESI$^+$)** *m/z* $[M+H]^+$ calculated for $C_{18}H_{26}O_2N$, 288.1958; found, 288.1959.

Cyclohexyl Sulfamate (4.12)[329]

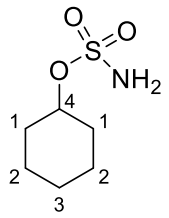

Formic acid (0.94 mL, 25 mmol) was added dropwise to chlorosulfonyl isocyanate (2.6 mL, 30 mmol) at 0 °C. The mixture solidified within 5 min and to the solid was added ACN (8 mL). The reaction mixture was allowed to warm to RT and stirred for an additional 4 h. The flask was cooled to 0 °C and cyclohexanol (1.0 mL, 10 mmol) in dry DMA (6.6 mL) was added to the solution. The mixture was stirred for 18 h and quenched by the addition of water (19 mL). The aqueous layers were extracted with diethyl ether (3 × 25 mL) and washed with water (25 mL) and brine (25 mL). The combined organic layers were dried with $MgSO_4$ and concentrated *in vacuo* to afford a white solid (457 mg, 26%). **R_f** 0.71 (50% EtOAc in pentane); **^{1}H NMR** δ_H (400 MHz, $CDCl_3$) 1.23 – 1.31 (1H, m, H-3), 1.32 – 1.44 (2H, m, H-2), 1.49 – 1.57 (1H, m, H-3), 1.58 – 1.70 (2H, m, H-1), 1.74 – 1.83 (2H, m, H-2), 1.97 – 2.04 (2H, m, H-1), 4.61 (1H, tt, *J* = 9.0, 4.0 Hz, H-4), 4.64 – 4.80 (2H, br. s, NH_2); **^{13}C NMR** δ_C (101 MHz, $CDCl_3$) 23.6 (C-2), 25.0 (C-3), 32.4 (C-1), 82.8 (C-4).

Cycloheptyl Sulfamate (4.13)

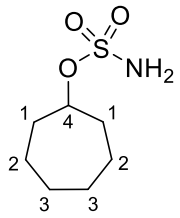

Formic acid (0.47 mL, 13 mmol) was added dropwise to chlorosulfonyl isocyanate (1.3 mL, 15 mmol) at 0 °C. The mixture solidified within 5 min and to the solid was added ACN (4 mL). The reaction mixture was allowed to warm to RT and stirred for an

additional 4 h. The flask was cooled to 0 °C and cycloheptanol (0.6 mL, 5.0 mmol) in dry DMA (3.3 mL) was added to the solution. The mixture was stirred for 18 h and quenched by the addition of water (3.8 mL). The aqueous layers were extracted with diethyl ether (3 × 25 mL) and washed with water (13 mL) and brine (13 mL). The combined organic layers were dried with $MgSO_4$ and concentrated *in vacuo* to afford a white solid (464 mg, 48%). **R_f** 0.77 (50% EtOAc in pentane); **IR** ν_{max} (thin film)/cm^{-1} 3323br, 1563m, 1433w, 1390m, ; **^{1}H NMR** δ_H (400 MHz, $CDCl_3$) 1.39 – 1.49 (2H, m, H-2), 1.51 – 1.61 (4H, m, H-3), 1.64 – 1.76 (2H, m, H-2), 1.83 – 1.93 (2H, m, H-1), 2.02 – 2.11 (2H, m, H-1), 4.76 (1H, tt, *J* = 8.5, 4.5 Hz, H-4), 4.91 (2H, br. s, NH_2); **^{13}C NMR** δ_C (101 MHz, $CDCl_3$) 22.4 (C-2), 28.2 (C-3), 34.6 (C-1), 85.7 (C-4); **HRMS (ESI$^+$)** *m/z* $[M+Na]^+$ calculated for $C_7H_{15}O_3NNaS$, 216.0665, found, 216.0665.

Pentyl Carbamate (4.20)[267]

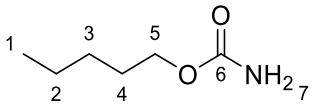

1-pentanol (1.1 mL, 10.0 mmol) was dissolved in DCM (20 mL) and was cooled to 0 °C. Trichloroacetyl isocyanate (1.4 mL, 12 mmol) was added dropwise to the mixture and warmed to RT. The reaction was stirred for 6 h and the solvent was removed *in vacuo*. The crude reaction mixture was dissolved in methanol (17 mL) and K_2CO_3 (0.14 g, 1.0 mmol) was added and stirred for 18 h. The mixture was diluted with DCM (10 mL) and quenched by addition of aq. sat. NH_4Cl (15 mL). The aqueous layers were extracted with DCM. The combined organic layers were washed with water, brine, and dried with $MgSO_4$. Purification by flash chromatography (30% → 35% EtOAc in pentane, with a gradient of 5%) afforded the title compound as a white solid (1.1 g, 87%). **R_f** 0.56 (50% EtOAc in pentane); **^{1}H NMR** δ_H (400 MHz, $CDCl_3$) 0.86 – 0.96 (3H, m, H-1), 1.27 – 1.41 (4H, m, H-2, H-3), 1.59 – 1.66 (2H, m, H-4), 4.05 (2H, t, *J* = 7.0 Hz, H-5), 4.57 (2H,

br. s, NH_2); **^{13}C NMR** δ_C (101 MHz, $CDCl_3$) 14.1 (C-1), 22.5 (C-2), 28.1 (C-3), 28.8 (C-4), 65.5 (C-5), 157.2 (C-6).

4-Propyloxazolidin-2-one (4.21)[267]

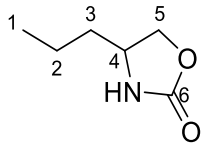

Into a flask was added $AgClO_4$ (1.1 mg, 0.52 mmol) and Me_4phen (1.9 mg, 0.0052 mmol) in DCM (5.2 mL). The mixture was stirred vigorously for 15 min at RT and activated 4 Å molecular sieves (0.52 g) was added. Carbamte **4.20** (68 mg, 0.52 mmol) was added whilst stirring, followed by the addition of iodosylbenzene (228 mg, 1.04 mmol). The mixture was heated to reflux for 18 h and filtered through a celite pad. The solvent was concentrated *in vacuo*. Purification by flash chromatography (30% → 50% EtOAc in pentane, with a gradient of 5%) afforded the title compound as a dark orange oil (14.1 mg, 21%). **R_f** 0.48 (80% EtOAc in pentane); **^{1}H NMR** δ_H (400 MHz, $CDCl_3$) 0.96 (3H, t, *J* = 7.5 Hz, H-1), 1.29 – 1.41 (2H, m, H-2), 1.52 – 1.60 (2H, m, H-3), 3.83 – 3.91 (1H, m, H-4), 4.02 (1H, dd, *J* = 8.5, 6.0 Hz, H-5), 4.49 (1H, t, *J* = 8.5 Hz, H-5), 5.58 (1H, br. s, NH); **^{13}C NMR** δ_C (101 MHz, $CDCl_3$) 14.0 (C-1), 18.7 (C-2), 37.5 (C-3), 52.5 (C-4), 70.5 (C-5), 160.2 (C-6).

Cyclohexyl Carbamate (4.29)[330]

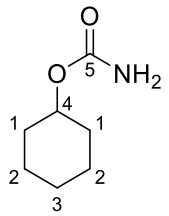

Cyclohexanol (1.0 mL, 10 mmol) was dissolved in DCM (20 mL) and was cooled to 0 ^oC. Trichloroacetyl isocyanate (1.4 mL, 12 mmol) was added dropwise to the mixture and warmed to RT. The reaction was stirred for 6 h and the solvent was removed *in vacuo*.

The crude reaction mixture was dissolved in methanol (17 mL) and K_2CO_3 (0.14 g, 1.0 mmol) was added and stirred for 18 h. The mixture was diluted with DCM (10 mL) and quenched by addition of sat. aq. NH_4Cl (15 mL). The aqueous layers were extracted with DCM. The combined organic layers were washed with water, brine, and dried with $MgSO_4$. Purification by flash chromatography (10% →50% EtOAc in pentane, with a gradient of 5%) afforded the title compound as a white solid (1.2 g, 84%). **R_f** 0.63 (50% EtOAc in pentane); **^{1}H NMR** δ_H (400 MHz, $CDCl_3$) 1.28 – 1.46 (4H, m, H-1, H-2), 1.49 – 1.61 (2H, m, H-3), 1.67 – 1.77 (2H, m, H-2), 1.86 – 1.93 (2H, m, H-1), 4.55 (2H, br. s, NH_2), 4.59 – 4.66 (1H, m, H-4); **^{13}C NMR** δ_C (101 MHz, $CDCl_3$) 24.0 (C-2), 25.5 (C-3), 32.1 (C-1), 73.6 (C-4), 161.3 (C-5).

Cycloheptyl Carbamate (4.30)

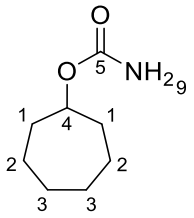

Cycloheptanol (1.2 mL, 10 mmol) was dissolved in DCM (20 mL) and was cooled to 0 ^oC. Trichloroacetyl isocyanate (1.4 mL, 12 mmol) was added dropwise to the mixture and warmed to RT. The reaction was stirred for 6 h and the solvent was removed *in vacuo*. The crude reaction mixture was dissolved in methanol (17 mL) and K_2CO_3 (0.14 g, 1.0 mmol) was added and stirred for 18 h. The mixture was diluted with DCM (10 mL) and quemched by addition of sat. aq. NH_4Cl (15 mL). The aqueous layers were extracted with DCM. The combined organic layers were washed with water, brine, and dried with $MgSO_4$. Purification by flash chromatography (10% →50% EtOAc in pentane, with a gradient of 5%) afforded the *title compound* as a white solid (1.0 g, 64%). **R_f** 0.65 (50% EtOAc in pentane); **IR** ν_{max} (thin film)/cm^{-1}) 3337br, 1750s, 1653m, 1229m, 1062m; **^{1}H NMR** δ_H (500 MHz, $CDCl_3$) 1.39 – 1.49 (2H, m, H-2), 1.54 – 1.57 (4H, m, H-3), 1.61 – 1.68 (4H, m, H-1, H-2), 1.91 – 1.97 (2H, m, H-1), 4.52 (2H, br. s, NH_2), 4.81 (1H, tt, *J* =

8.5, 4.5 Hz, H-4); **^{13}C NMR** δ_C (126 MHz, $CDCl_3$) 22.9 (C-2), 28.4 (C-3), 34.2 (C-1), 76.2 (C-4), 156.7 (C-5); **HRMS (ESI$^+$)** *m/z* $[M+H]^+$ calculated for $C_8H_{15}NO_2H$, 158.1176; found, 158.1177.

(2*R, 5*R**)-7-Benzyl-6-oxo-7-azaspiro[4.5]decan-2-yl carbamate (4.35)**

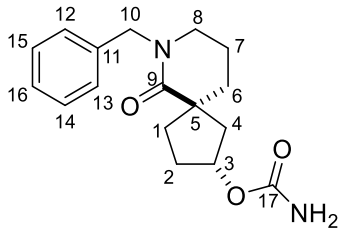

Lactam **3.13a** (38.9 mg, 0.150 mmol) was dissolved in DCM (0.3 mL) and was cooled to 0 ^oC. Trichloroacetyl isocyanate (20 µL, 0.18 mmol) was added dropwise to the mixture and warmed to RT. The reaction was stirred for 6 h and the solvent was removed *in vacuo*. The crude reaction mixture was dissolved in methanol (0.26 mL) and K_2CO_3 (2.1 mg, 0.015 mmol) was added and stirred for 18 h. The mixture was diluted with DCM (0.5 mL) and quenched by addition of sat. aq. NH_4Cl (1 mL). The aqueous layers were extracted with DCM. The combined organic layers were washed with water, brine, and dried with $MgSO_4$. Purification by flash chromatography (5% methanol in DCM) afforded the *title compound* as a white solid (15 mg, 32%). **R_f** 0.45 (5% methanol in DCM); **IR** ν_{max} (thin film)/cm^{-1} 3406br, 3204br, 1720s, 1615s, 1045m, 698m; **^{1}H NMR** δ_H (400 MHz, $CDCl_3$) 1.69 – 1.83 (4H, m, H-1, H-4, H-7), 1.83 – 1.92 (3H, m, H-2, H-6), 2.17 – 2.31 (2H, m, H-1, H-2), 2.63 (1H, dd, *J* = 14.5, 6.0 Hz, H-4), 3.21 (2H, t, *J* = 6.0 Hz, H-8), 4.51 (1H, d, *J* = 14.5 Hz, H-10), 4.55 – 4.63 (3H, m, H-10, NH_2), 5.25 – 5.29 (1H, m, H-3), 7.19 – 7.34 (5H, m, H-Ar); **^{13}C NMR** δ_C (101 MHz, $CDCl_3$) 20.7 (C-7), 33.2 (C-6), 36.2 (C-1), 37.9 (C-2), 44.9 (C-4), 47.8 (C-8), 48.7 (C-5), 50.7 (C-10), 78.8 (C-3), 127.4 (C-Ar), 128.0 (C-Ar), 128.7 (C-Ar), 137.7 (C-Ar), 156.7 (C-17), 176.0 (C-9); **HRMS (ESI$^+$)** *m/z* $[M+Na]^+$ calculated for $C_{17}H_{22}O_3N_2Na$, 325.1523; found, 325.1521.

Cyclopentyl 2,2,2-trichloroacetimidate (4.37) [207]

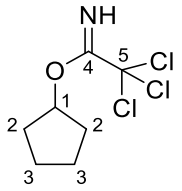

To a stirred mixture of cyclopentanol (0.45 mL, 5.0 mmol) in DCM (10 mL) was added trichloroacetonitrile (0.75 mL, 7.5 mmol) and DBU (70 µL, 0.50 mmol). The reaction mixture was stirred at RT for 18 h and diluted with water. The aqueous layers were extracted with DCM, and the combined organic layers were washed with water, brine, and dried with $MgSO_4$. The crude product was concentrated *in vacuo*. Purification by flash chromatography (20% EtOAc in pentane) afforded the title compound as a yellow oil (1.1 g, 97%). **R_f** 0.68 (10% EtOAc in pentane); **^{1}H NMR** δ_H (400 MHz, $CDCl_3$) 1.61 – 1.68 (2H, m, H-3), 1.73 – 1.84 (2H, m, H-3), 1.86 – 1.92 (4H, m, H-2), 5.30 (1H, quin, J = 4.0 Hz, H-1), 8.19 (1H, br. s, NH); **^{13}C NMR** δ_C (101 MHz, $CDCl_3$) 23.9 (C-3), 32.3 (C-1), 82.4 (C-1), 92.2 (C-5), 162.6 (C-4).

2,2,2-Trichloro-N-(2-hydroxycyclopentyl)acetamide (4.39)

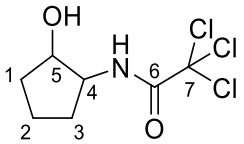

To a crude mixture of trichloro-oxazoline **4.38** (45.7 mg, 0.200 mmol) in pyridine and water (4:1, 2.9 mL) was added *p*-TsOH·H_2O (42.2 mg, 0.222 mmol). The mixture was heated to 80 °C for 5 h and cooled to RT. The solution was diluted with water (5 mL) and aq. sat. $NaHCO_3$ (5 mL) was added. The mixture was washed by ether (2 × 10 mL) and 5% aq.$CuSO_4$ solution (2 × 5 mL). The combined organic layers were washed with water, brine, and dried with $MgSO_4$. Purification by flash chromatography (20% → 40% EtOAc in pentane, with a gradient of 5%) afforded the *title compound* as a yellow oil (5.7 mg, 12%). **R_f** 0.69 (60% EtOAc in pentane); **IR** ν_{max} (thin film)/cm^{-1} 3393br, 1697s, 1511m,

822m; **^{1}H NMR** δ_H (500 MHz, $CDCl_3$) 1.62 – 1.69 (2H, m, H-2, H-3), 1.70 – 1.76 (1H, m, H-1), 1.87 – 1.95 (1H, m, H-2), 1.96 – 2.02 (1H, m, H-1), 2.12 – 2.19 (1H, m, H-3), 4.06 (1H, qd, *J* = 8.0, 5.0 Hz, H-4), 4.30 (1H, td, *J* = 5.0, 2.0 Hz, H-5), 7.27 – 7.33 (1H, br. s, NH); **^{13}C NMR** δ_C (126 MHz, $CDCl_3$) 20.7 (C-2), 29.2 (C-3), 33.7 (C-1), 55.7 (C-4), 72.6 (C-5), 92.9 (C-7), 161.9 (C-6); **HRMS (ESI$^+$)** *m/z* $[M+Na]^+$ calculated for $C_7H_{10}O_2NCl_3Na$, 267.9669, 269.9640, 271.9610, 273.9581; found, 267.9669, 269.9640, 271.9610, 275.1389.

(2*R, 5*R**)-7-Benzyl-6-oxo-7-azaspiro[4.5]decan-2-yl 2,2,2-trichloroacetimidate (4.45)**

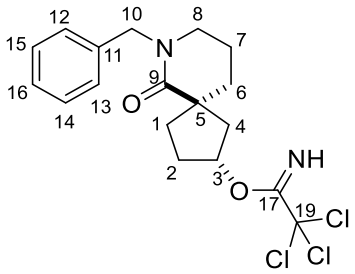

To a stirred mixture of lactam **3.13a** (51.9 mg, 0.200 mmol) in DCM (1 mL) was added trichloroacetonitrile (30 µL, 0.30 mmol) and DBU (3.0 µL, 0.020 mmol). The reaction mixture was stirred at RT for 18 h and diluted with water. The aqueous layers were extracted with DCM (2 × 1.5 mL), and the combined organic layers were washed with water, brine, and dried with $MgSO_4$. The crude product was concentrated *in vacuo*. Purification by flash chromatography (20% → 50% EtOAc in pentane, with a gradient of 5%) afforded the *title compound* as a yellow oil (22 mg, 27%). **R_f** 0.67 (50% EtOAc in pentane); **IR** ν_{max} (thin film)/cm^{-1} 2937s, 1730m, 1659m, 1630s, 1081m, 797m; **^{1}H NMR** δ_H (400 MHz, $CDCl_3$) 1.75 – 1.84 (3H, m, H-1, H-6), 1.84 – 1.89 (1H, m, H-4), 1.91 – 1.97 (2H, m, H-7), 2.03 – 2.11 (1H, m, H-2), 2.22 – 2.28 (1H, m, H-1), 2.31 – 2.37 (1H, m, H-2), 2.71 (1H, dd, *J* = 14.5, 6.0 Hz, H-4), 3.23 (2H, t, *J* = 6.0 Hz, H-8), 4.52 (1H, d, *J* = 14.5, H-10), 4.61 (1H, d, *J* = 14.5 Hz, H-10), 5.48 – 5.51 (1H, m, H-3), 7.21 – 7.36 (5H, m, H-Ar), 8.24 (1H, br. s, NH); **^{13}C NMR** δ_C (101 MHz, $CDCl_3$) 20.7 (C-6), 32.7

(C-2), 35.9 (C-7), 38.1 (C-1), 44.3 (C-4), 47.9 (C-8), 48.8 (C-5), 50.7 (C-10), 83.3 (C-3), 92.1 (C-19), 127.4 (C-Ar), 128.0 (C-Ar), 128.8 (C-Ar), 137.7 (C-Ar), 162.2 (C-17), 176.0 (C-9); **HRMS (ESI$^+$)** *m/z* $[M+Na]^+$ calculated for $C_{18}H_{21}O_2N_2Cl_3Na$, 425.0561, 427.0532, 429.0503, 430.0535; found, 425.0561, 427.0532, 429.0503,430.0537

(2*R, 5*R**)-7-Benzyl-6-oxo-7-azaspiro[4.5]decan-2-yl carbonazidate (4.48)**

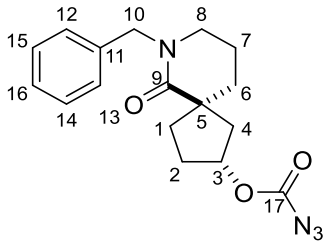

Lactam **3.13a** (25.9 mg, 0.100 mmol) was dissovled in THF (0.3 mL), followed by the addition of 1,1′-Carbonyldiimidazole (32.4 mg, 0.200 mmol). The mixture was stirred at RT for 5 h, and trimethylsilyl azide (0.13 mL, 1.0 mmol), EtOAc (0.3 mL), and water (0.3 mL) were added. After being stirred for 10 h, the mixture was diluted with water (2 mL), and the aqueous layers were extracted with EtOAc (3 × 5 mL). The combined organic layers were washed with water (5 mL), brine (5 mL), and dried with $MgSO_4$. Purification by flash chromatography (30% → 35% EtOAc in pentane, with a gradient of 5%) afforded the *title compound* as a yellow oil (10.8 mg, 33%). **R_f** 0.65 (60% EtOAc in pentane); **^{1}H NMR** δ_H (400 MHz, $CDCl_3$) 1.71 – 1.82 (4H, m, H-1, H-4, H-7), 1.84 – 1.89 (2H, m, H-6), 1.91 – 1.99 (1H, m, H-2), 2.16 – 2.25 (1H, m, H-1), 2.26 – 2.37 (1H, m, H-2), 2.70 (1H, dd, *J* = 14.5, 6.0 Hz, H-4), 3.22 (2H, t, *J* = 6.0 Hz, H-8), 4.48 (1H, d, *J* = 14.5 Hz, H-10), 4.62 (1H, d, *J* = 14.5 Hz, H-10), 5.40 (1H, tt, *J* = 6.0, 3.0 Hz, H-3), 7.19 – 7.34 (5H, m, H-Ar); **^{13}C NMR** δ_C (101 MHz, $CDCl_3$) 20.6 (C-7), 32.9 (C-2), 36.0 (C-6), 37.7 (C-1), 44.5 (C-4), 47.8 (C-8), 48.7 (C-5), 50.1 (C-10), 82.9 (C-3), 127.5 (C-Ar), 128.0 (C-Ar), 128.7 (C-Ar), 137.6 (C-Ar), 157.2 (C-17), 175.6 (C-9); **HRMS (ESI$^+$)** *m/z* $[M+H]^+$ calculated for $C_{17}H_{21}O_3N_4$, 329.1608; found, 329.1605.

(3a*R, 5*R**, 6a*S**)-1'-Benzyltetrahydrospiro[cyclopenta[*d*]oxazole-5,3'-piperidine]-2,2'(3H)-dione a (4.49) & (3a*S**, 4*R**, 6a*R**)-1'-Benzyltetrahydrospiro[cyclopenta[*d*]oxazole-4,3'-piperidine]-2,2'(3H)-dione b (4.50)**

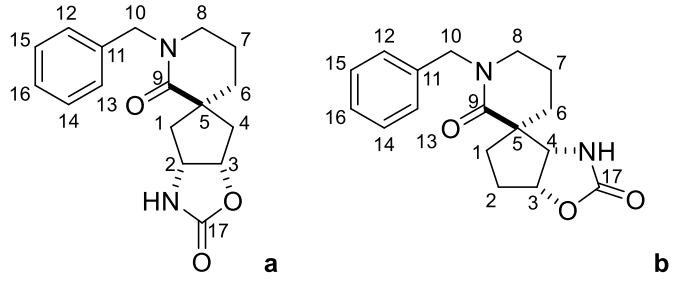

A solution of azidoformate **4.48** (15.3 mg, 0.047 mmol) in TCE (0.7 mL) was heated to reflux for 4 h. The reaction mixture was cooled down and the solvent was evaporated *in vacuo* and re-dissolved in EtOAc (1 mL). The solution was washed with water (2 × 1 mL), brine (1 mL), and dried with $MgSO_4$. Purification by flash chromatography (30% → 80% EtOAc in pentane, with a gradient of 5%) afforded the *title compounds* in a 2:1 ratio **a**:**b** of inseparable regioisomers, as a colourless oil.

Compounds **4.49** and **4.50** were isolated as an inseperable mixtures of isomers in a 2:1 ratio **a:b** (2.0 mg, 14%). $\mathbf{R_f}$ 0.35 (50% EtOAc in pentane); **IR** ν_{max} (thin film)/cm^{-1} 3687br, 1734s, 1700s, 1636m, 739m, 669m; **^{1}H NMR** δ_H (600 MHz, methanol-d_4) 1.77 (0.67H, dd, J = 14.0, 4.5 Hz, H-1$_a$), 1.80 – 1.85 (0.67H, m, H-1$_b$, H-6$_b$), 1.87 – 1.91 (1.34H, m, H-7$_a$), 1.91 – 1.96 (1.67H, m, H-4$_a$, H-6$_b$, H-7$_b$), 1.97 – 2.02 (1.67H, m, H-6$_a$, H-2$_b$), 2.15 – 2.21 (0.33H, m, H-1$_b$), 2.33 – 2.40 (0.33H, m, H-2$_b$), 2.54 (0.67H, dd, J = 14.0, 7.5 Hz, H-1$_a$), 2.63 – 2.69 (0.67H, m, H-4$_a$), 3.31 – 3.34 (2H, m, H-8$_a$, H-8$_b$), 4.36 (0.33H, d, J = 7.5 Hz, H-4$_b$), 4.44 – 4.50 (1H, m, H-2$_a$, H-10$_b$), 4.56 (0.67H, d, J = 15.0 Hz, H-10$_a$), 4.60 (0.67H, d, J = 15.0 Hz, H-10$_a$), 4.68 (0.33H, d, J = 15.0 Hz, H-10$_b$), 5.25 – 5.31 (1H, m, H-3$_a$, H-3$_b$), 7.24 – 7.39 (5H, m, H-Ar$_a$, H-Ar$_b$); **^{13}C NMR** δ_C (151 MHz, $CDCl_3$) 21.2 (C-7$_b$), 21.5 (C-7$_a$), 30.5 (C-6$_b$), 33.0 (C-2$_b$), 35.5 (C-6$_a$), 36.2 (C-1$_b$), 45.7 (C-4$_a$), 46.8 (C-1$_a$), 48.7 (C-8$_b$), 48.9 (C-8$_a$), 51.0 (C-10$_b$), 51.4 (C-5$_a$), 51.6 (C-10$_a$), 54.7 (C-5$_b$), 58.5 (C-2$_a$), 64.6 (C-4$_b$), 84.4 (C-3$_a$), 85.7 (C-3$_b$), 128.5 (C-Ar), 128.7 (C-Ar), 129.7 (C-Ar),

138.35 (C-11_a), 138.40 (C-11_b), 161.5 (C-17_a), 162.2 (C-17_b), 175.4 (C-9_b), 176.4 (C-9_a); **HRMS (ESI$^+$)** *m/z* $[M+H]^+$ calculated for $C_{17}H_{21}O_3N_2$, 301.1547; found, 301.1546.

tert-Butyl 2-oxopiperidine-1-carboxylate (4.51)[331]

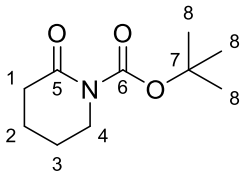

Dissolve valerolactam (0.09 mL, 1.00 mmol) in THF (12 mL) and cooled to −78 °C. *n*BuLi (0.66 mL, 1.6 M in hexanes, 1.00 mmol) was added dropwise and the resulting solution was stirred for 0.5 h. A solution of di-*tert*-butyl-dicarbonate (0.326 g, 1.50 mmol) in THF (3 mL) was added dropwise and the reaction was warmed to RT and stirred for 16 h. Aq. sat. NH_4Cl (2 mL) was added and the mixture was extracted with ether. The combined organic layers were washed with water, brine, and dried with $MgSO_4$. The crude product was concentrated *in vacuo*. Purification by flash chromatography (30% → 40% EtOAc in pentane, with a gradient of 10%) afforded the title compound as a colourless oil (0.19 g, quant.). **R_f** 0.38 (30% EtOAc in pentane); **^{1}H NMR** δ_H (400 MHz, $CDCl_3$) 1.52 (9H, s, H-8), 1.74 – 1.88 (4H, m, H-2, H-3), 2.46 – 2.54 (2H, m, H-1), 3.61 – 3.69 (2H, m, H-4); **^{13}C NMR** δ_C (101 MHz, $CDCl_3$) 20.5 (C-2), 22.8 (C-3), 28.0 (C-7), 34.9 (C-1), 46.3 (C-4), 82.8 (C-7), 152.8 (C-6), 171.3 (C-5).

4-Benzyl-4-azaspiro[2.5]octane (4.52 [332]

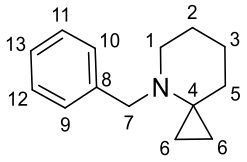

Benzylated-lactam **2.43** (1.89 g, 10.0 mmol) was dissolved in THF (30 mL) and cooled to −78 °C. Titanium isoproproxide (3.8 mL, 12.9 mmol) was added, followed by the dropwise addition of ethyl magnesium bromide (9.7 mL, 3.0 M solution in ether, 29.2

mmol). The mixture was then warmed to RT for 18 h and sat. aq. NH_4Cl (100 mL) was added. The resulting suspension was extracted with ether and the combined organic layers were washed with water, brine, and dried with $MgSO_4$. The solvent was removed *in vacuo*. Purification by flash chromatography (20% EtOAc in pentane) afforded the title compound as a colourless oil (1.4 g, 71%). **R_f** 0.71 (10% EtOAc in pentane); **^{1}H NMR** δ_H (400 MHz, $CDCl_3$) 0.34 – 0.38 (2H, m, H-6), 0.58 – 0.63 (2H, m, H-6), 1.38 – 1.53 (4H, m, H-2, H-3), 1.71 (2H, quin, *J* = 6.0 Hz, H-4), 2.69 – 2.74 (2H, m, H-1), 3.84 (2H, s, H-7), 7.17 – 7.23 (1H, m, H-Ar), 7.25 – 7.30 (4H, m, H-Ar); **^{13}C NMR** δ_C (101 MHz, $CDCl_3$) 14.7 (C-6), 18.4 (C-3), 24.6 (C-4), 27.9 (C-2), 42.9 (C-5), 47.8 (C-1), 54.1 (C-7), 126.6 (C-Ar), 128.1 (C-Ar), 128.7 (C-Ar), 140.7 (C-8).

tert-Butyl 4-azaspiro[2.5]octane-4-carboxylate (4.53)[333]

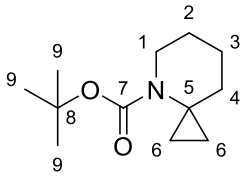

Benzylated-spiroamine **4.52** (0.550 g, 2.73 mmol) was dissolved in ethanol (12 mL) and 20% $Pd(OH)_2/C$ (82.8 mg) and di-*tert*-butyl-dicarbonate (298 mg, 1.37 mmol) were added. The mixture was stirred under hydrogen for 18 h at RT. The reaction was then filtered through a celite pad and concentrated *in vacuo*. Purification by flash chromatography (5% EtOAc in pentane) afforded the title compound as a colourless oil (0.254 g, 44%). **R_f** 0.82 (100% pentane); **^{1}H NMR** δ_H (400 MHz, $CDCl_3$) 0.55 – 0.61 (2H, m, H-6), 0.81 – 0.86 (2H, m, H-6), 1.38 – 1.43 (2H, m, H-4), 1.46 (9H, s, H-9), 1.51 (2H, quin, *J* = 6.0 Hz, H-2), 1.71 (2H, quin, *J* = 6.0 Hz, H-3), 3.41 (2H, t, *J* = 5.5 Hz, H-1); **^{13}C NMR** δ_C (100 MHz, $CDCl_3$) 14.5 (C-6), 24.3 (C-3), 25.5 (C-2), 28.6 (C-9), 32.9 (C-4), 38.8 (C-5), 47.0 (C-8), 79.3 (C-8),156.2 (C-7).

Isopropyl 5-((tert-butoxycarbonyl)amino)pentanoate (4.54)

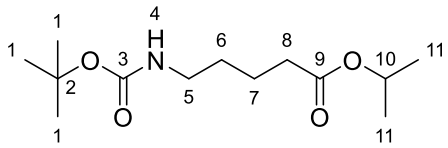

Boc-protected lactam **4.51** (23.8 mg, 0.119 mmol) was dissolved in THF (1 mL) and cooled to −78 °C. Titanium isoproproxide (50 µL, 0.15 mmol) was added, followed by the dropwise addition of ethyl magnesium bromide (0.12 mL, 3.0 M solution in ether, 0.35 mmol). The mixture was then warmed to RT for 18 h and aq. sat. NH_4Cl (1.2 mL) was added. The resulting suspension was extracted with ether and the combined organic layers were washed with water, brine, and dried with $MgSO_4$. The solvent was removed *in vacuo*. Purification by flash chromatography (5% → 10% EtOAc in pentane) afforded the *title compound* as a colourless oil (9.1 mg, 29%). **R_f** 0.59 (10% EtOAc in pentane); **IR** ν_{max} (thin film)/cm^{-1} 3367br, 1715s, 1521m, 1172s, 1109m; **^{1}H NMR** δ_H (400 MHz, $CDCl_3$) 1.22 (6H, d, *J* = 6.5 Hz, H-11), 1.43 (9H, s, H-1), 1.48 – 1.56 (2H, m, H-7), 1.59 – 1.69 (2H, m, H-6), 2.28 (2H, t, *J* = 7.5 Hz, H-5), 3.12 (2H, q, *J* = 6.5 Hz, H-8), 4.56 (1H, br, NH), 4.99 (1H, hept, *J* = 6.0 Hz, H-10); **^{13}C NMR** δ_C (101 MHz, $CDCl_3$) 22.0 (C-11), 22.3 (C-6), 28.6 (C-1), 29.6 (C-7), 34.3 (C-5), 40.3 (C-8), 67.7 (C-10), 79.3 (C-2), 156.1 (C-3), 173.1 (C-9); **HRMS (ESI$^+$)** *m/z* $[M+Na]^+$ calculated for $C_{13}H_{25}O_4NNa$, 282.1676; found, 282.1675.

7-Benzyl-7-azaspiro[4.5]decane-2,6-dione (4.57)

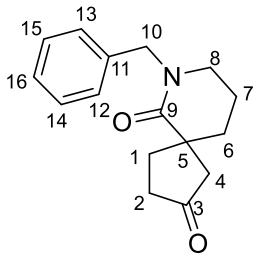

Dissolve alcohol **3.13a** (130 mg, 0.500 mmol) in DCM (5 mL), followed by the addition of $NaHCO_3$ (88.2 mg, 1.05 mmol). The mixture was cooled to 0°C and DMP (318 mg, 0.750 mmol) was added. The reaction was stirred for 12 h at RT and was washed with 1

M aq. NaOH solution twice. The aqueous layers were washed with DCM (3 × 10 mL) and the combined organic layers were washed with brine (10 mL) and dried with $MgSO_4$. Purification by flash chromatography (40% EtOAc in pentane) afforded the *titled compound* as a pale yellow oil (62 mg, 48%). **R_f** 0.40 (40% EtOAc in pentane); **IR** ν_{max} (thin film)/cm^{-1} 1742s, 1630s, 1234m, 736w; **^{1}H NMR** δ_H (400 MHz, $CDCl_3$) 1.72 – 1.82 (1H, m, H-7), 1.84 – 1.96 (4H, m, H-1, H-6, H-7), 2.09 – 2.12 (1H, m, H-4), 2.25 – 2.34 (1H, m, H-2), 2.49 – 2.69 (2H, m, H-1, H-2), 2.82 – 2.91 (1H, m, H-4), 3.22 – 3.32 (2H, m, H-8), 4.50 (1H, d, *J* = 14.5 Hz, H-10), 4.64 (1H, d, *J* = 14.5 Hz, H-10), 7.20 – 7.35 (5H, m, H-Ar); **^{13}C NMR** δ_C (101 MHz, $CDCl_3$) 19.9 (C-7), 33.9 (C-6), 34.2 (C-1), 36.4 (C-2), 46.3 (C-5), 47.6 (C-8), 50.3 (C-10), 50.5 (C-4), 127.5 (C-Ar), 128.0 (C-Ar), 128.7 (C-Ar), 137.2 (C-Ar), 174.1 (C-9), 217.2 (C-3); **HRMS (ESI$^+$)** *m/z* $[M+H]^+$ calculated for $C_{16}H_{20}O_2N$, 258.1489; found, 258.1491.

8-Benzyl-2-oxa-8-azaspiro[5.5]undecane-3,7-dione (4.58) & 2-Benzyl-9-oxa-2-azaspiro[5.5]undecane-1,8-dione (4.59)

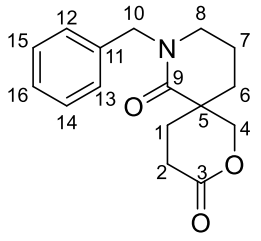

4.58

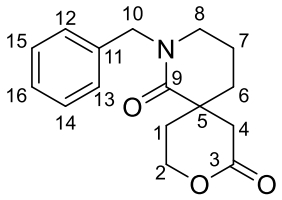

4.59

Ketone **4.57** (25.8 mg, 0.100 mmol) was dissolved in DCM (0.63 mL) and cooled to 0 °C. Then mcPBA (44.9 mg, 0.260 mmol) and TFA (7.7 µL, 0.10 mmol) were added whilst stirring. The reaction was warmed to RT and stirred for 7 h. An additional volume of DCM (1.9 mL) was added and the reaction was quenched with aq. sat. $NaHCO_3$ (1.9 mL). Organic layers were extracted with DCM (3 × 3.8 mL), washed with brine (3.8 mL), and dried with $MgSO_4$. The crude mixture was concentrated *in vacuo*. Purification by flash chromatography (30% → 35% EtOAc in pentane) afforded the *title compounds* in a 2:3 ratio **4.58**:**4.59**.

4.58: The *titled compound* was furnished as a colourless oil (5.4 mg, 20%). **R_f** 0.51 (35% EtOAc in pentane);); **IR** ν_{max} (thin film)/cm^{-1} 1738s, 1631s, 1263w, 702m; **^{1}H NMR** δ_H (500 MHz, $CDCl_3$) 1.67 – 1.72 (1H, m, H-1), 1.78 – 1.90 (4H, m, H-6, H-7), 2.50 – 2.62 (2H, m, H-1, H-2), 2.80 – 2.91 (1H, m, H-2), 3.21 – 3.30 (2H, m, H-8), 4.18 (1H, d, *J* = 11.5 Hz, H-4), 4.51 – 4.54 (1H, m, H-10), 4.61 (1H, d, *J* = 14.5 Hz, H-10), 4.67 – 4.70 (1H, m, H-4), 7.23 – 7.35 (5H, m, H-Ar); **^{13}C NMR** δ_C (126 MHz, $CDCl_3$) 18.8 (C-7), 27.8 (C-2), 30.6 (C-1), 30.9 (C-6), 39.8 (C-8), 41.2 (C-5), 50.7 (C-10), 73.6 (C-4),127.7 (C-Ar), 128.0 (C-Ar), 128.7 (C-Ar), 136.8 (C-11), 171.7 (C-3), 172.2 (C-9); **HRMS (ESI$^+$)** *m/z* $[M+H]^+$ calculated for $C_{22}H_{27}ON_2$, 335.2118; found, 335.2117.

4.59: The *titled compound* was furnished as a colourless oil (3.9 mg, 14%); **R_f** 0.46 (35% EtOAc in pentane); **IR** ν_{max} (thin film)/cm^{-1} 1728s, 1631s, 1241w, 754m, 702m; **^{1}H NMR** δ_H (400 MHz, $CDCl_3$) 1.71 – 1.80 (1H, m, H-1), 1.80 – 1.89 (4H, m, H-6, H-7), 2.31 – 2.35 (1H, m, H-1), 2.35 – 2.40 (1H, m, H-4), 3.15 (1H, d, *J* = 16.0 Hz, H-4), 3.26 (2H, t, *J* = 6.0 Hz, H-8), 4.36 (1H, dt, *J* = 11.5, 5.0 Hz, H-2), 4.46 (1H, d, *J* = 14.5 Hz, H-10), 4.51 – 4.58 (1H, m, H-2), 4.68 (1H, d, *J* = 14.5 Hz, H-10), 7.19 – 7.35 (5H, m, H-Ar); **^{13}C NMR** δ_C (126 MHz, $CDCl_3$) 18.8 (C-7), 34.0 (C-1), 34.8 (C-6), 39.8 (C-4), 40.7 (C-5), 47.5 (C-8), 50.7 (C-10), 66.4 (C-2), 127.7 (C-Ar), 128.0 (C-Ar), 128.8 (C-Ar), 136.9 (C-11), 171.3 (C-3), 172.9 (C-9); **HRMS (ESI$^+$)** *m/z* $[M+H]^+$ calculated for $C_{16}H_{20}O_3N$, 274.1438; found, 274.1439.

7-Benzyl-7-azaspiro[4.5]dec-3-ene-2,6-dione (4.60)

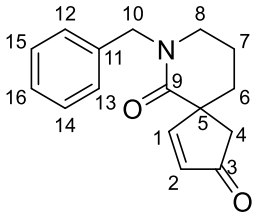

Acetic acid (0.42 mL) was added to ketone **4.57** (19.1 mg, 0.074 mmol), followed by NH_2SO_3H (23.1 mg, 0.204 mmol). The mixture was heated to reflux for 17 h and diluted

with DCM (2.5 mL). Aq. sat. $NaHCO_3$ was added (0.82 mL) and the mixture was extracted with DCM. The combined organic layers were washed with water, brine, and dried with $MgSO_4$. Purification by flash chromatogrphy (5% → 50% EtOAc in pentane, with a 5% gradient) afforded the *title compound* as a yellow oil (13 mg, 68%). **R_f** 0.39 (80% EtOAc in pentane); **IR** ν_{max} (thin film)/cm^{-1} 1716s, 1677w, 1634s, 1262m, 737w, 701w; **^{1}H NMR** δ_H (500 MHz, $CDCl_3$) 1.82 – 1.91 (2H, m, H-6, H-7), 1.93 – 2.08 (2H, m, H-6, H-7), 2.23 (1H, d, *J* = 18.0 Hz, H-4), 2.90 (1H, d, *J* = 18.0 Hz, H-4), 3.31 – 3.35 (2H, m, H-8), 4.54 (1H, d, *J* = 14.5 Hz, H-10), 4.64 (1H, d, *J* = 14.5 Hz, H-10), 6.27 (1H, d, *J* = 5.5 Hz, H-2), 7.23 – 7.36 (5H, m, H-Ar), 7.57 (1H, d, *J* = 5.5 Hz, H-1); **^{13}C NMR** δ_C (126 MHz, $CDCl_3$) 20.5 (C-7), 33.8 (C-6), 47.5 (C-4), 47.6 (C-8), 50.9 (C-10), 52.0 (C-5), 127.7 (C-Ar), 128.2 (C-Ar), 128.8 (C-Ar), 133.9 (C-2), 136.9 (C-Ar), 165.9 (C-1), 170.8 (C-9), 208.2 (C-3); **HRMS (ESI$^+$)** *m/z* $[M+H]^+$ calculated for $C_{16}H_{18}O_2N$, 256.1332; found, 256.1333.

2-Benzyl-2,8-diazaspiro[5.5]undecane-1,9-dione a (4.69) & 2-Benzyl-2,9-diazaspiro[5.5]undecane-1,8-dione b (4.70)

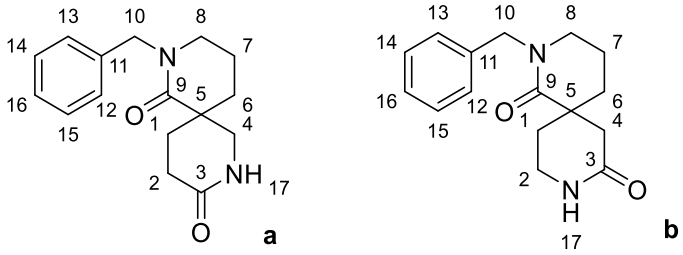

Ketone **4.57** (25.4 mg, 0.099 mmol), $NH_2OH{\cdot}HCl$ (24.0 mg, 0.346 mmol), and NaOAc (28.3 mg, 0.346 mmol) was dissovled in methanol (2.4 mL) and heated to reflux for 16 h. The reaction mixture was concentrated and re-dissolved in DCM. The organic layers were washed with water (5 mL), brine (5 mL), and dried with $MgSO_4$. The solvent was removed *in vacuo* and dissovled in ACN (0.5 mL). To the solution was added $HgCl_2$ (3.20 mg, 0.012 mmol) and the reaction was stirred at reflux for 16 h. The reaction was then cooled to RT and ACN was added to dissolve the solid formed. The solvent was removed *in vacuo*, and dissolved in DCM (4 × 2 mL). The combined organic layers were washed

with water (2 mL), brine (2 mL), and dried with $MgSO_4$. Purification by flash chromatography (0.5% → 2.5% methanol in DCM, with a gradient of 5%) afforded the *title compounds* in a 1:1 ratio **a:b** of inseparable regioisomers, as a colourless oil (3.7 mg, 14%). **R_f** 0.42 (5% methanol in DCM); **IR** ν_{max} (thin film)/cm^{-1} 3312br, 1683s, 1558m, 1243m, 736m; **^{1}H NMR** δ_H (500 MHz, $CDCl_3$) 1.73 – 1.84 (4H, m, H-1_a, H-6_a/H-6_b, H-7_a, H-7_b), 2.07 – 2.13 (0.5H, m, H-1_a), 2.25 – 2.34 (0.5H, m, H-1_b), 2.37 – 2.45 (1H, m, H-4_a, H-6_a/H-6_b), 2.49 – 2.60 (1.5H, m, H-2_a, H-2_b, H-4_b), 2.61 – 2.68 (0.5H, m, H-1_b), 2.79 – 2.89 (1H, m, H-2_b, H-4_a), 3.07 – 3.15 (1H, m, H-2_b, H-4_a), 3.21 – 3.29 (2H, m, H-8_a, H-8_b), 4.49 – 4.67 (2H, m, H-10_a, H-10_b), 7.19 – 7.36 (5H, m, H-Ar_a, H-Ar_b); **^{13}C NMR** δ_C (126 MHz, $CDCl_3$) 20.0/20.2 (C-7), 26.2 (C-4_b), 29.3 (C-2_a), 34.4 (C-6_a/C-6_b), 35.4 (C-6_a/C-6_b), 36.6 (C-1_b), 39.8 (C-2_b), 42.5 (C-4_a), 46.4 (C-5_a), 47.68 (C-8_a/C-8_b), 47.73 (C-8_a/C-8_b), 50.6 (C-10_a/C-10_b), 50.7 (C-10_a/C-10_b), 127.55 (C-Ar), 127.56 (C-Ar), 128.06 (C-Ar), 128.08 (C-Ar), 128.80 (C-Ar), 128.82 (C-Ar), 137.3 (C-11_a/C-11_b), 137.4 (C(11_a)/C(11_b)), 173.7 (C(3_a), C(3_b)), 174.1 (C(9_a), C(9_b)); **HRMS (ESI$^+$)** exact mass calculated for $[M+H]^+$ ($C_{16}H_{21}O_2N_2$) requires *m/z* 273.1598, found *m/z* 273.1597.

_N_-(8-Benzyl-7-oxo-2,8-diazaspiro[5.5]undec-2-en-3-yl)acetamide a (4.71) & _N_-(2-Benzyl-1-oxo-2,9-diazaspiro[5.5]undec-8-en-8-yl)acetamide b (4.72)

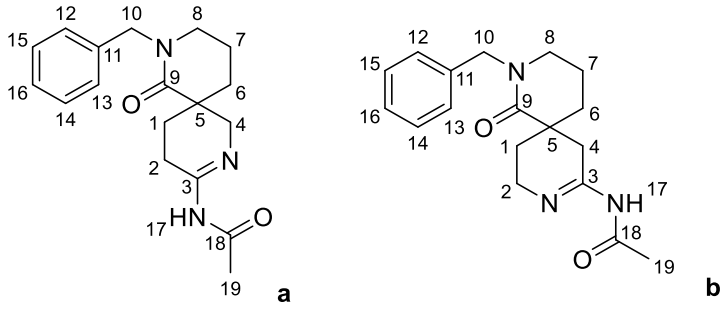

Ketone **4.57** (25.4 mg, 0.099 mmol), $NH_2OH{\cdot}HCl$ (24.0 mg, 0.346 mmol), and NaOAc (28.3 mg, 0.346 mmol) was dissovled in methanol (2.4 mL) and heated to reflux for 16 h. The reaction mixture was concentrated and re-dissolved in DCM. The organic layers were washed with water (5 mL), brine (5 mL), and dried with $MgSO_4$. The solvent was removed *in vacuo* and dissovled in ACN (0.5 mL). To the solution was added $HgCl_2$ (3.20

mg, 0.012 mmol) and the reaction was stirred at reflux for 16 h. The reaction was then cooled to RT and ACN was added to dissolve the solid formed. The solvent was removed *in vacuo*, and dissolved in DCM (4 × 2 mL). The combined organic layers were washed with water (2 mL), brine (2 mL), and dried with $MgSO_4$. Purification by flash chromatography (0.5% → 2.5% methanol in DCM, with a gradient of 5%) afforded the *title compounds* as a colourless oil.

Compounds **4.71** and **4.72** were isolated as an inseperable mixtures of isomers in a 3:1 ratio **a:b** (2.1 mg, 7%) as an unexpected side product (colourless oil) in the formation of lactams **4.69** and **4.70**. $\mathbf{R_f}$ 0.3 (5% methanol in DCM); **IR** ν_{max} (thin film)/cm^{-1} 3329br, 1717m, 1670m, 1634s, 1199m; **^{1}H NMR** δ_H (600 MHz, $CDCl_3$) 1.81 – 1.96 (5H, m, H-1_a, H-1_b, H-6_a, H-6_b, H-7_a, H-7_b), 2.10 – 2.15 (1.5H, m, H-4_a, H-19_b), 2.17 (2.25H, s, H-19_a), 2.29 – 2.36 (0.75H, m, H-2_a), 2.41 – 2.50 (0.25H, m, H-1_b), 2.51 – 2.60 (1H, m, H-1_a, H-4_b), 2.63 – 2.72 (1H, m, H-2_a, H-2_b), 2.89 (0.75H, d, J = 18.0 Hz, H-4_a), 3.18 – 3.25 (0.25H, m, H-4_b), 3.25 – 3.32 (2H, H-8_a, H-8_b), 4.53 (0.75H, d, J = 14.5 Hz, H-4_b), 4.63 (0.25H, d, J = 14.5 Hz, H-10_b), 4.63 (0.25H, d, J = 14.5 Hz, H-10_b), 4.67 (0.75H, d, J = 14.5 Hz, H-10_a), 7.22 – 7.38 (5H, m, H-Ar$_a$, H-Ar$_b$); **^{13}C NMR** δ_C (151 MHz, $CDCl_3$) 19.68/19.71* (C-16), 20.04 (C-7), 20.22/20.28* (C-6), 27.83* (C-2), 34.38 (C-1), 35.99* (C-1), 42.84* (C-4), 47.68*/47.75 (C-8), 48.15*/48.19 (C-5), 50.41 (C-4), 50.61/50.73* (C-10), 127.63 (C-Ar), 128.12 (C-Ar), 128.84 (C-Ar), 137.30*/137.32 (C-Ar), 168.79*/168.84 (C-3), 173.73/173.78 (C-18), 217.38 (C-9); **HRMS (ESI)** not found.

7-Benzyl-2-ethynyl-2-hydroxy-7-azaspiro[4.5]decan-6-one (4.78)

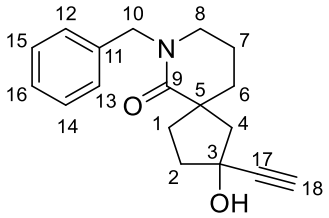

To a solution of ketone **4.57** (25.7 mg, 0.100 mmol) in THF (1 mL) was added ethylnylmagnesium bromide (0.24 mL, 0.5 M solution in THF) at 0 ^oC. The reaction was

allowed to warm to RT for 18 h and was quenched with aq. sat. NH_4Cl (0.5 mL) at 0°C. The aqueous layers were extracted with EtOAc and the combined organic layers were washed with water, brine, and dried with $MgSO_4$. The crude product was then concentrated *in vacuo.* Purification by flash chromatography (40% EtOAc in pentane) afforded the *title compound* as an inseparable diastereomic mixture, as a yellow oil (8.1 mg, 29%, *d.r.* = 2:1). **IR** ν_{max} (thin film)/cm^{-1} 3304s, 3283br, 2359w, 1603s, 1357m, 1230m, 702m; $\mathbf{R_f}$ 0.64 (40% EtOAc in pentane); **^{1}H NMR** δ_H (600 MHz, $CDCl_3$) (for major diastereomer) 1.78 – 1.85 (5H, m, H-1, H-6, H-7), 1.90 (1H, d, *J* = 14.0 Hz, H-4), 2.18 – 2.24 (1H, m, H-2), 2.25 – 2.34 (2H, m, H-1, H-2), 2.51 (1H, s, H-18), 2.53 (1H, d, *J* = 2.5 Hz, H-4), 3.23 – 3.29 (2H, m, H-8), 4.45 (1H, d, *J* = 14.5 Hz, H-10), 4.69 (1H, d, *J* = 14.5 Hz, H-10), 7.26 – 7.35 (5H, m, H-Ar); **^{13}C NMR** δ_C (151 MHz, $CDCl_3$) 20.6/20.9 (C-7), 36.2/36.7 (C-6), 37.6/38.7 (C-1), 42.8/43.1 (C-2), 47.8/47.9 (C-8), 48.9/49.0 (C-5), 50.7/51.0 (C-10), 53.1/53.9 (C-4), 70.5/71.7 (C-18), 73.7/75.2 (C-3), 86.5/86.6 (C-17), 127.4/127.8 (C-Ar), 128.0/128.1 (C-Ar), 128.7/128.9 (C-Ar), 136.9/137.7 (C-11), 176.1/177.8 (C-9); **HRMS (ESI$^+$)** *m/z* $[M+H]^+$ calculated for $C_{18}H_{22}O_2N$, 284.1645; found, 284.1643.

7-Benzyl-2-methylene-7-azaspiro[4.5]decan-6-one (4.83)

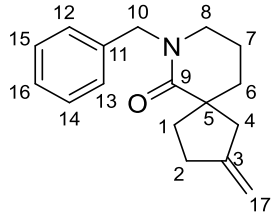

Dissolve ketone **4.57** (25.7 mg, 0.100 mmol) in THF (1 mL), followed by the addition of Dimethyltitanocene (5% in THF/ Toluene) (1.3 mL, 0.30 mmol) and heated to reflux for 18 h. The resulting mixture was diluted with petroleum ether and the orange-yellow precipitate were filtered. The filtrate was concentrated *in vacuo* and purification by flash chromatography (5% → 15% EtOAc in pentane, with a gradient of 5%, with 3% NEt_3) afforded the *title compound* (14 mg, 54%)

as a yellow oil. **R_f** 0.59 (20% EtOAc in pentane); **IR** ν_{max} (thin film)/cm^{-1} 3029s, 1632s, 1493m, 1353m, 1195m, 700m; **^{1}H NMR** δ_H (400 MHz, $CDCl_3$) 1.64 – 1.72 (3H, m, H-1, H-6), 1.72 – 1.81 (2H, m, H-7), 2.21 – 2.27 (1H, m, H-4), 2.29 – 2.41 (2H, m, H-1, H-2), 2.56 – 2.66 (1H, m, H-2), 2.93 – 3.01 (1H, m, H-4), 3.21 (2H, t, *J* = 6.0 Hz, H-8), 4.58 (2H, s, H-10), 4.85 – 4.91 (2H, m, H-17), 7.20 – 7.35 (5H, m, H-Ar); **^{13}C NMR** δ_C (101 MHz, $CDCl_3$) 20.2 (C-7), 31.0 (C-2), 32.8 (C-6), 37.5 (C-1), 45.6 (C-4), 47.8 (C-8), 49.1 (C-5), 50.7 (C-10), 106.2 (C-17), 127.4 (C-Ar), 128.0 (C-Ar), 128.7 (C-Ar), 137.8 (C-Ar), 151.4 (C-3), 175.1 (C-9); **HRMS (ESI$^+$)** *m/z* $[M+H]^+$ calculated for $C_{17}H_{22}ON$, 256.1696; found, 256.1696.

7.6 Single Crystal X-Ray Data

7.6.1 Crystal Data for Compound 3.10a

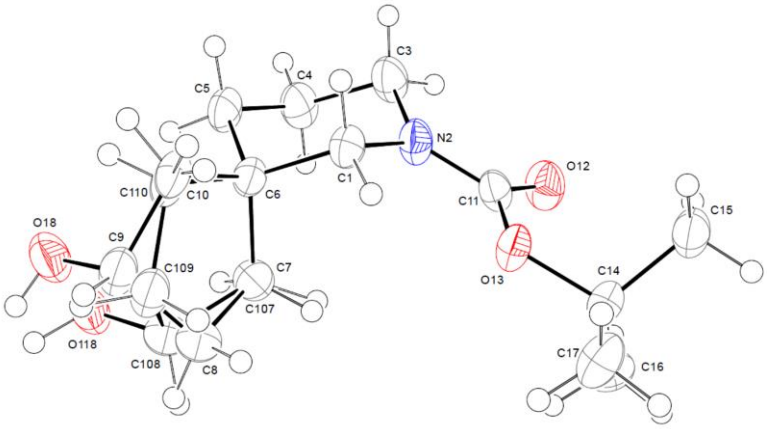

Empirical formula	C14 H25 N O3	
Formula weight	255.36	
Temperature	150 K	
Wavelength	1.54184 Å	
Crystal system	Monoclinic	
Space group	P 21/n	
Unit cell dimensions	a = 10.7816(3) Å	α= 90°.
	b = 10.5633(3) Å	β= 104.367(3)°.
	c = 13.0400(4) Å	γ = 90°.
Volume	1438.67(7) $Å^3$	
Z	4	
Density (calculated)	1.179 Mg/m^3	
Absorption coefficient	0.656 mm^{-1}	
F(000)	559.995	
Crystal size	0.20 x 0.10 x 0.07 mm^3	
Theta range for data collection	4.778 to 76.273°.	
Index ranges	-13<=h<=13, -10<=k<=13, -14<=l<=16	
Reflections collected	7940	
Independent reflections	2974 [R(int) = 0.026]	
Completeness to theta = 73.985°	99.8 %	
Absorption correction	Semi-empirical from equivalents	
Max. and min. transmission	0.96 and 0.77	
Refinement method	Full-matrix least-squares on F^2	
Data / restraints / parameters	2973 / 10 / 180	
Goodness-of-fit on F^2	1.0411	
Final R indices [I>2sigma(I)]	R1 = 0.0531, wR2 = 0.1278	
R indices (all data)	R1 = 0.0581, wR2 = 0.1329	
Extinction coefficient	18(4)	
Largest diff. peak and hole	0.30 and -0.31 $e.Å^{-3}$	

7.6.2 Cystal Data for Compound 4.57

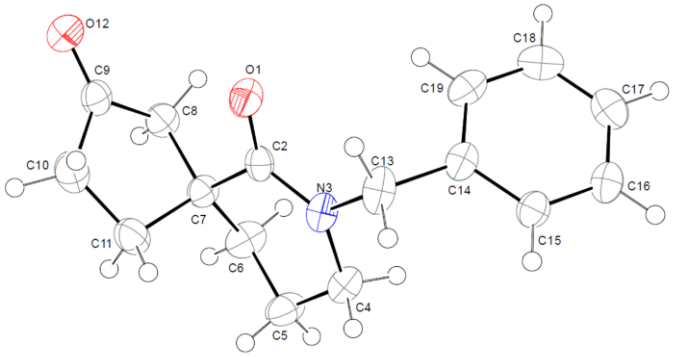

Empirical formula	C16 H19 N1 O2	
Formula weight	257.33	
Temperature	150 K	
Wavelength	1.54184 Å	
Crystal system	Orthorhombic	
Space group	P 21 21 21	
Unit cell dimensions	a = 7.9603(4) Å	α= 90°.
	b = 10.9712(5) Å	β= 90°.
	c = 15.3091(7) Å	γ = 90°.
Volume	1337.01(11) $Å^3$	
Z	4	
Density (calculated)	1.278 Mg/m^3	
Absorption coefficient	0.668 mm^{-1}	
F(000)	552	
Crystal size	0.22 x 0.20 x 0.19 mm^3	
Theta range for data collection	4.959 to 76.228°.	
Index ranges	-9<=h<=7, -13<=k<=13, -19<=l<=19	
Reflections collected	8268	
Independent reflections	2755 [R(int) = 0.028]	
Completeness to theta = 74.703°	99.8 %	
Absorption correction	Semi-empirical from equivalents	
Max. and min. transmission	0.88 and 0.75	
Refinement method	Full-matrix least-squares on F^2	
Data / restraints / parameters	2755 / 0 / 173	
Goodness-of-fit on F^2	1.0067	
Final R indices [I>2sigma(I)]	R1 = 0.0392, wR2 = 0.1035	
R indices (all data)	R1 = 0.0407, wR2 = 0.1051	
Absolute structure parameter	-0.10(13)	
Largest diff. peak and hole	0.20 and -0.14 $e.Å^{-3}$	

7.7 Mosher Ester NMR Analysis

7.7.1 Metabolite 3.10a from Mutant RT2

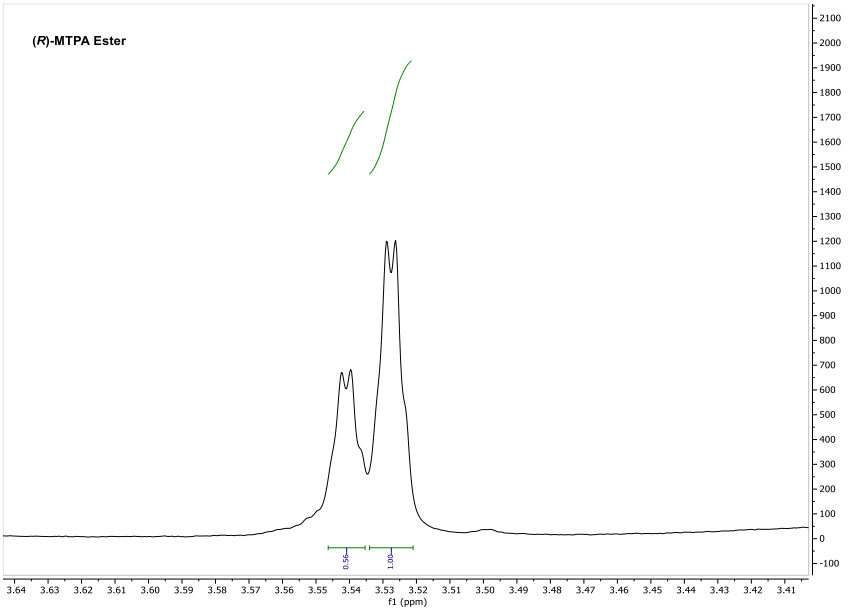

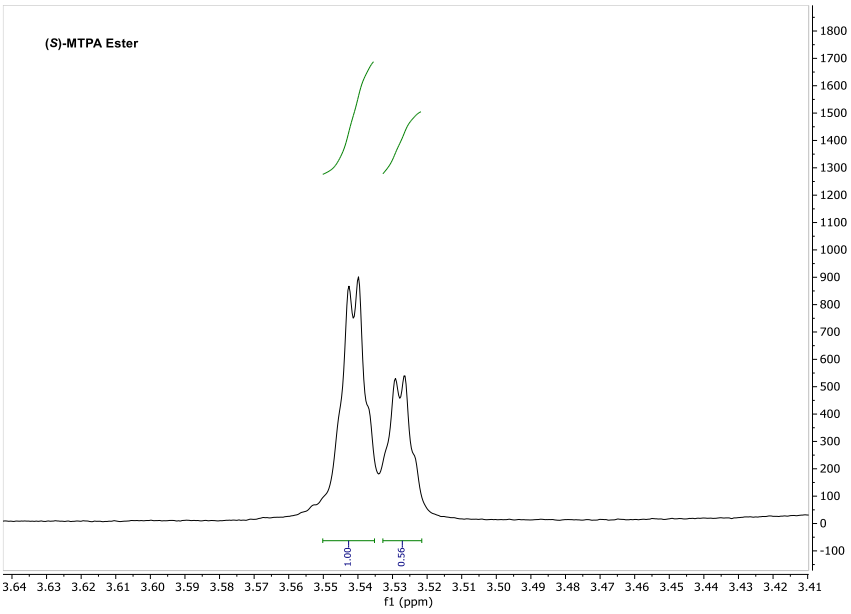

7.7.2 Metabolite 3.11a from Mutant R19/F87I

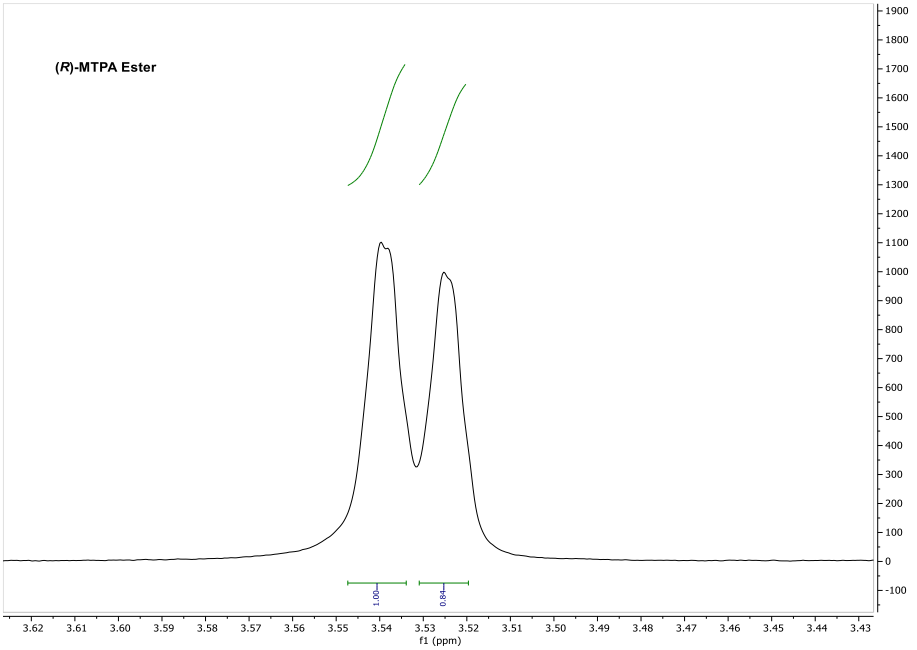

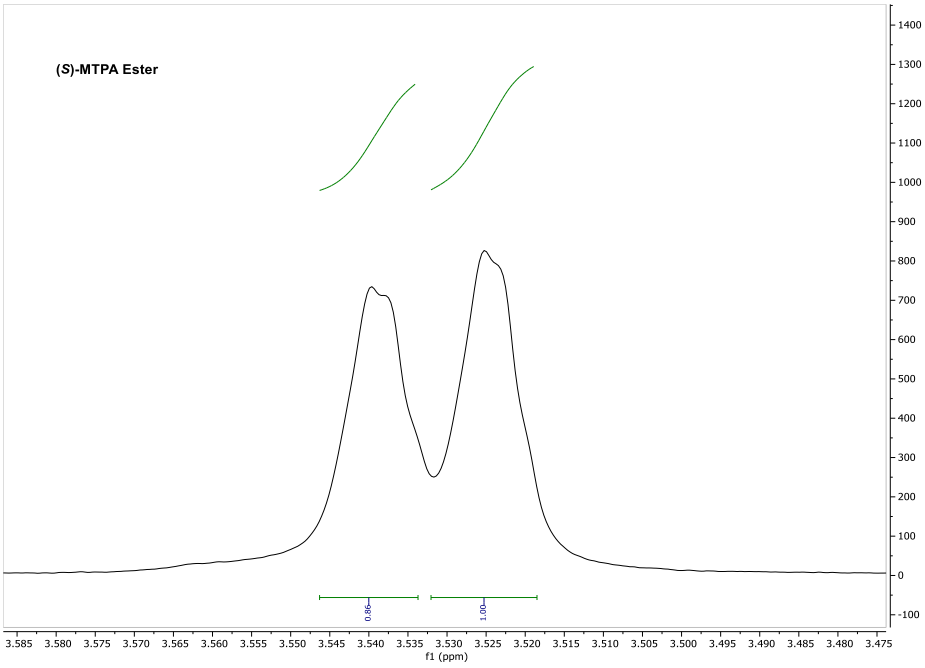

7.7.3 Metabolite 3.11b from Mutant GV/L188Q

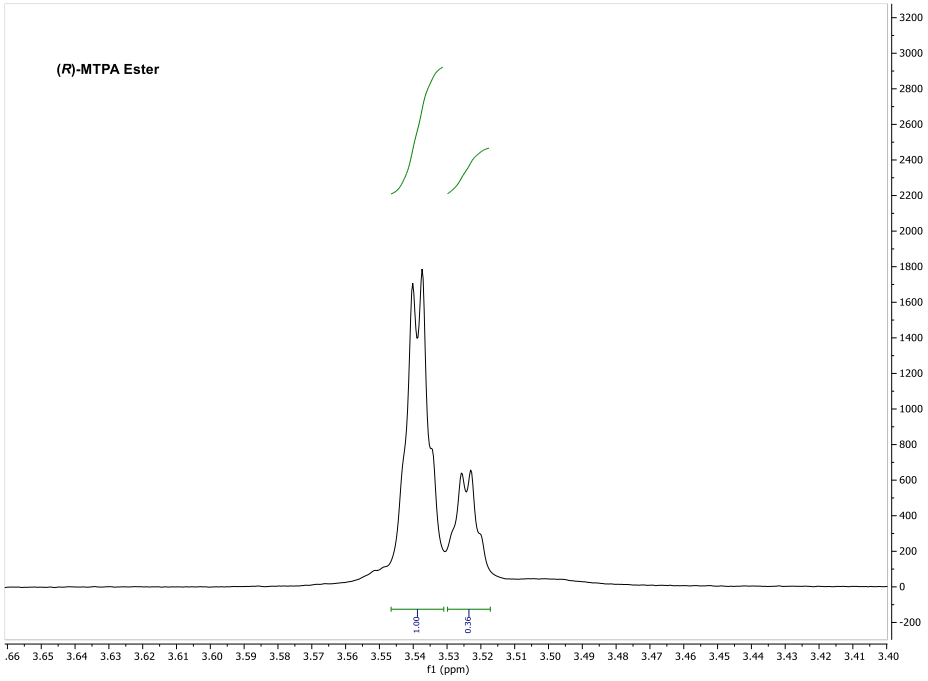

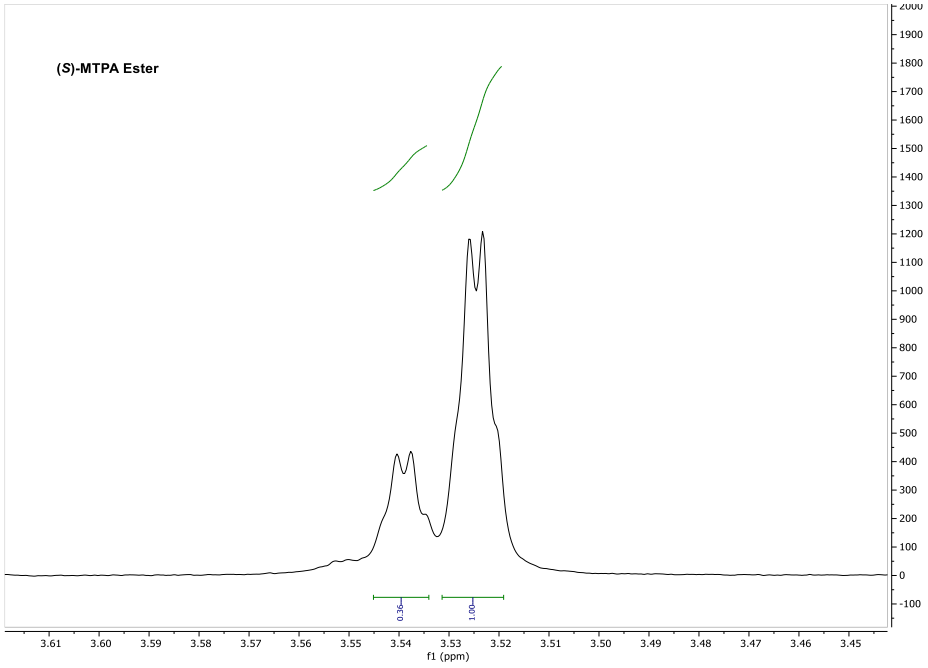

7.7.4 Metabolite 3.11c from Mutant R19/F87I

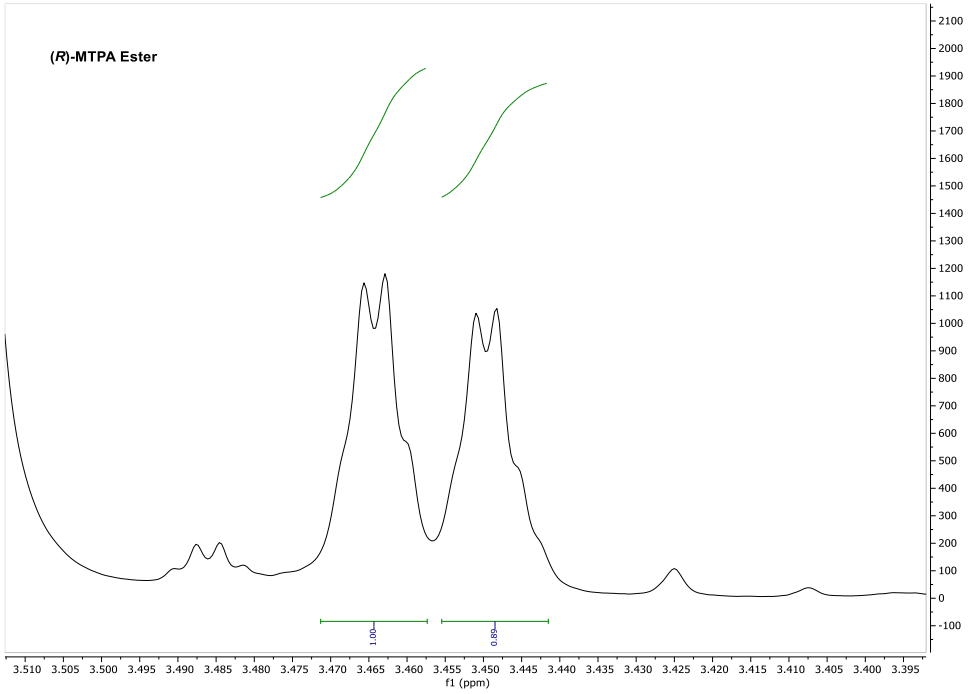

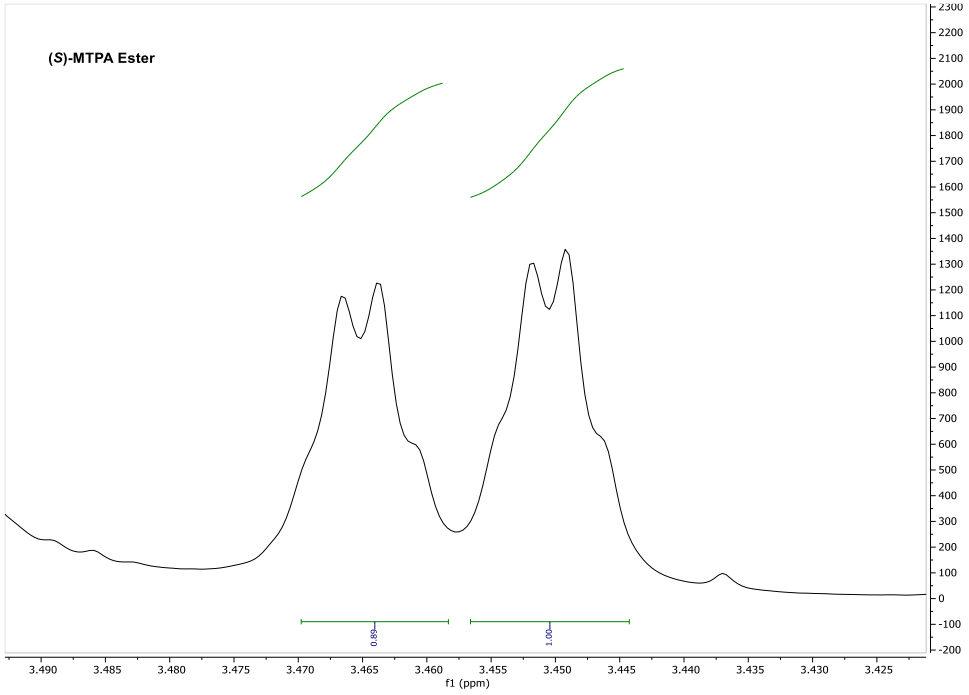

7.7.5 Metabolite 3.13a from Mutant R19/F87I

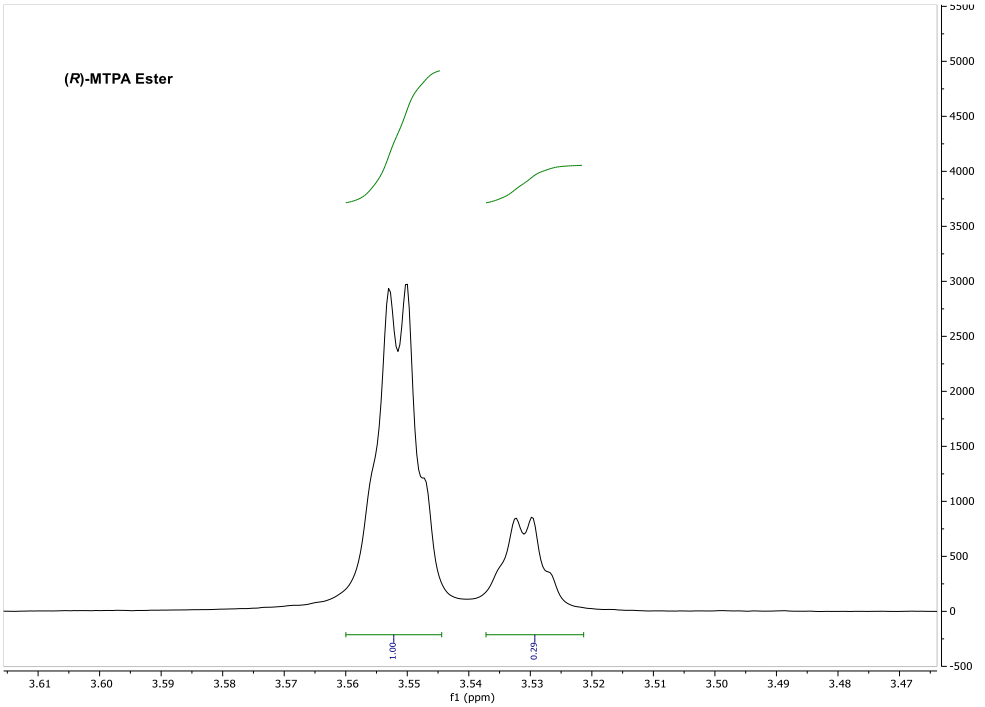

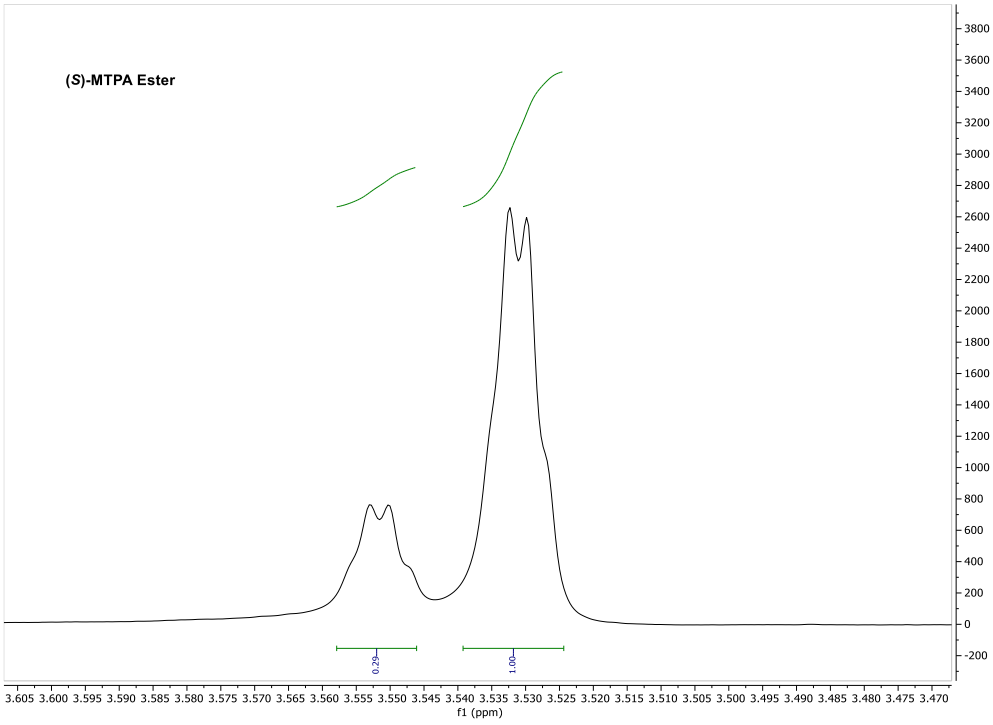

7.7.7 Metabolite 3.13b from Mutant R19/F87A/A184I

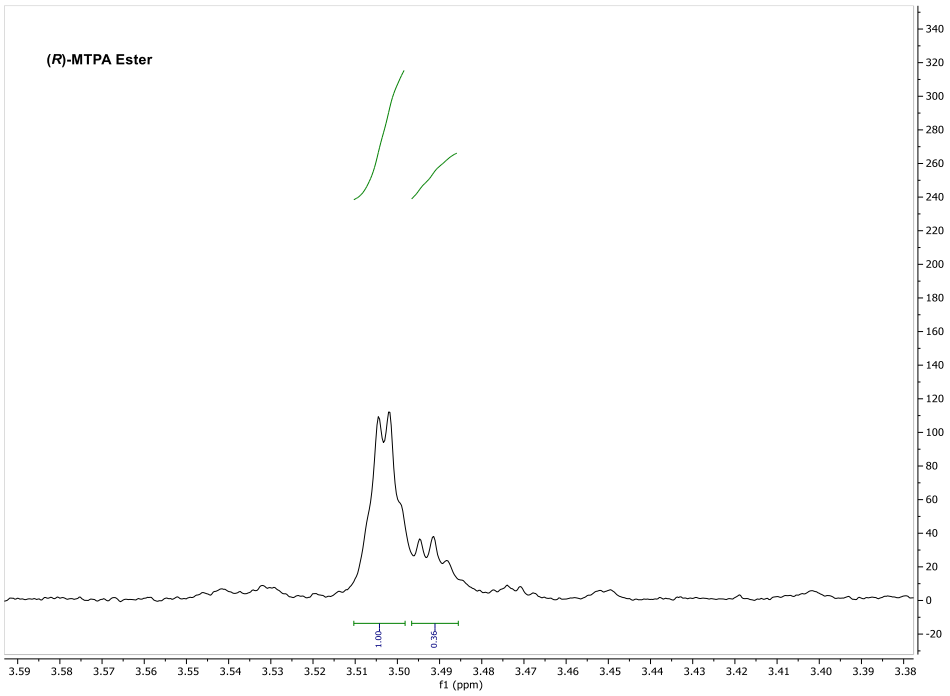

7.8 Chiral GC Data

7.8.1 Chiral GC Trace of 3.10a from Mutant R19/F87I

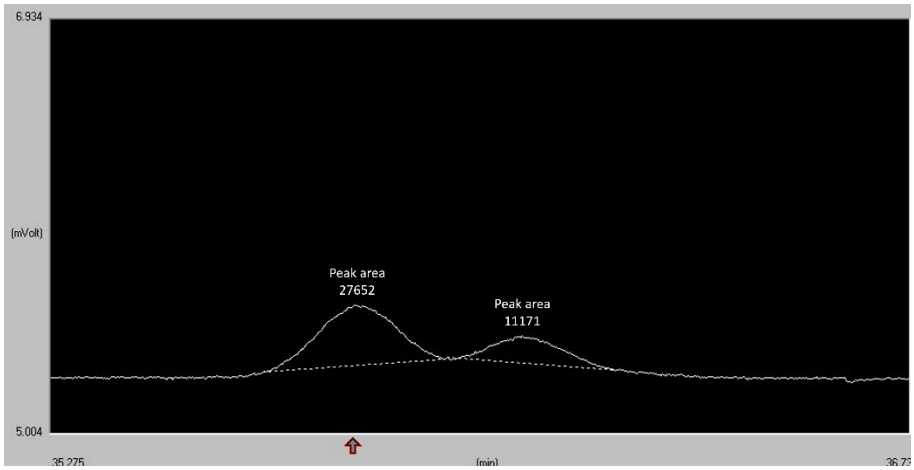

7.8.2 Chiral GC Trace of 3.10b

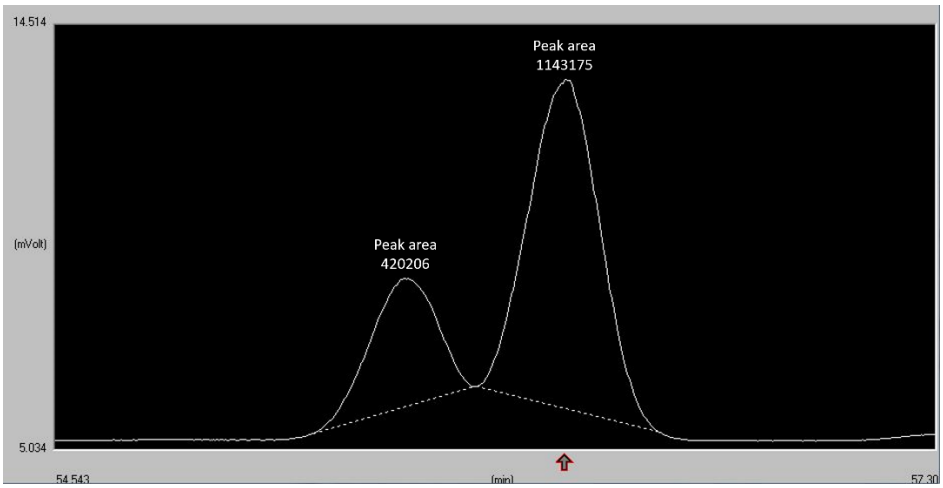

7.8.3 Chiral GC Trace of 3.10c

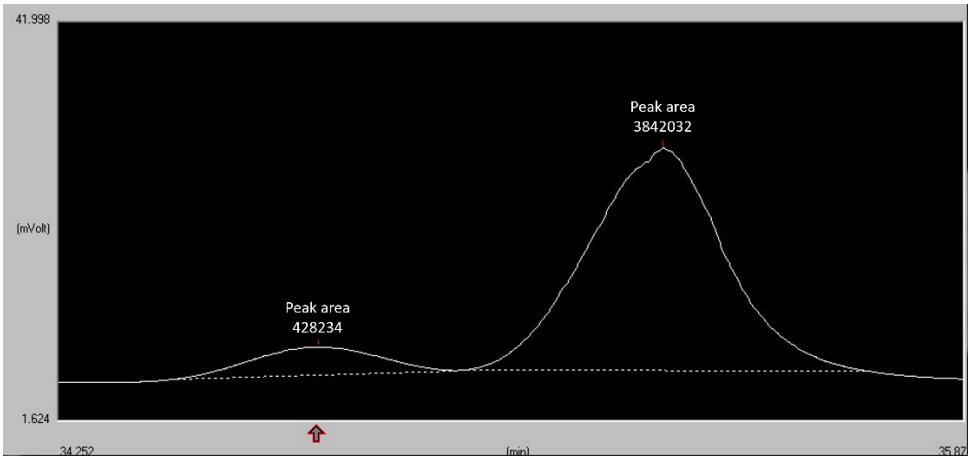

7.9 NOESY Spectra

7.9.1 Metabolite 2.24a from Mutant KT2/L188G/I263G

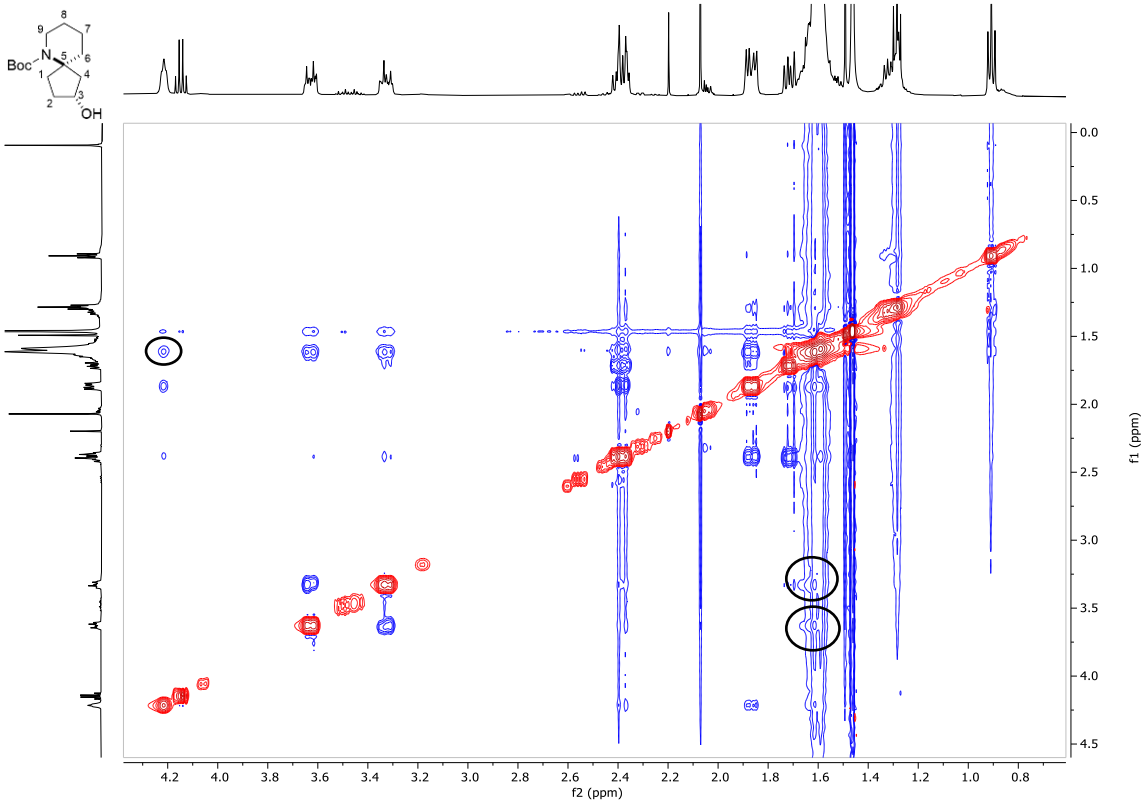

7.9.2 Metabolite 2.24b from Mutant GL/L188Q/I263G/A264G

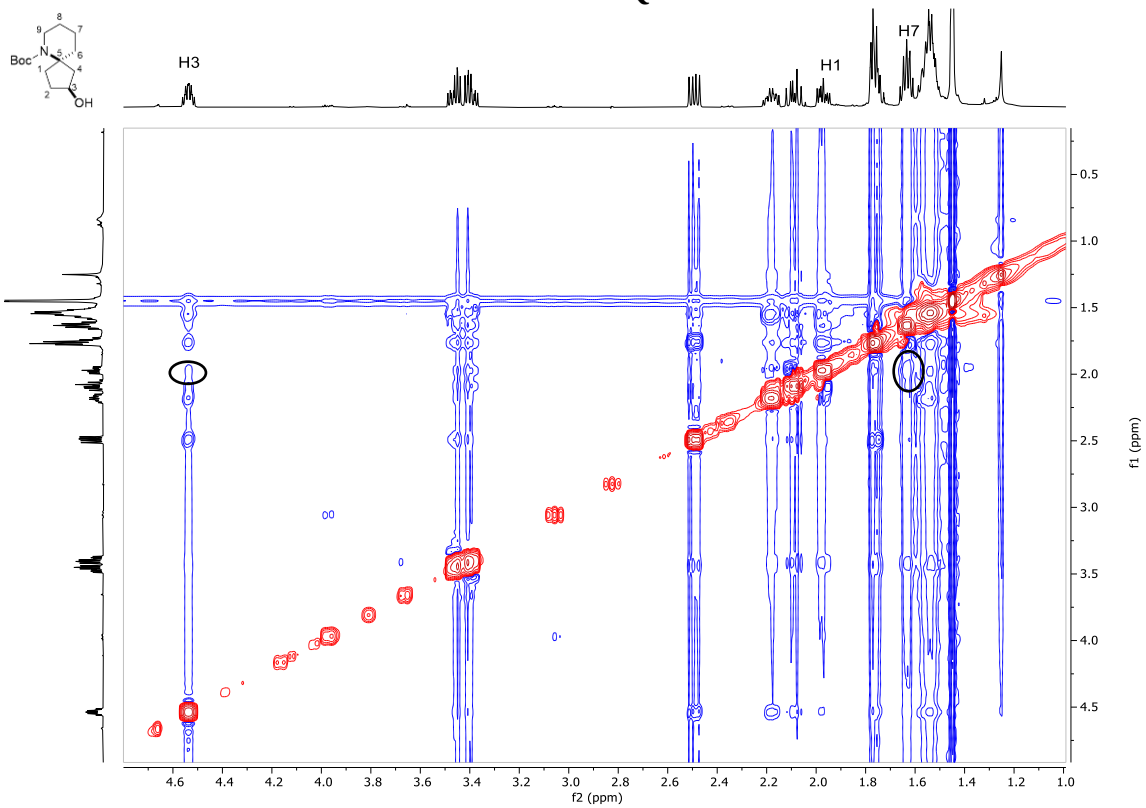

7.9.3 Metabolite 2.55a from Mutant A330P

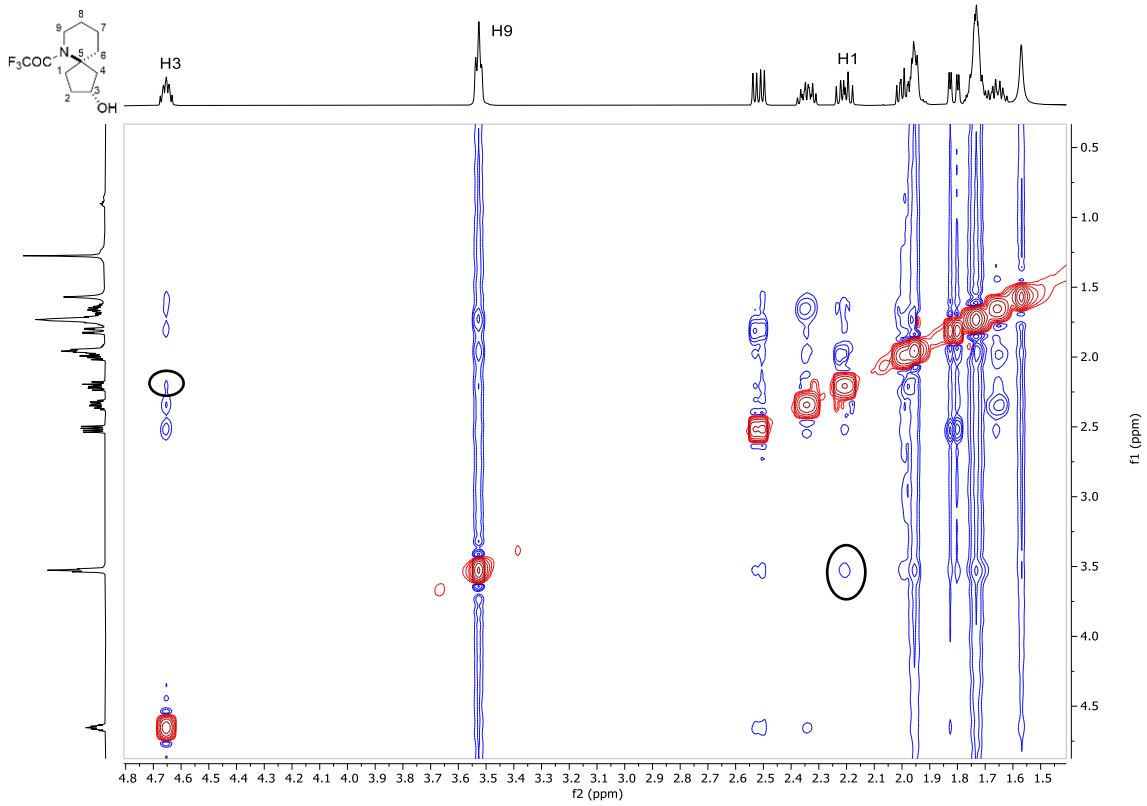

7.9.4 Metabolite 3.10a from Mutant R19/F87I

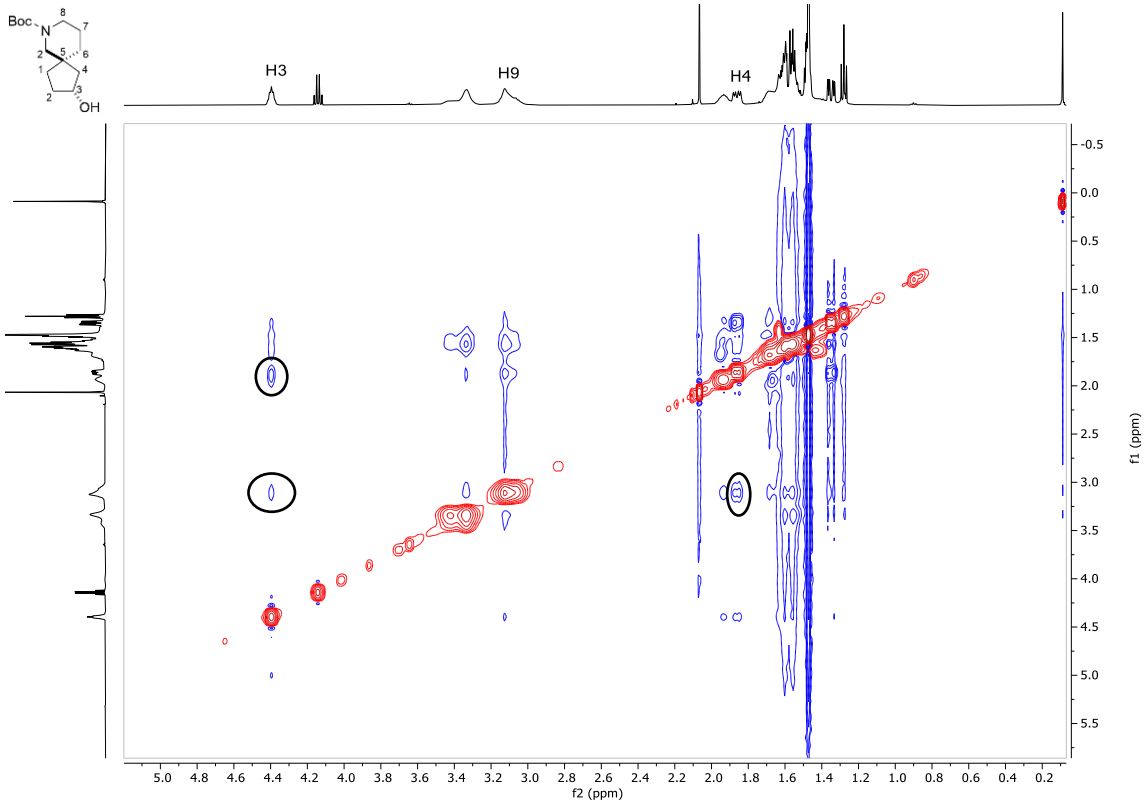

7.9.5 Metabolite 3.10c from Mutant RT2

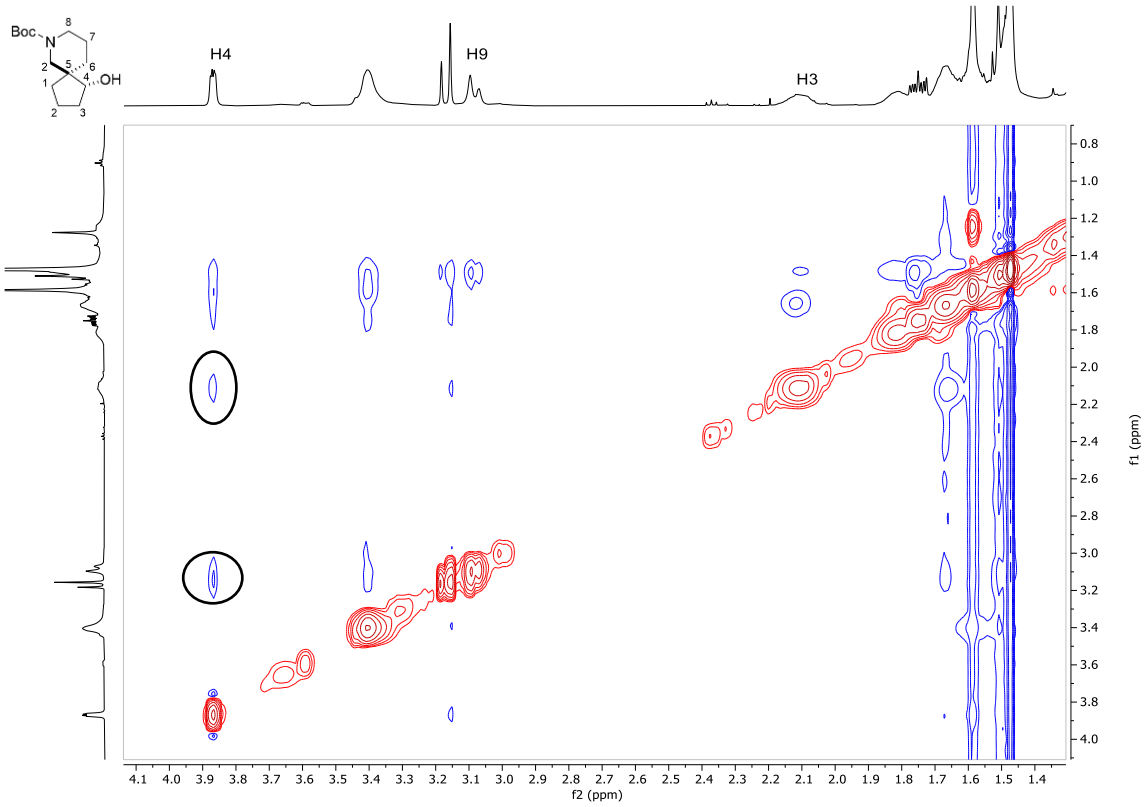

7.9.6 Metabolite 3.11a from Mutant R19/F87I

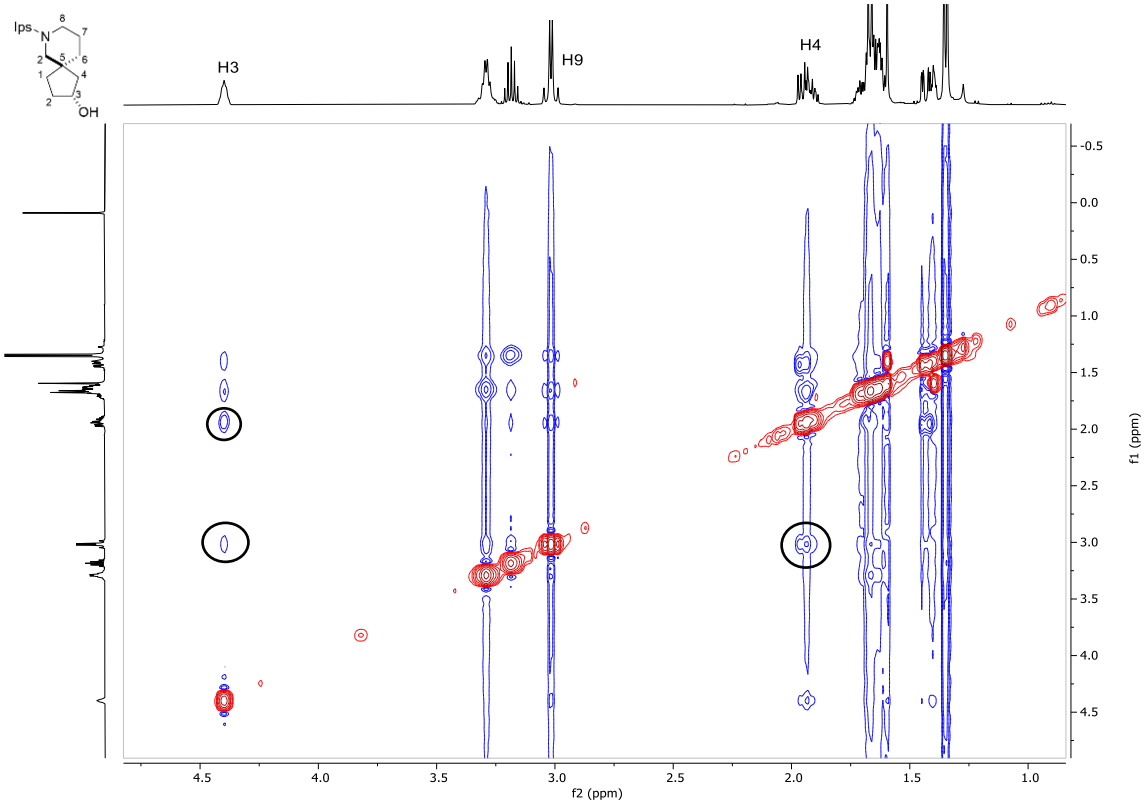

7.9.7 Metabolite 3.11b from Mutant R19/F87I

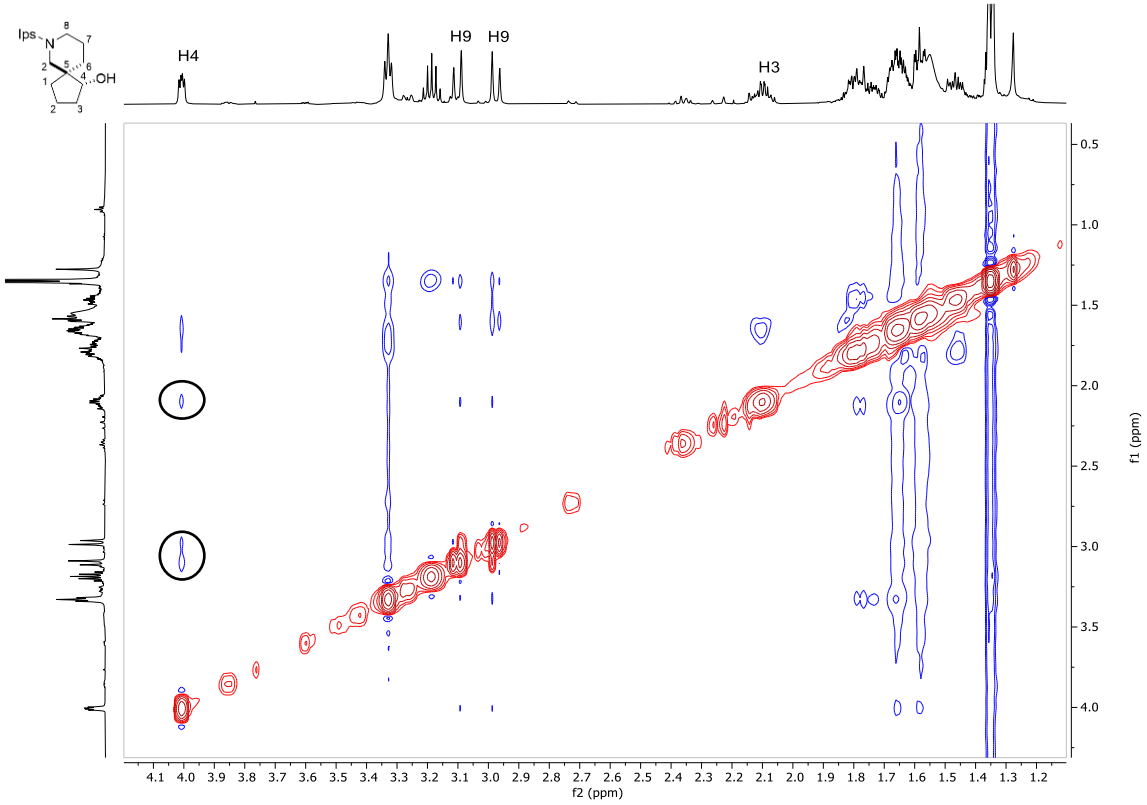

7.9.8 Metabolite 3.13a from Mutant R19/F87I

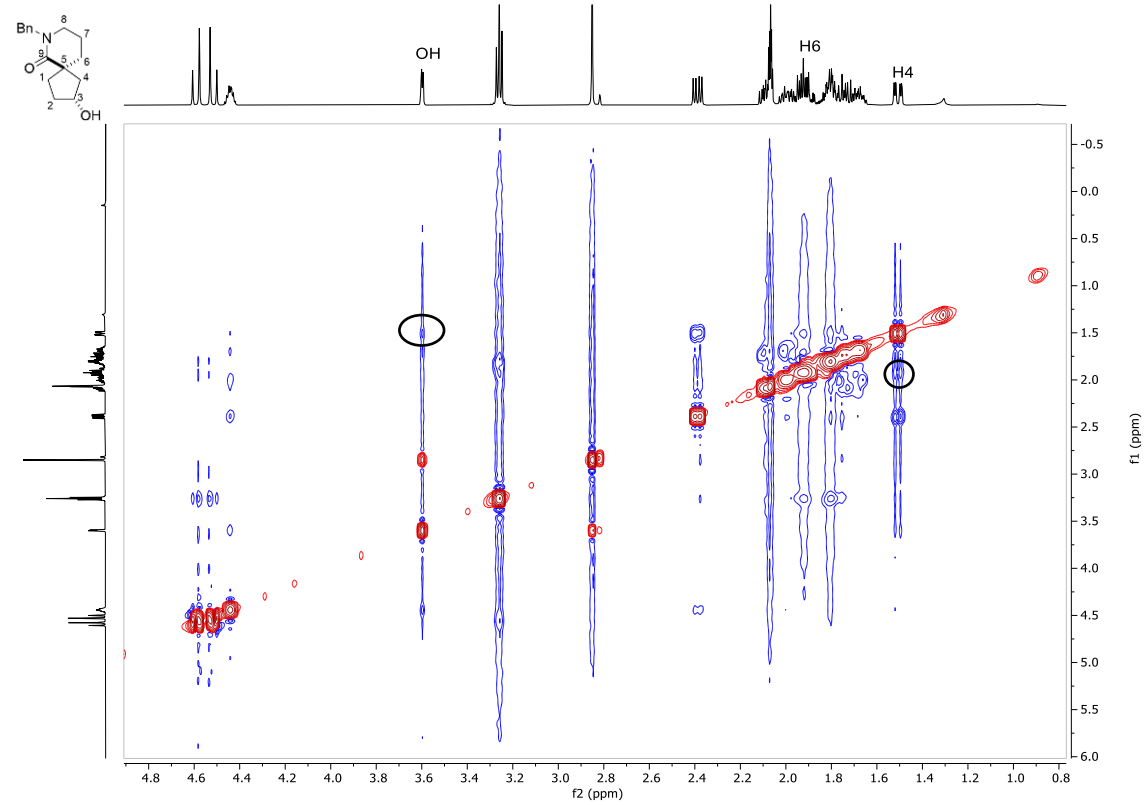

7.9.9 Compound 4.5

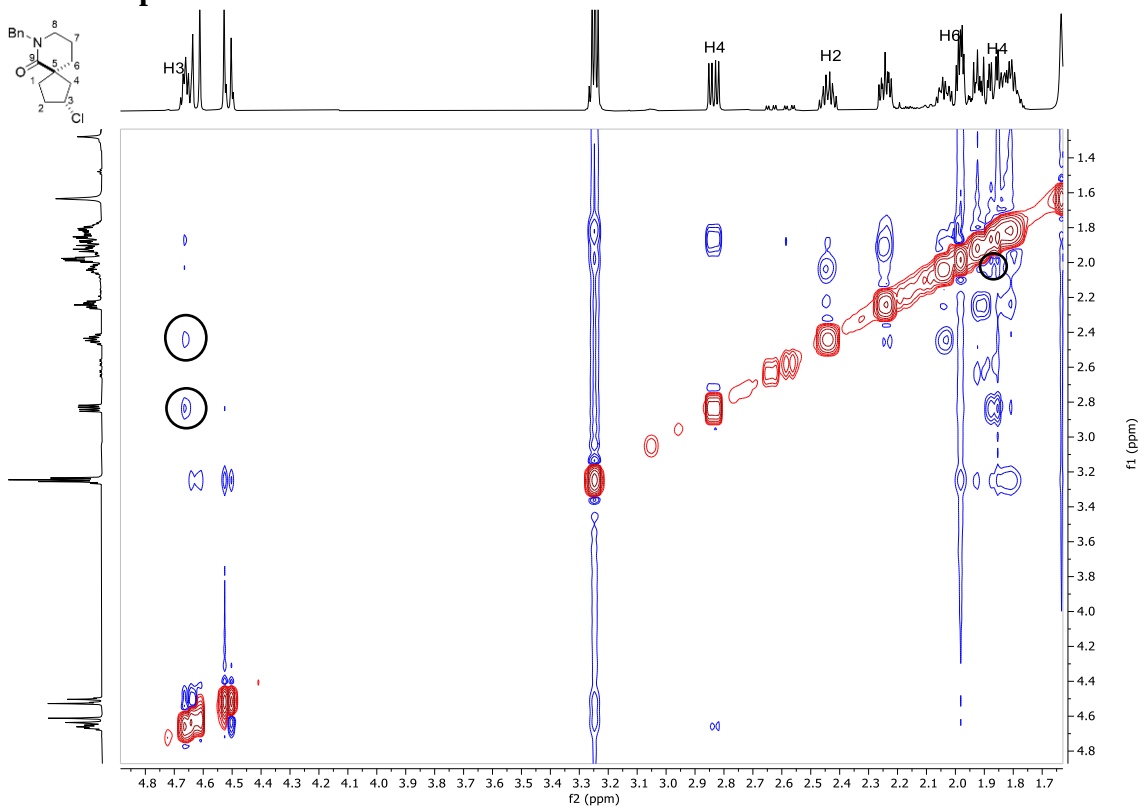

7.9.10 Compound 4.9

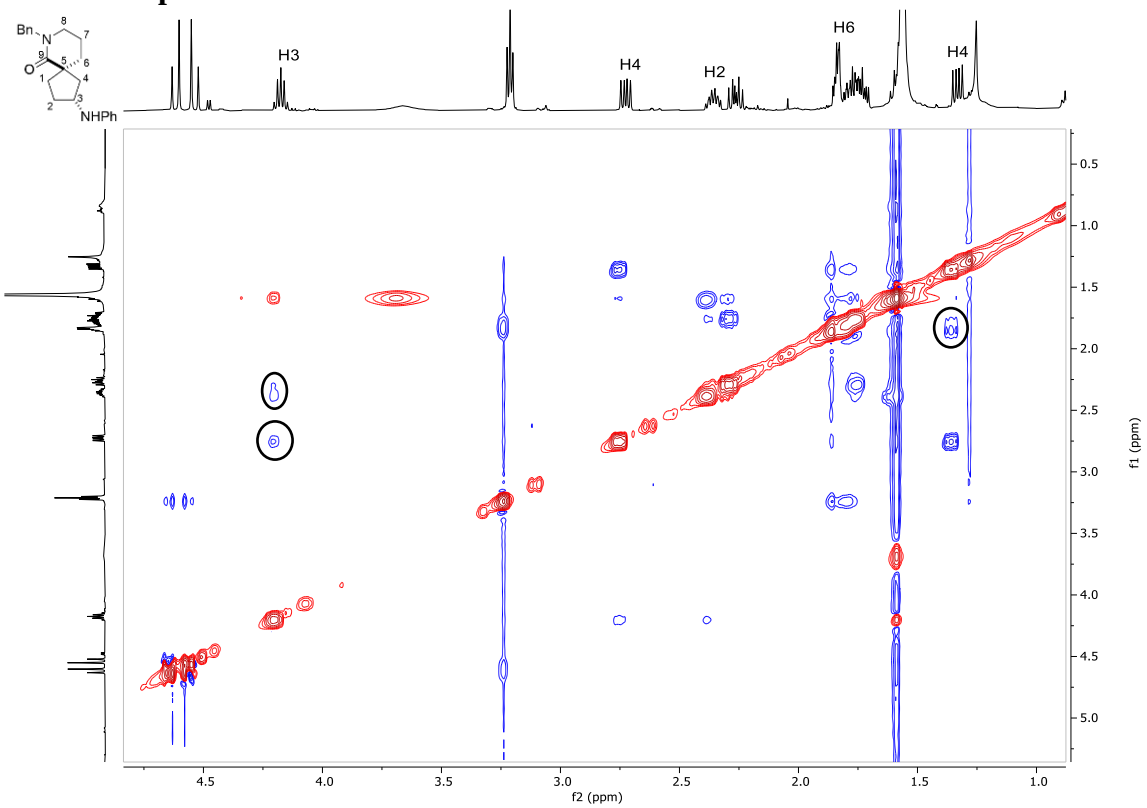

Chapter 8: Appendices

8.1 Screening Data

8.1.1. List of base mutations

Entry	Base Mutant	Mutations
1	G	A74G
2	GL	A74G/F87L
3	GQ	A74G/L188Q
4	GV	A74G/F87V
5	K19	H171L/Q307H/N319Y
6	KT2	R47L/Y51F/A191T/N239H/I259V/A276T/L353I
7	KU3	N239H/I259V/A276T
8	R19	R47L/Y51F/H171L/Q307H/N319Y
9	RT2	R47L/Y51F/A191T/N239H/I259V/A276T/L353I
10	VQ	F87V/L188Q

8.1.2 *N*-Ms Protected Spiroamine 2.37

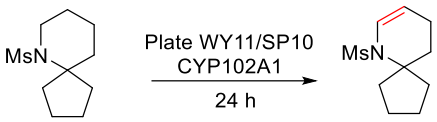

2.37 2.37a

Entry	Mutant	Conv. (%)	2.37a select. (%)	Others (%)
1	GV/A184I	100	36	64
2	GV/A184I/A264G	29	45	55
3	GV/A184I/A264G/A328G	43	13	87
4	GV/A184I/A328G	95	11	89
5	GV/A184I/I263G/A264G	25	2	98
6	GV/A184I/I263G/A328G	25	4	96
7	GV/L188Q	76	31	69
8	GV/L188Q/A328G	78	9	91
9	GV/L188Q/I263G/A264G/A328G	8	9	91
10	GV/L188Q/I263G/V78L	51	0	100
11	K19/F87A/A82M/A264G/A328G	100	97	3
12	K19/F87A/A82M/I263G	99	8	92
13	K19/F87A/A82M/I263G/A264G	100	2	98
14	K19/F87A/A82M/I263G/A264G/A328G	100	93	7
15	K19/F87A/A82M/I263G/A328G	100	91	9
16	K19/F87A/F81W	89	42	58
17	K19/F87A/I263A	0	0	100
18	K19/F87A/I263G	100	0	100

19	K19/F87V	72	28	72
20	K19/F87V/A328V	35	64	36
21	K19/F87V/E267V	100	4	96
22	K19/F87V/I263G	100	23	77
23	K19/F87V/Q403P	100	21	79
24	K19/F87A/A82M/I263G	12	31	69
25	KU3/A330P/I263A	5	0	100
26	KU3/A330P/S72W	29	21	79
27	R19	4	0	100
28	R19/A328L/A184I	100	1	99
29	R19/A330W	1	0	100
30	R19/F87A	100	59	41
31	R19/F87A/A184I	50	26	74
32	R19/F87A/A184I/A264G	98	43	57
33	R19/F87A/A184I/A264G/A328G	97	16	84
34	R19/F87A/A184I/I263G/A264G	48	29	71
35	R19/F87A/A184I/I263G/A264G/A328G	6	0	100
36	R19/F87A/A184I/I263G/A328G	30	27	73
37	R19/F87A/A184I/T260G/A328G	87	31	69
38	R19/F87A/A264G	91	35	65
39	R19/F87A/A328G	82	27	73
40	R19/F87A/A328G/P329G/A330G	100	15	85
41	R19/F87A/A328I/A264G	100	0	100
42	R19/F87A/I263G/A328G	27	21	79
43	R19/F87I	36	0	100
44	RP/H171L/I263G	95	10	90
45	RT2/A330P/V78I/A184I	29	65	35
46	RT2/S72G/A330W	40	26	74

8.1.3 *N*-Boc Protected Spiroamine 2.24

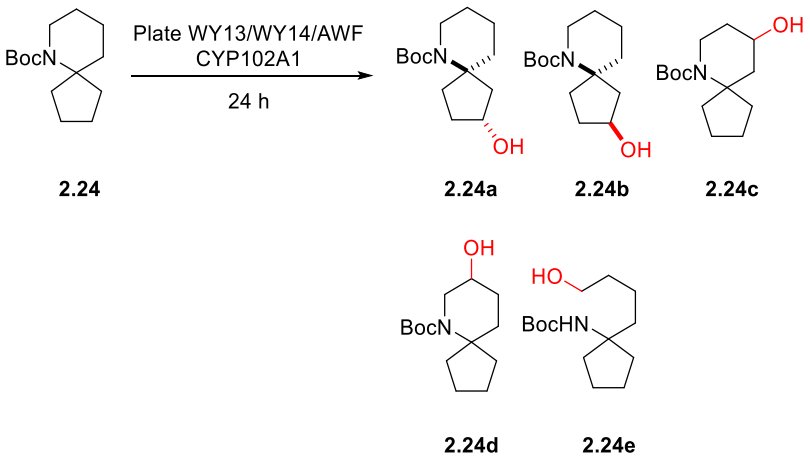

2.24 **2.24a** **2.24b** **2.24c** **2.24d** **2.24e**

Entry	Mutant	Conv. (%)	2.24					Others (%)
			a (%)	b (%)	c (%)	d (%)	e (%)	
1	A330P	0	0	0	0	0	0	100
2	GL/L188Q/	93	14	51	20	10	0	5

	I263G/A328G							
3	GV/A184I	97	3	1	47	0	0	49
4	GV/L188Q	98	12	3	56	2	0	27
5	GV/L188Q/ A264G	98	18	4	68	3	0	7
6	GV/L188Q/ A328G	96	12	6	59	3	0	21
7	GV/L188Q/ A330W	93	17	5	58	4	0	16
8	GV/L188Q/ I263G	94	10	37	43	3	0	8
9	GV/L188Q/ I263G/A328L	96	9	51	30	4	0	6
10	K19/F87A/ A82M/I263G	93	12	4	59	2	19	4
11	K19/F87A/ F81W	36	15	3	81	0	0	1
12	K19/F87A/ I263A	90	14	1	37	0	36	12
13	K19/F87A/ I263G	76	15	13	72	0	0	0
14	K19/F87V	93	20	7	70	4	0	0
15	K19/F87V/ A264G	100	12	0	5	4	0	78
16	K19/F87V/ E267V	91	8	12	22	4	0	54
17	K19/F87V/ E267V/V78I	73	33	22	35	10	0	0
18	K19/F87V/ I263G	95	6	21	37	2	0	34
19	K19/F87V/ Q403P	99	3	2	59	2	0	34
20	KT2/L188G/ I263G	93	66	4	23	3	0	5
21	KU3/A330P/ I263A	96	73	0	22	5	0	0
22	KU3/A330P/ S72W	95	39	2	45	3	0	11
23	R19	22	26	0	66	7	1	0
24	R19/A328L/ A184I	100	86	0	12	0	0	3
25	R19/A328L/ I263A	96	78	0	22	0	0	0
26	R19/A330W	100	31	0	54	14	0	0
27	R19/F87/A184I	100	3	11	28	3	0	55
28	R19/F87A	100	14	0	46	1	0	39
29	R19/F87A/ A184I	87	13	0	61	0	0	26
30	R19/F87A/ A328I/S72W	95	44	5	34	10	0	8
31	R19/F87A/A184I/T 260G/A328G	95	8	1	67	1	20	3

32	R19/F87A/A328I/ V78I	98	32	6	51	1	0	10
33	R19/F87A/ A328G	49	3	0	77	0	0	20
34	R19/F87A/ A328G/A264G	96	5	0	95	0	0	0
35	R19/F87A/ A328G/P329G/ A330G	97	8	3	85	0	0	3
36	R19/F87A/ A328L	49	24	5	59	8	0	3
37	R19/F87A/F81W/T 260G/ A328G	97	8	2	81	0	0	9
38	R19/F87A/ T260G	97	42	2	51	0	0	5
39	R19/F87I	100	5	9	21	5	5	55
40	R19/F87I/ A184F	100	7	4	27	6	0	55
41	R19/F87I/ A184M	100	2	10	22	2	0	63
42	R19/F87I/ A264F	97	15	0	24	10	0	51
43	R19/F87I/A328I	99	10	1	21	8	0	59
44	R19/F87I/A74L	100	1	3	37	1	0	58
45	R19/F87I/A82I	100	5	5	53	4	1	32
46	R19/F87I/A82M	100	8	6	0	9	1	76
47	R19/F87I/E267F	100	11	0	8	32	1	48
48	R19/F87I/F81W	0	0	0	0	0	0	100
49	R19/F87I/ I263W	100	0	0	0	0	1	99
50	R19/F87I/ K343W	100	7	4	32	6	1	50
51	R19/F87I/ L437LV	95	6	6	56	2	0	30
52	R19/F87I/ L437M	100	7	2	9	5	0	77
53	R19/F87I/ L437V	100	1	1	9	0	0	89
54	R19/F87I/ S332M	96	2	0	0	2	0	96
55	R19/F87I/S72V	100	9	1	19	4	0	67
56	R19/F87I/ T260G	99	30	0	10	18	0	40
57	R19/F87I/ T260L	100	9	3	7	10	0	71
58	R19/F87I/T438F	98	2	0	4	40	0	54
59	R19/S72G/ A330W	95	25	0	61	7	0	7
60	RP/A82M/ I263A	90	30	0	61	10	0	0
61	RP/H171L/	54	100	0	0	0	0	0

	I263G							
62	RP/H171L/ I263G/A184I	72	67	9	24	0	0	0
63	RP/I263A/ E267V	71	71	0	23	6	0	0
64	RT2/S72G/ A330W	19	27	1	60	12	0	0
65	VQ/S72G/ A330W	96	10	3	56	7	0	23
66	WT	0	0	0	0	0	0	100

8.1.4 *N*-Tfa Protected Spiroamine 2.55

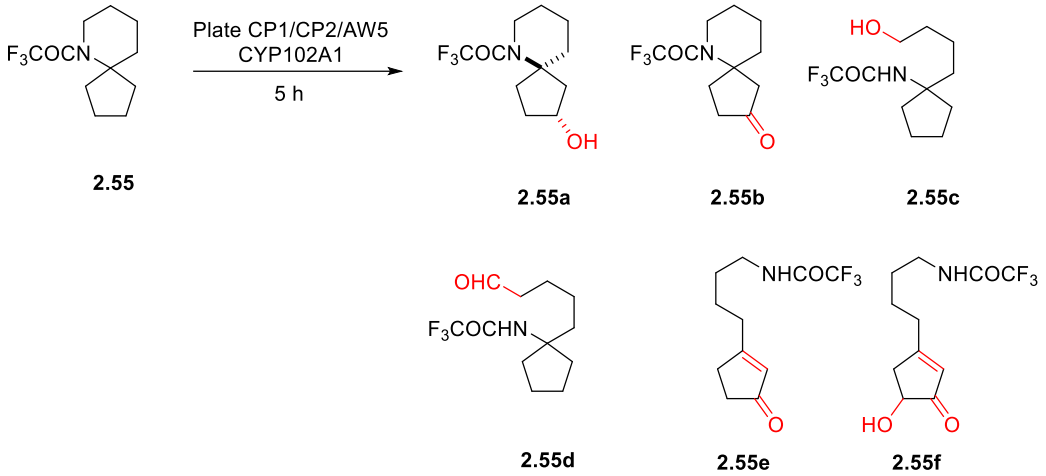

2.55 2.55a 2.55b 2.55c 2.55d 2.55e 2.55f

Entry	Mutant	Conv. (%)	2.55						Others (%)
			a (%)	b (%)	c (%)	d (%)	e (%)	f (%)	
1	A330P	100	95	2	0	0	0	3	100
2	GL/ L188Q/ I263G/ A328G	0	0	0	0	0	0	100	0
3	GQ/I263G/A328L/ A330L/S332F	100	78	2	0	1	0	19	100
4	GV/A184I	100	0	10	0	21	37	32	100
5	GV/A184I/I263G/ A328G	100	2	18	0	10	1	68	100
6	GV/ L188Q	100	0	5	0	10	37	47	100
7	GV/ L188Q/ A264G	100	15	15	13	15	1	40	100
8	GV/ L188Q/ A328G	100	0	7	0	10	9	74	100
9	GV/	100	0	5	0	12	28	55	100

	L188Q/ A330W								
10	GV/ L188Q/ I263G	100	1	14	0	9	1	74	100
11	GV/L188Q/I263G/ A328L	100	28	26	0	13	4	28	100
21	K19/F87A/A82M	100	0	4	6	10	0	79	100
13	K19/F87A/A82M/ I263G	100	0	16	21	17	4	43	100
14	K19/F87A/I263A	100	34	6	31	5	2	22	100
15	K19/F87A/I263G	100	6	30	6	21	4	33	100
16	K19/F87V	100	0	7	0	13	47	33	100
17	K19/F87V/A264G	100	33	1	10	12	1	43	100
18	K19/F87V/E267V	100	0	11	0	13	21	56	100
19	K19/F87V/E267V/ V78I	100	0	38	0	22	10	30	100
20	K19/F87V/I263G	100	0	20	0	9	9	61	100
21	K19/F87V/Q403P	100	0	4	0	17	43	36	100
22	KT2/L188G/ I263G	100	53	4	4	5	2	31	100
23	KU3/A330P/ I263A	100	89	5	0	2	0	4	100
24	KU3/A330P/ S72W	100	42	4	0	3	34	17	100
25	R19	61	0	0	0	0	0	100	61
26	R19/A328L/I263A	100	88	0	0	0	0	12	100
27	R19/ A330W	100	72	5	4	0	0	19	100
28	R19/F87A	100	0	0	0	4	7	88	100
29	R19/F87A/A184I	100	10	23	5	19	2	41	100
30	R19/F87A/A184I/ T260G/A328G	100	46	13	4	13	0	23	100
31	R19/F87A/A328G	100	0	13	0	8	4	75	100
32	R19/F87A/A328G/ P329G/A330G	100	3	6	6	11	5	69	100
33	R19/F87A/A328I/ S72W	100	17	29	6	25	4	18	100
34	R19/F87A/A328I/ V78I	100	11	15	3	25	11	34	100
35	R19/F87A/A328L	100	0	8	0	22	63	7	100
36	R19/F87A/F81W/ T260G/A328G	100	38	16	3	10	1	31	100
37	R19/F87A/I263G	100	0	19	0	24	20	36	100
38	R19/F87A/T260G	99	61	9	0	7	0	23	99
39	R19/F87I	100	0	34	0	28	4	35	100
40	R19/F87I/A184F	100	15	17	0	6	0	62	100
41	R19/F87I/A330F	100	0	46	0	21	7	26	100
42	R19/F87I/A330I	100	15	0	0	19	0	66	100
43	R19/F87I/A330I/ A184I	100	0	0	0	13	2	85	100
44	R19/F87I/A330P	100	0	55	0	22	6	16	100

45	R19/F87I/A330V	100	0	46	0	20	0	34	100
46	R19/F87I/A330V/ A184I	100	0	0	0	14	2	84	100
47	R19/F87I/A330V/ A82M	100	0	0	0	15	13	73	100
48	R19/F87I/A330W	100	0	44	0	20	3	33	100
49	R19/F87I/A330W/ A82M	100	0	0	0	14	3	83	100
50	R19/F87I/A330W/ A82M/I263G	100	0	28	0	9	0	63	100
51	R19/F87I/A330W/ I263G	100	0	19	0	3	0	78	100
52	R19/F87I/A82M/ A184I	100	0	49	0	21	4	26	100
53	R19/F87I/I263G/ A82M	100	2	35	0	11	0	53	100
54	R19/F87I/L437F	100	7	27	0	12	0	54	100
55	R19/F87I/L437LV	100	33	12	0	8	0	47	100
56	R19/F87I/L71M	100	0	44	0	22	4	31	100
57	R19/F87I/L75F	100	3	42	0	17	0	39	100
58	R19/F87I/L75M	100	0	54	0	25	2	20	100
59	R19/F87I/S332I	100	12	27	0	10	0	51	100
60	R19/F87I/S332L	100	12	18	0	2	0	68	100
61	R19/F87I/S72I	100	10	18	0	4	0	68	100
62	R19/F87I/S72L	100	0	0	0	16	11	73	100
63	R19/F87I/T438V	100	6	32	0	12	0	50	100
64	R19/S72G/A330W	100	81	3	4	2	0	10	100
65	RP/A82M/I263A	99	28	2	46	1	0	23	99
66	RP/H171L/I263G	100	0	0	0	14	0	86	100
67	RP/H171L/I263G/ A184I	100	76	5	4	3	1	13	100
68	RT2	100	59	6	6	8	1	19	100
69	VQ/S72G/A330W	100	0	0	0	7	34	59	100
70	WT	87	67	3	19	0	0	11	87

8.1.5 *N*-Boc-protected Spiroamine 3.10

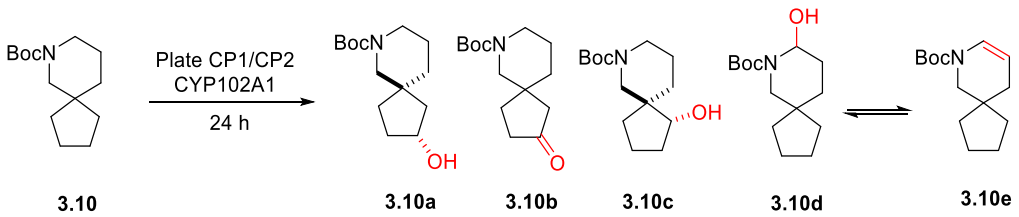

Entry	Mutant	Conv. (%)	3.10					Others (%)
			a (%)	b (%)	c (%)	d (%)	e (%)	
1	A330P	0	0	0	0	0	0	100
2	G/L188Q/I263G/	83	87	0	11	0	0	2

	A328L/A330L/ S332F							
3	G/L188Q/I263G/ A328G	0	0	0	0	0	0	100
4	GV/A184I	94	23	0	0	38	2	36
5	GV/A184I/I263G/ A328G	10	45	0	0	32	0	23
6	GV/L188Q	95	34	5	7	27	5	21
7	GV/L188Q/A264G	57	44	2	10	22	0	22
8	GV/L188Q/A328G	80	18	1	8	25	0	48
9	GV/L188Q/ A330W	97	10	2	1	9	4	73
10	GV/L188Q/I263G	69	75	0	0	6	0	18
11	GV/L188Q/I263G/ A328L	88	86	2	0	2	1	9
12	K19/F87A/A82M	82	8	0	3	24	6	59
13	K19/F87A/A82M/ I263G	66	53	0	0	36	5	6
14	K19/F87A/F81W	94	28	0	11	29	10	23
15	K19/F87A/I263A	93	14	0	0	56	6	24
16	K19/F87A/I263G	85	34	0	5	29	8	24
17	K19/F87V	98	5	0	2	4	3	85
18	K19/F87V/A264G	57	32	1	4	36	3	23
19	K19/F87V/A328V	73	56	0	5	26	9	5
20	K19/F87V/E267V	62	100	0	0	0	0	0
21	K19/F87V/E267V/ V78I	77	43	11	0	3	4	39
22	K19/F87V/I263G	72	53	1	2	7	0	36
23	K19/F87V/Q403P	97	22	4	4	26	4	40
24	KT2/L188G/I263G	64	63	0	7	7	2	21
25	KU3/A330P/A328I	0	0	0	0	0	0	100
26	KU3/A330P/I263A	3	89	0	11	0	0	0
27	KU3/A330P/S72W	11	75	0	25	0	0	0
28	R19	93	44	0	31	17	2	7
29	R19/A328L/A184I	28	58	3	40	0	0	0
30	R19/A328L/I263A	30	100	0	0	0	0	0
31	R19/A330W	23	67	0	0	33	0	0
32	R19/F87A	74	5	0	1	1	8	85
33	R19/F87A/A184I	23	28	0	0	26	6	40
34	R19/F87A/A328I/S 72W	55	100	0	0	0	0	0
35	R19/F87A/A184I/ T260/A328G	42	17	0	5	39	3	36
36	R19/F87A/A328I/ V78I	70	84	0	5	5	0	6
37	R19/F87A/A328G	93	26	0	5	36	8	25
38	R19/F87A/A328G/ P329G/A330G	69	28	0	0	36	6	29
39	R19/F87A/A328L	23	82	0	0	10	0	8
40	R19/F87A/F81W/ T260G/A328G	60	21	0	6	31	0	42

41	R19/F87A/ G265GG	74	45	0	4	37	4	11
42	R19/F87A/I263G	26	25	0	3	25	5	42
43	R19/F87A/I263G/ A264G	92	25	0	4	29	11	32
44	R19/F87A/T260G	67	29	0	8	24	4	35
45	R19/F87I	77	33	7	1	16	5	39
46	R19/F87I/L437F	75	60	0	2	11	10	17
47	R19/F87I/L437LV	67	65	2	7	4	12	10
48	R19/S72G/A330W	55	67	0	0	23	0	10
49	RP/A82M/I263A	67	18	0	27	23	0	32
50	RP/H171L/I263G	34	58	0	18	4	0	20
51	RP/H171L/I263G/ A184I	14	100	0	0	0	0	0
52	RT2	52	48	0	22	15	0	15
53	RT2/A330P/V78I/ A184I	36	81	4	0	14	0	1
54	VQ/S72G/A330W	97	13	2	0	9	5	71
55	WT	0	0	0	0	0	0	0

8.1.6 *N*-Ips-protected Spiroamine 3.11

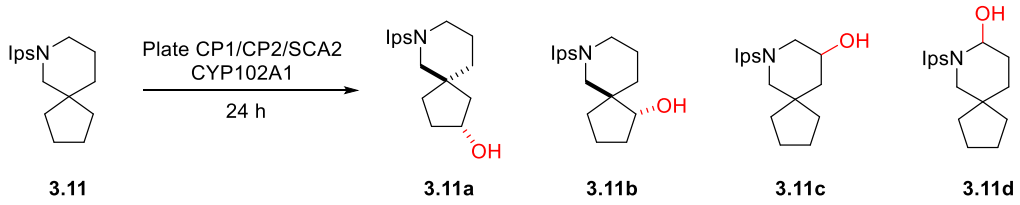

3.11 3.11a 3.11b 3.11c 3.11d

Entry	Mutant	Conv. (%)	3.11				Others (%)
			a (%)	b (%)	c (%)	d (%)	
1	A330P	18	86	7	0	0	7
2	GL/L188G/I263G/ A328G	3	0	0	0	0	100
3	GL/L188Q/S72W/I263G	12	24	48	0	0	28
4	GQ/I263G/A328L/A330L/S332F	47	91	0	0	0	9
5	GV/A184I	100	35	6	0	0	59
6	GV/A184I/I263G/A264G	67	1	1	5	36	57
7	GV/L188Q	100	56	8	0	0	36
8	GV/L188Q/A264G	70	48	22	2	17	10
9	GV/L188Q/A328G	99	5	5	1	33	56
10	GV/L188Q/A330W	100	28	32	2	0	38
11	GV/L188Q/I263G	99	23	2	1	5	69
12	GV/L188Q/I263G/A328L	61	80	1	0	0	19
13	K19/F87A/A82M	100	1	2	0	0	97
14	K19/F87A/A82M/A330W	100	11	7	0	3	79
15	K19/F87A/A82M/I263G	100	9	1	1	8	82
16	K19/F87A/F81W	37	10	4	0	53	33

17	K19/F87A/I263A	98	3	2	1	31	63
18	K19/F87A/I263G	100	2	8	0	2	88
19	K19/F87V	100	14	7	0	0	79
20	K19/F87V/A264G	63	54	11	1	21	13
21	K19/F87V/A328V	94	88	11	0	0	1
22	K19/F87V/E267V	100	55	5	0	0	40
23	K19/F87V/E267V/V78I	78	52	4	0	2	41
24	K19/F87V/I263G	100	17	6	0	3	74
25	K19/F87V/Q403P	100	17	5	0	0	78
26	KT2/L188G/I263G	99	71	2	0	2	26
27	KU3/A330P/A328I	5	91	3	0	0	6
28	KU3/A330P/I263A	29	88	3	0	3	7
29	KU3/A330P/S72W	96	85	9	0	1	5
30	L188Q/S72A/I263G/A328G	9	13	17	0	43	27
31	L188Q/S72H/I263G/A328G	9	10	21	0	41	28
32	R19	0	0	0	0	0	100
33	R19/A328L/I263A	12	91	0	0	0	9
34	R19/A330S	1	0	0	0	11	89
35	R19/A330W	87	7	42	0	34	17
36	R19/F87A	100	12	6	0	1	82
37	R19/F87A/A184I	100	6	2	0	7	86
48	R19/F87A/A184I/T260G/A328G	79	1	2	2	54	41
49	R19/F87A/A328G	100	7	2	1	2	89
40	R19/F87A/A328G/P329G/A330G	56	2	1	0	67	30
41	R19/F87A/A328I/S72W	52	62	6	0	12	20
42	R19/F87A/A328I/V78I	44	13	2	0	58	27
43	R19/F87A/A328L	59	68	10	0	10	12
44	R19/F87A/F81W/T260G/A328G	97	3	2	1	50	44
45	R19/F87A/G265GG	27	49	2	0	32	16
46	R19/F87A/I263G	100	0	3	0	0	97
47	R19/F87A/I263G/A264G	88	1	0	0	44	55
48	R19/F87A/T260G	44	26	2	0	47	25
49	R19/F87I	100	69	3	16	2	9
50	R19/F87I/L437F	94	88	2	0	1	9
51	R19/F87I/L437LV	37	72	4	15	3	7
52	R19/I263V/A330W	2	6	0	0	61	33
53	R19/S72A/A330W	31	32	2	8	39	19
54	R19/S72G/A330W	53	44	8	1	34	14
55	R19/S72H/A330W	11	52	1	4	18	25
56	R19/S72L/A330W	8	56	3	0	13	28
57	R19/S72P/A330W	13	0	1	6	0	93
58	R19/S72V/A330W	4	34	4	4	19	38
59	R19/S72W/A330W	54	39	2	13	34	12
60	RP/A82M/I263A	51	19	8	0	51	22
61	RP/A82M/I263A/A330W	25	19	2	2	3	74
62	RP/H171L/I263G	100	43	1	0	0	55
63	RP/H171L/I263G/A184I	51	77	1	0	0	22
64	RP/H171L/I263G/S72G	18	0	0	2	7	92
65	RP/H171L/I263G/S72W	22	87	1	1	3	8
66	RP/I263A/A330W	7	37	13	4	11	36
67	RP/V87I/E267V	100	71	25	1	1	3

68	RT2	96	68	10	0	15	7
69	RT2/I263A/A330W	12	27	1	0	43	29
70	RT2/S72Y/A330W	52	70	2	5	16	8
71	VQ/S72G/A330W	100	18	24	10	0	48
72	VQ/S72P/A330W	92	30	2	29	14	25
73	VQ/S72V/A330W	52	33	2	38	5	21
74	VQ/S72W/A330W	100	46	29	0	7	18
75	WT	3	0	0	0	0	100

8.1.7 *N*-Ms-protected Spiroamine 3.5

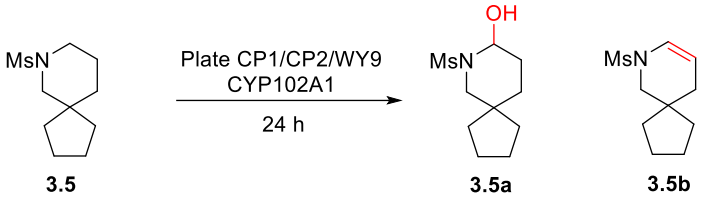

3.5 3.5a 3.5b

Entry	Mutant	Conv. (%)	Select. 3.5a (%)	Select. 3.5b (%)	Others (%)
1	A330P	58	72	11	17
2	G/L188Q/I263G/A328L/A330L/S332F	12	0	0	100
3	G/LQ/I263G/A328G	0	0	0	0
4	GV/A184I	100	5	0	95
5	GV/A184I/I263G/A328G	43	72	18	10
6	GV/L188Q	96	56	6	38
7	GV/L188Q/A264G	92	72	10	18
8	GV/L188Q/A328G	100	5	0	95
9	GV/L188Q/A330W	100	0	0	100
10	GV/L188Q/I263G	87	77	13	10
11	GV/L188Q/I263G/A328L	97	7	93	0
12	GV/L188Q/I263G/V78L	96	37	58	5
13	K19/F87A/A82M	100	0	0	100
14	K19/F87A/A82M/A330W	97	54	21	25
15	K19/F87A/A82M/I263G	100	41	8	51
16	K19/F87A/F81W	97	20	78	2
17	K19/F87A/I263A	86	82	16	2
18	K19/F87A/I263G	95	65	19	16
19	K19/F87V	99	50	9	41
20	K19/F87V/A264G	69	72	13	15
21	K19/F87V/A328V	99	71	14	15
22	K19/F87V/E267V	100	0	0	100
23	K19/F87V/E267V/V78I	79	51	6	42
24	K19/F87V/I263G	95	78	11	11
25	K19/F87V/Q403P	96	16	81	3
26	KT2/L188G/I263G	100	78	14	8
27	KU3/A330P/A328I	99	3	96	1
28	KU3/A330P/I263A	91	77	17	6

29	KU3/A330P/S72W	100	43	8	49
30	R19	0	0	0	0
31	R19/A328L/I263A	93	64	7	29
32	R19/A330W	85	60	22	17
33	R19/F87A	100	54	9	37
34	R19/F87A/A184I	89	77	15	8
35	R19/F87A/A328I/S72W	82	80	15	5
36	R19/F87A/A184I/T260G/A328G	47	34	10	56
37	R19/F87A/A328I/V78I	60	87	13	0
38	R19/F87A/A328G	96	61	5	34
39	R19/F87A/A328G/P329G/A330G	99	52	9	39
40	R19/F87A/A328L	98	32	40	29
41	R19/F87A/F81W/T260G/A328G	37	34	8	59
42	R19/F87A/G265GG	100	22	77	1
43	R19/F87A/I263G	100	56	10	34
44	R19/F87A/I263G/A264G	100	17	82	1
45	R19/F87A/T260G	11	40	12	49
46	R19/F87I	98	46	13	41
47	R19/F87I/L437F	77	15	2	82
48	R19/F87I/L437LV	22	44	9	47
49	R19/S72G/A330W	69	68	10	22
50	RP/A82M/I263A	81	80	12	8
51	RP/H171L/I263G	100	18	3	79
52	RP/H171L/I263G/A184I	40	73	11	17
53	RP/V78I/E267V	94	38	57	5
54	RT2	100	63	11	26
55	VQ/S72G/A330W	100	0	0	100
56	WT	48	79	14	7

8.1.8 *N*-DEP Protected Spiroamine 3.12

3.12 **3.12a**

Entry	Mutant	Conv. (%)	Select. 3.12a (%)	Others (%)
1	A330P	1	100	0
2	GL/L188Q/I263G/A328G	0	0	0
3	GQ/I263G/A328L/A330L/S332F	3	83	17
4	GV/A184I	100	14	86
5	GV/A184I/I263G/A328G	40	20	80
6	GV/L188Q/A264G	39	39	61
7	GV/L188Q/A328G	99	6	94
8	GV/L188Q/A330W	100	4	96
9	GV/L188Q/I263G	0	0	0

10	GV/L188Q/I263G/A328L	14	52	48
11	GV/L188Q	100	12	88
12	I263G	13	40	60
13	K19/F87A/I263A	20	16	84
14	K19/F87A/A82M	32	36	64
15	K19/F87A/A82M/E267F	20	35	65
16	K19/F87A/A82M	49	37	63
17	K19/F87A/A82M/I263G	50	61	39
18	K19/F87A/I263G	98	31	69
19	K19/F87V	100	1	99
20	K19/F87V/A264G	37	19	81
21	K19/F87V/E267V	100	68	32
22	K19/F87V/E267V/V78I	95	69	31
23	K19/F87V/I263G	92	28	72
24	K19/F87V/Q403P	100	6	94
25	KT2/L188G/I263G	25	47	53
26	KU3/A330P/I263A	8	66	34
27	KU3/A330P/S72W	5	78	22
28	R19	0	0	0
29	R19/A328L/I263A	2	100	0
30	R19/A328L/I263G	0	0	100
31	R19/A330W	3	31	69
32	R19/F87A	99	17	83
33	R19/F87A/A184I	96	27	73
34	R19/F87A/A328I/S72W	36	59	41
35	R19/F87A/A184I/T260G/A328G	55	6	94
36	R19/F87A/A328I/V78I	53	70	30
37	R19/F87A/A328F	2	0	100
38	R19/F87A/A328G	100	5	95
39	R19/F87A/A328G/A264G	9	0	100
40	R19/F87A/A328G/P329G/A330G	13	3	97
41	R19/F87A/A328L	44	22	78
42	R19/F87A/F81W/T260G/A328G	29	6	94
43	R19/F87A/I263G	100	23	77
44	R19/F87A/T260G	6	28	72
45	R19/F87I	100	72	29
46	R19/F87I/L437F	99	89	11
47	R19/F87I/L437LV	7	88	12
48	R19/S72G/A330W	1	100	0
49	RP/A82M/I263A	11	69	31
50	RP/A82M/I263A	1	0	100
51	RP/A82W/I263A	1	0	100
52	RP/F87V	22	0	100
53	RP/F87V/V78I	3	0	100
54	RP/H171L/I263G	33	65	35
55	RP/H171L/I263G/A184I	2	64	36
56	RP/H171L/I263G/F87V/V78I	89	41	59
40	RP/H171L/I263G/L437LV	6	29	71
41	RP/I263A/E267V	1	0	100
42	RP/V78I/E267V	71	8	92
43	RT2	16	79	21

44	RT2/S72W/A330W	0	0	100
45	VQ/S72G/A330W	100	7	93
46	WT	0	0	0
47	A330P	1	100	0
48	GL/L188Q/I263G/A328G	0	0	0
49	GQ/I263G/A328L/A330L/S332F	3	83	17
50	GV/A184I	100	14	86
51	GV/A184I/I263G/A328G	40	20	80
52	GV/L188Q/A264G	39	39	61
53	GV/L188Q/A328G	99	6	94
54	GV/L188Q/A330W	100	4	96
55	GV/L188Q/I263G	0	0	0
56	GV/L188Q/I263G/A328L	14	52	48
57	GV/L188Q	100	12	88
58	I263G	13	40	60
59	K19/F87A/I263A	20	16	84
60	K19/F87A/A82M	32	36	64
61	K19/F87A/A82M/E267F	20	35	65
62	K19/F87A/A82M	49	37	63
63	K19/F87A/A82M/I263G	50	61	39

8.1.9 Unprotected Spirocyclic Lactam 3.6

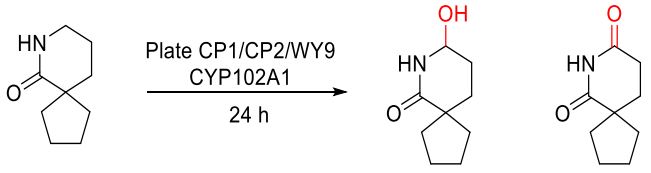

3.6 3.6a 3.6b

Entry	Mutant	Conv. (%)	Select. 3.6a (%)	Select. 3.6b (%)	Others (%)
1	A330P	18	21	8	70
2	GLQ/I263G/A328G	10	0	0	100
3	GQ/I263G/A328L/A330L/S332F	13	21	0	79
4	GV/A184I	90	61	26	13
5	GV/A184I/I263G/A328G	13	61	0	39
6	GV/L188Q	75	80	20	0
7	GV/L188Q/A264G	69	57	21	22
8	GV/L188Q/A328G	70	68	17	15
9	GV/L188Q/A330W	85	45	18	37
10	GV/L188Q/I263G	9	0	0	100
11	GV/L188Q/I263G/A328L	68	61	24	15
12	GV/L188Q/I263G/V78L	10	84	0	16
13	K19/F87A/A82M	100	0	0	100
14	K19/F87A/A82M/A330W	98	86	11	2
15	K19/F87A/A82M/I263G	59	62	20	18

16	K19/F87A/F81W	3	77	0	23
17	K19/F87A/I263A	33	46	15	39
18	K19/F87A/I263G	31	65	15	20
19	K19/F87V	88	70	18	12
20	K19/F87V/A264G	20	52	17	30
21	K19/F87V/A328V	36	100	0	0
22	K19/F87V/E267V	93	18	0	82
23	K19/F87V/E267V/V78I	94	11	0	89
24	K19/F87V/I263G	73	51	20	29
25	K19/F87V/Q403P	80	98	2	0
26	KT2/L188G/I263G	86	65	19	16
27	KU3/A330P/A328I	3	54	0	46
28	KU3/A330P/I263A	14	15	0	85
29	KU3/S72P/A330W	96	52	22	26
30	R19	11	0	0	100
31	R19/A328L/I263A	12	58	17	25
32	R19/A330W	11	57	0	43
33	R19/F87A	73	58	20	22
34	R19/F87A/A328I/S72W	57	69	27	4
35	R19/F87A/A328I/V78I	45	54	17	29
36	R19/F87A/A184I	94	75	25	0
37	R19/F87A/A184I/T260G/A328G	10	21	0	79
38	R19/F87A/A328G	71	41	10	49
39	R19/F87A/A328G/P329G/A330G	11	28	0	72
40	R19/F87A/A328L	94	62	24	14
41	R19/F87A/F81W/T260G/A328G	11	41	0	59
42	R19/F87A/G265GG	2	33	0	67
43	R19/F87A/I263G	81	33	10	57
44	R19/F87A/I263G/A264G	2	47	0	53
45	R19/F87A/T260G	8	0	0	100
46	R19/F87I	91	70	19	11
47	R19/F87I/L437F	20	28	10	62
48	R19/F87I/L437LV	14	36	11	53
49	R19/S72G/A330W	8	0	0	100
50	RP/A82M/I263A	44	67	23	11
51	RP/H171L/I263G	97	64	19	18
52	RP/H171L/I263G/A184I	47	64	23	13
53	RP/V87I/E267V	12	93	0	7
54	RT2	34	70	19	11
55	VQ/S72G/A330W	81	34	17	49
56	WT	9	0	0	100

8.1.10 *N*-Bn-protected Spirocyclic Lactam 3.13

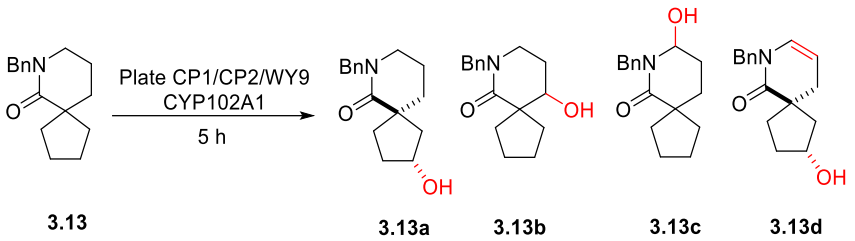

3.13 3.13a 3.13b 3.13c 3.13d

Entry	Mutant	Conv. (%)	3.13				Others (%)
			a (%)	b (%)	c (%)	d (%)	
1	A330P	100	0	0	0	0	100
2	GL/L188Q/I263G/A328G	100	0	0	0	0	100
3	GQ/I263G/A328L/A330L/S332F	4	67	0	0	1	32
4	GV/A184I	100	3	2	3	2	89
5	GV/A184I/I263G/A328G	15	27	0	19	19	35
6	GV/L188Q	100	3	1	8	9	79
7	GV/L188Q/A264G	13	2	1	8	14	75
8	GV/L188Q/A328G	100	0	0	3	2	95
9	GV/L188Q/A330W	10	0	0	0	0	100
10	GV/L188Q/I263G	34	0	0	0	0	100
11	GV/L188Q/I263G/A328L	19	69	0	0	0	31
12	GV/L188Q/I263G/V78L	19	4	0	48	12	36
13	K19/F87A/A82M	100	9	0	4	16	71
14	K19/F87A/A82M/A330W	91	13	10	43	22	12
15	K19/F87A/A82M/ I263G	97	7	5	27	3	58
16	K19/F87A/F81W	16	0	6	42	9	44
17	K19/F87A/I263A	98	3	0	37	45	15
18	K19/F87A/I263G	95	15	35	11	16	23
19	K19/F87V	100	2	1	13	10	73
20	K19/F87V/A264G	96	4	1	16	18	61
21	K19/F87V/A328V	66	75	14	5	3	4
22	K19/F87V/E267V	98	16	0	12	29	43
23	K19/F87V/E267V/V78I	48	18	2	17	24	39
24	K19/F87V/I263G	92	36	6	12	12	34
25	K19/F87V/Q403P	100	0	1	27	15	57
26	KT2/L188G/I263G	100	4	3	17	22	54
27	KU3/A330P/A328I	2	0	0	80	0	20
28	KU3/A330P/I263A	19	19	0	32	29	19
29	KU3/A330P/S7W	54	39	2	18	20	22
30	R19	1	0	0	0	0	100
31	R19/A328L/I263A	100	83	0	8	5	4
32	R19/A330W	90	2	4	39	47	9
33	R19/F87A	100	1	0	17	28	53
34	R19/F87A/A184I	100	4	1	37	22	35
35	R19/F87A/A184I/S72W	96	61	11	6	6	16
36	R19/F87A/A184I/	2	26	1	24	20	29

	V78I						
37	R19/F87A/A328G	100	4	0	16	24	56
38	R19/F87A/A328G/P329G/ A330G	96	0	0	62	33	5
39	R19/F87A/A328L	25	73	4	0	0	24
40	R19/F87A/F81W/ T260G/ A328G	6	4	0	33	38	25
41	R19/F87A/ G265GG	13	0	0	85	15	0
42	R19/F87A/I263G	100	4	11	4	17	64
43	R19/F87A/I263G/ A264G	34	20	0	28	1	51
44	R19/F87A/T260G	16	26	1	28	26	19
45	R19/F87A/T260G/A328G	100	1	0	35	47	17
46	R19/F87I	91	53	6	14	11	17
47	R19/F87I/L437F	70	53	0	1	1	45
48	R19/F87I/L437LV	100	79	2	0	1	18
49	R19/S72G/A330W	66	3	3	46	42	6
50	RP/A82M/I263A	30	25	0	37	32	6
51	RP/H171L/I263G	100	10	3	0	1	87
52	RP/H171L/I263G/A184I	2	9	3	24	27	37
53	RP/V87I/E267V	96	5	2	45	20	28
54	RT2	70	10	1	59	22	9
55	VQ/S72G/A330W	91	0	0	0	0	100
56	WT	91	0	0	42	33	25

8.2 Selectivity of α′-OH from Mutagenesis

8.2.1 First Generation Mutagenesis

Entry	Mutant	Conv. (%)	Select. 3.13c (%)
1	R19/A184I/A328L/I263R	6	6
2	R19/A184I/A328L/I263F	4	12
3	R19/A184I/A328L/T438L	20	19
4	R19/A184I/A328L/I263W	10	11
5	R19/A184I/A328L/I263S	86	8
6	R19/A184I/A328L/V26M	3	9
7	R19/A184I/A328L/V26L	30	28
8	R19/A184I/A328L/L181F	6	4
9	R19/A184I/A328L/ L181M	28	10
10	R19/A184I/A328L/T268S	15	56
11	R19/A184I/A328L/T438F	4	5
12	R19/A328L/V178W	11	8
13	R19/A184I/A328L/V178F	9	7
14	R19/A184I/A328L/A264F	5	5

15	R19/A184I/A328L/T436F	29	14
16	R19/A184I/A328L/V26F	2	0

8.2.2. Second Generation Mutagenesis

Entry	Mutant	Conv. (%)	Select. 3.13c (%)
1	R19/A184I/A328L/T268S/V26M	15	74
2	R19/A184I/A328L/T268S/V26F	0	0
3	R19/A184I/A328L/T268S/V26L	18	68
4	R19/A184I/A328L/T268S/V26H	0	0
5	R19/A184I/A328L/T268S/S72F	22	58
6	R19/A184I/A328L/T268S/S72W	34	65
7	R19/A184I/A328L/T268S/S72H	0	0
8	R19/A184I/A328L/T268S/S72Y	30	62
9	R19/A184I/A328L/T268S/S72D	0	0
10	R19/A184I/A328L/T268S/L437LV	0	0
11	R19/A184I/A328L/T268S/L437VL	0	0
12	R19/A184I/A328L/T268S/L437M	33	65
13	R19/A184I/A328L/T268S/L437LS	0	0
14	R19/A184I/A328L/T268S/L437F	25	67
15	R19/A184I/A328L/T268S/L437W	12	0
16	R19/A184I/A328L/T268S/L437D	22	0
17	R19/A184I/A328L/T268S/S332F	0	0
18	R19/A184I/T268S/P329W	27	73
19	R19/A184I/T268S/P329F	48	20
20	R19/A184I/A328L/T268S/M354F	0	0
21	R19/A184I/A328L/T268S/M354W	0	0

8.2.3 Third Generation Mutagenesis

Entry	Mutant	Conv. (%)	Select. 3.13c (%)
1	R19/A184I/P329W/I263R	12	6
2	R19/A184I/T268S/P329W/V78W	8	25
3	R19/A184I/A328L/T268S/V26M/S72W	32	64
4	R19/A184I/A328L/T268S/V26M/L188Q	14	54
5	R19/A184I/T268S/V26M/P329V/A330P	11	9
6	R19/A184I/T268S/P329W/V78N	28	55
7	R19/A184I/T268S/V26M/A330F	75	1
8	R19/A184I/T268S/P329W/V78M	7	10
9	R19/A184I/A328L/T268S/V26M/M354W	12	60
10	R19/A184I/A328L/T268S/V26M/L437M	42	57
11	R19/A184I/T268S/P329W/V78N	14	45

12	R19/A184I/A328L/T268S/V26M/A330L	31	52
13	R19/A184I/A328L/T268S/V26M/L437F	57	67
14	R19/A184I/T268S/P329W/S72F	36	47
15	R19/A184I/A328L/T268S/V26M/L437LV	6	30
16	R19/A184I/T268S/V26M/P329F	15	9
17	R19/A184I/A328L/T268S/V26M/S72F	6	36
18	R19/A184I/A328L/T268S/V26M/S72R	0	0
19	R19/A184I/A328L/T268S/V26M/L188F	1	43
20	R19/A328L/T268S/V26M/L181M	1	0
21	R19/A184I/A328L/T268S/V26M/M354F	2	28
22	R19/A184I/T268S/V26M/S332M	63	5
23	R19/A184I/A328L/T268S/V26M/L75F	83	24
24	R19/A184I/A328L/T268S/V26M/S332F	29	37
25	R19/A184I/A328L/T268S/V26M/T438F	2	6
26	R19/A184I/A328L/T268S/V26M/L188F	27	61

8.2.4 Fourth Generation Mutagenesis

Entry	Mutant	Conv. (%)	Select. 3.13c (%)
1	R19/A328L/T268S/V26M/L437F/L181M	13	44
2	R19/A184I/A328L/T268S/V26M/E435Q	71	17
3	R19/A184I/A328L/T268S/V26M/E435R	61	44
4	R19/A184I/A328L/T268S/V26M/L437F/M354W	70	17
5	R19/A184I/A328L/T268S/V26M/L437F/V78Q	63	16
6	R19/A328L/T268S/V26M/L437F/I184M	65	18
7	R19/A184I/A328L/T268S/V26M/E435H	71	17
8	R19/A328L/T268S/V26M/L437F/I184F	27	35
9	R19/A184I/A328L/T268S/V26M/L437F/V78W	6	20
10	R19/A184I/A328L/T268S/V26M/L437F/V78Y	12	18
11	R19/A184I/A328L/T268S/V26M/E435W	4	61
12	R19/A184I/A328L/T268S/V26M/L437F/A74G/V78F	13	10
13	R19/A184I/A328L/T268S/V26M/L437F/A74L	39	62
14	R19/A184I/A328L/T268S/V26M/E435M	65	0
15	R19/A184I/A328L/T268S/L437F/P25G	29	63
16	R19/A184I/A328L/T268S/V26M/L437F/L181F	0	0
17	R19/A184I/A328L/T268S/V26M/L437F/A74G/V78W	0	62
18	R19/A184I/A328L/T268S/V26M/E435F	3	73
19	R19/A184I/A328L/T268S/V26M/L437F/V78M	12	11
20	R19/A184I/A328L/T268S/V26M/L437F/A74V	28	64
21	R19/A184I/A328L/T268S/V26M/L437F/M354F	38	65

8.3 Flexible Residues in ADFR Docking Studies

8.3.1 *N*-Bn [6.3]-spirocycle 4.56

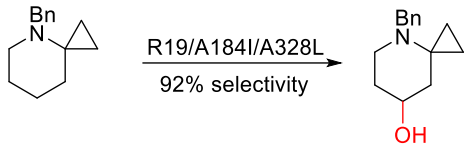

4.56 **4.56a**

Substrate	Mutant	Flexible Residues
4.56	R19/A184I/A328L	Phe87
		Ile184
		Leu328

8.3.2 Flexible Residues for Docking-Guided Mutagenesis Studies

8.3.2.1 First Generation Mutagenesis

Substrate	Mutant	Flexible Residues
3.13	R19/A184I/A328L/I263R	F87
		I184
		L328
		R263
	R19/A184I/A328L/I263F	F87
		I184
		L328
		F263
	R19/A184I/A328L/T438L	F87
		I184
		L328
		L438
	R19/A184I/A328L/I263W	F87
		I184
		L328
		W263
	R19/A184I/A328L/I263S	F87
		I184
		L328
		S263
	R19/A184I/A328L/V26M	F87
		I184

		L328
		M26
	R19/A184I/A328L/V26L	F87
		I184
		L328
		L26
	R19/A184I/A328L/L181F	F87
		I184
		L328
		F181
	R19/A184I/A328L/ L181M	F87
		I184
		L328
		M181
	R19/A184I/A328L/T268S	F87
		I184
		L328
		S268
	R19/A184I/A328L/T438F	F87
		I184
		L328
		F438
	R19/A328L/V178W	F87
		I184
		L328
		W178
	R19/A184I/A328L/V178F	F87
		I184
		L328
		F178
	R19/A184I/A328L/A264F	F87
		I184
		L328
		F264
	R19/A184I/A328L/T436F	F87
		I184
		L328
		F436
	R19/A184I/A328L/V26F	F87
		I184
		L328
		F26

8.3.2.2 Second Generation Mutagenesis

Substrate	Mutant	Flexible Residues
3.13	R19/A184I/A328L/T268S/V26M	F87
		I184
		L328
		S268
		M26
	R19/A184I/A328L/T268S/V26F	F87
		I184
		L328
		S268
		F26
	R19/A184I/A328L/T268S/V26L	F87
		I184
		L328
		S268
		L26
	R19/A184I/A328L/T268S/V26H	F87
		I184
		L328
		S268
		H26
	R19/A184I/A328L/T268S/S72F	F87
		I184
		L328
		S268
		F72
	R19/A184I/A328L/T268S/S72W	F87
		I184
		L328
		S268
		W72
	R19/A184I/A328L/T268S/S72H	F87
		I184
		L328
		S268
		H72
	R19/A184I/A328L/T268S/S72Y	F87
		I184
		L328
		S268
		Y72
	R19/A184I/A328L/T268S/S72D	F87
		I184
		L328
		S268
		D72
	R19/A184I/A328L/T268S/L437LV	F87
		I184

		L328
		S268
		V438
	R19/A184I/A328L/T268S/L437VL	ADFR was not performed due to lack of crystal structure with L437VL mutations
	R19/A184I/A328L/T268S/L437M	F87
		I184
		L328
		S268
		M437
	R19/A184I/A328L/T268S/L437LS	F87
		I184
		L328
		S268
		S438
	R19/A184I/A328L/T268S/L437F	F87
		I184
		L328
		S268
		F437
	R19/A184I/A328L/T268S/L437W	F87
		I184
		L328
		S268
		W437
	R19/A184I/A328L/T268S/L437D	F87
		I184
		L328
		S268
		D437
	R19/A184I/A328L/T268S/S332F	F87
		I184
		L328
		S268
		F332
	R19/A184I/T268S/P329W	F87
		I184
		L328
		S268
		W329
	R19/A184I/T268S/P329F	F87
		I184
		L328
		S268
		F329
	R19/A184I/A328L/T268S/M354F	F87
		I184

		L328
		S268
		F354
	R19/A184I/A328L/T268S/M354W	F87
		I184
		L328
		S268
		W354

8.3.3.3 Third Generation Mutagenesis

Substrate	Mutant	Flexible Residues
3.13	R19/A184I/P329W/I263R	F87
		I184
		W329
		R263
	R19/A184I/T268S/P329W/V78W	F87
		I184
		S268
		W329
		W78
	R19/A184I/A328L/T268S/V26M/S72W	F87
		I184
		L328
		S268
		M26
		W72
	R19/A184I/A328L/T268S/V26M/L188Q	F87
		I184
		L328
		S268
		M26
		Q188
	R19/A184I/T268S/V26M/P329V/A330P	F87
		I184
		S268
		M26
		V329
		P330
	R19/A184I/T268S/P329W/V78N	F87
		I184
		S268
		W329
		N78
	R19/A184I/T268S/V26M/A330F	F87
		I184
		S268
		M26

		F330
	R19/A184I/T268S/P329W/V78M	F87
		I184
		S268
		W329
		M78
	R19/A184I/A328L/T268S/V26M/M354W	F87
		I184
		L328
		S268
		M26
		W354
	R19/A184I/A328L/T268S/V26M/L437M	F87
		I184
		L328
		S268
		M26
		M437
	R19/A184I/T268S/P329W/V78N	F87
		I184
		S268
		W329
		N78
	R19/A184I/A328L/T268S/V26M/A330L	F87
		I184
		L328
		S268
		M26
		L330
	R19/A184I/A328L/T268S/V26M/L437F	F87
		I184
		L328
		S268
		M26
		F437
	R19/A184I/T268S/P329W/S72F	F87
		I184
		S268
		W329
		F72
	R19/A184I/A328L/T268S/V26M/L437LV	F87
		I184
		L328
		S268
		M26
		V438
	R19/A184I/T268S/V26M/P329F	F87
		I184
		S268
		M26
		F329

	R19/A184I/A328L/T268S/V26M/S72F	F87
		I184
		L328
		S268
		M26
		F72
	R19/A184I/A328L/T268S/V26M/S72R	F87
		I184
		L328
		S268
		M26
		R72
	R19/A184I/A328L/T268S/V26M/L188F	F87
		I184
		L328
		S268
		M26
		F188
	R19/A328L/T268S/V26M/L181M	F87
		L328
		S268
		M26
		M181
	R19/A184I/A328L/T268S/V26M/M354F	F87
		I184
		L328
		S268
		M26
		F354
	R19/A184I/T268S/V26M/S332M	F87
		I184
		S268
		M26
		M332
	R19/A184I/A328L/T268S/V26M/L75F	F87
		I184
		L328
		S268
		M26
		F75
	R19/A184I/A328L/T268S/V26M/S332F	F87
		I184
		L328
		S268
		M26
		F332
	R19/A184I/A328L/T268S/V26M/T438F	F87
		I184
		L328
		S268
		M26

		F438
	R19/A184I/A328L/T268S/V26M/L188F	F87
		I184
		L328
		S268
		M26
		F188

8.3.3.4 Fourth Generation Mutagenesis

Substrate	Mutant	Flexible Residues
3.13	R19/A328L/T268S/V26M/L437F/L181M	F87
		L328
		S268
		M26
		F437
		M181
	R19/A184I/A328L/T268S/V26M/E435Q	F87
		I184
		L328
		S268
		M26
		Q435
	R19/A184I/A328L/T268S/V26M/E435R	F87
		I184
		L328
		S268
		M26
		R435
	R19/A184I/A328L/T268S/V26M/L437F/M354W	F87
		I184
		L328
		S268
		M26
		F437
		W354
	R19/A184I/A328L/T268S/V26M/L437F/V78Q	F87
		I184
		L328
		S268
		M26
		F437
		Q78
	R19/A328L/T268S/V26M/L437F/I184M	F87
		L328
		S268
		M26
		F437

		M184
	R19/A184I/A328L/T268S/V26M/E435H	F87
		I184
		L328
		S268
		M26
		H435
	R19/A328L/T268S/V26M/L437F/I184F	F87
		L328
		S268
		M26
		F437
		F184
	R19/A184I/A328L/T268S/V26M/L437F/V78W	F87
		I184
		L328
		S268
		M26
		F437
		W78
	R19/A184I/A328L/T268S/V26M/L437F/V78Y	F87
		I184
		L328
		S268
		M26
		F437
		Y78
	R19/A184I/A328L/T268S/V26M/E435W	F87
		I184
		L328
		S268
		M26
		W435
	R19/A184I/A328L/T268S/V26M/L437F/A74G/V78F	F87
		I184
		L328
		S268
		M26
		F437
		F78
	R19/A184I/A328L/T268S/V26M/L437F/A74L	F87
		I184
		L328
		S268
		M26
		F437
		L74
	R19/A184I/A328L/T268S/V26M/E435M	F87
		I184
		L328
		S268

		M26
		M435
	R19/A184I/A328L/T268S/L437F/P25G	F87
		I184
		L328
		S268
		F437
	R19/A184I/A328L/T268S/V26M/L437F/L181F	F87
		I184
		L328
		S268
		M26
		F437
		F181
	R19/A184I/A328L/T268S/V26M/L437F/A74G/ V78W	F87
		I184
		L328
		S268
		M26
		F437
		W78
	R19/A184I/A328L/T268S/V26M/E435F	F87
		I184
		L328
		S268
		M26
		F435
	R19/A184I/A328L/T268S/V26M/L437F/V78M	F87
		I184
		L328
		S268
		M26
		F437
		M78
	R19/A184I/A328L/T268S/V26M/L437F/A74V	F87
		I184
		L328
		S268
		M26
		F437
		V74
	R19/A184I/A328L/T268S/V26M/L437F/M354F	F87
		I184
		L328
		S268
		M26
		F437
		F354
	R19/A328L/T268S/V26M/L437F/L181M	F87
		L328
		S268

		M26
		F437
		M181

References

1. Newman, D. J., Cragg, G. M. and Snader, K. M., *Nat Prod Rep*, 2000, **17**, 215-234.
2. Fowler, C. J., *Pharmacopoeia Londinensis*, Royal College of Physicians London, 1618.
3. Drews, J., *Science*, 2000, **287**, 1960-1964.
4. Moore, F. J., *A History of Chemistry*, McGraw-Hill, New York, 1918.
5. Roberts, A. M., *Seredipity*, Wiley, New York, 1989.
6. Parascandola, J. and R., J., *Bull. Hist. Med.*, 1974, **48**, 199-220.
7. Maehle, A. H., Prull, C. R. and Halliwell, R. F., *Nat. Rev. Drug Discov.*, 2002, **1**, 637-641.
8. Fleming, A., *Br. J. Exp. Pathol.*, 1920, **10**, 226-236.
9. Lombardino, J. G. and Lowe, J. A., 3rd, *Nat Rev Drug Discov*, 2004, **3**, 853-862.
10. Triggle, D. J., *Med Princ Pract*, 2007, **16**, 1-14.
11. Liu, R., Li, X. and Lam, K. S., *Curr Opin Chem Biol*, 2017, **38**, 117-126.
12. Consortium, I. H. G. S., *Nature*, 2001, 860-921.
13. Consortium, I. H. G. S., *Nature*, 2004, **431**, 931-945.
14. Szymanski, P., Markowicz, M. and Mikiciuk-Olasik, E., *Int J Mol Sci*, 2012, **13**, 427-452.
15. Barker, A., Kettle, J. G., Nowak, T. and Pease, J. E., *Drug Discov Today*, 2013, **18**, 298-304.
16. McGovern, S. L., Caselli, E., Grigorieff, N. and Shoichet, B. K., *J. Med. Chem.*, 2002, **45**, 1712-1722.
17. Paul, S. M., Mytelka, D. S., Dunwiddie, C. T., Persinger, C. C., Munos, B. H., Lindborg, S. R. and Schacht, A. L., *Nat Rev Drug Discov*, 2010, **9**, 203-214.
18. Fox, S., Farr-Jones, S., Sopchak, L., Boggs, A., Nicely, H. W., Khoury, R. and Biros, M., *J Biomol Screen*, 2006, **11**, 864-869.
19. Macarron, R., *Drug Discov Today*, 2006, **11**, 277-279.
20. Macarron, R., Banks, M. N., Bojanic, D., Burns, D. J., Cirovic, D. A., Garyantes, T., Green, D. V., Hertzberg, R. P., Janzen, W. P., Paslay, J. W., Schopfer, U. and Sittampalam, G. S., *Nat Rev Drug Discov*, 2011, **10**, 188-195.
21. Bollag, G., Hirth, P., Tsai, J., Zhang, J., Ibrahim, P. N., Cho, H., Spevak, W., Zhang, C., Zhang, Y., Habets, G., Burton, E. A., Wong, B., Tsang, G., West, B. L., Powell, B., Shellooe, R., Marimuthu, A., Nguyen, H., Zhang, K. Y., Artis, D. R., Schlessinger, J., Su, F., Higgins, B., Iyer, R., D'Andrea, K., Koehler, A., Stumm, M., Lin, P. S., Lee, R. J., Grippo, J., Puzanov, I., Kim, K. B., Ribas, A., McArthur, G. A., Sosman, J. A., Chapman, P. B., Flaherty, K. T., Xu, X., Nathanson, K. L. and Nolop, K., *Nature*, 2010, **467**, 596-599.
22. Bollag, G., Tsai, J., Zhang, J., Zhang, C., Ibrahim, P., Nolop, K. and Hirth, P., *Nat Rev Drug Discov*, 2012, **11**, 873-886.
23. Erlanson, D. A., Fesik, S. W., Hubbard, R. E., Jahnke, W. and Jhoti, H., *Nat Rev Drug Discov*, 2016, **15**, 605-619.
24. Erlanson, D. A., McDowell, R. S. and O'brien, T., *J. Med. Chem.*, 2004, **47**.
25. Murray, C. W. and Rees, D. C., *Nat Chem*, 2009, **1**, 187-192.
26. Doak, B. C., Morton, C. J., Simpson, J. S. and Scanlon, M. J., *Australian Journal of Chemistry*, 2013, **66**.
27. Jacquemard, C. and Kellenberger, E., *Expert Opin Drug Discov*, 2019, **14**, 413-416.
28. S., B. R., McMartin, C. and Guida, W. C., *Med. Res. Rev.*, 1996, **16**, 3-50.
29. Fink, T., Bruggesser, H. and Reymond, J. L., *Angew Chem Int Ed Engl*, 2005, **44**, 1504-1508.

30. Hann, M. M. and Oprea, T. I., *Curr Opin Chem Biol*, 2004, **8**, 255-263.
31. Kuntz, I. D., Chen, K., Sharp, K. A. and Kollman, P. A., *Proc. Natl. Acad. Sci. USA*, 1999, **96**, 9997-10002.
32. Reynolds, C. H., Bembenek, S. D. and Tounge, B. A., *Bioorg Med Chem Lett*, 2007, **17**, 4258-4261.
33. Bembenek, S. D., Tounge, B. A. and Reynolds, C. H., *Drug Discov Today*, 2009, **14**, 278-283.
34. Tsai, J., Lee, J. T., Wang, W., Zhang, J., Cho, H., Mamo, S., Bremer, R., Gillette, S., Kong, J., Haass, N. K., Sproesser, K., Li, L., Smalley, K. S. M., Fong, D., Zhu, Y. L., Marimuthu, A., Nguyen, H., Lam, B., Liu, J., Cheung, I., Rice, J., Suzuki, Y. and Bollag, G., *Proc. Natl. Acad. Sci. USA*, 2008, **105**, 3041-3046.
35. Zhang, C., Ibrahim, P. N., Zhang, J., Burton, E. A., Habets, G., Zhang, Y., Powell, B., West, B. L., Matusow, B., Tsang, G., Shellooe, R., Carias, H., Nguyen, H., Marimuthu, A., Zhang, K. Y., Oh, A., Bremer, R., Hurt, C. R., Artis, D. R., Wu, G., Nespi, M., Spevak, W., Lin, P., Nolop, K., Hirth, P., Tesch, G. H. and Bollag, G., *Proc Natl Acad Sci U S A*, 2013, **110**, 5689-5694.
36. Souers, A. J., Leverson, J. D., Boghaert, E. R., Ackler, S. L., Catron, N. D., Chen, J., Dayton, B. D., Ding, H., Enschede, S. H., Fairbrother, W. J., Huang, D. C., Hymowitz, S. G., Jin, S., Khaw, S. L., Kovar, P. J., Lam, L. T., Lee, J., Maecker, H. L., Marsh, K. C., Mason, K. D., Mitten, M. J., Nimmer, P. M., Oleksijew, A., Park, C. H., Park, C. M., Phillips, D. C., Roberts, A. W., Sampath, D., Seymour, J. F., Smith, M. L., Sullivan, G. M., Tahir, S. K., Tse, C., Wendt, M. D., Xiao, Y., Xue, J. C., Zhang, H., Humerickhouse, R. A., Rosenberg, S. H. and Elmore, S. W., *Nat Med*, 2013, **19**, 202-208.
37. Murray, C. W., Newell, D. R. and Angibaud, P., *MedChemComm*, 2019, **10**, 1509-1511.
38. Morley, A. D., Pugliese, A., Birchall, K., Bower, J., Brennan, P., Brown, N., Chapman, T., Drysdale, M., Gilbert, I. H., Hoelder, S., Jordan, A., Ley, S. V., Merritt, A., Miller, D., Swarbrick, M. E. and Wyatt, P. G., *Drug Discov Today*, 2013, **18**, 1221-1227.
39. Leung, C. S., Leung, S. S., Tirado-Rives, J. and Jorgensen, W. L., *J Med Chem*, 2012, **55**, 4489-4500.
40. Zhao, H., Serby, M. D., Xin, Z., Szczepankiewicz, B. G., Liu, M., Kosogof, C., Liu, B., Nelson, L. T. J., Johnson, E. F., Wang, S., Pederson, T., Gum, R. J., Clampit, J. E., Haasch, D. L., Zapatero, C. A., Fry, E. H., Rondinone, C., Trevillyan, J. M., Sham, H. L. and Liu, G., *J. Med. Chem.*, 2006, **49**, 4455-4458.
41. Wood, W. J. L., Patterson, A. W., Tsuruoka, H., Jain, R. K. and Ellman, J. A., *J. Am. Chem. Soc.*, 2005, **127**, 15521-15527.
42. Ward, Y. D., Thomson, D. S., Frye, L. L., Cywin, C. L., Morwick, T., Emmanuel, M. J., Zindell, R., McNeil, D., Bekkali, Y., Girardot, M., Hrapchak, M., DeTuri, M., Crane, K., White, D., Pav, S., Wang, Y., Hao, M. H. and Spero, D. M., *J. Med. Chem.*, 2002, **45**, 5471-5482.
43. Jhoti, H., Cleasby, A., Verdonk, M. and Williams, G., *Curr Opin Chem Biol*, 2007, **11**, 485-493.
44. Forino, M., Johnson, S., Wong, T. Y., Rozanov, D. V., Savinov, A. Y., Li, W., Fattorusso, R., Becattini, B., Orry, A. J., Jung, D., Abagyan, R. A., Smith, J. W., Alibek, K., Liddington, R. C., Strongin, A. Y. and Pellecchia, M., *Proc. Natl. Acad. Sci. USA*, 2005, **102**, 9499-9504.
45. Wyss, D. F., Arasappan, A., Senior, M. M., Wang, Y. S., Beyer, B. M., Njoroge, F. G. and McCoy, M. A., *J. Med. Chem.*, 2004, **47**, 2486-2498.

46. Erlanson, D. A., Lam, J. W., Wiesmann, C., Luong, T. N., Simmons, R. L., DeLano, W. L., Choong, I. C., Burdett, M. T., Flanagan, W. M., Lee, D., Gordon, E. M. and O'Brien, T., *Nat Biotechnol*, 2003, **21**, 308-314.
47. O'Brien, T., Fahr, B. T., Sopko, M. M., Lam, J. W., Waal, N. D., Raimundo, B. C., Purkey, H. E., Pham, P. and Romanowski, M. J., *Acta Crystallogr Sect F Struct Biol Cryst Commun*, 2005, **61**, 451-458.
48. Masters, S. L., Simon, A., Aksentijevich, I. and Kastner, D. L., *Annu Rev Immunol*, 2009, **27**, 621-668.
49. Li, Q., *Front Mol Biosci*, 2020, **7**, 180.
50. Hudson, S. A., McLean, K. J., Surade, S., Yang, Y. Q., Leys, D., Ciulli, A., Munro, A. W. and Abell, C., *Angew Chem Int Ed Engl*, 2012, **51**, 9311-9316.
51. Miyake, Y., Itoh, Y., Hatanaka, A., Suzuma, Y., Suzuki, M., Kodama, H., Arai, Y. and Suzuki, T., *Bioorg Med Chem*, 2019, **27**, 1119-1129.
52. Jenuwein, T. and Allis, C. D., *Science*, 2001, **293**, 1074-1080.
53. Itoh, Y., Sawada, H., Suzuki, M., Tojo, T., Sasaki, R., Hasegawa, M., Mizukami, T. and Suzuki, T., *ACS Med Chem Lett*, 2015, **6**, 665-670.
54. Lovering, F., Bikker, J. and Humblet, C., *J Med Chem*, 2009, **52**, 6752-6756.
55. Marson, C. M., *Chem Soc Rev*, 2011, **40**, 5514-5533.
56. Muller, G., Berkenbosch, T., Benningshof, J. C., Stumpfe, D. and Bajorath, J., *Chemistry*, 2017, **23**, 703-710.
57. Jampilek, J., *Molecules*, 2019, **24**.
58. Vitaku, E., Smith, D. T. and Njardarson, J. T., *J Med Chem*, 2014, **57**, 10257-10274.
59. Walsh, C. T., *Tetrahedron Letters*, 2015, **56**, 3075-3081.
60. Zheng, Y., Tice, C. M. and Singh, S. B., *Bioorg Med Chem Lett*, 2014, **24**, 3673-3682.
61. Thomas, A. W., Krafft, E. A., Kurt, A., Maier, A. and Zimmerli, D., *Synthesis*, 2005, DOI: 10.1055/s-2005-918454, 3245-3252.
62. Zheng, Y. J. and Tice, C. M., *Expert Opin Drug Discov*, 2016, **11**, 831-834.
63. Sveiczer, A., North, A. J. P., Mateu, N., Kidd, S. L., Sore, H. F. and Spring, D. R., *Org Lett*, 2019, **21**, 4600-4604.
64. Geoghegan, K. and Bode, J. W., *Org Lett*, 2015, **17**, 1934-1937.
65. Melnykov, K. P., Artemenko, A. N., Ivanenko, B. O., Sokolenko, Y. M., Nosik, P. S., Ostapchuk, E. N., Grygorenko, O. O., Volochnyuk, D. M. and Ryabukhin, S. V., *ACS Omega*, 2019, **4**, 7498-7515.
66. Mullen, P., Miel, H. and Anthony McKervey, M., *Tetrahedron Letters*, 2010, **51**, 3216-3217.
67. Emmons, W. D., *J. Am. Chem. Soc.*, 1953, **75**, 4623-4624.
68. Kolocouris, N., Kolocouris, A., Foscolos, G. B., Fytas, G., Neyts, J., Padalko, E., Balzarini, J., Snoeck, R., Andrei, G. and De Clercq, E., *J. Med. Chem.*, 1996, **39**, 3307-3318.
69. Lesma, G., Landoni, N., Sacchetti, A. and Silvani, A., *Tetrahedron*, 2010, **66**, 4474-4478.
70. Martinez-Alsina, L. A., Murray, J. C., Buzon, L. M., Bundesmann, M. W., Young, J. M. and O'Neill, B. T., *J Org Chem*, 2017, **82**, 12246-12256.
71. Palmer, N., Peakman, T. M., Norton, D. and Rees, D. C., *Org Biomol Chem*, 2016, **14**, 1599-1610.
72. Congreve, M., Carr, R., Murray, C. and Jhoti, H., *Drug Discovery Today*, 2003, **8**, 876-877.
73. Jenkins, I. D., Lacrampe, F., Ripper, J., Alcaraz, L., Van Le, P., Nikolakopoulous, G., Leone, P. A., White, R. H. and Quinn, R. J., *J. Org. Chem.*, 2009, **74**, 1304-1313.
74. Pfefferkorn, J. A. and Choi, C., *Tetrahedron Letters*, 2008, **49**, 4372-4373.

75. Guazzelli, G., Duffy, L. A. and Procter, D. J., *Org. Lett.*, 2008, **10**, 4291-4294.
76. Vo, C. V., Mikutis, G. and Bode, J. W., *Angew Chem Int Ed Engl*, 2013, **52**, 1705-1708.
77. Luescher, M. U. and Bode, J. W., *Org Lett*, 2016, **18**, 2652-2655.
78. Lin, M.-N., Wu, S.-H. and Yeh, M.-C. P., *Advanced Synthesis & Catalysis*, 2011, **353**, 3290-3294.
79. Huard, K., Bagley, S. W., Menhaji-Klotz, E., Preville, C., Southers, J. A., Jr., Smith, A. C., Edmonds, D. J., Lucas, J. C., Dunn, M. F., Allanson, N. M., Blaney, E. L., Garcia-Irizarry, C. N., Kohrt, J. T., Griffith, D. A. and Dow, R. L., *J Org Chem*, 2012, **77**, 10050-10057.
80. King, T. A., Stewart, H. L., Mortensen, K. T., North, A. J. P., Sore, H. F. and Spring, D. R., *European J Org Chem*, 2019, **2019**, 5219-5229.
81. Griggs, S. D., Tape, D. T. and Clarke, P. A., *Org Biomol Chem*, 2018, **16**, 6620-6633.
82. Godula, K. and Sames, D., *Science*, 2006, **312**.
83. Wencel-Delord, J. and Glorius, F., *Nat Chem*, 2013, **5**, 369-375.
84. Chu, J. C. K. and Rovis, T., *Angew Chem Int Ed Engl*, 2018, **57**, 62-101.
85. Friese, F. W., Muck-Lichtenfeld, C. and Studer, A., *Nat Commun*, 2018, **9**, 2808.
86. Hong, B., Li, C., Wang, Z., Chen, J., Li, H. and Lei, X., *J Am Chem Soc*, 2015, **137**, 11946-11949.
87. Breslow, R. and Gellman, S. H., *J. Am. Chem. Soc.*, 1983, **105**, 6728-6729.
88. Espino, C. G. and Du Bois, J., *Angew. Chem. Int. Ed.*, 2001, **40**, 598-600.
89. Espino, C. G., Fiori, K. W., Kim, M. and Du Bois, J., *J. Am. Chem. Soc.*, 2004, **126**, 15378-15379.
90. Roizen, J. L., Harvey, M. E. and Du Bois, J., *Acc. Chem. Res.*, 2012, **45**, 911-922.
91. Hrdina, R., Metz, F. M., Larrosa, M., Berndt, J.-P., Zhygadlo, Y. Y., Becker, S. and Becker, J., *European Journal of Organic Chemistry*, 2015, **2015**, 6231-6236.
92. Sofack-Kreutzer, J., Martin, N., Renaudat, A., Jazzar, R. and Baudoin, O., *Angew Chem Int Ed Engl*, 2012, **51**, 10399-10402.
93. Topczewski, J. J., Cabrera, P. J., Saper, N. I. and Sanford, M. S., *Nature*, 2016, **531**, 220-224.
94. Sharpe, R. J. and Johnson, J. S., *J Am Chem Soc*, 2015, **137**, 4968-4971.
95. Larfrance, M., Gorelsky, S. I. and Fagnou, K., *J. Am. Chem. Soc.*, 2007, **129**, 14570-14571.
96. Simmons, E. M. and Hartwig, J. F., *Nature*, 2012, **483**, 70-73.
97. Huang, X., Wang, Y., Lan, J. and You, J., *Angew Chem Int Ed Engl*, 2015, **54**, 9404-9408.
98. Zaitsev, V. G., Shabashov, D. and Daugulis, O., *J. Am. Chem. Soc.*, 2005, **127**, 13154-13155.
99. Rej, S., Das, A. and Chatani, N., *Coordination Chemistry Reviews*, 2021, **431**.
100. Arana-Pena, S., Carballares, D., Morellon-Sterlling, R., Berenguer-Murcia, A., Alcantara, A. R., Rodrigues, R. C. and Fernandez-Lafuente, R., *Biotechnol Adv*, 2021, **51**, 107584.
101. Hollmann, F., Opperman, D. J. and Paul, C. E., *Angew Chem Int Ed Engl*, 2021, **60**, 5644-5665.
102. Bell, E. L., Finnigan, W., France, S. P., Green, A. P., Hayes, M. A., Hepworth, L. J., Lovelock, S. L., Niikura, H., Osuna, S., Romero, E., Ryan, K. S., Turner, N. J. and Flitsch, S. L., *Nature Reviews Methods Primers*, 2021, **1**.
103. Zwick, C. R., 3rd and Renata, H., *J Am Chem Soc*, 2018, **140**, 1165-1169.

104. Loskot, S. A., Romney, D. K., Arnold, F. H. and Stoltz, B. M., *J Am Chem Soc*, 2017, **139**, 10196-10199.
105. Singh, R., Kolev, J. N., Sutera, P. A. and Fasan, R., *ACS Catal*, 2015, **5**, 1685-1691.
106. Jia, Z. J., Gao, S. and Arnold, F. H., *J Am Chem Soc*, 2020, **142**, 10279-10283.
107. Agarwal, V., Miles, Z. D., Winter, J. M., Eustaquio, A. S., El Gamal, A. A. and Moore, B. S., *Chem Rev*, 2017, **117**, 5619-5674.
108. Latham, J., Brandenburger, E., Shepherd, S. A., Menon, B. R. K. and Micklefield, J., *Chem Rev*, 2018, **118**, 232-269.
109. Yokoyama, K. and Lilla, E. A., *Nat Prod Rep*, 2018, **35**, 660-694.
110. Villorbina, G., Roura, L., Camps, F., Joglar, J. and Fabrias, G., *J. Org. Chem.*, 2003, **68**, 2820-2829.
111. Gonzalez, F. J. and Gelboin, H. V., *Environ. Health Perspect.*, 1992, **98**, 81-85.
112. Klingenberg, M., *Arch. Biochem. Biophys.*, 1958, **75**, 376-386.
113. Cooper, D. Y., Levin, S., Narasimhulu, S., Rosenthal, O. and Estabrook, R. W., *Science*, 1965, **147**, 400-402.
114. Lewis, D. F. V. and Hlavica, P., *Biochim. Biophys. Acta*, 2000, **1460**, 353-374.
115. McDonnell, A. M. and Dang, C. H., *J. Adv. Pract. Oncol.* , 2013, **4**, 263-268.
116. Hasemann, C. A., Kurumbali, R. G., Boddupalli, S. S., Peterson, J. A. and Deisenhofer, J., *Structure*, 1995, **2**, 41-62.
117. Rupasinghe, S., Schuler, M. A., Kagawa, N., Yuan, H., Lei, L., Zhao, B., Kelly, S. L., Waterman, M. R. and Lamb, D. C., *FEBS Lett*, 2006, **580**, 6338-6342.
118. Oritz, P. R. and Montellano, O., *Chem. Rev.*, 2010, **110**, 932-948.
119. Sadler, N. C., Nandikonda, P., Webb-Robertson, B. J., Ansong, C., Anderson, L. N., Smith, J. N., Corley, R. A. and Wright, A. T., *Drug Metab. Dispos.*, 2016, **44**, 984-991.
120. Nelson, D. R., Kamataki, T., Waxman, D. J., Guengerich, F. P., Estabrook, R. W., Feyereisen, R., Gongzalez, F. J., Coon, M. J., Gunsalus, I. C., Gotoh, O., Okuda, K. and Nebert, D. W., *DNA Cell Biol.*, 1993, **12**, 1-51.
121. McGourty, J. C. and Silas, J. H., *Br. J. Clin. Pharmac.*, 1985, **20**, 555-566.
122. Leeder, J. S., *Epilepsia*, 1998, **39**, S8-S16.
123. Guengerich, F. P., *Chem. Res. Toxicol.*, 2000, **14**, 611-650.
124. Waterman, M. R. and Keeney, D. S., *Horm. Res.*, 1992, **38**, 217-221.
125. Whitehouse, C. J., Bell, S. G. and Wong, L. L., *Chem Soc Rev*, 2012, **41**, 1218-1260.
126. Buchana, J. F. and Fulco, A. J., *Biochem. Biophys. Res. Commun.*, 1978, **85**, 1254-1260.
127. Ho, P. P. and Fulco, A. J., *Biochim. Biophys. Acta*, 1976, **431**, 249-256.
128. Miura, Y. and Fulco, A. J., *Journal of Biological Chemistry*, 1974, **249**, 1880-1888.
129. Narhi, L. O. and Fulco, A. J., *Journal of Biological Chemistry*, 1986, **261**, 7160-7169.
130. Narhi, L. O., Kim, K. B., Stevenson, P. M. and Fulco, A. J., *Biochem. Biophys. Res. Commun.*, 1983, **116**, 851-858.
131. Omura, K., Aiba, Y., Onoda, H., Stanfield, J. K., Ariyasu, S., Sugimoto, H., Shiro, Y., Shoji, O. and Watanabe, Y., *Chem Commun (Camb)*, 2018, **54**, 7892-7895.
132. McLean, K. J., Girvan, H. M. and Munro, A. W., *Expert Opin. Drug Metab. Toxicol.*, 2007, **3**, 847-863.
133. Solé, J., Caminal, G., Schürmann, M., Álvaro, G. and Guillén, M., *Journal of Chemical Technology & Biotechnology*, 2019, **94**, 244-255.
134. Li, H. and Poulos, T. L., *Nat. Struct. Biol.*, 1997, **4**, 140-146.

135. Cowart, L. A., Falck, J. R. and Capdevila, J. H., *Archives of Biochemistry and Biophysics*, 2001, **387**, 117-124.
136. Noble, M. A., Miles, C. S., Chapman, S. K., Lysek, D. A., Mackay, A. C., Reid, G. A., Hanzlik, R. P. and Munro, A. W., *Biochem. J.* , 1999, **339**, 371-379.
137. Ost, T. W. B., Miles, C. S., Murdoch, J., Cheung, Y. F., Reid, G. A., Chapman, S. K. and Munro, A. W., *FEBS Lett.*, 2000, **486**, 173-177.
138. Carmichael, A. B. and Wong, L. L., *Eur. J. Biochem.*, 2001, **268**, 3117-3125.
139. Haines, D. C., Tomchick, D. R., Machius, M. and Peterson, J. A., *Biochemistry*, 2001, **40**.
140. Kuper, J., Tee, K. L., Wilmanns, M., Roccatano, D., Schwaneberg, U. and Wong, T. S., *Acta Crystallographica Section F Structural Biology and Crystallization Communications*, 2012, **68**, 1013-1017.
141. Warman, A. J., Neeli, R., Roitel, O., Girvan, H. M., Seward, H. E., Murray, S. A., McLean, K. J., Joyce, M. G., Toogood, H., Holt, R. A. and Munro, A. W., *Biochem. Soc. Trans.*, 2005, **33**, 747-753.
142. Ruettinger, R. T., Wen, L. P. and Fulco, A. J., *Journal of Biological Chemistry*, 1989, **264**, 10987-10995.
143. Uhlmann, H., Kraft, R. and Bernhardt, R., *Journal of Biological Chemistry*, 1994, **269**, 22557-22564.
144. Sherman, D. H., Li, S., Yermalitskaya, L. V., Kim, Y., Smith, J. A., Waterman, M. R. and Podust, L. M., *J Biol Chem*, 2006, **281**, 26289-26297.
145. Li, S., Chaulagain, M. R., Knauff, A. R., Podust, L. M., Montgomery, J. and Sherman, D. H., *Proc. Natl. Acad. Sci. USA*, 2009, **106**, 18463-18468.
146. Menard, A., Fabra, C., Huang, Y. and Auclair, K., *Chembiochem*, 2012, **13**, 2527-2536.
147. Braunegg, G., Raadt, A., Feichtenhofer, S., Grengl, H., Kopper, I., Lehmann, A. and Weber, H. J., *Angew. Chem. Int. Ed.*, 1999, **38**, 2763-2766.
148. Raadt, A., Griengl, H. and Weber, H., *Chem. Eur. J.*, 2001, **7**, 27-31.
149. Landwehr, M., Hochrein, L., Otey, C. R., A., K., Backvall, J. E. and Arnold, F. H., *J. Am. Chem. Soc.*, 2006, **128**, 6058-6059.
150. Munzer, D. F., Meinhold, P., Peters, M. W., Feichtenhofer, S., Griengl, H., Arnold, F. H., Glieder, A. and de Raadt, A., *Chem Commun (Camb)*, 2005, DOI: 10.1039/b501527h, 2597-2599.
151. Li, Z., Jiang, Y., Guengerich, F. P., Ma, L., Li, S. and Zhang, W., *J Biol Chem*, 2020, **295**, 833-849.
152. Bornscheuer, U. T., Huisman, G. W., Kazlauskas, R. J., Lutz, S., Moore, J. C. and Robins, K., *Nature*, 2012, **485**, 185-194.
153. Giver, L., Gershenson, A., Freskgard, P. O. and Arnold, F. H., *Proc. Natl. Acad. Sci. USA*, 1998, **95**, 12809-12813.
154. Farinas, E. T., Schwaneberg, U., Glieder, A. and Arnold, F. H., *Adv. Synth. Catal.*, 2001, **343**, 601-606.
155. Glieder, A., Farinas, E. T. and Arnold, F. H., *Nat Biotechnol*, 2002, **20**, 1135-1139.
156. Meinhold, P., Peters, M. W., Chen, M. M., Takahashi, K. and Arnold, F. H., *Chembiochem*, 2005, **6**, 1765-1768.
157. Fasan, R., Chen, M. M., Crook, N. C. and Arnold, F. H., *Angew Chem Int Ed Engl*, 2007, **46**, 8414-8418.
158. Wang, Z. J., Renata, H., Peck, N. E., Farwell, C. C., Coelho, P. S. and Arnold, F. H., *Angew Chem Int Ed Engl*, 2014, **53**, 6810-6813.
159. Zhang, R. K., Chen, K., Huang, X., Wohlschlager, L., Renata, H. and Arnold, F. H., *Nature*, 2019, **565**, 67-72.
160. Dunham, N. P. and Arnold, F. H., *ACS Catal*, 2020, **10**, 12239-12255.

161. Coelho, P. S., Wang, Z. J., Ener, M. E., Baril, S. A., Kannan, A., Arnold, F. H. and Brustad, E. M., *Nat. Chem. Biol.*, 2013, **9**, 485-487.
162. Brandenberg, O. F., Chen, K. and Arnold, F. H., *J Am Chem Soc*, 2019, **141**, 8989-8995.
163. Hecht, M. H., Richardson, J. S., Richardson, D. C. and Ogden, R. C., *Science*, 1990, **249**, 884-891.
164. Bryson, J. W., Betz, S. F., Lu, H. S., Suich, D. J., Zhou, H. X., O'Neil, K. T. and DeGrado, W. F., *Science*, 1995, **270**, 935-941.
165. Seifert, A., Vomund, S., Grohmann, K., Kriening, S., Urlacher, V. B., Laschat, S. and Pleiss, J., *Chembiochem*, 2009, **10**, 853-861.
166. Whitehouse, C. J., Bell, S. G., Tufton, H. G., Kenny, R. J., Ogilvie, L. C. and Wong, L. L., *Chem Commun (Camb)*, 2008, DOI: 10.1039/b718124h, 966-968.
167. Whitehouse, C. J., Bell, S. G., Yang, W., Yorke, J. A., Blanford, C. F., Strong, A. J., Morse, E. J., Bartlam, M., Rao, Z. and Wong, L. L., *Chembiochem*, 2009, **10**, 1654-1656.
168. Ren, X., Yorke, J. A., Taylor, E., Zhang, T., Zhou, W. and Wong, L. L., *Chemistry*, 2015, **21**, 15039-15047.
169. Ren, X., O'Hanlon, J. A., Morris, M., Robertson, J. and Wong, L. L., *ACS Catalysis*, 2016, **6**, 6833-6837.
170. Syntrivanis, L.-D., Wong, L. L. and Robertson, J., *European Journal of Organic Chemistry*, 2018, **2018**, 6369-6378.
171. Li, Y. and Wong, L. L., *Angew Chem Int Ed Engl*, 2019, **58**, 9551-9555.
172. Karplus, M. and McCammon, J. A., *Nat. Struct. Biol.*, 2002, **9**, 646-652.
173. Hollingsworth, S. A. and Dror, R. O., *Neuron*, 2018, **99**, 1129-1143.
174. DPhil thesis of Yuan Zhang, University of Oxford, 2022.
175. McCammon, J. A., Gelin, B. R. and Karplus, M., *Nature*, 1977, **267**, 585-590.
176. Hospital, A., Goni, J. R., Orozco, M. and Gelpi, J. L., *Adv Appl Bioinform Chem*, 2015, **8**, 37-47.
177. Roy, K., Kar, S. and Das, R. N., in *Understanding the Basics of QSAR for Applications in Pharmaceutical Sciences and Risk Assessment*, Elsevier Inc., New York, 2015, pp. 357-425.
178. Meng, X. Y., Zhang, H. X., Mezei, M. and Cui, M., *Curr. Comput. Aided Drug Des.*, 2011, **7**, 146-157.
179. Fischer, E., *Ber. Dtsch. Chem. Ges.*, 1894, **27**, 2985-2993.
180. Koshland, D. E., *Proc. Natl. Acad. Sci. USA*, 1958, **44**, 98-104.
181. Kille, S., Zilly, F. E., Acevedo, J. P. and Reetz, M. T., *Nat Chem*, 2011, **3**, 738-743.
182. Chen, W., Fisher, M. J., Leung, A., Cao, Y. and Wong, L. L., *ACS Catalysis*, 2020, **10**, 8334-8343.
183. Peng, Y., Gao, C., Zhang, Z., Wu, S., Zhao, J. and Li, A., *ACS Catalysis*, 2022, **12**, 2907-2914.
184. Bovino, M. T., Liwosz, T. W., Kendel, N. E., Miller, Y., Tyminska, N., Zurek, E. and Chemler, S. R., *Angew Chem Int Ed Engl*, 2014, **53**, 6383-6387.
185. Acton, J. J., Bao, J., Egbertson, M., Harrison, S. T., Knowles, S. L., Li, C., Lo, M. M. C., Mazzola, R. D., Meng, Z., Rudd, M. T., Selyutin, O. 3-(lH-Pyrazol-4-yl)pyridineallosteric Modulators of the M4 Muscarinic Acetylcholine Receptor. WO2017/107089A1, June 29, 2017.
186. Stevens, K., Tyrrell, A. J., Skerratt, S. and Robertson, J., *Org. Lett.*, 2011, **13**, 5964 - 5967.
187. SBM CDT Report of Xinlan Cook, University of Oxford, 2017.
188. Hill, R. K. and Conley, R. T., *J. Am. Chem. Soc.* , 1960, **82**, 645 - 652.
189. Hilmey, D. G. and Paquette, L. A., *Org. Lett.*, 2005, **7**, 2067 - 2069.

190. Kanaoka, Y., Yonemitsu, O., Sato, E. and Ban, Y., *Chem. Pharm. Bull.*, 1968, **16**, 280 - 284.
191. Niemczak, M., Czerniak, K. and Kopczyński, T., *New Journal of Chemistry*, 2015, **39**, 1868-1873.
192. Dixon, L. A. Encyclopedia of Reagents for Organic Synthesis - Polyphosphate Ester. John Wiley & Sons, Ltd.: New York, 2001.
193. Cava, M. P., Lakshmikantham, M. V. and Mitchell, M. J., *J. Org. Chem.*, 1969, **34**, 2665 - 2667.
194. Kornblum, N. and Powers, J. W., *J. Org. Chem.*, 1957, **22**, 455 - 456.
195. Ono, N., Kamimura, A., Miyake, H., Hamamoto, I. and Kaji, A., *J. Org. Chem.*, 1985, **50**, 3692 - 3698.
196. DPhil thesis of Leonidas Syntrivanis, University of Oxford, 2017.
197. Wu, H., Zhang, H. and Zhao, G., *Tetrahedron*, 2007, **63**, 6454-6461.
198. Kong, D. Spiro and other derivatives of diamondoids posessing therapeutic activity in the treatment of viral disorders. EP1995227A1, March 31, 2008.
199. Wang, T., Yin, Z., Zhang, Z., Johnson, B. L., Kadow, J. F., Well, N. A. Piperazine and Homopiperazine Derivatives as HIV Attachment Inhibitors, WO2014/160689, October 2, 2014.
200. Dolman, S. J., Schrock, R. R. and Hoveyda, A. H., *Org. Lett.*, 2003, **5**, 4899 - 4902.
201. Connolly, T., Wang, Z., Walker, M. A., McDonald, I. M. and Peese, K. M., *Org Lett*, 2014, **16**, 4444-4447.
202. Li, B., Harjani, J. R., Cormier, N. S., Madarati, H., Atkinson, J., Cosa, G. and Pratt, D. A., *J Am Chem Soc*, 2013, **135**, 1394-1405.
203. Xiao, K. J., Luo, J. M., Xia, X. E., Wang, Y. and Huang, P. Q., *Chemistry*, 2013, **19**, 13075-13086.
204. Clark, R. D., Ray, N. C., Blaney, P. M., Hurley, C. A., Williams, K. Fused Ring Azadecalin Glucocorticoid Receptor Modulators, CA02558899, February 5, 2013.
205. Pouliquen, M., Blanchet, J., Lasne, M. C. and Rouden, J., *Org. Lett.*, 2008, **10**, 1029 - 1032.
206. SBM CDT Report of Pol Hernandez Llado, University of Oxford, 2018.
207. He, X., Jiang, Y., Zhang, Y., Wu, S., Dong, G., Liu, N., Liu, Y., Yao, J., Miao, Z., Wang, Y., Zhang, W. and Sheng, C., *MedChemComm*, 2015, **6**, 653-664.
208. O'Hanlon, J. A., Ren, X., Morris, M., Wong, L. L. and Robertson, J., *Org Biomol Chem*, 2017, **15**, 8780-8787.
209. Chang, D., Feiten, H. J., Engesser, K. H., Van Beilen, J. B. and Witholt, B., *Org. Lett.*, 2002, **4**, 1859-1862.
210. Li, H. and Poulos, T. L., *Nat. Struct. Biol.*, 1997, **4**, 140-146.
211. Fisher, M.
212. Huang, W. C., Westlake, A. C., Marechal, J. D., Joyce, M. G., Moody, P. C. and Roberts, G. C., *J Mol Biol*, 2007, **373**, 633-651.
213. Ravichandran, K. G., Boddupalli, S. S., Hasermann, C. A., Peterson, J. A. and Deisenhofer, J., *Science*, 1993, **261**, 731 - 736.
214. Woods, M. and Sherry, D., *Inorg. Chem.*, 2003, **42**, 4401-4408.
215. Martin, A., Vors, J.-P. and Baudoin, O., *ACS Catalysis*, 2016, **6**, 3941-3945.
216. Zhang, C., Wang, Y., Song, Y., Gao, H., Sun, Y., Sun, X., Yang, Y., He, M., Yang, Z., Zhan, L., Yu, Z.-X. and Rao, Y., *CCS Chemistry*, 2019, **1**, 352-364.
217. Wilkinson, S. M., Barron, M. L., O'Brien-Brown, J., Janssen, B., Stokes, L., Werry, E. L., Chishty, M., Skarratt, K. K., Ong, J. A., Hibbs, D. E., Vugts, D. J., Fuller, S., Windhorst, A. D. and Kassiou, M., *ACS Chem Neurosci*, 2017, **8**, 2374-2380.
218. DPhil thesis of John Liddon, University of Oxford, 2015.

219. Kong, D., Lam, F. W., Sciamanna, S. F., Shelton, E., Liu, S., Carlson, R. M. Spiro and Other Derivatives of Diamondoids Possessing Therapeutic Activity in the Treatment of Viral Disorders, US2008/0293685, November 27, 2008.
220. Beck, H. P., Booker, S. K., Bregman, H., Cee, V. J., Chakka, N., Cushing, T. D., Epstein, O., Fox, B. M., Geuns-Meyer, S., Hao, X., Hibiya, K., Hirata, J., Hua, 309 Z., Human, J., Kakuda, S. Pyrazole Amide Derivative, WO2015/129926A1, September 3, 2015.
221. Yoo, S. E. and Lee, S. H., *Synlett*, 1990, **7**, 419-420.
222. Prakash rao, H. S. and Siva, P., *Synthetic Communications*, 1994, **24**, 549-555.
223. Ganem, B. and Osby, J. O., *Chem. Rev.*, 1986, **86**, 763-780.
224. Rao, H. S. P. and Bharathi, B., *Indian J. Chem.*, 2002, **41B**, 1072-1074.
225. Glavee, G. N., Klabunde, K. J., Sorensen, C. M. and Hadjipanayis, G. C., *Langmuir*, 1994, **10**, 4726-4730.
226. Hodgson, H. H., *Chem. Rev.*, 1947, **40**, 251-277.
227. Acevedo-Rocha, C. G., Gamble, C. G., Lonsdale, R., Li, A., Nett, N., Hoebenreich, S., Lingnau, J. B., Wirtz, C., Fares, C., Hinrichs, H., Deege, A., Mulholland, A. J., Nov, Y., Leys, D., McLean, K. J., Munro, A. W. and Reetz, M. T., *ACS Catalysis*, 2018, **8**, 3395-3410.
228. Watanabe, Y., Laschat, S., Budde, M., Affolter, O., Shimada, Y. and Urlacher, V. B., *Tetrahedron*, 2007, **63**, 9413-9422.
229. Schewe, H., Holtmann, D. and Schrader, J., *Appl Microbiol Biotechnol*, 2009, **83**, 849-857.
230. Bernhardt, R., *J Biotechnol*, 2006, **124**, 128-145.
231. Jung, S. T., Lauchli, R. and Arnold, F. H., *Curr Opin Biotechnol*, 2011, **22**, 809-817.
232. Roiban, G. D. and Reetz, M. T., *Chem Commun (Camb)*, 2015, **51**, 2208-2224.
233. Rea, V., Dragovic, S., Boerma, J. S., de Kanter, F. J., Vermeulen, N. P. and Commandeur, J. N., *Drug Metab Dispos*, 2011, **39**, 2411-2420.
234. Vottero, E., Rea, V., Lastdrager, J., Honing, M., Vermeulen, N. P. and Commandeur, J. N., *J Biol Inorg Chem*, 2011, **16**, 899-912.
235. Graham-Lorence, S., Truan, G., Peterson, J. A., Falck, J. R., Wei, S., Helvig, C. and Capdevila, J. H., *J Biol Chem*, 1997, **272**, 1127-1135.
236. Calandra, N. A., King, S. M. and Herzon, S. B., *J Org Chem*, 2013, **78**, 10031-10057.
237. Zou, C.-L., Cai, L., Ji, H., Xie, G.-B., Wang, F.-P., Jian, X.-X., Song, L., Liu, X.-Y., Chen, D.-L. and Chen, Q.-H., *Tetrahedron*, 2008, **64**, 7594-7604.
238. Kimura, Y., Atarashi, S., Kawakami, K., Sato, K. and Hayakawa, I., *J. Med. Chem.*, 1994, **37**, 3344 - 3352.
239. Dong, L., Xu, Y. J., Cun, L. F., Cui, X., Mi, A. Q., Jiang, Y. Z. and Gong, L. Z., *Org. Lett.*, 2005, **7**, 4285 - 4288.
240. Semple, J. E., Wang, P. C., Lysenko, Z. and Jouillie, M. M., *J. Am. Chem. Soc.*, 1980, **102**, 7505 - 7510.
241. Yamamoto, Y., Shimizu, E., Ban, K., Wada, Y., Mizusaki, T., Yoshimura, M., Takagi, Y., Sawama, Y. and Sajiki, H., *ACS Omega*, 2020, **5**, 2699-2709.
242. Ji, H., Jing, Q., Huang, J. and Silverman, R. B., *Tetrahedron*, 2012, **68**, 1359-1366.
243. Li, Y., Manickam, G., Ghoshal, A. and Subramaniam, P., *Synthetic Communications*, 2006, **36**, 925-928.
244. Wei, L., He, G.-G., Liu, L., Tang, M., Zhang, T., Bai, H. and Du, Z.-T., *Russian Journal of Organic Chemistry*, 2020, **56**, 1089-1095.
245. Bull, S. D., Davies, S. G., Fenton, G., Mulvaney, A. W., Prasad, R. S. and Smith, A. D., *Journal of the Chemical Society, Perkin Transactions 1*, 2000.
246. Moriyama, K., Nakamura, Y. and Togo, H., *Org Lett*, 2014, **16**, 3812-3815.

247. Wall, M. J., Player, M. R., Patch, R. J., Meegalla, S., Liu, J., Illig, C. R., Cheung, W., Chen, J. S., Asgari, D. Quinolinone Derivatives as Inhibitors of c-fms Kinase, WO2005/009967A2, February, 3, 2005.
248. Humphries, P. S., Bersot, R., Kincaid, J., Mabery, E., McCluskie, K., Park, T., Renner, T., Riegler, E., Steinfeld, T., Turtle, E. D., Wei, Z. L. and Willis, E., *Bioorg Med Chem Lett*, 2018, **28**, 293-297.
249. Rombouts, F., Franken, D., Martínez-Lamenca, C., Braeken, M., Zavattaro, C., Chen, J. and Trabanco, A. A., *Tetrahedron Letters*, 2010, **51**, 4815-4818.
250. Tokuyama, H., Okano, K., Okuyama, K.-i. and Fukuyama, T., *Synlett*, 2008, **2008**, 1977-1980.
251. Amat, M., Guignard, G., Llor, N. and Bosch, J., *J Org Chem*, 2014, **79**, 2792-2802.
252. Inoue, M., Sumii, Y. and Shibata, N., *ACS Omega*, 2020, **5**, 10633-10640.
253. Database, K. D., https://www.genome.jp/kegg/drug/).
254. Alonso, P., Pardo, P., Fontaneda, R., Fananas, F. J. and Rodriguez, F., *Chemistry*, 2017, **23**, 13158-13163.
255. Fontaneda, R., Fananas, F. J. and Rodriguez, F., *Chem Commun (Camb)*, 2018, **54**, 11025-11028.
256. Buchwald, S. L., LaMaire, S. J., Nielsen, R. B., Watson, B. T. and King, S. M., *Tetrahedron Lett.*, 1987, **28**, 3895-3898.
257. Reed-Berendt, B. G., Latham, D. E., Dambatta, M. B. and Morrill, L. C., *ACS Cent Sci*, 2021, **7**, 570-585.
258. Balcells, D., Nova, A., Clot, E., Gnanamgari, D., Crabtree, R. H. and Eisenstein, O., *Organometallics*, 2008, **27**, 2529 - 2535.
259. Li, Z. and Zhang, Y., *Tetrahedron*, 2002, **58**, 5301 - 5306.
260. Zhang, X., 2022.
261. Tavanti, M., Mangas-Sanchez, J., Montgomery, S. L., Thompson, M. P. and Turner, N. J., *Org Biomol Chem*, 2017, **15**, 9790-9793.
262. Heravi, M. M. and Zadsirjan, V., *RSC Advances*, 2020, **10**, 44247-44311.
263. Hazelard, D., Nocquet, P.-A. and Compain, P., *Org. Chem. Front.*, 2017, **4**, 2500-2521.
264. Bois, J. D., *Org Process Res Dev*, 2011, **15**, 758-762.
265. Alderson, J. M., Phelps, A. M., Scamp, R. J., Dolan, N. S. and Schomaker, J. M., *J Am Chem Soc*, 2014, **136**, 16720-16723.
266. Ju, M., Huang, M., Vine, L. E., Dehghany, M., Roberts, J. M. and Schomaker, J. M., *Nature Catalysis*, 2019, **2**, 899-908.
267. Schomaker, J. M., Vine, L. E. and Zerull, E. E., *Synlett*, 2020, **32**, 30-44.
268. Mou, X. Q., Chen, X. Y., Chen, G. and He, G., *Chem Commun (Camb)*, 2018, **54**, 515-518.
269. Stateman, L. M., Wappes, E. A., Nakafuku, K. M., Edwards, K. M. and Nagib, D. A., *Chem Sci*, 2019, **10**, 2693-2699.
270. Wappes, E. A., Nakafuku, K. M. and Nagib, D. A., *J Am Chem Soc*, 2017, **139**, 10204-10207.
271. Grigorjeva, L., Maleckis, A., Klimovica, K., Skvorcova, M., Ivdra, N., Leitis, G. and Jirgensons, A., *Chem. heterocycl. compounds*, 2012, **48**, 919-924.
272. Breslow, D. S., Edwards, E. I., Leone, R., Schleyer, P. R. , *J. Am. Chem. Soc.*, 1968, **90**.
273. Talele, T. T., *J Med Chem*, 2016, **59**, 8712-8756.
274. Taylor, R. D., MacCoss, M. and Lawson, A. D., *J Med Chem*, 2014, **57**, 5845-5859.
275. Blanksby, S. J. and Ellison, G. B., *Acc. Chem. Res.*, 2003, **36**, 255-263.

276. Grimm, M. L., Suleman, N. K., Hancock, A. N., Spencer, J. N., Dudding, T., Rowshanpour, R., Castagnoli, N., Jr. and Tanko, J. M., *J Am Chem Soc*, 2020, **142**, 2640-2652.
277. Cavani, F., Raabova, K., Bigi, F. and Quarantelli, C., *Chemistry*, 2010, **16**, 12962-12969.
278. White, N. A. and Rovis, T., *J Am Chem Soc*, 2015, **137**, 10112-10115.
279. Kaur, K. and Srivastava, S., *New Journal of Chemistry*, 2020, **44**, 18530-18572.
280. Ali, I., Saleem, K., Gaitonde, V. D., Aboul-Enein, H. Y. and Hussain, I., *Chirality*, 2010, **22**, 24-28.
281. Randle, E., 2022.
282. Luo, J., Ling, Y., Zhang, P., Sun, L. and Lai, W., *Synthesis*, 2014, **46**, 2225-2233.
283. Ramalingan, C. and Park, Y. T., *J. Org. Chem.*, 2007, **72**, 4536-4538.
284. Sze, Y. K. and Irish, D. E., *Can. J. Chem.* , 1975, **53**, 427-436.
285. Peltzer, R. M., Gauss, J., Eisenstein, O. and Cascella, M., *J Am Chem Soc*, 2020, **142**, 2984-2994.
286. Harada, S., Matsuda, D., Morikawa, T. and Nishida, A., *Synlett*, 2020, **31**, 1372-1377.
287. Lebel, H., Guay, D., Paquet, V. and Huard, K., *Org. Lett.*, 2004, **5**.
288. Rivkin, A., Yoshimura, F., Gabarda, A. E., Chou, T. C., Dong, H., Tong, W. P. and Danishefsky, S. J., *J. Am. Chem. Soc.*, 2003, **125**, 2899-2901.
289. Claridge, T. D. W., Davies, S. G., Lee, J. A., Nicholson, R. L., Roberts, P. M., Russell, A. J., Smith, A. D. and Toms, S. M., *Org. Lett.*, 2008, **10**, 5437-5440.
290. Petasis, N. A. and Bzowej, E. I., *J. Am. Chem. Soc.*, 1990, **112**, 6392-6394.
291. Hartley, R. C., Li, J., Main, C. A. and McKiernan, G. J., *Tetrahedron*, 2007, **63**, 4825-4864.
292. Zhou, W., Qian, P., Zhao, J., Fang, H., Han, J. and Pan, Y., *Org Lett*, 2015, **17**, 1160-1163.
293. Chawner, S. J., Cases-Thomas, M. J. and Bull, J. A., *European J Org Chem*, 2017, **2017**, 5015-5024.
294. Ravindranath, P. A., Forli, S., Goodsell, D. S., Olson, A. J. and Sanner, M. F., *PLoS Comput Biol*, 2015, **11**, e1004586.
295. Bach, R. D. and Dmitrenko, O., *J. Am. Chem. Soc.*, 2004, **126**, 4444-4452.
296. Tian, Z., Fattahi, A., Lis, L. and Kass, S. R., *J. Am. Chem. Soc.*, 2006, **128**, 17087-17092.
297. Valentine, A. M., LeTadic-Biadatti, M. H., Toy, P. H., Newcomb, M. and Lippard, S. J., *J Biol Chem*, 1999, **274**, 10771-10776.
298. Ruzicka, F., Huang, D. S., Donnelly, M. I. and Frey, P. A., *Biochemistry*, 1990, **29**, 1696-1700.
299. Clark, J. P., Miles, C. S., Mowat, C. G., Walkinshaw, M. D., Reid, G. A., Daff, S. N. and Chapman, S. K., *J Inorg Biochem*, 2006, **100**, 1075-1090.
300. Volz, T. J., Rock, D. A. and Jones, J. P., *J. Am. Chem. Soc.*, 2002, **124**, 9724 - 9725.
301. Cryle, M. J. and De Voss, J. J., *Angew Chem Int Ed Engl*, 2006, **45**, 8221-8223.
302. Shahrokh, K., Orendt, A., Yost, G. S. and Cheatham, T. E., 3rd, *J. Comput. Chem.*, 2012, **33**, 119-133.
303. Guengerich, F. P., Martin, M. V., Sohl, C. D. and Cheng, Q., *Nat Protoc*, 2009, **4**, 1245-1251.
304. Abraham, M. J., Murtola, T., Schulz, R., Páll, S., Smith, J. C., Hess, B. and Lindahl, E., *SoftwareX*, 2015, **1-2**, 19-25.
305. Whitehouse, C. J., Yang, W., Yorke, J. A., Rowlatt, B. C., Strong, A. J., Blanford, C. F., Bell, S. G., Bartlam, M., Wong, L. L. and Rao, Z., *Chembiochem*, 2010, **11**, 2549-2556.

306. Shahrokh, K., Orendt, A., Yost, G. S. and Cheatham, T. E., 3rd, *J Comput Chem*, 2012, **33**, 119-133.
307. Lindorff-Larsen, K., Piana, S., Palmo, K., Maragakis, P., Klepeis, J. L., Dror, R. O. and Shaw, D. E., *Proteins*, 2010, **78**, 1950-1958.
308. Jorgensen, W. L., Chandrasekhar, J., Madura, J. D., Impey, R. W. and Klein, M. L., *The Journal of Chemical Physics*, 1983, **79**, 926-935.
309. Darden, T., York, D. and Pedersen, L., *The Journal of Chemical Physics*, 1993, **98**, 10089-10092.
310. Hess, B., *J. Chem. Theory Comput.*, 2008, **4**, 435-447.
311. Bussi, G., Donadio, D. and Parrinello, M., *J Chem Phys*, 2007, **126**, 014101.
312. Yang, Y. I., Shao, Q., Zhang, J., Yang, L. and Gao, Y. Q., *J Chem Phys*, 2019, **151**, 070902.
313. Parrinello, M. and Rahman, A., *Journal of Applied Physics*, 1981, **52**, 7182-7190.
314. Daura, X., Gademann, K., Jaun, B., Seebach, D., van Gunsteren, W. F. and Mark, A. E., *Angewandte Chemie International Edition*, 1999, **38**, 236-240.
315. Trott, O. and Olson, A. J., *J Comput Chem*, 2010, **31**, 455-461.
316. Sidduri, A., Lou, J. P., Campbell, R., Rowan, K. and Tilley, J. W., *Tetrahedron Lett.*, 2001, **42**, 8757-8760.
317. Escudero, J., Bellosta, V. and Cossy, J., *Angew Chem Int Ed Engl*, 2018, **57**, 574-578.
318. Saadabad, H. R. and Akhlaghinia, B., *Chem. Pap.* , 2015, **69**, 479-485.
319. Brandt, J. C. and Wirth, T., *Beilstein J Org Chem*, 2009, **5**, 30.
320. Nielsen, S. D., Smith, G., Begtrup, M. and Kristensen, J. L., *European Journal of Organic Chemistry*, 2010, **2010**, 3704-3710.
321. Pearson, W. H. and Walavalkar, R., *Tetrahedron*, 2001, **57**, 5081 - 5089.
322. Widjaja, T., Fitjer, L., Pal, A., Schmidt, H. G., Noltemeyer, M., Deidrich, C. and Grimme, S., *J. Org. Chem.*, 2007, **72**, 9264 - 9277.
323. Wu, X., Riedel, J. and Dong, V. M., *Angew Chem Int Ed Engl*, 2017, **56**, 11589-11593.
324. Wolckenhauer, S. A. and Rychnovsky, S. D., *Org. Lett.*, 2004, **6**, 2745 - 2748.
325. Natarajan, P., Chaudhary, R. and Venugopalan, P., *J Org Chem*, 2015, **80**, 10498-10504.
326. de Filippis, A., Gomez Pardo, D. and Cossy, J., *Tetrahedron*, 2004, **60**, 9757-9767.
327. Winter, D. K., Drouin, A., Lessard, J. and Spino, C., *J Org Chem*, 2010, **75**, 2610-2618.
328. Kim, S., Joe, G. H. and Do, J. Y., *J. Am. Chem. Soc.*, 1993, **115**, 3328-3329.
329. Yamamoto, H., Ho, E., Sasaki, I., Mitsutake, M., Takagi, Y., Imagawa, H. and Nishizawa, M., *Eur. J. Org. Chem.*, 2011, **2011**, 2417-2420.
330. Inaloo, I. D., Majnooni, S. and Esmaeilpour, M., *Eur. J. Org. Chem.*, 2018, **2018**, 3481-3488.
331. Duchemin, N., Buccafusca, R., Daumas, M., Ferey, V. and Arseniyadis, S., *Org Lett*, 2019, **21**, 8205-8210.
332. Lin, K. W., Yan, S., Hsieh, I. L. and Yan, T. H., *Org. Lett.*, 2006, **8**, 2265-2267.
333. Park, Y. S. and Beak, P., *Tetrahedron*, 1996, **52**, 12333-12350.